THE PHYSICAL REVIEW

VOLUME 88 Second S N

OCTOBER 1 1952

Published for

AMERICAN PHYSICAL SOCIETY

Information for Contributors

Manuscripts

Send manuscripts to S. A. Goudsmit, Brookhaven National Laboratory, Upton, Long Island, New York.

Each article submitted will in general consist of (a) textual material, i.e., all material which is to be set in type, and (b) drawings or photographs from which zinc etchings or copper halftones will be made. Textual material will consist of an abstract, the body of the paper, tabular material, references, and figure captions. All of this material must be in English, typewritten (except mathematical expressions) double spaced with wide margins (for editorial instructions to the printer) on a durable, white paper, preferably letter size. The original copy, not the carbon, should be submitted.

For general style, spellings, abbreviations, and form, recent issues of this journal should be consulted.

The prime requisite is that the copy shall be clear to the typesetter, who is neither a physicist nor a mathematician.

Abstracts

An abstract must accompany each article. It should be adequate as an index and as a summary. As an index, it should give all subjects, major and minor, concerning which new information is presented. As a summary it should give the conclusions of the article and all numerical results of general interest.

Mathematical Expressions

All but the simplest mathematical expressions should be carefully printed in by hand. Be sure to distinguish between capital and small letters. Indicate clearly superscripts and subscripts by inverted carets and carets, respectively. Avoid complicated superscripts and subscripts. Avoid repetition of a complicated expression by representing it by some convenient symbol. Identify in the margin Greek letters and unusual symbols. Use fractional exponents instead of root signs. Use the solidus (/) for fractions wherever its use will save vertical space.

References

References should appear as footnotes, numbered consecutively, and arranged thus:

[1] A. B. Smith, Phys. Rev. 61, 852 (1932).
[2] H. Lamb, *Hydrodynamics* (Cambridge University Press, Cambridge, England, 1940), sixth edition, pp. 573, 645.

Tables

All but the simplest tabular material should be organized in tabular form rather than as a part of the running text. Tables may be typewritten on sheets separate from the running text with indications in the margin of the running text where the table is to be inserted. Each table must have a caption which will make the data in the table intelligible without reference to the text. Avoid complicated column headings; if necessary, use symbols which are explained in the table caption.

Figures

Wherever possible figures should be planned for the width of a column of the *Physical Review* (3 inches). A convenient reduction ratio is about 2:1 or 3:1. The original drawings or photographs should therefore be in general about 6 to 9 inches wide and the lettering and symbols should be large enough on the original that when reduced they shall not be less than about $\frac{1}{16}$ in. (~1.5 mm). If the reduction is 3:1, the original lettering should be not less than $\frac{1}{8}$ in. high.

The process of making zinc etchings or copper halftones is a black and white photographic one. Therefore line drawings must be in *india ink* on white paper or tracing cloth. Coordinate paper is not desirable but if used must be blue lined and the coordinate lines which are to show must be inked over.

Photographs should have maximum black and white contrast.

Plan figures to use space efficiently. Avoid wasting space, particularly at the top or bottom.

Identify on the black or other suitable place each original drawing or photograph with the author's name and the figure number. Figures should be numbered consecutively and their approximate position indicated in the margin of the running text. Figure captions should be typed and included with the manuscript (not as part of the figure).

Avoid round and oval photographs.

Alterations

Take great care that each manuscript is typographically accurate. A limited number of alterations in proof are unavoidable, but the cost of making extensive alterations after the article has been set in type will be charged to the author.

Proof and all correspondence concerning papers in the process of publication should be addressed to the Publication Manager, American Institute of Physics, 57 East 55 Street, New York 22, New York.

THE PHYSICAL REVIEW

A journal of experimental and theoretical physics established by E. L. Nichols in 1893

VOLUME 88

Second Series

OCTOBER 1–DECEMBER 15, 1952

Published for the

AMERICAN PHYSICAL SOCIETY

by the

AMERICAN INSTITUTE OF PHYSICS
Incorporated

THE PHYSICAL REVIEW

A journal of experimental and theoretical physics established by E. L. Nichols in 1893

Published by the American Institute of Physics for the

AMERICAN PHYSICAL SOCIETY

Officers

President

J. H. VAN VLECK
Harvard University
Cambridge, Massachusetts

Vice-President

ENRICO FERMI
Institute for Nuclear Studies
University of Chicago
Chicago 37, Illinois

Secretary

K. K. DARROW
Bell Telephone Laboratories
Office:
Columbia University
New York 27, New York

Treasurer

G. B. PEGRAM
Columbia University
New York 27, New York

Local Secretary for the Pacific Coast

J. KAPLAN
University of California at Los Angeles
Los Angeles, California

Managing Editor

S. A. GOUDSMIT
Brookhaven National Laboratory
Upton, Long Island
New York

BOARD OF EDITORS

Editor

S. A. GOUDSMIT

Assistant Editor

S. PASTERNACK

Associate Editors

HARVEY BROOKS
R. F. CHRISTY
C. L. CRITCHFIELD
M. DEUTSCH
T. H. JOHNSON
BRUNO ROSSI
M. GOLDHABER
R. HOFSTADTER
A. W. LAWSON
A. PAIS
R. SERBER
C. H. TOWNES
W. P. ALLIS
F. G. BRICKWEDDE
W. B. FRETTER
CONYERS HERRING
H. W. LEVERENZ
ARNOLD NORDSIECK

Manuscripts for publication should be submitted to S. A. GOUDSMIT, Brookhaven National Laboratory, Upton, Long Island, New York. The authors' institutions are requested to pay a publication charge of $15 per page which, if honored, entitles them to 100 free reprints. Instructions will be sent with galley proofs.

Proof and all correspondence concerning papers in the process of publication should be addressed to the Publication Manager, American Institute of Physics, 57 East 55 Street, New York 22, New York.

Subscription Price

United States and Canada $30.00
Elsewhere $32.00

Back Numbers [1]

Yearly back number rate when complete year is available:
Prior to 1949: $25.00
Thereafter: $33.00
Single copies: $3.00 each, prior to July, 1929;
$1.50 each, July, 1929–December, 1941;
$3.00 each, January, 1942–December, 1946;
$1.50 each, thereafter.
General index, 1893–1920: $4.00.

Subscriptions, renewals, and orders for back numbers should be addressed to the American Institute of Physics, 57 East 55 Street, New York 22, New York.

Changes of address in the case of members of the American Physical Society should be addressed to the Treasurer; in the case of other subscribers to the American Institute of Physics.

[1] For Series 1 inquire of Physics Department, Cornell University, Ithaca, New York.

The Physical Review is published semi-monthly at Prince and Lemon Streets, Lancaster, Pennsylvania.

Entered as second-class matter March 6, 1947, at the Post Office at Lancaster, Pennsylvania, under the Act of March 3, 1879.

Acceptance for mailing at special rate of postage provided for in paragraph (d-2), section 34.40, P. L. & R. of 1948, authorized January 27, 1933.

THE
PHYSICAL REVIEW

A journal of experimental and theoretical physics established by E. L. Nichols in 1893

SECOND SERIES, VOL. 88, NO. 1 OCTOBER 1, 1952

Neutron Energy Distributions from Be, C, and Pb Bombarded by 245-Mev Protons*

B. K. NELSON,† G. GUERNSEY,‡ AND G. MOTT§
Department of Physics, University of Rochester, Rochester, New York
(Received March 10, 1952)

The energy distribution of the neutrons radiated by targets bombarded by protons of energy 244 Mev has been measured. Neutrons in the forward direction from Be, C, and Pb targets were observed, and in a direction 15° forward from Be and C targets.

The neutrons were allowed to bombard a polyethylene radiator; scattered protons were observed by a scintillation counter coincidence telescope of four anthracene crystals. The effect of the carbon in the polyethylene was determined by taking similar data with a carbon radiator. The last counter in the telescope was used as a proportional counter, proton energies being determined by measuring the height of the scintillation pulse in this crystal. A gated amplifier, turned on by a coincidence among the four crystals of the telescope, assured that only those pulses in the proportional counter corresponding to protons traversing the telescope from the radiator were counted. The entire neutron spectrum from about 120 to 240 Mev was measured at once by measuring the spectrum of pulses in the proportional crystal with a 24-channel pulse-height analyzer.

All the spectra observed were found to be peaked, the energies at the peaks being about 215, 195, and 180 Mev for Be, C, and Pb, respectively, in the forward direction, and at about 175 and 165 for Be and C at 15°.

The carbon and lead spectra were more broadly peaked than the beryllium spectra, and the 15° spectra were broader than the 0° spectra, the full widths at half-maximum being 27 percent, 33 percent, and 49 percent for Be, C, and Pb forward spectra, and 40 percent and 42 percent for Be and C at 15°.

INTRODUCTION

THIS experiment is one of a group of three performed with the same equipment; the others were the measurement of the total neutron cross section in hydrogen and carbon at various energies in the range from 90 to 220 Mev,[1] and the measurement of the differential n-p scattering cross section at 180 and 220 Mev.[2]

The experiments make use of an anthracene scintillation crystal in the measurement of the energy of the protons from n-p scattering; since the intensity of the scintillation is a monotonic function of the energy loss of the proton in the crystal, which in turn is a function of the incident energy of the proton; it is possible, by measuring the height of the scintillation pulse, to determine the energy of the proton. This method of determining the proton energy presents certain advantages over the use of absorbers, namely, the large and somewhat uncertain corrections for losses in the absorbers do not have to be made, and further, it is possible to obtain information concerning a large part of the neutron spectrum at one time.

APPARATUS

The Neutron Source

Three targets were mounted on flip coils arranged in a circle so that any one of them could be raised into the same position in the proton beam. They were a 1-in. Be target, a 0.781-in. carbon target, and a 0.309-in. Pb target, located at the 58-in. radius of the Rochester 130-in. cyclotron, where the energy of the proton beam, calculated from the magnetic field at that radius, is about 244 Mev. Two of the sets of data reported were obtained with a fourth, ½-in. Be target, at a radius of 58¼ in., where the proton energy is about 245 Mev.

Collimator

A three-foot cube of copper, with a 1-in.×1-in. hole through it, was used to collimate the neutron beam and shield the counters from the direct radiation from the

* This research was supported by the AEC.
† Now at Massachusetts Institute of Technology (Project Lincoln), Cambridge, Massachusetts.
‡ Now at Massachusetts Institute of Technology (Project Lincoln), Cambridge, Massachusetts.
§ Now at Medical Center, University of Rochester, Rochester, New York.
[1] Mott, Guernsey, and Nelson, following paper [Phys. Rev. 88, 9 (1952)].
[2] Guernsey, Nelson, and Mott, accompanying paper [Phys. Rev. 88, 15 (1952)].

cyclotron. This shielding was essential for reduction of the background.

Radiator and Counter Telescope

Two *n-p* radiators, one polyethylene and one carbon, were mounted on a wheel in such a way that by selsyn control from the research room either one could be inserted in the neutron beam behind the collimator, or no radiator at all. The polyethylene radiator was $\frac{1}{2}$ in. thick, the carbon radiator of such a thickness as to have the same number of carbon nuclei per square centimeter as the other.

Protons scattered from the radiator were detected by a counter telescope consisting of four anthracene crystals with RCA 5819 photomultipliers. The photomultipliers and their associated preamplifiers were provided with magnetic shields consisting of three concentric iron cylinders, for operation in the stray magnetic field of the cyclotron. The first three crystals were mounted on Lucite light pipes to remove their shields from the neutron beam. The fourth crystal was mounted directly on the photomultiplier, adjacent to the photocathode, for maximum pulse-height resolution.

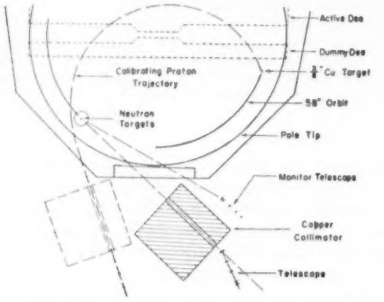

FIG. 1(a). Experimental arrangement. The dotted lines indicate the position of the equipment during the calibration, the solid lines the position during the run.

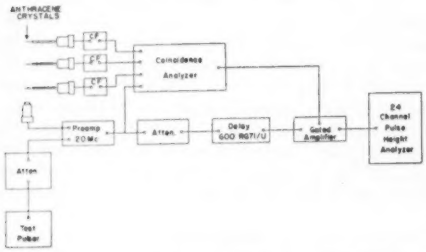

FIG. 1(b). Block diagram of electronics. During the calibration with the test pulser, an additional connection was made between the pulser and the coincidence analyzer, so the gated amplifier was turned on in the same way as during a run.

Alignment

The equipment was designed so that the collimator could be put in a predetermined position by rolling it into place along tracks which had been aligned with lines scribed in the coil dust cover. The counter telescope and radiator support wheel, in a separate assembly, were then supported on the tracks behind the collimator, a slight amount of adjustment being allowed to center the radiator in the beam. The telescope assembly was constructed so that the entire telescope could be rotated about a vertical axis through the radiator.

Figure 1(a) is a diagram of the experimental arrangement.

Electronics[3]

A fourfold coincidence circuit with a resolving time δ of 4×10^{-8} second was used with the telescope. Pulses from this circuit were used to trigger a gated amplifier which was part of a highly stabilized (by negative feedback) chain of amplifiers driven by the fourth, or proportional, crystal. The length of the gate was 0.75 microsecond. The output of this amplifier chain was analyzed by a 24-channel pulse-height analyzer.[4]

Cathode followers were used to couple the first three photomultipliers to the 93-ohm cable between cyclotron and research rooms, while for increased stability under line voltage changes, a three-stage feed-back amplifier with unity gain was used with the fourth.

A delay of 600 feet of 93-ohm coaxial cable was used in the proportional chain ahead of the gated amplifier, to assure the arrival of the pulse in the middle of the gate.

After the coincidence circuit was adjusted for proper discrimination against triples, counting rate *versus* voltage data were taken with each photomultiplier separately; the tubes were then operated at voltages on the plateaux of these curves. The high voltage for the photomultipliers was supplied by a regulated power supply. Figure 1(b) shows a block diagram of the electronics.

Calibration

The equipment was calibrated both with electrically generated pulses simulating the shape of a scintillation pulse, and with monoenergetic protons.

The electronic pulses were generated by discharging a condenser into a 93-ohm cable connected to the input of the photomultiplier preamplifier. Additional outputs from the pulser were used to trigger the coincidence circuit during calibration in a manner similar to that obtaining during a run. The voltage to which the condenser was charged was used as an indication of the size of the pulse. By varying this voltage and observing

[3] Guernsey, Mott, Nelson, and Roberts, Rev. Sci. Instr. **23**, 476 (1952).

[4] H. Logemann (to be published). The 24-channel pulse-height analyzer described in this paper uses the principle described by D. H. Wilkinson, Proc. Cambridge Phil. Soc. **46**, 508 (1949).

the response of the pulse-height selector, the response of the entire amplifier chain to pulses at its input was calibrated.

Monoenergetic protons were obtained by using the collimator and magnetic field as a mass spectrometer, detecting protons scattered from a target properly placed in the internal proton beam (see Fig. 1). The telescope was aligned with the collimator hole and the radiators removed. The response of the proportional crystal to these protons could then be observed. Additional proton energies for calibration were obtained by putting various thicknesses of copper in the proton beam, as well as by using a second target in the cyclotron, scattered protons from which had a trajectory of different radius to the collimator.

The energy of the protons was determined by measuring their range in copper,[5] and in the case of the higher energy group, by calculation from their known trajectory in the field. These two methods agreed within one percent, giving as the energy at the crystal, 193±1.5 Mev.

Information concerning the resolution of the response of the equipment to monoenergetic protons was also obtained simultaneously with calibrating data.

The finite resolution is due largely to statistical fluctuations of the energy loss of the protons in the crystal. This has been treated theoretically in an unpublished thesis by K. R. Symon, Harvard, 1948; calculations based on this treatment indicate that resolutions between 10 and 15 percent are to be expected, improving with increasing pulse height. The resolution observed with monoenergetic protons is plotted as a function of pulse height in Fig. 2. The resolution is of the right order of magnitude to agree with Symon's thesis, and does improve with increasing pulse height, though not so fast as the theory predicts, namely from 15 percent at pulse height 16.2 to 10 percent at pulse height 23.4. The effect of straggling of the protons in the copper absorber can be seen in the increase in the width of the resolution for pulses greater than pulse height 30.

In the calculations of neutron energy spectra from scintillation pulse-height spectra, the resolution has been taken as given by the straight line, $\Delta h\sqrt{h}$ constant, in Fig. 2.

This line has been drawn somewhat below most of the points corresponding to data obtained with the 193-Mev protons. This was done because there was evidence that part of the width of the response curves was due to the fact that this proton group was not completely monoenergetic. Preliminary data taken with a larger hole in the collimator had indicated a second group of protons, just resolved, of energy about 170 Mev; it appeared that these came from some other source in the cyclotron than the target, as for example, one of the dees, and they were almost completely

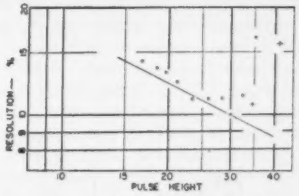

FIG. 2. Resolution of equipment *versus* scintillation pulse height. The circles indicate data obtained with 193-Mev protons from one target, degraded by various amounts of copper; the crosses indicate data obtained with 77-Mev protons from a second target, similarly degraded. The straight line is of the form $(\Delta h)\sqrt{h}$ constant.

removed when the collimator opening was reduced to the 1-in.×1-in. size used throughout the experiment. But it appeared that perhaps they were not completely removed. The line is drawn through the point at pulse height 30, 10 percent resolution, because this point corresponds to data obtained with the undegraded 77-Mev group of protons from the second proton target, which had exhibited no such low energy contamination.

The anthracene crystal used was the best available at the time of the experiment. The resolution obtained left much to be desired, as it was sometimes almost as great as the width of the spectra to be observed. The theory indicates that a thicker crystal would improve this situation, the resolution being better with the corresponding increased energy loss. The limit in this direction will be set by experimental difficulties in light collection and by nuclear interactions of the protons with the crystal.

Monitor

The monitor used was a scintillation counter telescope similar to the main telescope. This telescope was set up alongside the collimator, which shielded its counters from direct ionizing radiation from the cyclotron, as indicated in Fig. 1. There were four anthracene crystals and a polyethylene radiator. 1P21 photomultipliers were used. The proper operating voltages were determined, as before, by using a voltage on the plateau of a counting rate *versus* voltage curve for each counter.

EXPERIMENTAL PROCEDURE

The procedure adopted was as follows: First the response of the equipment to calibrating protons was observed. Then the telescope was set to some convenient angle, a neutron target raised, and with the polyethylene radiator in place, a pulse-height spectrum taken. The polyethylene was then replaced by the carbon radiator and a second pulse-height spectrum taken. This alternation between CH_2 and C radiators was then repeated until a reasonable compromise was reached between excessively long running time with good counting statistics and a short running time with poor counting

[5] Aron, Hoffman, and Williams, *Range-Energy Data*, University of California Radiation Laboratory Report No. 121 (unpublished) (1949).

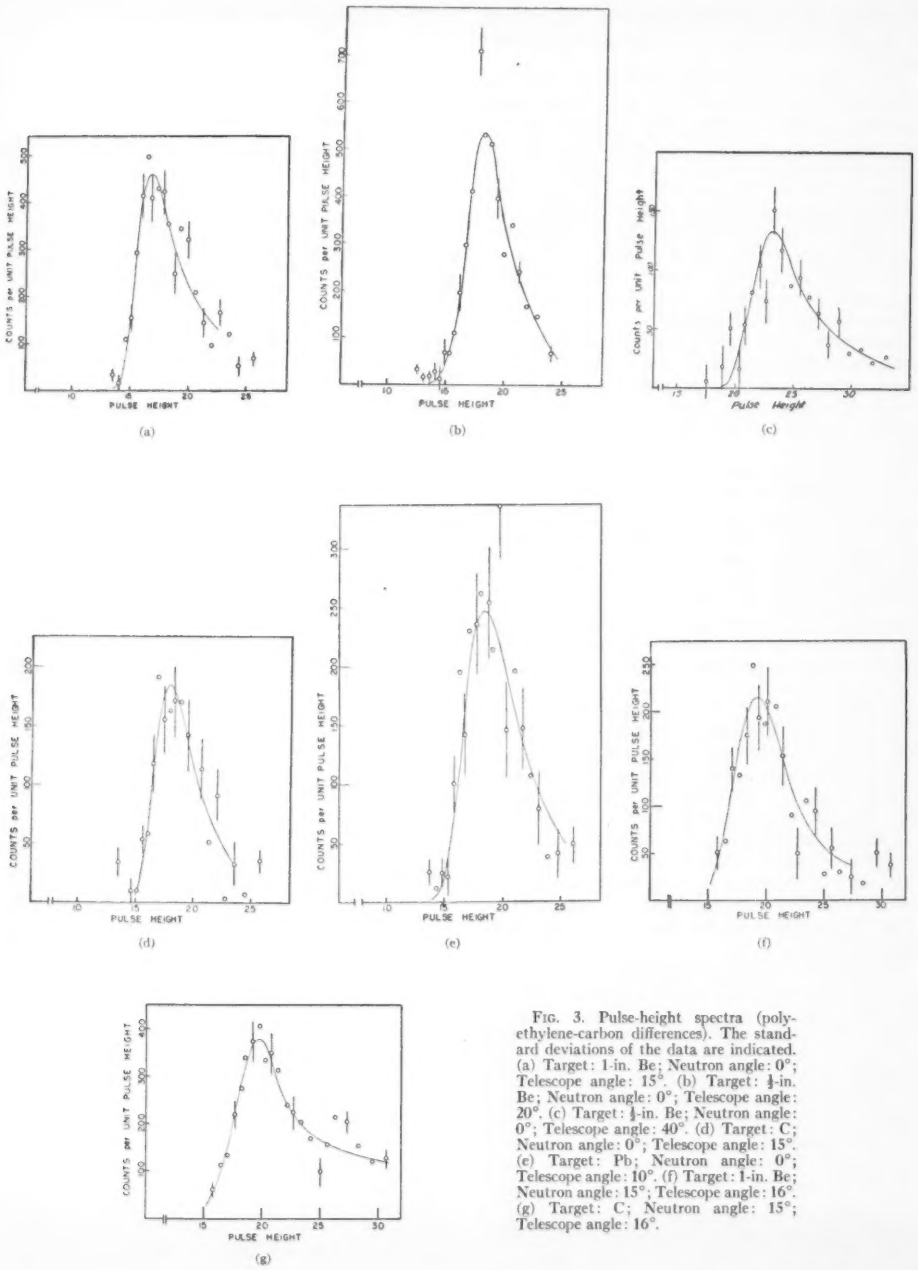

FIG. 3. Pulse-height spectra (polyethylene-carbon differences). The standard deviations of the data are indicated. (a) Target: 1-in. Be; Neutron angle: 0°; Telescope angle: 15°. (b) Target: ½-in. Be; Neutron angle: 0°; Telescope angle: 20°. (c) Target: ½-in. Be; Neutron angle: 0°; Telescope angle: 40°. (d) Target: C; Neutron angle: 0°; Telescope angle: 15°. (e) Target: Pb; Neutron angle: 0°; Telescope angle: 10°. (f) Target: 1-in. Be; Neutron angle: 15°; Telescope angle: 16°. (g) Target: C; Neutron angle: 15°; Telescope angle: 16°.

statistics. The response to the calibrating protons was then checked again.

Run Calibration

There was evidence of drift of the response of the photomultiplier during the course of the experiment, hence the calibration check for each run as outlined above.

For the two sets of data obtained with the ½-in. Be target at the 58¼-in. radius, the geometry was the same as that during the original calibration, and the run calibrating protons had the same energy, 193 Mev. For the data obtained with the other three targets, however, the geometry of the set-up was different, and the calibrating protons were of different energy. Since they were to be used to check the calibration, their energy could not be determined by direct reference to the calibration curve. The original calibration data were used, however, to determine the energy in a very simple manner. A copper absorber of known thickness was inserted in half of the proton beam, so that at the proportional crystal the proton spectrum consisted of two monoenergetic groups. The ratio of the scintillation pulse heights of these two groups is correctly given by the original calibration curves (of pulse height *versus* pulse-height selector channel number) even under a drift in the response of the photomultiplier, since such a drift will be one in gain. Having this ratio, the amount of absorber used, and the original pulse height-*vs*-proton energy curve, one can calculate the energy of the protons. It was found to be 113±1 Mev, under varying conditions of thickness of absorber and photomultiplier high voltage.

One final check on the calibration is available when the neutron spectrum is calculated from the pulse height spectrum. There must be no neutrons of energy greater than (E_p+Q), E_p being the bombarding proton energy and $-Q$ being the threshold of the (p,n) reaction in the target. As it turns out, application of this criterion indicates that there was a systematic error in pulse-height determination, of about 6 percent for those runs calibrated with the 113-Mev protons, and about 3 percent for those runs calibrated with 193-Mev protons. Apparently there was a 3 percent error in the high energy portion of the initial calibration curve, and an additional 3 percent error in the determination of the energy of the "113"-Mev protons.

The neutron spectra reported here are as calculated with these corrections applied to the pulse-height scale.

Treatment of Background

The background in this equipment can be classed in two categories as due to either fast random coincidences or slow random coincidences. In the first group, the gate is opened by a random quadruple registered in the "fast" fourfold coincidence circuit (as for example a particle traversing the first three counters accompanied by a chance coincidence in the fourth). In the second group, the gate is opened by either a true or random fast fourfold coincidence, and a particle traverses the fourth crystal by chance at such a time that its pulse reaches the gated amplifier during the time its gate is open. Of the two, because of the longer resolving time, the latter should be the more numerous. Measured, by removing the pulse-timing delay from the proportional channel, it was found, with the polyethylene radiator, to be of the order of 10 percent of the total. Its spectrum, however, exhibited the same shape as that of the total spectrum, indicating that in large part it arose from protons originating in the radiator, and hence, though measured in a random way, really consisted of a part of the true spectrum. It need not, then, be subtracted. Thus, the random background which should be subtracted is small compared with 10 percent of the total counting rate with the CH_2 radiator; it will be of the same order of magnitude with the carbon radiator, and save for a correction too small to be justified by the counting statistics attained, the random background correction will be made automatically with the carbon background subtraction.

EXPERIMENTAL RESULTS

The pulse-height spectra obtained (CH_2-C differences) are presented in Figs. 3(a) to 3(g). The standard deviations of the data are indicated. The data are plotted as obtained with pulse-height corrections made as indicated by the run calibration checks. The smooth curves are those corresponding to the neutron spectra of Figs. 4(a) to 4(g).

METHOD OF ANALYSIS OF DATA

The following steps are followed in calculation of a neutron spectrum from an observed pulse-height spectrum: (a) Correction is made for the finite pulse-height resolution of the response to monoenergetic protons (this correction is described below). (b) The corrected pulse-height spectrum is transformed to a proton energy spectrum, making use of the pulse-*vs*-energy calibration curve and its slope: $dN/dE=(dN/dh)(\partial h/\partial E)$. (c) The proton energy spectrum at the proportional crystal, just obtained, is transformed to a proton energy spectrum at the radiator, correction being made for the energy loss in the first three crystals of the telescope and in the radiator. (d) Correction is made for the finite angular resolution of the telescope because of the finite spread in proton energies scattered into the telescope by a monoenergetic neutron beam. This correction is similar to that of step (a). (e) From this proton spectrum, of form dN_p/dE_p, is calculated a spectrum of protons per unit neutron energy interval, of form dN_p/dE; proton energy as a function of neutron energy being obtained from the relativistic expression

$$E_p=\frac{E}{1+(\tan^2\theta)(1+E_n/2Mc^2)}.$$

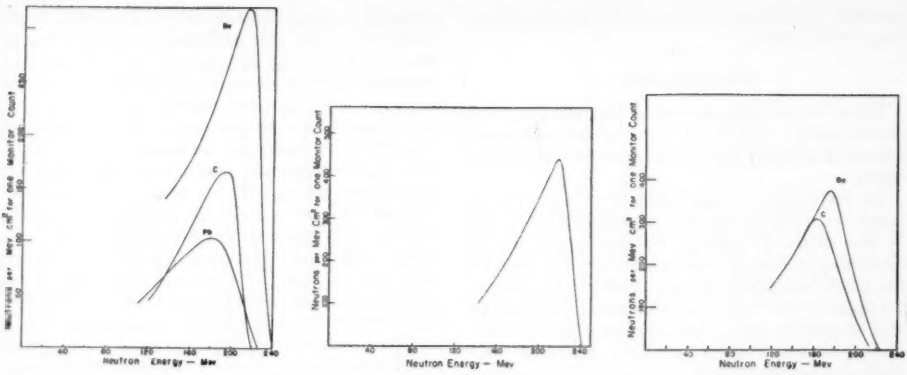

FIG. 4. Neutron energy spectra corresponding to the pulse-height spectra of Fig. 3. (a) Spectra in the forward direction from 1-in. Be, 0.781-in. C, and 0.309-in. Pb targets. (b) Spectrum in the forward direction from ½-in. Be target [corresponds to Figs. 3(b) and 3(c)]. (c) Spectra at 15° from 1-in. Be and 0.781-in. C targets.

(f) Finally, the neutron spectrum is calculated from this by

$$\frac{dN}{dE}=\left(\frac{dN_p}{dE}\right)\left(\frac{1}{k\sigma_{np}(E,\theta)}\right).$$

The cross section, $\sigma_{np}(E,\theta)$ was obtained by interpolation from the Berkeley data[6] for the differential n-p scattering cross section at 40, 90, and 260 Mev. The constant k is the product of the number of H nuclei in the radiator times the solid angle of the telescope as seen by each such nucleus.

The correction for finite resolution is the solution of the integral equation,

$$F(h)=\int_{-\infty}^{\infty} g(\eta)f(h-\eta)d\eta,$$

for $f(h)$, where $F(h)$ is the observed spectrum, and $g(\eta)$ is the resolution curve of the instrument, $g(\eta)\Delta\eta$ being the probability for recording at height h a pulse which should be recorded between height $h-\eta$ and $h-(\eta+\Delta\eta)$. This equation was solved numerically, $g(\eta)$ being obtained from the response of the equipment to monoenergetic protons.

NEUTRON SPECTRA

The spectra obtained are presented in Figs. 4(a) to 4(c). As remarked before, they are plotted as corresponding to pulse-height spectra with pulse-height scale 1.06 times that of the pulse-height spectra observed (the correction is 1.03 for the two Be spectra with 20° and 40° telescope angle).

In Fig. 5 is the spectrum of Fig. 4(a) plotted together with the spectra reported from Harvard,[7] Harwell,[8] and Berkeley,[9] from beryllium bombarded by protons of energies 114, 149, and 360 Mev, respectively.

NEUTRON SPECTRUM TO BE EXPECTED FROM A MONOENERGETIC PROTON BEAM

In the course of an experiment on meson yields of various targets,[10] D. Clark has made measurements of the recirculation of the cyclotron beam. His data indicate that with a 1-in. Be target, one would expect a recirculation of 1.24, i.e., the beam intensity is 1.24 times that which would obtain without recirculation. With this information, and the known energy loss in the target, one can calculate a reasonable energy spectrum for the proton beam. It is presented in Fig. 6(a). The widths of the steps of this histogram are the energy loss in the target (15.7 Mev for 244-Mev protons in 1-in. of Be), and the heights of the successive steps constitute a geometric progression whose sum is 1.24, the height of the largest step being unity.

By making use of this spectrum and the neutron spectrum observed with this target [Fig. 4(a)], one can calculate the neutron spectrum that would arise from a monoenergetic proton spectrum. The calculation is of the same sort as that used in treating the finite pulse and angular resolutions in calculating the neutron spectra. This neutron spectrum is given in Fig. 6(a). For ease of calculation it has been somewhat idealized, but its important features are correctly represented.

It is, of course, possible to do this again, using the neutron spectrum observed with the ½-in. Be target. However, what has been done in this case is to use the neutron spectrum just calculated as corresponding to monoenergetic protons, and the hypothetical proton spectrum corresponding to a ½-in. Be target (recircu-

[6] Kelley, Leith, Segre, and Wiegand, Phys. Rev. **79**, 96 (1950).
[7] L. Bodansky, Phys. Rev. **80**, 481 (1950).
[8] J. M. Cassels, *et al.*, Phil. Mag. **42**, 215 (1951).
[9] Fox, Leith, and Wouters, Phys. Rev. **80**, 23 (1950).
[10] D. L. Clark, Phys. Rev. **87**, 157 (1952).

lation 1.50, energy loss 7.8 Mev), and calculate the neutron energy spectrum one would expect to observe with this target. This can then be compared with the spectrum already reported for this target, Fig. 4(b), to get some idea of the validity of the neutron spectrum for monoenergetic protons of Fig. 6(a). The various spectra involved in this process are presented in Fig. 6(b); the observed spectrum, *D*, has been expanded vertically by a factor of 1.07, not a severe renormalization since the monitor geometry was slightly different in the two runs.

It is to be observed that the two spectra are not identical. The difference, particularly at the low energy end, is a bit greater than is to be expected from a consideration of the uncertainty of the shapes of the two reported neutron spectra.

The difficulty probably lies in the simplicity of approach to the energy spectrum of the proton beam. No consideration was taken of the inhomogeneity of the primary proton beam, due, for example, to radial oscillations. The assumption was implicitly made that the target was aligned exactly tangent to the proton orbit, so that all the protons traversed the same target thickness; this assumption is not justified. Also, the two targets were not in the same position in the cyclotron, so that the effect of the radial oscillations might have been different for the two. In view of these considerations, the disagreement is perhaps not so bad. There is, in this disagreement, an indication of the uncertainty of the spectra of Figs. 6 reported as corresponding to monoenergetic protons.

UNCERTAINTY IN SHAPE OF SPECTRA

Because of the nature of the calculations it is impossible to present observed points with their statistical spreads on the neutron spectra of Figs. 4(a) to 4(g). As an indication of the uncertainty in the knowledge of the shape of these spectra, then, the pulse-height spectra corresponding to two idealized neutron spectra have been calculated. These spectra, Figs. 7, have about the same width at half-maximum as the spectra of Fig. 4, but one has its peak at a higher energy and one at a lower energy. The pulse-height spectra are plotted in Figs. 8, along with the experimental data, and the smooth curves from which the spectra of Fig. 4 were calculated.

Some idea of the precision obtained is given by these curves; the extremes shown are clearly poor fits to the data.

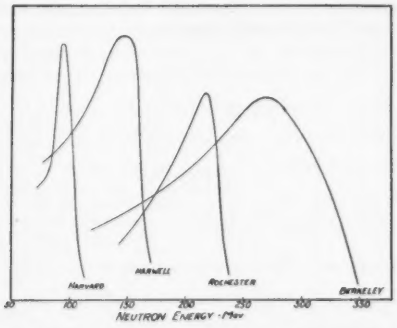

FIG. 5. Comparison of our neutron energy spectrum from Be with those reported by Harvard, Harwell, and Berkeley. The spectrum labeled Rochester is that of Fig. 4(b). The others are from references 7, 8, and 9.

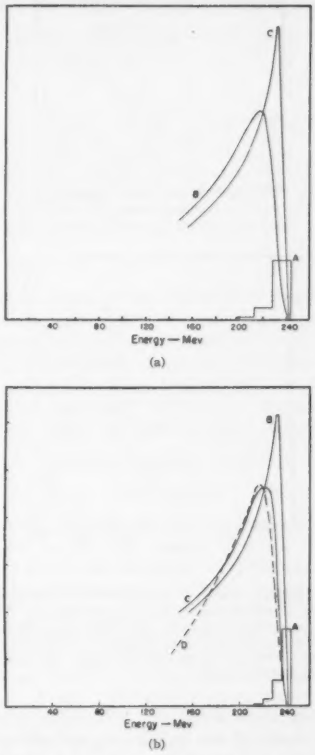

FIG. 6. Neutron spectrum corresponding to monoenergetic proton beam. (a) Spectra associated with 1-in. Be target. *A*: Hypothetical proton spectrum calculated from data on recirculation of cyclotron proton beam. *B*: Neutron spectrum of Fig. 4(a). *C*: Neutron spectrum corresponding to monoenergetic proton spectrum, calculated from *A* and *B*. (b) Spectra associated with ½-in. Be target. *A*: Hypothetical proton spectrum calculated from recirculation data. *B*: Neutron spectrum corresponding to monoenergetic protons, from Fig. 6a. *C*: Neutron spectrum to be expected from *A* and *B*. *D*: Observed neutron spectrum, from Fig. 4(b), to compare with *C*.

ACKNOWLEDGMENT

It is a pleasure to acknowledge the help that was received from various quarters. Professor A. Roberts

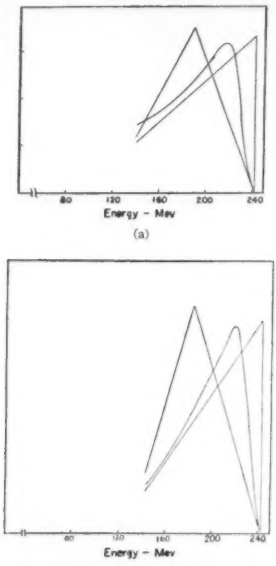

FIG. 7. Extreme neutron spectra for an indication of the uncertainty of the shape of the reported spectra. The pulse-height spectra corresponding to these neutron spectra are given, with the observed data, in Figs. 8; they do not fit the data well. (a) Spectra corresponding to 1-in. Be target. (b) Spectra corresponding to ½-in. Be target.

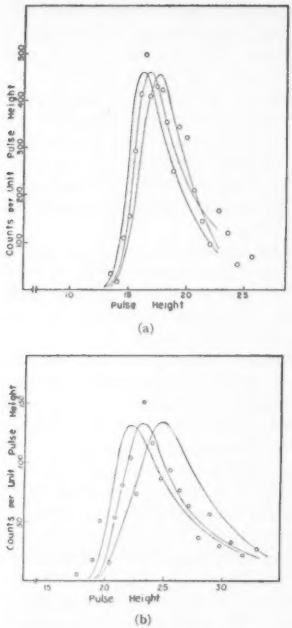

FIG. 8. Pulse-height spectra corresponding to the neutron spectra of Fig. 7. The circles indicate the observed data, and the solid lines the spectra corresponding to the neutron spectra of Fig. 7. The small pulse-height spectrum corresponds to the high energy spectrum. (a) Spectra corresponding to 1-in. Be target data. (b) Spectra corresponding to ½-in. Be target data (40° telescope).

was very generous with advice and assistance throughout the course of the experiment, and offered many valuable suggestions during the preparation of this paper. We are indebted to Mr. D. Clark for the use of his coincidence equipment with our monitor telescope, and for the information on recirculation of the cyclotron proton beam used herein. The personnel of the Electronics Shop and of the Engineering Department constructed much of the equipment used. Mr. L. Momo of the Engineering Department was responsible for the detail design of the collimator and telescope mount and support.

The senior author, B. K. Nelson, wishes to express his gratitude for the aid provided by a two year tenure of an AEC Predoctoral Fellowship.

Total Cross Sections of Carbon and Hydrogen for High Energy Neutrons*

GEORGE R. MOTT,† GORDON L. GUERNSEY,‡ AND BRUCE K. NELSON§
Department of Physics, University of Rochester, Rochester, New York
(Received March 10, 1952)

Measurements of the total cross sections of carbon and hydrogen have been made at neutron energies of 97±5, 117±5, 140±5, 156±5, 180±7, and 220±10 Mev, using a calibrated anthracene crystal as an energy sensitive detector for recoil protons. This proportional crystal was used as the fourth of a quadruple coincidence anthracene scintillation counter telescope which detected recoil protons scattered at 20° from a polyethylene radiator in the collimated neutron beam from the University of Rochester 130-in. synchrocyclotron. The methods employed permit the simultaneous measurement of total cross sections over a continuous spectrum of neutron energies. The results are in general agreement with previously reported data.

I. INTRODUCTION

THE total n-p cross section was measured at 220 Mev to enable normalization of the differential cross-section data to an absolute scale. In view of the relative lack of experimental values for the total n-p scattering cross sections in the energy range from 100 to 200 Mev, it was decided to repeat the measurements at lower energies. The unique method of detection of recoil protons used in this experiment has made feasible the measurement of total cross sections over a spectrum of neutron energies simultaneously. The data for neutron energies from 140 to 220 Mev have been obtained from runs using the neutron beam produced by protons of 240 Mev, and the values corresponding to 97 and 117 Mev have been obtained from neutron beams from targets bombarded by lower energy protons at small cyclotron radii.

All measurements have been made by observing the attenuation of a colimated beam of neutrons in carbon and paraffin, using the source and detector in good geometry.

Previous investigators in performing similar experiments have used various detectors, including gas-filled counters,[1,2] carbon activation,[3] bismuth fission chambers,[4–6] and anthracene scintillation counters.[7] In some instances the effective neutron energy has been set for the experiment by means of absorbers, while others have used the energy dependence of the $C^{12}(n-2n)C^{11}$ and bismuth fission reactions. By establishing a pulse height *vs* proton energy calibration for a 1-cm anthracene crystal, it has proven feasible to ascertain neutron energies to better than 10 percent using a counter telescope containing no thick absorbers, thus obviating the necessity for making uncertain corrections. The proton calibration curve obtained for the crystal has as its major uncertainty the present information concerning the range of protons in copper and anthracene.

II. EXPERIMENTAL METHOD

A. Principle

Basically, the same principle underlies the present experiment as has been used by others in performing the same type of measurement. Namely, one measures the exponential decrease in intensity of a well-collimated beam of monoenergetic neutrons, as the thickness of material traversed by the neutrons is increased. Since only heterogeneous neutron beams are available from high energy proton bombardment, methods must be incorporated into the experiment to insure counting only recoil protons of a given energy interval, and hence set the range of effective neutron energies. One method of accomplishing this has been to use absorbers in conjunction with the recoil proton detector, usually a hydrogenous radiator and counter telescope.

It has been shown that a moderately thick anthracene crystal can be used in a proportional fashion by utilizing the variation with energy of specific ionization by protons.[8] One is thus provided with a method of proton energy determination by measurement of the amplitude of the scintillation pulses, once a suitable calibration has been made. A discussion of the calibration procedure used is given in the preceding paper, and the resulting curve giving pulse height *vs* proton energy is shown in Fig. 1.

The agreement between the observed widths of the calibrating proton pulse-height distributions and the theoretical values for the energy loss widths expected for protons in anthracene as calculated by the method given Symon[9] is indicated in Table I. $\Delta P/P$ is the percent width at half-maximum for a set of observed pulse-height distributions, and $(E-E_p)/E_p$ is the

* This research was assisted by the joint program of the AEC and ONR.
† Now at Medical Center, University of Rochester, Rochester, New York.
‡ Now at Massachusetts Institute of Technology (Project Lincoln), Cambridge, Massachusetts.
§ AEC pre-doctoral fellow, now at Massachusetts Institute of Technology (Project Lincoln), Cambridge, Massachusetts.
[1] Hadley, Kelly, Leith, Segré, Wiegand, and York, Phys. Rev. **75**, 351 (1949).
[2] Taylor, Pickavance, Cassels, and Randle, Phil. Mag. **42**, 20 (1951).
[3] Cook, McMillan, Peterson, and Sewell, Phys. Rev. **75**, 7 (1949).
[4] J. DeJuren and N. Knable, Phys. Rev. **77**, 606 (1950).
[5] J. DeJuren and B. J. Moyer, Phys. Rev. **81**, 919 (1951).
[6] J. DeJuren, Phys. Rev. **80**, 27 (1950).
[7] Fox, Leith, and Wouters, Phys. Rev. **80**, 23 (1950).
[8] Guernsey, Mott, and Nelson, Rev. Sci. Instr. **23**, 476 (1952).
[9] K. R. Symon, Doctor's dissertation, Harvard University (1949).

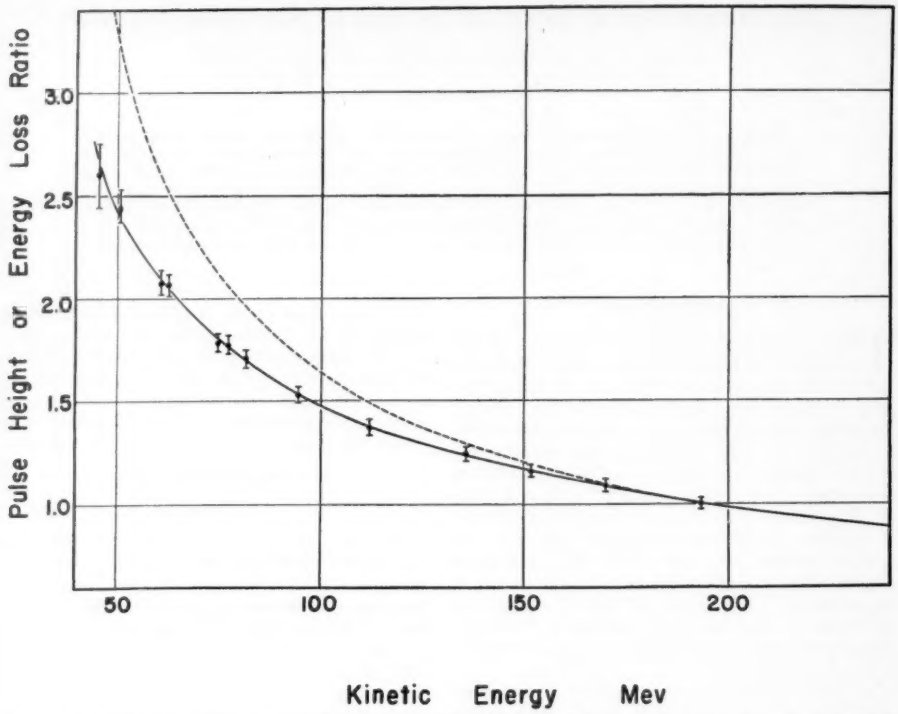

FIG. 1. Pulse height *vs* proton energy for 1.09-cm anthracene. The dashed line indicates theoretical energy loss by ionization adjusted for unity energy loss at 6.2-Mev for 193.5-Mev protons. Errors assigned to points indicate total spreads equivalent to two full channel widths of 24 channel pulse-height analyzer.

percent width at half-maximum, given to the nearest integer, for the energy loss distribution function calculated for the corresponding proton energies and the anthracene thickness used. Only the small-thickness calculation has been made, i.e., the special case wherein the energy loss is of the order of, or smaller than one-tenth of the kinetic energy of the incident proton. For this reason, many of the observed widths are not directly comparable to the corresponding theoretical values. To make these comparisons, the general case of the calculation must be employed. A few of the pulse-height spectra obtained during the calibration runs are shown in Fig. 2. Smooth curves have been drawn through the experimental points, these curves being very nearly Gaussian.

TABLE I. Widths of experimental pulse-height distributions for protons incident on 1.09 cm anthracene and comparison with "small-thickness" calculation using method of K. R. Symon.

E_p (Mev)	$\Delta P/P$ (%)	$(E-E_p)/E_p$ (%)	
Target 4 E_p=193 Mev at proportional crystal			
193	15.7	15	
170	16	13	
152	13.5	12	
135	13.7	11	
112	11.5	10	
94.5	11.7	—	"small-thickness" calculation invalid
81.5	12.1	—	
74.5	11.2	—	
60.5	18	—	
45.5	27	—	
Target 2 E_p=77 Mev at proportional crystal			
E_p (Mev)		$\Delta P/P$ (%)	
77		9.8	
62.5		10	
51		16	

The pulse-height analyzer was a 24-channel device[10] which presented a spectrum of pulse heights corresponding to the energy spectrum of the recoil protons, in view of the aforementioned calibration. Calculations for the range-energy relation in anthracene were made using $I=11.5Z$ ev.[8,11] This information was used to

[10] H. Logemann, Rev. Sci. Instr. (to be published).
[11] H. A. Bethe, Revs. Modern Phys. **9**, 263 (1937), Eqs. (749), (749a), and (750).

estimate the energy losses for protons traversing the crystals of the telescope. Figure 3 indicates the relation between the energy of a proton scattered in the radiator and the corresponding energy when incident on the last crystal, as inferred from the range-energy data. This curve was obtained by assuming that the total absorption was due not only to the crystals of the telescope, but also to half the radiator thickness, on the average. It has further been assumed that the stopping power of polyethylene is so nearly equal to that of anthracene, that allowances for this difference would constitute a negligible correction to the energy determination.

The neutron energy E_n appropriate to the observed scattered proton energy E_p and laboratory recoil angle ϕ was calculated using the relativistic formula. This

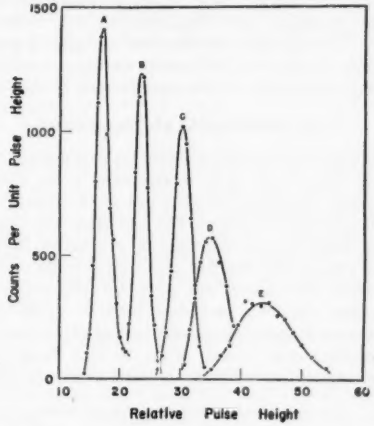

FIG. 2. Pulse-height distributions for calibration protons. Typical data for protons of different energies at proportional crystal: *A* 193 Mev, *B* 112 Mev, *C* 74 Mev, *D* 60 Mev, and *E* 45 Mev.

data is shown in Fig. 4. To use this information for this particular experiment, E_n *vs* E_p for $\phi = 20°$ was plotted.

Since numbers proportional to neutron intensity over an entire spectrum of neutron energies are furnished by the pulse-height analyzer, one needs only to use in the calculations for the cross sections the ordinates to the recoil proton pulse-height spectra, corresponding to various attenuator thicknesses, at the appropriate pulse height. Backgrounds are determined in the same manner.

To be rigorously correct, one must use proton spectra which correspond only to recoils from hydrogen. This is customarily done by counting protons first from a polyethylene radiator and then from a graphite radiator containing the same number of carbon atoms. Subtracting the carbon spectrum from the polyethylene spectrum yields the hydrogen effect, provided the runs

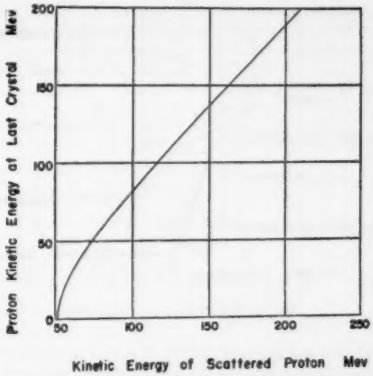

FIG. 3. Theoretical relation between energy of scattered protons and the corresponding energies at the proportional crystal.

are properly timed by the monitoring procedure. A preliminary attenuation run was made using copper with thicknesses ranging from zero to about 1.3 mean free paths for 220-Mev neutrons. For each attenuator, runs were made using both the polyethylene and graphite radiators. Pulse-height spectra for both polyethylene and polycarbon differences were plotted for each attenuator, and it was found that the ratio of the polyethylene counts to the hydrogen counts at a given pulse height was constant within the errors over the range of attenuator thicknesses used. The constancy of these ratios was observed to hold over an interval of pulse heights corresponding to neutrons from the peak energy of 220 Mev down to 140 Mev, near the end of the data for the spectra. Evidently the cross sections

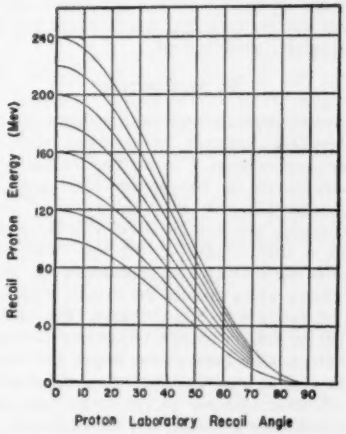

FIG. 4. Recoil proton energy *vs* laboratory recoil angle $E_p(E_n, \phi) = E_n/[1+(E_n/2mc^2+1)\tan^2\phi]$.

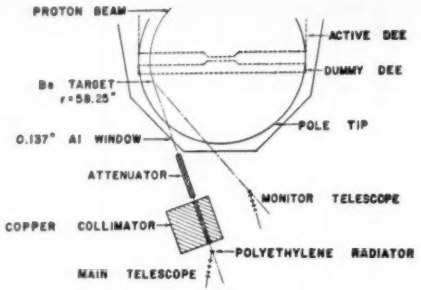

FIG. 5. Experimental arrangement.

for elastic and inelastic processes occurring in the carbon content of the polyethylene radiator do not vary sufficiently rapidly with energy to alter the ratios significantly as the neutron spectrum at the radiator was modified by the attenuator. In view of these observations, all subsequent measurements were made using only the polyethylene radiator. This afforded the attainment of reasonable accuracy at a considerable saving in cyclotron operating time.

In treating the data, it has been found convenient to draw a smooth curve through the experimental points for each spectrum and take values for the calculations from it. The uncertainty introduced by this procedure was reduced by repeating each spectrum several times and using the average values in the computations.

Measurements were made for graphite and paraffin attenuators separately, and the value for the hydrogen cross section deduced in the usual way:

$$\sigma_H=(\sigma_p-\sigma_C)/f,$$

where σ_C = total cross section for carbon, σ_H = total cross section for hydrogen, $\sigma_p=\sigma_C+f\sigma_H$, and $f=2.08$ for the paraffin samples used.

B. Arrangement

The experimental arrangement is shown in Fig. 5. A $\frac{1}{2}$-in. beryllium target at $58\frac{1}{4}$-in. radius intercepts the 240-Mev proton beam. The resulting neutron spectrum has been shown by Nelson (previous paper), to be peaked near 220 Mev with half-intensity points at approximately 170 and 230 Mev. This beam emerged through a thin window in the tank wall and was collimated by a 1-in.×1-in. aperture in the three-foot copper block which shielded the counter telescope from direct radiation from the cyclotron. The attenuators of either graphite or paraffin blocks were interposed in the neutron beam between the target and collimator. The line of sight from the polyethylene radiator through the collimator aperture to the target was carefully established using a transit, and the equipment was so designed that it could be dismantled and reassembled along the same line without the necessity for making further measurements. The attenuator samples were maintained in alignment with the reference direction by a support consisting of thin Dural rails.

C. Counter Telescope

D. Electronics

Since the telescope and electronics, including the monitor, were common to the three present experiments, the reader is referred to the preceding paper for a complete discussion.

E. The Neutron Attenuators

The attenuators consisted of carefully machined blocks of graphite and paraffin 2 in.×2 in. of assorted lengths to provide a diversity of transmission values for the neutron energies used. Maximum attenuator thicknesses employed were approximately two mean free paths. The analyst's report showed negligible impurities in both the graphite and paraffin samples, and that the average composition of the paraffin was: $(CH_{2.08})_n$.

III. EXPERIMENTAL PROCEDURE

The method of collecting data for a complete attenuation curve consisted of interspersing a run with the reference attenuator between groups of repeated runs with various attenuators. The procedure was repeated until data for several values of attenuator thickness were taken. The average of all runs made with the reference attenuator was used for the undegraded intensity since this procedure tends to minimize the effect of systematic errors arising from slight changes in monitoring over periods of six to eight hours which were required to complete an entire attenuation curve.

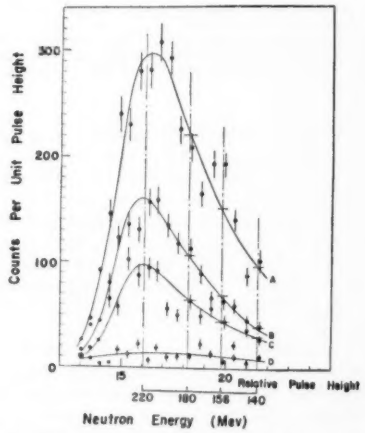

FIG. 6. Typical polyethylene spectra. A: Reference attenuator (8.4 cm carbon). B: $X=26.6$ cm carbon. C: $X=53.4$ cm carbon. D: Background (18 inches Pb).

The background was determined for each run by replacing the attenuator with lead absorbers slightly longer than four mean free paths for the highest neutron energies used. The background rates observed under these conditions amounted to several times the expected value, or approximately 5 percent of the counting rates with no attenuation in the worst case. The possibility of slight leaks in the collimator or scattering around the collimator from extraneous neutron sources in the cyclotron may be possible contributing factors to this discrepancy. Subtraction of this background, however, gave attenuation curves which were linear within the experimental errors.

Preliminary runs at 220 Mev with the most intense beams available from the cyclotron resulted in attenuation curves displaying excellent linearity among all points except the no attenuator value, which was too high to be compatible with the rest. Possibly the high singles counting rates in the first crystals were contributing to random gate openings and hence the excessive counting rate observed. However, attenuation of the beam with several centimeters of material provided sufficient reduction of intensity to reduce the effect to negligible proportions. This value of attenuator was used as the "reference attenuator" for subsequent runs at 220 Mev. For runs made with lower energy neutrons from targets at smaller radii, the beams available were less intense, and this effect was not observed; all points including the no attenuator values of these attenuation curves being consistent with a linear relation.

IV. DETERMINATION OF THE NEUTRON ENERGY

Prior to making the total cross-section runs, an electrical calibration of the entire proportional channel was made as described in the preceding paper. This calibration enabled the transforming of the counts per channel data furnished by the pulse-height analyzer to a counts per unit pulse-height spectrum for the proton recoils. In addition, the 200-Mev calibrating proton beam was intercepted by the telescope at 0° and a run was made to locate the peak of the 193-Mev proton pulse-height distribution on the pulse-height scale previously established. By using this pulse height as a reference, all pulse heights in the recoil spectrum could be expressed as ratios to the reference.

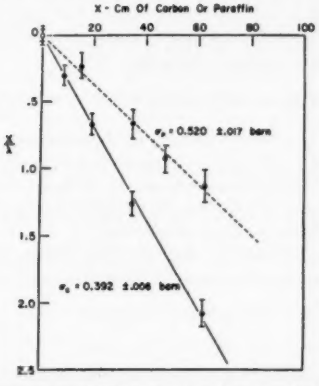

FIG. 7 Attenuation of 120-Mev neutrons in carbon and paraffin.

TABLE II. Summary of experimental results.

Attenuator	Primary determinations: Neutron energy (Mev)	Primary determinations: σ_{total} (barns)	Hydrogen differences: Neutron energy (Mev)	Hydrogen differences: σ_{total} (barns)
carbon	220±7	0.297±0.004	220±10	0.0413±0.0035
paraffin	216±6	0.383±0.006		
carbon	216±6	0.296±0.005	220±10	0.0413±0.0037
paraffin	216±6	0.382±0.006		
carbon	180±7	0.311±0.009	180±7	0.044 ±0.012
paraffin	180±7	0.403±0.022		
carbon	156±5	0.325±0.010	156±5	0.0505±0.0083
paraffin	156±5	0.430±0.014		
carbon	140±5	0.349±0.004	140±5	0.0485±0.0056
paraffin	140±5	0.450±0.011		
carbon	121±4	0.392±0.006	117±5	0.0615±0.0086
paraffin	113±3	0.520±0.017		
carbon	95±3	0.502±0.012	97±5	0.074 ±0.010
paraffin	100±3	0.656±0.017		

The steps involved in determining the neutron energy associated with any given pulse height in the recoil spectrum are as follows: 1. Determination of proton energy incident on the last crystal. Figure 1 gives proton energy at the last crystal *vs* pulse-height ratio. 2. Determination of proton energy when scattered. Using the value of proton energy at the last crystal from step 1, Fig. 3 gives the corresponding energy when scattered in the radiator. 3. Determination of primary neutron energy. Using the energy of the scattered proton from step 2 together with the telescope angle used, Fig. 4 gives the corresponding neutron energy.

The errors assigned to the neutron energies have been obtained from the standard deviation in the average pulse heights for both the recoil and the 193-Mev proton peaks, and allowances have been made for possible inaccuracies in the range-energy relation.

V. SCATTERING CORRECTIONS

Effects arising from elastic and inelastic scattering into the detector have been estimated for the geometry and found to be sufficiently small, compared to the stated probable errors, so that these corrections have not been applied to the experimental values.[12]

[12] E. M. McMillan and D. Sewell, unpublished USAEC report MDDC-1558 (1947).

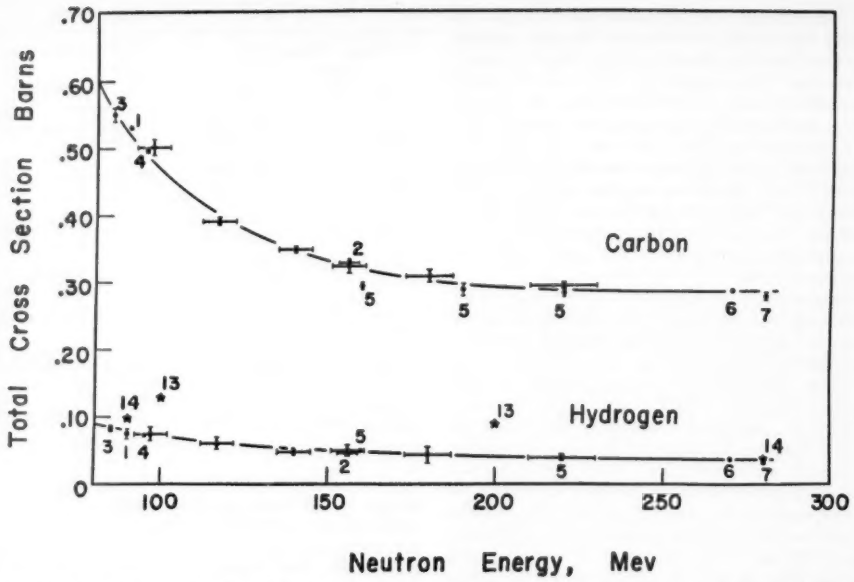

FIG. 8. Total neutrons cross sections for carbon and hydrogen. The large crosses give values and associated experimental errors from the present work. The numbers opposite the smaller points indicate the reference to the work reporting the data.

VI. RESULTS

Sample pulse-height spectra for protons from the polyethylene radiator exposed to the full energy neutron beam are shown in Fig. 6, and typical attenuation curves for carbon and paraffin are shown in Fig. 7. All experimental results are summarized in Table II, and these points are indicated in Fig. 8 together with previously reported values in the energy interval 80 to 280 Mev. It may be remarked that the agreement in energy and cross-section values is good in most cases.

The experimental values in the region from 100 to 200 Mev are approximately half the n-p total cross sections predicted by Ashkin and Wu[13] using tensor force and the symmetrical Rarita-Schwinger exchange model in the rigorous scattering theory. The results of this calculation for neutron energies of 100 and 200 Mev are also shown in Fig. 8. The values from the Born approximation calculation are still farther from the measured values.

The cross sections calculated by Christian and Hart[14] using tensor force and a Yukawa potential ($R=1.35\times10^{-13}$ cm) for $E_n=90$ and 280 Mev constitute a better fit to experimental data, however. These values are also indicated in Fig. 8.

A purely empirical formula has been obtained for the variation of the n-p total cross section with energy. This formula has been found to fit not only the data of the present report, but also all existing total cross-section data from neutron energies of 1 Mev to 280 Mev. In nearly every case the empirical fit falls within the stated errors of the experimental value, the average departure from all available data being about 6 percent.

This formula may prove useful for interpolating between experimental data to estimate the total cross section at some particular energy. It is:

$$\sigma=[2.55+0.028E+10(e^{-0.0165E}-e^{-0.2E})]/E,$$

where E is the neutron energy in the laboratory system in Mev and σ is the total cross section in barns.

The author wishes to thank Dr. Arthur Roberts for his guidance of this work, Mr. Hugo Logemann for his helpful discussions and development of the 24-channel pulse-height analyzer, and Mr. Fred Palmer and the cyclotron operating crew for their cooperation during the runs.

[13] J. Ashkin and Ta-You Wu, Phys. Rev. **73**, 973 (1948).
[14] R. S. Christian and E. W. Hart, Phys. Rev. **77**, 441 (1950).

Differential n-p Scattering Cross Section for 220-Mev Neutrons*

G. GUERNSEY,† G. MOTT,‡ AND B. K. NELSON§
Department of Physics, University of Rochester, Rochester, New York
(Received March 10, 1952)

The differential neutron-proton scattering cross section as a function of angle has been investigated for neutron energies of 220 Mev and 180 Mev. A ½-inch Be target at the 58½-inch radius in the University of Rochester 130-in. cyclotron was used to produce a beam of neutrons. This neutron beam scattered protons from a polyethylene scatterer which were detected by a four scintillation counter coincidence telescope. A measurement of the pulse height from the last counter was used to determine the energy of the scattered proton. The effect of the carbon in the polyethylene was subtracted by taking runs with a carbon scatterer calculated to have the same number of carbon atoms per cm² as had the polyethylene. Runs were taken from 0° to 50° for the proton angle in the laboratory coordinate system. A comparison is made of the 220-Mev angular distribution with the Berkeley 260-Mev data which indicates essential agreement of the shapes.

INTRODUCTION

THE characteristic of the neutron-proton scattering problem which has become increasingly difficult to cope with, as experiments have advanced to higher energies, is that of specifying the energy of the neutron which is being scattered. It is, of course, desirable to do this with as high a counting efficiency as possible, and still determine the energy accurately. The problem has been solved in this experiment by detecting protons with a scintillation counter telescope, the last counter of which was calibrated for its pulse-height response to proton energy. Since only thin crystal anthracene counters need be used in the quadruple coincidence telescope, the protons lost to the detector are negligible. Also, since the shape of the resolution curve for monoenergetic protons can be determined for the last counter as well as its pulse-height response *versus* proton energy, the proton energy determination can be made to a few percent.

This experiment is one of a group of three high energy neutron studies and the methods and apparatus used are in general the same as those described in the first two[1,2] and in a subsequent paper.[3] The methods will be described only where they differ from those of reference 1. The notations for angles and the kinematic relations of the neutron and proton are those given in the paper by Hadley *et al.*[4] The definition of angles is repeated here for convenience: Φ is the angle that the proton makes in the laboratory system with the direction of the incident neutron and θ is the center-of-mass angle of the scattered neutron.

The geometry of the counter telescope employed is presented in Fig. 1. It is the scatterer S and counter C_3 that determine the maximum spread $\delta\Phi$ in the angle Φ, and the distance from S to C_3 as well as the area of C_3 that determine the solid angle $\Delta\omega$ for any point in the scatterer. The angular resolution curve is essentially triangular in the approximation that $\tan\delta\Phi=\delta\Phi$ and that the widths of S and C_3 are equal. For the geometry shown, $\delta_{max}\Phi=5°$ full width at the base of the triangle and $\Delta\omega=1.8\times10^{-3}$ steradian. For the short telescope run (Group B), to be mentioned later, $\Delta\omega=5.85\times10^{-3}$ steradian.

The pulse-height spectra for protons scattered into the counter telescope have been recorded for telescope angles of from 0° to 50° as measured from the incident neutron direction. From this the number of protons per unit pulse height, at pulse heights corresponding to a constant neutron energy, has been determined for each angle. This number of protons is then transformed to a proton energy scale and finally to a neutron energy scale from the kinematics of the scattering. The number of protons per Mev of the incident neutron energy is proportional to the laboratory system cross section and can be converted to the center-of-mass system by multiplying by the appropriate value of $d(\cos\Phi)/d(\cos\theta)$. If we call this $R(\theta)$, then $R(\theta)$ is related to the absolute value of the cross section $\sigma(\theta)$ by requiring that

$$\int KR(\theta)d\omega=\sigma_{tot}, \quad \text{for} \quad \sigma(\theta)=KR(\theta). \qquad (1)$$

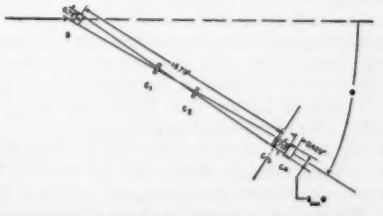

FIG. 1. Counter geometry.

* This work was assisted by the research program of the AEC.
† Now at Massachusetts Institute of Technology (Project Lincoln), Cambridge, Massachusetts.
‡ Now at Medical Center, University of Rochester, Rochester, New York.
§ Now at Massachusetts Institute of Technology (Project Lincoln), Cambridge, Massachusetts.
[1] Nelson, Mott, and Guernsey, accompanying paper [Phys. Rev. 88, 1 (1952)].
[2] Mott, Guernsey, and Nelson, preceding paper [Phys. Rev. 88, 9 (1952)].
[3] Guernsey, Mott, Nelson, and Roberts, Rev. Sci. Instr. 23, 476 (1952).
[4] Hadley, Kelly, Leith, Segrè, Wiegand, and York, Phys. Rev. 75, 351 (1949).

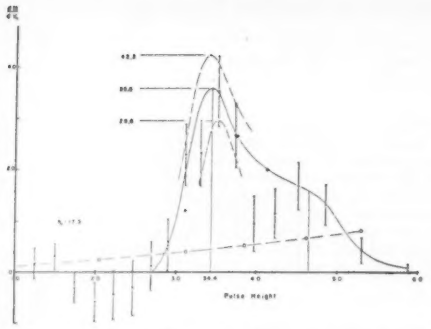

FIG. 2. Pulse-height distribution for $\Phi=50°$, recoil protons, showing the low energy contribution. The small solid circles represent the observed number of protons per unit pulse height with their statistical uncertainties. The large circles correspond to contributions from neutron energies below 166 Mev, the crosses to contributions from neutron energies above 166 Mev, both of which have been computed from a measured neutron spectrum.

NEUTRON SPECTRUM

The energy spectrum of the incident neutrons is that of Fig. 4(b) in reference 1, and is described in detail in reference 1. (See also Fig. 3 of this paper.)

ANALYSIS OF THE DATA

The method of analysis applied to the data is essentially that of steps (a) through (e) in reference 1 with the exception that here we were concerned with obtaining dN_p/dE_n for a particular value of E_n rather than for the entire spectrum. The value of E_n considered was 220 Mev since this corresponded to the peak of the neutron spectrum (and thus the peaks of the pulse-height distributions) where the counting statistics were of course the best. Data for $E_n=180$ Mev were also considered and are presented here only as an illustration of the further possibilities of this method. For the neutron spectrum used, the counting rates in the pulse-height spectra were appreciably lower at 180 Mev, and thus the statistics are quite poor.

The energy determination was made by averaging the neutron energies corresponding to the pulse heights at the peaks of eighteen pulse-height spectra. This gives an average deviation from the average of 2.2 percent and is an indication of the relative accuracy of the determination. However, the absolute value is in doubt through some, as yet, unknown error and is believed to be 215 Mev for the peak of the spectrum used here. One is referred to the Run Calibration section of reference 1 for comment on this discrepancy.

In Fig. 2 is an example of the data recorded in the form of a pulse-height distribution for $\Phi=50°$. This particular distribution has rather poor statistical accuracy. However, it is a good example of an important characteristic of this method of detection. The number of protons per unit pulse height at the peak, $dN_p/dV_0 = 35.8\pm6.2$, is the number to be transformed to a value of dN_p/dE_n which is proportional to $\sigma(\Phi=50°)$. The observed position of the peak is 34.4 volts (on an arbitrary scale) and the 17.5 is from the associated calibrating proton run, indicating that 193-Mev protons appear at 17.5 volts rather than the standard 16.95 and the pulse-height scale must undergo a corresponding linear transformation.

DOUBLE-VALUED PULSE-HEIGHT SPECTRUM

Consider the energy of the proton scattered by a neutron of energy E_n. The proton will lose energy as it passes through the remainder of the scatterer, the three coincidence crystals and into the last (proportional) counter crystal. Thus for some value of E_n, at a given angle Φ, the protons will stop at the far face of the last counter, losing the maximum energy in the crystal and thus giving the maximum pulse height. Protons, from neutrons above this energy (E_{nc}) as well as from neutrons below E_{nc}, will lose less energy and so give smaller pulse heights. Therefore, it is evident that the pulse-height distribution is double valued. For small angles Φ, and the counter 4 crystal thickness used (1.09 cm), E_{nc} is quite small. Since the low energy end of the neutron spectrum is sparsely populated, this means that the contribution to the pulse-height spectrum from the low energy end of the neutron spectrum is also quite small. However, for large laboratory angles, E_{nc} includes an appreciable portion of the neutron spectrum (at $\Phi=50°$, $E_{nc}=166$ Mev) and the low energy contribution is no longer negligible. In Fig. 2 the protons scattered by neutrons of energy below 166 Mev are shown by the dashed line.

The neutron spectrum referred to above is shown in Fig. 3. The measured values extend to 142 Mev and

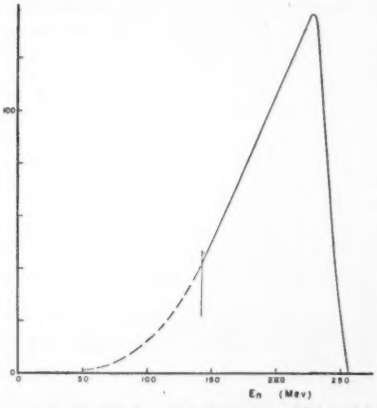

FIG. 3. The differential neutron spectrum, at 0° from ½-in. Be target, assumed as effective in the scattering experiment including the extrapolation used for the low energy corrections. The solid line is an observed spectrum (reference 1).

have been extrapolated as shown by the dashed line. This spectrum was transformed by the inverse of the steps described in reference 1 into a proton pulse-height distribution for the value of Φ in question. For this correction, it was assumed that the cross section is proportional to $1/E$. Also, it was necessary to assume something about the response of counter 4 to protons of energy below about 45 Mev, the low energy end of our calibration.

The largest pulses observed correspond to protons of energy 37.5 Mev which have a range of 1.09 cm of anthracene. (See appendix of reference 3.) The calibration curve was, therefore, extrapolated to a pulse height of 51.3 volts for 37.5 Mev, as obtained from a $\Phi=50°$ recoil proton spectrum from a carbon scatterer. This had a reasonably sharp cutoff at 51.3 units of pulse height. The remainder of the pulse height *versus* energy curve was assumed to follow a straight line, pulse height in volts = 1.368 times the proton energy in Mev, from 0 to 37.5 Mev.

The points indicated by large circles in Fig. 2 correspond to neutron energies below $E_{nc}(50°)=166$ Mev and the three crosses refer to points above 166 Mev. The low energy points were normalized by requiring that the three high energy points, with the low energy contribution added, should fit the observed pulse-height spectrum. The correct number per unit pulse height is obtained by subtracting the low energy contribution from the observed value, as $35.8\pm6.2-4.5=31.3\pm6.2$ counts per unit pulse height. This correction amounts to about 12 percent for $\Phi=50°$, $E_n=220$ Mev, 40 percent at the same angle for $E_n=180$ Mev. Since, this correction is less than 1.5 percent for $\Phi=40°$, $E_n=220$ Mev and 4 percent for $\Phi=40°$, $E_n=180$ Mev, it was not made for angles less than $\Phi=40°$.

EXPERIMENTAL RESULTS

All values of $\sigma(\theta)$ obtained from $E_n=220$ Mev are presented in Table I. Group B data were run with a wider acceptance angle telescope and has been normalized to a smooth curve through the five points of Group A. The average deviation of the Group B data from the normalizing ratio was 2.0 percent. The two

TABLE I. $\sigma(\theta)$ in 10^{-27} cm²/sterad for $E_n=215$ Mev. $\sigma(\theta)=KR(\theta)$, $K=0.0468$.

Φ	$\frac{d\sigma\cos\theta}{d\cos\theta}$	$\sigma(\theta)$[a] $A_\circ$	$B\square$	$C*$	$D\triangle$	Weighted average	θ
0	0.2238				13.4 ±2.8	13.4 ±2.8	180
7.5	0.2266	8.89±0.84		8.84±1.03		8.89±0.66	164.2
10	0.2288				7.58±0.75	7.58±0.75	158.8
10.7	0.2296		6.97±1.31			6.97±1.31	157.3
15	0.2353	5.43±0.66		4.77±0.89		5.38±0.47	148.4
				5.90±1.03			
19.1	0.2427		4.23±0.48			4.18±0.35	139.9
			4.13±0.52				
29.8	0.2730		2.53±0.37			2.53±0.37	117.7
30	0.2737	2.47±0.42		2.29±0.51		2.40±0.32	117.2
40	0.3211	1.29±0.20	1.41±0.20	1.19±0.25		1.31±0.12	96.9
50	0.3976	1.43±0.28	1.47±0.39			1.45±0.22	76.9

[a] Columns A through D are results of four different runs [see text]. The symbols refer to Fig. 4.

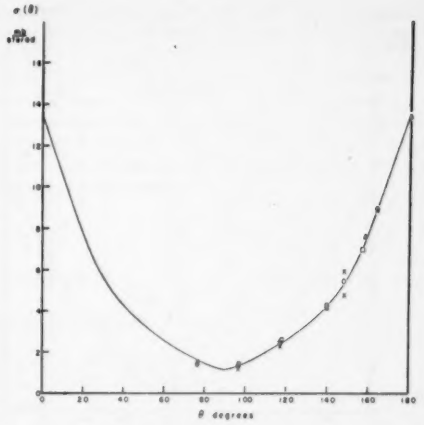

FIG. 4. All experimental determinations of differential cross section for 220-Mev neutron energy. The symbols refer to Table I. The smooth curve is an empirical fit used only for normalization to the total cross section.

points of Group D were also normalized to Group A using the 10° point of Group D (the only point in the range common to both, which was 5.5 percent higher than the smooth curve for Group A. Group C is presented just as obtained per 1000 monitor counts with no renormalization.

The errors given are the result of counting statistics alone. They correspond very closely to the standard deviations on the individual points in the original polyethylene-carbon differences, but in most cases are derived from two extreme curves drawn for the pulse-height distributions. (See the upper and lower partial curves in Fig. 2.)

The variation of the cross section over the angular width of the telescope is negligible except for the point at $\Phi=0°$. At 0°, however, the cross section falls off rapidly over the entire 2π of directions from 0° and, as a result, the value of $(dN_p/dE_n)(\Phi=0°)$ would give a too low value of $\sigma(180°)$. This effect has been calculated using the triangular window for Φ mentioned above and a straight line for $(dN_p/dE_n)(\Phi)$ required to contain the $\Phi=7.5°$ point. The correction amounts to an increase of 4.4 percent and has been applied to the value of $\sigma(\theta=180°)$ given in Table I.

NORMALIZATION TO THE TOTAL CROSS SECTION

Since the experimental points do not extend very far below $\theta=90°$, it is difficult to make an extrapolation of the points to $\theta=0°$. Therefore, a smooth curve was drawn through the weighted averages of the points from 180° to 90° and Eq. (1) was rewritten as

$$\sigma_{tot}\simeq 2\pi K\cdot\frac{2\pi}{18}\sum_{n=0}^{8}R(95+10n)\sin(95+10n).$$

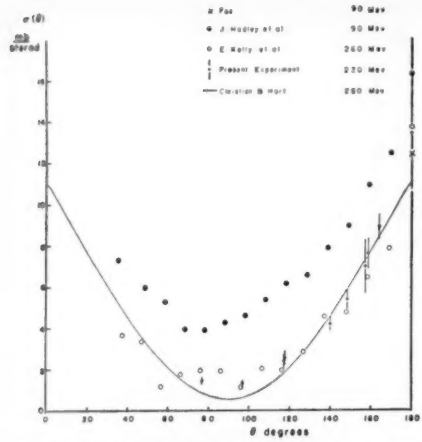

FIG. 5. The weighted averages of the 220-Mev data, plotted for comparison of the shapes with the Berkeley data and the theoretical prediction of Christian and Hart for a tensor force model. The absolute values are not directly comparable, since the 220-Mev data have been normalized for 90° symmetry and the 260-Mev data for $\theta<90°$ symmetry.

For the curve shown in Fig. 4, $K=0.0468$, when the total n-p cross section is taken equal to $41.3\pm3.5\times10^{-27}$ cm². This is the value given in reference 2 for $E_n=220$ Mev. Figure 4 also presents all the values of $\sigma(\theta)$ given in Table I.

If the data had been normalized to the same shape curve but symmetric about 85° instead of symmetric about 90°, the absolute values of the points would then be 13 percent higher. The ±8.5 percent assigned to the total cross section also contributes to the error in the absolute values of $\sigma(\theta)$.

Unfortunately, one can say nothing much from the data regarding symmetry about 90°. However, from whatever minimum is evident in going as far as $\theta=77°$, the data are in essential agreement with the finding by Christian and Hart[5] of slightly greater than 50 percent

TABLE II. $\sigma(\theta)$, 10^{-27} cm²/sterad. $E_n=172$ Mev $K=0.144$.

Φ	$\frac{d\ \text{corr}}{d\ \cos\theta}$	$\sigma(\theta)$[a] A^*	$B^\square$	C^+	D^Δ	Weighted average	θ
0	0.2282				16.6±6.8	16.6±6.8	180
7.5	0.2311	9.7±1.3		13.0±3.0		10.9±1.4	164.5
10	0.2330				7.6±1.5	7.6±1.5	159.3
10.7	0.2338		7.0±1.2			7.0±1.2	157.8
15	0.2392	4.8±1.0		4.9±1.3		5.3±0.8	148.8
				6.4±1.8			
19.1	0.2464		4.2±1.2			3.5±0.9	140.5
			2.5±1.1				
29.8	0.2758		2.1±0.9			2.1±0.9	118.2
30	0.2762	2.8±0.8		2.0±1.0		2.5±0.6	117.7
40	0.3219	3.0±0.6	2.1±0.6			2.4±0.4	97.4
50	0.3960	2.3±0.7				2.3±0.7	77.5

[a] Data corresponding to values in columns A through D are identified in text in connection with Table I. Symbols refer to Fig. 6.

[5] R. S. Christian and E. W. Hart, Phys. Rev. 77, 441 (1950).

exchange force giving a good fit to the high energy angular distributions.

One may compare the weighted averages of our data for $E_n=220$-Mev, taken from Table I, with the Berkeley data for 90-Mev[4,6] and 260 Mev[7] by referring to Fig. 5. The additional 90-Mev point at 180° was obtained from Fig. 12 of reference 6 and is due to Fox.[8] The 220-Mev data overlap to some extent, but are on the average higher than that at 260 Mev. It may be noted that the ratios $\sigma(180°)/\sigma(90°)$ are about equal for the 220-Mev and 260-Mev distributions. However, since the ratios are so large at these energies, the experimental errors do not justify a precise comparison.

The solid curve in Fig. 5 is a theoretical prediction of Christian and Hart[5] for n-p scattering from a Yukawa potential at 280-Mev neutron energy, with

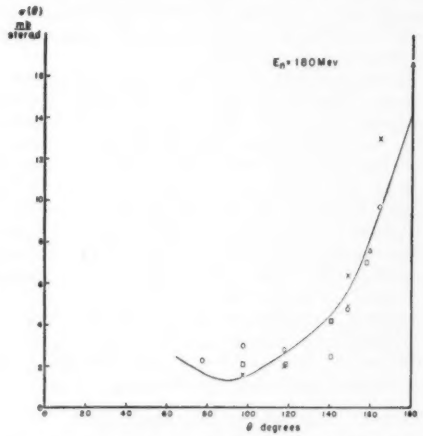

FIG. 6. Values of $\sigma(\theta)$ obtained from the pulse-height distribution data at a pulse height other than that of the maximum of the distribution. The solid curve is the same shape used for normalizing the 220-Mev data. The symbols refer to Table II.

inclusion of tensor force, for a $\sigma_{tot}=37\times10^{-27}$ cm² and has been copied from Fig. 3 of reference 6. One observes that, for the symmetric normalization used in the case of $\sigma(\theta, 220$ Mev), this curve is about as good a fit to the 220-Mev data as it is to the 260-Mev data of the Berkeley group. An additional comment may be made regarding the shape of the angular distribution presented here. It seems to satisfy the description of being V-shaped rather than U-shaped, thus being consistent with the inclusion of a tensor interaction in the potential model.

The values of $\sigma(\theta)$ for $E_n=180$ Mev, obtained from the pulse-height spectra which furnished the $E_n=220$-

[6] Chamberlain, Segrè, and Wiegand, Phys. Rev. 83, 923 (1951).
[7] Kelly, Leith, Segrè, and Wiegand, Phys. Rev. 79, 96 (1950).
[8] R. H. Fox, unpublished USAEC Report No. UCRL-867 (1950).

Mev information, are presented in Table II. They have been calculated in the same way as were the values for $E_n = 220$, except that the effects of finite pulse-height resolution and angular resolution have been neglected. This is justified when the pulse-height spectra do not change slope rapidly compared with the resolution widths. These values of $\sigma(\theta)$ for 180 Mev are plotted in Fig. 6, in which the solid curve is the same as was used for integration of the 220-Mev data but normalized to a total cross section of 44 mb.[2] The value of K taken for these data was 0.144, which fitted the points to the normalizing curve more or less closely. This distribution exhibits the expected gross features, but details of shape, unfortunately, are not significant.

The authors wish to express their appreciation to Professor A. Roberts for his interest in this problem and his generous assistance with the performance and analysis of the experiment.

PHYSICAL REVIEW VOLUME 88, NUMBER 1 OCTOBER 1, 1952

Excitation Functions to 100 Mev*

NORTON M. HINTZ† AND NORMAN F. RAMSEY
Nuclear Laboratory, Harvard University, Cambridge, Massachusetts
(Received June 2, 1952)

A method is described for obtaining excitation functions using the stacked foil technique with an internal cyclotron beam. The method, which utilizes multiple Coulomb scattering for deflection and 180° focusing for energy separation, has the advantages of good energy resolution, high intensity, and low background. Equations are presented for the particle orbits from which are derived the energy resolution and efficiency attainable. Absolute excitation curves are given for the reactions, $C^{13}(p,pn)C^{11}$; Na^{24}, Na^{22}, and F^{18} from Al^{27}; $B^{11}(p,n)C^{11}$; and $S^{34}(p,n)Cl^{34}$. Absolute cross sections are determined using the monitor reaction, $C^{13}(p,pn)C^{11}$, and the ratio of the β-counting rates. Various corrections to the relative and absolute excitation curves are discussed. A brief interpretation of the results is given in which it is argued that they are consistent with present ideas about high energy nuclear reactions.

1. INTRODUCTION

THE sparsity of data on excitation functions of nuclear reactions above 30 Mev made it worthwhile to begin a systematic study in this field with the 100-Mev protons from the Harvard cyclotron. Some of the results of this investigation have already been published[1–3] together with a brief account of the method used. It is the purpose of this paper to describe the method more fully and to present some additional excitation curves.

At energies of a few tens of Mev one expects individual variations in nuclear structure to have little effect on the excitation curves, the main features of which should depend on the more general properties of nuclei such as the average nucleon density, the momentum distribution of the nucleons, the mean free path of fast nucleons in nuclear matter, and the average level density at large excitation. Accordingly, it was felt that a method should be devised by means of which a few reactions could be done with reasonably high accuracy, especially those which were of particular use in monitoring high energy proton flux, and by means of which the main features of a large number of other reactions could be obtained quickly and with economy of cyclotron time.

The classical method of stacked foils[4] satisfies these requirements well at low energies where no special difficulties are met with in beam deflection, extraction, and intensity. However, at 100 Mev, the present techniques of extraction are highly inefficient and therefore lead to serious problems of intensity or energy resolution. To overcome these difficulties it was decided to use the stacked foil method with the internal cyclotron beam, making use of the focusing properties of the uniform magnetic field to provide a nearly monochromatic beam of reasonable intensity. A somewhat similar technique has been used by Chupp and McMillan[5] with the protons stripped from fast deuterons. However, due to the broad energy distribution of their protons, the choice of carbon as an absorber, and the high neutron background their results were inaccurate.

2. EXPERIMENTAL GEOMETRY AND PARTICLE ORBITS

The method of stacked foils is unsatisfactory for use directly with the circulating beam of a frequency modulated cyclotron for two reasons. First, the small gain in orbit radius per turn (~1 mil) makes it impossible to align the foil and absorber assembly in such a way that all targets receive the same proton flux.

* Assisted by the joint program of the ONR and AEC.
† Present address: Department of Physics, University of Minnesota, Minneapolis, Minnesota.
[1] Norton M. Hintz, Phys. Rev. **83**, 185 (1951).
[2] J. W. Meadows and R. B. Holt, Phys. Rev. **83**, 47 (1951).
[3] J. W. Meadows and R. B. Holt, Phys. Rev. **83**, 1257 (1951).
[4] E. O. Lawrence, Phys. Rev. **47**, 17 (1935).
[5] W. W. Chupp and E. M. McMillan, Phys. Rev. **72**, 873 (1947).

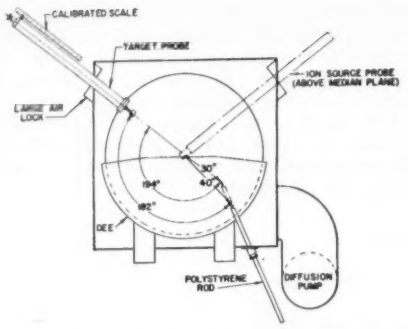

FIG. 1. Geometry of scattering and target probes in "180°" arrangement.

Second, the energy spread of the primary beam, which is probably due to radial oscillations, results in very poor energy resolution, especially for foils well down in the absorber stack. This is because an initial energy spread, ΔE_0, increases approximately as $1/E$ as the particles penetrate the absorbers, due to the $1/E$ dependence of the stopping cross section. Since the range spread, ΔR_0, corresponding to ΔE_0, remains constant as the particles pass through the absorber, the fractional energy width $\Delta E/E$ is approximately,

$$\Delta E/E=(\Delta R_0/E)(dE/dR)_E\simeq(\Delta E_0/E_0)(E_0/E)^2, \quad (1)$$

and so increases very rapidly down the absorber stack. A 100-Mev proton beam must be monochromatic to better than 1 percent initially if the energy resolution is to be limited by ordinary range straggling.

Both of these difficulties can be overcome f the protons are first deflected by multiple Coulomb scattering in a thin foil placed in the median plane. The stack of absorbers and targets can then be placed above or below the median plane of the cyclotron beam at an angular position, relative to the scatterer, which results in particles from a narrow momentum interval being focused on the target face. The actual geometry used is shown in Fig. 1. The target and absorber assembly is inserted on a calibrated radial probe which passes through a large vacuum lock. The assembly is held above or below the median plane a distance which is determined by two factors. The maximum amplitude of the vertical oscillations sets a lower limit and the aperture of the dee system an upper limit. Since the circulating beam must expand to a radius somewhat greater than that of the targets, it is essential that no protons strike the absorber assembly as they pass by it on their way to the scatterer. This would result in protons of lower energy than that defined by the scatter reaching the targets. For the Harvard cyclotron, virtually all of the protons have vertical oscillations less than $\frac{3}{4}$ in. at a radius of 30 in. At this same radius the dee aperture is $\pm 1\frac{3}{4}$ in. Thus the target assembly could lie between about $\frac{3}{4}$ in. and $1\frac{3}{8}$ in., allowing a small margin for error in placement. This fixes the maximum foil diameter and hence the maximum efficiency attainable.

The scatterer consists of a strip of tantalum foil, of approximately the thickness for maximum scattering efficiency ($\sim$5 mils), fixed to the end of a polystyrene rod which passes through an existing hole in the cyclotron dee. This hole, which almost completely determined the scatterer position, was fortunately located very near the correct angle for energy focusing.

The equations which describe the proton orbits before and after scattering will be given briefly for their use in determining the target and scatterer positions, the scatterer thickness, and the expected energy resolution and efficiency.

If the magnetic field is nearly uniform,

$$[n=(r/H)\partial H/\partial r\ll 1],$$

the proton orbits may be taken as circles upon which are superposed small periodic radial and vertical displacements[6] of frequencies ω_r and ω_v and amplitudes A_r and A_v. These frequencies are given by

$$\omega_r=\omega_0(1-n)^{\frac{1}{2}}, \quad \omega_v=\omega_0(n)^{\frac{1}{2}}, \quad (2)$$

where ω_0 is the orbital frequency. If A_r and A_v are small relative to r, we may discuss the radial and vertical motions independently.

We first consider the particle orbits projected in the median plane. The orbital angle, θ_0, is to be measured from the scatterer position; the radial co-ordinate, r, from the cyclotron center. Just before scattering the orbit may be described by

$$r=r_0+A_r\cos(\theta_r+\delta_r), \quad (3)$$

where $\theta_r=\omega_r t=\theta_0(1-n)^{\frac{1}{2}}$ and r_0 is the radius of a particle of the same energy in a stable orbit. The phase factor, δ_r, is small since all particles will be nearly at the maximum in their radial oscillation when intercepted by the scatterer as a consequence of the small gain in orbit radius per revolution. A calculation shows $\delta_r\simeq 10^{-2}$ radian as a maximum value. When a proton passes through the scatterer its direction will change and it will lose energy. The change in direction corresponds to an additional radial oscillation of phase zero and amplitude, A_s, which is to be superposed on that already present. The energy loss will correspond to a sudden decrease in the stable orbit radius by an amount Δr_0, but since the radial coordinate of the particle does not change, an additional radial oscillation of amplitude Δr_0 and phase $\pi/2$ must be superposed. Thus, after scattering, the orbit may be written

$$r=r_0+\Delta r_0(\cos\theta_r-1)+A_r\cos(\theta_r+\delta_r)+A_s\sin\theta_r. \quad (4)$$

The scattering induced radial oscillation amplitude, A_s, will be related to the projected scattering angle,

[6] D. W. Kerst and R. Serber, Phys. Rev. **60**, 53 (1941).

α_r, by

$$\alpha_r=\left[\left(\frac{dr}{d\theta_0}\right)_f-\left(\frac{dr}{d\theta_0}\right)_i\right]\Big/ r,$$

evaluated at $\theta_0=0$. The subscripts i and f indicate the derivative before and after scattering. This gives

$$A_s=r_s\alpha_r(1-n)^{-\frac{1}{2}}, \tag{5}$$

where r_s, the scatterer radius, is written

$$r_s=r_0+A_r\cos\delta_r.$$

At $\theta_r=2\pi$, or $\theta_0=2\pi(1-n)^{-\frac{1}{2}}$, $r=r_s$ from Eq. (4) and particles of all energy are refocused at the scatterer radius. This is the proper target position for maximum intensity and minimum energy resolution. In practice, the targets may be placed directly above or below the scatterer when maximum intensity is desired since $(1-n)^{-\frac{1}{2}}\simeq 1$ and the scattered beam will be refocused to within the target width at $\theta_0=2\pi$.

At $\theta_r=\pi$, or $\theta_0=\pi(1-n)^{-\frac{1}{2}}$, Eq. (4) gives $r=2(r_0-\Delta r_0)-r_s$, which is the same for all particles of the same energy independent of A_r, α_r, and δ_r. This is the well-known result for "180°" focusing, to first order, of particles from a line source in a uniform magnetic field. The innermost edge of the scatterer corresponds to the line source.

The over-all efficiency of the "180°" and "360°" arrangements will be determined by the motion of the particles in the vertical direction and, in the case of "180°" focusing, by the energy spectrum of the primary circulating beam. By analogy with the above, the motion in the Z direction, perpendicular to the median plane, will be given by

$$Z=A_v\sin(\theta_v+\delta_v)+A_s'\sin\theta_v \tag{6}$$

after scattering. A_s' is the scattering induced vertical oscillation given by

$$A_s'=r_s\alpha_v n^{-\frac{1}{2}} \tag{7}$$

where α_v is the projected vertical scattering deflection. Here δ_v will not in general be small since the particles will strike the scatterer at all phases in their vertical oscillation.

The distribution in α_r and α_v will be approximately Gaussian,[7] with

$$\langle\alpha_r^2\rangle_{Av}=\langle\alpha_v^2\rangle_{Av}=\langle\alpha^2\rangle_{Av}=B\log(\theta_2/\theta_1). \tag{8}$$

θ_1, θ_2, and B are defined in the reference. If the innermost edge of the scatterer is aligned vertically, the δ_v will be distributed randomly, and the mean square value of Z after scattering and at an angle θ_0 will be

$$\langle Z^2\rangle_{Av}=\tfrac{1}{2}\langle A_v^2\rangle_{Av}+r_s^2n^{-1}\langle\alpha_v^2\rangle_{Av}\sin^2(\theta_0n^{\frac{1}{2}}). \tag{9}$$

If the distribution in A_v can be taken as approximately Gaussian, the fraction of the particles which are scattered into the angular range defined by the vertical dimension of the target will be, for a single traversal of the scatterer,

$$I=(2\pi\langle Z^2\rangle_{Av})^{-\frac{1}{2}}\int_{Z_1}^{Z_2}\exp[Z^2/2\langle Z^2\rangle_{Av}]dZ. \tag{10}$$

Z_1 and Z_2 are the coordinates of the vertical extremes of the target. I will be a maximum, for a given Z_1 and Z_2, if the scatterer thickness is chosen so that $\langle Z^2\rangle_{Av}^{\frac{1}{2}}$, as calculated from Eq. (9), is equal to $\frac{1}{2}(Z_1+Z_2)$, i.e., a particle which is scattered through the rms scattering angle should just be able to enter the target center. Actually, I is a rather slowly varying function of $\langle Z^2\rangle_{Av}$ so a single scatterer can be used over a fairly wide energy range. A scatterer of high nuclear charge should be used to minimize the energy loss for a given rms scattering angle.

Not all particles which are scattered into the range defined by Z_1 and Z_2 will enter the targets since they must have the correct radial coordinate as well. In the "360°" case ($\theta_0=2\pi(1-n)^{-\frac{1}{2}}$) all particles will have the correct radius and the efficiency of the arrangement as calculated from Eq. (10) will be about 7 percent for $\frac{5}{16}$-in. diameter targets placed with their center one inch from the median plane. For the "180°" case the efficiency is roughly 0.7 percent, as determined by Eq. (10) and the fraction of all particles which lie within the energy range subtended by the targets. The intensity available with this method, even with the rather broad energy spectrum of the Harvard cyclotron, is of the order of 10^{-9} amp/cm^2 which is considerably greater than that which can be obtained in an external magnetically analyzed beam.

As stated previously, the targets could not be placed exactly at the correct angles for "180°" focusing because of cyclotron geometry. However, due to the small angular aperture of the Coulomb scattered beam, the focusing error was never greater than the target width. In the "180°" case, if β is the angle by which the actual geometry differs from $\pi(1-n)^{-\frac{1}{2}}$, the focusing error, Δf, is from Eq. (4):

$$\Delta f=\tfrac{1}{2}\beta^2(\Delta r_0+A_r)-\beta A_s. \tag{11}$$

Δf is defined as the radial width, at the target position, of a group of scattered particles of the same energy. For $\beta=10°$, the maximum deviation used, the rms value of Δf is about 0.1 in., which is roughly equal to the half-width of the targets when $\frac{5}{16}$-in. diameter foils are used. Thus the energy resolution is determined primarily by the target width and range straggling. A small contribution to the energy width at the targets can come from a finite source width due to penetration of the primary particles back from the innermost edge of the scatterer.[8,9] A radioautograph of the scatterer showed ~90 percent of the activity to be concentrated

[7] E. J. Williams, Proc. Roy. Soc. (London) **169**, 531 (1939).

[8] W. J. Knox, Phys. Rev. **81**, 693 (1951).

[9] Cassels, Dickensen, and Howlett, Proc. Phys. Soc. **B64**, 590 (1951).

within 1 mm of the edge. An experiment to measure the energy distribution of the scattered beam is discussed in Appendix A.

3. TARGET ASSEMBLY AND BOMBARDMENT PROCEDURE

The choice of an absorber material to degrade the proton energy was based on the following considerations. For a given energy loss in the absorbers it is desired to (1) minimize loss of particles due to multiple scattering, (2) minimize nuclear interactions in the absorbers which would give neutron and proton secondaries and decrease the incident proton flux. To satisfy requirement (1) the mean square displacement, after traversing a given energy range, should be minimized. This is best done using elements of low nuclear charge and high density, the latter being more important. In this respect, copper and uranium are about equally good and about twice as good as aluminum or carbon. In respect to (2), one gains steadily by going to heavier elements but only as $A^{\frac{1}{3}}$, so factor (1) is more important. Considering availability and machinability, brass is an excellent choice. Fortunately the relative stopping power of zinc to copper is unity to within one part in one thousand over the crucial energy range, so the computed range-energy curves for copper could be used. A relatively heavy element is also desired in order to minimize contamination of the targets due to nuclear recoils from the absorbers. Occasionally thin aluminum absorbers were used for small energy steps but only over a small range interval so that losses due to multiple scattering were small. Since the dispersion in energy, due to range-straggling, is approximately independent of the substance for a given energy loss this factor does not enter into the choice of the absorber material.

The absorber-target geometry should be such that all foils should receive the same proton flux and all protons which can activate the foils should pass through the same absorber thickness. This is usually done by placing the foils and absorbers behind a collimating hole of smaller diameter. However, it was found that any material in front of the targets spoiled the energy resolution and increased the neutron background. Consequently, the absorbers were made $\frac{1}{16}$ in. larger in diameter than the foils and no collimation used. Each absorber was recessed slightly to take the target foil or pellet and a cap, with a raised center portion, was fitted so that the total absorber thickness was the same everywhere. By having the absorbers slightly larger than the foils, protons scattered out of the foil area are partly compensated for by protons scattered in from the surrounding absorber area. This will be discussed in Appendix B.

The absorber density was determined by a volumetric and a gravimetric method, the two results checking to within 0.3 percent. The foils were punched with a precision ground dowel pin fitting into a jig bushing. Pellets were pressed with a similar arrangement. The foils or pellets were weighed, usually after counting, on a microbalance to ± 0.02 mg. For irradiation, the stack of absorbers and targets was fitted into a brass capsule. This was then held at a suitable distance from the median plane on a radial probe (Fig. 1, reference 1). Altogether the foils were then surrounded by $\frac{3}{16}$ in. of brass giving shielding against low energy protons entering the stack sideways. The background due to such protons was then found to be less than 0.1 percent.

Several such targets can be irradiated simultaneously above and below the median plane when more efficient use of cyclotron time is desired. Since the width of the radial oscillation distribution is about 2.5 in. for the Harvard cyclotron, the radial half-width of the scattered beam at $\theta_0=\pi(1-n)^{-\frac{1}{2}}$ is 5 in., allowing room for several targets at slightly different radii.

When the yield of one reaction was being used to calibrate the cross section for another, the irradiation time was kept short relative to the shorter of the two half-lives and the cyclotron was given a preliminary warm-up to ensure steadiness during the run. Zero time was taken at the midpoint of the bombarding interval.

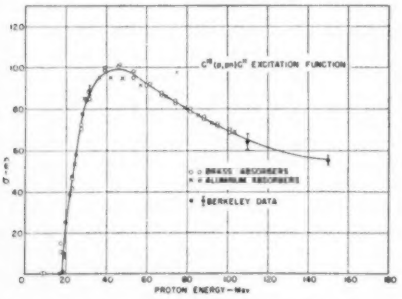

FIG. 2. Data for $C^{12}(p,pn)C^{11}$ reaction normalized to Berkeley data (Aamodt *et al.*, reference 9) at 32 Mev.

4. RELATIVE EXCITATION FUNCTIONS

After irradiation the samples were counted in well-defined geometry in a shielded sample changer containing a thin mica end-window Geiger tube. The short and long term stability of the counter was checked from time to time with a standard source and found to be within the statistical limits if the Geiger tube was left continuously at the operating voltage.

The raw counter data was corrected for counter background, dead time losses, decay since zero time, and neutron induced activity. The latter was evidenced by activity in foils placed beyond the proton range and was usually of the order of 2 percent.

After these corrections, two further ones must be considered before the corrected counting rates for a given activity can be taken as a relative excitation function. These are. the losses of protons from the foil

area caused by nuclear collisions and by Coulomb scattering. As will be discussed in Appendix B, the latter can be made negligible by surrounding the foils with material whose thickness is several times larger than the rms displacement of protons which traverse the absorber stack. The loss of protons due to nuclear effects is difficult to determine since the second foil of the stack is in "very poor" geometry relative to the first while the last is intermediate between "poor" and "good" geometry. Somewhat arbitrarily the data have been corrected using $\sigma_a = \pi R^2$ as the nuclear absorption cross section. A value of $R = 1.4 \times 10^{-13} A^{\frac{1}{3}}$ has been chosen. This should over correct for the first few foils and undercorrect for the last few. Since the maximum correction for nuclear absorption was about 10 percent, the overall uncertainty in the relative cross section should be not more than ~3 percent. Some evidence to support this comes from the fit obtained to the absolute cross sections measured at 32 Mev and 110 Mev[10] when our data are so corrected. This is shown in Fig. 2.

The energy of the protons at each target foil was calculated from the average radius and magnetic field for the scattered protons together with range-energy curves calculated from the Bethe-Bloch formula.[11] Allowance was made for the stopping effect of the target foils or pellets. The magnetic field was measured by U. E. Kruse and G. Watkins to within 0.01 percent using a nuclear resonance method.

5. ABSOLUTE CROSS SECTIONS

Because of effects resulting from rf pick-up and neutron background, a direct measurement of the proton current to the targets, from inside of the cyclotron vacuum system, was not feasible and it was decided to use the $C^{12}(p,pn)C^{11}$ reaction in order to monitor the proton current. By normalizing the relative excitation function for C^{11}, obtained as described here, to the absolute values at 32 and 110 Mev of Aamodt *et al.*,[10] a curve resulted which gave the absolute cross section in the region from the threshold to 100 Mev to within 5–10 percent.

The monitor foils of polyethylene or polystyrene were the same diameter, $\frac{5}{16}$ in. or $\frac{7}{16}$ in., as the target foils and from 3 to 5 mils in thickness. They were placed either in contact with or in separate absorbers from the target foils. If the monitor foil is placed near the target foil, so that both receive the same proton flux, the cross section for a reaction, Z, in terms of the monitor reaction, M, is:

$$\sigma_Z = \sigma_M R_Z n_M \tau_Z / R_M n_Z \tau_M, \qquad (12)$$

where R is the disintegration rate extrapolated to zero time, n the number of target nuclei per cm² and τ the half-life. It is assumed that the irradiation time is short as compared with the τ's.

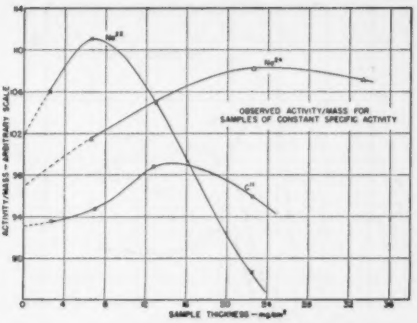
OBSERVED ACTIVITY/MASS FOR
SAMPLES OF CONSTANT SPECIFIC ACTIVITY
ACTIVITY/MASS — ARBITRARY SCALE
SAMPLE THICKNESS — mg/cm²

FIG. 3. Curves to determine correction for self absorption and scattering in β-ray samples.

The ratio R_Z/R_M was determined by counting the β-activity of the residual nuclei. The target and monitor foils were mounted on Lucite or copper planchets, of sufficient thickness to ensure saturation backscattering,[12] and counted in identical geometry with the same Geiger tube. The general procedure for applying corrections to the observed counting rates for absorption and scattering have been discussed by several authors[12–14] and will be mentioned only briefly. The correction for absorption of the β-rays in the air and window of the counter was made from an absorption curve taken on a thin source (5–10 mg/cm²) with the absorbers placed against the counter window to insure linearity. The scattering effect of the air between sample and window has been found to be less than 1 percent for the geometry used in this experiment.[12] The correction for absorption and scattering of the β-rays in the sample itself is determined by extrapolating to zero sample thickness a curve of counting rate *vs* sample thickness for samples of constant specific activity. Such samples are produced by irradiating targets of various thicknesses at the same position in the absorber stack. Resultant curves for several activities are shown in Fig. 3. The increase of counting rate due to back-scattering has been found to be independent of β-ray energy for β-distributions of maximum energy greater than 0.3 Mev provided the sample backing is of sufficient thickness to give saturation backscattering.[13] However, some recent work[15] has shown a possible difference in the saturation backscattering of electrons and positrons which, if it exists, would give an error of ~+10 percent in the absolute values for the Na^{24} cross section. The aluminum counter

[10] Aamodt, Peterson, and Phillips, unpublished University of California Radiation Laboratory Report No. 1400.
[11] Aron, Hoffman, and Williams, unpublished University of California Radiation Laboratory Report No. 121.
[13] L. R. Zumwalt, unpublished Atomic Energy Commission Unclassified Report No. 567.
[13] B. P. Burtt, Nucleonics **5**, 28 (1949).
[14] Conference on Absolute β-Counting, unpublished Report No. 8, National Research Council (1950).
[15] H. H. Seliger, J. Research Natl. Bur. Standards **47**, 41 (1951).

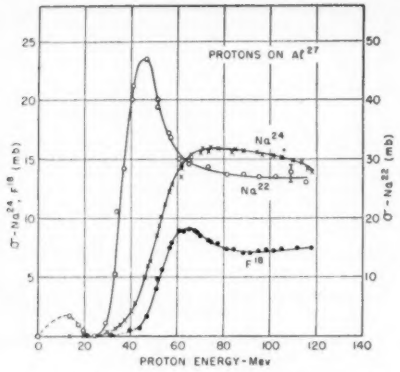

FIG. 4. Multiple particle reactions from protons on Al^{27}. Note ordinate scale at right for Na^{22} yield.

housing has been found to have a negligible effect on the counting rates if the samples are close to the window.[14]

If the corrections mentioned above are made on the observed counting rates, the counter efficiency has been shown to be independent of β-ray energy from 0.3 to 2.3 Mev maximum.[12] The over-all accuracy of this procedure is certainly not better than 10 percent for β-rays above 1 Mev and probably 20 percent for those of lower energy.

As an independent check on the value of the cross section for the reaction $Al^{27}(p,3pn)Na^{24}$ obtained from the corrected β-ray count, a direct β-γ coincidence calibration was made of the ratio $R(Na^{24})/R(C^{11})$. In the case of C^{11}, which emits no γ-rays, the positrons were counted in coincidence with the annihilation radiation.[16] The Na^{24} source was coincidence-calibrated in the usual way. When corrections of a few percent were made for the γ-sensitivity of the β-crystal, the ratio $R(Na^{24})/R(C^{11})$ agreed to within 3 percent with that determined as described above. This result does not imply the same reliability for the other absolute cross sections, since in general the corrections for absorption and scattering of the β-rays were greater than in the case of the Na^{24}/C^{11} ratio. However, it seems to rule out the possibility of gross errors in the extrapolations involved in determining these absorption corrections.

6. RESULTS

A. $C^{12}(p,pn)C^{11}$

The final data for this reaction is shown in Fig. 2. Bombardments of one or two minutes were sufficient to give 1 percent statistics in a one minute counting interval with 0.005-in. polystyrene foils so that as many as twenty foils could be run in the stack. The smooth fit of our data to the results of Aamodt *et al.*[10] at 110 Mev and 32 Mev gives good evidence for the over-all reliability of the method and provides a check on our absolute energy scale and resolution. A shift of 1 Mev at the bombarding energy of 100 Mev would give a noticeable discrepancy with the linear accelerator data at the threshold.

B. Na^{24}, Na^{22}, and F^{18} from Al^{27}

These nuclei were identified by their half-lives, absorption characteristics and chemistry and were easily resolved from the decay curves without chemical separation. Considerable 10 and 20-minute activity was also present in the aluminum foils, presumably due to fission reactions leading to C^{11} and N^{13}, but this could not be resolved. To determine the absolute cross sections, polyethylene monitor foils were included in the target assembly. A bombardment of 4–6 min gave sufficient activity to obtain the ratios $\sigma(C^{11})/\sigma(Na^{24})$ and $\sigma(C^{11})/\sigma(F^{18})$. The Na^{24} yield was then used as a secondary monitor in the longer runs of several hours needed to give sufficient Na^{22} intensity. The absolute excitation functions for these reactions are shown in Fig. 4 where the combined results of several runs for each curve are plotted. The rise of the Na^{22} curve below 20 Mev is probably a contamination effect since it occurs at a rather low energy for even a (p,Li^6) reaction. There is some evidence[17] for K-capture in the decay of F^{18} which, if it exists, would raise the value of $\sigma(F^{18})$ shown in Fig. 4. Some doubt has arisen as to the correctness of the Na^{22} absolute cross section. J. B. Harding[18] has determined the ratio $\sigma(Na^{22})/\sigma(Na^{24})$ by counting the γ-radiation in both cases with a calibrated scintillation crystal. He obtains a value of about half of ours. The cause of this discrepancy is not known.

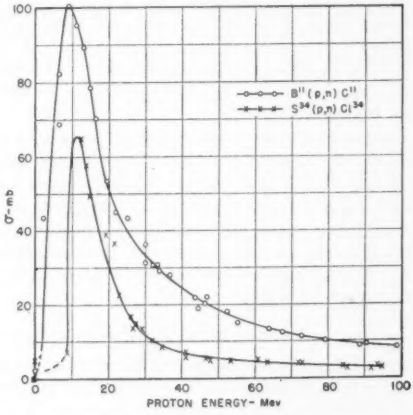

FIG. 5. Excitation functions for two (p,n) reactions.

[16] Birge, Kruse, and Ramsey, Phys. Rev. **83**, 274 (1951).

[17] Z. W. Ho, Compt. rend. **226**, 1187 (1948).

[18] A. E. R. E. Harwell (private communication).

C. $B^{11}(p,n)C^{11}$ and $S^{34}(p,n)Cl^{34}$

After the rather complicated reactions on aluminum, it was thought worthwhile to look at a simple reaction, (p,n), for several nuclei. The results of the first two such reactions are shown in Fig. 5. Even simpler reactions of the type $X(p,p')X^*$ could be studied by the activation technique using such stable nuclei as Sr^{81}, Rh^{103}, In^{115}, etc., which have isomeric states.

Powdered natural boron (81 percent B^{11}) was used for the $B^{11}(p,n)C^{11}$ reaction. The C^{11} yield from the 19 percent of B^{10} by a (p,γ) reaction should be negligible except below the (p,n) threshold. The powdered boron could not be pressed into pellets, so recessed absorbers with tight fitting caps were used to hold the powder. Two runs were made at 100 Mev to obtain the main features of the excitation curve above 30 Mev. After this, numerous runs were made at an incident energy of 60 Mev, shifting the energy scale slightly at each run by adding a thin absorber to obtain detail in the low energy peak. Each run was separately monitored with the C^{11} reaction, and all points reduced to absolute cross sections for plotting. The absolute cross sections, in terms of that of C^{11}, should be quite accurate since in both cases the same activity was being counted and the samples were adjusted to have the same thickness. The points below 10 Mev are badly smeared because of straggling and should not be taken seriously. The activity of boron samples beyond the proton range was less than 0.05 percent of the peak. This is evidence for the very small background of protons which might have entered the absorber stack from the side.

The reaction $S^{34}(p,n)Cl^{34}$ leads to an energetic (3–5 Mev) β-emitter with a 32-min period whose decay scheme is not well known.[19] Natural sulfur (4.2 percent S^{34}) was used although isotopic enrichment would have improved the accuracy. The interfering activities (P^{32}, Si^{31}) were eliminated by counting the samples through a thick absorber. If a small 15-hour background was subtracted the samples decayed from about 50 min to 4 hours with a slope of 32 ± 0.5 min. This half-life was checked against a purified Cl^{34} source obtained by irradiating Na_2SO_4 and precipitating AgCl. This gave a period of 32.5 ± 0.5 min over 10 half-lives. The absolute values shown in Fig. 5 are rather approximate (±25 percent) since thick samples and absorbers were used, resulting in rather large corrections to the β-count. In calculating $\sigma(Cl^{34})$, one β-ray per disintegration was assumed.

An excitation curve for Cu^{62} (10.2 min, β^+) from natural copper is shown in Fig. 6. This was taken as a preliminary to work in progress on the separated isotopes. The large peak at 25 Mev is the result of the $Cu^{63}(p,pn)Cu^{62}$ reaction while the smaller peak at 50 Mev is probably the $Cu^{65}(p,p3n)Cu^{62}$ reaction.

[19] L. Ruby and J. R. Richardson, Phys. Rev. **83**, 698 (1951).

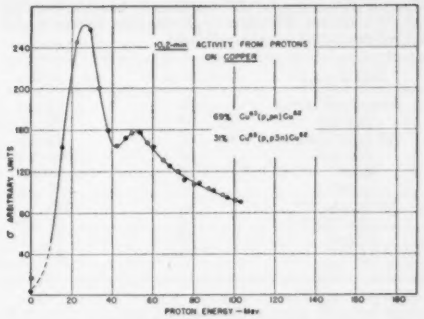

FIG. 6. Cu^{62} from natural copper.

7. ERRORS

A possible error in both the relative and absolute cross sections is the loss of nuclei from the target foils due to recoil or evaporation during bombardment. The first of these has been discussed in another paper in connection with its use to determine the momentum transfer in high energy nuclear reactions.[20] For the C^{11} and Na^{24} reactions the loss is about 5–10 percent for 1-mil foils. Since 5-mil foils were generally used, the recoil loss is less than the uncertainty in the proton absorption correction, and further, tends to cancel in the ratio R_Z/R_M. This will also be true for the F^{18} and Na^{22} reactions. The recoil losses for the two (p,n) reactions should be even less since a smaller momentum transfer to the residual nucleus is expected. There will in these cases be an error of a few percent in the absolute cross sections due to recoil losses from the monitor foil.

The loss of product nuclei by evaporation from the targets during irradiation has been reported to be small if the targets are not overheated.[21,22] An experiment was performed to measure the F^{18} and Cl^{34} yield when the targets were held at atmospheric pressure in a vacuum-tight capsule during irradiation. The values obtained were 10 percent high for F^{18} and 15 percent high for Cl^{34} as compared to the average values from several runs in which vacuum-tight capsules were not used. Although these corrections are within the errors in the absolute ratio of the β-counts they have been included in the curves presented. Other sources of error in the relative excitation curves would be the finite energy width of the scattered beam and the subsequent straggling in the absorber as well as any errors in the absolute energy scale. The spectrum of the "180°" scattered protons was measured at the target position. The method and results are given in Appendix A. Protons initially monochromatic at 100 Mev will have a dispersion of 4 Mev at 20 Mev, which will lower the peaks in the (p,n) reactions by ~15

[20] N. M. Hintz, Phys. Rev. **86**, 1042 (1952).
[21] Brown, Irvine, and Livingston, J. Chem. Phys. **12**, 132 (1944).
[22] J. D. Seagrave, Phys. Rev. **84**, 1219 (1951).

TABLE I. Thresholds for Al^{27} reactions in laboratory system calculated from mass differences ($-Q$) and mass differences plus total Coulomb barrier heights ($-Q+V_B$).

Mode of decay	$-Q$, Mev	$-Q+V_B$, Mev
$Al^{27}(p,3pn)Na^{24}$	32	44
(p,pHe^3)	24	36
$Al^{27}(p,3p3n)Na^{22}$	52	64
$(p,T\,He^3)$	35	47
$(p,\alpha d)$	20	32
(p,Li^6)	18.5	30
$Al^{27}(p,5p5n)F^{18}$	91	110
$(p,\alpha T\,He^3)$	45	54
$(p,2\alpha d)$	30	49
(p,B^{10})	24	41

percent but will have little effect on the reactions with higher thresholds.

In summary, it is believed the relative values at different energies are correct to within ± 5 percent, except in the case of the (p,n) peaks, the principal uncertainty being in the proton absorption correction. The absolute values should be within ± 15 percent for Na^{24} and for C^{11} from B^{11} and ± 25 percent for F^{18}, Na^{22}, and Cl^{34}, the uncertainty being in the absorption and scattering corrections to the β-ray count.

8. CONCLUSIONS

The reaction $C^{12}(p,pn)C^{11}$ has been discussed theoretically by Heckrotte and Wolff[23] using the evaporation theory at low energy and a rough independent particle model at higher energy. They predict a peak at 45 Mev to be followed by a slowly varying cross section up to 140 Mev where their calculations terminate. The peak found here is in fair agreement with their calculation. The earlier curve of Chupp and McMillan[18] did not show this peak due to the poorer energy resolution and higher neutron background. The slowly decreasing cross section above 45 Mev does not agree with the calculations of Heckrotte and Wolff, who predict a cross section which rises slowly above the peak and which has about half the value observed. The reason for the discrepancy is not clear from their brief account of the calculation. In any independent particle model the cross section must ultimately decrease approximately as $1/E$. The contribution to the C^{11} yield from a (p,d) reaction[24] would give a decreasing term of about 25 mb at 90 Mev.

The detailed interpretation of the reactions on Al^{27} along the lines of the C^{11} calculation would be quite difficult because of the many ways in which the reaction may proceed. In addition to the evaporation and fast knock-on neutrons and protons there is an appreciable contribution from the emission of α-particles, or other compound nuclei, as can be seen from an inspection of Table I in which the reaction thresholds for various modes of decay have been calculated. From Fig. 4 it seems likely that Na^{24} is produced mostly by a $(p,3pn)$ reaction although there is some evidence at the threshold for a (p,pHe^3) reaction. Na^{22} must definitely result in part from reactions of the kind $(p,\alpha pn)$ or (p,Li^6). Similarly, F^{18} cannot be made by a $(p,5p5n)$ process below 91 Mev, even allowing for barrier penetration. The slowly varying yield at high energy in these curves may then be due to an increasing contribution from processes in which the nucleons leave as individuals, superimposed on a decreasing tail from the evaporation of heavier fragments from a compound nucleus. This effect can be seen in a striking way in Fig. 1, reference 3, in which the (p,α) contribution to the production of Na^{22} from Mg^{25} has reached a very small value before the threshold of the $(p,2p2n)$ reaction occurs. A high probability for the evaporation of α-particles and other light fragments follows directly from phase-space and level density arguments alone[25] if these units are thought of as having at least a transient existence in the nucleus. In addition, because of increasing non-capture excitation at high energies as predicted by Serber[26] and verified by nuclear recoil measurements,[20] there is a tendency for the actual excitation of the nucleus to vary more slowly than the energy of the incident particle.

The two (p,n) reactions (Fig. 5) should be much simpler in their interpretation. The sharp peak at low energy would result from capture of the incident particle followed by the evaporation of a single neutron. This contribution becomes very small above ~ 30 Mev because of competition from the emission of several particles. Here the yield should be almost entirely from a single exchange collision in the nucleus with small momentum transfer. An analysis of the curves should give evidence as to whether the same ratio of ordinary to exchange forces as is required to explain free n-p

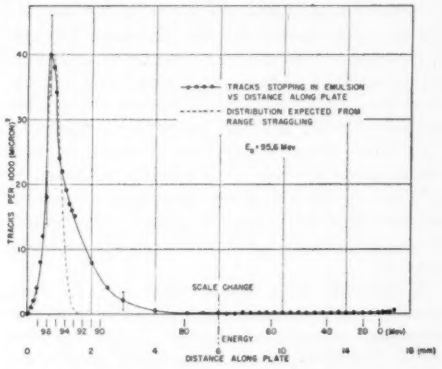

FIG. 7. Tracks stopping in NTA plate behind tapered absorber at 95.6 Mev.

[23] W. Heckrotte and P. Wolff, Phys. Rev. **73**, 264 (1948).
[24] G. F. Chew and M. L. Goldberger, Phys. Rev. **77**, 470 (1950); J. Hadley and H. York, Phys. Rev. **80**, 345 (1950).
[25] K. J. Le Couteur, Proc. Phys. Soc. (London) **A63**, 259 (1950).
[26] R. Serber, Phys. Rev. **72**, 1114 (1947).

scattering can be used to account for the p-n collisions between an incident particle and one in the nucleus.

The authors wish to thank Dr. Karl Strauch for his suggestion of the boron reaction and his help with this and other aspects of the experiment. Dr. Ralph Waniek and Dr. James Meadows have given considerable technical aid. Professor N. Bloembergen, Dr. P. J. van Heerden, and U. E. Kruse, were responsible for some very fruitful discussions. Arthur Hansen and Archie Grant were very helpful in the construction of apparatus and in the numerous cyclotron bombardments.

APPENDIX A

An estimate of the energy distribution of the "180°" scattered beam at the target position was obtained by exposing an Eastman NTA plate behind a tapered absorber.[37] The plate was then scanned along the direction of the taper, which was perpendicular to a cyclotron radius. The number of tracks which stopped in the emulsion, per unit length along the taper direction, was then proportional to the number of protons per unit range interval. The results are shown in Fig. 7 with standard deviations for typical points. The dotted line shows the distribution expected from range straggling alone if this distribution is normalized at the peak. The calculated broadening due to focusing error and width of plate scanned is negligible. The results seem to indicate the presence of a group of particles from 3–5 Mev less in energy and roughly 30 percent of the peak intensity. However, in order to limit the track density, even with $\frac{1}{16}$ sec exposure, it was necessary to detune the timing of the ion source pulsed high voltage to a point corresponding to a reduction by a factor of 30 in the normal beam, and to substitute helium for hydrogen as the ion source gas. This adjustment would drastically reduce the normal beam but have only a small effect on the spurious particles[38] which do not originate at the ion source. In addition, the peak of Fig. 7 was probably underestimated in relation to the rest of the curve since the high track density in that area would cause some tracks which stopped to be overlooked. The results here should be regarded as an upper limit to the energy width under normal operation conditions. The low energy protons may be the result of particles on a second or third traversal of the scatterer which penetrate beyond its innermost edge or to particles doubly scattered from the dee structure. A spread of as much as 2 or 3 Mev would be easily seen in a discrepancy with the linear accelerator data[9] at the threshold. However, from this experiment it can be concluded that the values of the (p,n) cross sections at high energy cannot be in error by more than 10 percent because of the presence of low energy protons at the targets.

APPENDIX B

The loss of protons from the foil area of the absorber assembly by multiple Coulomb scattering has been mentioned as a source of error in the relative excitation functions. A brief summary is given here of an approximate calculation and an experiment bearing on this effect.

[37] N. Bloembergen and P. J. van Heerden, Phys. Rev. **83**, 561 1951).

[38] Kruse, Mack, and Ramsey, Rev. Sci. Instr. **22**, 839 (1951).

TABLE II. Results of calculation showing scattering losses $F(\tau)$, for various foil radii, r_f, and absorber radii, r_a.

Case	$\langle\Delta r^2\rangle_{Av}^{\frac{1}{2}}$ cm	r_f cm	r_a cm	$(r_a-r_f)/\langle\Delta r^2\rangle_{Av}^{\frac{1}{2}}$	$F(\tau)$ %
1. Brass	0.10	0.397	0.556	1.6	2
2. Brass	0.10	0.556	0.715	1.6	1.3
3. Brass	0.10	0.397	0.715	3.2	1
4. Aluminum	0.17	0.556	0.715	0.9	7.3
5. Aluminum	0.17	0.397	0.715	1.9	2.6

The multiple scattering theory of Williams[7] modified by Dickinson and Dodder[39] to include energy loss is used because of its analytical simplicity. The geometry of the target and absorber assembly is taken as a series of thin foils of radius, r_f, embedded coaxially in a solid cylinder of absorber of radius, r_a. It is assumed that only those protons are lost from the foil area whose displacements after penetrating a depth, τ, are such that they are found outside of the absorber area. Those protons which stray into the region between r_f and r_a are assumed to be approximately replaced by protons which are initially in this region and are scattered into the foil area.

Protons incident at a distance from the absorber center, r, will have, at a depth, τ, a displacement, Δr, projected along a radius. The distribution of Δr is Gaussian with the mean square displacement, $\langle\Delta r^2\rangle_{Av}$, given by[39] $\langle\Delta r^2\rangle_{Av}=\langle\alpha^2\rangle_{Av}\tau^2/3$, where $\langle\alpha^2\rangle_{Av}$ is the mean square projected scattering angle at a depth τ. $\langle\alpha^2\rangle_{Av}$ can be calculated from the formulas of Dickinson and Dodder. When the circular geometry is approximately taken into account, the fractional loss after a depth τ is

$$F(\tau)=\int_0^{\rho_f}\rho\rho_f^{-2}[1-\mathrm{erf}(\rho_a)]d\rho,$$

where $\rho_a=\frac{1}{2}[(2\rho_a-\rho^2)^{\frac{1}{2}}-\rho]$, the ρ's being the r's, defined above, in units of $\langle\Delta r^2\rangle_{Av}^{\frac{1}{2}}$. $F(\tau)$ was evaluated numerically for several values of r_f and r_a for brass and aluminum, each for an absorber thickness, τ, corresponding to an energy interval from 100 to 20 Mev. The results are shown in Table II.

This shows clearly the desirability of brass over aluminum absorbers and the critical dependence of F on the amount by which the absorber diameter exceeds the foil diameter (column 5). For most of the data presented here the geometry corresponds to case 3 for which the scattering loss is negligible. When aluminum absorbers were used to obtain small energy steps at low energy, a small discrepancy could be seen with the points taken with brass absorbers of the order of magnitude shown in Table II. This is shown in Fig. 2 where the final curve is drawn favoring the brass absorber points. An experiment to check the values calculated above was performed using $\frac{1}{16}$-in. foils in $\frac{1}{8}$-in. absorbers. After irradiation, the center $\frac{1}{8}$-in. diameter was punched out and the inner and outer areas counted separately. Since the scattering losses are almost entirely from the periphery of the foils, the ratio of the inner to outer area activities gives an estimate of $F(\tau)$. The result for a geometry resembling case 3 (brass absorbers) was $F\leq 1$ percent while for a geometry intermediate between cases 4 and 5 was $F=2\pm 1$ percent, in rough agreement with the calculated values.

[39] W. C. Dickinson and D. C. Dodder, Los Alamos Report No. 1182 (1950).

[39] B. Rossi and K. Greisen, Revs. Modern Phys. **13**, 240 (1941).

A New Gyromagnetic Effect in Permalloy and Iron

S. J. BARNETT AND LOUIS A. GIAMBOMI*
University of California, Los Angeles, California and *California Institute of Technology, Pasadena, California*
(Received September 11, 1950)

A long circular cylinder of compressed ferromagnetic powder is magnetized along its axis to an intensity of magnetization J_s, near saturation, so that the moments of all of the magnetic elements point essentially in the same direction Z. In a direction X, normal to Z, a small magnetic intensity H_x with frequency f, such that $1/f$ is much greater than the relaxation time, is applied. This causes the intensity of magnetization to oscillate synchronously through a small angle in the XZ-plane; and this leads to the development of an intensity of magnetization J_y in the transverse direction Y and proportional to H_x. From measurements of J_y, or the corresponding magnetic induction B_y, the longitudinal magnetization J_s, the frequency f, and the transverse permeability $\mu_x=\mu_y$, the gyromagnetic ratio ρ can be calculated for approximate saturation. For both Permalloy and iron rods, steadily magnetized longitudinally in very intense fields and cross magnetized at frequencies of 22 and 30 kc/sec in very weak fields, the values obtained for ρ do not differ by more than the experimental error from those obtained for the same substances (though in a different physical state) in experiments on the Barnett and Einstein-de Haas effects.

I. INTRODUCTION

IT has been known since 1914[1] that a rod of iron becomes magnetized by mere rotation about an axis precisely as it would be magnetized by applying to it in the direction of the axis a magnetic field with the intensity

$$H=\rho d\theta/dt, \tag{1}$$

where $d\theta/dt$ is the angular velocity in radians per second and ρ is a constant for the given substance. The quantity ρ is the ratio of the angular momentum of the elementary magnet to its magnetic moment, and it is known as the *gyromagnetic ratio* of the substance.

Since 1914 many other ferromagnetic substances have been magnetized by rotation, and their gyromagnetic ratios have been found to be comprised approximately between the limits $1.00\times m/e$ (Heusler alloy) and $1.09\times m/e$ (cobalt), in electromagnetic units, m and e being the mass and the charge, respectively, of a Lorentz electron. The results have been confirmed by numerous experiments on the converse effect, first suggested in 1907 by O. W. Richardson, but first obtained experimentally by Einstein and de Haas in 1915 and 1916 (the rough magnitude of the ratio in 1915, the sign also in 1916).[2]

The magnetization produced by rotation as above cannot, however, be attributed to the rotation of the rod as a whole, but rather to the rotation impressed on its magnetic elements, which are entrained in the motion. Thus, the idea arose that if the rod were initially magnetized along a diameter and the vector intensity of magnetization rotated about the axis while the rod itself remained at rest, a gyromagnetic intensity of magnetization should be developed along the axis. *Conceivably* this could be done in at least two ways:

(1) The fixed rod might be placed in a steady magnetic field directed normally to the axis, and the field-producing agent could be rotated about this axis. This would rotate the vector intensity of magnetization and *might* be expected to produce a gyromagnetic intensity of magnetization along the axis.

(2) Or, if the rod were magnetized transversely by each of two similar coils with axes normal to the rod and perpendicular to one another and supplied with equal currents by a two-phase electric generator, rotation of the vector intensity of magnetization would result, and a gyromagnetic intensity of magnetization along the axis *might* be expected.

Closely related to (1) and (2) is a third process, (3). The rod might be steadily magnetized to approximate saturation along its axis so that the moments of all the elementary magnets would be aligned practically in this direction (Z) and placed in a weak alternating magnetic field with lines of magnetic induction normal to the rod (direction X). This would produce a small oscillation of the magnetic elements about axes in the direction Y normal to X and Z and thus produce an alternating gyromagnetic intensity of magnetization in the direction Y. This could be observed by means of a surrounding coil of wire with the planes of its turns normal to Y.

Experiments by method (1) offer no certain advantages over those in which the rotation is affected mechanically, and certain serious disadvantages are evident. Such experiments have apparently never been made.

Experiments by method (2) have an advantage over those involving the actual rotation of the rod in that very much higher frequencies can be used and the gyromagnetic intensity is proportional to the frequency.

Two groups of high frequency experiments by this method were made in the interval 1922–1925[3] by J. W. Fisher, who expected to find, even with rods only weakly magnetized at right angles to their axes, longitudinal magnetization equal to that which would have resulted

* Now with the Rand Corporation, Santa Monica, California.
[1] S. J. Barnett, Phys. Rev. **6**, 239 (1915).
[2] See S. J. Barnett, Proc. Am. Acad. Arts Sci. **73**, 401 (1940); **75**, 109 (1944); and Phys. Rev. **66**, 224 (1944).
[3] J. W. Fisher, Proc. Phys. Soc. (London) **34**, 177 (1922); Proc. Roy. Soc. (London) **A109**, 7 (1925).

from rotating the *rods*, initially unmagnetized, at the same high frequencies. However, only small deflections, a few mm and less, and in the wrong direction, were obtained at frequencies up to 5×10^4 per sec, at which the rotation of the rods would have given 13 to 35 cm.

It was shown by one of us,[4] however, that Fisher's expected deflection, on the most favorable hypothesis possible, should be multiplied by the small factor $3I_\perp/2I_\infty$, where $I_\perp$ is the cross magnetization and I_∞ the saturation magnetization of the rods. On this most favorable (and quite improbable) hypothesis, deflections of the order of one cm only could be expected.

More elaborate and precise experiments by one of us,[4] made on Permalloy and iron powders with the assistance of Dr. V. Hoover, also gave, as was expected, deflections far smaller than the values calculated on the most favorable hypothesis.

In discussing this type of experiment with one of us a number of years ago Professor Einstein suggested that the magnetic elements do not rotate with the intensity of magnetization vector at all, but have their moments periodically reversed by the rotating field.

Thus, for simplicity (in an XYZ coordinate system, X and Y horizontal, Z vertical) we may imagine the rod to be unmagnetized in the Z directions, while half the elements have moments with X components only, and half moments with Y components only. The alternating X intensity will then change the X cross magnetization by reversing the moments of the first group, and the alternating Y intensity will change the horizontal cross magnetization by reversing the moments of the Y group. Thus, in the two-phase system, the magnetization vector will rotate but without any rotation of the elements, and thus without the production of any longitudinal (Z) magnetization by a gyromagnetic process. Bloch and Becker have more recently suggested essentially the same explanation of the null effect.[5]

As is well known, there have long been other indications favoring the hypothesis that in the early part of the magnetizing process (weak fields) the magnetization proceeds by such quantum jumps, or reversals, of the elements, and not by changes in their orientation; and the work by method (2), which has to do with weak fields only, supports the other evidence.

In strong fields, however, the indications are that changes of magnetization are due to gradual changes in the orientation of the elements. If this is the case, a repetition of the investigations by this method (2), but with fields strong enough nearly to saturate the magnetic material, should yield positive results instead of a null effect. However, there are obviously considerable difficulties in the way of such an investigation.

In connection with the discussion just mentioned, Professor Einstein suggested the type of experiment described under method (3), and this paper deals chiefly with an investigation made by this method.

In all the experiments mentioned above only relatively slow processes are contemplated, the times involved in producing the maximum changes in magnetization being very great in comparison with the relaxation times, so that in each change the magnetization is essentially and continuously in equilibrium with the impressed speed or field.

In quite recent years several related experiments using microresonance phenomena have been devised to measure gyromagnetic ratios of atomic nuclei and of electrons. Thus:

Rabi and others have developed atomic beam resonance methods to measure the gyromagnetic ratios of nuclei and other elementary particles.

Bloch and others have measured gyromagnetic ratios of nuclei by applying oscillating fields normal to steady fields and detecting the gyromagnetic intensity by induction, somewhat as in the experiments described in this paper. Closely related experiments have been made by Purcell and his collaborators.

Griffiths and others have used microresonance methods to measure gyromagnetic ratios for the elements in highly magnetized ferromagnetic substances. In some of these experiments, one plane wall of a resonant cavity is constructed of the substance to be studied and highly magnetized in a direction X parallel to the surface. The cavity is excited in a mode of oscillation such that the oscillating magnetic intensity close to the wall has the direction Y normal to X. In the combined fields the elements in the substance precess. When the frequency of the cavity is equal to the precessional frequency, the energy absorbed by the wall is increased to a maximum. By measuring the absorption of the cavity as a function of the intensity of the impressed field the gyromagnetic ratio can be calculated.

The fundamental principle involved in all these gyromagnetic experiments is the same. The nature of the magnetic element (whether simple spinning electron, spinning electron with orbital participation, nucleus, or other element), the strength of the supplementary or applied field if any is present, the degree of saturation of the material in such an applied field if any is present, the time involved in producing the gyromagnetic effect, and its relation to the relaxation time or to the resonance period, as well as the methods[6] of

[4] See S. J. Barnett, Phys. Rev. **27**, 115 (1926); and Proc. Am. Acad. Arts Sci. **68**, 229 (1933).

[5] Or we may perhaps proceed as follows: With respect to the axis of the cylinder, some of the elements might revolve clockwise and some counterclockwise as they jumped from one orientation to the other. There is no *a priori* reason to expect either clockwise or counterclockwise rotations to predominate. The clockwise rotating elements would give rise to a gyromagnetic effect in one direction along the axis, while the counterclockwise rotating ones would give rise to an effect in the opposite direction. The macroscopic gyromagnetic intensity of magnetization would be close to zero.

[6] These methods can be varied greatly. For example, in experiments on magnetization by rotation, the rod may be oscillated about its axis instead of being set into continuous unidirectional rotation, and the alternating electromotive force thus developed

detection, differ from one type of experiment to another. Different values of the gyromagnetic ratio may thus be obtained for a substance from different types of experiment. But the fundamental idea in all is identical with that of the experiments on magnetization by rotation.

Not very long after Einstein's suggestion was made, the approximate theory was developed and experiments were instituted to test its validity and to measure the gyromagnetic ratios of continuously and highly magnetized compressed iron and Permalloy powders. These materials were chosen on account of the necessity of freedom from eddy currents in the rather high frequency fields employed. Circumstances, however, made it necessary to postpone the work in its early stages, and it was only recently that it became practicable to resume it. Although in the recent work many improvements have been made, we had hoped to make still further and important changes, but this has been prevented by the pressure of other matters. For the sake of brevity, the discussion here will be restricted, so far as experiments are concerned, almost entirely to the newer work.

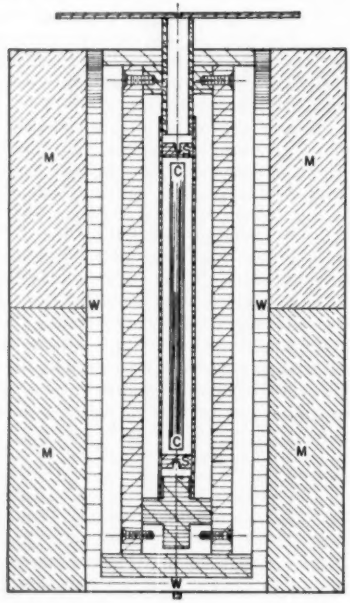

FIG. 1. Central cross section showing rod, rod holder, magnetizing coil, water jacket, etc.

in the surrounding coil of wire may be compared with the electromotive force produced by an alternating field of known intensity and the same frequency, an amplifier being used to increase the sensitivity if needed. See S. J. Barnett, Bull Nat. Research Council 3, Part 2, 245 (1922).

II. GENERAL DESCRIPTION AND THEORY

In the experiments a long circular cylinder c of compressed iron powder, or Permalloy powder, is placed with its axis vertical (Z direction of a right-hand rectangular coordinate system XYZ) and is magnetized in this direction to intensity of magnetization J_s, approximately that of saturation, by a large coaxial solenoidal electric coil M[7] surrounding it symmetrically (see Fig. 1).

The magnetic cylinder lies symmetrically at the center of a second coil PP', Fig. 2, Helmholtz type, but long, narrow and rectangular, with its turns in vertical planes parallel to YZ. When the rod is absent there is produced through the agency of this coil, traversed by an alternating electric current I, with frequency $f=\omega/2\pi$, throughout the region normally occupied by the rod, a small and approximately uniform magnetic intensity H_x in the X direction. When the rod is in place there results in the rod an approximately uniform intensity of magnetization J_x in the X direction, synchronous with I and H_x. An equilibrium theory is assumed (see above) because the period $1/f$ is large in comparison with the relaxation time.

It is easy to show that when the length of the rod, with transverse permeability μ_x $(=\mu_y)$, is great in comparison with its diameter, and the demagnetizing factor is thus essentially equal to 2π, the intensity of magnetization J_x is given by the relation

$$J_x=\frac{1}{2\pi}\left(\frac{\mu_x-1}{\mu_x+1}\right)H_x. \tag{2}$$

When the ratio of the length of the rod to its diameter is not very great, as is the case in this investigation, the mean demagnetizing factor N_x will be somewhat less than 2π. We shall write

$$N_x=2\pi(1-\delta), \tag{3}$$

where δ is small in comparison with unity. Thus, in place of (2) we may write with all sufficient precision

$$J_x=\frac{1}{2\pi}\left(\frac{\mu_x-1}{\mu_x+1}\right)(1+\delta)H_x. \tag{4}$$

The alternating horizontal intensity H_x causes the axes of the elementary magnets—always lined up almost completely with their axes in the direction Z—to execute small oscillations in planes normal to X and Z about horizontal axes in the direction Y. Thus, there exists a gyromagnetic intensity G in the direction Y, producing a gyromagnetic intensity of magnetization J_y, proportional to G.

A third coil S, which may or may not be similar to PP', is similarly situated but with the planes of its turns normal to those of PP' and linked with the flux ϕ due to J_y. It has, therefore, induced in it an electro-

[7] S. J. Barnett, Phys. Rev. 27, 425 (1908).

motive force E which may be measured, after amplification if necessary, and will make possible the determination of J_y or the corresponding magnetic induction B_y. For the intensity of magnetization J_y, we have

$$J_y=\frac{1}{2\pi}\left(\frac{\mu_x-1}{\mu_x+1}\right)(1+\delta)G. \tag{5}$$

Let θ designate the mean angle made by the axes of the elementary magnets with Z at any time t, and θ_0 its amplitude. Then θ is given by the relation

$$\theta=\frac{J_x}{J_s}=\frac{1}{2\pi J_s}\left(\frac{\mu_x-1}{\mu_x+1}\right)(1+\delta)H_x. \tag{6}$$

The angular velocity of the axes of the elements at the time t is

$$\frac{d\theta}{dt}=\frac{1}{J_s}\frac{dJ_x}{dt}=\frac{1}{2\pi J_s}\left(\frac{\mu_x-1}{\mu_x+1}\right)(1+\delta)\frac{dH_x}{dt}. \tag{7}$$

In accordance with Eq. (1), the gyromagnetic intensity G is given by the relation

$$G=\rho\frac{d\theta}{dt}=\frac{\rho}{2\pi J_s}\left(\frac{\mu_x-1}{\mu_x+1}\right)(1+\delta)\frac{dH_x}{dt}. \tag{8}$$

From Eqs. (5) and (8) we get

$$J_y=\frac{\rho}{4\pi^2 J_s}\left(\frac{\mu_x-1}{\mu_x+1}\right)^2(1+2\delta)\frac{dH_x}{dt}. \tag{9}$$

The magnetic induction B_y produced in the rod by G is

$$B_y=4\pi J_y-NJ_y=2\pi(1+\delta)J_y. \tag{10}$$

Suppose the intensity H_x produced (primarily by the coil PP') in the space to be occupied by the rod to be given by the equation

$$H_x=H_{x0}\sin\omega t, \tag{11}$$

so that

$$dH_x/dt=\omega H_{x0}\cos\omega t; \tag{12}$$

then

$$J_x=\frac{1}{2\pi}\left(\frac{\mu_x-1}{\mu_x+1}\right)(1+\delta)H_{x0}\sin\omega t\equiv J_{x0}\sin\omega t, \tag{13}$$

$$J_y=\frac{\rho\omega}{4\pi^2 J_s}\left(\frac{\mu_x-1}{\mu_x+1}\right)^2(1+2\delta)H_{x0}\cos\omega t\equiv J_{y0}\cos\omega t, \tag{14}$$

and

$$B_y=\frac{\rho\omega}{2\pi J_s}\left(\frac{\mu_x-1}{\mu_x+1}\right)^2(1+3\delta)H_{x0}\cos\omega t\equiv B_{y0}\cos\omega t. \tag{15}$$

When Eqs. (14) and (15) are solved for ρ we obtain

$$\rho_J=\frac{4\pi^2 J_s J_{y0}}{\omega H_{x0}}\left(\frac{\mu_x+1}{\mu_x-1}\right)^2(1-2\delta), \tag{16}$$

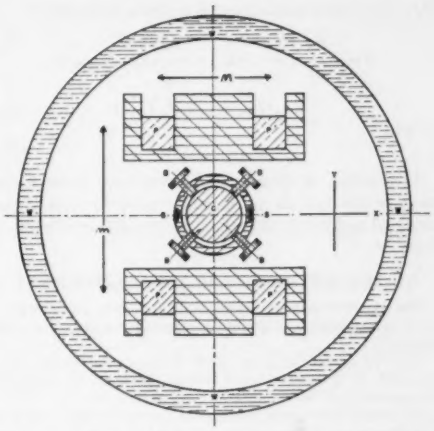

Fig 2. Cross section of primary coils PP, P'P', rod C, secondary coil S, adjusting screws B, and cooling jacket W.

and

$$\rho_B=\frac{2\pi J_s B_{y0}}{\omega H_{x0}}\left(\frac{\mu_x+1}{\mu_x-1}\right)^2(1-3\delta). \tag{17}$$

All the unknown quantities on the right-hand side of either Eq. (16) or Eq. (17) can be found experimentally by methods whose principles are well known, and thus ρ can be determined. The phase relations between X, J_y, etc., can be determined with an oscilloscope. The methods used are described below. The quantity J_y or the quantity B_y is determined, as indicated above, by measuring the emf E induced in the coil S when H_x varies.

If the coil S is so constructed that its constant γ is uniform throughout the space normally occupied by the material of the rod, Eq. (14) will be used. The flux ϕ through the coil will be given by the relation

$$\phi=\gamma VJ_y=\gamma VJ_{y0}\cos\omega t, \tag{18}$$

where V is the volume of the rod and γVJ_y is its magnetic moment, with the amplitude γVJ_{y0}.

If the coil S is a narrow flat coil wound symmetrically in (essentially) a plane through the axis of the rod and infinitely close to its surface, the flux will be given by the relation

$$\phi=B_y dl\cdot N=B_y S=B_{y0}S\cos\omega t, \tag{19}$$

where d is the diameter of the rod, l its length, N the number of turns in the coil, and S the total area of the coil.

The emf E induced in the coil in the first case is

$$E=-d\phi/dt=-(d/dt)(\gamma VJ_{y0}\cos\omega t)$$
$$=\omega\gamma VJ_{y0}\sin\omega t=E_0\sin\omega t, \tag{20}$$

so that

$$J_{y0}=E_0/\omega\gamma V. \tag{21}$$

The emf E induced in the coil in the second case is

$$E = -\frac{d\phi}{dt} = -\frac{d}{dt}(SB_y) = -\frac{d}{dt}(SB_{y0}\cos\omega t)$$

$$= \omega SB_{y0}\sin\omega t = E_0\sin\omega t, \qquad (22)$$

so that

$$B_{y0} = E_0/\omega S. \qquad (23)$$

In practice, of course, corrections have to be made because the coils do not satisfy exactly the conditions assumed and the demagnetizing factor differs somewhat from 2π.

III. THE APPARATUS AND ITS ARRANGEMENT

The apparatus may be divided into several groups as follows:

(A) The first group includes the magnetic materials that were studied.

(B) The second, the large coil M of copper wire which, when traversed by a steady electric current, produced the magnetic intensity H_z and the intensity of magnetization J_z.

(C) The third, the equipment for producing the high frequency power necessary to energize the coils which produced the oscillating magnetic intensity H_z.

(D) The fourth, the (primary) coils for producing the magnetic intensity H_z, the (secondary) coils used for the measurement of the gyromagnetic induction B_y or gyromagnetic magnetization J_y and for other measurements; also thermal devices to control the temperatures of these coils and the magnetic materials.

(E) The fifth, the amplifier used to increase the strength of the gyromagnetic signal appearing in the secondary coil, and devices to measure the magnitude, phase, and frequency of this signal.

(A) The Magnetic Materials

Three rods of compressed powdered ferromagnetic materials were used in the experiments. These same rods, from material supplied by the Bell Telephone Laboratories, were used by one of us in the experiments with rotating magnetic fields referred to above. They were cylindrical in shape, about 25 cm in length, and 1.41 cm in diameter. The rods were formed from small disks of compressed iron and compressed Permalloy dust. Disks were cut from the compressed material and packed closely, with cement between them, in Bakelite tubes $\frac{1}{8}$-inch outside diameter and $\frac{1}{32}$ inch thick. The disks were squeezed together in a vise while the cement hardened. The lengths of the rods are listed below:

(1)[8]	Permalloy	25.1 cm
(2)	Permalloy	24.0 cm
(3)	Iron	24.0 cm.

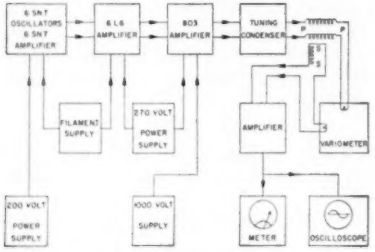

FIG. 3. Block diagram of primary and secondary circuits.

[8] In the course of the experimental work, rod No. (1) was accidentally broken so that it became necessary to make part of the Permalloy experiments on rod No. (1) and part on rod No. (2). The existence of the gyromagnetic effect was established with all the rods.

(B) The Coil for Producing the Steady Magnetic Field

This coil M (Fig. 1), a circular cylinder in form, was wound on a brass bobbin from about 300 pounds of *DCC* copper wire in 3900 turns, and had a resistance of 10.4 ohms at room temperature. It produced a magnetic field of approixmately 90.2 gausses per ampere averaged over the region in which the sample was placed. The coil was mounted with the axis approximately vertical.

On top of the bobbin, screw adjustments were provided which made it possible to rotate the sample and secondary coil through small angles, as described below.

The intensity external to the large coil fell off so rapidly with distance that its effect upon the meters and the rest of the apparatus could be neglected.

The large coil M, as well as the primary coil, at first became very hot and made it necessary to install a cooling jacket (see Fig. 1). For this jacket, coils were wound in the form of a helix from $\frac{1}{4}$-inch copper tubing, on the curved surfaces and bottom of a brass tube $4\frac{1}{2}$ inches in diameter and 20 inches long, with large quantities of soft solder filling the space between turns. The entire assembly fitted tightly in the circular hole of the large coil. Couplings were provided so that tap water could be forced through the coils from bottom to top. The primary coil and assembly were placed inside this tube and held there by machined bakelite disks bolted to the primary coil and fittng closely to the brass tube. The remainder of the space inside the brass tube was filled with transformer oil. In this way, temperature changes in the region inside the cylinder could be kept to less than a tenth of a degree during all experiments.

(C) Equipment for Producing the High Frequency Power (Fig. 3)

It was necessary to employ frequencies low enough to prevent disturbances from eddy currents and to insure that the time of an oscillation was much greater than the relaxation time of the material. On the other hand, since the gyromagnetic voltage is proportional to the square of the frequency, it was desirable to use as high frequencies as practicable. From these considerations frequencies ranging from 20 to 32 kc/sec were chosen. To prevent purely electrical disturbances from getting through it was necessary to use screen grid tubes and to make the apparatus as nearly symmetrical as possible. Push-pull tube arrangements were used throughout. The arrangements adopted produced steady voltages at constant frequencies and provided ready means for changing the frequency at will.

The oscillator consisted essentially of a 6SN7 vacuum tube in a multivibrator circuit, with an attached tank, as first used by Reich. We have had considerable experience with this kind of oscillator and have always found it to perform very satisfactorily. The oscillator could be so adjusted that its frequency changed by only 0.1 percent in the course of an experiment.

The oscillator was followed by a loosely coupled 6SN7 push-pull buffer amplifier, and this was followed by the other equipment necessary to produce the high frequency power. All this was of standard design, built from high grade materials, and properly screened in iron and copper boxes. The output of the final power amplifier was fed through a transformer into a tuned series resonant circuit. The inductance was that of the Helmholtz coil pair (described in the next section) which furnished the oscillating magnetic field and a small variometer in series therewith; the capacity was that of two variable condensers, with a small trimmer attached to one of them.

The oscillator could be so adjusted that its frequency changed by only about 0.1 percent in the course of an experiment.

(D) The Alternating Current Coils

The fourth group of apparatus consisted of several coils and thermal devices. Some of the components showed microphonic behavior and were placed on special tables, separate from the rest of the apparatus.

Primary Coils

These coils PP', the two halves of the Helmholtz pair referred to in the last section, were constructed with precision from highly insulating materials and had the approximate sizes and shapes indicated in Fig. 2. In the framework accurately machined holes and screws were provided by means of which the specimen under study could be inserted, removed, rotated, aligned, and centered.

Secondary Coils

The main secondary coil C was constructed much like one-half of the primary, but with shape, size, and windings suitable for its different purpose (see Fig. 2).

The coil, with the sample inside, was placed in the center of the primary Helmholtz coils PP' in such a position that the mutual inductance between primary and secondary was close to zero. A Bakelite bearing was provided to fasten the bottom of the secondary coil to the bottom of the frame of the primary coil. At the top of the secondary coil another Bakelite tube was fastened to the secondary coil with Bakelite screws. This tube served to hold and turn the secondary coil into any selected azimuth.

In order to detect the small gyromagnetic signal it was important to reduce to small values all extraneous voltages in the secondary coil. To do this, first the secondary coil was mechanically rotated into a position of approximate minimum mutual inductance with the primary and clamped in this position. To reduce the coupling between the two coils further, a variable mutual inductance was used by which any induced voltage could be reduced to a small quantity.

(E) Apparatus and Arrangements for Measuring the Gyromagnetic Electromotive Force ψ

The apparatus in this group included an amplifier to increase the strength of the gyromagnetic signal from a few tenths of a millivolt to a magnitude more convenient to measure by standard instruments. The amplifier finally adopted employed a 6SJ7 vacuum tube with a tuned-grid tuned-plate circuit. For this single stage amplifier the gain was 10.6 at 22 kc/sec and 17.5 at 30 kc/sec.

High Q parallel resonant circuits were used to peak the amplifier and allow only a narrow band of frequencies to be amplified. In this way background noise, always troublesome, was greatly reduced.

An oscilloscope and an electron voltmeter were attached to the output of the amplifier to measure the phase and magnitude of the signal. The oscilloscope was operated on external sweep, with a synchronizing signal tapped from the output of the 803 power amplifier.

IV. MEASUREMENT OF THE QUANTITIES NEEDED FOR THE DETERMINATION OF THE GYROMAGNETIC RATIO

If the secondary coil S were a narrow flat coil wound symmetrically in (essentially) a plane through the axis of the rod, and (infinitely) close to its surface, the quantity ρ could be determined from an equation formed by combining Eqs. (17) and (23) as follows:

$$\rho=\frac{2\pi E_0 J_s}{S\omega^2 H_{x_0}}\left(\frac{\mu_s+1}{\mu_s-1}\right)^2(1-3\delta), \qquad (24)$$

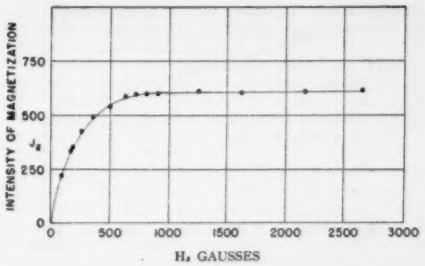

FIG. 4. Magnetization curve for powered Permalloy.

where S is the total area of the ideal coil. Corrections resulting from the departure of the shape and location of the coil from ideal conditions will be applied later.

(*1*) The frequency $f=\omega/2\pi$ of the 6N7 Reich oscillator was determined by comparison with the highly constant 60/sec frequency of the mains by standard procedure with the assistance of two commercial oscillators, an oscilloscope, and a frequency meter. The two frequencies used in most of the work were found to be 21.75 kc and 30.50 kc with an error not greater than about 0.1 percent.

(*2*) The amplitude H_{x_0} of the oscillating horizontal intensity produced by the current I, with amplitude I_0, in the primary coil was determined as follows:

A specially constructed test coil was placed in the region occupied in the main experiment by the rod being tested, and a high impedance voltmeter was placed across its terminals. The voltage could then be read as a function of the current in the primary coil. In a preliminary experiment the test coil was rotated until the voltage was a maximum, when it was locked in place.

Numerous readings of the voltage E' were then taken with various values of I', the primary current, at each of the frequencies of the experiment. Then for each frequency an average value of the amplitude of H_x was computed for each value of E' and the corresponding value of I'. With this information it was easy to determine the effective constant K of the coil for each frequency used. Then we have

$$H_{x_0}=KI_0, \qquad (25)$$

where I_0 is the primary current producing the gyromagnetic emf in the main experiment.

It was, of course, impossible to proceed in the usual way to determine the constant of the coil on account of the presence of the surrounding conducting tube. Also, it is to be noted that in the method adopted an absolute calibration of the ammeter is not needed.

(*3*) *The longitudinal magnetization* J_s. In the case of each rod, placed symmetrically in the large coil M, J_s was determined ballistically for various magnitudes of the current in the coil. For Permalloy a curve for J_s against H_s is plotted in Fig. 4.

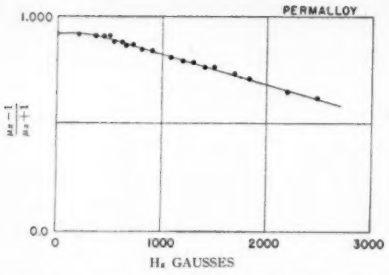

FIG. 5. Transverse permeability function for Permalloy.

(4) *The longitudinal permeability μ_z in weak fields.* While this quantity is not needed directly for the calculation of ρ, we have used it indirectly for the calculation of μ_x which, in weak fields where our rods are essentially isotropic, is equal to μ_z. The quantity μ_z is determined as follows.

Let H_{zi} designate the mean magnetic intensity in the rod in the field of strength H_z. Then,

$$H_{zi}=H_z-N_zJ_z,$$

and

$$\mu_z=4\pi J_z/(H_z-N_zJ_z)+1.$$

The demagnetizing factor N_z, which is easily measured but which can also be obtained with sufficient precision from the tables, is 0.07.

(5) *The transverse demagnetizing factor $2\pi(1-\delta)$.* The demagnetizing factor is a purely geometric quantity, but, of course, it requires magnetic measurements for its experimental determination. To determine δ we use the approximate equation

$$\delta=\frac{\mu_x+1}{2\mu_x}\frac{B_x{}^i}{H_{x0}}-1, \tag{26}$$

and proceed with weak fields, in which the transverse permeability is identical with the longitudinal permeability, already determined as indicated in (4). We measure B_{xi}/H_{x0} for both small and large magnitudes of H_x, either ballistically or with the high frequencies of the principal experiments.

The results gave for δ the value 0.01.

(6) *The transverse permeability and the permeability function* $(\mu_x-1)/(\mu_x+1)$. When δ is small it is readily shown that

$$(\mu_x-1)/(\mu_x+1)=(B_x{}^i/H_{x0}-1)(1-2\delta), \tag{27}$$

an equation from which we can obtain both the transverse permeability μ_x and the permeability function $(\mu_x-1)/(\mu_x+1)$. The vertical curve of $(\mu-1)/(\mu+1)$ against H_z is plotted in Fig. 5.

(7) *The gyromagnetic* emf ψ *developed in the actual secondary coil when the* emf E *would be developed in the ideal coil of area S.* In all of the final work the secondary coil was flat and rectangular like the ideal coil of area S, but it was longer than the rod and considerably wider. This coil will be designated in this section as coil (1).

From the actual emf ψ developed in this coil in the main experiment we have to find the emf E which would have been developed in the ideal coil of Eq. (24).

For this purpose experiments were made with three secondary coils, *viz.*, (1) the actual secondary coil, (2) the coil wound closely on the rod and approximating closely the ideal coil of Eq. (24), and (3) a coil exactly like coil (2) but wound on Bakelite. Each coil had the same number of turns N as the ideal coil and in the experiments with it was symmetrically mounted with the planes of its turns parallel to those of the primary coil, which was traversed by an alternating current of known amplitude. The fluxes through the three coils will be designated by ϕ_1, ϕ_2, ϕ_3.

For ϕ_1 we have

$$\phi_1=\phi_{1x}+\phi_{1Jz}, \tag{28a}$$

and thus

$$\phi_{1Jz}=\phi_1-\phi_{1z}, \tag{28b}$$

where ϕ_{1z} is the flux when the rod is absent, and ϕ_{1J} is the part of the flux due to the presence of the rod.

For ϕ_2 we have similarly

$$\phi_2=\phi_{2x}+\phi_{2J}=\phi_3+\phi_{2J}; \tag{28c}$$

since ϕ_3 is identical with the flux ϕ_{2x}, the flux would thread coil (2) if the rod were removed. Thus, we obtain

$$\phi_{2J}=\phi_2-\phi_3 \tag{28d}$$

for the flux through coil b due to the rod only.

The flux ϕ_{2J} (due to the intensity of magnetization only) is made up of two parts, *viz.*, the flux ϕ_b which crosses the central section of the rod and would be the total flux through the coil (2) if it were wound from infinitely thin wire, and ϕ_Δ, the reverse flux through the small area $2\Delta l$ between the coil and the rod.

The flux through the first is

$$\phi_b=+BS, \tag{28e}$$

and that through the second is

$$\phi_\Delta=-BS\Delta/[b(1+\delta)]. \tag{28f}$$

Thus,

$$\phi_{2J}=BS\{1-\Delta/[b(1+\delta)]\}=BS(1-\Delta/b). \tag{28g}$$

The fluxes ϕ_1, ϕ_{1x}, ϕ_2, and ϕ_3 were calculated from the voltages induced in the appropriate coils, and then the quantity C was calculated from the equation

$$C=(\phi_2-\phi_3)/(\phi_1-\phi_{1x}).$$

Then

$$\phi_{2J}=\phi_{1J}C. \tag{28h}$$

From Eqs. (28g) and (28h) we obtain

$$\phi_{2J}=BS[1-(\Delta/b)]=\phi_{1J}C, \tag{28i}$$

and thus

$$BS=\phi_{1J}C(1+\Delta/b). \tag{28j}$$

From Eq. (28j) we see that

$$E/\psi=BS/\psi_{1J}=C[1+(\Delta/b)], \tag{28k}$$

or

$$E=C\psi[1+(\Delta/b)]. \tag{28l}$$

Substituting in Eq. (24) the vlaue of E from (28l), we obtain

$$\rho=\frac{C\psi_0 J_s}{\omega^2 S H_{x0}}\left(\frac{\mu+1}{\mu-1}\right)^2\left(1-3\delta+\frac{\Delta}{b}\right). \tag{29}$$

Many experiments also were made with direct currents in the primary coil, a galvanometer being used to measure the fluxes.

The values for C obtained for the Permalloy and iron rods are contained in Table I. The voltage across the terminals of the secondary coil, which would equal the gyromagnetic voltage if there were no extraneous voltages in the secondary, was increased by the amplifier, whose gain was carefully determined for both frequencies, and then measured by an electron voltmeter.

V. EXTRANEOUS ELECTROMOTIVE FORCES IN THE SECONDARY CIRCUIT AND PRELIMINARY ADJUSTMENTS

In what follows, for convenience, emfs in phase with or in opposition to the gyromagnetic emf will be referred to as in-phase emfs and those in quadrature therewith as quadrature emfs.

The extraneous effects originate fundamentally through residual mutual induction and capacity coupling between primary and secondary circuits. These were minimized by making the arrangements as nearly symmetrical as practicable; partly by the use of variometers and variable condensers. But it would have been difficult, if not impossible, to eliminate their effects sufficiently except that the induction effect is in quadrature with the gyromagnetic effect and that all the disturbing effects are independent of the direction of J_s, while the gyromagnetic effect reverses its sign with J_s.

In preliminary experiments a secondary coil A, wound on a Bakelite frame, was placed inside the primary coil. This coil assembly was, in turn, placed inside the hole in the bobbin of the coil M. The secondary coil was rotated in azimuth, varying the mutual inductance between the primary and secondary coils, until an induced (quadrature) voltage of convenient amplitude was obtained.

The amplifier was connected to the terminals of this coil A. The electron voltmeter and the vertical deflection terminals (Y deflection) of an oscilloscope were connected to the output of the amplifier. In order to synchronize the sweep (X deflection) of the oscilloscope with the current in the primary circuit, the oscilloscope was operated on "external sweep." The synchronizing signal, obtained from the terminals of the transformer in the primary circuit, was attenuated by a resistance network, and applied to the oscilloscope.

The positions (X coordinate) of the maximum and minimum of the induced voltages were noted on the oscilloscope screen. These extremes furnished a standard with which to compare phase relations of any other sine wave appearing across the output of the amplifier.

The secondary coil A was then removed from the apparatus, and the ferromagnetic sample, with a surrounding secondary coil B, was placed inside the hole in the bobbin of the coil M. The amplifier was connected to the terminals of this secondary coil. The electron voltmeter and synchronized oscilloscope were again connected to the amplifier output.

The secondary coil B and magnetic sample were rotated by means of the controls provided until an approximate minimum mutual inductance was obtained between the primary and secondary coils. With the screw adjustments previously described, this coil could be adjusted to within ten minutes of arc of any desired azimuth.

The residual voltage in the secondary circuit contained chiefly a quadrature component arising from the remaining mutual inductance and an in-phase component arising from the gyromagnetic effect, and other causes referred to below. To reduce the voltage still further, the variometer was adjusted until the output voltage was brought to a minimum by reduction of its quadrature component.

When this minimum was reached, it was found that the remaining voltage was an in-phase voltage and could not be removed by readjusting the variometer. It contained both the gyromagnetic effect and an in-phase disturbing effect.

This in-phase disturbance was attributed mostly to electric asymmetry in the amplifier and to the eddy currents flowing in the conducting walls of the container surrounding and close to the primary and secondary coils. The coils of the variometer, on the other hand, were placed in a large iron box, in such a manner that the coils were comparatively remote from the walls and their field affected but little by them. In seeking to remove the residual in-phase voltage, it was found that altering the capacity of one of the terminal condensers in the primary circuit could be made to change symmetry conditions in such a way as to produce (if desired) a large voltage, consisting of both a quadrature component and a small in-phase component (less than one-twentieth as large). The quadrature component could be eliminated by readjusting the variometer, leaving a small in-phase component added to or subtracted from the residual voltage.

By a series of adjustments, first by turning the condenser one way or the other, and then by removing the quadrature voltage by adjusting the variometer, the magnitude of the in-phase voltage by adjusting the variometer, the magnitude of the in-phase voltage in the output of the amplifier could be set to any desired small value E_1, and the quadrature component could be eliminated.

VI. THE MEASUREMENT OF THE GYROMAGNETIC EMF

The method finally adopted enabled the measurements to be made in spite of a troublesome quadrature disturbance due to the action on the magnetic material of the intense magnetic field in which it was placed. The method will be described first as if the disturbance were not present. Then the modifications necessitated by it will be discussed.

The sample and the secondary coil were placed in the apparatus, as described above. The current in the large coil M was set to some predetermined value, producing a steady magnetic intensity H_s and an intensity of magnetization J_s along the axis of the rod. The variometer and condenser were adjusted, as described above, until the output meter indicated a small in-phase voltage E_1. The current in the coil M was then reversed, changing H_s to $-H_s$, and also changing J_s to $-J_s$. With this change in J_s, the gyromagnetic voltage changed from ψ to $-\psi$. The output meter, which was originally reading E_1, would then change its reading to E_2, where $E_2-E_1=2\psi$ if the above-mentioned dis-

TABLE I.

	Permalloy	Iron
Direct current	2.27	2.21
23 kc/sec	2.17	2.12
32 kc/sec	1.98	1.93

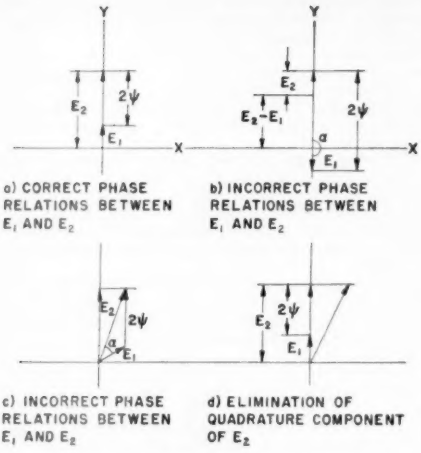

FIG. 6. Correct and incorrect phase relations.

turbances were absent. Certain precautions were necessary to eliminate possible errors due to disturbances. They can be explained with the help of the diagrams in Fig. 6. In these diagrams in-phase voltages are plotted along the Y axis, and quadrature voltages along the X axis.

Figure 6a shows the relations desired between E_1 and E_2, with the phase angle between E_1 and E_2 equal to zero. With this phase relation $E_2-E_1=2\psi$.

Figure 6b displays an incorrect phase relation between E_1 and E_2, where the phase angle between them is an arbitrary value α. Here $E_1-E_2\neq 2\psi$.

In order to insure that the phase angle between E_1 and E_2 was zero, it was necessary to check continually this phase relation with the oscilloscope. The residual voltage E_1 was not reduced to zero, but was made large enough to permit its phase to be determined on the oscilloscope. To eliminate any possible quadrature component of E_1, the variometer was adjusted until a minimum voltage appeared on the output meter. It was found that this minimum occurred when all of the quadrature component was eliminated, only an in-phase component of E_1 being left.

In general, the quadrature disturbance modified the procedure. If E_1 was in phase with the gyromagnetic effect, the voltage E_2 appearing upon reversing the magnetic field H_s would, in general, not be exactly in phase but would have a quadrature component (Fig. 6d).

The appearance of this quadrature component can be understood by considering the effect of H_s and of its reversal upon the apparatus.

We made a very elaborate study of this quadrature effect and concluded that it was due at least chiefly to the change of mutual inductance caused by motions of the rod as a whole and the relative motions of its various parts produced by the entire magnetic field of the coil. Neither rod nor field was entirely homogeneous, symmetry was not perfect, and neither the rod nor its mountings possessed perfect rigidity. Minute motions of the rod could be observed with a microscope when the magnetic field was produced, and the emfs resulting were similar to those produced by giving to the rod mechanically displacements of the same order. These motions due to the magnetic forces occurred in spite of great care to make the construction as rigid as possible. The application of the magnetic field produced similar electromotive forces—even when the whole tube containing the coils was filled with solid paraffin, which may indicate that internal distortion of the rod was largely responsible.[9]

Fortunately, while the gyromagnetic emf reverses with H_s (or J_s), the distortion or motion of the materials due to the action of the intense magnetic field, like all the other disturbances, is identical for both directions of the field, and thus can be eliminated. It is not to be expected, however, that after the reversal of the field the material will return precisely to its previous configuration, and thus the quadrature effect produced by the reversal must be removed before reading E_s. The actual procedure for obtaining 2ψ was as follows: The current in the coil M was set to some predetermined value, and the emf E_1 was measured as indicated above. Next, the reversing switch in the circuit of the coil M was thrown, and the meter reading E_s was obtained, but not until the variometer had been adjusted to remove any quadrature emf imparted by the abrupt reversal of H_s. Then the reversing switch was thrown back to its original position, and another reading for E_1 was obtained. This process was repeated for four or more throws of the reversing switch, accompanied by four or more readings of E_1 and E_2, within a minute's time. The switch was thrown at approximately equally spaced times so as to minimize the effects of systematic drifts. It is exceedingly important to remark that the value of 2ψ obtained from this process is independent of the magnitude of E_1 and also of the magnitude of the quadrature emf which had to be eliminated before reading E_2.

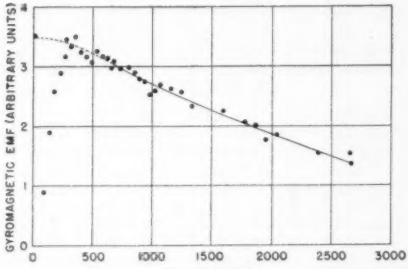

FIG. 7. Gyromagnetic emf for Permalloy at 30 kc/sec.

[9] The very great effect on the mutual inductance produced by even a minute change in the orientation of the rod with regard to the direction of H_s can be seen as follows:

Suppose the axis of the rod, in the plane of the paper, to have the direction of the magnetic intensity H_s; suppose the long axis of the primary coil, in the direction CD, and the planes of its turns to make the small angle θ_1 with AB; and suppose the axis EF of the secondary coil and the planes of its turns to make the small angle θ_2, in any plane with AB. Then the primary coil, traversed by an electric current, will produce in the rod an (extra) longitudinal moment

$$M_1=A\theta_1.$$

where A is a constant.

The moment M_1 will send through the secondary coil a flux

$$\phi_2=BM_1\theta_2,$$

where B is a constant.

Therefore, on account of the asymmetry, that is, on account of the existence of the angles θ_1 and θ_2, the primary will send through the secondary a flux

$$\phi_2=AB\theta_1\theta_2.$$

The flux ϕ_2 vanishes when either θ_1 or $\theta_2=0$, but when neither vanishes it may have a consideralbe value on account of the small longitudinal demagnetizing factor of the rod, and the consequent large value of A.

Thus, even very small angular displacements of the rod relative to the coils may produce large changes in the mutual inductance of the two.

For the single value of the primary current, an average value for E_1 and an average value for E_2 were calculated. The differences between these averages was equal to 2ψ.

For each set of four or more readings, the value of the primary current I_p was recorded so that H_z could be computed as described in Sec. IV. Also, the value of the current in the coil M was recorded, so that the proper value of $(\mu_z+1)/(\mu_z-1)$ could be selected.

Many repeated readings of 2ψ were taken for many values of H_z between zero and 2700 gausses. Figures 7 and 8 display graphs of $2\psi/H_{0z}$ plotted against H_z for Permalloy and iron, respectively. Also, in these figures are shown the curves expected for $2\psi/H_{0z}$ in a heavy black line, as predicted by Eq. (27). To calculate this curve, the value $\rho=0.96$ for Permalloy and $\rho=0.98$ for iron were used in Eq. (27), with other quantities appearing on the right-hand side of the equation determined as described earlier.

VII. THE GYROMAGNETIC RATIO AND ITS EXPERIMENTAL ERROR

The experimental values of ρ for Permalloy and iron were obtained by substituting in the right side of Eq. (24) the experimental values of the various quantities involved. Multiplication by the standard value of e/m gave $\rho e/m$, which is the gyromagnetic ratio in terms of that of a Lorentz electron spinning on a diameter. In the case of Permalloy the voltage rises to a maximum before approximate saturation at $H_z=ca$ 800 gausses is reached (see Figs. 4 and 7)—while values computed from the data obtained between 400 and 800 gausses are in close agreement with the results obtained in stronger fields. Only these latter data were included in the calculations of the final value of ρ since the equations are not strictly valid except for essential saturation.

The experimental error was computed in the usual way from the square root of the sum of the squares of errors arising from various sources, and was found to be $\delta\rho/\rho=\pm 0.08$.

As a result of the work on Permalloy we find for its gyromagnetic ratio

$$\rho=(0.96\pm 0.08)m/e.$$

It was not possible to saturate the iron sample with the magnetic fields obtainable, so that the formula could not be applied with certainty. However, it was possible to obtain a rough determination of the gyromagnetic ratio for iron in the region available. (See Fig. 8.) As H_z increased, the emf started from zero, reached a maximum, and then decreased in magnitude in much the same way as did the emf for Permalloy.

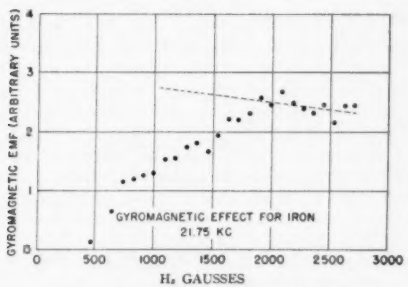

FIG. 8. Gyromagnetic emf for iron at 21.75 kc/sec.

TABLE II.

	ρ (Permalloy)	ρ (Iron)
Present study	$(0.96\ \pm 0.08\ )m/e$	$(0.98\ \pm 0.11\ )m/e$
Barnett effect	$(1.048\pm 0.006)m/e$	$(1.038\pm 0.010)m/e$
Einstein-de Haas effect	$(1.046\pm 0.003)m/e$	$(1.032\pm 0.004)m/e$

Since saturation J_s could not be obtained, it was not possible to apply, with certainty, Eq. (27) to iron. By assuming that the gyromagnetic ratio could be calculated from the values of E obtained after the maximum value of E had been reached (as was observed for Permalloy), and by assuming also that the correct saturation value of J_s could be obtained by extrapolating the data obtainable, the value

$$\rho=(0.98\pm 0.11)m/e$$

was obtained for iron.

The error was computed in the same way as for Permalloy.

In view of the large experimental error, there is no significant disagreement between these results, obtained with very intense steady fields, and the results obtained from the Barnett effect, with rotational frequencies equivalent to exceedingly minute magnetic intensities, and from the Einstein-de Haas effect, with both weak and moderately strong fields.

Table II lists the results obtained from the three effects.

On account of the magnitude of the experimental errors, no differences between the values of ρ which were observed at the two frequencies can be considered significant. The value of ρ presented is a weighted value obtained from measurements at both frequencies. Also, in view of the large experimental errors, no significance can be attached to the differences between the numerical results presented here and those given in a preliminary report[10] published before the completion of new, more extensive, and more reliable calibrations on which the above calculations are based.

The work described here has been carried out in the Norman Bridge Laboratory of the California Institute of Technology under the auspices of the University of California and the Institute, and with important help from the Carnegie Institution of Washington, the National Research Council, and the ONR.

[10] S. J. Barnett and L. A. Giamboni, Phys. Rev. **76**, 1542 (1949).

Discontinuities in the Binding Energies of Neutrons and Protons in Light Nuclei

MARTIN G. REDLICH
Palmer Physical Laboratory, Princeton University, Princeton, New Jersey
(Received May 16, 1952)

Apart from even-odd variations, there is a peak in the binding energies of neutrons at $N=7$, and of protons at $Z=7$. Smaller peaks may exist at N or $Z=11$ and 14.

THE most pronounced fluctuations in several nuclear properties appear around certain neutron and proton numbers which have been called magic. According to the shell model of the nucleus, they are the counterparts of electron numbers of atoms with closed shells. The ionization potential of an atom or an ion fluctuates markedly and regularly with atomic number: It increases gradually up to a closed shell, and then drops abruptly. Apart from even-odd variations, the same behavior would be expected at the magic numbers.

Limited data indicate that there exist substantial declines in the binding energies of protons after $Z=82$ and in the binding energies of neutrons after $N=126$. The stage is set for an examination of these properties for light nuclei: Tables of some masses obtained from nuclear reactions[1] and mass spectroscopy[2] have been published and are in excellent agreement. A table of masses of atoms from S^{31} to Zn^{66} is available,[3] as well as an earlier one which covers most isotopes of elements to zinc.[4] Experimental uncertainties range approximately from 0.03 mmu for stable nuclei up to F^{20} to 0.3 mmu

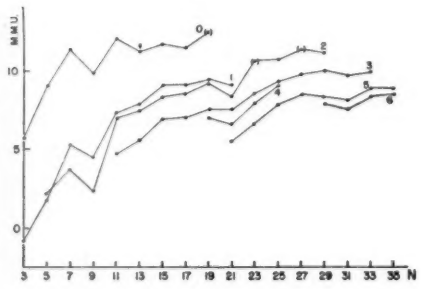

FIG. 1. Binding energy of a neutron *vs* N for N odd. The numbers on the curves indicate $N-Z$.

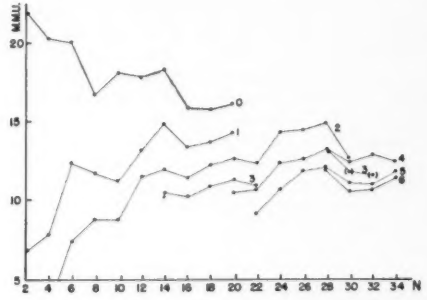

FIG. 2. Binding energy of a neutron *vs* N for N even. The numbers on the curves indicate $N-Z$.

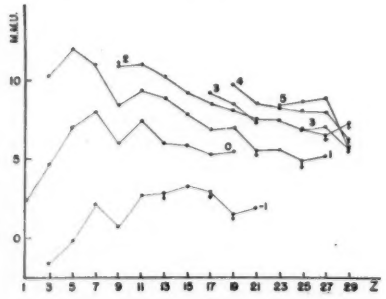

FIG. 3. Binding energy of a proton *vs* Z for Z odd. The numbers on the curves indicate $N-Z$.

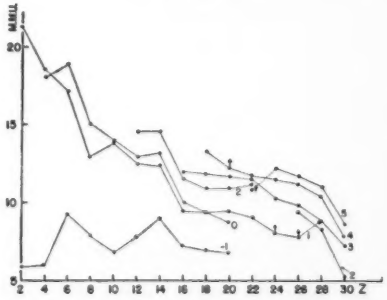

FIG 4. Binding energy of a proton *vs* Z for Z even. The numbers on the curves indicate $N-Z$.

[1] Li, Fowler, and Lauritsen, Phys. Rev. **83**, 512 (1951).
[2] H. Ewald, Z. Naturforsch. **6a**, 293 (1951).
[3] Collins, Nier, and Johnson, Phys. Rev. **86**, 408 (1952).
[4] Obtainable from Dr. A. H. Wapstra.

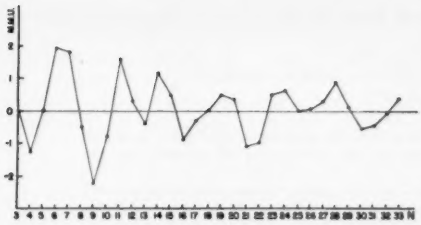

FIG. 5. $\langle\Delta(N)\rangle_{Av}$ vs N.

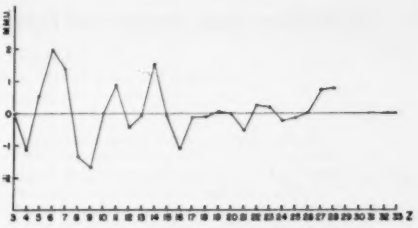

FIG. 6. $\langle\Delta(Z)\rangle_{Av}$ vs Z.

for a few of the heavier ones. Some masses calculated from beta-decay energies are uncertain because the final state may be excited.

Binding energies of neutrons are plotted against N in Figs. 1 and 2; binding energies of protons against Z in Figs 3 and 4. To circumvent the even-odd variation, one set of curves joining points of equal $N-Z$ is drawn for odd N or Z (Figs. 1 and 3), and another for even N or Z (Figs. 2 and 4). If a binding energy has been obtained from two masses, one of which is based upon a questionable beta-decay, an arrow at the binding energy point indicates the direction of possible correction; if both masses are in doubt, the point is enclosed by parentheses.

The most prominent peak appears at N or $Z=7$. This means, for $N=Z$ for instance, that a neutron (or proton) in N^{14} is more tightly bound than in either B^{10} or F^{18}. There are smaller peaks at 11 and 14. Conspicuous declines occur from N or $Z=28$ to 30, but only for Z from 27 to 29. There are increases before $N=23$ and 24.

These fluctuations are pictured in more detail in Figs. 5 and 6. $\Delta(N)$ is the difference between the binding energy of a neutron, $B(N)$, in a nucleus with even (or odd) N and the average of that of its two neighbors with the same $N-Z$ and even (or odd) N. In symbols,

$$\Delta(N)=B(N)-\tfrac{1}{2}[B(N+2)+B(N-2)].$$

The average of $\Delta(N)$ for all available $N-Z$ curves is denoted $\langle\Delta(N)\rangle_{Av}$ and plotted against N; $\langle\Delta(Z)\rangle_{Av}$ is defined analogously and plotted against Z. Since points have been obtained from the two curves of binding energies for each $N-Z$, both even and odd N or Z appear on the abscissas of Figs. 5 or 6. An idealized curve of binding energies of protons adjusted for zero even-odd variation and the corresponding curve for $\Delta(Z)$ are given in Fig. 7 in order to indicate the expected behavior of $\Delta(Z)$ near a magic number $Z=a$. The curves of $\Delta(Z)$ for binding energies of electrons in an atom defined as for protons in a nucleus vary in essentially the same way around Z for a closed shell, such as 10.

The shape of the curve of $\langle\Delta(Z)\rangle_{Av}$ from $Z=5$ to 10 (Fig. 6) is very similar to that of $\Delta(Z)$ obtained from the idealized binding energies. It indicates that $Z=7$ is a magic number. The integrated curve for $\langle\Delta(N)\rangle_{Av}$ in this region would indicate a rise up to $N=7$ with a sharp drop from 7 to 8 and a smaller drop from 8 to 9.

The behavior for N and for Z from 10 to 17 is that to be expected for magic numbers at 11 and 14. Peaks at 6 and 14 were previously noticed[8] on curves of binding energies of neutrons to nuclei with even N. The peaks at 7 and 11 were not reported, however, since no curves for odd N were drawn.

Beyond 17 the curves for $\langle\Delta(N)\rangle_{Av}$ and $\langle\Delta(Z)\rangle_{Av}$ have only a small rise up to 28 in common. A decline

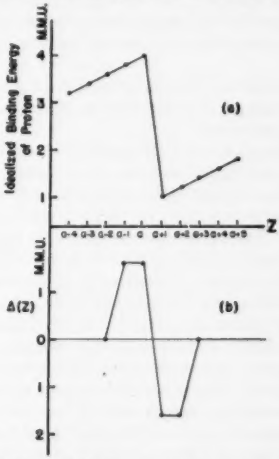

FIG. 7. (a) Idealized binding energy of a proton, adjusted for zero even-odd variation vs Z. (b) The corresponding curve for $\Delta(Z)$ vs Z.

from 20 to 21 and a rise from 22 to 23 appear primarily on the neutron curve.

The fractional decreases in binding energy after nuclear magic numbers are much smaller than those following closed atomic shells. The variations at 7, 11, 14, and probably 28 are, however, of the same magnitude as those at 82 and 126.

It is with pleasure that I thank Professor E. P. Wigner for suggesting this investigation and for his continued advice and interest.

[8] J. Sanada and Y. Yoshizawa, Phys. Rev. **83**, 663 (1951).

Production Cross Section and Frequency of Neutral Mesons in Cosmic Rays*

G. Salvini† and Y. B. Kim
Palmer Physical Laboratory, Princeton University, Princeton, New Jersey
(Received June 9, 1952)

Nuclear interactions have been observed in a large cloud chamber operated at Echo Lake, Colorado, altitude 10,500 ft. The events were produced by ionizing particles (protons) in NaI crystals inside the cloud chamber, and were detected by photomultipliers.

In this paper the electromagnetic component associated with the nuclear events is studied as evidence for the properties of the neutral meson whose decay is assumed to be the source of this component. The results are consistent with the assumption that the π^0 mesons are the main source of the photons associated with the nuclear events. The probability of production of π^0 mesons is in agreement with the theoretical results of Fermi, within the limits of the large experimental errors. The ratio of the number of neutral π^0 mesons to the number of the charged $\pi^{\pm}$ mesons is estimated in events of different multiplicities of shower particles and it is found to be close to 0.5 for events with multiplicity varying from 1 to 5 or more (corresponding to energies of from 1 to about 20 Bev for the producing protons).

These results agree with the results of other experimenters, if all the possible systematic errors are taken into account. The estimated energy distribution of the π^0 mesons emitted is given.

INTRODUCTION

THIS paper reports the results of our experimental research performed during the summer of 1951, with a cloud chamber controlled by scintillation crystals inside. We studied the production of the neutral mesons in the nuclear events produced by the cosmic-ray protons.

In the following we will summarize the present state of knowledge of neutral mesons, before giving and discussing our results.

The first indication of the existence of neutral mesons in cosmic rays came from the cloud-chamber work of Fretter, Chao, Bridge, Rossi, and Hazen.[1] From their results it appeared that the frequency of the electromagnetic[2] component associated with high energy nuclear events seemed too high to be accounted for by some kind of purely e.m. mechanism. Successive support for the neutral meson hypothesis came from the work of Fretter,[3] Tinlot and Gregory,[4] and Lovati *et al.*[5] The results of Tinlot and Gregory, for example, indicated that, in certain favorable cases, the e.m. component associated with nuclear events is in agreement with the neutral meson hypothesis, and the number of neutral mesons deduced from the frequency of the e.m. components is equal to about one-third of the penetrating particles in the penetrating showers.

Significant work on neutral mesons has been done by the Bristol group[6] by means of nuclear plates. They succeeded in determining (a) an indirect estimate of the mass of the neutral meson, (b) a ratio of the numbers of charged and neutral mesons, (c) an upper limit for the decay time of the neutral mesons, and (d) an indication of the energy distribution of the neutral mesons in the air, at high altitude. One may consider results (b) and (c) to be more direct and reliable than those of (a) and (d).

Strictly speaking, one cannot take these results as direct evidence for neutral mesons in cosmic radiation. The situation is the same for cloud-chamber observations: namely, one can only say that there are cases in which the general aspect of the e.m. component emitted really indicates a two-photon decay of a neutral particle of between 200–400 electron masses. However, since nearly conclusive evidence of the proposed neutral meson properties has been furnished by experiments involving machine made mesons,[7] one may take these cosmic-ray results as fairly reliable.

The nuclear plate technique has a low efficiency in detecting neutral mesons. In fact, with a decay into two photons: $\pi^0 \rightarrow 2\gamma$, most of the photons will go out of the region of detection before materializing. Even when photons are found to materialize within this region the inferences concerning the parent neutral mesons are rather difficult to make. In this respect, a multi-plate cloud chamber has an advantage over the nuclear plates since, here, one can in most cases follow the decay photons through their electromagnetic development and, moreover, can correlate them to a particular event in both time and space. But one must pay careful attention to the bias introduced in triggering the cloud chamber with a particular detection arrangement. Most of the previous cloud-chamber work employed G-M counter controlled triggering in one form or another and unavoidably introduced unknown biases in detection.

In using multiplate cloud chambers, one must look for all the events that could have contained charged or

* Assisted by the joint program of the AEC and ONR.
† Now at Cagliari University, Cagliari, Italy.
[1] W. B. Fretter, Phys. Rev. **73**, 41 (1948); Bridge, Hazen, and Rossi, Phys. Rev. **73**, 179 (1948); C. Y. Chao, Phys. Rev. **75**, 581 (1948).
[2] Hereafter referred to as e.m.
[3] W. B. Fretter, Phys. Rev. **76**, 511 (1949).
[4] B. P. Gregory and J. H. Tinlot, Phys. Rev. **81**, 667 (1951). (References to previous work may be found in this article.)
[5] Lovati, Mura, Salvini, and Tagliaferri, Nuovo cimento **7**, 943 (1950). Lovati, Mura, and Tagliaferri, Nuovo cimento **9**, 205 (1952).
[6] Carlson, Hooper, and King, Phil. Mag. **41**, 701 (1950).
[7] Steinberger, Panofsky, and Steller, Phys. Rev. **78**, 802 (1950).

neutral mesons, irrespective of the number of penetrating secondary particles emitted. Therefore, if one triggers the cloud chamber by means of conventional G-M counters on the basis of the number of penetrating secondaries, the results obtained will be quite far from the real distribution, especially at the lower energies.

In order to get around this difficulty, an apparatus has been built to permit a relatively unbiased selection of the events to be studied. Such unbiased selection compares favorably with that obtained by nuclear plates, and allows us to correlate in a more definite manner the results of the cloud chamber with those obtained by nuclear plates.

I. EXPERIMENTAL DISPOSITION

The technique utilizes a proportional scintillation counter placed inside a cloud chamber. The cloud chamber is triggered by means of the signal from photomultipliers viewing the crystal, when that signal indicates that at least one heavily ionizing particle has resulted from an interaction in the crystal. In this way, selection is made on the basis of the energy of the heavily ionizing particles resulting from the interaction (the "evaporation" particles), regardless of the detailed behavior of the secondary particles of higher energies, so that the bias is no more severe in regard to protons of fairly high energy (100 Mev up), and to mesons, than the bias usually introduced in the nuclear plate technique.

The cloud chamber used in these experiments was a rear illuminated type, with an illuminated region 46×46×20 cm³. The general construction is not much different from other cloud chambers of this type.[8] NaI crystals, each 7×10×0.6 cm³, were used for the scintillation counter. They were enveloped with aluminum foil and glass and mounted in an aluminum plate. We placed this crystal plate under a glass window located in the cloud-chamber ceiling (Figs. 1 and 7). The light emitted by the crystal was collected by six 1P21 photomultiplier tubes. The high voltage supplied to the photomultiplier tubes was adjusted in order to discriminate against events giving up less than a certain amount of energy in the crystal. Most of the time the bias corresponded to about 12 Mev ionization energy loss in the crystal. This amount of energy loss is much lower than the average energy loss of a nuclear star caused by a proton in the crystal. Since the energy dissipation by a nuclear star in the crystal will be mainly that of the evaporation particles and gray particles, the triggering will be independent of the number or nature of the fast secondary particles emitted. Also the bias is enough to discriminate against the abundant fast cosmic-ray particles traversing the crystals such as μ-mesons, since at least three or four fast particles must traverse the crystal simultaneously in order that the energy dissipation exceeds that set by the bias.

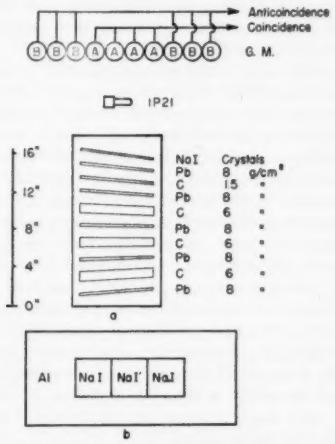

FIG. 1. (a) Crystals and plates assembly in the cloud chamber. (b) Top view of the Al plate containing the NaI crystals.

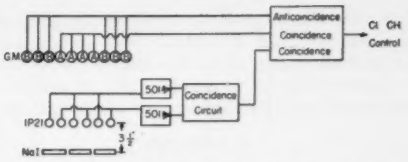

FIG. 2. Block diagram of the circuits and counters used for triggering the cloud chamber.

In order to reduce the background noise, the photomultipliers were arranged in two groups of three each in a twofold coincidence. The block diagram of the circuitry used for the scintillation crystals is given in Fig. 2, which also shows the Geiger counters involved.

The triggering occurred when there was a pulse in the crystal above the bias level in coincidence with one or more counters in A and in anticoincidence with B. We adopted this scheme in order to avoid the many small stars due to neutrons and the frequent air showers. Thus, we collected the events due mainly to proton interactions.

The experiment was carried out during the summer of 1951 at Echo Lake, Colorado (altitude 10,500 feet). The actual running time of the cloud chamber was about 1200 hours.

Part of the time we took oscilloscope pictures of crystal pulses in order to correlate the pulse heights with the different kinds of nuclear events. A short description of this pulse-height distribution for different

[8] R. R. Rau, Princeton Cosmic Ray Group, Tech. Report No. 4 (unpublished); M. B. Gottlieb, Phys. Rev. 82, 349 (1951).

kinds of events is given in the Appendix. The cloud chamber contained Pb plates and carbon plates mounted alternately, of the thickness indicated in Fig. 1. Carbon plates are intended to give information on the interactions of the secondary particles in light nuclei.

II. ANALYSIS

1. In the analysis of the photographs obtained with the apparatus described above, we were mainly interested in the observation of the fast protons and of all the π-mesons, charged or neutral, emitted from the crystal. For the following discussion it is important to distinguish clearly between these fast particles and the slow tracks which usually appear in nuclear interactions. This distinction, with somewhat different limits in energy will be similar to the distinction between "shower particles" and black and gray particles which was made by Camerini *et al.*[9] In the following, we will designate as penetrating particles (abbreviated p.p.) those charged particles emitted directly from the nuclear interactions, with an ionization loss close to the minimum. The estimate of the ionization alone is a poor index of the energy of the particle. In order to get a better definition of the p.p. we considered each track whose ionization was between one and two times the minimum on the assumption it was either a proton or a meson. This examination was made by estimating the Coulomb scattering from plate to plate and the eventual change in ionization of the track in going through the plates. With these assumptions concerning the nature of the particle, we could in turn estimate the ionization of the particle again, and assign an upper limit to it.

With the limits of our cloud chamber in the estimate of the ionization and of the Coulomb scattering, we could go so far as to consider as a p.p. a particle whose "estimated ionization" was less than 1.7 the minimum (>290 Mev for protons, and >45 Mev for the mesons). Thus we define for the purpose of this paper a p.p. as a particle ionizing ≤ 1.7 minimum. The possible error involved in this estimate is quite important in the estimate of the ratio of neutral to charged mesons and will be considered in detail in Sec. IV.

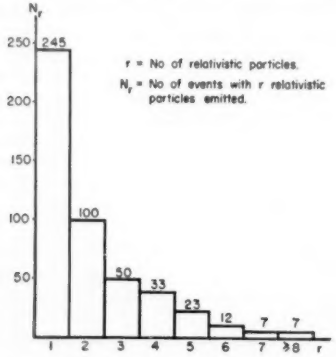

FIG. 3. Distribution of the nuclear events according to the total number of the relativistic particles (π^0 mesons+penetrating particles). Due to the character of our measurements this distribution can be considered the real one at 10,500 feet above sea level.

[9] Camerini, Davis, Fowler, Franzinetti, Muirhead, Lock, Perkins, and Yekutieli, Phil. Mag. **42**, 1241 (1951).

The particles going out of the illuminated region after traversing only one or two plates below the crystals (Plates 2 and 3) were the most difficult to classify according to our method. But, due to the favorable location of the crystals (Fig. 1) these were only a small percentage of the total number of shower particles. We did not include in the statistics the events whose primary proton was inclined more than 50° with respect to the vertical.

Also an intense development of an electromagnetic component may be counted as an obstacle in judging the penetrating particles, since under this condition the picture will be more or less obscured. This effect, however, was not significant for our energy range.

The presence of electromagnetic components emitted from the nuclear events in the crystal was identified from the electromagnetic cascade generally starting from the first plate of lead (Plate 2). We classified an event as containing an electromagnetic component when at least one pair of electrons or at least one relativistic electron was observed, as judged by the strong scattering in going through the plates. Care was taken to rule out accidental electron tracks by comparing the different regions of the cloud chamber.

Gray tracks and heavy tracks were estimated from the density of ionization. They are, however, not too important for the present discussion. In each nuclear event in the crystal, we also looked for electrons emitted directly as well as other kinds of particles.

2. Classification of Events. All events in the crystal were considered in which we could identify at least one penetrating particle or at least one electromagnetic component. These events were classified according to the number of p.p.'s emitted (see Table I, row a). In each group we also listed the number of events which contained electromagnetic components (row b) and the total number of neutral mesons estimated (row c). For instance, we observed 239 of N_1 events (namely events containing one p.p.), and 35 events out of these 239 contained electromagnetic components. Our estimate of the corresponding total number of neutral mesons was 45 and the number corrected for missed cascades is 50. (The correction procedure is described below.)

In estimating the number of π^0 mesons from the number of observed electromagnetic components, we assumed the decay scheme for π^0 to be: $\pi^0 \rightarrow 2\gamma$. The energy and angle relation in this process has been discussed by many authors.[3,5]

In about 40 percent of the cases, we actually could see two e.m. cores originating from the nuclear events

in the crystal, and in a few cases we were able to verify the relation:

$$(2\sin\tfrac{1}{2}\psi)^2=(\mu c^2)^2/E_1E_2, \qquad (1)$$

holding between the two cores. In Eq. (1), ψ is the angle subtended by the two decay photons and E_1, E_2 are their energies, and μc^2 is the π^0 rest energy. When three e.m. cores were clearly correlated to the nuclear event concerned, we assumed that there were two π^0 decays. In no case, was there evidence for the existence of more than four e.m. cores in a single nuclear event. This could be due to the difficulty in resolving the more complicated events. However, due to the low frequency of the complicated events this limitation will not alter our statistical results. This method of estimating the number of π^0 mesons is subject to two types of errors. One is the geometry factor; π^0 mesons emitted with angle wider than $60°\sim70°$ from the vertical will escape detection. In Table I, we did not make any correction arising from this geometry factor, since we will also miss shower particles with about equal probability. However, we have to estimate a systematic error arising from the fluctuation of the electromagnetic cascade developments. The cascade process is essentially a statistical affair, therefore we may sometimes miss π^0 mesons because the decay photons did not convert to electrons at all. According to the recent work of Wilson[10] the average number of electrons to be observed from a photon initiated shower is smaller than the number one would expect from conventional shower theories, and this effect becomes important for low energy showers. Thus our error may become quite appreciable for low energy π^0 mesons. Using Wilson's data, we have estimated the probability P of missing a π^0 meson, emitted in an interaction in the crystal of our cloud chamber. For a π^0 meson of a given energy, we estimated this probability by considering various energy divisions among the two decay photons. We found that the probability P is relatively high ($P=0.4$) for a low energy π^0 and approaches zero for a π^0 of total energy above 400 Mev. Assuming that the π^0 energy distribution is similar to that of the charged mesons, we estimated the average missing probability P to be ~0.12 and have applied this correction to the number of observed neutral mesons. To understand the relatively low value of P, one must remember that we considered as evidence for the presence of one π^0 meson the appearance of one electron or one e.m. pair below the first Pb plate.

Another source of small error in the opposite direction may be the knock-on electrons from the p.p. traversing the Pb plates. An estimate of the knock-on error combined with P resulted in a final correction of 0.10 to the results of Table I, row *c*, leading to the final corrected values for the π^0 meson, given in row *d* of Table I.

[10] Robert R. Wilson, Phys. Rev. **86**, 261 (1952). We are very grateful to Professor Wilson for sending his results to us before publication.

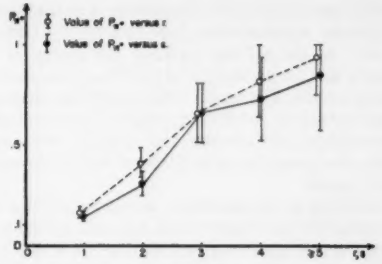

FIG. 4. Probability of emission of at least one neutral meson in nuclear events of different multiplicities. On the abscissa the numbers of the penetrating particles, indicated by s, and the numbers of relativistic particles, indicated by r, are reported.

In estimating the number of neutral mesons from the observed number of electromagnetic showers, we explicitly assumed that all the electromagnetic component comes from π^0 decays. If any appreciable amount of electromagnetic component arises from some other source besides π^0 decays, then the estimate of the number of π^0 mesons will be too high.

The number listed under the column $s=0$ is subject to a greater error since this kind of event is generally hard to identify. Therefore its normalization with the other numbers is doubtful.

From Table I, and again because of the unbiased condition of our triggering system, we can derive the frequency distribution of the number of nuclear events *versus* the number of the relativistic particles. Here, and in later discussions, relativistic particles include the neutral mesons and the p.p. The observed distribution is given in Fig. 3.

III. CROSS SECTION FOR PRODUCTION OF THE NEUTRAL MESONS

In comparing rows *a* and *b* in Table I, we notice the fact that the probability of emission of electromagnetic component becomes higher as the multiplicity increases. This indicates that the production of the neutral mesons becomes more probable for large size stars. To express this effect quantitatively we form the π^0 production probability $P_{\pi^0}(s)$ by dividing the number in row *b* by that of row a, i.e.,

$$P_{\pi^0}(s)=b/a,$$

for different multiplicities, s.

This will give us the probability of producing at least one π^0 meson in a nuclear event containing s p.p.'s. In Fig. 4 is shown a plot of P_{π^0} *vs* s. In the same Fig. 4 (broken line), we also plot $P_{\pi^0}(r)$, which is the probability of finding at least one π^0 meson in an event with r relativistic particles. The quantity $P_{\pi^0}(r)$ is not biased in favor of the charged particles as the quantity $P_{\pi^0}(s)$ is.

In order to obtain some information on the cross section $\sigma_{p\pi}$ for the production of $\geq1\pi^0$ meson, we now

consider our results on the production of neutral mesons by protons, together with those obtained by Camerini *et al.*,[9] on the relation between the energy of the primary and the multiplicity of p.p.'s for proton-induced nuclear events. The results obtained will be affected by large statistical errors and will be only indicative. Nevertheless, we consider the attempt worthwhile, due to the present complete lack of direct information on this point.

According to the results of Camerini *et al.*,[9] for each multiplicity s, one can attribute a certain spread of the energy of the producing proton. Since it is not likely that our nuclear events differ statistically from those produced in the nuclear plates, we will use the energy-multiplicity relation derived in the emulsion work.

Thus, for each s, we estimate the region of energy inside which most of the events ($\sim$70 percent) with s p.p.'s fall. This region is the horizontal dimension of each rectangle indicated in Fig. 5; the corresponding multiplicity s is indicated by the number inside each rectangle. In the limits of our estimate we can assume that $P_{\pi^0}(s)$ is equal to the ratio between $\sigma_{\rm pr}(E)$, cross section for π^0 production, and the total cross section for nuclear interaction of the impinging protons, which we can assume to be close to the geometrical, $\sigma_{\rm geo}$:

$$\sigma_{\rm pr}(E)=P_{\pi^0}(s)\sigma_{\rm geo},$$

where E is an energy inside the limits of the width of the rectangle s. Each rectangle s is located in Fig. 5 at an ordinate equal to $\sigma_{\rm pr}(E)$, and the height of the rectangle is equal to the statistical error of this quantity. So, the rectangles of Fig. 5 show the behavior of $\sigma_{\rm pr}$ *versus* the energy in the sense that the real cross section $\sigma_{\rm pr}$ for emission of at least one π^0 meson is a line which should be contained in the region of the diagram delimited from these rectangles.

The experimental point given at 345 Mev was obtained by Moyer.[11] The geometrical cross section in the crystal is the average of the geometrical cross sections in Na and I:

$$\sigma_{\rm geo}=\tfrac{1}{2}\pi r_0^2(A_{\rm Na}^{\frac{1}{3}}+A_{\rm I}^{\frac{1}{3}})\cong 10^{-24}\ {\rm cm}^2.$$

In Fig. 5 we show also the energy dependence of the cross section for production of at least one charged meson, which we will indicate as $\sigma_{\rm pr}'$, obtained from the same results of Camerini *et al.* We can see from comparing the position of the dots with that of the rectangles that $\sigma_{\rm pr}$ is lower than $\sigma_{\rm pr}'$. The cross section for production of $\geq 1\pi^0$ meson by protons of 1–2 Bev is about 0.1–0.2 the geometrical value of the cross section.

In Fig. 5 we also plot the cross sections *versus* the primary proton energies predicted by the Fermi model.[12] In this calculation, we assumed that any of the three types of mesons will be emitted with equal probability in nuclear interactions. Curve I is the cross section for the production of at least one charged mesons, and Curve II is the cross section for the production of at least one neutral meson.

The estimate of $\sigma_{\rm pr}$ as a function of the energy given in Fig. 5 is only indicative, in view of the large horizontal spread of the energies that we mentioned, and also because of the many data that had to be supplied from experiments with the nuclear plates, which were performed at higher altitude.

TABLE I. Distribution of the nuclear events, N_s.

No. of penetrating particles, s		0	1	2	3	4	5	≥ 6
N_s, no. of nuclear events containing s penetrating particles	a	?	239	103	50	26	11	9
No. of nuclear events N_s having electromagnetic component	b	(45)	35	32	33	19	9	8
No. of estimated π^0 mesons	c	(49)	45	41	43	27	15	14
No. of π^0 mesons corrected	d	54	50	45	47	30	16	15

IV. RATIO OF NEUTRAL TO CHARGED π-MESONS

1. We will indicate by R the ratio of the number of π^0 mesons to the number of charged π-mesons:

$$R=\pi^0/(\pi^+ + \pi^-).$$

A few remarks should be made before results are discussed. The measurement of R is of such a nature that the real error is likely to be bigger than the statistical error. This is because the identification of the neutral and the charged mesons is based on different kinds of evidence. The main difficulty in counting the charged mesons lies in the indistinguishability of the charged mesons from protons at high energy; whereas, in the case of the π^0 mesons, the main difficulty is that of missing low energy π^0's, because of the low energy of the decay photons and the large angular spread. For these reasons, the error attributed to each estimate of R will be increased in order to take into account the possible systematic errors.

The value of R has already been estimated by a few groups of experimenters, using several different methods. Carlson *et al.*,[6] gave a value $R=0.45\pm 0.1$ obtained by counting the pairs in the neighborhood of the nuclear explosions for events with three or more shower particles. (The error quoted is purely the statistical error.)

Gregory and Tinlot[4] found a value 0.3 for the ratio of neutral mesons to penetrating particles. If we assume that the charged π-mesons are about $\frac{3}{4}$ of the shower particles, their result gives $R=0.4$. The numbers above refer to events with at least 3 shower particles, produced by protons or neutrons.

Recently Camerini *et al.*,[9] repeated the estimate of R from another point of view, which is more indirect, but still very interesting, for it at least makes it possible to fix an upper limit to the value of this difficult ratio R. Here an estimate was made of the number of π^0 mesons

[11] Burton J. Moyer (private communication). The result was obtained by bombarding carbon with 345-Mev protons.

[12] E. Fermi, Prog. Theor. Phys. **5**, 570 (1950).

in events whose primaries had energies ≤ 10 Bev, and whose multiplicity s was ≤ 4. On the basis of the balance of energy between the primary proton and the charged secondaries, they concluded that the neutral mesons are about as numerous as the charged mesons. Due to the character of this measurement we would indicate their result in the following way: $R \leq 1 \pm 0.3$.

A preliminary estimate of R based on results using the present technique has already been given by us in a previous note.[13] This value was reported as $R_3 = 0.37 \pm 0.08$ (statistical error only) for nuclear events with three or more shower particles produced by protons. This measurement was affected by some slight systematic error which will be discussed in the following.

2. The data of Table I will now be considered, taking into account the possible sources of systematic errors which occur in the estimate of R. We consider first events with three or more penetrating particles.

These events show 368 shower particles, and for them we estimated 109 (corrected number[14]) neutral mesons, corresponding to 30 percent of the penetrating particles. If we want to estimate R we have to know how many of these penetrating particles are charged π-mesons.

This number can hardly be estimated directly in our cloud chamber, where we can distinguish between $\pi^{\pm}$ mesons and protons on the basis of the Coulomb scattering and the intensity of ionization only up to about 400 Mev in the most favorable cases. Therefore, we estimated the percentage of the $\pi^{\pm}$ mesons on the shower particles using the results of other experiments. As has already been stated (Sec. II), our shower particles are protons of energy higher than 290 Mev, and charged π-mesons of energy higher than 45 Mev. From the map of Camerini *et al.*,[15] giving the distribution in energy of the protons and charged π-mesons of the nuclear interactions, we deduce that 65 percent of our p.p. are charged π-mesons. On the one hand, an estimate of the percentage of charged π-mesons among the penetrating particles has been made by Annis and Bridge in a cloud chamber similar to, but larger than ours.[16] They found that 75 percent of the fast secondary particles of nuclear interactions are $\pi^{\pm}$ mesons. Their results corresponded to energies higher than ours, so we can consider that 75 percent is an upper limit for the percentage of the $\pi^{\pm}$ mesons among our p.p.'s.

On the other hand, a percentage of 50 (half the p.p. are $\pi^{\pm}$ mesons) would certainly be a lower limit. In fact, according to the map given by Camerini this would correspond to assuming that we considered as p.p. all the particles ionizing ≤ 2.2 times the minimum (protons ≥ 200 Mev). On the contrary, we can conclude, on the basis of the comparisons made with electrons and recognized protons and π-mesons, that most of the tracks ionizing two times the minimum were rejected in our selection of the p.p., and therefore 50 percent for the relative number of $\pi^{\pm}$ mesons and p.p. is a lower limit.

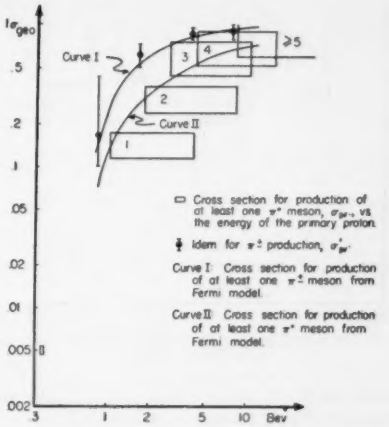

FIG. 5. π^0 production cross section vs primary proton energies. The points indicated by dots are values reported by Camerini *et al.* (see reference 9) in the nuclear plates work. Solid lines are the cross sections for charged (Curve I) and neutral mesons (Curve II) predicted by the Fermi model (see reference 12) of meson production.

On this basis, the values of R for nuclear events with three or more shower particles, which will be designated as R_3^{∞}, is as follows:

$$R_3^{\infty} = 109/(368)(0.5) = 0.59 \pm 0.08 \text{ upper limit of } R_3^{\infty},$$

supposing that 50 percent only of the p.p. are mesons:

$$R_{3P} = 109/(368)(0.65) = 0.45 \pm 0.07 \text{ most probable value according to our measurement}$$

$$R_3^{\infty} = 109/(368)(0.75) = 0.39 \pm 0.06 \text{ lower limit of } R_3^{\infty}.$$

3. We can now try to estimate the value of R for lower multiplicities, therefore lower energies. For this purpose, we consider the events of columns 0 to 4 in Table I (events with four or less shower particles). The ratio r_0^4 of the π^0 mesons to the number of the penetrating particles is:

$$r_0^4 = 226/699 = 0.32 \pm 0.03.$$

Again the most uncertain point is the percentage of the $\pi^{\pm}$ mesons among the pp. An indication of how much the percentage of the $\pi^{\pm}$ mesons among the shower particles changes with the size of the nuclear events comes from Camerini *et al.*[9] From these results we deduce that the $\pi^{\pm}$ mesons are about 60 percent of our p.p.'s in this range of multiplicity (the previous estimate for the events of multiplicity $3-\infty$ was 65

[13] G. Salvini and Y. Kim, Phys. Rev. **85**, 921 (1952).

[14] The number of the π^0 mesons is higher here than in the previous report (see reference 13). The main corrections come from the re-estimates of the probability of missing the neutral meson, based on the results of the Monte Carlo method (see reference 10).

[15] Camerini, Fowler, Lock, and Muirhead, Phil. Mag. **41**, 413 (1950).

[16] M. Annis and H. S. Bridge, Phys. Rev. **86**, 589(A) (1952).

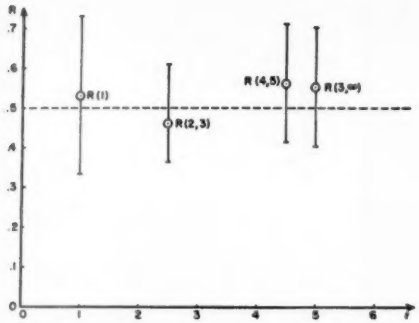

FIG. 6. The ratio of neutral to charged mesons *vs* multiplicities in relativistic particles.

percent). With the same criteria as in the estimate of R_3^∞ we give for R_0^4 the values (see Table I):

$R_0^4 = 226/699 \times 0.5 = 0.65 \pm 0.08$ (upper limit of R_0^4)
$R_0^4 = 226/699 \times 0.6 = 0.54 \pm 0.07$ (most probable value)
$R_0^4 = 226/699 \times 0.75 = 0.43 \pm 0.07$ (lower limit of R_0^4).

In our earlier estimate[13] we found $R_0^4 = 0.4 \pm 0.1$. The earlier result was not corrected for the fluctuations in the cascade of the decay photons, for the final results of the Monte Carlo method[10] were not known to us at that time. The present value seems to be lower (but almost within the errors) than the one estimated by Camerini *et al.*[9] In the comparison of the two values, we have to keep in mind the following facts: The difference in the energy spectrum of the protons at high altitude (Camerini *et al.*) and at mountain altitude (our results) is likely to affect the difference between their value of R_0^4 and ours. Their value $R_0^4 = 1 \pm 0.3$ has to be considered in our opinion as an upper limit, for there is no sure evidence yet that the "missing energy" goes only into production of neutral mesons.[17]

4. A less biased estimate of R can be obtained from the following considerations: The general question implicit in the value of R is the dependence of R on the size of the nuclear events, and therefore on the energy of the primary protons. Should we find that R is fairly constant for different multiplicities and close to $\frac{1}{2}$, this would indicate that the cross section for production of π^0 mesons goes with the energy as the cross section for production of the charged mesons of each sign. To resolve the question, we can now estimate the value of R in a way which differs from the previous estimates, and which can be used because of the very low bias of our disposition. It is easy to see that the selections of the type we used before (0 to 4, or 3 to ∞ p.p.'s) are going to favor the neutral mesons or the charged mesons in an appreciable way. This systematic error already was pointed out by Camerini *et al.*[9] We are free to a large extent from these errors if we obtain the ratio R from events of equal numbers of relativistic particles, without any choice in favor of the charged or neutral mesons. By relativistic particles we mean here the neutral mesons and the p.p. In computing, for instance, the number of the events with two relativistic particles, we will include the events with $2\pi^0$ only, $1\pi^0$ and 1 p.p., 2 p.p.'s only. Moreover, what we want now is the ratio of the π^0's to the total number of $\pi^\pm$ mesons. Therefore, we have to add to the number of $\pi^\pm$ mesons estimated among the p.p.'s the $\pi^\pm$ mesons of energy <45 Mev (see Sec. II). The number of these low energy $\pi^\pm$ mesons can be estimated from our results. It constitutes a small correction: the $\pi^\pm$ mesons below 45 Mev are about 10 percent of the total number of $\pi^\pm$ mesons. We will indicate by $R(m, n)$ the value of R referred to events with m, $m+1$, $\cdots n$ relativistic particles.

Value of $R(2, 3)$

We indicate by $R(2, 3)$ the ratio R obtained for the events with two or three relativistic particles, including the $\pi^\pm$ mesons with energy <45 Mev. From our events, reported in Table I and Fig. 3, we obtain

$$R(2, 3) = 83/180 = 0.46^{+0.15}_{-0.1}.$$

We assume in this computation that the $\pi^\pm$ mesons are 60 percent of the p.p.'s. The large errors attempt to include the possible systematic errors which have already been outlined in the preceding paragraph.

TABLE II. Ratio R of the number of the $\pi^\pm$ mesons, among nuclear events of different multiplicity. R_3^∞ = value of R for events with three or more penetrating particles. $R(2, 3)$ = value of R for events with two or three "relativistic particles." The other symbols are obvious.

	Authors	Value
R_3^∞	Gregory and Tinlot[a]	0.4 ± 0.1[d,e]
R_3^∞	Carlson *et al.*[b]	0.45 ± 0.1[f,e]
R_3^∞	Salvini and Kim present experiment	$0.45^{+0.15}_{-0.1}$[g,e]
R_0^4	Camerini *et al.*[c]	1 ± 0.3[b]
R_0^4	Salvini and Kim present experiment	$0.54^{+0.15}_{-0.1}$[g,i,h]
$R(3, \infty)$	Salvini and Kim present experiment	0.54 ± 0.15[g,i]
$R(4, 5)$	Salvini and Kim present experiment	0.55 ± 0.15[g,i]
$R(2, 3)$	Salvini and Kim present experiment	$0.46^{+0.15}_{-0.1}$[g,i]
$R(1)$	Salvini and Kim present experiment	0.53 ± 0.2[g,i]

[a] See reference 4.
[b] See reference 6.
[c] See reference 9.
[d] Estimated by us on the basis of their results.
[e] This measurement is biased in favor of the charged π-mesons.
[f] Only the statistical error reported.
[g] The error given here is larger than the statistical, for allowing for the possible systematic errors (see the text).
[h] This measurement is biased in favor of the π^0 mesons.
[i] The π^0 mesons of energy ≤ 45 Mev were included.

[17] In a conversation with one of us Dr. Perkins kindly discussed our results and their previous results (see reference 9). He told us that in a recent, more direct estimate they found a value close to our value (2). We are indebted to him for a general discussion of the problem of the determination of R.

Value of $R(4, 5)$

In the same way as above we find, for events with four or five shower particles: (We assume now that the charged mesons are 65 percent of the p.p.).

$$R(4, 5)=0.55^{+0.15}_{-0.1}.$$

For $R(3, \infty)$ we find:

$$R(3, \infty)=0.54^{+0.15}_{-0.1}.$$

It is interesting to note how this less biased value differs from R_3 given in (2).

5. A more direct estimate can be obtained in the following way: Consider first the value of $R(1)$. Among the events with only one p.p. (Table I), we identified $29\pi^{\pm}$ mesons of a kinetic energy lower than 100 Mev. On the basis of the energy spectrum of the $\pi^{\pm}$ mesons (Camerini *et al.*[15]) these mesons should be $\sim\frac{1}{3}$ of the total number of $\pi^{\pm}$ mesons. So we have about $87\pi^{\pm}$ mesons from the events with one p.p. only. We have to compare this number with the number of the events of Table I in column (0) with only one π^0 meson emitted. The ratio results:

$$R(1)=46/87=0.53\pm0.2.$$

The large errors take into account the possible systematic errors in the estimate of the number of the π^0's and of the energy of the $\pi^{\pm}$ mesons.

6. Conclusions on the value R. In Table II we give the values for the ratio R as estimated in different regions of multiplicity from different observers.

Figure 6 shows the dependence of R on the multiplicity. The circles represent the values $R(1)$, R (2, 3), $R(3, \infty)$, $R(4, 5)$, which are the only ones of Table II really unbiased from selections in favor of the π^0 or of the $\pi^{\pm}$ mesons.

Our conclusion is that the value R is fairly constant for multiplicities from 1 to about 6, and is close to 0.5. In terms of the energy of the primary protons, this means that R is close to 0.5 for events produced by protons of energy between 2 and 20 Bev.

The differences in the previous results of many authors can be understood on the basis of the different selections and the systematic errors which can easily be made in a measurement as difficult as this one. These results for R are consistent with those found in Sec. III, for the probability of the production of the neutral and the charged π-mesons.

V. ENERGY OF THE π^0 MESONS. EXAMINATION OF THE ELECTROMAGNETIC CORES

We consider now the e.m. cores emitted from nuclear events in the crystals. This will lead to an estimate of the energies of the π^0's emitted in events of different multiplicities, and establish an upper limit for the percentage of the e.m. component which may be due to some source other than the π^0 decay.

TABLE III. Energy distribution of the π^0 mesons in events with different numbers of penetrating particles. E=total energy (rest mass+kinetic) of the π^0 meson. The energy was measured by the method described in the text. The numbers given are the numbers of the π^0 mesons for each energy interval. Generally speaking, row (2) refers to events produced mainly by protons of about 1–4 Bev, row (3), to events mainly above 4 Bev.

	(a)	(b)	(c)
(1) Energy interval (Mev)	$400\leq E<700$	$700\leq E<1000$	$E\geq 1000$
(2) $0\leq s\leq 2$	14	6	7
(3) $s\geq 3$	8	5	8

Energy of the π^0 Mesons Emitted from Events with Different Multiplicities

It is difficult to make an absolute estimate of the energy of each π^0 meson emitted in the nuclear events, but it is relatively easy to compare the e.m. cores observed in events with different multiplicities in order to conclude if the energy distributions of the π^0 mesons taken from events of different multiplicities are the same or not, and in what sense they differ.

For the following estimates, which mainly involve the estimate of the energy of the decay photons from their e.m. development, we established a scale of energy which probably is close to the correct one, but which, since it is the same for events with different multiplicities, may not coincide with the correct one. We summarized here the criteria used in establishing this scale.

We considered the events with at least two e.m. cores, each of them going through at least four plates (including two lead plates) corresponding to a total of at least three radiation lengths. We estimated the energy of each of these cores, on the basis of the results of the Monte Carlo method[10] allowing for the possible fluctuations, which can be very large, with standard rules prepared in advance for all the events. For energies larger than 500 Mev we extrapolated the results of Wilson.[9] This extrapolation was used up to about 1000 Mev and it was made by assuming that the number of the electrons at maximum was proportional to the energy of the primary photons from 500 to 1000 Mev. The correction for the presence of the carbon plates was made by adding to the estimated energy an amount corresponding to the ionization losses of the electrons in traversing the carbon plates.

In this way, the energy was estimated for the π^0 mesons in events with different multiplicity. The energy of the two e.m. cores was estimated using the criteria given above, and each case was considered on the basis of the relation (1). We estimate that the energy calculated by us is in each case within a factor 2 of the real value. The results for the events with multiplicities s from 0 to 2 and from 3 to ∞ are given in Table III. The energies which were measured here were from 400

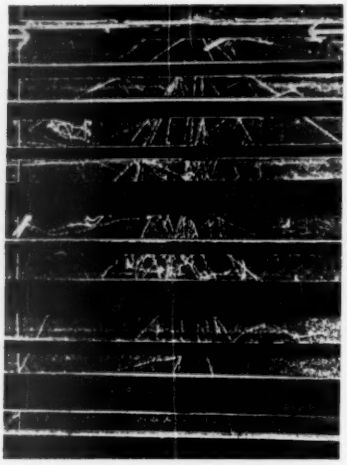

FIG. 7. A representative cloud-chamber photograph. The crystal plate is indicated by the arrows. This is a nuclear event in which no p.p. and one π^0 were created. The two electromagnetic cores are clearly due to photons: the π^0 had an energy higher than 1000 Mev.

Mev up. It is seen from the table that the energies of the π^0 mesons do not differ too much in the events of different multiplicities. This seems to agree with the corresponding result on charged π-mesons.[9]

An experiment designed to enable the estimate of the total energy distribution of the neutral mesons more directly is being prepared by one of us. A preliminary result of the present experiment is that the total energy distribution of the π^0 mesons is rather close to the energy distribution of the charged mesons.[15] In this sense the preliminary indications of Carlson *et al.*[6] concerning neutral mesons from 200 Mev to 600, and of our experiment concerning neutral mesons from 300 Mev and above[13] are confirmed.

Consideration of the Possibility of a Different Origin of the e.m. Component

Evidence that neutral unstable particles of mass close to 300 Mev are at least in good part responsible for the e.m. component in the cosmic radiation has already been given in an indirect but very suggestive way by Carlson *et al.*[6] The doubt that could still remain in their treatment is that the behavior of the e.m. cascade in the air and the Compton effect on the photons of low energy traveling in the air could simulate the existence of an unstable neutral mass decaying into two photons, and that part of the e.m. component from the nuclear events has an origin other than the π^0 mesons. It thus appears worthwhile to check this point again in a more direct way.

For this purpose we examined 39 e.m. cores, which traversed at least three lead plates (at least five plates in the cloud chamber). We searched around each of them for a second core, which should have been present if their only origin was from the decay photons of the π^0 mesons. We found the second core in 24 out of the 39 cases. Consideration of the fluctuations in the e.m. cascade and of the possible angles between the cores, as estimated on the basis of (1), and of the possibility for the second core escaping observation may explain at least 10 of the remaining 39–24 cases.

From this examination we conclude that the π^0 mesons are at least the main and may be the only source of the photons from the nuclear events. If single photons are emitted from the nuclear events of our energies (1–20 Bev), these photons should be ≤ 20 percent of the photons resulting from the decay of π^0's.

Nuclear Events with Only Electromagnetic Component Emitted (Events N_0)

In this category we include those events which do not show any ionizing penetrating particles. They were recognized on the basis either of the grey tracks usually coming out of the crystals, or of the presence of more than one core of e.m. component, pointing with a non-ionizing (photon) link to one point in the crystal. The first criterion was the more common. Examples of these pictures are shown in Figs. 7 and 8.

These events were examined quite carefully, since

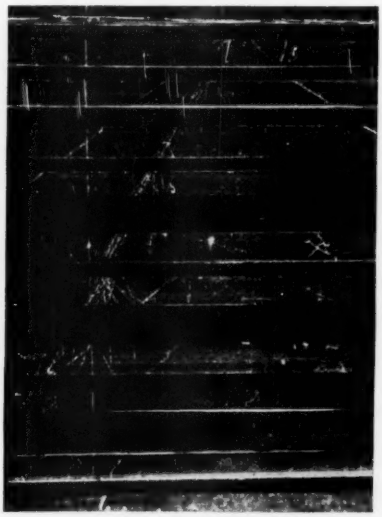

FIG. 8. A nuclear event with two protons and only e.m. component emitted. Events like this and like the one of Fig. 7 would escape the conventional Geiger-Müller control or the nuclear plates.

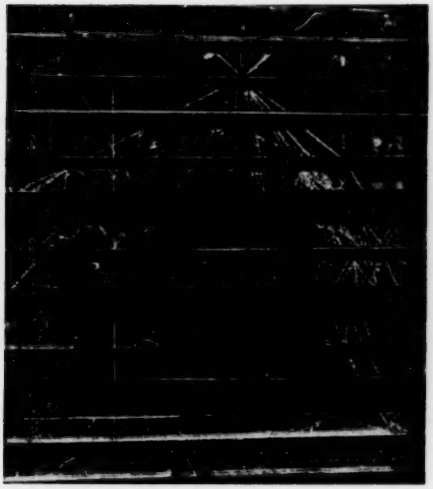

FIG. 9. An event produced in the first lead plate. We have a few of these events, which indicate how the crystal could be an efficient detector also for interactions produced outside.

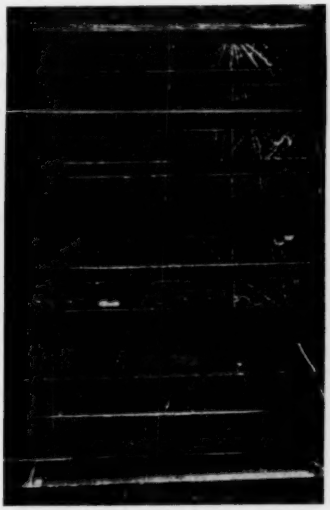

FIG. 10. A nuclear event in the crystal with two p.p. emitted. One of them interacts in the seventh plate (carbon) to give a heavy prong and one light particle, probably one $\pi^{\pm}$ meson directed upward.

they will usually escape observation in the nuclear plates and the Geiger-Müller triggered cloud chambers. The evidence for π^0 mesons in these events was about as strong as in the other nuclear collisions.

Two other events of interest are shown in Figs. 9 and 10.

CONCLUSIONS

On the basis of our experiment and of the evidence already existing we can now fix certain points regarding the existence and properties of the π^0 mesons.

The π^0 mesons are definitely the main source of the photons associated with the nuclear events. An upper limit for the number of photons associated with nuclear events having an origin other than π^0 decay can be set at 20 percent.

The cross section $\sigma_{pr}(E)$ for production of the π^0 mesons increases with the energy of the producing protons, in the way indicated by Fig. 5. This estimate of the cross section was obtained in an indirect way, and involves rather large corrections. In these limits it appears that $\sigma_{pr}(E)$ depends on energy in a way that would be expected from the assumption that the π^0 meson has, at energies above 1 Bev, the same probability of production as each of the positive and negative π-mesons. The predictions of Fermi[12] concerning the cross section for production of the neutral and charged π-mesons are confirmed. The value of the cross section for production of at least one π^0 meson is about 0.1–0.2 of the geometrical for incident protons of 1–2 Bev.

The ratio $R=\pi^0/(\pi^+ + \pi^-)$ of the total number of neutral mesons to the total number of charged mesons is close to 0.5 for multiplicities ranging from one to five or six, that is, for different energies of the producing protons between 2 and 20 Bev. This result agrees with almost all the results of previous experiments when these are corrected for the bias introduced in the selection of the events.

TABLE IV. Pulse-heights distribution for various kinds of events.

Pulse height: Events	12–17	18–23	24–29	≥30	Total
Nuclear interactions[a]	38	53	49	77	217
No visible track[b]	13	23	10	14	60
Charged slow particles stopping in the crystals[c]	26	32	38	9	105
Charged particles traversing the crystals[d]	74	94	53	27	248
Electromagnetic showers[e]	83	85	54	36	258
Doubtful cases[f]	35	34	18	13	100
					988

[a] Nuclear interactions occurred in the NaI crystals, with visible prongs coming out of the crystals. About 75 percent of them appear to be due to ionizing particles (protons).

[b] No visible track. Events included in this class may consist of the following types: (a) small stars produced by neutral particles whose prongs end in the crystal; (b) relativistic particles traveling in an almost horizontal direction.

[c] Charged slow particles stopping in the crystals. These events may consist of either simple stoppings or small evaporation stars.

[d] Charged particles traversing the crystals. The following kinds of events were included in this class: (a) unrelated penetrating particles going through the crystals; (b) particles from nuclear events produced above the crystals.

[e] Electromagnetic showers. Mostly produced above the crystal either by cloud-chamber walls or by materials above the cloud chamber.

[f] Doubtful cases. Cases in which it is hard to estimate the origin of the pulse. Some of them could be due to radioactive contamination.

The behavior of R *versus* the multiplicity of relativistic particles (π^0 mesons plus penetrating particles) calculated on the basis of our results, is given in Fig. 6.

The energy distribution of the π^0 mesons from events of low and high multiplicity is about the same, within the statistics of 48 cases selected only on the criterion of being near the center of the cloud chamber. This is similar to the results for $\pi^{\pm}$ mesons. Also, the total energy distribution of the π^0 mesons seems to be close to the total energy distribution of the charged mesons.[12]

ACKNOWLEDGMENTS

The authors are deeply indebted to Professor G. T. Reynolds for continuous discussion and encouragement.

He worked with us at the beginning of this experiment, on the preparation of the scintillation crystals and the discussion of the project.

We also wish to express our gratitude to Professor R. Rau for his help in the solution of many technical problems connected with the technique of rear illuminated cloud chambers.

APPENDIX

We studied about one thousand oscilloscope pictures of chamber events. The results are tabulated in Table IV with the description of the terminologies used in the table. The pulse-height scale is comparative, and for pulse heights higher than 30, a saturation effect exists.

The useful events for us (nuclear events) are only about 14 percent of the cloud-chamber pictures taken. The actual events we took into our analysis are about 10 percent of the total pictures taken. It is true that if we used a higher bias (for instance, required pulses higher than 24 or so), then we could have increased the efficiency by eliminating a rather large percentage of undesired events at low pulse heights, but we feared that this might bring in some bias in our selection.

PHYSICAL REVIEW VOLUME 88, NUMBER 1 OCTOBER 1, 1952

The Variational Method for Problems of Neutron Diffusion and of Radiative Transfer

SU-SHU HUANG*
Berkeley Astronomical Department, University of California, Berkeley, California
(Received June 17, 1952)

The functional as proposed by R. E. Marshak for solving certain inhomogeneous integral equations by the variational method is modified in such a way that the simultaneous equations which determine the parameters become linear. Thus we can solve this type of integral equations with an accuracy as high as required without much labor. As an illustration we obtain by the present method an approximate solution of Milne's integral equation for the neutron density (or for the source function in the problem of radiative transfer) in a simple form. Our approximate solution agrees (for the first four figures) everywhere with the one computed by C. Mark from the exact solution.

MARSHAK[1] has formulated a variational method for certain inhomogeneous integral equations concerned with neutron diffusion problems. Let the inhomogeneous integral equation be

$$q_0(x)=\int K(x,x')q_0(x')dx'+f(x), \tag{1}$$

where $K(x,x')$ is a positive symmetric kernel, and $f(x)$ is bounded so that $\int|f(x)|dx$ exists. Marshak finds that the functional,

$$\frac{\int q(x)\left\{q(x)-\int K(x,x')q(x')dx'\right\}dx}{\left[\int q(x)f(x)dx\right]^2}, \tag{2}$$

is an extremum[2] for the actual solution, $q_0(x)$, and can be equated to $k_1/[q_0(\infty)-k_2]$ provided that we can write

$$q_0(\infty)=k_1\int q_0(x)f(x)dx+k_2, \tag{3}$$

where k_1 and k_2 are two constants. LeCaine[3] applies this method to Milne's problem and obtains an approximate solution in simple analytical form with high accuracy.

As can be seen from (2), variation of Marshak's functional leads to a set of simultaneous equations of second degree for the varying parameters. Hence it would be very difficult to solve these simultaneous equations when we have more than two parameters in the trial function. We shall here slightly modify the functional in order to linearize the equations which determine the parameters.

Assume that $q_0(x)$ approaches zero rapidly so that $\int x^n q_0(x)dx$ exists (n is a positive integer). We define

* J. S. Guggenheim Memorial Foundation Fellow.
[1] R. E. Marshak, Phys. Rev. **71**, 688 (1947).
[2] B. Davison, Phys. Rev. **71**, 694 (1947), has discussed the conditions under which (2) is a minimum.
[3] J. LeCaine, Phys. Rev. **72**, 564 (1947).

a new functional as follows:

$$\mathfrak{F}=\int q(x)\left[q(x)-\int K(x,x')q(x')dx'\right]dx - 2\int q(x)f(x)dx. \quad (4)$$

It can be easily seen that $\mathfrak{F}$ is an extremum for the actual solution $q_0(x)$. If $\int q_0(x)f(x)dx$ can be expressed in terms of a characteristic constant involved in the integral equation (1), we can determine this constant by

$$\mathfrak{F}=-\int q_0(x)f(x)dx. \quad (5)$$

The integral equation for the neutron density (or the source function in the case of radiative transfer), $\rho_0(x)$, in the Milne problem is

$$\rho_0(x)=\tfrac{1}{2}\int_0^\infty E_1(|x-x'|)\rho_0(x')dx', \quad (6)$$

with

$$E_n(x)=\int_1^\infty \frac{e^{-xv}}{v^n}dv.$$

Since the asymptotic neutron density is linear,[4] we may write

$$\rho_0(x)=x+\alpha+q_0(x), \quad (7)$$

where α is a constant and $q_0(x)$ approaches zero for large x. Thus the integral equation for $q_0(x)$ assumes the following form:

$$q_0(x)=\frac{1}{2}\int_0^\infty E_1(|x-x'|)q_0(x')dx'-\frac{\alpha}{2}E_2(x)+\frac{1}{2}E_3(x). \quad (8)$$

The functional $\mathfrak{F}$ associated with (8) is simply

$$\mathfrak{F}=\int_0^\infty q(x)\left\{q(x)-\tfrac{1}{2}\int_0^\infty E_1(|x-x'|)q(x')dx'\right\}dx - \int_0^\infty q(x)[E_3(x)-\alpha E_2(x)]dx. \quad (9)$$

In order to express $\frac{1}{2}\int_0^\infty q_0(x)[E_3(x)-\alpha E_2(x)]dx$ in terms of α, we integrate Eq. (8) both directly and after multiplication at both sides by x. Thus we find

$$\mathfrak{F}=-\frac{1}{2}\int_0^\infty q_0(x)[E_3(x)-\alpha E_2(x)]dx=\frac{1}{8}-\frac{\alpha^2}{4}, \quad (10)$$

which is the equation determining α. Thus we can see that α enters into (8) as a characteristic constant and that we are encountering an eigenvalue problem.

If we assume $q(x)=0$ (i.e., no variation in the functional) we have (discarding the negative root)

$$\alpha=\tfrac{1}{2}\sqrt{2}=0.7071, \quad (11)$$

which is only 0.5 percent less than the correct value. (Marshak's functional leads to an even better value, 0.7083, with the same trial function.) For comparison, the value obtained by Chandrasekhar[5] in the fourth approximation of his method is 0.7069.

Following LeCaine[3] we now introduce a trial function with two parameters:

$$q(x)=aE_2(x)+bE_3(x). \quad (12)$$

Thus

$$\mathfrak{F}=\left(\frac{1}{2}-\frac{\pi^2}{24}\right)a^2+\frac{1}{3}(1-\ln 2)ab+\left(-\frac{13}{144}-\frac{2}{9}\ln 2+\frac{\pi^2}{36}\right)b^2 - \frac{1}{8}a+\frac{2}{3}(1-\ln 2)\alpha a+\frac{1}{5}(1-2\ln 2)b+\frac{1}{8}\alpha b. \quad (13)$$

$\partial\mathfrak{F}/\partial a=0$ and $\partial\mathfrak{F}/\partial b=0$ give two linear equations

TABLE I. Evaluation of $\rho_0(x)$.

x	$\rho_0(x)$ Present calc	Mark's calc
0	0.577439	0.577350
0.01	0.598240	0.5982
0.02	0.615380	0.6154
0.03	0.631227	0.6312
0.04	0.646272	...
0.05	0.660745	0.6607
0.06	0.674779	...
0.07	0.688460	...
0.08	0.701849	...
0.09	0.714990	...
0.1	0.727918	0.7279
0.12	0.753236	...
0.14	0.777962	...
0.16	0.802207	...
0.18	0.826052	...
0.2	0.849558	0.8495
0.25	0.907127	...
0.3	0.963372	0.9633
0.35	1.018620	...
0.4	1.073093	1.0731
0.45	1.126946	...
0.5	1.180292	1.1803
0.6	1.285799	1.2858
0.7	1.390106	1.3901
0.8	1.493532	1.4935
0.9	1.596292	1.5963
1	1.698539	1.6985
1.2	1.901911	1.9019
1.5	2.205135	2.2051
2	2.707923	2.7079
2.5	3.209199	3.2092
3	3.709812	3.7098
3.5	4.210117	4.2101
4	4.710272	4.7102
5	5.710396	...

[4] G. Placzek and W. Seidel, Phys. Rev. **72**, 550 (1947); also E. Hopf, *Mathematical Problems of Radiative Equilibrium*, Cambridge tract No. 31 (Cambridge University Press, Cambridge, 1934).

[5] S. Chandrasekhar, Astrophys. J. **100**, 76 (1944); *Radiative Transfer* (Oxford University Press, London, 1950), p. 80.

which determine a and b:

$$a=4.259399\alpha-3.268660,$$
$$b=6.895438-9.392962\alpha. \tag{14}$$

The equation determining α is

$$-\tfrac{1}{16}a+\tfrac{1}{3}(1-\ln 2)a\alpha-\tfrac{1}{10}(2\ln 2-1)b+\tfrac{1}{16}b\alpha = \tfrac{1}{8}-\tfrac{1}{4}\alpha^2, \tag{15}$$

which together with (14) gives

$$\alpha=0.71044596, \tag{16}$$

as compared with the value 0.71044609 computed by Placzek and Seidel[4] from the exact definite integral, 0.7104457 by LeCaine,[3] and 0.7104494 by Menzel and Sen.[6] It follows from (12), (14), and (16) that

$$q(x)=-0.242586E_2(x)+0.222244E_3(x). \tag{17}$$

As the variational calculation of the value of α and of the approximate solution of (8) by the present functional is extremely simple, we can easily compute the solution with four parameters. Let

$$q(x)=aE_2(x)+bE_3(x)+cE_4(x)+dE_5(x). \tag{18}$$

The corresponding functional $\mathfrak{F}$ and the equation for determining α now assume, respectively, the forms:

$$\begin{aligned}\mathfrak{F}=&\frac{1}{2}\left(1-\frac{\pi^2}{12}\right)a^2+\frac{1}{2}\left(-\frac{13}{72}-\frac{4}{9}\ln 2+\frac{\pi^2}{18}\right)b^2\\&+\frac{1}{2}\left(\frac{23}{90}+\frac{4}{15}\ln 2-\frac{\pi^2}{24}\right)c^2\\&+\frac{1}{2}\left(-\frac{10419}{151200}-\frac{552}{1575}\ln 2+\frac{\pi^2}{30}\right)d^2+\frac{1}{3}(1-\ln 2)ab\\&+\left(\frac{67}{144}+\frac{2}{9}\ln 2-\frac{\pi^2}{18}\right)ac+\left(\frac{111}{360}-\frac{11}{30}\ln 2\right)ad+\frac{1}{24}bc\\&+\left(-\frac{49}{480}-\frac{2}{5}\ln 2+\frac{\pi^2}{24}\right)bd+\left(\frac{11}{120}-\frac{1}{10}\ln 2\right)cd\\&-\frac{1}{8}a+\left(\frac{1}{5}-\frac{2}{5}\ln 2\right)b-\frac{1}{18}c+\left(\frac{13}{84}-\frac{2}{7}\ln 2\right)d\\&+\alpha\left[\frac{2}{3}(1-\ln 2)a+\frac{1}{8}b+\left(\frac{11}{30}-\frac{2}{5}\ln 2\right)c+\frac{5}{72}d\right],\end{aligned} \tag{19}$$

and

$$\begin{aligned}&-\frac{1}{16}a+\left(\frac{1}{10}-\frac{1}{5}\ln 2\right)b-\frac{1}{36}c+\left(\frac{13}{168}-\frac{1}{7}\ln 2\right)d\\&+\alpha\left[\frac{1}{3}(1-\ln 2)a+\frac{1}{16}b+\left(\frac{11}{60}-\frac{1}{5}\ln 2\right)c\right.\\&\left.+\frac{5}{144}d\right]=\frac{1}{8}-\frac{1}{4}\alpha^2.\end{aligned} \tag{20}$$

[6] D. H. Menzel and H. K. Sen, Astrophys. J. **110**, 1 (1949).

The final result is

$$\alpha=0.7104460894, \tag{21}$$

$$\begin{aligned}q(x)=&-0.27891881E_2(x)+0.52732328E_3(x)\\&-0.61602263E_4(x)+0.35036496E_5(x),\end{aligned} \tag{22}$$

and

$$\rho_0(x)=0.71044609+x+q(x). \tag{23}$$

The solution $\rho_0(x)$ of Eq. (6) has been calculated by various methods.[7] We have computed $\rho_0(x)$ according to (23) and (22), the result being given in Table I, where Mark's value[7] computed from the exact analytic solution[4] is listed also for comparison. We can see that our result agrees nearly everywhere with Mark's. The present approximate solution has therefore a simple analytic form with high accuracy. The functions $E_n(x)$ have been tabulated extensively.[8]

The emergent angular distribution $\varphi(\mu)$ can be directly obtained from (23) and (22). Normalizing it such that

$$\int_0^1 \varphi(\mu)d\mu=1, \tag{24}$$

we obtain

$$\begin{aligned}\varphi(\mu)=&0.50007629+0.57495310\mu-0.38177815\mu^2\\&-0.30342447\mu^3+(0.24155039\mu\\&+0.45667462\mu^2+0.53349039\mu^3\\&+0.30342447\mu^4)\ln[(1+\mu)/\mu].\end{aligned} \tag{25}$$

Comparison with the table[9] computed from the exact analytic expression[4] shows that the maximum error is 0.016 percent at $\mu=0$, and the error at $\mu=0.01$ is already reduced to 0.004 percent. For the whole range $0.1\leq\mu\leq 1$ the error involved in (25) is about one part in one million.

The approximate solution we have given here is similar in form to one given recently by Menzel and Sen.[6] It is interesting to note that although the methods of determining the parameters (i.e., a, b, c, $\cdots$) by them and by us are fundamentally different, both give accurate numerical results.

Applications of the same method to the problem of formation of spectral lines in stellar atmospheres will appear elsewhere.

I wish to thank Professor Otto Struve for his encouragement and for the facilities which he has rendered to me during the present investigation.

[7] For a recent review see reference 6 or C. Mark, Phys. Rev. **72**, 558 (1947).

[8] G. Placzek, *The Functions $E_n(x)$, MT-1* (National Research Council of Canada, Ottawa, Canada, 1946).

[9] G. Placzek, Phys. Rev. **72**, 556 (1947).

Natural Line Shape

FRANCIS LOW*
Institute for Advanced Study, Princeton, New Jersey
(Received May 9, 1952)

The covariant methods of Feynman and Dyson are applied to the problem of line shape. It is shown that the line center depends almost completely on the form of the S_{F_e}' function, that is the Feynman-type Green's function for the electron interacting with an external field A_μ^e and with the quantized radiation field. A finite equation for S_{F_e}' is derived, from which the line center and shape may be calculated to any desired accuracy. The method is illustrated by two examples: the elastic scattering of photons by a one electron atom in its ground state and the emission of photons by the same type of atom following thermal excitation.

INTRODUCTION

THE shape of atomic spectral lines has been discussed by Weisskopf and Wigner.[1] Their results are inconclusive in three respects. In the first place, the time dependent formalism which they use leaves some doubt as to the correct choice of boundary conditions in a decay problem in which the excitation of the system (by electron bombardment, for instance, as in a discharge tube) is considered to be an independent, unspecified process. In the second place, although the line width found by these authors is finite and in agreement with experiment, the line center is shifted by an infinite energy, obviously corresponding to the infinite self-energy of an electron interacting with its own radiation field. Finally, within the Weisskopf-Wigner formalism, it would be extremely difficult to calculate a next approximation. This might conceivably be of some practical interest in an experiment such as the Lamb shift, where the accuracy of the measurement is a small fraction of the line width, and where it is not at all clear, beyond the lowest order, what the measured "energy" of the excited state corresponds to in the language of quantum-mechanical perturbation theory.

In order to discuss the problem in such a way that all our results will be finite we will make use of the computational techniques of Feynman[2] and Dyson.[3] The experiment which we shall discuss is the elastic scattering cross section for photons of frequency k of a one-electron atom in its ground state ψ_0; that is we shall calculate radiative corrections to the Kramers-Heisenberg dispersion formula. The emitted line shape can be obtained from this calculation by replacing the incoming photon by a time dependent external field whose frequency distribution corresponds roughly to that of the mode of excitation preceding the measured emission of photons.

The two questions that are of primary interest concern the symmetry of the line shape and the position of its center. The line center k_0 is here defined as the frequency corresponding to the maximum cross section in the neighborhood of a resonance E_n. In first approximation, of course, any line is symmetric about this point. One may, however, introduce, as a measure of asymmetry, the quantity

$$\delta=[\sigma(k_0+\Gamma)-\sigma(k_0-\Gamma)]/\sigma(k_0),$$

where Γ is the half-width of the line.

A convenient unit of an experimentally measurable order of magnitude is the Lamb unit, $\pounds\cong\alpha^3z^2(E-m)\cong\alpha^5z^4m$. In general, $\Gamma\cong\pounds$ for all but metastable states. We shall find that up to (but not including) terms of order $\alpha^3z^2\pounds$, the line center k_0 is shifted only by Lamb-shift-like effects, and that to this accuracy all the terms contributing to the shift (before renormalization) are in one to one correspondence with those predicted by stationary state perturbation theory, even though the "energy" of the "state" is only defined to within $\Gamma\approx\pounds$.

I. THE KRAMERS-HEISENBERG DISPERSION FORMULA

We shall begin by deriving the Kramers-Heisenberg dispersion formula within the framework of the S-matrix theory of Feynman and Dyson. This will immediately make it clear how radiative corrections must be calculated.

We shall work in the Furry[4] interaction representation; that is all electron operators ψ have their time dependence given by the external field A_μ^e, which we assume to be time independent:

$$[\gamma_\mu(\partial/\partial x_\mu-ieA_\mu^e(x))+m]\psi=0. \quad (1)$$

The stationary solutions of (1), $\psi_n(\mathbf{x})e^{-iE_nt}$, constitute a complete set of spinor functions of $\mathbf{x}$ at any one time.

The Feynman Green's function for the external field is given by

$$S_{F_e}(x_1,x_2)=S_{F_e}(\mathbf{x}_1,\mathbf{x}_2;t_1-t_2)$$
$$=\epsilon(t_1,t_2)\langle V|P[\psi(x_1)\bar{\psi}(x_2)]|V\rangle, \quad (2)$$

where $|V\rangle$ is the exact vacuum state of the external field, $\epsilon(t_1,t_2)=\pm1$ according to whether $t_1>t_2$ or $t_1<t_2$,

* Present address: Department of Physics, University of Illinois, Urbana, Illinois.

[1] V. Weisskopf and E. Wigner, Z. Physik **63**, 54 (1930); **65**, 18 (1930).

[2] R. Feynman, Phys. Rev. **76**, 749, 769 (1949).

[3] F. Dyson, Phys. Rev. **75**, 486, 1736 (1949).

[4] W. Furry, Phys. Rev. **81**, 115 (1950).

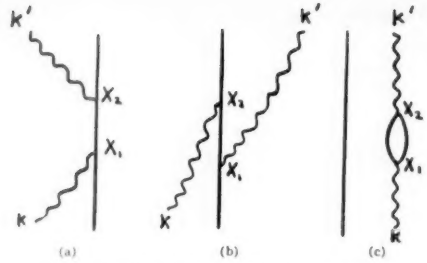

FIG. 1. (a) and (b): Kramers-Heisenberg scattering. (c): Delbrück scattering.

and P is Dyson's time ordering operator. We note, using (2), that

$$\begin{aligned} S_{Fe}(x_1, x_2) &= \sum_{n+} \psi_n(\mathbf{x}_1)\bar{\psi}_n(\mathbf{x}_2)e^{-iE_n(t_1-t_2)} \text{ for } t_1>t_2 \\ &= -\sum_{n-} \psi_n(\mathbf{x}_1)\bar{\psi}_n(\mathbf{x}_2)e^{-iE_n(t_1-t_2)} \text{ for } t_1<t_2 \\ &= \frac{1}{2\pi i}\sum_n \int_{-\infty}^{\infty} \frac{d\omega e^{i\omega(t_1-t_2)}}{E_n(1-i\epsilon)+\omega}\psi_n(\mathbf{x}_1)\bar{\psi}_n(x_2), \end{aligned} \tag{3}$$

where ϵ is to approach zero after the ω integration has been done. Finally, S_{Fe} satisfies the integral equation:

$$S_{Fe}(1,2) = S_F(1,2) - \int S_F(1,3)e\gamma_\mu A_\mu^e(3)S_{Fe}(3,2)dx_3. \tag{4}$$

The S-matrix element from a state with a photon of four-momentum $\mathbf{k}$, k to one of four-momentum $\mathbf{k}'$, k', the atom remaining in its ground state ψ_0, is

$$\begin{aligned} (k', 0|S|k, 0) = \sum_{n=0} \frac{(-i)^n}{n!} \int_{-\infty}^{\infty} dx_1 \cdots dx_n \\ \times (k', 0|P[H_I(x_1)\cdots H_I(x_n)]|k, 0), \end{aligned} \tag{5}$$

where

$$H_I(x) = j_\mu(x)A_\mu(x), \tag{6}$$

with $j_\mu(x) = ie\bar{\psi}(x)\gamma_\mu\psi(x)$. The first nonvanishing approximation to (5) is represented by the three Feynman graphs, Figs. 1(a), (b), and (c), where of course the electron propagates from x_1 to x_2 according to S_{Fe}, not S_F. Figure 1(c) corresponds to the scattering of light by the external field A_μ^e and will not be discussed here. The matrix elements of 1(a) and 1(b) are

$$\begin{aligned} S_a &= \frac{2\pi e^2}{(kk')^{\frac{1}{2}}} \int_{-\infty}^{\infty} d\mathbf{x}_1 d\mathbf{x}_2 dt_1 dt_2 \bar{\psi}_0(\mathbf{x}_2)e^{-i\mathbf{k}'\cdot\mathbf{x}_2}\gamma_\mu e_\mu' \\ &\quad \cdot S_{Fe}(x_1, x_2)\gamma_\nu e_\nu e^{i\mathbf{k}\cdot\mathbf{x}_1}\psi_0(\mathbf{x}_1)e^{i(E_0+k')t_2}e^{-i(E_0+k)t_1} \\ &= \frac{2\pi e^2}{(kk')^{\frac{1}{2}}} \sum_n (0|\,\boldsymbol{\alpha}\cdot\hat{e}_\lambda' e^{-i\mathbf{k}'\cdot\mathbf{x}}|n)(n|\,\boldsymbol{\alpha}\cdot\hat{e}_\lambda e^{i\mathbf{k}\cdot\mathbf{x}}|0) \\ &\quad \times \int_{-\infty}^{\infty} dt_1 dt_2 e^{i(E_0+k')t_1}e^{-i(E_0+k)t_2} \frac{e^{i\omega(t_2-t_1)}}{2\pi i(E_n+\omega)}d\omega \end{aligned}$$

or

$$S_a = \frac{(2\pi)^2 e^2}{ki}\delta(k-k')\sum_n \left(0\left|\boldsymbol{\alpha}\cdot\hat{e}_\lambda' \frac{e^{-i\mathbf{k}'\cdot\mathbf{x}}}{E_n-E_0-k}\right|n\right) \times (n|\,\boldsymbol{\alpha}\cdot\hat{e}_\lambda e^{i\mathbf{k}\cdot\mathbf{x}}|0).$$

Similarly,

$$\begin{aligned} S_a+S_b = -i\delta(k-k')(2\pi e)^2[k\textstyle\sum_n[0|\,\boldsymbol{\alpha}\cdot\hat{e}_\lambda' e^{-i\mathbf{k}'\cdot\mathbf{x}}|n) \\ \times (n|\,\boldsymbol{\alpha}\cdot\hat{e}_\lambda e^{i\mathbf{k}\cdot\mathbf{x}}|0)/(E_n-E_0-k) \\ +(0|\,\boldsymbol{\alpha}\cdot\hat{e}_\lambda e^{i\mathbf{k}\cdot\mathbf{x}}|n) \\ \times (n|\,\boldsymbol{\alpha}\cdot\hat{e}_\lambda' e^{-i\mathbf{k}'\cdot\mathbf{x}}|0)/(E_n-E_0+k)], \end{aligned} \tag{7}$$

leading to a scattering cross section

$$d\sigma = (e^2/m)^2 d\Omega\,|H'|^2,$$

where

$$\begin{aligned} H' = m\sum_n \Big\{ &\frac{(0|\,\boldsymbol{\alpha}\cdot\hat{e}_\lambda' e^{-i\mathbf{k}'\cdot\mathbf{x}}|n)(n|\,\boldsymbol{\alpha}\cdot\hat{e}_\lambda e^{i\mathbf{k}\cdot\mathbf{x}}|0)}{E_n-E_0-k} \\ &+\frac{(0|\,\boldsymbol{\alpha}\cdot\hat{e}_\lambda e^{i\mathbf{k}\cdot\mathbf{x}}|n)(n|\,\boldsymbol{\alpha}\cdot\hat{e}_\lambda' e^{-i\mathbf{k}'\cdot\mathbf{x}}|0)}{E_n-E_0+k}\Big\}. \end{aligned} \tag{8}$$

In nonrelativistic approximation $\boldsymbol{\alpha}$ is replaced by $\mathbf{p}/m$ in the sum over positive states. The negative energy sum leads in well-known fashion to the nonrelativistic A^2 term in the scattering cross section.

We may anticipate later results at this point to ask for the effect of nonresonant terms on the line shape near a resonance E_n, where the energy denominator in (8) must be replaced by

$$\frac{1}{E_n-E_0-k} \to \frac{1}{E_n-E_0-k-i\Gamma_n}.$$

One finds that the effect of a nonresonant level E_m is to shift the line center by

$$\delta k_0 \cong \alpha^6 z^4 (E_n-E_0) \simeq \alpha^3 z^2 \mathcal{L},$$

and to distort the line shape by $\delta \simeq \alpha^3 z^2$. These orders of magnitude are the same whether or not the level E_m is removed from E_n by a fine structure splitting, since in that case the matrix element will be smaller by $\alpha^2 z^2$,

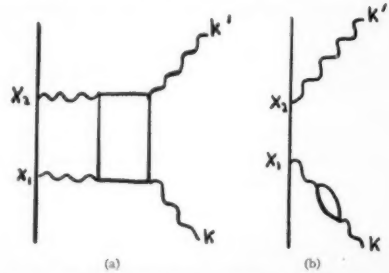

FIG. 2. Vacuum polarization corrections to scattering.

exactly compensating the smaller energy difference in the denominator.

The effect of the frequency variation of the matrix element

$$H' = (0|\,\boldsymbol{\alpha}\cdot\hat{\boldsymbol{e}}_\lambda \exp(i\mathbf{k}\cdot\mathbf{x})\,|n)$$

is even smaller, since parity allows only even or odd terms to appear for a given transition. One finds a shift

$$\delta k_0 \approx \alpha^6 z^6 (E_n - E_0) \approx \alpha^5 z^4 \mathfrak{L},$$

together with an asymmetry $\delta \approx \alpha^5 z^4$. Both of these corrections are much too small to be of interest at present.

II. GENERAL DISCUSSION OF RADIATIVE CORRECTIONS

When the photon frequency approaches any excitation energy of the atom (8) breaks down; for $k = E_n - E_0$ the scattering it predicts is infinite. We must therefore recalculate graph 1(a) together with its radiative corrections. These corrections can be of four types.

(1) Corrections due to vacuum polarization by the incoming and outgoing photons, such as shown in Figs. 2(a) and (b).

Aside from an unobservable renormalization of the photon wave functions, these graphs produce corrections considerably smaller than those discussed in I.

(2) Corrections to γ_μ, such as shown in Figs. 3(a) and 3(b). These are also small, and the same remarks apply as those of the preceding paragraph.

(3) Corrections to the incoming or out-going atom as in graph 3(c). These are important, but require no calculation. They replace $\psi_0(\mathbf{x})e^{-iE_0t}$ by $\langle v|\psi_H(x)|g\rangle = Z_2^{\frac{1}{2}}\psi_g(\mathbf{x})e^{-iE_0t}$, where ψ_H is a Heisenberg representation operator, $|V\rangle$ is the exact vacuum state and $|g\rangle$ the exact ground state of the atom, including all radiative corrections; $Z_2^{\frac{1}{2}}$ is the infinite (or zero) renormalization of probability amplitude discussed by Dyson. ψ_g is finite when it is expressed as a function of the renormalized mass and charge; once this is done it differs from ψ_0 by small corrections which are no longer of interest since they affect the resonant behavior even less than those discussed in I. In the future we shall therefore disregard these graphs and write $\psi_0 e^{-iE_0t}$ for the incoming, $\bar{\psi}_0 e^{iE_0t}$ for the outgoing atom, remembering that E_0 is the exact ground-state energy (which is of course a well-defined number).

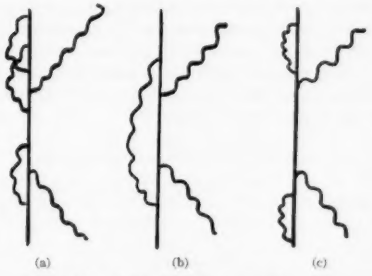

FIG. 3. (a) and (b): Radiative corrections to γ_μ. (c): Radiative corrections to ψ_0, $\bar{\psi}_0$ and E_0.

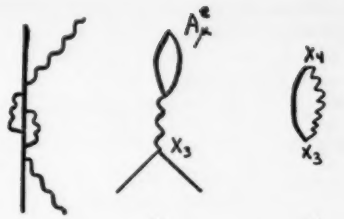

FIG. 4. (a): Radiative corrections to S_{Fe}'. (b): Vacuum polarization contribution to Σ_e. (c): Lowest order dynamic contribution to Σ_e.

(4) Finally we have corrections of the type shown in Fig. 4(a).

We note that these can be calculated in exactly the same manner as $(k'|S_A|k)$ in I, except that S_{Fe} must be replaced by S_{Fe}', where

$$S_{Fe}'(x_1, x_2) = \epsilon(1, 2)\langle 0|\,P[\psi_H(x_1)\bar{\psi}_H(x_2)]\,|0\rangle,$$

and where $|0\rangle$ is the exact vacuum state and ψ_H is in the Heisenberg representation.

III. CALCULATION OF S_{Fe}'

Dyson has shown that for $A_\mu^e = 0$, S_F' satisfies an integral equation

$$S_F'(1-2) = S_F(1-2) + \int S_F(1-3)\Sigma(3-4)S_F'(4-2)d(34). \quad (9)$$

In fact it is in terms of the kernel of this equation, $\Sigma(3-4)$, that his renormalization procedure is defined.

When an external field is present, we may still write

$$S_{Fe}'(1, 2) = S_{Fe}(1, 2) + \int S_{Fe}(1, 3)\sum_e(3, 4)S_{Fe}'(4, 2)d(34), \quad (10)$$

where $\sum_e$ is no longer a function of the difference $x_3 - x_4$, but of $\mathbf{x}_3$, $\mathbf{x}_4$ and $t_3 - t_4$.

$\sum_e$ will contain a whole new series of diagrams arising from vacuum polarization by the external field, of which the lowest order is shown in Fig. 4(b), and, after renormalization, is given by $\sum_P = iA_\mu^{e\prime}(x_3)\delta(x_3 - x_4)$, where

$$A_\mu^{e\prime} \cong (e^2/15\pi m^2)\partial^2 A_\mu^e/\partial x_\nu^2$$

as shown by Schwinger.[5]

Otherwise the diagrams appearing in $\sum_e$ will be precisely those appearing in $\sum$, and can be renormalized appropriately.

[5] J. Schwinger, Phys. Rev. **76**, 790 (1949).

For instance, in lowest order one has, corresponding to the diagram of Fig. 4(c)

$$\sum_e = -\gamma_\mu S_{F_e}(x_3, x_4)\gamma_\nu D_{F_{\mu\nu}}(x_3-x_4),$$
$$D_{F_{\mu\nu}} = \langle 0|P[A_\mu(x_3)A_\nu(x_4)]|0\rangle, \quad (11)$$

or, using (4),

$$\sum_e = \gamma_\mu S_F(x_3-x_4)\gamma_\mu D_F(x_3-x_4)$$
$$-\int \gamma_\mu S_F(x_3-x_5)e\gamma_\mu A_\mu^e(x_5)$$
$$\times S_F(x_5+x_4)\gamma_\nu \cdot D_F(x_3-x_4)dx_5$$
$$+\int \gamma_\lambda S_F(3-5)e\gamma_\mu A_\mu^e(5)S_F(5-6)$$
$$\times\gamma_\nu A_\nu^e(6)S_{F_e}(6,4)\gamma_\lambda D_F(3-4)dx_5dx_6,$$

in which the divergences have been isolated in the first two terms, to which known methods apply. The last term is finite, and contains no renormalization. The same method can in principle be applied to any term in $\sum_e$, so that we may take $\sum_e(x_3, x_4)$ to be finite and known.

The equation we have to solve is thus

$$S_{F_e}'(1,2) = S_{F_e}(1,2) + \int S_{F_e}(1,3)\sum_e(3,4)S_{F_e}'(42)d(34). \quad (10)$$

To solve (10) we set

$$S_{F_e}'(1,2) = \frac{1}{2\pi i}\sum_n \int d\omega f_{nn}(\omega)e^{i\omega(t_1-t_2)}\psi_n(\mathbf{x}_1)\bar{\psi}_n(\mathbf{x}_2)$$
$$+\frac{1}{2\pi i}\sum_{n\neq m}\int d\omega f_{nm}(\omega)e^{i\omega(t_1-t_2)}\psi_n(\mathbf{x}_1)\bar{\psi}_m(\mathbf{x}_2), \quad (11)$$

where $f_{nn}(\omega)$ and $f_{nm}(\omega)$ are to be determined so that (10) is satisfied. So far (11) involves no approximations, since the ψ_n's form a complete set.

Substituting (11) into (10) we find, using (3), and taking the inner product with $\bar{\psi}_n(\mathbf{x}_1)\beta\cdots\beta\psi_n(\mathbf{x}_2)$,

$$\frac{1}{2\pi i}\int e^{i\omega(t_1-t_2)}d\omega f_{nn}(\omega)$$
$$= \frac{1}{2\pi i}\int \frac{e^{i\omega(t_1-t_2)}}{\omega+E_n}d\omega + \frac{1}{2\pi i}\int \frac{d\omega_1 e^{i\omega_1(t_1-t_2)}}{E_n+\omega_1}$$
$$\times\frac{d\omega_2 e^{i\omega_2(t_4-t_2)}}{2\pi i}dt_3dt_4d\mathbf{x}_3d\mathbf{x}_4\bar{\psi}_n(\mathbf{x}_2)$$
$$\cdot\sum_e(\mathbf{x}_3,\mathbf{x}_4,t_3-t_4)\{\psi_n(\mathbf{x}_4)f_{nn}(\omega_2)$$
$$+\sum_{m\neq n}\psi_m(\mathbf{x}_4)f_{mn}(\omega_2)\}, \quad (12)$$

or if we call

$$\int \bar{\psi}_n(\mathbf{x}_3)\sum_e(\mathbf{x}_3,\mathbf{x}_4,t_3-t_4)\psi_m(\mathbf{x}_4)d\mathbf{x}_3d\mathbf{x}_4 = H_{nm}(t_3-t_4), \quad (13)$$

(12) becomes

$$\int e^{i\omega(t_1-t_2)}d\omega f_{nn}(\omega)$$
$$= \int \frac{e^{i\omega(t_1-t_2)}}{E_n+\omega}d\omega + \frac{1}{i}\int \frac{d\omega e^{i\omega(t_1-t_2)}}{E_n+\omega}\cdot H_{nn}(-\omega)$$
$$\cdot f_{nn}(\omega) + \frac{1}{i}\int \frac{d\omega e^{i\omega(t_1-t_2)}}{E_n+\omega}\sum_{m\neq n}H_{nm}(-\omega)f_{mn}(\omega),$$

where

$$H_{nm}(\omega) = \int_{-\infty}^{\infty} dt e^{i\omega t}H_{nm}(t),$$

or finally

$$f_{nn}(\omega) = \frac{1}{E_n+\omega} + \frac{1}{i}\frac{H_{nn}(-\omega)f_{nn}(\omega)}{E_n+\omega}$$
$$+\frac{1}{i}\sum_{m\neq n}\frac{H_{nm}(-\omega)f_{mn}(\omega)}{E_n+\omega}. \quad (14)$$

By taking the inner product with $\bar{\psi}_n\beta\cdots\beta\psi_m$, we obtain a second equation:

$$\frac{1}{2\pi i}\int d\omega f_{nm}(\omega)e^{i\omega(t_1-t_2)}$$
$$= \left(\frac{1}{2\pi i}\right)^2\int \frac{d\omega_3}{E_n+\omega_1}e^{i\omega_1(t_1-t_2)}d\omega_2 e^{i\omega_2(t_4-t_2)}$$
$$\cdot dt_3dt_4[H_{nm}(t_3-t_4)f_{mm}(\omega_2)$$
$$+\sum_{p\neq m}H_{np}(t_3-t_4)f_{pm}(\omega_2)], \quad (15)$$

$$f_{nm}(\omega) = \frac{-i}{E_n+\omega}[H_{nm}(-\omega)f_{mm}(\omega)$$
$$+\sum_{p\neq m}H_{np}(-\omega)f_{pm}(\omega)]. \quad (16)$$

In principle (16) and (14) determine S_{F_e}', and can be solved to any desired accuracy. In particular, if we neglect quadratic terms in $H_{nm}(n\neq m)$, corresponding to neglecting higher order Lamb shifts (but not higher order radiative corrections), we obtain a very simple solution of the expected type:

$$f_{nn} = 1/[E_n+\omega+W_{nn}(-\omega)+\cdots], \quad (17)$$

where

$$W_{nn} = iH_{nn}(-\omega) - \sum_{m\neq n}\frac{iH_{nm}(-\omega)iH_{mn}(-\omega)}{E_m+\omega}+\cdots,$$
$$f_{mn} = \frac{-iH_{mn}(-\omega)+\cdots}{[E_m+\omega+W_{mm}(-\omega)][E_n+\omega+W_{nn}(-\omega)]}. \quad (18)$$

IV. RESONANCE SCATTERING

We may now rederive Eq. (7). S_a becomes, if we neglect f_{mn} compared to f_{nn} (a neglect corresponding to a line shift $\delta k_0 \approx \alpha^3 z^6 \Delta E \approx \alpha^6 z^4 \mathfrak{L}$ and asymmetry $\delta \approx \alpha^6 z^4$).

$$S_a = \frac{2\pi e^2}{(kk')^{\frac{1}{2}}} \int_{-\infty}^{\infty} d\mathbf{x}_1 d\mathbf{x}_2 dt_1 dt_2 \bar{\psi}_0(x_2) e^{-i\mathbf{k}'\cdot\mathbf{x}_2} \gamma_\mu e_\mu' \cdot S_{Fe}'(x_1, x_2) \gamma_\nu e_\nu e^{i\mathbf{k}\cdot\mathbf{x}_1} \psi_0(\mathbf{x}_1) \times e^{i(E_0+k')t_1} e^{-i(E_0+k)t_2}$$

$$= \frac{1}{i} \frac{(2\pi e)^2}{k} \sum_n \frac{(0|\,\boldsymbol{\alpha}\cdot\hat{e}_\lambda' e^{-i\mathbf{k}'\cdot\mathbf{x}}|\,n)(n|\,\boldsymbol{\alpha}\cdot\hat{e}_\lambda e^{i\mathbf{k}\cdot\mathbf{x}}|\,0)}{E_n - E_0 - k + W_{nn}(E_0+k)}, \quad (19)$$

and the resonance scattering is given by

$$d\sigma_n = (e^2/m)^2 d\Omega\, |(0|\,\boldsymbol{\alpha}\cdot\hat{e}_\lambda' e^{-i\mathbf{k}'\cdot\mathbf{x}}|\,n)(n|\,\boldsymbol{\alpha}\cdot\hat{e}_\lambda e^{i\mathbf{k}\cdot\mathbf{x}}|\,0)\cdot m|^2 \cdot 1/[(E_n - E_0 - k + \delta E_n(E_0+k))^2 + \Gamma_n^2(E_0+k)], \quad (20)$$

in the neighborhood of $k = E_n - E_0$, where δE_n and $-i\Gamma_n$ are the real and imaginary parts of $W_{nn}(E_0+k)$.

The line shape and center are therefore effectively determined by the energy denominator in (20). In the fourth-order term,

$$-\sum_{m \neq n} \frac{iH_{nm}(E_0+k) iH_{mn}(E_0+k)}{E_m - E_0 - k},$$

one may set $k + E_0 \cong E_n$ and obtain a shift of order of magnitude

$$\delta k_0 \approx z^3 \alpha^5 (E_n - E_0) \approx z\alpha^2 \mathfrak{L}.$$

The fourth-order renormalization term obtained by expanding

$$iH_{nn}(E_0+k) = iH_{nn}(E_n) + (E_0 + k - E_n)(\partial/\partial E_n) iH_{nn}(E_n),$$

leaves the line shape symmetric but shifts its center by

$$\delta k_0 \approx z^4 \alpha^6 (E_n - E_0) \approx z^2 \alpha^3 \mathfrak{L}.$$

To within present experimental accuracy, therefore, the entire observable effect arises from the term $iH_{nn}(E_n)$. This term is a power series in e^2 (but not in v/c as were the off-diagonal and renormalization terms). The first approximation in e^2 corresponds to the conventional Lamb-shift calculations. The shift due to the second approximation to $\sum_e$ is of order $e^2\mathfrak{L}$ and has been calculated by Berson, Kroll, and Weneser. Finally, the imaginary part of $iH_{nn}(E_n)$ is different from zero, and in lowest order is unaffected by the renormalization subtractions, which are real: i.e., the self-mass and the Z_2 renormalization, which subtracts a real multiple of $E_n - E_0 - k$ from $iH_{nn}(E_0+k)$, change iH_{nn} by a real number, so that $-i\Gamma_n$ may be computed in lowest order without renormalization. This is most easily done using the conventional sum over states which can easily be derived from (21). The Feynman prescription for going around poles will give an imaginary contribution to the sum from each state that has lower energy than E_n, this contribution being $-i/2$ times the transition probability per unit time from the state ψ_n to the state in question.

V. EMISSION LINE-SHAPE

We replace the incoming photon by an effective thermal excitation potential $V(x,t) = \int I(\omega) e^{-i\omega t} d\omega V(x)$. Then the probability of radiation of a photon of frequency k with the atom in its ground state is $|(k|S|0)|^2$ where

$$(k|S|0) = e\left(\frac{2\pi}{k}\right)^{\frac{1}{2}} \int_{-\infty}^{\infty} d\mathbf{x}_1 d\mathbf{x}_2 dt_1 dt_2 \bar{\psi}_0(\mathbf{x}_2) \times e^{-i\mathbf{k}\cdot\mathbf{x}_2} \gamma_\mu e_\mu S_{Fe}'(x_1, x_2) \beta V(\mathbf{x}_1) I(\omega) d\omega \times \psi_0(\mathbf{x}_1) e^{i(E_0+k)t_1} e^{-iE_0 t_2} e^{-i\omega t_2} \quad (21)$$

$$\approx \frac{1}{(k)^{\frac{1}{2}}} \sum_n (0|\,\boldsymbol{\alpha}\cdot\hat{e}_\lambda e^{-i\mathbf{k}\cdot\mathbf{x}}|\,n)(n|\,V(\mathbf{x})\,|0) \times \int dt_1 dt_2 d\omega d\nu e^{i(E_0+k)t_1} \times \frac{e^{-i(E_0+\omega)t_2} e^{i\nu(t_1-t_2)} I(\omega)}{E_n + \nu + W_{nn}(-\nu)} \quad (22)$$

$$= \frac{I(k)}{(k)^{\frac{1}{2}}} \sum_n \frac{(0|\,\alpha\cdot\hat{e}_\lambda e^{-i\mathbf{k}\cdot\mathbf{x}}|\,n)(n|\,V|\,0)}{E_n - E_0 - k + W_{nn}(E_0+k)}, \quad (23)$$

and the probability of radiation of a photon of frequency k is

$$P(k) \approx \frac{|I(k)|^2}{k} \left| \sum_n \frac{(0|\,\boldsymbol{\alpha}\cdot\hat{e}_\lambda e^{-i\mathbf{k}\cdot\mathbf{x}}|\,n)(n|\,V|\,0)}{E_n - E_0 - k + W_{nn}(E_0+k)} \right|^2. \quad (24)$$

When $k - E_n - E_0 \approx 0$, $1/W_{nn} \approx 1/[z^2\alpha^3(E_n - E_0)]$. Thus, if one of the terms in the sum is large, the others are very small, so that

$$P(k) \approx \frac{|I(k)|^2}{k} \sum_n \left| \frac{(0|H'|n)(n|V|0)}{(E_n - E_0 - k + \delta E_n)^2 + \Gamma_n^2} \right|^2, \quad (25)$$

where each term contributes only when k is very near resonance. If $I(k)$ is such as to excite many states, but varies slowly over the line width, this is the expected result.

The author would like to express his gratitude to Dr. J. R. Oppenheimer and to the Institute for Advanced Study for their hospitality during his stay in Princeton.

Photoconduction in Anodic Ta_2O_5

L. Apker and E. A. Taft
General Electric Research Laboratory, Schenectady, New York

(Received May 26, 1952)

Interference phenomena in films of anodic Ta_2O_5 show that fundamental optical absorption occurs for $h\nu > 4.6$ ev. The resultant photoconduction between electrolyte and tantalum substrate shows a quantum yield near 0.5 when the field in the film is of order 10^7 volts/cm.

WE have observed photoconduction in thin films of Ta_2O_5 formed by anodizing Ta metal sheet in the well-known manner.[1] The electrolyte was 0.1 normal citric acid buffered to *p*H5 with sodium citrate, a solution transparent in the ultraviolet to $h\nu \sim 5$ ev. Thus radiation penetrated the liquid to the oxidized Ta plate. The film thickness was roughly 15A per volt of forming potential applied between the Ta and a Pt cathode,[2] the field in the Ta_2O_5 film being of order 10^7 volts/cm.

Figure 1 shows the behavior of the photoconduction at $h\nu = 4.89$ ev with incident radiation fluxes near 10^{14} quanta/sec. As indicated by the solid curve, photocurrents increased with increasing forming potential up to ~ 10 volts (and hence with increasing film thickness up to ~ 150A). The full forming potential was applied during these photoconduction measurements. Above 10 volts, the photoconductive yield remained practically constant near 0.5 electron/incident quantum. At a fixed film thickness (and hence, in the range below a fixed forming potential), the photoconduction was proportional to the applied voltage as shown by dashed lines of Fig. 1.

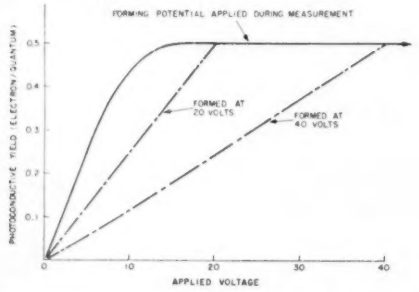

FIG. 1. General behavior of photoconduction in anodic Ta_2O_5 film with radiation levels near 10^{14} quanta/sec cm^2 at $h\nu = 4.89$ ev. With full forming potentials applied, data follow solid line; experimental deviations were of order 20 percent. Data in range below two typical fixed forming potentials are dashed; deviations from these lines were less serious. Hysteresis at very low voltage is ignored.

(At very small voltages deviations appeared. Small but measurable currents could still be drawn at zero applied voltage. In fact, a retarding voltage (Ta−, Pt+) of ~ 1 volt was necessary to stop the photoconduction. The same was true for a very small leakage current driven by chemical action. Some hysteresis was evident in this region.)

This relatively efficient photoconduction was observed only for photon energies $> h\nu \sim 4.6$ ev. Measurements of the reflecting power of anodic Ta_2O_5 films of various thicknesses on bright Ta substrates showed that interference effects typical of a transparent film were prominent for $h\nu < 4.6$ ev. These abruptly ceased at 4.6 ev. Beyond this point, the reflecting power exhibited only the slow variation typical of first-surface reflection from an opaque film. One concludes that the fundamental absorption edge of anodic Ta_2O_5 is close to 4.6 ev and that this absorption is responsible for the observed photoconduction. Further, the absorption constant for $h\nu > 4.6$ ev exceeds 10^5 cm^{-1}. At $h\nu = 4.89$ ev, most of the radiation that enters a film thicker than about 150A is absorbed. Thus, the absorption and the photoconductive quantum yield does not change with forming voltage above 10 volts. Below this value, the film is too thin to absorb all of the entering radiation, and the photoconduction decreases with decreasing forming voltage.

The small photocurrent drawn at zero applied voltage may be classed as a kind of photovoltaic or Becquerel effect. We may safely assume that there is a gradient in chemical composition as we progress from Ta to electrolyte in the Ta_2O_5 film.[3] The oxide should become less *n*-type (or more *p*-type) in this same direction. An electrostatic field is thus present, and the energy of an electron at the bottom of the conduction band increases from the Ta side to the electrolyte side of the film. Charges freed by the absorption of light will thus migrate even when no voltage is applied externally, and a photocurrent results. This current will only be stopped when an external voltage is applied in the retarding direction and is sufficient to level the bottom of the

[1] A. Guntherschulze and H. Betz, *Electrolytic Condensers* (M. Krayn, Berlin, 1947).

[2] D. A. Vermilyea, private communication. The value given in reference 1 is apparently too small.

[3] H. E. Haring, J. Electrochem. Soc. **99**, 30 (1952) and references cited there.

conduction band. This naive model neglects, of course, such possibly important influences as electronic work functions and other surface properties at the interfaces. Nevertheless, it is useful in correlating some of the main features of the film behavior.

The linear variation of photocurrent with voltage below the forming potential is of interest, particularly since the leakage current is very nonlinear. The situation appears somewhat similar to that in thin semiconductor films in vacuum.[4]

We wish to thank J. K. Bragg, M. H. Hebb, J. P. Howe, D. Turnbull, and D. A. Vermilyea for valuable conversations.

[4] P. K. Weimer and A. D. Cope, RCA Rev. **12**, 326 (September, 1951); Forgue, Goodrich, and Cope, RCA Rev. **12**, 338 (September, 1951).

PHYSICAL REVIEW VOLUME 88, NUMBER 1 OCTOBER 1, 1952

Multiple Scattering of Fast Protons in Photographic Emulsions*†

MARTIN J. BERGER‡
Department of Physics and Institute for Nuclear Studies, University of Chicago, Chicago, Illinois
(Received April 21, 1952)

Measurements have been made of the multiple Coulomb scattering of protons with energies of 337±1 Mev and 218±2 Mev in Ilford G-5 emulsions. A total of 261 tracks with a combined length of 130.4 cm were analyzed by the determination of the lateral multiple scattering deflections according to the "coordinate method." The results are summarized in terms of the customary scattering factors which, for a given cell length, indicate the proportionality of the average multiple scattering deflection to the quantity "charge/momentum×velocity" of the scattered particle. Scattering factors are given for cell lengths of 250, 500, 750, and 1000 microns. These results are compared with the predictions of various theories of multiple scattering, including those of Moliere, Snyder, and Scott, as well as a proposed extension of the theory of Goudsmit and Saunderson, which has the advantage of being directly and conveniently applicable to the analysis of lateral multiple scattering deflections. The predicted theoretical scattering factors are in fair agreement with the experimental values, but slightly larger; the discrepancies are either within, or just outside of, the limits of the experimental error (3–6 percent).

I. INTRODUCTION

THE energy of charged particles can be determined by the measurement of the deflections of their tracks in photographic plates caused by multiple scattering, i.e., frequent and predominantly small-angle Coulomb scattering. This method has been developed by various investigators in the course of cosmic ray research[1–5] and has more recently been applied to fast electrons from nuclear reactions and from accelerators.[6,7] It was the purpose of this investigation to determine the multiple scattering of artificially accelerated high energy protons. A preliminary account of some of the results of the experiment has been presented in a previous communication.[8] Measurements of the multiple scattering of fast protons under controlled conditions have also been reported by Gottstein *et al.*[9]

The evidence presented here is based on the analysis of the lateral multiple scattering deflections that occurred in 130.4 cm of track of protons with energies of 337±1 Mev and 218±2 Mev in Ilford G-5 emulsions that had been exposed to the external beam of the 184-in. Berkeley cyclotron.[10] Since the energy of this beam is known with an accuracy of 0.3 percent, the multiple scattering calibration was thus freed of the error introduced by the uncertainty of the particle energy that occurs with cosmic-ray particles whose energies must be determined by grain counts or range measurements, or with fast electrons which may suffer considerable radiative energy loss.

II. ANALYSIS OF THE TRACKS

The method of determining the multiple scattering from the deflections of the tracks is illustrated by Fig. 1. The heavy winding curve represents a track of a particle passing successively through points P_1, P_2, and P_3, as projected onto a plane parallel to the surface of the emulsion. Point P_2 divides the portion of track shown

* This work was supported by the joint program of the ONR and AEC.
† Based on a doctoral dissertation submitted to the University of Chicago.
‡ Now Postdoctoral Fellow in statistics and physics, University of Chicago, Chicago, Illinois.
[1] Goldschmidt-Clermont, King, Muirhead, and Ritson, Proc. Phys. Soc. (London) **61**, 183 (1948).
[2] S. Lattimore, Nature **161**, 518 (1948).
[3] Y. Goldschmidt-Clermont, Nuovo cimento **7**, 331 (1950).
[4] P. H. Fowler, Phil. Mag. **41**, 169, 413 (1950).
[5] R. L. Setti, Nuovo cimento **8**, 96 (1951).
[6] D. R. Corson, Phys. Rev. **84**, 605 (1951).
[7] L. Voyvodic and E. Pickup, Phys. Rev. **81**, 471, 890 (1951); **85**, 91 (1952).
[8] Berger, Lord, and Schein, Phys. Rev. **83**, 850 (1951).
[9] Gottstein, Menon, Mulvey, O'Ceallaigh, and Rochat, Phil. Mag. **42**, 708 (1951).
[10] The plate exposures were obtained through the courtesy of Professors E. O. Lawrence and W. Barkas of the Radiation Laboratory of the University of California.

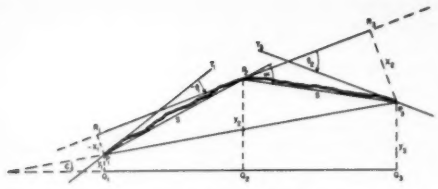

FIG. 1. Geometrical analysis of a track.

in Fig. 1 into two equal cells of length s. Lines P_1T_1, R_1R_3, and T_3P_3 are tangent to the track at P_1, P_2, and P_3, respectively. Line Q_1Q_3 is a reference line, approximately parallel to the track with respect to which the coordinates of the points P_1, P_2, and P_3 are, respectively, y_1, y_2, and y_3.[11] In the absence of scattering the track would be rectilinear. Hence in Fig. 1, $-x_1$ and x_2 are the lateral spatial multiple scattering deflections in cells (P_1, P_2) and (P_2, P_3), as projected on planes containing the direction of emergence, respectively, incidence, of the particle.[12] The probability distributions of $-x_1$ and x_2 are the same, provided one averages over all possible directions of incidence in cell (P_1, P_2) and emergence in cell (P_2, P_3) (see Appendix, Sec. C).

It follows from simple geometric considerations that, if the multiple scattering deflections are small, the angle α between successive chords P_1P_2 and P_2P_3 is

$$\alpha=(x_2-x_1)/s, \tag{1}$$

and that

$$x_2-x_1=(2y_2-y_1-y_3)=-\Delta^2y_1.^{13} \tag{2}$$

Let y_t $(t=1,2,\cdots,k+1)$ be the set of coordinates of a track divided into k cells of lengths s. Then the lateral multiple scattering is specified by the set of second coordinate differences Δ^2y_t, or chord-angles α_t $(t=1,2,\cdots,k-1)$. It has become customary to express this information in terms of a scattering factor as follows:

$$K=\langle\Delta^2y\rangle\frac{1}{s}\left(\frac{100}{s}\right)^{\frac{1}{2}}\frac{pv}{Z}=\langle\alpha\rangle\left(\frac{100}{s}\right)^{\frac{1}{2}}\frac{pv}{Z}, \tag{3}$$

where Z, p, and v are the charge, momentum, and velocity of the scattered particle. The numerical values of the scattering factor K are given for the case that $\langle\alpha\rangle$ is expressed in degrees, s in microns and (pv) in Mev. The use of such a scattering factor is motivated by the fact that K is approximately constant, and thus expresses the universal scattering properties of the photographic emulsion.[14] The average values $\langle\Delta^2y\rangle$ and $\langle\alpha\rangle$ used in expression (3) may be defined in a number of different ways. We shall in this paper consider the following averages:

(a) Arithmetic mean

$$\langle|\Delta^2y|\rangle=\frac{1}{k-1}\sum_{t=1}^{k-1}|\Delta^2y_t|.$$

(b) Arithmetic mean with cutoff

$$\langle|\Delta^2y|\rangle_c=\frac{1}{k'}\sum_{t=1}^{k-1}W_t'|\Delta^2y_t|,$$

where

$$W_t'=1 \quad \text{if} \quad |\Delta^2y_t|\leq 4\langle|\Delta^2y|\rangle_c,$$
$$W_t'=0 \quad \text{otherwise};$$
$$k'=\text{number of nonzero } W_t'\text{s}.$$

(c) Root mean square value with cutoff

$$\langle(\Delta^2y)^2\rangle_c^{\frac{1}{2}}=\left\{\frac{1}{k''}\sum_{t=1}^{k-1}W_t''(\Delta^2y_t)^2\right\}^{\frac{1}{2}},$$

where

$$W_t''=1 \quad \text{if} \quad |\Delta^2y_t|\leq 4\langle(\Delta^2y)^2\rangle_c^{\frac{1}{2}},$$
$$W_t''=0 \quad \text{otherise};$$
$$k''=\text{number of nonzero } W_t''\text{s}.$$

The corresponding scattering factors for these three cases are K_1, K_1^c, and K_2^c, respectively. The averages of α are defined in an analogous fashion in the three cases. The purpose of the truncated averages (b) and (c) is to reduce the statistical fluctuations caused by the comparatively rare large single scattering deflections which may give rise to occasional very large second coordinate differences or chord-angles. Previous experimental multiple scattering determinations have been mainly concerned with the scattering factors K_1 and K_1^c, while the theory outlined in the next section is applicable to K_2^c.

III. THEORIES OF MULTIPLE SCATTERING

A. General Remarks

Multiple scattering deflections are the sum of numerous small and a few comparatively large single scattering deflections. Hence their probability distribution is approximately Gaussian with an added "single scattering tail." The Gaussian part of the distribution has been determined in the approximate theories of Williams and Fermi as presented by Rossi and Greisen.[15] The ac-

[11] In the present experiment, the angle ϵ between the chord to the track and the reference line was always smaller than 1°.

[12] The convention has been adopted of giving a negative (positive) algebraic sign to deflections projected on a plane containing the direction of emergence (incidence) when they are directed toward the reference line with respect to which the coordinates are determined, and the opposite sign when the deflections are directed away from the reference line.

Actually it is not strictly true that $-x_1$ and x_2 are deflections projected on the planes of emergence or incidence, since the tracks are slightly inclined with respect to the plane of projection. But the tracks used in this experiment were long ($\geq$8000 microns) compared to the thickness of the emulsion ($\leq$600), so that the angle of dip was less than 4°, and the error caused by it negligible.

[13] Δ is a difference operator: $\Delta y_t=y_{t+1}-y_t$, $\Delta^2y_t=\Delta(\Delta y_t)=y_{t+2}-2y_{t+1}+y_t$, etc.

[14] Actually K is slightly dependent on s and (pv). Hence it seems preferable to use the term "scattering factor" instead of the term "scattering constant" often found in the literature.

[15] B. Rossi and K. Greisen, Revs. Modern Phys. **13**, 241 (1941); this paper contains a presentation of the calculations of Fermi, and of a simplified version of the theory of E. J. Williams.

curacy of the multiple scattering measurements in photographic emulsions is such, however, that it becomes necessary to use the more detailed theories such as those of Williams,[16] Moliere,[17] and Snyder and Scott,[18,19] which also take into account the single scattering tail. In these theories the increased accuracy had to be obtained at the expense of increased complexity, their results being given to a large extent in numerical rather than analytical form. All of the treatments mentioned so far give the distribution of the angular multiple scattering deflection; the distribution of the lateral deflections is only given by the theories of Fermi, and of Snyder and Scott (who have not worked it out in quite the same numerical detail as the angular distribution, however). In order to make the exact angular distributions applicable to the method of track analysis in terms of second coordinate differences or chord-angles as described in the previous section, one may use the relation between the mean square angular and lateral projected multiple scattering deflections

$$s^2\langle\phi^2\rangle = 3\langle x^2\rangle, \tag{4}$$

predicted by the theory of Fermi and generally valid in the small angle approximation. In Fig. 1, the projected angular deflections corresponding to the lateral deflections $-x_1$ and x_2 are designated $-\phi_1$ and ϕ_2. It follows readily from (1) and (4) that $\langle\alpha^2\rangle^{\frac{1}{2}} = (2/3)^{\frac{1}{2}}\langle\phi^2\rangle^{\frac{1}{2}}$. The same factor of proportionality $(2/3)^{\frac{1}{2}}$ has in previous multiple scattering determinations using photographic plates also been assumed to hold for the mean angular and lateral deflections (both with and without a cutoff). This is an accurate approximation justified by the theory of Snyder and Scott.

B. An Extension of the General Theory of Goudsmit and Saunderson

Both the theories of Moliere, and of Snyder and Scott, have been shown to be special cases (small angle approximation) of the more general theory of Goudsmit and Saunderson.[20] This theory, which gives the angular multiple scattering distribution, has the following advantages: (1) The theory can be used in conjunction with an arbitrary underlying single scattering law, which makes it easy to take into account—to any desired degree of approximation—the modifications introduced into the Coulomb scattering of charged particles by atoms as the result of screening of the nuclear charge by the atomic electrons, and of the interference effects caused by the finite size of the nucleus; (2) Goudsmit and Saunderson's theory can readily be extended to provide simple expressions for the average lateral multiple scattering deflection, and thus can be made applicable to the coordinate method of analyzing tracks in photographic emulsions.

Consider a particle traversing a path length s in a scattering medium, and let x be the lateral multiple scattering deflection as projected on a plane containing the direction of incidence (direction of motion at $s=0$). It is shown in the Appendix [see Eq. (A26)] that the following expression holds for the average deflection as function of the path length s, provided that the particle is scattered in a thin layer of matter and predominantly in the forward direction (as is the case for fast charged particles undergoing multiple Coulomb scattering in photographic emulsions):

$$\langle x^k|s\rangle = k\int_0^s (s-s')^{k-1}\langle\sin^k\theta\cos^k\varphi|s'\rangle ds'. \tag{5}$$

In Eq. (5) $\langle\sin^k\theta\cos^k\varphi|s\rangle$ is an average angular multiple scattering deflection; it can be found from the theory of Goudsmit and Saunderson, according to which the probability $F(\theta,\varphi|s)\sin\theta d\theta d\varphi$ that a particle moving initially (at $s=0$) in the z direction, will be deflected by multiple scattering into direction $(\theta,\theta+d\theta)$, and $(\varphi,\varphi+d\varphi)$, is given by

$$F(\theta,\varphi|s)\sin\theta d\theta d\varphi = \sum_{n=0}^{\infty}\frac{2n+1}{4\pi}P_n(\cos\theta) \times\exp\left\{-N\int_0^s ds'\int_0^{s'}\sin\theta' d\theta' I(\theta') \times[1-P_n(\cos\theta')]\right\}\sin\theta d\theta d\varphi, \tag{6}$$

where P_n is the nth Legendre polynomial, N is the number of scattering centers per unit volume, and $I(\theta)$ is the underlying single scattering law.

In the Appendix, a more complicated expression is also derived for $\langle x^k|s\rangle$ which holds without any approximation. It can be used when one is dealing with slow particles in photographic emulsions, while it reduces to the simpler expression (5) for fast particles.

C. Application to Multiple Coulomb Scattering

In applying the foregoing results to multiple Coulomb scattering we shall follow Williams[16] in assuming for the interaction between charged particles and atoms a potential

$$V(r) = \frac{ZZ'e^2}{r}e^{-r/a}(1-e^{-2r/b}), \tag{7}$$

which can be shown to give, in the Born approximation, a single scattering cross section,

$$I(\theta) = \frac{2\pi Z^2Z'^2e^4}{p^2v^2} \times\left\{\frac{1}{\sin^2\frac{1}{2}\theta+\frac{1}{4}\omega_0^2}-\frac{1}{\sin^2\frac{1}{2}\theta+\frac{1}{4}\omega_0^2(1+2\omega_2/\omega_0)^2}\right\}^2. \tag{8}$$

[16] E. J. Williams, Proc. Roy. Soc. (London) **A169**, 531 (1939); Phys. Rev. **58**, 292 (1940).
[17] G. Moliere, Z. Naturforsch. **3a**, 78 (1948).
[18] H. S. Snyder and W. T. Scott, Phys. Rev. **76**, 220 (1949); **78**, 223 (1950).
[19] W. T. Scott, Phys. Rev. **85**, 245 (1952).
[20] S. Goudsmit and J. L. Saunderson, Phys. Rev. **57**, 24 (1940); **58**, 36 (1940).

Notations: Z' and A: atomic number and weight of the scattering atom; Z, p, V and $2\pi\lambda$: charge number, momentum, velocity, and de Broglie wavelength of the scattered particle; e and m: charge and mass of the electron; h: Planck's constant; c: velocity of light; a and b: maximum and minimum impact parameters.

$$\omega_0=\lambda/a \quad \text{and} \quad \omega_2=\lambda/b.$$

In the potential (7) the factor $\exp(-r/a)$ takes into account the screening of the nucleus by the atomic electrons, which sharply reduces the scattering cross section for angles less than ω_0; the factor $[1-e^{-2\pi r/b}]$, derived on the assumption that the electric charge of the nucleus is distributed uniformly over a sphere of radius b, takes into account the interference effects resulting from the finite size of the nucleus which cut down the scattering for angles larger than ω_2. We shall set the maximum impact parameter

$$a=0.881a_0[1.13+3.76(ZZ'e/137v)^2]^{-\frac{1}{2}}, \qquad (9)$$

where $a_0=(h^2/me^2)(Z')^{-\frac{1}{3}}$ is the first Bohr radius of the atom. Moliere[21] has shown that in the case $b=0$ (nuclear point charge) the use of an impact parameter of this form will assure the validity of the scattering law (8), even if the condition for the applicability of the Born approximation ($ZZ'e/137v\ll 1$) is not strictly fulfilled, a circumstance that may easily arise with photographic emulsions in which most of the scattering is due to silver ($Z'=47$) and bromine ($Z'=35$). It seems plausible that for the case $b\neq 0$ the impact parameter a given by (9) is also adequate. Finally, we set the nuclear radius $b=1.4\times 10^{-13}A^{\frac{1}{3}}$.

Substituting (8) into (6), computing from (6) the value of $\langle \sin^k\theta\cos^k\varphi|s\rangle$ and substituting it into (5), one finds by a straightforward calculation that

$$\langle x^2|s\rangle=\tfrac{1}{3}n\omega_0^2s^2\log\left[\frac{\omega_2}{\omega_0}\left(1+2\frac{\omega_0}{\omega_2}\right)^{-1}\frac{2}{e}\right], \qquad (10)$$

where $n=4\pi Na^2s(ZZ'e/137v)^2$ denotes the average number of individual collisions which the particle makes in traversing a distance s. This result is the same as that predicted by the theory of Fermi, except for the correction factor $(2/e)(1+2\omega_0/\omega_2)^{-1}$ in the logarithm. But the distribution of the lateral multiple scattering deflections will in general not be Gaussian, unless the particle traverses a very large thickness of material, even though the finite size of the nucleus provides a cutoff ω_2 for the size of the individual angular single scattering deflections. This can easily be seen by considering the ratio $M=\langle x^4|s\rangle/\langle x^2|s\rangle^2$ which for a Gaussian distribution has the numerical value 3. We find from (5), (6), and (8) that

$$M=\frac{2.7}{n}\left\{\log\left[\frac{\omega_2}{\omega_0}\left(1+2\frac{\omega_0}{\omega_2}\right)^{-1}\frac{2}{e}\right]\right\}^{-2}\left(\frac{\omega_2}{\omega_0}\right)^2+1.8. \qquad (11)$$

[21] G. Moliere, Z. Naturforsch. **2a**, 133 (1947).

Numerical example: 340-Mev protons in Ilford G-5 emulsion.

	Silver	Bromine
Density in emulsion	1.85 g/cm³	1.36 g/cm³
n = number of collisions in path length of s microns	$2.60s$	$2.22s$
ω_2/ω_0	1324	1834
$M(s)$	$1.8+3.85\times 10^4/s$	$1.8+7.88\times 10^4/s$
M(2000 microns)	21.0	41.2

D. Mean Square Lateral Deflection with Cutoff

The mean square lateral multiple scattering deflection,

$$\langle x^2\rangle=\frac{1}{k}\sum_{i=1}^{k}x_i^2,$$

estimated from k observed deflections $x_1, x_2\cdots, x_k$, has a standard deviation equal to $\langle x^2\rangle[(M-1)/k]^{\frac{1}{2}}$. Thus if M is large the statistical fluctuations are also large. As has already been mentioned, this situation is remedied and M reduced by the use of a weighted average in which multiple scattering deflections larger in absolute value than some chosen limit (say, four times the root mean square deflection)[22] are given weight zero. We proceed to derive a theoretical expression for a mean square deflection with such a cutoff.

According to (8), the magnitudes of the angular single scattering deflections are essentially confined to the range (ω_0, ω_2); we note that $\omega_2/\omega_0=a/b\gg 1$. Let us choose an angle ω, such that $\omega_0\ll\omega_1\ll\omega_2$. Then the probability p_k that a particle traversing a distance s in a scattering medium will be deflected exactly k times through angles $\theta>\omega$, is given by the Poisson law:

$$p_k=\frac{1}{k!}\left[n\left(\frac{\omega_0}{\omega_1}\right)^2\right]^k\exp\left[-n\left(\frac{\omega_0}{\omega_1}\right)^2\right],$$

where n is the average number of all deflections. Let $f_k(x)$ be the distribution of lateral multiple scattering deflections corresponding to this contingency. Then the general lateral multiple scattering distribution may be written:

$$f(x)=\sum_{k=0}^{\infty}f_k(x)p_k.$$

If we furthermore require that $n(\omega_0/\omega_1)^2\ll 1$,

$$f(x)\cong[1-n(\omega_0/\omega_1)^2]f_0(x)+n(\omega_0/\omega_1)^2f_1(x). \qquad (12)$$

If the multiple scattering deflections are small, it is a good approximation to set

$$\int x^2f_1(x)dx=\int x^2f_0(x)dx+\int x^2h(x)dx, \qquad (13)$$

where $h(x)$ is the lateral single scattering distribution

[22] Under the conditions of the present experiment, on the order of 1 percent of the data were lost by such a cutoff. A smaller cutoff would have resulted in a slight further reduction of M, which would have been more than counterbalanced, however, by the increased loss of data.

corresponding to one Coulomb collision resulting in an angular deflection in the range (ω_1, ω_2). Thus, according to (12) and (13),

$$\langle x^2\rangle = \int x^2 f(x)dx = \int x^2 f_0(x)dx + n\left(\frac{\omega_0}{\omega_1}\right)^2 \int x^2 h(x)dx. \quad (14)$$

This separation of the mean square deflection into a true multiple scattering component $\langle x^2\rangle_0 = \int x^2 f_0(x)dx$ and a single scattering component $\langle x^2\rangle_1 = n(\omega_0/\omega_1)^2 \times \int x^2 h(x)dx$ has the advantage that a properly chosen cutoff may be applied, which—as we shall see—will affect the single scattering component $\langle x^2\rangle_1$ only.

The moments of $f_0(x)$ can be calculated by means of the general multiple scattering theory. The only differences compared to the previous calculation leading to formulas (10) and (11) is the use of a sharp cutoff ω_1 for the individual angular deflections instead of the more gradual cutoff at ω_2. With the use of the single scattering law

$$I(\theta) = \frac{2\pi Z'^2 Z^2 e^4}{p^2v^2} \frac{1}{(\sin^2\frac{1}{2}\theta + \frac{1}{4}\omega_0^2)^2} \quad \text{if} \quad 0 \leq \theta \leq \omega_1, \quad (15)$$

$$I(\theta) = 0 \quad \text{if} \quad \theta > \omega_1,$$

one finds

$$\langle x^2 | s\rangle_0 = \tfrac{1}{3} n\omega_0^2 s^2 [\log(\omega_1/\omega_0) - \tfrac{1}{2}] \quad (16)$$

and

$$M_0 = \langle x^4 | s\rangle_0 / \langle x^2 | s\rangle_0^2 = \frac{2.7}{n[\log(\omega_1/\omega_2) - \frac{1}{2}]^2}\left(\frac{\omega_1}{\omega_0}\right)^2 + 1.8. \quad (17)$$

The numerical value of M_0 is of interest. Let us assume, for the sake of concreteness, that ω_1 is chosen so that $n\omega_0/\omega_1 = 1/20$. This means that the probability of the occurrence of two or more collisions in the path length s, resulting in deflections larger than ω_1, is equal to $1-\exp(-1/20)-(1/20)\times\exp(-1/20) = 0.12$ percent. Corresponding to $n = 10^2$, 10^3, or 10^4 collisions one finds that $M_0 = 3.04$, 2.48, and 2.23, respectively. Now for a normal distribution ($M = 3$) a cutoff at four times the standard deviation will reduce the second moment by only 0.11 percent. But $f_0(x)$ has a dispersion (as indicated by M_0) less than a normal distribution for $n > 100$; hence $\langle x^2\rangle_0$ will practically not be affected by the introduction of such a cutoff.

It remains to determine $h(x)$. Employing now the small angle approximation, we consider a particle traveling in the direction of the z axis, which while traversing a layer of matter of thickness s makes one collision with a resulting angular deflection in the range (ω_1, ω_2) at a random point in the layer, after it has traveled a distance $s-t$. The lateral deflection resulting from such a collision is $x = \theta t \cos\varphi$. The joint probability density of ϑ, φ, and t is, approximately,

$$g(\theta, \varphi, t)d\theta d\varphi dt = \frac{\omega_1^2}{\pi\{1-(\omega_1/\omega_2)^2\}} \frac{d\theta}{\theta^3} d\varphi dt, \quad (18)$$

$$\omega_2 \geq \theta \geq \omega_1, \quad s \geq t \geq 0, \quad \pi \geq \varphi \geq -\pi.$$

By transforming (18) into a joint probability density for x, φ, and t, and integrating over t and φ, with due regard for the inequalities for the variables in (18), one finds

$$h(x)dx = dx \int dt \int d\varphi g\left(\frac{x}{t\cos\varphi}, \varphi, t\right) \frac{\partial(\theta, \varphi, t)}{\partial(x, \varphi, t)}$$

$$= \frac{1}{3\pi\{1-(\omega_1/\omega_2)^2\}} \frac{dx}{\omega_1 s}\left\{H\left(\frac{x}{\omega_1 s}\right) - \left(\frac{\omega_1}{\omega_2}\right)^3 H\left(\frac{x}{\omega_2 s}\right)\right\} \quad \text{if} \quad |x| \leq \omega_1 s,$$

$$= \frac{1}{3\pi\{1-(\omega_1/\omega_2)^2\}} \frac{dx}{\omega_1 s}\left\{\frac{\pi}{2}\left(\frac{\omega_1 s}{x}\right)^3 - \left(\frac{\omega_1}{\omega_2}\right)^3 H\left(\frac{x}{\omega_2 s}\right)\right\} \quad \text{if} \quad \omega_1 s \leq |x| \leq \omega_2 s, \quad (19)$$

$$= 0 \quad \text{if} \quad |x| \geq \omega_2 s,$$

where

$$H(x) = \log\left[\frac{1+(1-x^2)^{\frac{1}{2}}}{1-(1-x^2)^{\frac{1}{2}}}\right] + \tfrac{1}{3}[\sin^{-1}x - x(1-x^2)^{\frac{1}{2}}].$$

According to (19),

$$\int_{-u}^{u} x^2 h(x)dx = \frac{\omega_1^2 s^2}{6}\left[\log\left(\frac{2u}{s\omega_1}\right)^2 - \frac{1}{3}\right], \quad (20)$$

provided that $u \geq \omega_1 s$. The final result, obtained by combining (14), (13), and (20), is

$$\langle x^2 | s, u\rangle = \int_{-u}^{u} x^2 f(x)dx = \frac{1}{3}\omega_0^2 s^2 n\left(\log\frac{2u}{s\omega_0} - \frac{2}{3}\right). \quad (21)$$

In accordance with experimental practice, u is then chosen so as to satisfy the implicit relation $u = u_0 = 4\langle x^2 | s, u_0\rangle^{\frac{1}{2}}$.

It is a satisfactory feature that the angle ω_1 which was introduced as an artifice to facilitate the calculation but which has no clear-cut physical significance, has disappeared from the final result.

Formula (21) has been compared with the predictions of other theories. Calculations based on numerical values given by Moliere, and by Snyder and Scott for the angular scattering distribution, and on the relation $3\langle x^2\rangle = s^2\langle\phi^2\rangle$ between lateral and angular mean square deflections, gave results for $\langle x^2 | s, u_0\rangle$ that agreed to within the limits of error of the computation (1–2 percent) with Eq. (21). This equivalence was found to hold

under a wide range of conditions (n=av. no. of collisions ranging from 100 to 84000). Expression (21) thus provides a convenient substitute for numerical calculations. Moreover, the same approach may readily be adapted for use in conjunction with some other assumed form of the underlying single scattering law.

A calculation of $\langle x^4|s_1u_0\rangle$ (with $u_0=4\langle x^2|s_1u_0\rangle^4$), either by a method similar to that used above for $\langle x^2|s_1u_0\rangle$, or with the use of the numerical tables given by Snyder and Scott, indicates that $M(u_0)=\langle x^4|s_1u_0\rangle/\langle x^2|s_1u_0\rangle^2\sim 3.7$, so that the cutoff will considerably reduce the statistical fluctuations.

For scattering by a mixture of substances, as in photographic emulsions, we shall follow Snyder and Scott in using an effective average number of collisions n_{eff}, and an effective minimum angle ω_{0eff}, defined by

$$n_{eff}=\sum_i n_i, \tag{22}$$

$$n_{eff}\omega_{0eff}^2=\sum_i n_i\omega_{0i}^2, \tag{23}$$

where n_i and ω_{0i} are the parameters appropriate for the i'th substance. A cutoff may then be applied after the substitution of n_{eff} and ω_{0eff} in (21).

IV. EXPERIMENTAL PROCEDURES

A. Source of Data

The proton tracks to be analyzed were obtained by the exposure of Ilford G-5 plates that were dropped through the proton beam of the Berkeley 184-in. cyclotron, which has an energy of 340.0±0.8 Mev.[23] In some of the exposures, the protons were first slowed down by a block of aluminum with a thickness of 42.210 g/cm² before entering the plates, which reduced their energies to 222±2 Mev.[24] The direction of entry of the protons into the plates was almost parallel to the emulsion surface. Most of the tracks were longer than 8000 microns. In order to avoid the effects of possible emulsion distortion in the edge zones of the plates, the multiple scattering was determined only in a portion of the tracks, averaging 5000 microns in length, that followed the first 1500 microns of track as measured from the point of entry of the protons into the emulsion, whereby sections of track lying closer than 50 microns to the surface of the emulsion were practically also excluded. Otherwise the selection of tracks was random. The direction of motion of the protons in the emulsion could easily be determined from the occasional stars which they produced. Energy loss in the emulsion was calculated to reduce the mean proton energy in the measured portion of each track to 337 Mev without, and 218 Mev with the intermediate aluminum layer. Nine different plates were used, with thicknesses of 200, 400, and 600 microns and surface areas of 2 in.×4 in. and 3 in.×4 in.

[23] R. L. Mather, Phys. Rev. **83**, 895 (1951).

[24] This follows from Bethe's theoretical expression for energy loss by ionization as evaluated numerically by J. H. Smith [Phys. Rev. **71**, 32 (1947)]. The increase in the energy spread is due to straggling.

B. Apparatus and Measurements

The measurements were made with a Zeiss "Lumipan" microscope using a 90-power oil immersion lens. The total magnification was 1350, and the field of view had a diameter of 140 microns. The ocular of the microscope was provided with a filar micrometer, by means of which distances of the order of 0.001 micron could be measured. The regular microscope stage was mounted on a specially built stage[25] that could be moved rectilinearly in two directions at right angles to each other by means of two precision screws. By means of measurements with an interferometer it was found that the deviation from rectilinearity of the motion of the stage was less than 0.03 micron when the stage was moved over a distance of one centimeter. The microscope was mounted on a solid bench anchored to the ground in order to eliminate vibrations, and was located in a well-insulated cork-lined basement room in which the temperature was found to vary not more than 2° over periods of several days.

The procedure used for measuring the track deflections was the following. The track under consideration was lined up so that it was very nearly parallel to one of the directions of motion of the microscope stage. The thread of the filar micrometer of the eyepiece, also approximately parallel to the track, was lined up to lie across the center of a grain of the track. The stage was then moved through a distance equal to the cell length, which resulted in a displacement of the thread from the track. The distance through which the thread had to be shifted in order to be again centered on the track gave the lateral displacement or change in the y coordinate of the track with respect to the reference line (the direction of motion of the stage) (see Fig. 1). Since the ionization density of the tracks was low, it was sometimes necessary to center the thread not on a grain but on the estimated position of the track between two adjacent grains. The basic cell length was chosen to be 250 microns, while the analysis of the measurements was carried out for multiples of this unit: 250, 500, 750, and 1000 microns.

The experimentally measured scattering includes both the true multiple scattering and spurious scattering. This spurious scattering may in turn be considered to consist of two components of different origin. One of them, usually designated by the term noise level, is approximately random, and results from errors in the experimental determination of the trajectory of the particle in the photographic plate. The other component is more or less systematic and results from emulsion distortion.

The noise level, expressed in terms of a spurious average second coordinate difference, is found to be approximately independent of the cell length. It can be determined, therefore, by repeated measurements of the same track, using different cell lengths, provided

[25] Used in a previous investigation by Dr. J. Lord.

that the dependence of the true multiple scattering on the cell length is quite accurately known. Since the determination of this dependence was one of the objects of this experiment, this approach was not used. Instead, reliance was placed on measurements carried out on the tracks of particles with energies so high that any apparent scattering was certain to be spurious.[26] These measurements had to be made on plates other than those containing the proton tracks, but the experimental evidence indicates that the noise level is essentially determined by the measuring apparatus and is not affected by the idiosyncracies of individual emulsions. Numerous noise level calibrations were made periodically throughout the course of the experiment in order to make sure that the apparatus was in good working order.

The spurious second coordinate difference due to noise was found to have a root mean square value $E=0.182$ micron, and an absolute mean value $E'=0.150$ micron. The ratio $E'/E=0.824$ is compatible with the assumption that the noise level deflections have a Gaussian distribution. Variations of the cell length from 125 to 1000 microns did not result in a significant change of the noise level. The correction applied to the proton data consisted of subtracting E^2 from the observed $\langle(\Delta^2 y)^2\rangle$, and E'^2 from the observed $\langle|\Delta^2 y|\rangle^2$ and $\langle|\Delta^2 y|\rangle_c^2$.

In order to detect the possible presence of emulsion distortion, the distribution of the algebraic signs of the observed second coordinate differences was examined. Under the hypothesis that there is no emulsion distortion, positive and negative $\Delta^2 y_t$'s are equally likely; moreover, alternate $\Delta^2 y_t$'s are independent of each other; and the probability that an actually observed distribution of algebraic signs may have arisen under this hypothesis due to chance fluctuations may be calculated with the aid of formulas for the probability distribution of the number of "runs" of alternate $\Delta^2 y_t$'s.[27]

[26] The tracks used for this purpose included those of mesons with energies estimated to be 250 Bev or more that were produced in a nucleon-nucleon collision [Lord, Fainberg, and Schein, Phys. Rev. **80**, 970 (1950)], and the track of an oxygen nucleus with an estimated energy of more than 15 Bev, found in the cosmic radiation by M. Schein and J. Lord (private communication).

[27] In the sequence of second coordinate differences $\Delta^2 y_t$ $(t=1,2,\cdots)$ obtained from a track, successive $\Delta^2 y_t$'s are correlated:

$$\langle\Delta^2 y_t \cdot \Delta^2 y_{t+1}\rangle = \langle(x_{t+1}-x_t)(x_{t+2}-x_{t+1})\rangle = -\langle x_{t+1}{}^2\rangle$$

But in subsequence of alternate $\Delta^2 y_t$'s (e.g., $t=2T$, $T=1,2\cdots$) all elements are uncorrelated and independent; moreover, each is equally likely to be positive or negative. Let $P(r,k|R)$ denote the probability that in an observed ordered sequence of R alternate $\Delta^2 y_t$'s there are exactly $\Delta^2 y_t$'s with a positive sign, and that the sequence contains exactly k runs. The number of runs is equal to the number of blocks containing $\Delta^2 y_t$'s of like sign, into which the sequence can be divided; e.g., in the sequence $-++---+$, there are four runs: $-$, $++$, $---$, $+$. It can be shown [see A. M. Mood, Ann. Math. Stat. **11**, 367 (1940)] that

$$\text{if } k=2m \quad P(r,k|R)=2^{1-R}\binom{R-r-1}{m-1}\binom{r-1}{m-1};$$

$$\text{if } k=2m+1 \quad P(r,k|R)=2^{-R}\left\{\binom{R-r-1}{m}\binom{r-1}{m-1}+\binom{R-r-1}{m-1}\binom{r-1}{m}\right\}.$$

Given R, one can compute with the aid of these formulas the probability that k and r will lie in a specified range.

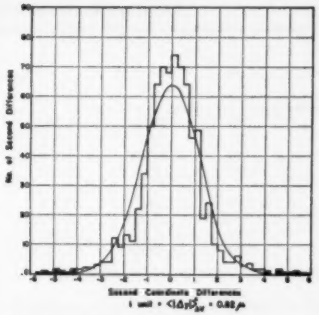

FIG. 2. Distribution of 795 uncorrelated second coordinate differences obtained from the tracks of 337-Mev protons divided into cells with a length of 500 microns.

Such a statistical analysis was applied individually to the results obtained with each of the nine plates used in this experiment. For eight of these plates the hypothesis of no distortion had a probability of 75 percent or better. For one plate (2 in.×4 in., 600 microns thick) this probability was as low as 15 percent so that, because of the suspicion of emulsion distortion, the results from this plate were not used for the computation of the scattering factors.

V. RESULTS AND CONCLUSIONS

A. Distribution of Lateral Multiple Scattering Deflections

Each second coordinate difference $\Delta^2 y_t$ is the difference of two independent lateral multiple scattering deflections. The histogram in Fig. 2 shows the distribution of 795 $\Delta^2 y_t$'s obtained from measurements on the tracks of 337-Mev protons divided into 500-micron cells. Only alternate $\Delta^2 y_t$'s were used in plotting the histogram in order to avoid correlation effects, successive $\Delta^2 y_t$'s being correlated since they have one lateral deflection in common. The scale of the abscissa is in units of $\langle|\Delta^2 y|\rangle_c$; the shaded areas to the left of -4 and to the right of $+4$ on the abscissa represent the 1.4 percent of the data eliminated when the cutoff was introduced. The curve in Fig. 2 represents a Gaussian distribution with an absolute mean value equal to $\langle|\Delta^2 y|\rangle_c$. It is seen that the experimental histogram exceeds this curve in the center and at the tails, while it is lower in the intermediary region. This is consistent with the theoretically predicted non-Gaussian shape of the distribution curve of the lateral deflections.

B. Scattering Factors

The results of the measurements are summarized in Table I, which gives, for cell lengths $s=250$, 500, 750, and 1000 microns, the number of cells included in the analysis, and the multiple scattering in Ilford G-5 emulsions, as expressed in terms of the average second

TABLE I. Multiple scattering of protons in Ilford G-5 photographic plates.

Energy T (Mev)	Cell length s (microns)	No. of cells k	Mean deflections (no cutoff) $\langle\|\Delta^2y\|\rangle$ (microns)	K_1	Mean deflections (with cutoff) $\langle\|\Delta^2y\|\rangle_c$ (microns)	$K_1{}^c$	rms deflections (with cutoff) $\langle(\Delta^2y)^2\rangle_c^{\frac{1}{2}}$ (microns)	$K_2{}^c$
337	250	3620	0.310	26.2±0.9	0.289	24.4±0.7	0.383	32.4±0.9
	500	1682	0.878	26.3±1.0	0.820	24.5±0.8	1.101	32.9±1.1
	750	1140	1.636	26.6±1.1	1.512	24.6±0.9	2.035	33.1±1.2
	1000	815	2.602	27.5±1.2	2.395	25.3±1.0	3.189	33.7±1.3
218	250	1607	0.464	26.5±1.0	0.437	25.0±0.8	0.579	33.1±1.2
	500	756	1.347	27.2±1.3	1.257	25.4±1.0	1.683	34.0±1.4
	750	496	2.509	27.6±1.5	2.337	25.7±1.2	3.127	34.4±1.6
	1000	360	3.933	28.1±1.7	3.681	26.3±1.4	4.913	35.1±1.9

coordinate differences and the corresponding scattering factors. The last two of these quantities are listed for the following three cases (see Sec. II): (a) average of absolute values without cutoff ($\langle|\Delta^2y|\rangle$ and K_1); (b) average of absolute values with cutoff at four times the experimental mean value ($\langle\Delta^2y|\rangle_c$ and $K_1{}^c$); (c) root mean square average with cutoff at four times the experimental root mean square value ($\langle(\Delta^2y)^2\rangle_c^{\frac{1}{2}}$ and $K_2{}^c$). The values given are those obtained after correcting for spurious scattering (noise level) according to the procedure described in Sec. IV B, by subtracting E'^2 from the observed $\langle|\Delta^2y|\rangle^2$ and $\langle|\Delta^2y|\rangle_c{}^2$, and E'^2 from the observed $\langle(\Delta^2y)^2\rangle_c$. ($E'=0.150$ micron, $E=0.182$ micron.) The indicated standard errors of the scattering factors were calculated on the assumption that the total error has the following three independent components whose squares are to be added: (1) the statistical error, arising from the circumstance that the scattering factors are determined from a limited number of cells;[28] (2) an error of 2 percent resulting from the expected variation of the composition of the emulsion from the nominal composition (density variations; humidity effects); (3) the error resulting from the uncertainty of the proton energy, which was assumed to be 1 percent for the 337-Mev protons, and 2 percent for the 218-Mev protons, considering the spread in the proton beam energy as well as energy loss in the emulsions.

In Fig. 3, the experimental values of the scattering factors K_1 and $K_1{}^c$ are compared with the theoretical values predicted both by the theory of Moliere,[17] and the equivalent theory of Snyder and Scott (as modified by Scott).[19] It can be seen that the experimental values are in fair agreement with, though somewhat lower than, those predicted theoretically, the discrepancies being just outside the limits of error (3–4 percent) for 337-Mev protons, and within the limits of error (3–6 percent) for the 218-Mev protons. The rise of the scattering factors with increasing cell length is less than predicted. The simple version of the theory of Williams (as presented by Rossi and Greisen) would give $K_1{}^c=32.7$ (regardless of the cell length and proton energy), which is 24 percent to 34 percent higher than the experimental results. According to calculations by Goldschmidt,[3] and Voyvodic and Pickup,[7] the more exact form of the theory of Williams is in close agreement with that of Moliere, and therefore is also consistent with the results of this experiment.

In Fig. 4, the experimental values of the scattering factor $K_2{}^c$ are compared with the corresponding theoretical values. The latter were obtained by first computing $\langle x^2|s,u_0\rangle$ with the use of (21), multiplying this result by a factor of two to obtain $\langle(\Delta^2y)^2\rangle_c$, from which $K_2{}^c$ is then found according to (3).[29] Again the experimental values are seen to lie somewhat below the theoretical curve, the discrepancy being within or just outside the probable experimental error.

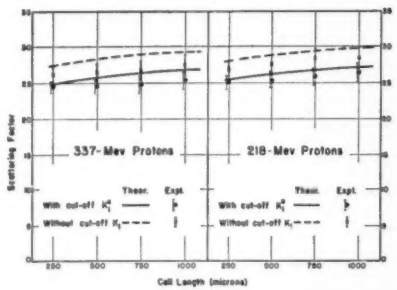

FIG. 3. Scattering factors K_1 and $K_1{}^c$ for Ilford G-5 emulsions. Comparison of the experimental results with the theory of Moliere and the equivalent theory of Snyder and Scott.

[28] The following expression can be shown to hold for the statistical error:

$$\delta K_2{}^c/K_2{}^c=\tfrac{1}{2}[(k-\tfrac{1}{2})(M-3)+(3k-4)(1+\mu^4/s^8)]^{\frac{1}{2}}(k-1)^{-1},$$

where $\delta K_2{}^c$ = standard deviation of $K_2{}^c$; k = number of cells; s = cell length (microns); $M=3.7$; $\mu=10E\ pv/K_2{}^cZs$; E = noise level (microns). The ratios $\delta K_1{}^c/K_1{}^c$ and $\delta K_1/K_1$, being based on averages of absolute values, cannot be easily calculated, but may be assumed to be of the same order of magnitude as $\delta K_2{}^c/K_2{}^c$.

[29] This step in the calculation involves a slight approximation. For the cutoff is applied to x_i theoretically, and to Δx_i experimentally. But it may be shown that the following relation holds for the distribution functions of Δx_i and x_i

$$f(\Delta x_i/A)d(\Delta x_i/A)\sim f(x_i/A')d(x_i/A'),$$

for $|\Delta x_i|\geq 4A$ and $|x_i|\geq 4A'$, where A and A' are the truncated root mean square values of Δx_i and x_i, respectively. Hence $A^2=2A'^2$. It was estimated that under the conditions of the present experiment, this approximation will introduce an error less than 1 percent into the calculated value of $K_2{}^c$.

TABLE II. Scattering factors: results of various calibrations.

Particle	Cell length (microns)	K_2^c	K_1	Reference
Electrons				
Pairs from 14.8- and 17.6-Mev Be^8 gamma-rays	15–70	21.3±1.0		Voyvodic and Pickup[a]
Electrons and positrons				
40 to 283 Mev (weighted average)		25.1±0.6		Corson[b]
Positrons				
105 Mev	200	26.2±0.6	26.7±0.6	Gottstein *et al.*[c]
185 Mev	400	24.0±0.8	24.9±0.8	Gottstein *et al.*[c]
Protons				
336 Mev	600	29.2±1.0	30.7±1.0	Gottstein *et al.*[c]
337 Mev	500	24.5±0.7	26.2±0.9	This work
218 Mev	500	25.4±1.0	27.2±1.3	This work

[a] See reference 7.
[b] See reference 6.
[c] See reference 8.

It should be mentioned that the results obtained for different plates were consistent; no significant variations of the value of the scattering constants were found beyond those to be expected on account of statistical fluctuations.

In Table II a listing is given of the scattering factors for Ilford G-5 emulsions found by various investigators under conditions such that the particle energy was controlled and approximately constant. The values obtained in this experiment which are quoted for comparison are those for a cell length of 500 microns; these are regarded as the most reliable values because their statistics are good while the noise level corrections were quite small (1.4 percent for the 337-Mev protons, and 0.7 percent for the 218-Mev protons). As previous results for photographic emulsions have been given in terms of the mean rather than the root mean square deflections, the comparison is confined to the factors K_1^c and K_1.

C. Accuracy of Energy Determinations by the Scattering Method

The measurement of a large number of tracks of particles with identical properties provided an opportunity of making an experimental check of the accuracy with which energies can be determined by the multiple scattering technique. For this purpose a group of 128 tracks of 337-Mev protons, all in one plate with dimensions 3 in.×4 in.×400 microns, were selected. Each track had a measured portion 5000 microns long and was divided into twenty cells with a length of 250 microns. With the use of the experimentally determined scattering factor K_2^c an apparent energy was computed for each track from the observed root mean square second coordinate difference (with cutoff). The resultant energy spectrum is shown in Fig. 5. The peak of the spectrum is at approximately 330 Mev, and 50 percent of the tracks underwent deflections indicating apparent energies in the range from 285 Mev to 395 Mev. The slight asymmetry of the histogram is not due to an asymmetry of the scattering deflections, but arises from the transformation to a kinetic energy scale. The histogram in Fig. 5 may also be interpreted to represent the inherent uncertainty of an energy determination based on the knowledge of the true scattering factor and measurements made on a single track 5000 microns long and divided into 20 cells, the probable error in this case being approximately 20 percent.

ACKNOWLEDGMENTS

The author takes pleasure in acknowledging the encouragement and valuable advice received from Professor Marcel Schein. He is also indebted to Professors E. O. Lawrence and W. Barkas for arranging for the exposure of the plates to the beam of the Berkeley cyclotron, to Dr. J. J. Lord for help and advice in matters of photographic plate technique, and to Mr. Roy Berg and Mr. Lewis Leder for their assistance with the measurements.

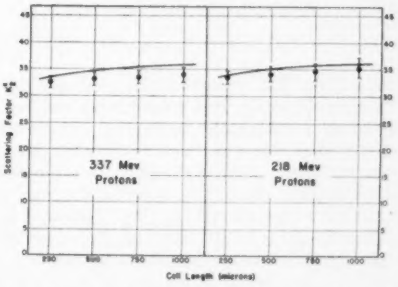

FIG. 4. Scattering factor K_2^c for Ilford G-5 emulsions. Comparison of the experimental results with the theoretical value calculated from Eq. (21).

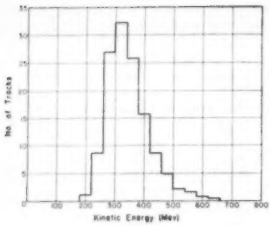

FIG. 5. Apparent energy spectrum for 128 protons with a true energy of 337 Mev, obtained by the multiple scattering method.

APPENDIX: LATERAL MULTIPLE SCATTERING DEFLECTIONS

A. General Theory

Let us consider a particle traveling in an infinite medium in which scattering centers are distributed at random. We describe the state of the particle by the probability density $F(\theta,\varphi,x,y,z|s)$ which is conditional on the path length s traversed by the particle; s is measured from a reference point on the trajectory which is also taken to be the origin of a Cartesian coordinate system (x,y,z) specifying the position, and a spherical coordinate system (θ,φ) specifying the direction of motion of the particle. If the particle is initially, at $s=0$, moving in the z direction, the x coordinate may be used to represent the lateral deflection as projected on the $x-z$ plane (a plane parallel to the surface of the emulsion as discussed in Sec. II). The dependence of F on y and z is then of no interest to us, and we shall ignore these coordinates from now on. The stochastic equation governing the probability density F is

$$\begin{aligned}F(\theta,\varphi,x|s+\Delta s)&=[1-NQ(s)\Delta s]F(\theta,\varphi,x-\sin\theta\cos\varphi\Delta s|s)\\&+NQ(s)\Delta s\int_0^{2\pi}d\varphi'\int_0^{\pi}d\theta'F(\theta',\varphi',x\\&-\sin\theta'\cos\varphi'\Delta s|s)\cdot\psi(\theta',\varphi';\theta,\varphi|s).\end{aligned}\quad(A1)$$

The initial condition is assumed to be

$$F(\theta,\varphi,x|0)=(2\pi)^{-1}\delta(x)\delta(\theta)\quad(A2)$$

where $\delta(x)$ and $\delta(\theta)$ are delta-functions. The first term on the right side of Eq. (A1) takes into account the case in which the particle makes no collision in the interval $(s,s+\Delta s)$, while the second term refers to the case that the particle makes one collision by which it is deflected into the direction (θ,φ). The probability of more than one collision in the interval $(s,s+\Delta s)$ is assumed to be negligibly small. N is the number of scattering centers per unit volume of the medium, $Q(s)$ is the total cross section for the underlying single scattering process, and $\psi(\theta',\varphi';\theta,\varphi|s)$ is the transition probability density for a change of direction from (θ',φ') to (θ,φ) in a single collision. ψ is assumed to obey the following conditions:

$$\psi(\theta',\varphi';\theta,\varphi|s)=\psi(\theta,\varphi;\theta',\varphi'|s)\quad\text{(symmetry)},\quad(A3)$$

$$\int_0^{2\pi}d\varphi\int_0^{\pi}d\theta\psi(\theta',\varphi';\theta,\varphi|s)=1\ \text{(normalization)}.\quad(A4)$$

The dependence of Q and ψ on s may be used to express their energy dependence, if the energy for some value of s and the energy loss as a continuous function of s are known.

From the difference equation (A1) one obtains, by going to the limit $\Delta s\to 0$, the integro-differential equation

$$\begin{aligned}\frac{\partial F(\theta,\varphi,x|s)}{\partial s}&=NQ(s)\int_0^{2\pi}d\varphi'\int_0^{\pi}d\theta'[F(\theta',\varphi',x|s)\\&\times\psi(\theta',\varphi';\theta,\varphi|s)]-NQ(s)F(\theta,\varphi,x|s)\\&-\sin\theta\cos\varphi\frac{\partial F(\theta,\varphi,x|s)}{\partial x}.\end{aligned}\quad(A5)$$

The kernel ψ, positive and symmetric in (θ,φ) and (θ',φ'), can be expanded in terms of its eigenfunctions:

$$\psi(\theta',\varphi';\theta,\varphi|s)=\sum_{n=0}^{\infty}c_n(s)\phi_n(\theta',\varphi')\phi_n(\theta,\varphi).\quad(A6)$$

The eigenfunctions ϕ_n are solutions of the integral equation

$$\begin{aligned}\phi_n(\theta,\varphi)=\frac{1}{c_n(s)}\int_0^{2\pi}d\varphi'\int_0^{\pi}d\theta'\phi_n(\theta',\varphi')\\\times\psi(\theta',\varphi';\theta,\varphi|s).\end{aligned}\quad(A7)$$

They form an orthogonal system, and will be assumed to be normalized. All the eigenvalues are real and positive. One eigenfunction, $\phi_0=1/(4\pi)^{\frac{1}{2}}$, can be found by inspection with the help of the normalization equation (A4) of the text. The corresponding eigenvalue $c_0=1$ is the largest eigenvalue since it belongs to the eigenfunction with no node.

Multiplying Eq. (A5) by x^k, substituting the expansion (A6), and integrating with respect to θ,φ and x, one finds

$$\begin{aligned}\int_0^{2\pi}d\varphi\int_0^{\pi}d\theta\int_{-z}^{z}dx\left[\frac{\partial}{\partial s}+NQ(1-c_n)\right]x^k\phi_nF\\=-\int_0^{2\pi}d\varphi\int_0^{\pi}d\vartheta\int_{-z}^{z}dx\,x^k\sin\theta\cos\varphi\phi_n\frac{\partial F}{\partial x}\\(n=0,1,2,\cdots).\end{aligned}\quad(A8)$$

The initial condition (A2) implies that

$$F(\theta,\varphi,\pm s|s)=0, \tag{A9}$$

so that

$$\frac{\partial}{\partial s}\int_{-s}^{s}x^kF\,dx=\int_{-s}^{s}x^k\frac{\partial F}{\partial S}dx$$

and

$$\int_{-s}^{s}x^k\frac{\partial F}{\partial x}dx=-k\int_{-s}^{s}x^{k-1}F\,dx.$$

Hence

$$\left[\frac{\partial}{\partial s}+NQ(1-c_n)\right]\int_0^{2\pi}d\varphi\int_0^{\pi}d\theta\int_{-s}^{s}x^k\phi_nF\,dx$$

$$=k\int_0^{2\pi}d\varphi\int_0^{\pi}d\theta\int_{-s}^{s}x^{k-1}\sin\theta\cos\varphi\phi_nF. \tag{A10}$$

It is convenient to use the notation

$$\langle f|s\rangle=\int_0^{2\pi}d\varphi\int_0^{\pi}d\theta\int_{-s}^{s}dx f(\theta,\varphi,x,s)F(\theta,\varphi,x|s),$$

$$R_n(s)=\exp\left\{-N\int_0^{s}Q(s')[1-c_n(s')]ds'\right\},$$

in terms of which the solution of (A10) may be written

$$\langle x^k\phi_n|s\rangle=kR_n(s)\int_0^{s}\frac{ds_1}{R_n(s_1)}\langle x^{k-1}\sin\theta\cos\varphi\phi_n|s_1\rangle. \tag{A11}$$

If the expansion

$$\sin\theta\cos\varphi\phi_n=\sum_{j_1}A_{j_1}{}^n\phi_{j_1} \tag{A12}$$

is substituted in (A11), the result is

$$\langle x^k\phi_n|s\rangle=kR_n(s)\sum_{j_1}A_{j_1}{}^n\int_0^{s}\frac{ds_1}{R_n(s_1)}\langle x^{k-1}\phi_{j_1}|s_1\rangle. \tag{A13}$$

Repeated application of this recursion relation yields

$$\langle x^k\phi_n|s\rangle=k!R_n(s)$$

$$\times\sum_{j_1j_2\cdots j_k}\left\{A_{j_1}{}^nA_{j_2}{}^{j_1}\cdots A_{j_k}{}^{j_{k-1}}\cdot\int_0^{s}ds_1\frac{R_{j_1}(s_1)}{R_n(s_1)}\right.$$

$$\left.\times\int_0^{s_1}ds_2\frac{R_{j_2}(s_2)}{R_{j_1}(s_2)}\cdots\int_0^{s_{k-1}}ds_k\frac{\langle\phi_{j_k}|s_k\rangle}{R_{j_k}(s_k)}\right\}. \tag{A14}$$

The remaining problem is to determine $\langle\phi_{j_k}|s\rangle$. Let

$$G(\theta,\varphi|s)=\int_{-s}^{s}dxF(\theta,\varphi,x|s).$$

It follows from (A5) and (A9), that

$$\frac{\partial G(\theta,\varphi|s)}{\partial s}=NQ(s)\int_0^{2\pi}d\varphi'\int_0^{\pi}d\theta'[G(\theta',\varphi'|s)$$

$$\times\psi(\theta',\varphi';\theta,\varphi|s)]-NQ(s)G(\theta,\varphi|s). \tag{A15}$$

Substituting in (A15) the expansion

$$G(\theta,\varphi|s)=\sum_{n=0}^{\infty}A_n(s)\phi_n(\theta,\varphi), \tag{A16}$$

and the eigenfunction expansion (A6) for the kernel ψ, one obtains the differential equations

$$[d/ds+NQ(1-c_n)]a_n=0. \tag{A17}$$

Solving for the coefficients a_n and substituting the solutions in (A16), one obtains

$$G(\theta,\varphi|s)=\sum_{n=0}^{\infty}\langle\phi_n|0\rangle\phi_n(\theta,\varphi)R_n(s), \tag{A18}$$

where

$$\langle\phi_n|0\rangle=\int_0^{2\pi}d\varphi\int_0^{\pi}d\theta G(\theta,\varphi|0)\phi_n(\theta,\varphi). \tag{A19}$$

Thus, since the ϕ_n are orthogonal,

$$\langle\phi_{j_k}|s\rangle=\langle\phi_{j_k}|0\rangle R_n(s), \tag{A20}$$

so that finally

$$\langle x^k\phi_n|s\rangle=k!R_n(s)\sum_{j_1j_2\cdots j_k}A_{j_1}{}^nA_{j_2}{}^{j_1}\cdots A_{j_k}{}^{j_{k-1}}$$

$$\times\langle\phi_{j_k}|0\rangle T_{j_1j_2\cdots j_k}{}^n, \tag{A21}$$

where

$$T_{j_1j_2\cdots j_k}{}^n=\int_0^{s}ds_1\frac{R_{j_1}(s_1)}{R_n(s_1)}\int_0^{s_1}ds_2\frac{R_{j_2}(s_2)}{R_{j_1}(s_1)}\cdots$$

$$\times\int_0^{s_{k-1}}ds_k\frac{R_{j_k}(s_k)}{R_{j_{k-1}}(s_k)}.$$

This expression gives not only the moments of x (for $n=0$), but also the product moments of x and the eigenfunctions $\phi_n(\theta,\varphi)$. It should be noted that (A18) is a generalization of the angular distribution function of Goudsmit and Saunderson [Eq. (6) of the text], to which it reduces if the underlying single scattering law

is axially symmetric so that $\psi=\psi(\cos\chi)$, where $\cos\chi=\cos\theta\cos\theta'-\sin\theta\sin\theta'\cos(\varphi-\varphi')$. In this case spherical harmonics

$$Y_{nm}=\frac{1}{2\pi}\left\{\frac{2n+1}{2}\frac{(n-m)!}{(n+m)!}\right\}^{\frac{1}{2}}P_n(\cos\theta)e^{im\varphi},$$

are the normalized eigenfunctions satisfying the integral Eq. (A5). Since these eigenfunctions are characterized by two indexes, m and n, the corresponding matrix elements in Eq. (A21) will have four indexes:

$$\left.\begin{aligned}
&A_{j_n{}^{fn}}=\int_0^{2\pi}d\varphi\int_0^{\pi}d\theta\phi_{jn}\sin\theta\cos\varphi\phi_{j_n{}'}\\
&\to A_{n'm'}{}^{fn,m}=\int_0^{2\pi}d\varphi\int_0^{\pi}d\theta Y_{nm}\sin\theta\cos\varphi Y_{n'm'}{}^{*}\\
&A_{n+1,m+1}{}^{n,m}=\frac{1}{2}\left\{\frac{(n+m+1)(n+m+2)}{(2n+1)(2n+3)}\right\}^{\frac{1}{2}},\\
&A_{n-1,m+1}{}^{n,m}=-\frac{1}{2}\left\{\frac{(n-m)(n-m+1)}{(2n+1)(2n-1)}\right\}^{\frac{1}{2}}\\
&A_{n+1,m-1}{}^{n,m}=-\frac{1}{2}\left\{\frac{(n-m+1)(n-m+2)}{(2n+1)(2n+3)}\right\}^{\frac{1}{2}},\\
&A_{n-1,m-1}{}^{n,m}=\frac{1}{2}\left\{\frac{(n+m)(n+m-1)}{(2n+1)(2n-1)}\right\}^{\frac{1}{2}}\\
&A_{n',m'}{}^{n,m}=0\quad\text{if}\quad\begin{cases}m\neq m'\pm1\\ n\neq n'\pm1\end{cases}.
\end{aligned}\right\}\text{(A22)}$$

The moments $\langle x^k\rangle$ for the case of axial symmetry have also been dealt with by Lewis,[30] who expanded them into infinite series whose coefficients are shown to obey an infinite set of coupled differential equations that can be solved recursively. The explicit solution of these equations would yield a result equivalent to (A21) with the matrix elements (A22).

B. Approximation

If the underlying single scattering is predominantly in the forward direction (which implies that (c_n-1) is small), and if the layer of matter traversed by the particle is thin (s small), then we may set

$$R_n(s)=\exp\left\{-N\int_0^s Q(1-c_n)ds\right\}=1-\delta_n s,\quad\text{(A23)}$$

where δ_n is assumed to be sufficiently small that we may neglect its second and higher powers. Then

$$\begin{aligned}
T_{j_1j_2\cdots j_k}&\cong\int_0^s ds_1\int_0^{s_1}ds_2\cdots\int_0^{s_{k-1}}ds_k\\
&\times(1+\delta_n-\delta_{j_1})(1+\delta_{j_1}-\delta_{j_2})\cdots(1+\delta_{j_{k-1}}-\delta_{j_k})\\
&\cong\int_0^s ds_1\int_0^{s_1}ds_2\cdots\int_0^{s_{k-1}}ds_k(1+\delta_n-\delta_{j_k})\\
&\cong\int_0^s ds_1\int_0^{s_1}ds_2\cdots\int_0^{s_{k-1}}ds_k\frac{R_{j_k}(s_k)}{R_{j_n}(s_k)}.
\end{aligned}\quad\text{(A24)}$$

But because of (A12) and (A21),

$$\begin{aligned}
\sum_{j_1j_2\cdots j_k}&A_{j_1{}^n}A_{j_2{}^{j_1}}\cdots A_{j_k{}^{j_{k-1}}}\langle\phi_{j_k}|0\rangle R_{j_k}(s)\\
&=\langle\sin^k\theta\cos^k\varphi\phi_n|s\rangle,
\end{aligned}\quad\text{(A25)}$$

so that

$$\begin{aligned}
\langle x^k\phi_n|s\rangle=k!\int_0^s ds_1\int_0^{s_1}ds_2\cdots\int_0^{s_{k-1}}ds_k\\
\times\langle\sin^k\theta\cos^k\varphi\phi_n|s\rangle.
\end{aligned}\quad\text{(A26)}$$

By a simple integral transformation[31] one obtains from (A26) Eq. (5) of the text (which corresponds to the case $n=0$).

C. Reversibility

In addition to the "forward" stochastic Eq. (5) of the text, one can also write down the "backward" equation

$$\begin{aligned}
F(\theta,\varphi,x|s-\Delta s)&=(1-NQ\Delta s)F(\theta,\varphi,x+\sin\theta\cos\varphi\Delta s|s)\\
&+NQ\Delta s\int_0^{2\pi}d\varphi'\int_0^{\pi}d\theta'F(\theta',\varphi',x\\
&+\sin\theta'\cos\varphi'\Delta s|s)\psi(\theta',\varphi;\theta',\varphi'|s),
\end{aligned}\quad\text{(A27)}$$

and the corresponding integro-differential equation

$$\begin{aligned}
-\frac{\partial F}{\partial s}=NQ\int_0^{2\pi}d\varphi'\int_0^{\pi}d\theta'[F(\theta',\varphi',x|s)\\
\times\psi(\theta,\varphi;\theta',\varphi'|s)]-NQF+\cos\varphi\sin\theta\partial F/\partial x.
\end{aligned}\quad\text{(A28)}$$

Let us assume that ψ and Q do not depend on s (no energy loss). Since $\psi(\theta',\varphi';\theta,\varphi)=\psi(\theta,\varphi|\theta'\varphi')$, the substitution $s'\to(-s)$ and $x'\to(-x)$ will transform (A28) into the "forward" equation (A5). Hence the solutions of the "backward" equation will be the same as that of the "forward" equation, except that the "initial" conditions (at $s=0$) become "final" conditions (at $s'=0$), i.e., refer to the direction of emergence instead of the direction of incidence of the particle.

[30] H. W. Lewis, Phys. Rev. **78**, 526 (1950).

[31] See, for example, B. Van der Pol and H. Bremmer, *Operational Calculus* (Cambridge University Press, Cambridge, 1950), p. 52.

Fission Asymmetry as a Function of Excitation Energy of the Compound Nucleus

J. L. FOWLER, W. H. JONES,* AND J. H. PAEHLER
Oak Ridge National Laboratory, Oak Ridge, Tennessee
(Received May 22, 1952)

The yield of Mo^{99} and Ag^{111} relative to Ba^{140} has been measured for proton produced fission in normal uranium. For this type of fission, as well as for fission obtained in other ways, the variation with compound nucleus excitation energy of the ratio of the yield of Ag^{111} to that of Ba^{140} is discussed in terms of the statistical theory of nuclei.

A PRELIMINARY investigation of asymmetry of fragment mass distribution from proton induced fission has been made as a function of energy in the range 11–18 Mev. Foils of normal uranium (100 mg/cm²) separated by aluminum were bombarded at a fixed radius with the internal beam of the 86-inch cyclotron. In different experiments, the energy of the proton beam at the bombarding radius was found from the known p,n and $p,2n$ excitation curves of Cu^{63} [1] and the range energy relations in copper. The 2.5 cm×0.6 cm foils of uranium and aluminum were supported behind a 11-mil window of a water-cooled Al probe, and the energy of the protons at each foil was found to ±1.0 Mev from the incident proton energy and the range energy curves in U and Al.

For each U foil, the fission yields of Mo^{99} and Ag^{111} relative to Ba^{140} were determined by use of radiochemical procedures.[2] Mo^{99} and Ba^{140} occur at the peaks of the thermal neutron fission mass distribution; Ag^{111} occurs in the valley of this distribution. Relative yields were obtained in terms of known yields by performing the identical radiochemical analysis for thermal neutron fission in similar quantities of normal uranium. Neutron fission background was found in foils placed beyond the proton range.

The ratio, Yield Mo^{99}/Yield Ba^{140}, is almost constant as a function of proton energy and is the order of 60 percent higher than in the case of thermal neutron fission in U^{235}. The ratio, Yield Ag^{111}/Yield Ba^{140}, varies with proton energy in such a way as to indicate that the probability of symmetrical fission increases rapidly with excitation energy. In Fig. 1, the asymmetry of fission as produced in a number of ways is compared. As ordinate on log scale, the ratio, Yield Ag^{111}/Yield Ba^{140}, is plotted against the quantity $(E_x-5)^{-\frac{1}{2}}$, where E_x is the bombarding particle energy plus its binding energy in Mev. The binding energies are calculated from semi-empirical mass tables.[3] The abscissa, which varies inversely as the square root of energy, suggests reciprocal nuclear temperature. The quantity 5 Mev which is subtracted from the excitation energy to give a linear relationship on the semilog plot is interpreted as the effect of cooling of the nucleus as it is distorted to give fission. This checks with the γ-ray fission threshold, which is about 5 Mev.

With $(E_x-5)^{\frac{1}{2}}=bT$, where T is the nuclear temperature of the distorted nucleus, Fig. 1 shows Yield Ag^{111}/Yield Ba^{140} varies as $3.5\exp(-9.6/bT)$. Since in the case of nuclear phenomena as well as in atomic phenomena, the relative probability of two states separated in energy by ΔE is of the form $\exp(-\Delta E/T)$, $9.6/b$ is interpreted as the energy difference between the asymmetrical mode of oscillation of the distorted uranium

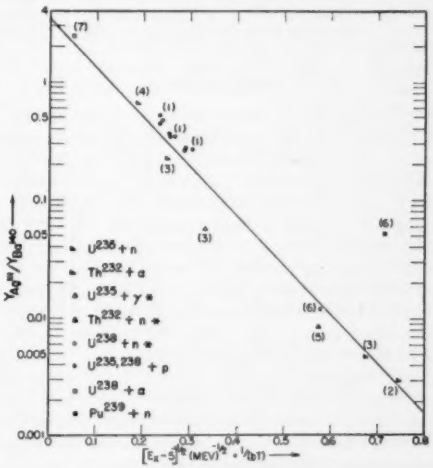

FIG. 1. Fission asymmetry as a function of excitation energy of the compound nucleus. (*) Average over neutron energy spectrum. References: (1) Jones, Fowler, and Paehler, Phys. Rev. **87**, 174 (1952); (2) Revs. Modern Phys. **18**, 513 (1946); (3) R. W Spence, unpublished Atomic Energy Commission report AECU 645 (1949); (4) A. S. Newton, Phys. Rev. **75**, 17 (1949); (5) A. Turkevich and J. B. Niday, Phys. Rev. **84**, 52 (1951); (6) Appendix B, *Radiochemical Studies: The Fission Products* (McGraw-Hill Book Company, Inc., New York, 1950), National Nuclear Energy Series, Plutonium Project Record, Vol. 9, Div. IV; (7) P. R. O'Connor and G. T. Seaborg, Phys. Rev. **74**, 1189 (1948).

* Research Participant from Emory University, Atlanta, Georgia.

[1] S. N. Ghoshal, Phys. Rev. **80**, 939 (1950).

[2] W. W. Meinke, unpublished Atomic Energy Commission report AECD 2738 (1949).

[3] N. Metropolis and G. Reilwiesner, unpublished Atomic Energy Commission report NP 1980 (1950).

nucleus and the symmetrical mode. Nuclear temperature, defined by $1/T=d\ln\omega(E)/dE$, can be estimated from the expression for nuclear level densities; $\omega(E)=C\exp[2(E/a)^{\frac{1}{2}}]$. For uranium $C=10$ and $a=0.244$ gives the observed 5 electron volt spacing of levels at excitation energy of about 6 Mev. Under the assumption that the energy level density in the distorted nucleus varies in the same way, b becomes $(0.244)^{-1}$ and ΔE is 4.7 Mev. Figure 1 then indicates that the symmetrical mode of fission requires the order of 4.7 Mev more energy than the asymmetrical mode.[4]

The authors wish to express their thanks to Professor John A. Wheeler of Princeton University for his very valuable discussion and suggestions concerning the theoretical interpretation.

[4] *Note added in proof.*—Professor V. F. Weisskopf (private communication) uses $C=0.005$ and $a=0.08$ for the level densities in uranium. With these constants, ΔE becomes 2.7 Mev.

PHYSICAL REVIEW VOLUME 88, NUMBER 1 OCTOBER 1, 1952

Non-Adiabatic Treatment of the Relativistic Two-Body Problem

MAURICE M. LÉVY
Institute for Advanced Study, Princeton, New Jersey

(Received June 2, 1952)

The method of Tamm and Dancoff, for the non-adiabatic treatment of the relativistic interaction of two nucleons, is generalized in order to include nucleon pair creation and higher order effects in the exchange of mesons. This generalized form of the Tamm-Dancoff method is shown to give results which are equivalent to those obtained from the relativistic equation of Bethe and Salpeter. A detailed study is made of two limiting cases: (a) no pair of nucleons is created in the intermediate states, but an arbitrary number of mesons can be present at the same time; (b) the maximum number of mesons present at a given time is one, but the number of pairs is unrestricted.

The two methods are applied to the calculation of the lowest order correction to the scalar meson interaction of two nucleons. It is shown that the exact correction, which is of the second order in the nucleon velocities, can only be obtained through the inclusion of the fourth- and sixth-order interaction processes involving, in the corresponding Feynman diagrams, the crossing of the meson lines.

1. INTRODUCTION

THE study of a system of two bound particles interacting through a quantized field has usually been done by means of the so-called "adiabatic" approximation, that is: an effective potential between the interacting particles is calculated, neglecting their motion during the exchange of field quanta; this potential is then introduced into a wave equation, and the motion of the interacting particles is worked out as a second step. This method yields good results for nonrelativistic potentials but fails in the case of intrinsically relativistic interactions, such as that yielded by the pseudoscalar meson theory. It has been shown, in this case,[1] that the adiabatic approximation does not allow the system to bind, even if a relativistic calculation is made to the second order in the coupling constant. Furthermore, the notion of effective potential becomes ambiguous when higher order effects are considered.[2]

Since the physical evidence has focused the attention on the pseudoscalar meson theory, it is important to calculate the energy levels of a system of two bound nucleons by means of a method which does not separate the calculation of the interaction to a given order in the coupling constant, from the derivation of the equations of motion, valid to the same order. Such an approach has first been made independently by Tamm[3] and Dancoff,[4] who derived an approximate second-order equation for two particles interacting through a scalar meson field. Another way to treat non-adiabatically a bound system of two particles is provided by the covariant equation which has been proposed by Bethe and Salpeter[5] and subsequently derived from field theory by Gell-Mann and Low.[6]

It is the purpose of the present paper:

(a) to generalize the method of Tamm and Dancoff (abbreviated as T.D. in the following) as to include pair creation and higher order effects in the exchange of mesons, in order to bring it into a suitable form for the study of the pseudoscalar meson interaction between nucleons;

(b) to compare this extended form of the T.D. formalism, where the physical meaning of all quantities is clear at all stages, with the results obtained from the equation of Bethe and Salpeter (abbreviated as B.S. in the following); it will be shown that both descriptions are equivalent, although the way in which the interaction is expanded in powers of the coupling constant is quite different;

[1] M. M. Lévy, Phys. Rev. **84**, 441 (1951).
[2] Y. Nambu, Prog. Theor. Phys. **5**, 614 (1950).
[3] I. Tamm, J. Phys. (U.S.S.R.) **9**, 449 (1945).
[4] S. M. Dancoff, Phys. Rev. **78**, 382 (1950).
[5] E. Salpeter and H. A. Bethe, Phys. Rev. **84**, 1232 (1951).
[6] M. Gell-Mann and F. Low, Phys. Rev. **84**, 350 (1951).

(c) to illustrate this equivalence and to compare the practical value of the two methods, by calculating the lowest order non-adiabatic corrections to the scalar meson interaction between two nucleons; it will be shown that the "ladder" approximation, in the B.S. equation, as well as the second-order approximation in the T.D. formalism, give rise to corrections of the first order in nucleon velocities; however, when the fourth-order effects in the exchange of mesons, especially those which correspond to interaction diagrams involving meson lines crossings, are taken into account, the non-adiabatic corrections of the first order in v/c are cancelled exactly, and the remaining corrections are of the order of v^2/c^2.

From the preceding study it will be concluded that it is more convenient to use the T.D. method when only convergent processes are taken into account; on the other hand, when renormalizations of mass and charge have to be carried out explicitly, it appears easier to use the B.S. equation. The results of the present paper provide a correspondence between the two methods, and therefore make it possible to use them concurrently, depending on the effects which have to be calculated.

The application of the general theory to the analysis of the pseudoscalar meson interaction of two nucleons and the calculation of the low energy properties of the neutron-proton system will be considered in a subsequent paper.

2. EXTENSION OF THE TAMM-DANCOFF FORMALISM

2.1. General Equations

Let us consider two nucleons (1) and (2), with wave fields $\psi(1)$ and $\psi(2)$ interacting through a neutral meson[7] field ϕ. We write the Schrödinger equation for the wave-functional Ψ of the system:[8]

$$-i\delta\Psi/\delta t=(H_0+H')\Psi, \tag{1}$$

in which H_0 is the free Hamiltonian

$$H_0=\int\{\bar{\psi}(1)H_1\psi(1)+\bar{\psi}(2)H_2\psi(2) +[\pi^2+(\nabla\phi)^2+\mu^2\phi^2]\}d^3x_1d^3x_2, \tag{2}$$

where H_1 and H_2 are the free Hamiltonian operators of particles (1) and (2), and π the field canonically conjugate to ϕ. H' is an interaction Hamiltonian, the matrix element of which describe the simultaneous creation (or annihilation) of one meson and zero or one pair of nucleons. Looking for stationary expressions of Ψ, as a function of the (common) time t, we expand it as a series of the complete and orthonormal set of eigenfunctions of H_0:

$$\Psi(t)=\sum_{\lambda,m,n} a_\lambda^{(m,n)}\psi_\lambda^{(m,n)}e^{iWt}. \tag{3}$$

In this equation, W is the total energy of the system, m the number of mesons present in the free state which is considered, n the corresponding number of pairs of nucleons; λ is a variable which specifies the momenta, spins, etc., $\cdots$ of the particles of the systems and $a_\lambda^{(m,n)}$ the quantized probability amplitude[9] of the state (λ, m, n). The solution of Eq. (1) leads to the following set of coupled integral equations:

$$[W-E_\lambda^{(m,n)}]a_\lambda^{(m,n)} =\sum_{q=n-1}^{n+1}\sum_{p=m\pm1}\sum_{\mu}(\lambda, m, n|H'|\mu, p, q)a_\mu^{(p,q)}, \tag{4}$$

where we have put:

$$(\lambda, m, n|H'|\mu, p, q)=(\psi_\mu^{(p,q)}, H'\psi_\lambda^{(m,n)}). \tag{5}$$

One of the ways of solving the system of Eqs. (4) [other ways will be considered later] consists in eliminating all the amplitudes except $a_\lambda^{(0,0)}$, by means of successive substitutions. The resulting equation is of the following form:

$$[W-E_\lambda^{(0,0)}]a_\lambda^{(0,0)}=\sum_{p,q}\sum_{\lambda'}\Delta^{(p,q)}(\lambda,\lambda')a_{\lambda'}^{(0,0)}, \tag{6}$$

where $\Delta^{(p,q)}(\lambda,\lambda')$ is an interaction term which is proportional to the $2p$th power of the coupling constant G, and which results from a series of virtual processes such that the maximum numbers of mesons and nucleon pairs in the intermediate states are, respectively, p and q.

The series on the right-hand side of (6) includes all kinds of divergent processes, such as self-energy, vacuum polarization, etc. In the framework of the present formalism, it is not possible, even if the meson interaction belongs to a renormalizable type,[10] to separate covariantly these divergences and to reinterpret them as renormalization effects of mass and charge.[11] It is possible, however, to treat them separately, by using the correspondence between the present formalism and the covariant equation of Bethe and Salpeter, which will be discussed in Sec. 3.

In the remaining paragraphs of this Section, we shall only consider virtual processes which, in quantum electrodynamics and spinless meson theories, are essentially convergent. We shall further limit ourselves to two special cases:

[7] The words "nucleon" and "meson" are used, in this section, as a matter of convenience. The formalism applies generally to two Fermi-Dirac particles interacting through a Boson field.

[8] A system of units in which $\hbar=c=1$ is used throughout this paper.

[9] These amplitudes have, of course, to be properly symmetrized. The two originally interacting nucleons are treated separately from the virtual pairs, since they cannot annihilate each other.

[10] P. T. Matthews, Phil. Mag. **41**, 185 (1950); A. Salam, Phys. **82**, 217 (1951); **84**, 426 (1951).

[11] A covariant form of the configuration space treatment of the two-body problem has recently been proposed by S. Schweber and A. Wightman (to be published). Renormalization becomes possible in their formalism, but meets with considerable difficulties, mainly because of the vacuum fluctuations of which some finite parts, depending on the total energy of the system, have to be separated and re-interpreted. The simplest way to treat radiative effects seems to be to use the equivalence between the T.D. formalism and the B.S. equation (see Sec. 3).

(a) No pair of nucleons can be produced, but an arbitrary number of mesons can simultaneously be present in the system.

(b) The maximum number of mesons at any time is one, but an arbitrary number of nucleon pairs can be present at the same time.

2.2. Higher Order Effects in the Exchange of Mesons (No Pairs Present)

For this problem we have to put $n=q=0$ in (5). The two special cases $m\leqslant 1$ and $m\leqslant 2$ will first be discussed in detail, as the results will be needed in Sec. 4, for the calculation of the relativistic corrections to the scalar interaction.

2.21. $m\leqslant 1$

This simple case has been treated by Tamm[3] and Dancoff.[4] The system (4) contains only two equations connecting $a_\lambda^{(0,0)}$ and $a_\mu^{(1,0)}$. Eliminating the latter, one obtains an equation like (6), with only one interaction term:

$$\Delta_2^{(1,0)}=\left.\begin{aligned}&\frac{(\mathbf{p}_1,\mathbf{p}_2,s_1,s_2|H'|\mathbf{p}_1-\boldsymbol{\kappa},\mathbf{p}_2,s_1',s_2)(\mathbf{p}_1-\boldsymbol{\kappa},\mathbf{p}_2,s_1',s_2|H'|\mathbf{p}_1-\boldsymbol{\kappa},\mathbf{p}_2+\boldsymbol{\kappa},s_1',s_2')}{W-E_{p_1-\kappa}-E_{p_2}-\omega_\kappa}\\ &+\text{a symmetrical term with respect to }\mathbf{p}_1\text{ and }\mathbf{p}_2,\end{aligned}\right\}\quad(7)$$

which can be considered, in the momentum representation, as an "equivalent potential," valid to the second order in G. In this equation, $\mathbf{p}_1$, $\mathbf{p}_2$ are the momenta of the nucleons, M their mass, $\boldsymbol{\kappa}$ the momentum of the exchanged meson; s_1, s_2, s_1', s_2' represent the spin states of the nucleons. We have set

$$E_p=(p^2+M^2)^{\frac{1}{2}},\quad \omega_\kappa=(\kappa^2+\mu^2)^{\frac{1}{2}}.$$

2.22. $m\leqslant 2$

The elimination of $a_\mu^{(1,0)}$ and $a_\nu^{(2,0)}$ would already lead, at this stage, to an Eq. (6) with an infinite series of interaction terms. It is, however, possible to replace this series by an interaction kernel obeying an integral equation. By eliminating $a_\nu^{(2,0)}$, one first gets an inhomogeneous integral equation for $a_\mu^{(1,0)}$:

$$[W-E_\mu^{(1,0)}]a_\mu^{(1,0)}=\sum_{\lambda'}(\mu,1,0|H'|\lambda',0,0)a_{\lambda'}^{(0,0)}+\sum_{\nu,\mu'}\frac{(\mu,1,0|H'|\nu,2,0)(\nu,2,0|H'|\mu',1,0)}{W-E_\nu^{(2,0)}}a_{\mu'}^{(1,0)}.\quad(8)$$

Calculating the Neuman-Liouville series corresponding to this equation, one finds that $a_\mu^{(1,0)}$ can be written in the form:

$$[W-E_\mu^{(1,0)}]a_\mu^{(1,0)}=\sum_{\lambda'}K_{\mu\lambda'^{(1)}}a_{\lambda'}^{(0,0)},\quad(9)$$

where $K_{\mu\lambda'^{(1)}}$ is a solution of the following equation:[12]

$$K_{\mu\lambda'^{(1)}}=(\mu,1,0|H'|\lambda',0,0)+\sum_{\nu,\mu'}\frac{(\mu,1,0|H'|\nu,2,0)(\nu,2,0|H'|\mu',1,0)}{[W-E_\nu^{(2,0)}][W-E_{\mu'}^{(1,0)}]}K_{\mu'\lambda'^{(1)}}.\quad(10)$$

By substituting (9) in the first equation of (5), one finally obtains the equation for $a_\lambda^{(0,0)}$:

$$[W-E_\lambda^{(0,0)}]a_\lambda^{(0,0)}=\sum_{\mu,\lambda'}\frac{(\lambda,0,0|H'|\mu,1,0)}{W-E_\mu^{(1,0)}}K_{\mu\lambda'^{(1)}}a_{\lambda'}^{(0,0)}.\quad(11)$$

The other amplitudes can then simply be expressed as functions of $a_\lambda^{(0,0)}$.

It should be noted that, to this order (where only terms up to the fourth order in the coupling constant are correctly taken into account), it is entirely consistent to replace $K_{\mu\lambda'^{(1)}}$ by its first Born approximation. This leads again to an equation like (6), with two interaction terms: the first one is identical with Δ_2, defined by (7); the second can be split into two parts $\Delta_4^{(a)}$ and $\Delta_4^{(b)}$, which can be written explicitly:

$$\Delta_4^{(a)}=2\frac{(\mathbf{p}_1,\mathbf{p}_2,s_1,s_2|H'|\mathbf{p}_1-\boldsymbol{\kappa},\mathbf{p}_2,s_1',s_2)(\mathbf{p}_1-\boldsymbol{\kappa},\mathbf{p}_2,s_1',s_2|H'|\mathbf{p}_1-\boldsymbol{\kappa}-\boldsymbol{\kappa}',\mathbf{p}_2,s_1'',s_2)}{(W-E_{p_1-\kappa}-E_{p_2}-\omega_\kappa)(W-E_{p_1-\kappa-\kappa'}-E_{p_2}-\omega_\kappa-\omega_{\kappa'})}$$
$$\times\frac{(\mathbf{p}_1-\boldsymbol{\kappa}-\boldsymbol{\kappa}',\mathbf{p}_2,s_1'',s_2|H'|\mathbf{p}_1-\boldsymbol{\kappa}-\boldsymbol{\kappa}',\mathbf{p}_2+\boldsymbol{\kappa},s_1'',s_2')\times(\mathbf{p}_1-\boldsymbol{\kappa}-\boldsymbol{\kappa}',\mathbf{p}_2+\boldsymbol{\kappa},s_1'',s_2'|H'|\mathbf{p}-\boldsymbol{\kappa}-\boldsymbol{\kappa}',\mathbf{p}_2+\boldsymbol{\kappa}+\boldsymbol{\kappa}',s_1'',s_2'')}{(W-E_{p_1-\kappa-\kappa'}-E_{p_2+\kappa}-\omega_{\kappa'})},\quad(12a)$$

$$\Delta_4^{(b)}=2\frac{(\mathbf{p}_1,\mathbf{p}_2,s_1,s_2|H'|\mathbf{p}_1-\boldsymbol{\kappa}',\mathbf{p}_2,s_1',s_2)(\mathbf{p}_1-\boldsymbol{\kappa}',\mathbf{p}_2,s_1',s_2|H'|\mathbf{p}_1-\boldsymbol{\kappa}-\boldsymbol{\kappa}',\mathbf{p}_2,s_1'',s_2)}{(W-E_{p_1-\kappa'}-E_{p_2}-\omega_{\kappa'})(W-E_{p_1-\kappa-\kappa'}-E_{p_2}-\omega_\kappa-\omega_{\kappa'})}$$
$$\times\frac{(\mathbf{p}_1-\boldsymbol{\kappa}-\boldsymbol{\kappa}',\mathbf{p}_2,s_1'',s_2|H'|\mathbf{p}_1-\boldsymbol{\kappa}-\boldsymbol{\kappa}',\mathbf{p}_2+\boldsymbol{\kappa},s_1'',s_2')\times(\mathbf{p}_1-\boldsymbol{\kappa}-\boldsymbol{\kappa}',\mathbf{p}_2+\boldsymbol{\kappa},s_1'',s_2'|H'|\mathbf{p}_1-\boldsymbol{\kappa}-\boldsymbol{\kappa}',\mathbf{p}_2+\boldsymbol{\kappa}+\boldsymbol{\kappa}',s_1'',s_2'')}{(W-E_{p_1-\kappa-\kappa'}-E_{p_2+\kappa}-\omega_{\kappa'})}\quad(12b)$$

[12] It is to be noted that, when the Neuman-Liouville expansion does not converge, Eq. (10) continues to have a meaning.

plus the symmetrical terms with respect to $\mathbf{p}_1$ and $\mathbf{p}_2$. These interaction terms correspond to virtual processes which are illustrated[13] in Fig. 1: $\Delta_4^{(a)}$ corresponds to graphs (a) and (a'); $\Delta_4^{(b)}$ to (b) and (b').

The process where meson κ' is absorbed by particle (1) before κ has been emitted has already been taken care of in the first term of the right-hand side of (6). This can be seen by iterating Eq. (6) an arbitrary number of times. An important feature of the present formalism is, consequently, that an infinite number of virtual processes is already included in a single interaction term. It is, therefore, suited to the treatment of bound states problems, where the interaction between the nucleons occurs during a long time.

2.23. *m Arbitrary*

We first suppose that the probability amplitudes of the states where the number of mesons is higher than $N+1$ (N being an arbitrary positive integer) are sufficiently small and can be neglected. The system (5) consists, in this case, in a set of $N+2$ coupled equations, the mth of which connects $a_\lambda^{(m-1,0)}$, $a_\mu^{(m,0)}$ and $a_\nu^{(m+1,0)}$. By eliminating all the amplitudes except $a_\lambda^{(0,0)}$, one gets for the latter amplitude an equation identical with (9); but the kernel $K_{\mu\lambda'}^{(1)}$, does not satisfy any longer Eq. (10). Instead, one introduces a series of kernels

$$K_{\lambda_1\mu_1}^{(1)}, \cdots, K_{\lambda_{N+1}\mu_{N+1}}^{(N+1)},$$

defined by the following equations:

$$K_{\lambda\mu}^{(m)} = (\lambda, m, 0|H'|\mu, m-1, 0) + \sum_{\mu',\lambda'} \frac{(\lambda, m, 0|H'|\mu', m+1, 0)}{[W-E_{\mu'}^{(m+1,0)}][W-E_{\lambda'}^{(m,0)}]} K_{\mu'\lambda'}^{(m+1)} K_{\lambda'\mu}^{(m)}, \tag{13}$$

with $m=1, 2\cdots N+1$, and $K_{\lambda\mu}^{(N+2)}=0$. All the amplitudes $a_\lambda^{(m,0)}$ are then expressed as functions of $a_{\lambda'}^{(0,0)}$, through the kernels $K^{(1)}, \cdots, K^{(m)}$, by means of the equation:

$$[W-E_\lambda^{(m,0)}]a_\lambda^{(m,0)} = \sum_{\mu_1,\cdots\mu_{m-1},\lambda'} \frac{K_{\lambda\mu_1}^{(m)} K_{\mu_1\mu_2}^{(m-1)} \cdots K_{\mu_{m-1},\lambda'}^{(1)}}{[W-E_{\mu_1}^{(m-1,0)}]\cdots[W-E_{\mu_{m-1}}^{(1,0)}]} a_{\lambda'}^{(0,0)}. \tag{14}$$

These equations are valid for any value of the coupling constant G, if there exist a finite number of intermediate states having higher probability amplitudes than all the others. On the other hand, they are more convenient than the system (5), because one has now to solve a set of uncoupled equations, the kernel of each one being defined by the solution of the preceding one. The first N equations are inhomogeneous; the eigenvalue problem occurs only in the solution of the last one [Eq. (9)], which is homogeneous. Furthermore, the problem is now all set for an application of perturbation theory: having solved the system of equations corresponding to $m \leq N+1$, it is possible, by doing only some integrations, to calculate the correction to the energy levels which is provided by the system corresponding to $m \leq N+2$.

When it is possible to expand the interaction in powers of G^2, one can replace Eqs. (9) and (13) by Eq. (6), with $q=0$ and

$$\Delta^{(p,0)}(\lambda, \lambda') = \sum_{\mu_i} \sum_{(r_i)} \frac{(\lambda, 0, 0|H'|\mu_1, 1, 0)(\mu_1, 1, 0|H'|\mu_2, 2, 0)}{[W-E_{\mu_1}^{(1,0)}][W-E_{\mu_2}^{(2,0)}]} \times \left\{\prod \frac{(\mu_{i-1}, r_{i-1}, 0|H'|\mu_i, r_i, 0)}{[W-E_{\mu_i}^{(r_i,0)}]}\right\} \times \frac{(\mu_{2p-2}, 2, 0|H'|\mu_{2p-1}, 1, 0)(\mu_{2p-1}, 1, 0|H'|\lambda', 0, 0)}{[W-E_{\mu_{2p-1}}^{(1,0)}]}. \tag{15}$$

FIG. 1. Virtual processes involving two mesons (and no pairs) in the intermediate states.

The summation of the right-hand side is extended on all possible sets of $2p-4$ numbers (r_i), with $i=3, \cdots, 2p-2$, which satisfy the following conditions: $r_i \leq p$, $r_{i+1}=r_i \pm 1$, $r_2=r_{2p-2}=2$. The formal expression (15) might allow, in certain cases, the summation of the interaction terms which appear on the right-hand side of (6).

2.3. Lowest Order Pair Creation Effects

We consider the case where the maximum number of mesons which can be present at a given time in the intermediate states is one, the number of nucleon pairs simultaneously present being unrestricted. This case includes the lowest order exchange processes in which virtual pair creation can affect the interaction of the two particles of the system, and not merely their self-energy. After a brief study of the general equations, we shall derive in an explicit fashion the effective interaction resulting from the creation of two virtual pairs.

2.31. *General Equations for $m \leq 1$, n Arbitrary*

For each value of n, the system (4) includes two equations, defining the amplitudes $a_\lambda^{(0,n)}$ and $a_\lambda^{(1,n)}$. The

[13] In the graphical description of the virtual exchange effects, a conventional time ordering is used by which the emission and absorption of mesons, the creation or annihilation of pairs, occur in the same order as the corresponding matrix elements in $\Delta^{(p,q)}(\lambda, \lambda')$, counted from the right to the left.

latter can be eliminated so that the transformed system contains only the probability amplitudes of states where no meson is present:

$$[W-E_\lambda^{(0,n)}]a_\lambda^{(0,n)} = \sum_{0\leqq n'=n-2}^{n+2}\sum_{\lambda'} Q^{(n,n')}(\lambda,\lambda')a_{\lambda'}^{(0,n')}, \quad (16)$$

where we have set:

$$Q^{(n,n')}(\lambda,\lambda') = \sum_{p=n-1}^{n+1}\sum_{\mu}\frac{(\lambda,0,n|H'|\mu,1,p)(\mu,1,p|H'|\lambda',0,n')}{[W-E_\mu^{(1,p)}]}, \quad (17)$$

in which p and n' are restricted by the inequalities: $n-1\leq p\leq n+1$, $p-1\leq n'\leq p+1$. $Q^{(n,n')}(\lambda,\lambda')$ is a "reduced" matrix element for the transitions between two states where n' and n nucleon pairs are present respectively.

The form of Eqs. (16) is such that it is possible to apply to them the method of integral equations and successive kernels developed in Sec. 2.23. The situation

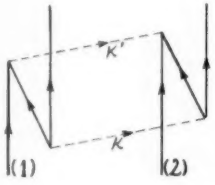

FIG. 2. A virtual process involving two pairs, in the intermediate states, but not more than one meson at a given time.

is, however, a little more complicated, since the summation of the right-hand side extends over five amplitudes, instead of just two as in the case where no pairs are present. Two series of kernels have to be defined, by means of the equations:

$$[W-E_\lambda^{(0,n)}]a_\lambda^{(0,n)} = \sum_{\lambda'}L^{(n)}(\lambda,\lambda')a_{\lambda'}^{(0,n-1)}+M^{(n)}(\lambda,\lambda')a_{\lambda'}^{(0,n-2)}, \quad (18)$$

and these kernels are solutions of integral equations, the kernels of which are functions of other kernels corresponding to higher values of n.

When it is possible to expand the interaction in powers of G^2, one can replace Eqs. (16) by Eq. (6) with $p=1$, where the interaction terms $\Delta^{(1,q)}$ can be written explicitly:

$$\Delta^{(1,q)}(\lambda,\lambda') = \sum_{\alpha=1,2}\sum_{\beta=1,2}\sum_{(r_i)}\sum_{\mu}\frac{Q^{(0,\alpha)}(\lambda,\mu_1)}{W-E_{\mu_1}^{(0,\alpha)}} \times\left\{\prod_{i=1}^{q-2}\frac{Q^{(r_i,r_{i+1})}(\mu_i,\mu_{i+1})}{W-E_{\mu_{i+1}}^{(0,r_{i+1})}}\right\}Q^{(\beta,0)}(\mu_{q-1},\lambda'). \quad (19)$$

The summation of the right-hand side extends over all possible sets of $q-1$ positive integers (r_i), with $i=1,2,\cdots,q-1$, which satisfy the conditions: $0<r_i\leq q$, $r_i-2\leq r_{i+1}\leq r_i+2$, $r_1=\alpha$, $r_{q-1}=\beta$.

The generalization of Eqs. (16) and (19) to the case where more than one meson is present at one time is straightforward, although the equations become complicated. The only modification which has to be made is in the form of $Q^{(n,n')}(\lambda,\lambda')$, which becomes analogous to $\Delta^{(p,0)}(\lambda,\lambda')$ of Eq. (15).

2.32. Effective Interaction Resulting from the Creation of Two Virtual Pairs

This calculation, which illustrates the formal equations of the preceding paragraph, will also be used in the next section for comparison with the results obtained from the B.S. equation: it will then provide an example of the analytical differences which occur between the two treatments when virtual nucleon pairs are present in the intermediate states.

After inserting in the system (4) the conditions $m\leq 1$, $n=0$ or 2, we obtain for $a_\lambda^{(0,0)}$, an equation like (6), with two interaction terms on the right-hand side. The first is identical with $\Delta_2^{(1,0)}$ of (7); the second, which results from the virtual process illustrated in Fig. 2 (plus those which are symmetrical with respect to particles 1 and 2), has the following expression:

$$\Delta_4^{(1,2)} = \frac{1}{2V^2}\frac{\Gamma_{12}^{(1)}(\mathbf{p}_1,-\mathbf{p}_1-\boldsymbol{\kappa}')\Gamma_{12}^{(2)}(\mathbf{p}_2,-\mathbf{p}_2+\boldsymbol{\kappa}')\Gamma_{21}^{(1)}(-\mathbf{p}_1-\boldsymbol{\kappa}',\mathbf{p}_1+\boldsymbol{\kappa}+\boldsymbol{\kappa}')\Gamma_{21}^{(2)}(-\mathbf{p}_2+\boldsymbol{\kappa}',\mathbf{p}_2-\boldsymbol{\kappa}-\boldsymbol{\kappa}')}{\omega_\kappa\omega_{\kappa'}[W-E_{p1}-E_{p2}-E_{p2-\kappa'}-E_{p2-\kappa-\kappa'}-\omega_\kappa]} \times[W-E_{p1}-E_{p2}-E_{p1+\kappa'}-E_{p2-\kappa'}-E_{p1+\kappa+\kappa'}-E_{p2-\kappa-\kappa'}] \times[W-E_{p1}-E_{p1+\kappa'}-E_{p1+\kappa+\kappa'}-E_{p2-\kappa-\kappa'}-\omega_{\kappa'}] \quad (20)$$

where we have used the notation

$$(\lambda,0,0|H'|\mu,1,1)=[2V\omega_\kappa]^{-\frac{1}{2}}\Gamma_{12}^{(r)}(\mathbf{p}_r,-\mathbf{p}_r-\boldsymbol{\kappa}), \quad (21)$$

for the matrix element describing the creation of one meson and one nucleon pair; $\mathbf{p}_r$ is the initial momentum of nucleon (r), $\boldsymbol{\kappa}$ the momentum of the emitted meson and V the volume in which the nucleon wave functions are normalized. We have set $\omega_\kappa=(\kappa^2+\mu^2)^{\frac{1}{2}}$. Another slightly more general definition of $\Gamma_{ij}^{(r)}(\mathbf{p},\mathbf{p}')$ will be given in 3.1.

3. NON-ADIABATIC CORRECTIONS IN THE BETHE AND SALPETER EQUATION

We write B.S. equation, in coordinate space, as follows:[14]

$$\chi(x_1, x_2) = -\int S_F^{(1)}(x_1, x_1')S_F^{(2)}(x_2, x_2')$$

$$\times G(x_1', x_2'; x_1'', x_2'')\chi(x_1'', x_2'')dx_1'dx_2'dx_1''dx_2'', \quad (22)$$

where the indices (1) and (2) refer to the nucleons. For the interaction kernel G, which is a covariant function of $x_1'-x_2'$, $x_1''-x_2''$, Bethe and Salpeter have proposed an expansion in powers of the coupling constant:

$$G=G_2+G_4+\cdots \quad (23)$$

where G_2 is the Feynman expression corresponding to the second-order diagram of the S-matrix:

$$G_2(x_1', x_2'; x_1'', x_2'')$$
$$=G^2\Delta_F(x_1'-x_2')\delta(x_1', x_1'')\delta(x_2', x_2''). \quad (24)$$

The functions S_F and Δ_F, which appear in (22) and (24) are defined according to Dyson.[15] The replacement of G by G_2 corresponds to the so-called "ladder approximation," to which we shall restrict ourselves in the following. The extension of our calculations to the other terms of the interaction can be carried out in a straightforward way.

3.1. Expression of Eq. (22) in the Momentum Representation

The "wave function" $\chi(x_1, x_2)$ is expanded by means of its Fourier coefficients, in the following way:

$$\chi(x_1, x_2)=\sum_{i,j}\sum_{p_1,p_2}\frac{1}{V}A_{ij}(p_1, p_2)$$
$$\times u_i^{(1)}(\mathbf{p}_1)u_j^{(2)}(\mathbf{p}_2)e^{i(p_1x_1+p_2x_2)}, \quad (25)$$

where the function $u_i^{(r)}(p_r)$ is the amplitude of the Dirac spinor, obeying the following equation:

$$[i\boldsymbol{\gamma}^{(r)}\cdot\mathbf{p}_r+\gamma_4^{(r)}E_i+M]u_i^{(r)}(\mathbf{p}_r)=0. \quad (26)$$

The indices i, j can take the values 1, 2. We have set $E_1(\mathbf{p}_r)=-E_2(\mathbf{p}_r)=E_{p_r}$. Substituting (25) into (22), using the momentum representation of the S_F and Δ_F functions and multiplying both sides on the right with $\bar{u}_i^{(1)}(\mathbf{p}_1)\bar{u}_j^{(2)}(\mathbf{p}_2)(i\gamma_\mu^{(1)}p_\mu^{(1)}+M)(i\gamma_\nu^{(2)}p_\nu^{(2)}+M)$, the following equation is obtained:

$$A_{ij}(p_1, p_2)$$
$$=\frac{-iG^2}{2V[E^{(1)}-E_i(\mathbf{p}_1)+i\epsilon_i\eta][E^{(2)}-E_j(\mathbf{p}_2)+i\epsilon_j\eta]}$$
$$\times\sum_{k,l}\sum_{\kappa}\frac{\Gamma_{ik}^{(1)}\Gamma_{jl}^{(2)}A_{kl}(p_1-\kappa, p_2+\kappa)}{\kappa^2+\mu^2-i\eta}, \quad (27)$$

+symmetrical term with respect to particles (1) and (2), where the following notations have been used:

$$E^{(r)}=-ip_4^{(r)}$$

and

$$\Gamma_{ik}^{(r)}=\bar{u}_i^{(r)}(\mathbf{p}_r)\gamma_4^{(r)}\mathcal{O}^{(r)}u_k^{(r)}(\mathbf{p}_r+\epsilon_r\boldsymbol{\kappa}),$$

$\mathcal{O}^{(r)}$ being an operator connected with the properties of the meson field which is considered: $\mathcal{O}^{(r)}=1$ for scalar, $i\gamma_5^{(r)}$ for pseudoscalar, $\gamma_\mu^{(r)}$ for vector fields, etc. We have also $\epsilon_1=+1$, $\epsilon_2=-1$, η is a small positive quantity which tends to zero after the summation over κ on the right hand side of (27) has been carried out.

We use in the following the center of gravity system, defined as: $p^{(1)}+p^{(2)}=P(0,0,0,W)$, $p^{(1)}-p^{(2)}=p(\mathbf{p}, ip_0)$. By going to the limit of a continuous distribution of the momenta, we obtain the equation:

$$A_{ij}(\mathbf{p}, p_0)=\frac{1}{[\Lambda_i(\mathbf{p})-p_0][\Lambda_j(\mathbf{p})+p_0]}\sum_{k,l}\frac{-iG^2}{(2\pi)^4}$$
$$\times\int\frac{\Gamma_{ik}^{(1)}\Gamma_{jl}^{(2)}A_{kl}(\mathbf{p}+\boldsymbol{\kappa}, p_0+\kappa_0)d^3\kappa d\kappa_0}{\omega_\kappa^2-\kappa_0^2-i\eta}, \quad (28)$$

where we have put:

$$\Lambda_i(\mathbf{p})=\tfrac{1}{2}W-E_i(\mathbf{p})+i\epsilon_i\eta. \quad (29)$$

When the times of the two particles are equalled in $\chi(x_1, x_2)$ the corresponding amplitude is given by:

$$a_{ij}(\mathbf{p})=\frac{1}{2\pi i}\int_{-\infty}^{+\infty}A_{ij}(\mathbf{p}, p_0)dp_0. \quad (30)$$

3.2. Adiabatic Approximation in the B.S. Equation

In order to obtain the adiabatic approximations to Eq. (28), we neglect the motion of the nucleons while the mesons are in flight. Mathematically, this corresponds to replacing Δ_F, in Eq. (22), by its time integral, multiplied by a δ-function operating on the time coordinate.

$$\Delta_F(x)\rightarrow\delta(x_4)\int_{-\infty}^{+\infty}\Delta_F(\mathbf{x}, x_4)dx_4. \quad (31)$$

As is well known, the integral of the right-hand side of (31) is equal to the Yukawa potential. With the help of

[14] From Eq. (22) to Eq. (31) inclusive, light type is used for 4-dimensional quantities, heavy type for three-dimensional ones. In the rest of the paper, light type is used for one-dimensional quantities, unless otherwise stated.

[15] F. J. Dyson, Phys. Rev. **75**, 486, 1736 (1949).

(30), Eq. (28) becomes:

$$A_{ij}^{(0)}(\mathbf{p}, p_0)=\frac{F_{ij}^{(0)}(\mathbf{p})}{[\Lambda_i(\mathbf{p})-p_0][\Lambda_j(\mathbf{p})+p_0]}, \tag{32}$$

where we have put:

$$F_{ij}^{(0)}(\mathbf{p})=\lambda\sum_{k,l}\int\frac{\Gamma_{ik}^{(1)}\Gamma_{jl}^{(2)}a_{kl}^{(0)}(\mathbf{p}+\boldsymbol{\kappa})d^3\kappa}{\omega_\kappa^2}, \tag{33}$$

with $\lambda=G^2(2\pi)^{-3}$. In this approximation, the "odd" components of a_{ij} (corresponding to $i\neq j$) vanish. The "even" components obey the equation:

$$[W-2E_i(\mathbf{p})]a_{ii}^{(0)}(\mathbf{p})=-\lambda\epsilon_i\sum_k\int\frac{\Gamma_{ik}^{(1)}\Gamma_{ik}^{(2)}a_{kk}^{(0)}(\mathbf{p}+\boldsymbol{\kappa})d^3\kappa}{\omega_\kappa^2}. \tag{34}$$

This equation does not exactly correspond to the non-relativistic limit of (28), because it still involves the exact spin matrix elements and one small component of the amplitude. Its form is that of a two-particle Dirac equation, where the "odd" components[16] of the wave-function are equalled to zero.

3.3. Non-Adiabatic Corrections (Pairs Excluded)

The non-adiabatic corrections to Eq. (34) are calculated by inserting on the right-hand side the "adiabatic" approximation and iterating the equation an arbitrary number of times. When no pairs are created during the interaction of the two nucleons, Eq. (28) is restricted to the "large" components of the amplitude $A_{ij}(i=j=1)$. In this subsection, all the indices will be dropped; we shall write, for example, $A_{11}=A$, $a_{11}=a$, $\Lambda_1(\mathbf{p})=\Lambda_p$, $\Gamma_{11}^{(r)}(\mathbf{p}, \mathbf{p}')=\Gamma^{(r)}(\mathbf{p}, \mathbf{p}')$ etc.

In order to calculate the first non-adiabatic correction, we insert in the right-hand side of (28) the trial-function $A(\mathbf{p}, p_0)=-2\Lambda_p a(\mathbf{p})[{\Lambda_p}^2-{p_0}^2]^{-1}$, which has the same dependence on p_0 as the adiabatic solution, and satisfies Eq. (30). Integrating over κ_0 yields the equation:

$$A(\mathbf{p}, p_0)=\frac{i\lambda}{{\Lambda_p}^2-{p_0}^2}\int\frac{\Gamma^{(1)}(\mathbf{p}, \mathbf{p}+\boldsymbol{\kappa})\Gamma^{(2)}(-\mathbf{p}, -\mathbf{p}-\boldsymbol{\kappa})[\Lambda_{p+\kappa}-\omega_\kappa]a(\mathbf{p}+\boldsymbol{\kappa})d^3\kappa}{\omega_\kappa[(\Lambda_{p+\kappa}-\omega_\kappa)^2-{p_0}^2]}. \tag{35}$$

Inserting this expression into the right-hand side of (30) leads to an equation for $a(\mathbf{p})$ which can be written, with the help of (29), as follows:

$$(W-2E_p)a(\mathbf{p})=\lambda\int\frac{\Gamma^{(1)}(\mathbf{p}, \mathbf{p}+\boldsymbol{\kappa})\Gamma^{(2)}(-\mathbf{p}, -\mathbf{p}-\boldsymbol{\kappa})a(\mathbf{p}+\boldsymbol{\kappa})d^3\kappa}{\omega_\kappa(W-E_p-E_{p+\kappa}-\omega_\kappa)}. \tag{36}$$

The interaction term is readily found to be identical with (7) if the latter is written in the center-of-mass system ($\mathbf{p}_1=+\mathbf{p}$, $\mathbf{p}_2=-\mathbf{p}$). The second approximation to Eq. (34) is obtained by inserting in the right-hand side of (28) the expression (35) which has just been calculated for $A(\mathbf{p}, p_0)$. By making use of (30), one obtains the equation:

$$\begin{aligned}(W-2E_p)a(\mathbf{p})=&\lambda\int\frac{\Gamma^{(1)}(\mathbf{p}, \mathbf{p}+\boldsymbol{\kappa})\Gamma^{(2)}(-\mathbf{p}, -\mathbf{p}-\boldsymbol{\kappa})a(\mathbf{p}+\boldsymbol{\kappa})d^3\kappa}{\omega_\kappa(W-E_p-E_{p+\kappa}-\omega_\kappa)}\\&+\frac{\lambda^2}{2}\int\frac{\Gamma^{(1)}(\mathbf{p}, \mathbf{p}+\boldsymbol{\kappa})\Gamma^{(2)}(-\mathbf{p}, -\mathbf{p}-\boldsymbol{\kappa})\Gamma^{(1)}(\mathbf{p}+\boldsymbol{\kappa}, \mathbf{p}+\boldsymbol{\kappa}+\boldsymbol{\kappa}')\Gamma^{(2)}(-\mathbf{p}-\boldsymbol{\kappa}, -\mathbf{p}-\boldsymbol{\kappa}-\boldsymbol{\kappa}')a(\mathbf{p}+\boldsymbol{\kappa}+\boldsymbol{\kappa}')d^3\kappa d^3\kappa'}{\omega_\kappa\omega_{\kappa'}(W-E_{p+\kappa}-E_{p+\kappa+\kappa'}-\omega_\kappa)(W-E_p-E_{p+\kappa+\kappa'}-\omega_\kappa-\omega_{\kappa'})(W-E_p-E_{p+\kappa'}-\omega_{\kappa'})}.\end{aligned} \tag{37}$$

On the right-hand side, the kernel of the first term is again identical with (7); the kernel of the second term is equal to $\frac{1}{2}\Delta_4^{(a)}$, defined by (12a), and corresponds to the virtual process where two mesons can be present at the same time, without crossing of meson lines illustrated in Fig. 1(a).

The previous procedure can be continued to all orders in the coupling constant. The amplitude $a(\mathbf{p})$ obeys the following general equation, for which a recurrence proof can be given through lengthy but straightforward calculations:

$$(W-2E_p)a(\mathbf{p})=2\sum_{n=1}^{\infty}\left(\frac{\lambda}{2}\right)^n\int\frac{D^{(n)}(\mathbf{p}, \boldsymbol{\kappa}_1, \cdots, \boldsymbol{\kappa}_n)}{\omega_{\kappa_1}\cdots\omega_{\kappa_n}}a(\mathbf{p}+\boldsymbol{\kappa}_1+\cdots+\boldsymbol{\kappa}_n)d^3\kappa_1\cdots d^3\kappa_n \tag{38}$$

with

$$D^{(n)}=\frac{\prod_{q=1}^{n-1}[\Gamma^{(1)}(\mathbf{p}+\boldsymbol{\kappa}_1+\cdots+\boldsymbol{\kappa}_q, \mathbf{p}+\boldsymbol{\kappa}_1+\cdots+\boldsymbol{\kappa}_q)\Gamma^{(2)}(-\mathbf{p}-\boldsymbol{\kappa}_1-\cdots-\boldsymbol{\kappa}_q, -\mathbf{p}-\boldsymbol{\kappa}_1-\cdots-\boldsymbol{\kappa}_q)}{\prod_{q=1}^{n}[W-E(\mathbf{p}+\boldsymbol{\kappa}_q+\cdots+\boldsymbol{\kappa}_n)-E(\mathbf{p}+\boldsymbol{\kappa}_1+\cdots+\boldsymbol{\kappa}_n)-\omega_{\kappa_1}-\cdots-\omega_{\kappa_q}]\times\prod_{q=1}^{n-1}[W-E_p-E(\mathbf{p}+\boldsymbol{\kappa}_{q+1}+\cdots+\boldsymbol{\kappa}_n)-\omega_{q+1}-\cdots-\omega_{\kappa_n}]}. \tag{39}$$

[16] Namely, those which correspond to $i\neq j$.

Equation (38) is identical with Eqs. (6) and (15) for $a_\lambda^{(0,0)}$ if, in all the processes formally included in the latter, only the exchange effects with no meson lines crossing are taken into account. In the ladder approximation, when no pairs are present, one has therefore the result:

$$a^{(0,0)}(\mathbf{p}, -\mathbf{p}) = a(\mathbf{p}); \tag{40}$$

the Fourier coefficient of the wave function corresponding to equal times of the particles is identical with the probability amplitude of the state where only two nucleons, and no meson, are present.

3.4. Calculation of the First Non-Adiabatic Approximation, Pair Creation Being Included

In this case, the whole set of components of A_{ij} must be considered. One inserts on the right-hand side of (28) the adiabatic solution defined by (32). Making use of (30) and (33), the equation for the amplitude corresponding to equal times of the particles is obtained:

$$[W - E_i(\mathbf{p}) - E_j(\mathbf{p})]a_{ij}(\mathbf{p}) = -\lambda \sum_{k,l} \int \Gamma_{ik}^{(1)} \Gamma_{jl}^{(2)} K_{ij}^{kl}(\mathbf{p}, \mathbf{p}+\boldsymbol{\kappa}) a_{kl}(\mathbf{p}+\boldsymbol{\kappa}) d^3\kappa, \tag{41}$$

where the kernel has the following expression:

$$K_{ij}^{kl} = \frac{1 - \frac{1}{4}(\epsilon_i - \epsilon_j)(\epsilon_k - \epsilon_l)}{4\omega_\kappa} \times \sum_{\substack{\mu = i,j \\ \nu = k,l}} \frac{\epsilon_\mu \epsilon_\nu}{\omega_\kappa - \epsilon_\mu \Lambda_\mu(\mathbf{p}) - \epsilon_\nu \Lambda_\nu(\mathbf{p}+\boldsymbol{\kappa})}. \tag{42}$$

By eliminating all the amplitudes except a_{11} by means of successive substitution, one obtains an equation of the general form:

$$(W - 2E_p)a_{11}(\mathbf{p}) = \sum_n \lambda^n \int \Delta_n(\mathbf{p}, \mathbf{p}') a_{11}(\mathbf{p}') d^3p', \tag{43}$$

where all the interaction kernels corresponding to virtual processes which do not involve pair creation are identical with those defined by Eq. (15). When nucleon pairs are created in the intermediate states, the corresponding kernels of Eq. (43) coincide with those defined by Eq. (19) only in the nonrelativistic limit. For example, the process illustrated by Fig. 2 leads to the interaction term:

$$\Delta_4^{(1,2)}(\mathbf{p}, \mathbf{p}') = \int \frac{\Gamma_{12}^{(1)}(\mathbf{p}, \mathbf{p}'') \Gamma_{12}^{(2)}(-\mathbf{p}, -\mathbf{p}'') \Gamma_{21}^{(1)}(\mathbf{p}'', \mathbf{p}') \Gamma_{21}^{(2)}(-\mathbf{p}'', -\mathbf{p}') d^3p''}{\omega(\mathbf{p}, \mathbf{p}'') \omega(\mathbf{p}'', \mathbf{p}') (W + 2E_{p''}) (\omega_{p, p''} + E_p + E_{p''}) (\omega_{p'', p'} + E_{p''} + E_{p'})} \tag{44}$$

which differs from the corresponding expression (20) in the T.D. formalism by corrections proportional to $(2E_p - W)$ or $(2E_{p'} - W)$. These differences tend to zero in the nonrelativistic limit, since, in that case, the amplitudes $a_{11}(\mathbf{p})$ and $a_{11}(\mathbf{p}')$ are mainly concentrated in the region of low momenta.[17]

4. RELATIVISTIC CORRECTIONS TO THE SCALAR MESON INTERACTION OF TWO NUCLEONS

In this section we calculate the lowest order relativistic corrections to the scalar neutral meson interaction of two nucleons. The purpose of this application is to compare in practical calculations the two nonadiabatic methods which have been discussed, in general terms, in Secs. 2 and 3.

Before relativistic "corrections" can be calculated, it is necessary to define briefly the nonrelativistic equation, wave function and coupling constant which have to be corrected.

4.1. Nonrelativistic Schrödinger Equation

In the scalar (neutral) meson theory, the nonrelativistic amplitude $a_0(\mathbf{p})$ is constituted by four "large" components, all of them obeying the same equation (there is no spin-separation between the stationary states):

$$[p^2 + M|w|]a_0(\mathbf{p}) = \lambda_0 M \int \frac{a_0(\mathbf{p}+\boldsymbol{\kappa}) d^3\kappa}{\omega_\kappa^2}, \tag{45}$$

where w is the binding energy: $w = W - 2M$. The simplest approximation to the solution of this equation[18] is provided by the "trial"-function of Wilson:[19] $a_0(\mathbf{p}) \sim (p^2 + \gamma^2)^{-2}$. The eigenvalue corresponding to the ground state is obtained by means of the variational principle:[20] $\delta\lambda_0 = 0$, where λ_0 is defined by:

$$\frac{1}{\lambda_0} = \frac{\int a_0^*(\mathbf{p}) \omega_\kappa^{-2} a_0(\mathbf{p}+\boldsymbol{\kappa}) d^3p d^3\kappa}{\int a_0^*(\mathbf{p}) [p^2 + M|w|] a_0(\mathbf{p}) d^3p}. \tag{46}$$

The corresponding values of the constants are as follows: $\mu = 140.25$ Mev, $(\mu/M = 0.150)$, $|w| = 2.185$ Mev,

[17] These differences result from the fact that the "one-meson part" of the "ladder" approximation includes a small fraction of the contributions of the exchange effects where, in the intermediate states, more than two pairs are present. It is to be noted that the difference $2E_{p''} - W$, where $\mathbf{p}''$ is the intermediate momentum which appears in Eq. (44), cannot be considered as small, even in the non-relativistic limit. Terms involving $\mathbf{p}''$ are in fact, identical in both expressions (20) and (44).

[18] For a general study of the solution of this equation in the momentum representation, see: M. M. Lévy, Proc. Roy. Soc. (London) **A204**, 145 (1950), and J. phys. et radium (to be published).

[19] A. H. Wilson, Proc. Cambridge Phil. Soc. **34**, 365 (1938).

[20] It is simpler, and more in accordance with the practical situation, where the binding energy is known, and the coupling constant unknown, to vary λ_0 instead of $|w|$.

$\gamma=0.843\mu, G^2/4\pi=2\pi^2\lambda_0=2.453(\mu/M)$. The mean value of the momentum is given by: $\langle p^2/M^2\rangle=\gamma^2/M^2$. Consequently, $G^2/4\pi$, $\langle p/M\rangle=\langle v/c\rangle$ and μ/M are all of the same order of magnitude.

4.2. Variational Principle in a Perturbation Expansion

We need a formula which defines, through a variational principle, the corrections to λ_0 introduced by a relativistic correction to the potential. When only one large amplitude $a(\mathbf{p})$ is involved, it obeys an integral equation which can be written in general:

$$T(\mathbf{p})a(\mathbf{p})=\lambda\int K(\mathbf{p},\,\mathbf{p}+\boldsymbol{\kappa})a(\mathbf{p}+\boldsymbol{\kappa})d^3\kappa. \tag{47}$$

We suppose that the kernel of this equation can be split into two parts:

$$K=K_0(\mathbf{p},\,\mathbf{p}+\boldsymbol{\kappa})+K_1(\mathbf{p},\,\mathbf{p}+\boldsymbol{\kappa}), \tag{48}$$

where $K_0=\omega_\kappa^{-2}$, and K_1 is a relativistic correction which is supposed to be small. We write: $a(\mathbf{p})=a_0(\mathbf{p})+a_1(\mathbf{p})$, $\lambda=\lambda_0+\lambda_1$. Multiplying both sides of (47) with $a_0^*(\mathbf{p})$, and integrating over $\mathbf{p}$, we obtain by taking into account the fact that $a_0(\mathbf{p})$ is solution of the variational principle (46), the following expression:

$$\frac{\lambda_1}{\lambda_0^2}=-\frac{\int a_0^*(\mathbf{p})K_1(\mathbf{p},\,\mathbf{p}+\boldsymbol{\kappa})a_0(\mathbf{p}+\boldsymbol{\kappa})d^3pd^3\kappa}{\int a_0^*(\mathbf{p})K_0(\mathbf{p},\,\mathbf{p}+\boldsymbol{\kappa})a_0(\mathbf{p}+\boldsymbol{\kappa})d^3pd^3\kappa}. \tag{49}$$

In the general case where the amplitude $a(\mathbf{p})$ has "large" and "small" components $a_{ij}(\mathbf{p})$, the generalizations of Eqs. (47) and (49) are as follows:

$$T_{ij}a_{ij}(\mathbf{p})=\lambda\sum_{k,l}\int\Gamma_{ik}^{(1)}\Gamma_{jl}^{(2)}K_{ij}^{kl}(\mathbf{p},\,\mathbf{p}+\boldsymbol{\kappa})a_{kl}(\mathbf{p}+\boldsymbol{\kappa})d^3\kappa, \tag{47g}$$

$$\frac{1}{\lambda_0}-\frac{\lambda_1}{\lambda_0^2}=\frac{\sum_{i,j,k,l}\int a_{ij}^{(0)*}(\mathbf{p})\Gamma_{ik}^{(1)}\Gamma_{jl}^{(2)}K_{ij}^{kl}(\mathbf{p},\,\mathbf{p}+\boldsymbol{\kappa})a_{kl}^{(0)}(\mathbf{p}+\boldsymbol{\kappa})d^3pd^3\kappa}{\sum_{i,j}\int a_{ij}^{(0)}(\mathbf{p})T_{ij}(\mathbf{p})a_{ij}^{(0)}(\mathbf{p})d^3p}. \tag{49g}$$

In this last formula, $a_{ij}^{(0)}$ is the solution of the equation:

$$T_{ij}a_{ij}^{(0)}(\mathbf{p})=\lambda_0\sum_{kl}\int\Gamma_{ik}^{(1)}\Gamma_{jl}^{(2)}\omega_\kappa^{-2}a_{kl}^{(0)}(\mathbf{p}+\boldsymbol{\kappa})d^3\kappa, \tag{50}$$

and $\Gamma_{ik}^{(r)}$ are the spin matrix elements defined by Eq. (28).

4.3. Relativistic Corrections (Pair Formation Neglected)

In this sub-section, the corrections which come from the retardation of the meson field, and those contributed by the relativistic part of the spin-matrix elements connecting positive energy states, are estimated.

The spin matrix elements are easily calculated in the scalar case. One gets, for example, for particle (1):

$$\Gamma_{ik}^{(1)}=\left\{\frac{[M+E_i(\mathbf{p})][M+E_k(\mathbf{p}+\boldsymbol{\kappa})]}{4E_i(\mathbf{p})E_k(\mathbf{p}+\boldsymbol{\kappa})}\right\}^{\frac{1}{2}}\times\{1-\mathbf{R}_i(\mathbf{p})\cdot\mathbf{R}_k(\mathbf{p}+\boldsymbol{\kappa})+i\boldsymbol{\sigma}^{(1)}\cdot[\mathbf{R}_i(\mathbf{p})\times\mathbf{R}_k(\mathbf{p}+\boldsymbol{\kappa})]\}, \tag{51}$$

with $\mathbf{R}_i(\mathbf{p})=[M+E_i(\mathbf{p})]^{-1}\cdot\mathbf{p}$. The relativistic part of the matrix elements which connect positive energy states only ($i=j=k=l=1$) contributes corrections which are clearly of the order of v^2/c^2, or higher. The separation singlet-triplet is also of the same order.

4.31. Lowest Order Correction in the B.S. *Equation*

It is convenient, in order to calculate the relativistic corrections included in the B.S. equation, to use Eq. (38), which involves only the amplitude $a(\mathbf{p})$. The two first terms of the expansion of the right-hand side are written more explicitly in Eq. (37). On the right-hand side of this equation, the first term includes the Yukawa potential, plus an interaction term which is of the order of v/c, since:

$$\langle(E_p+E_{p+\kappa}-W)/\omega_\kappa\rangle\sim\langle p^2/M\mu\rangle\sim(\mu/M).$$

The contribution of the second term is also a correction of the order of v/c, since λ_0 is itself of the order of μ/M. In this last term, all the differences between W and the sum of two free energies of the interacting particles can be dropped in the denominator of the kernel. The higher order terms, in the expansion of the right of (55), are proportional to $(\lambda/2)^n$, with $n\geqslant 3$. They are, therefore, of the order v^3/c^3, or higher. The equation which, in the "ladder" approximation of the B.S. equation, includes all the corrections of the first order in v/c is, consequently, of the form (47) with:

$$K_1(\mathbf{p},\,\mathbf{p}+\boldsymbol{\kappa})=\frac{W-E_p-E_{p+\kappa}}{\omega_\kappa^2}+\frac{\lambda_0}{2}\int\frac{d^3\kappa'}{\omega_{\kappa'}^2\omega_{\kappa-\kappa'}^2(\omega_{\kappa'}+\omega_{\kappa-\kappa'})}. \tag{52}$$

If this expression is introduced into (49), the resulting value of λ_1/λ_0 is obviously of the order of μ/M. Incidentally, the equation which was derived by Tamm[3] and Dancoff[4] for the scalar meson theory included, as a non-adiabatic correction, only the first term of the right-hand side of (52). The second one, which is proper to the "ladder" approximation of the B.S. equation, corresponds to the exchange process illustrated in graph (1a). Both terms are of the same order of magnitude.[21]

4.32. *Calculation of the Exact Correction (In the Absence of Pair Formation)*

In the calculation of the preceding sub-section, three contributions to the relativistic corrections of the order of v/c have been neglected: these come from the exchange processes illustrated by diagrams (1a′), (1b), (1b′), which involve meson lines crossings. They can be taken into account if one considers instead of Eq. (38) the general Eq. (6) obtained, in the T.D. formalism, for $a_\lambda^{(0,0)}$. The interaction terms of that equation are written up to the fourth order in Eqs. (7), (12a), and (12b). Adding these terms, and keeping only the parts which are of the order of μ/M, the following equation is obtained:

$$\frac{p^2+M|w|}{M}a(\mathbf{p}) = \lambda\int\frac{1}{\omega_\kappa{}^2}\left(1-\frac{E_p+E_{p+\kappa}-W}{\omega_\kappa}\right)a(\mathbf{p}+\boldsymbol{\kappa})d^3\kappa + \lambda^2\int\frac{a(\mathbf{p}+\boldsymbol{\kappa}+\boldsymbol{\kappa}')d^3\kappa d^3\kappa'}{\omega_\kappa{}^3\omega_{\kappa'}{}^2}. \quad (53)$$

The second term of the right-hand side includes, in the limit where all the differences between W and the sum of two free energies are equalled to zero, the contributions of the kernels $\Delta_4^{(a)}$, $\Delta_4^{(b)}$ of Eq. (12). Since we are using perturbation theory, we can replace $a(\mathbf{p}+\boldsymbol{\kappa}+\boldsymbol{\kappa}')$ by $a_0(\mathbf{p}+\boldsymbol{\kappa}+\boldsymbol{\kappa}')$. After integrating over $\boldsymbol{\kappa}'$, with the help of (45), Eq. (53) becomes of the form (47), with: $K_1(\mathbf{p},\,\mathbf{p}+\boldsymbol{\kappa})=[\mathbf{p}+\boldsymbol{\kappa})^2-\mathbf{p}^2]/2M\omega_\kappa{}^3$. Introducing this expression into (49), we get, because of the symmetry of the integrations over $\mathbf{p}$ and $\mathbf{p}+\boldsymbol{\kappa}$: $\lambda_1=0$. We see therefore that the contributions of the order of v/c coming from all the exchange processes which do not involve pair formation cancel each other, leaving a correction of the order of v^2/c^2 only.

This result is valid for neutral and symmetrically charged scalar meson theories.[22] It is not valid for a purely charged theory, since the diagrams involving meson lines crossings are, in this case, excluded by charge conservation. In the present state of the physical evidence, however, it is not easy to justify a purely charged meson theory.

4.4. Corrections Arising from Pair Formation

We finally want to prove that, for the scalar meson interaction, pair formation contributes only corrections of the order of $(v/c)^4$ to the corrective ratio λ_1/λ_0. The most convenient way is, in this case, to use Eq. (41), which belongs to the general type (47g), and to calculate λ_1/λ_0 from Eq. (49g).

The introduction of the small components of $a_{ij}(\mathbf{p})$ produces a singlet-triplet separation. It is, however, easy to see that the corrections to the coupling constant are of the same order for both kinds of states. It is, therefore, sufficient and simpler to consider singlet states only. In this case, the nonvanishing components of the zero-order amplitude defined by (45) are: $a_{11}{}^{(2)}=-a_{11}{}^{(3)}=a_0(\mathbf{p})$. The amplitude $a_{ij}{}^{(0)}(\mathbf{p})$ however, which satisfies Eq. (50), possesses, in addition, the components:[23]

$$a_{12}{}^{(1)}=-a_{21}{}^{(1)}=u_1(\mathbf{p}),\quad a_{12}{}^{(2)}=-a_{21}{}^{(3)}=u_2(\mathbf{p}),$$
$$a_{12}{}^{(3)}=-a_{21}{}^{(2)}=u_3(\mathbf{p}),\quad a_{12}{}^{(4)}=-a_{21}{}^{(4)}=u_4(\mathbf{p}),$$

with the following definition:

$$u_1=u_4{}^*=\frac{i\lambda_0}{W}\int\frac{|\mathbf{p}+\boldsymbol{\kappa}|}{2M}[S_\kappa{}^{(1)}-iS_\kappa{}^{(2)}]\frac{a_0(\mathbf{p}+\boldsymbol{\kappa})}{\omega_\kappa{}^2}d^3\kappa,$$

$$u_2=-u_3{}^*=-\frac{p}{2M}\frac{[p^2+M|w|]}{MW}a_0(\mathbf{p}) - \frac{\lambda_0}{W}\int\frac{|\mathbf{p}+\boldsymbol{\kappa}|}{2M}\left[\frac{\mathbf{p}\cdot(\mathbf{p}+\boldsymbol{\kappa})}{|\mathbf{p}|\cdot|\mathbf{p}+\boldsymbol{\kappa}|}+iS_\kappa{}^{(3)}\right]\frac{a_0(\mathbf{p}+\boldsymbol{\kappa})}{\omega_\kappa{}^2}d^3\kappa, \quad (54)$$

where $\mathbf{S}_\kappa=[\mathbf{p}\times(\mathbf{p}+\boldsymbol{\kappa})]\cdot[|\mathbf{p}|\cdot|\mathbf{p}+\boldsymbol{\kappa}|]^{-1}$. Using Eq.

[21] Another way to obtain the correction λ_1/λ_0 from the B.S. equation would be to solve directly Eq. (28), by means of a variational principle. It is clear, however, that as far as the scalar interaction is concerned, the method would give results identical with those obtained above: firstly because, when pair formation is not considered, Eqs. (28) and (38) are equivalent; secondly, because, to obtain the expression (52) of $K_1(\mathbf{p},\,\mathbf{p}+\boldsymbol{\kappa})$, only terms of the order of v^2/c^2 or higher have been neglected. Furthermore, a direct solution of Eq. (28) by means of a variational principle is not only unnecessary in the present case, but also hazardous, since any "trial" function is likely to become a bad approximation in the immediate neighborhood of the poles of $A(\mathbf{p},\,\mathbf{p}_0)$. A large number of variation-iterations are necessary, in order to test the accuracy of the value of λ which is obtained. Otherwise, the errors introduced by the variational principle might well be of the same order as (if not bigger than) the "correction" which one wants to calculate.

[22] It holds for quantum electrodynamics and neutral vector meson theory, because the spin matrix elements give also, in these cases, corrections of the order of v^2/c^2.

[23] The amplitude a_{ij} possesses, for every value of i and j, 4 spin-components $a_{ij}{}^{(r)}$, $r=1,\,2,\,3,\,4$. The components a_{22} have been dropped everywhere, since they are of a still higher order in v/c. See reference 1.

(49g), the following value of λ_1/λ_0 is obtained:

$$\frac{\lambda_1}{\lambda_0} = \frac{\lambda_0^2/2MW}{\int a_0^*(\mathbf{p})[p^2+M|w|]a_0(\mathbf{p})d^3p}$$

$$\times\int\frac{a_0^*(\mathbf{p})a_0(\mathbf{p}+\boldsymbol{\kappa}+\boldsymbol{\kappa}')}{\omega_\kappa^2\omega_{\kappa'}^2}\{|\mathbf{p}|\cdot|\mathbf{p}+\boldsymbol{\kappa}+\boldsymbol{\kappa}'|\mathbf{S}_\kappa\cdot\mathbf{S}_{\kappa'}$$

$$-|\mathbf{p}+\boldsymbol{\kappa}|^{-2}[|\mathbf{p}+\boldsymbol{\kappa}|^2+\mathbf{p}\cdot(\mathbf{p}+\boldsymbol{\kappa})][|\mathbf{p}+\boldsymbol{\kappa}|^2$$

$$+(\mathbf{p}+\boldsymbol{\kappa})\cdot(\mathbf{p}+\boldsymbol{\kappa}+\boldsymbol{\kappa}']d^3pd^3\kappa d^3\kappa'\}. \quad (55)$$

The right-hand side of this equation is of the order of $(\mu/M)^4\sim(v/c)^4$. Since pair formation does not contribute to the corrections of the order of v^2/c^2, these can be obtained exactly by considering:

(a) the exchange processes, including those which involve meson lines crossings, represented by Δ_2, $\Delta_4^{(a,b)}$ and Δ_6, in Eqs. (7), (12a), (12b), (15).

(b) the relativistic part of the spin matrix elements connected positive energy states, in the expression of Δ_2 only. This contribution produces the lowest order singlet-triplet separation, which is, therefore, of the order of v^2/c^2.

5. SUMMARY AND CONCLUSION

The results of the investigation described in this paper can be summarized as follows:

(1) The T.D. formalism can be used for the non-adiabatic treatment of the relativistic two-body problem, even if it is physically necessary to take into account virtual pair formation and higher order exchange effects. It has been shown that the T.D. formalism provides, through the natural play of the equations of motion, an iteration of the exchange processes included in these equations; so that, to any order in the coupling constant, it describes an infinite series of exchange effects. This makes it suitable to the description of bound systems, in which the interaction operates during a long time.

(2) The B.S. equation has been found to give, within the limits of the "ladder" approximation, results which are equivalent to those which can be obtained, with the same approximation, from the T.D. formalism. While, in the absence of pair creation, these results are identical in both methods, there exist, when pair formation is taken into account, some small analytical differences, which, however, tend to zero in the nonrelativistic limit.

(3) A detailed study of the relativistic corrections to the scalar meson interaction of two nucleons shows that the "ladder" approximation of the B.S. equation leads to wrong results, because it neglects the processes involving meson lines crossings, which are thus physically important.

The general methods developed in this paper will be used subsequently for the treatment of the neutron-proton system in the case of the symmetrical pseudoscalar meson interaction. While most of the interaction processes will be investigated in the framework of the T.D. formalism, the equivalence between this formalism and the B.S. equation will be used in order to calculate the radiative corrections to the interaction, where an explicit renormalization of mass and charge has to be carried out.

The author would like to express his gratitude to Professor Oppenheimer, for the hospitality extended to him at the Institute for Advanced Study, and for the continued and stimulating interest which he has taken in this work. He is also very indebted to the late Professor Dancoff, for many useful discussions in connection with his method. His thanks are finally due to Professor Pais and the members of the Physics group of the Institute for Advanced Study for stimulating discussions and helpful suggestions.

Total Cross Sections of Heavy Nuclei for Fast Neutrons*

D. W. MILLER,† R. K. ADAIR, C. K. BOCKELMAN,‡ and S. E. DARDEN
University of Wisconsin, Madison, Wisconsin

(Received March 31, 1952)

The total neutron cross sections of twenty-three heavy elements from iron to bismuth have been determined as a function of neutron energy from about 0.05 Mev to 3.2 Mev. Every element whose major isotope (>50 percent abundant) has a closed neutron shell of 50, 82, or 126 neutrons is included among the elements investigated. Below 1.4 Mev, neutrons having an energy spread of 20 kev were employed to take measurements at 20-kev intervals on strontium, yttrium, barium, lanthanum, cerium, and praseodymium. Niobium and molybdenum were also investigated in this region using energy intervals of 70 kev between measurements. These measurements and earlier low energy measurements on fifteen other heavy elements were extended to 3.2 Mev, using an energy spread of 20 kev and intervals between points of about 200 kev. The most unusual feature of the results is a very broad maximum which is clearly observed in the total cross sections of thirteen of the elements studied. This maximum appears to move to higher neutron energies with increasing mass number. The position and shape of the maximum seems to be independent of all other nuclear details, such as the nuclear spin or the binding energy of the added neutron. When averaged over resonances, the total cross sections of the closed-shell nuclei do not appear to be different from the total cross sections of other nuclei of about the same masses. There is some indication that the spacing of resonances in the total cross sections of the closed-shell nuclei is greater than observed in the cross sections of other nuclei.

I. INTRODUCTION

THE observed energy dependence of the total cross sections of nuclei for fast neutrons can be compared with theory most readily in the cases of very light or very heavy nuclei. Nuclear dispersion theory predicts the variations in the total cross section caused by the presence of excited states in the compound nucleus of the reaction. This theory has been successfully compared with experiment repeatedly in cases of light nuclei with widely spaced levels. For heavy nuclei, Feshbach, Peaslee, and Weisskopf[1,2] have developed a continuum theory which predicts the energy dependence of the total cross section averaged over resonances. Only two parameters are required in this theory, the nuclear radius and the wave number of the incident neutron within the nucleus. The most important result of this theory for the present study is that the predicted total cross section is a monotonically decreasing function of neutron energy, regardless of the choice of nuclear parameters. Before the present investigation was begun, the total cross sections of heavy elements then known indicated that the validity of the theory was uncertain. Although qualitative agreement was found in some cases, the total cross sections of the elements indium, tin, antimony, and iodine up to 1.4-Mev neutron energy did not show the predicted monotonic decrease.

To provide further results for comparison with the continuum theory, in the present work the energy dependence of the total cross section was determined for 23 heavy elements. In addition to an investigation of nine elements containing neutron closed shells, the measurements previously made at Wisconsin on 12 heavy elements[3] were extended to 3.2-Mev neutron energy. These twelve elements are iron, nickel, copper, zinc, silver, indium, tin, antimony, iodine, tantalum, wolfram, and radiogenic lead. The total cross sections of the elements niobium and molybdenum were also determined in the present experiment over the entire energy range from 0.12 to 3.2 Mev.

More than one-third of the heavy elements included in the study were chosen because they consist primarily of nuclei with closed shells in neutrons. This choice allows one to make a comparison between the total cross sections of closed-shell nuclei and nonmagic nuclei, in order to determine if any differences can be observed. Because the binding energy of a neutron added to a closed-shell nucleus is abnormally small, the closed-shell-plus-one compound nucleus is formed at a lower excitation energy than its neighbors. One therefore expects the total cross section of a closed-shell nucleus to exhibit fewer resonances than other nearby nuclei. Individual resonances in the cross sections of nuclei as heavy as those investigated here usually cannot be resolved in the fast-neutron energy region. This makes direct measurements of level densities impossible. However, if one is able to observe any structure at all in the cross sections of heavy closed-shell nuclei, it will indicate fewer resonances than have been observed for heavy nonclosed-shell nuclei.

At high excitation energies the closed-shell cores are expected to be broken up, so that highly excited states of closed-shell-plus-one nuclei are not expected to differ from the highly excited states of other nuclei. Since the smallest binding energy of a neutron added to any nucleus investigated in this work is 3.9 Mev, the compound nucleus is in all cases excited well above its ground state, and no closed-shell peculiarities other than reduced level densities were anticipated.

The elements investigated in this work included all

* Work supported by the AEC and the Wisconsin Alumni Research Foundation.

† AEC Predoctoral Fellow. Now at Indiana University, Bloomington, Indiana.

‡ Now at Massachusetts Institute of Technology, Cambridge, Massachusetts.

[1] Feshbach, Peaslee, and Weisskopf, Phys. Rev. 71, 145 (1947).

[2] H. Feshbach and V. F. Weisskopf, Phys. Rev. 76, 1550 (1949).

[3] See R. K. Adair, Revs. Modern Phys. 22, 249 (1950) for references.

of the nine elements in which the major isotope (>50 percent abundant) has a closed shell of 50, 82, or 126 neutrons. These elements are strontium, yttrium, zirconium, barium, lanthanum, cerium, praseodymium, lead, and bismuth. Measurements of the total cross sections of some of these elements in the energy range covered by the present investigation have been published earlier.[3-5]

It was hoped that the present investigation would provide a test for the statistical theories, and at the same time determine if the total cross sections of closed-shell nuclei exhibit any special deviations.

II. EXPERIMENTAL PROCEDURE

All but six of the scattering samples used in the present experiment were metallic cylinders 1.75 inches in diameter. The niobium samples were in the form of 1.375-inch diameter cylinders. Antimony, iodine, yttrium oxide, strontium, and barium were enclosed in cylindrical brass containers of 1.688-inch outside diameter and 0.024-inch wall thickness. In all cases the samples were made from the element except for yttrium, which was available only in the form of yttrium oxide.

Samples of lanthanum and praseodymium, already machined to the proper dimensions, were provided by Dr. F. H. Spedding of the Ames Laboratory of the Atomic Energy Commission. Dr. Spedding's analysis stated that these samples were very pure, having a metal content greater than 99 percent. Rare earth and other metal impurities were present in such small amounts that they were not detectable by spectrographic means, or at most could be detected only in negligible amounts. Dr. Spedding also supplied the yttrium oxide, which was 99.7 percent pure and contained only traces of other rare earths. In order to drive off any water or carbon dioxide which might have been adsorbed, the yttrium-oxide powder was heated to red heat in a platinum dish immediately before being packed into the sample containers. A sample of zirconium, machined to the correct dimensions for the present experiment, was supplied by Argonne National Laboratory.

Cerium, barium, and strontium were obtained from commercial sources and machined to the proper dimensions. The analysis of the cerium metal was quoted by the supplier as 92.6 percent cerium, 1.1 percent iron, balance—other rare earth metals. For the barium the supplier gave the following analysis: 97.8 percent barium, 2.0 percent strontium and calcium. To prevent oxidation, the barium and strontium samples were sealed in brass containers immediately after machining. Samples of copper, zinc, and tin were machined from regular stocks of these metals. Antimony and iodine were pulverized and packed into brass containers. Samples of all of the remaining twelve elements were available from earlier experiments performed at Wisconsin.[6-10]

Since measurements in this experiment were taken on yttrium oxide (Y_2O_3), it was necessary to determine the oxygen cross section at each energy before the yttrium cross section could be calculated. If the oxygen cross section had been read from a curve, a small shift between the energy scales used in the earlier oxygen measurements[11] and the present measurements on yttrium oxide could have resulted in large errors in the yttrium cross section, because resonances produce rapid variations of the cross section of oxygen with energy. As a consequence, the oxygen cross section was redetermined at every energy immediately before or after the measurements on yttrium oxide. For this purpose, the transmission of neutrons through a brass can containing beryllium-oxide powder was compared with that through a brass can containing beryllium metal. The results obtained for the oxygen cross section were in excellent agreement with the earlier measurements.[11]

Cross sections were computed from the observed transmissions under the assumption that the neutron intensity decreases exponentially in the scatterer. The measurements at neutron energies above 1 Mev were carried out following the procedure described earlier,[11] using the $T(p,n)$ reaction as a neutron source. For neutron energies below 1 Mev, neutrons were obtained from the $Li(p,n)$ reaction. In most of the measurements, the neutrons were detected by observing proton-recoil pulses produced in a cylindrical ionization chamber.[11] For neutron energies above 1 Mev, the counter was filled with purified hydrogen at a pressure of 425 psi. In order to reduce the gamma-ray background, the hydrogen pressure was reduced as the neutron energy was decreased below 1 Mev. At low pressures the chamber was operated as a proportional counter in order to improve the signal-to-noise ratio.

Neutrons emitted from the target in the forward direction were used for all measurements above 0.12 Mev. Measurements were taken at an angle of 115 degrees with respect to the proton beam for neutron energies below 0.12 Mev, since $Li(p,n)$ neutrons emitted in the forward direction are not monoergic below this energy.

For measurements on lanthanum, niobium, and molybdenum below 1 Mev, and on cerium below 1.3 Mev, a BF_3 counter was used.[8] Measured backgrounds for the BF_3 counter varied from 8 percent of the direct neutron flux in the forward direction to 25 percent in the 115-degree direction. All data taken with the BF_3

[4] S. Kikuchi and H. Aoki, Proc. Phys. Math. Soc. Japan **21**, 75 (1939); H. Aoki, Proc. Phys. Math. Soc. Japan **21**, 232 (1939).
[5] Zinn, Seely, and Cohen, Phys. Rev. **56**, 260 (1939).
[6] Barschall, Bockelman, and Seagondollar, Phys. Rev. **73**, 659 (1948).
[7] Bockelman, Peterson, Adair, and Barschall, Phys. Rev. **76**, 277 (1949).
[8] Barschall, Bockelman, Peterson, and Adair, Phys. Rev. **76**, 1146 (1949).
[9] R. K. Adair, Phys. Rev. **77**, 748 (1950).
[10] Peterson, Adair, and Barschall, Phys. Rev. **79**, 935 (1950).
[11] Bockelman, Miller, Adair, and Barschall, Phys. Rev. **84**, 69 (1951).

counter were corrected for background. No background corrections were applied to data taken with the recoil counter in the forward direction, because in this case the background was negligible. It was necessary, however, to make a correction to the measurements taken with the recoil counter in the 115-degree direction, where the background was of the order of 9 percent.

The scattering samples were placed midway between the target and the center of the active volume of the counter. For the recoil counter, the distance from the target to the center of the active counting volume was 14 inches, while for the BF_3 counter a distance of 10 inches was used. In addition to the background corrections, a correction was applied for the effects of neutrons scattered into the counter by the sample. The latter correction was made on the assumption that the neutrons were scattered isotropically from the sample. With this assumption, 1.5 percent of the scattered neutrons enter the counter in the 14-inch geometry and 3 percent in the 10-inch geometry.

For most of the low energy data taken in this investigation, lithium targets causing a 20-kev energy loss for protons of threshold energy were used. The only exceptions were niobium and molybdenum from 0.15 to 1.0 Mev (85-kev lithium target) and cerium from 0.006 to 0.110 Mev (8-kev lithium target). All of the high energy measurements employed a Zr−T target which caused an energy loss of 35 kev for 1-Mev protons.[11] Over most of the energy range investigated, however, the target thickness of the Zr−T target was about 20 kev.

For measurements above 1.4 Mev, widely-spaced points were taken in order to determine the energy dependence of the average cross section. In general, it is desirable to use a neutron energy spread which is equal to the spacing between measurements in order to obtain a smooth variation of the experimental cross section with a minimum number of measurements. Smaller neutron energy spreads are also wasteful of generator time, since the neutron yield and counting rate decrease with decreasing target thickness. In this investigation, however, the thickest Zr−T target available caused a neutron energy spread nearly ten times smaller than the energy intervals at which measurements were performed above 1.4 Mev. This disadvantage was partly offset by a small gain of information; namely, if the widely-spaced points indicated considerable variations in the cross section, one could conclude that the level spacing was comparable to or greater than the energy spread used. This statement should not be taken to imply that the level spacing was smaller than the neutron energy spread if the widely-spaced points exhibited no appreciable fluctuations, for narrow levels could easily have been missed.

III. RESULTS

The total cross sections of the elements studied are plotted as a function of neutron energy in Figs. 1 and 2. In those cases where experimental points are not indicated below 1 Mev, the solid curves reproduce the results of the earlier Wisconsin measurements.[6–11] Vertical bars indicate data obtained in the present investigation, the length of each vertical bar representing the standard statistical error in the measurement. The approximate neutron energy spread employed is represented by the length of the base of the large triangle in each energy region. It should be emphasized that the solid curve drawn above 1 Mev in each case represents an estimate of the cross section *averaged over resonances*. The best smooth curve was drawn through the experimental points obtained in the present work. Since the energy spread of the neutrons utilized in this region was usually less than the spacing between experimental points, fluctuations of the experimental points considerably beyond the statistical error from the solid curve indicate the presence of resonance structure.

Iron, the lightest element included in this study, is the only element investigated which shows appreciable structure at high neutron energies except for a few elements which consist principally of closed-shell nuclei. The experimental curve seems to indicate that the average cross section of iron reaches a minimum value at about 1.2 Mev, and then increases with increasing neutron energy to 3.2 Mev. This increase may not be significant because of the uncertainty in the average cross section introduced by the large number of resonances. The average cross section of nickel, the second element beyond iron in the periodic table, does not increase at high energies, but rather decreases with increasing neutron energy to about 1.5 Mev and is nearly constant from 1.5 to 3.2 Mev. With the neutron energy spread used, there is much less evidence at high neutron energies for structure in the nickel cross section than in the iron cross section. This may be caused partly by the presence of two isotopes in nickel.

The earlier Wisconsin results[9] for copper and zinc, indicated by the solid curves below 1 Mev, were obtained with thick lithium targets, which precluded the observation of individual resonances. It will be noted that the cross sections of nickel, copper, and zinc at high neutron energies are almost identical in shape and magnitude.

The principal isotope of each of the next three elements investigated, strontium, yttrium, and zirconium, contains 50 neutrons. Four peaks are observed in the strontium cross section below 0.7 Mev. It is not at all clear that these peaks are actually individual resonances; in fact, the shape of the peak at 0.33 Mev indicates the superposition of two or more resonances. The widths of the peaks at 0.12, 0.44, and 0.53 Mev are all about 40 kev, or twice the experimental energy spread. No attempt was made to study in detail the variations in the strontium cross section above 0.7 Mev. The solid curve drawn above this energy therefore represents the cross section averaged over resonances. Above 0.7 Mev, the large fluctuations in the experi-

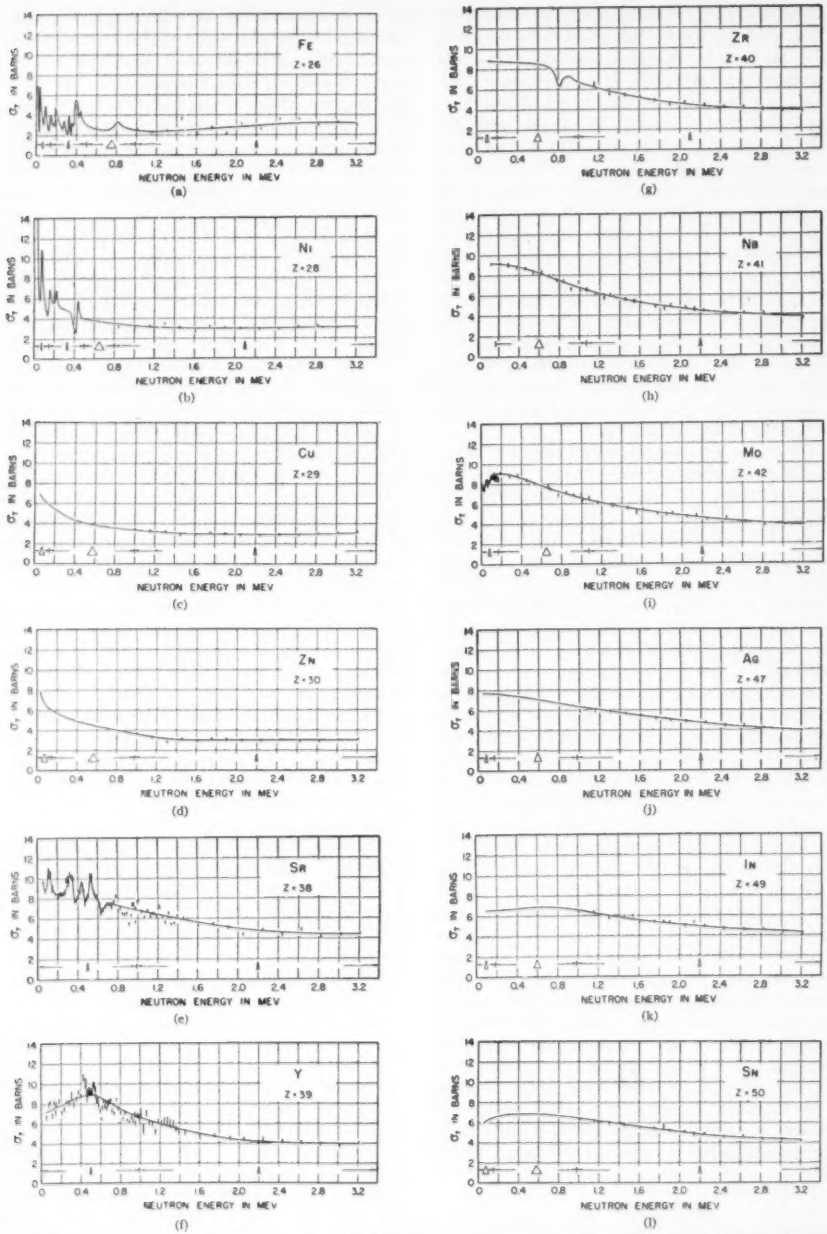

FIG. 1. Total cross sections for fast neutrons of iron, nickel, copper, zinc, strontium, yttrium, zirconium, niobium, molybdenum, silver, indium, and tin. See the first paragraph of Sec. III in the text for explanation of symbols and curves.

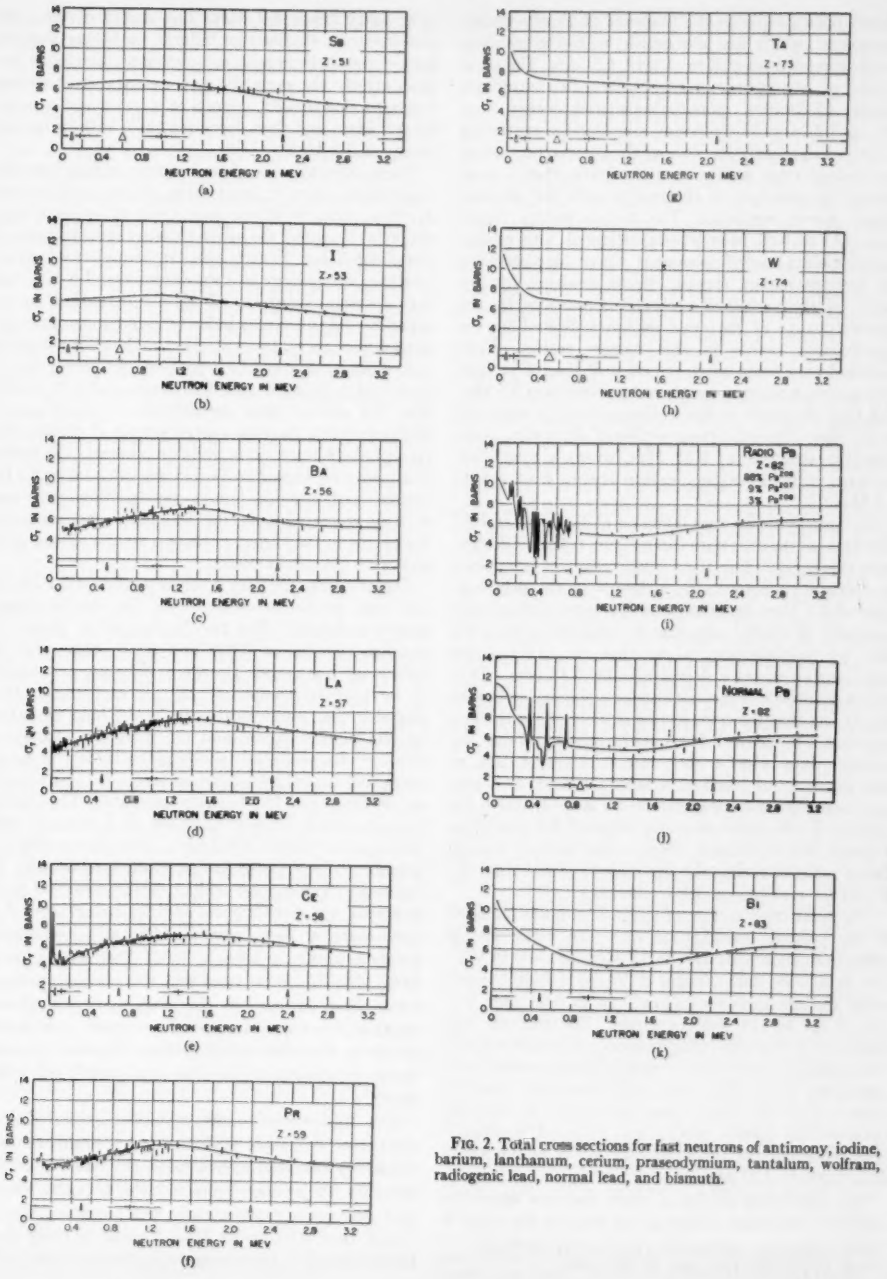

FIG. 2. Total cross sections for fast neutrons of antimony, iodine, barium, lanthanum, cerium, praseodymium, tantalum, wolfram, radiogenic lead, normal lead, and bismuth.

mental points indicate the presence of closely-spaced resonances, which are observable with the neutron energy spread employed to at least 1.5 Mev. The cross section of strontium averaged over this structure appears to decrease monotonically with energy from 0.05 to 3.2 Mev. For yttrium, considerable scattering of the experimental points about the curve representing the average cross section again indicates that a large amount of structure is observable with the neutron energy spread employed. The narrow energy region from 0.45 to 0.67 Mev was investigated with experimental points spaced somewhat closer together than the neutron energy spread. Strong evidence for the reality of the variations observed is provided by the smooth change of the cross section indicated by the experimental points in this narrow region. When averaged over resonances, the cross section of yttrium increases with neutron energy to a maximum at 0.5 Mev and then decreases as the neutron energy is increased to 3.2 Mev. The total cross section of zirconium, apart from the structure at 0.85 Mev, shows a monotonic decrease with increasing neutron energy from 0.1 to 3.2 Mev.

No measurements were taken on niobium in the 115° direction, so that the data extend from 0.12 to 3.2 Mev. Over this energy range the average cross section appears to decrease monotonically, although in the neighborhood of 0.2 Mev the cross section appears to be nearly constant. A similar behavior is indicated around 0.2 Mev by molybdenum, except that the molybdenum cross section shows a decrease below 0.12 Mev. That such a decrease might occur also for niobium is indicated by the fact that the cross section of niobium for thermal neutrons is 6.7 barns.[12] It should be mentioned that the niobium data below 1 Mev were thick target data, so that no structure could have been observed. As a consequence, no comparison should be made between the amount of resonance structure observed for strontium, yttrium, and zirconium, whose major isotopes contain closed neutron shells, and the amount of structure observed for niobium, which is nonmagic.

The total cross section of molybdenum was obtained in the present investigation over the entire energy range from about 0.02 Mev to 3.2 Mev. Below 0.16 Mev, the data were taken using a 30-kev lithium target, while the measurements from 0.16 to 0.98 Mev employed an 85-kev lithium target. No structure was observed in the low energy region with these targets. The average cross section of molybdenum increases to a maximum at 0.2 Mev, and then decreases smoothly from 0.2 to 3.2 Mev. Good agreement is obtained between the present results and those of Stubbins,[13] who measured the total cross section of molybdenum from 0.010 to 1.23 Mev.

The total cross section of silver does not appear to exhibit a maximum, although the slope of the curve is quite small below 0.2 Mev. The shapes of the cross section curves obtained for indium, tin (whose isotopes have closed shells in protons), antimony, and iodine are qualitatively the same. In each case the cross section increases slowly with energy to a maximum around 0.5–1.0 Mev, and then decreases again with increasing energy to 3.2 Mev.

The principal isotope of each of the next four elements investigated, barium, lanthanum, cerium, and praseodymium, contains 82 neutrons. Over the entire energy region investigated, the neutron energy spread employed was about 20 kev. In each case, the average cross section increases with energy to a maximum near 1.4 Mev and then decreases again to 3.2 Mev. Fluctuations in the experimental points may indicate the presence of closely-spaced resonances. In an attempt to determine whether individual levels could be separated, the energy ranges from 0.35 to 0.58 Mev for lanthanum and 0.40 to 0.61 Mev for cerium were reexamined at closely-spaced energies with a neutron energy spread of 10 kev, but no reproducible structure could be resolved. The results obtained with higher resolution are not plotted in the figures, but smooth curves representing the cross sections averaged over the resonance and statistical variations in the higher resolution results agreed quite well with the curves shown.

Definite structure may be observed below 0.1 Mev in the cross section of cerium with the neutron energy spread employed. The two peaks, which appear at neutron energies of 0.024 and 0.097 Mev, may be individual resonances. However, they are too narrow to be resolved completely in this experiment. It is probable that elastic scattering is the only important process in this region, and the minimum changes in cross section predicted by resonance theory for elastic scattering caused by individual levels at these energies are 98 barns and 24.2 barns, respectively. The changes in cross section actually observed are 5 barns at 0.024 Mev and 1.2 barns at 0.097 Mev. Since the experimental heights of these peaks are so much smaller than the theoretical values, the widths of the observed peaks represent the experimental neutron energy spread at these energies. The observed widths at half-maximum for these peaks are 5 kev at 0.024 Mev and 13 kev at 0.097 Mev. It will be noted that there is some evidence for a sharp increase in the cross section of praseodymium below 0.1 Mev, possibly caused by structure similar to that observed in cerium. However, measurements on praseodymium were not carried below 0.05 Mev.

The thick-target results obtained earlier[7] for the total cross sections of tantalum and wolfram are represented by the solid curves below 0.7 Mev. For these elements, the average cross sections are quite similar, both decreasing monotonically with increasing neutron energy from 0.02 to 3.2 Mev. Neither of them shows the maximum in the average cross section exhibited by

[12] Wu, Rainwater, and Havens, Phys. Rev. **71**, 174 (1947).
[13] W. F. Stubbins, Phys. Rev. **84**, 902 (1951).

all elements heavier than silver which were investigated in this experiment.

Radiogenic lead and normal lead both contain closed shells in protons, but the isotope Pb^{208}, which also contains a closed shell in neutrons, is 52 percent abundant in normal lead and nearly absent in radio lead. When averaged over resonances, the cross sections of normal lead and radio lead exhibit very similar behavior. Both cross sections reach a minimum near 1.3 Mev, and then increase with increasing neutron energy to 3.2 Mev, where the curves appear to have zero slope. For normal lead some resonance structure, observable with the neutron energy spread employed, is indicated at high neutron energies by the scatter of experimental points. A reproducible high point at 1.75 Mev indicates the presence of one or more peaks in the lead cross section at about this energy. The solid line above 1 Mev represents the cross section averaged over this resonance structure.

Measurements on lead at the Massachusetts Institute of Technology[14] cover an energy region in common with the present experiment from 1.0 to 2.35 Mev. The M.I.T. data do not show the increase with energy indicated in the present measurements above 1.4 Mev. However, an investigation carried out by Stafford[15] shows an increase of the total cross section in this energy region similar to that obtained in the present measurements.

Bismuth is similar to normal lead in that its principal isotope contains a closed shell of 126 neutrons; however, bismuth does not contain a closed proton shell. The energy dependence of the average cross section of bismuth is qualitatively the same as found for radiogenic lead and normal lead, exhibiting a definite minimum around 1.2 Mev.

Aoki[4] and Zinn *et al.*,[5] obtained results for some of the elements included in this investigation using $D+D$ neutrons. In six comparisons made with the values obtained by Zinn *et al.*, agreement within the sum of the statistical errors quoted in the two experiments is found in five cases. The value obtained by Zinn *et al.*, for zinc is somewhat higher than that found in the present investigation. On the other hand, Aoki's measurements differ from the curves in Figs. 1 and 2 by more than the sum of the statistical errors in all of the thirteen cases compared. In twelve of the comparisons his results are lower than the present measurements, the only exception being barium.

The differences between the values obtained by Aoki and by Zinn *et al.*, can be explained in terms of the geometry and the inscattering corrections used in the two experiments.[16] In their experiments as well as in the present investigation, corrections for scattering into the detector were calculated on the assumption that the distribution of scattered neutrons was isotropic. This assumption is not expected to be correct at higher energies because of anisotropic diffraction scattering. As a result, the cross sections reported in all three experiments are expected to be low. If one is to retain the assumption of isotropic scattering, the error in the final result will be smaller if the geometry of the experiment can be improved; i.e., if the solid angle subtended by the scatterer at the detector can be reduced. In the three experiments under consideration, this solid angle was as follows: Zinn *et al.*, $d\Omega/4\pi=0.0025$; present investigation, $d\Omega/4\pi=0.0039$; Aoki, $d\Omega/4\pi=0.0055$. As a consequence, one expects the results of Zinn *et al.*, to be slightly higher and those of Aoki to be lower than the values obtained in the present measurement. This may explain the differences between the results of the three experiments.

The error in the cross section resulting from the failure of the inscattering correction to take diffraction scattering into account is expected to be largest for the heaviest elements and the highest energies. An investigation of this effect indicated that the maximum error introduced into the results by an isotropic inscattering correction amounts to about 10 percent in the worst cases.[17]

For the measurements on lanthanum, praseodymium, and zirconium, only thin samples were available for the present investigation. As a consequence, the high transmission caused a larger statistical error for these elements. Since the yttrium cross section was obtained from two separate measurements, the statistical error in the yttrium cross section was also high. The standard statistical error in nearly all of the measurements was between 2 and 4 percent.

IV. DISCUSSION

The outstanding features of the results of the present investigation concern the energy dependence of the total cross section averaged over resonances. In the energy region investigated, the total cross sections of neighboring elements show a striking similarity both in shape and in magnitude. Furthermore, a slow variation of the shape and magnitude of the cross section takes place with increasing nuclear mass or size.[18] The average cross section does not seem to depend strongly upon other characteristics of the nucleus, such as the nuclear spin, binding energy of the added neutron, or the closed-shell property. For example, the average total cross sections of niobium (single isotope) and molybdenum (seven isotopes) are almost identical. Again, the average cross section of lead, whose major isotope has a closed shell in neutrons, is nearly the same as that of radiogenic lead, whose major isotope is not neutron-magic. The binding energies of a neutron added to the

[14] Willard, Preston, and Goodman, unpublished Technical Report No. 45, Mass. Inst. Tech. (1950).
[15] G. H. Stafford, Proc. Phys. Soc. (London) **64A**, 388 (1951).
[16] R. K. Adair, Revs. Modern Phys. **22**, 249 (1950).
[17] M. Walt, private communication.
[18] This behavior is summarized by a three-dimensional representation of the cross section as a function of neutron energy and nuclear mass. See H. H. Barschall, Phys. Rev. **86**, 431 (1952).

principal isotopes of lead and radiogenic lead are also quite different; Harvey[19] lists them as about 3.9 and 6.8 Mev, respectively. A further illustration of the spin independence of the cross section when averaged over resonances is given by the similarity of the cross sections of lead, whose major isotope probably has spin zero, and bismuth, which has a spin of 9/2.

Another interesting feature of the experimental results is a very broad maximum which occurs in the cross sections of at least 13 of the 23 elements studied. In particular, such a maximum is observed for all elements heavier than silver which were included in the investigation, with the exceptions of tantalum and wolfram. In addition, this maximum appears to move to higher neutron energies with increasing mass number.

The rise in the cross sections of radiogenic lead, normal lead, and bismuth at high neutron energies is preceded by a minimum. It is interesting to note that the magnitude of the cross section at this minimum at 1.2 Mev is about $2\pi R^2$, which is much smaller than expected at this energy. This may result from some sort of interference effect, possibly similar to that observed between resonance and potential scattering of neutrons. It is not clear from the present results whether one should describe the cross-section curves for radio lead, normal lead, and bismuth as representing maxima at 3.2 Mev or minima at about 1.2 Mev. However, the results obtained by Stafford[15] for normal lead indicate that the cross section drops off again fairly rapidly at neutron energies higher than attained in the present investigation, the center of the resultant maximum occurring at 3.2 Mev, in agreement with the curve drawn in Fig. 2.

It may not be surprising that the average total cross section appears to be largely a function of the nuclear size at high energies where optical diffraction effects are prominent. However, one cannot readily explain the change in the position of the maximum in the average cross section using an optical model. If one assumes that the maximum represents evidence for some nuclear property, according to an optical model this property would be expected to depend only on R/λ. With this hypothesis, the maximum would be expected to shift to larger wavelengths or lower energies with increasing nuclear radius. Yet the results described above show the opposite behavior; the maximum appears to move to higher energies with increasing nuclear size.

It has been pointed out earlier that the continuum theory formulated by Feshbach, Peaslee, and Weisskopf[1,2] predicts a monotonic decrease in the total cross section as a function of neutron energy. At least thirteen of the twenty-three elements investigated in this work do not exhibit this behavior, but instead show a broad maximum in the total cross section. Results for cadmium obtained earlier by Fields *et al.*,[20] using photoneutrons, exhibit a similar behavior, making at least fourteen elements whose cross sections disagree with the theory in this respect. It would seem to be worthwhile, then, to attempt to find a modification of the theory which will account for the observed deviations. Such a modification has recently been proposed by Weisskopf.[21]

There is some evidence that the spacings between resonances exhibited by the total cross sections of the closed-shell nuclei are larger than shown by nonclosed-shell nuclei, in agreement with the considerations discussed earlier. Since the level densities of the compound nucleus near the energy of binding of the last neutron to the nucleus depend strongly upon the odd-even or even-even character of the target nucleus,[22] the effect of a closed shell will be superimposed upon this variation. The results of the present investigation show that the level densities indicated by the cross sections of strontium, primarily an even-even closed-shell nucleus, and yttrium, an even-odd closed-shell nucleus, are comparable to that shown by iron, a much lighter nonclosed-shell even-even nucleus. Again, cerium, an even-even closed-shell nucleus, exhibits some structure at low neutron energies, which indicates a level spacing much greater than one would expect for nuclei of this mass. The contrast between the level spacings indicated by the total cross sections of lead and radiogenic lead at low energies provides further evidence for reduced resonance densities in the cross sections of closed-shell nuclei.[10]

V. ACKNOWLEDGMENTS

The authors wish to thank Professor H. H. Barschall for advice and suggestions concerning this investigation. Helpful discussions of the results with Professor E. P. Wigner are gratefully acknowledged. They also wish to thank Dr. F. H. Spedding of the Ames Laboratory for taking a keen interest in the investigation of the closed-shell nuclei, and Jack Powell, Adrian Daane, and W. J. McGinnis, members of Dr. Spedding's research group, who prepared the samples of lanthanum, praseodymium, and yttrium, under Dr. Spedding's direction. The authors are also indebted to Professor D. J. Mack of the University of Wisconsin Department of Mining and Metallurgy for helpful suggestions concerning the preparation of the cerium, barium, and strontium samples.

[19] J. A. Harvey, Phys. Rev. **81**, 353 (1951).

[20] Fields, Russell, Sachs, and Wattenberg, Phys. Rev. **71**, 508 (1947).

[21] V. F. Weisskopf, Phys. Rev. **86**, 582 (1952).

[22] H. Hurwitz and H. A. Bethe, Phys. Rev. **81**, 898 (1951).

Pulse-Free Discharges in Negative Point-to-Plane Corona

ALLAN GREENWOOD
Department of Electrical Engineering, The University, Leeds, England
(Received April 24, 1952)

Near breakdown the negative point-to-plane corona discharge has been observed to adopt a pulse-free mode. The physical characteristics of this phase are described, but no attempt is made to explain the transition from the pulsating discharge.

IN a paper dealing with point-to-plane corona in dry air, Bandel[1] refers to a "pulseless Townsend discharge" which he has observed with a negative point near breakdown. Similar observations have been made independently in this Department during studies on high current, negative point-to-plane discharges, with short gaps. Using a suitable optical system, it has been possible to investigate the precise structure of the discharge, and also obtain photographs of the phenomenon. Tests have been made with both steel and platinum points, 1 mm in diameter, with a gap length of 1 cm.

The ring discharge described by Greenwood,[2] is modified with increasing gap voltage, until, at about 13 kv with the particular electrode geometry considered, an extensive cap over the end of the point, bounded roughly by the limits of the preceding ring, is covered with a turbulent array of discharge. The change from this phase to the pulse-free discharge is comparatively abrupt, although the transition is frequently signalled by sharp filamentary spikes which appear amongst the general glow just described.

The Townsend type discharge is remarkable for its great luminosity compared with the previous modes. It has a small intense button of negative glow adjacent to the point, a short but well-defined dark space, and then a spike-like jet of positive column associated with a fan. The spike passes centrally through this fan and is clearly visible beyond. As the gap voltage is increased this becomes more noticeable, and ultimately, when flashover occurs, it is along this channel that the main spark travels.

The principal dimensions of the discharge on a 1 mm diameter point are shown in Fig. 1. They serve to illustrate well a point mentioned by Bandel,—the way in which the main stem is constricted laterally in the region beyond the Faraday dark space. Much effort has been devoted to producing a photograph showing clearly the sharp boundaries of the dark space, but this has so far eluded us. The intensity of the adjoining portions of the discharge is so great, that even with short exposures, these regions merge, and the intervening dark space is lost. Conditions are aggravated by the reflected glare from the polished surface of the point. In Fig. 2 the clarity of this part of the discharge has been sacrificed to some extent in order to bring out more sharply the fan and the cigar-shaped central spike. There is no distinct limit to the discharge on the side remote from the point, indeed a faint cone of diffused light stretches right across the gap to the anode.

The spike discharge forms more readily on steel points than on points made of platinum. On platinum

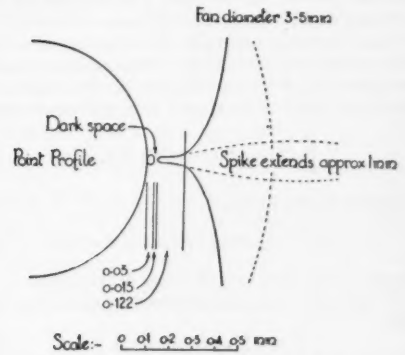

FIG. 1. Leading dimensions of the spike discharge.

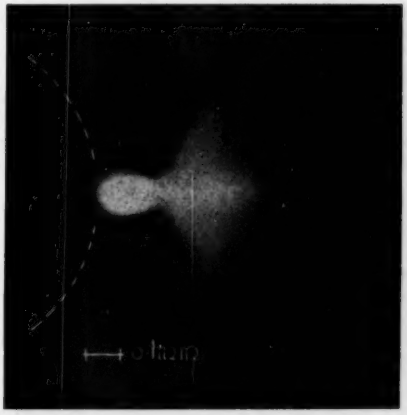

FIG. 2. Spike discharge on a 1-mm diameter point, gap voltage 14.8 kv, current 165 μa.

[1] H. W. Bandel, Phys. Rev. **84**, 92 (1951).
[2] A. N. Greenwood, Nature **168**, 41 (1951).

points the spike rarely settles, but oscillates about the surface with great rapidity. With steel points, on the other hand, the discharge frequently anchors itself to one spot, and there remains quite steady, only moving about when the field is increased almost to flashover. It is not unusual for the stem to take up a position off, and inclined to, the axis of symmetry. When the point is subsequently examined under the microscope it is usually found that the spot favored by the root of the discharge, coincides with a small crater on the surface. These form more readily on steel than on platinum, the process no doubt being assisted by chemical action, and this may account for the effect referred to.

Discourse on the mechanism of the transition from the Trichel pulse regime to the pulse-free discharge would be little more than speculation at this stage, comment is therefore reserved until a more thorough investigation of the phenomenon has been made. It is perhaps worth stating that too much importance should not be attached to the changes in shape of the induced Trichel pulses as the transition is approached, since these are largely conditioned by the circuit.

PHYSICAL REVIEW VOLUME 88, NUMBER 1 OCTOBER 1, 1952

Electronic States in Crystals under Large Over-All Perturbations*

PAULA FEUER
Purdue University, Lafayette, Indiana
(Received May 15, 1952)

Solutions of the three-dimensional Schrödinger equation are discussed for a potential which is the sum of a potential with the periodicity of the crystal lattice plus a perturbing potential. A general theory of large over-all perturbations, such that the energy lies close to one permitted band in one region of the crystal and close to a second permitted band in another, is developed. The theory is then applied to a one-dimensional crystal in a uniform electric field, using the narrow band approximation; the probability for an electron to cross a forbidden energy band is calculated. These results are considered in connection with the interpretation of the current-voltage characteristic of an $N-P$ junction of germanium at high electric fields.

I. INTRODUCTION

A METHOD for obtaining solutions of the perturbed periodic wave equation

$$-(\hbar^2/2m)\nabla^2\psi-\{E-V_P(\mathbf{r})-V(\mathbf{r})\}\psi=0, \qquad (1)$$

where $V_P(\mathbf{r})$ is a periodic potential associated with a crystal lattice and $V(\mathbf{r})$ is some sort of perturbing potential, has been described by Slater.[1]

The method consists of expanding ψ in terms of localized functions, originally used by Wannier[2] in connection with the theory of the exciton, and defined as follows: Let $\psi_0(\mathbf{p};\mathbf{r})$ represent a solution of the periodic wave equation [Eq. (1) with $V(\mathbf{r})=0$] corresponding to the effective momentum $\mathbf{p}$ and such that

$$\int\psi_0^*(\mathbf{p};\mathbf{r})\psi_0(\mathbf{p};\mathbf{r})dV=1,$$

the integration being taken over the volume of the crystal. In a permitted band $\mathbf{p}$ assumes values given by $N_i\mathbf{p}\cdot\boldsymbol{\tau}_i=n_i\hbar$, where the n_i are integers which have values $0, \pm1, \pm2, \cdots$, the $\boldsymbol{\tau}_i$ are the primitive lattice translations, and each N_i is the number of cells of the crystal extending along an axis parallel to $\boldsymbol{\tau}_i$. Now, if the phases of the $\psi_0(\mathbf{p};\mathbf{r})$ are properly chosen,

$$a(\mathbf{r}-\mathbf{r}_k)=N^{-\frac{1}{2}}\textstyle\sum_{\mathbf{p}}\exp[-(i/\hbar)\mathbf{p}\cdot\mathbf{r}_k]\psi_0(\mathbf{p};\mathbf{r}) \qquad (2)$$

represents a function localized around the kth atom of the crystal. (The choice of phases of the ψ_0 is very important and will be discussed in considerable detail in the appendix.) The number of atoms of the crystal is N and the sum is taken over all values of $\mathbf{p}$ in a particular permitted band. Thus, corresponding to each permitted band of the crystal, there is a Wannier function for each atom of the crystal. It is easily shown that

$$\int a^*(\mathbf{r}-\mathbf{r}_k)a(\mathbf{r}-\mathbf{r}_m)dV=\delta_{km}. \qquad (3)$$

It can also be shown that

$$\psi_0(\mathbf{p};\mathbf{r})=\textstyle\sum_k\exp[(i/\hbar)\mathbf{p}\cdot\mathbf{r}_k]a(\mathbf{r}-\mathbf{r}_k), \qquad (4)$$

the sum being taken over all atoms of the crystal.

The solution of Eq. (1) proposed by Slater has the form

$$\psi(\mathbf{r})=\textstyle\sum_k\phi(\mathbf{r}_k)a(\mathbf{r}-\mathbf{r}_k). \qquad (5)$$

Slater shows that if this expansion is valid and if $V(\mathbf{r})$ is so slowly varying as to be considered constant over a distance comparable with the range of the Wan-

* This work was supported in part by the Signal Corps and is based on a thesis presented in partial fulfillment of the requirements for the degree of Doctor of Philosophy at Purdue University.

[1] J. C. Slater, Phys. Rev. **76**, 1592 (1949).

[2] G. H. Wannier, Phys. Rev. **52**, 191 (1937).

nier functions, the $\phi(\mathbf{r}_k)$ can be obtained by solving the set of difference equations

$$-E\phi(\mathbf{r}_k)+\sum_s A(\mathbf{r}_k-\mathbf{r}_s)\phi(\mathbf{r}_s)+V(\mathbf{r}_k)\phi(\mathbf{r}_k)=0. \quad (6)$$

The A's depend on the unperturbed problem only and have a simple interpretation. Let $E(\mathbf{p})$ represent the energy of the unperturbed problem as a function of the momentum. If a single permitted band is considered, $E(\mathbf{p})$ can be treated as a periodic function of $\mathbf{p}$, and it can be shown that

$$A(\mathbf{r}_s)=N^{-1}\sum_{\mathbf{p}} \exp[(i/\hbar)\mathbf{p}\cdot\mathbf{r}_s]E(\mathbf{p}) \quad (7)$$

and

$$E(\mathbf{p})=\sum_s \exp[-(i/\hbar)\mathbf{p}\cdot\mathbf{r}_s]A(\mathbf{r}_s). \quad (8)$$

Thus the A's are just Fourier coefficients in the expansion of the energy of the unperturbed problem as a function of the effective momentum.

The following criticism[3] of Slater's theory can be made, however. If Eq. (2) is substituted into Eq. (5), we obtain

$$\psi(\mathbf{r})=\sum_{\mathbf{p}} c(\mathbf{p})\psi_0(\mathbf{p};\mathbf{r}), \quad (9)$$

where

$$c(\mathbf{p})=N^{-1}\sum_k \phi(\mathbf{r}_k)\exp[-(i/\hbar)\mathbf{p}\cdot\mathbf{r}_k].$$

Now, all the well-behaved solutions of the periodic problem form a complete set, but those corresponding to one permitted band do not; thus Eq. (9) and Eq. (5) represent an expansion of $\psi(\mathbf{r})$ in terms of an incomplete set of functions. It is a good approximate solution provided that the energy considered lies always close to only one permitted energy band. (The Wannier functions used in Eq. (5) must then be those which correspond to this particular permitted band.) If the energy considered lies close to two overlapping permitted bands or if the energy lies close to one permitted band in one region of the crystal and close to a second permitted band in another, the approximation is no longer a good one.

This limitation of Slater's theory has also been pointed out by Adams,[4] who has considered the perturbed periodic problem for the general case of a perturbing potential which is a function of both position and momentum. Adams expresses the solution of the perturbed periodic wave equation in the form

$$\psi=\sum_{k,n}\phi_n(\mathbf{r}_k)a_n(\mathbf{r}-\mathbf{r}_k), \quad (10)$$

where the sum over k is taken over all atoms of the crystal [as in Eq. (5)]; $a_n(\mathbf{r}-\mathbf{r}_k)$ are the Wannier functions corresponding to the nth permitted band and the sum over n is taken over all permitted bands of the crystal. The wave function ψ is thus expanded in terms of a complete set of functions. Adams then derives a set of simultaneous differential equations from which the $\phi_n(\mathbf{r}_k)$, considered as continuous functions of $\mathbf{r}$, can be determined.

It is the purpose of this paper to present an alternate formulation of the problem, for the case in which the perturbing potential is a function of position only. The solutions ψ of Eq. (1) will be expressed in the form of Eq. (10) and difference equations will be derived for the $\phi_n(\mathbf{r}_k)$. The general theory will then be used to discuss a special model of a one-dimensional crystal under a uniform electric field, and the probability per unit time for an electron to cross a forbidden energy band will be calculated.

II. THE DIFFERENCE EQUATIONS

Substituting Eq. (10) into Eq. (1), we obtain

$$\{H_0-E+V(\mathbf{r})\}\sum_{k,n}\phi_n(\mathbf{r}_k)a_n(\mathbf{r}-\mathbf{r}_k)=0, \quad (11)$$

where

$$H_0=-(\hbar^2/2m)\nabla^2+V_P(\mathbf{r})$$

is the unperturbed Hamiltonian. To obtain difference equations for the $\phi_n(\mathbf{r}_k)$ we multiply Eq. (11) by $a_l^*(\mathbf{r}-\mathbf{r}_m)$ and integrate over the volume of the crystal. The following integrals are then of interest. It can easily be seen that

$$\int a_l^*(\mathbf{r}-\mathbf{r}_m)a_n(\mathbf{r}-\mathbf{r}_k)dV=\delta_{nl}\delta_{km}. \quad (12)$$

For, according to Eq. (2), $a_n(\mathbf{r}-\mathbf{r}_k)$ is a linear combination of unperturbed wave functions $\psi_{0n}(\mathbf{p};\mathbf{r})$, the subscript n being used to denote the nth permitted band; similarly $a_l(\mathbf{r}-\mathbf{r}_k)$ is a linear combination of unperturbed wave functions $\psi_{0l}(\mathbf{p};\mathbf{r})$ of the lth permitted band. When $n\neq l$, all functions ψ_{0n} and ψ_{0l} are orthogonal and hence the integral above vanishes for all values of k and m. When $n=l$, Eq. (12) is the same as Eq. (3). Consider

$$I_{ln}(\mathbf{r}_m-\mathbf{r}_k)=\int a_l^*(\mathbf{r}-\mathbf{r}_m)H_0a_n(\mathbf{r}-\mathbf{r}_k)dV.$$

Using Eq. (2)

$$I_{ln}(\mathbf{r}_m-\mathbf{r}_k)=N^{-1}\sum_{\mathbf{p},\mathbf{p}'}\exp[(i/\hbar)\mathbf{p}\cdot\mathbf{r}_m]$$

$$\times\exp[-(i/\hbar)\mathbf{p}'\cdot\mathbf{r}_k]\int\psi_{0l}^*(\mathbf{p};\mathbf{r})H_0\psi_{0n}(\mathbf{p}';\mathbf{r})dV.$$

When the unperturbed Hamiltonian operates on $\psi_{0n}(\mathbf{p}';\mathbf{r})$, the wave function is just multiplied by the energy corresponding to the effective momentum $\mathbf{p}'$. Thus

$$I_{ln}(\mathbf{r}_m-\mathbf{r}_k)=N^{-1}\sum_{\mathbf{p},\mathbf{p}'}\exp[(i/\hbar)\mathbf{p}\cdot\mathbf{r}_m]$$

$$\times\exp[-(i/\hbar)\mathbf{p}'\cdot\mathbf{r}_k]E_n(\mathbf{p}')\int\psi_{0l}^*(\mathbf{p};\mathbf{r})\psi_{0n}(\mathbf{p}';\mathbf{r})dV.$$

Since all ψ_{0l} and ψ_{0n} are orthogonal for $n\neq l$, $I_{ln}=0$ for

[3] The discussion of the limitations of Slater's theory, the general theory of large over-all perturbations, and the application of the general theory to a crystal in a uniform electric field, which follow, were presented on October 27, 1951, at the 308th meeting of the American Physical Society.

[4] E. N. Adams II, Phys. Rev. **85**, 41 (1952).

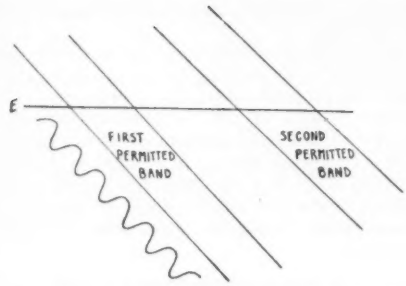

FIG. 1. Potential and energy bands in a periodic potential perturbed by a linear potential.

$n \neq l$. When $n=l$,

$$\int \psi_{0l}^*(\mathbf{p};\mathbf{r})\psi_{0l}(\mathbf{p}';\mathbf{r})dV=\delta_{\mathbf{p}\mathbf{p}'}. \quad (13)$$

Thus

$$I_{ll}(\mathbf{r}_m-\mathbf{r}_k)=N^{-1}\sum_{\mathbf{p}} \exp[(i/\hbar)\mathbf{p}\cdot(\mathbf{r}_m-\mathbf{r}_k)]E_l(\mathbf{p}).$$

Comparison of this with Eq. (7) shows that

$$I_{ll}(\mathbf{r}_m-\mathbf{r}_k)=A_l(\mathbf{r}_m-\mathbf{r}_k). \quad (14)$$

Using Eqs. (11), (12), and (14), we then obtain the difference equations

$$-E\phi_l(\mathbf{r}_m)+\sum_k \phi_l(\mathbf{r}_k)A_l(\mathbf{r}_m-\mathbf{r}_k)+\sum_{k,n}\phi_n(\mathbf{r}_k) \times\left\{\int a_l^*(\mathbf{r}-\mathbf{r}_m)V(\mathbf{r})a_n(\mathbf{r}-\mathbf{r}_k)dV\right\}=0, \quad (15)$$

which must be satisfied for all values of $\mathbf{r}_m$. There is a set of such equations corresponding to each permitted band of the crystal, that is, for each value of l. These are the basic equations for further discussion.

It will now be shown that the type of approximation used by Slater is not sufficiently accurate in the present case. Suppose we approximate the integrals in Eq. (15) by replacing $V(\mathbf{r})$ by $V(\mathbf{r}_m)$. Then, because of the orthogonality properties of the a's, Eq. (15) becomes

$$-E\phi_l(\mathbf{r}_m)+\sum_k \phi_l(\mathbf{r}_k)A_l(\mathbf{r}_m-\mathbf{r}_k)+V(\mathbf{r}_m)\phi_l(\mathbf{r}_m)=0. \quad (16)$$

The above procedure amounts to expanding $V(\mathbf{r})$ in a Taylor series around $\mathbf{r}=\mathbf{r}_m$ and neglecting all terms in the expansion except the first. But Eq. (16) represents the Slater difference equations corresponding to the lth permitted band. There is a set of such difference equations corresponding to each permitted band, that is, corresponding to $l=1, 2, 3, \cdots$. But these sets are, respectively, independent equations in $\phi_1(\mathbf{r}_m)$, $\phi_2(\mathbf{r}_m)$, $\phi_3(\mathbf{r}_m)\cdots$. They would be satisfied by solutions of the type $\phi_2=\phi_3=\cdots=0$ and $\phi_1(\mathbf{r}_m)$ determined by Eq. (16) with $l=1$, or by $\phi_1=\phi_3=\cdots=0$ and $\phi_2(\mathbf{r}_m)$ determined by Eq. (16) with $l=2$, etc. Such solutions correspond to states which would exist if one permitted band were present without the others. In order to obtain a solution which is a good approximation when the energy lies close to one permitted band in one region of the crystal and close to a second permitted band in another, it is thus necessary to consider variation in the potential over a distance comparable with the range of the Wannier functions; that is, it is necessary to include more terms in the Taylor expansion of $V(\mathbf{r})$. (The formulation of Adams[4] leads to a similar conclusion.) The simplest case to consider is that for which the potential energy varies uniformly with distance, as it does when a uniform electric field is applied to the crystal.

III. ELECTRONIC STATES IN A CRYSTAL UNDER AN APPLIED ELECTRIC FIELD

A. General Theory

We now consider the difference equations, Eq. (15), for a one-dimensional crystal when the perturbing potential is $V(x)=eFx$ where F is the electric field strength. Thus, we consider solutions of the one-dimension Schrödinger equation,

$$-(\hbar^2/2m)d^2\psi/dx^2-\{E-V_P(x)-eFx\}\psi=0. \quad (17)$$

The periodic potential and the energy bands under a strong perturbing electric field are sketched in Fig. 1. As indicated there, we will restrict our attention to a region of the crystal such that the energy lies close to the first permitted band in one part of the region and close to the second permitted band in another. In this region, a good approximate wave function will be

$$\psi=\sum_k\{\phi_1(x_k)a_1(x-x_k)+\phi_2(x_k)a_2(x-x_k)\}, \quad (18)$$

which is just the one-dimensional analog of Eq. (10), with contributions from bands other than the first or second neglected. In evaluating the integrals in the difference equations which are the one-dimensional analogs of Eq. (15), it is convenient to use the Taylor expansion $V(x)=eFx_m+eF(x-x_m)$. We have then to evaluate integrals of the type

$$B_{ln}(x_m-x_k)=\int a_l^*(x-x_m)(x-x_m)a_n(x-x_k)dx. \quad (19)$$

These integrals can possess useful symmetry properties. If the periodic potential is symmetric about the cell centers, it can be shown that by proper choice of the phases of the ψ_0 of Eq. (2), the Wannier functions $a(x-x_k)$ can be made real and either symmetric or antisymmetric around $x=x_k$. (This is discussed in detail in the appendix.) It is then easily deduced that

$$B_{nn}(x_i)=B_{nn}(-x_i), \quad B_{ln}(x_i)=B_{nl}(-x_i), \quad (20)$$

$$B_{nn}(0)=0. \quad (21)$$

Moreover, when $a_l(x-x_k)$ and $a_n(x-x_k)$ have opposite symmetries around $x=x_k$, it can be shown that

$$B_{nl}(x_i)=B_{nl}(-x_i). \quad (22)$$

The difference equations for the ϕ_1 and ϕ_2 which correspond, respectively, to Eq. (15) with $l=1$ and $l=2$ (with contributions from permitted bands other than the first and second neglected) then become

$$-E\phi_1(x_m)+eFx_m\phi_1(x_m)+\sum_s A_1(x_s)\phi_1(x_m-x_s)$$
$$+eF\sum_s B_{11}(x_s)\phi_1(x_m-x_s)$$
$$+eF\sum_s B_{12}(x_s)\phi_2(x_m-x_s)=0, \quad (23)$$

$$-E\phi_2(x_m)+eFx_m\phi_2(x_m)+\sum_s A_2(x_s)\phi_2(x_m-x_s)$$
$$+eF\sum_s B_{22}(x_s)\phi_2(x_m-x_s)$$
$$+eF\sum_s B_{12}(x_s)\phi_1(x_m-x_s)=0. \quad (24)$$

In the sums over k which appear in Eq. (15), k has been set equal to $m-s$, and the sums taken over s. In order to obtain specific expressions for the A's and for the Wannier functions, a particular crystal model must be considered. The difference equations, Eqs. (23) and (24), will now be examined using the so-called narrow band approximation.

B. Unperturbed Wave Functions and Wannier Functions

Katsura, Hatta, and Morita[5] have discussed solutions of the Schrödinger equation, Eq. (17), and have used the narrow band approximation to show that, in this approximation, there is no distortion of the energy bands when a uniform field is applied to the crystal. These authors had not read Slater's paper at the time their work was done. Their method consists of expressing the ψ of Eq. (17) as a sum of atomic orbitals, multiplied by coefficients. Difference equations are then obtained for these coefficients. (The method is similar to but less general than that of Slater. After completing their work, Katsura, Hatta, and Morita[6] became aware that their calculations could be improved by using an expansion in terms of Wannier functions rather than atomic orbitals.) They considered, however, only a range of x such that E lies always close to a particular permitted band; thus interaction between the bands was not discussed and only one set of difference equations was obtained.

In the narrow band approximation,[7] it is assumed that the crystal atoms are far apart and the solution of the unperturbed periodic wave equation,

$$-(\hbar^2/2m)d^2\psi/dx^2-\{E-V_P(x)\}\psi=0, \quad (25)$$

is written as

$$\psi_0(p;x)=N^{-\frac{1}{2}}c(p)\sum_n \exp[(i/\hbar)px_n]u(x-x_n). \quad (26)$$

The u's are wave functions characteristic of the atoms before they are brought together to form the crystal, and are solutions of

$$-\frac{\hbar^2}{2m}\frac{d^2u(x-x_n)}{dx^2}-\{E_0-U(x-x_n)\}u(x-x_n)=0, \quad (27)$$

where $U(x-x_n)$ is the potential associated with the isolated atom. The constant $c(p)$ is determined by the normalization condition

$$\int\psi_0^*(p;x)\psi_0(p;x)dx=1.$$

Assuming that

$$\int u^*(x-x_m)u(x-x_n)dx=1 \quad \text{for} \quad m=n,$$
$$=\delta \quad \text{for} \quad m=n\pm1, \quad (28)$$
$$=0 \quad \text{otherwise},$$

it easily follows that

$$c(p)=e^{i\theta}[1+2\delta\cos(pa/\hbar)]^{-\frac{1}{2}}, \quad (29)$$

where $e^{i\theta}$ is an arbitrary phase factor.

The energy E as a function of the effective momentum p is then given by

$$E(p)=\int\psi_0^*(p;x)\left\{-\frac{\hbar^2}{2m}\frac{d^2}{dx^2}+V_P(x)\right\}\psi_0(p;x)dx.$$

Using Eqs. (27) and (28) and letting

$$\int u^*(x-x_m)\{V_P(x)-U(x-x_n)\}u(x-x_n)dx$$
$$=-\alpha \quad \text{for} \quad m=n,$$
$$=-\gamma_0 \quad \text{for} \quad m=n\pm1, \quad (30)$$
$$=0 \quad \text{otherwise},$$

it is easily shown that

$$E(p)=\frac{E_0-\alpha+2(\delta E_0-\gamma_0)\cos(pa/\hbar)}{1+2\delta\cos(pa/\hbar)}.$$

Assuming δ is small, we have

$$E(p)\cong E_0-\alpha-2\gamma\cos(pa/\hbar), \quad (31)$$

where $\gamma=\gamma_0-\alpha\delta$. Equation (31) defines a narrow permitted band of width $4|\gamma|$. If $u(x-x_n)$ is a function symmetric around $x=x_n$, $\gamma>0$; if antisymmetric, $\gamma<0$.

The Wannier functions corresponding to such a permitted band are given by the one-dimensional analog of Eq. (2), the sum being taken over values of $p=sh/Na$, $s=0,\pm1,\pm2,\cdots\pm N/2$. Inserting Eq. (26) into Eq. (2) with $p=sh/Na$, using Eq. (29), $x_n=na$,

[5] Katsura, Hatta, and Morita, Sci. Repts. Tôhuku Imp. Univ., Series I, Vol. XXXIV, No. 1, 19 (1950).
[6] Katsura, Hatta, and Morita, private communication.
[7] F. Seitz, *Modern Theory of Solids* (McGraw-Hill Book Company, Inc., New York, 1940), pp. 303–307.

$x_k=ka$, and $\hbar=h/2\pi$, we obtain

$$a(x-x_k)=\sum_n b_{n-k}u(x-x_n), \tag{32}$$

where

$$b_{n-k}=\frac{1}{N}\sum_s \frac{\exp[2\pi i(s/N)(n-k)]}{[1+2\delta\cos(2\pi s/N)]^{\frac{1}{2}}}.$$

In the expression for $c(p)$, θ has been set equal to zero; it will be shown that when this is done, $a(x-x_k)$ has the desired localization around $x=x_k$. The sum over s can be replaced by an integral. Letting $y=2\pi s/N$,

$$b_{n-k}\cong\frac{1}{\pi}\int_0^\pi \frac{\cos(n-k)y}{[1+2\delta\cos y]^{\frac{1}{2}}}dy.$$

This integral can be expressed in terms of the hypergeometric function

$$F=F\left(\tfrac{1}{2};n-k+\tfrac{1}{2};n-k+1;\frac{4\delta^2}{[1+(1-4\delta^2)^{\frac{1}{2}}]^2}\right);$$

it can be shown that

$$b_{n-k}=(-1)^{n-k}\frac{(2n-2k-1)!!}{(2n-2k)!!}\times\left\{\frac{2}{1+(1-4\delta^2)^{\frac{1}{2}}}\right\}^{\frac{1}{2}}\left\{\frac{2\delta}{1+(1-4\delta^2)^{\frac{1}{2}}}\right\}^{n-k}F, \tag{33}$$

where $2m!!=(2m)(2m-2)(2m-4)\cdots 2$. The hypergeometric function is rather insensitive to changes in n and, for small values of δ, b_{n-k} decreases with $n-k$ essentially as δ^{n-k}. Thus, in Eq. (32), the term involving $u(x-x_k)$ is the most important; the other $u(x-x_n)$ of the sum are multiplied by coefficients which are smaller the greater the distance of the nth atom from the kth. Thus $a(x-x_k)$ has the desired localization around the kth atom.

C. Solution of the Difference Equations

Consider now a crystal of the type described in Part B, under an applied uniform electric field. Let the first and second permitted bands be characterized by equations of the form of Eq. (31):

$$E_1(p)=E_{01}-\alpha_1-2\gamma_1\cos(pa/h),$$
$$E_2(p)=E_{02}-\alpha_2+2\gamma_2\cos(pa/h). \tag{34}$$

The unperturbed wave functions $\psi_{01}(p;x)$ corresponding to the first permitted band have the form of Eq. (26), with orbitals $u_1(x-x_n)$ symmetric about $x=x_n$; the unperturbed wave functions $\psi_{02}(p;x)$ are similarly constructed from orbitals $u_2(x-x_n)$ which are antisymmetric about $x=x_n$. (This accounts for the opposite signs of the third terms of $E_1(p)$ and $E_2(p)$ where both γ_1 and γ_2 are positive.) The Wannier functions $a_1(x-x_k)$ and $a_2(x-x_k)$ have the form of Eq. (32). The solution of the Schrödinger equation, Eq. (17), is given by Eq. (18) with the $\phi_1(x_k)$ and $\phi_2(x_k)$ determined by the difference equations, Eqs. (23) and (24). The A's of the difference equations satisfy equations which are the one-dimensional analogs of Eqs. (7) and (8). Comparison of Eq. (34) with Eq. (8) indicates that

$$A_1(0)=E_{01}-\alpha_1,\quad A_1(a)=A_1(-a)=-\gamma_1,$$
$$A_2(0)=E_{02}-\alpha_2,\quad A_2(a)=A_2(-a)=\gamma_2, \tag{35}$$

and that all the other A's are zero. In dealing with the coefficients B in this approximation, integrals involving overlap between Wannier functions associated with atoms further apart than nearest neighbors will be neglected. We thus include terms involving $B(0)$ and $B(a)$ and neglect all other B's. Then, using Eqs. (21) and (35) and setting $x_m=ma$, the difference equations, Eqs. (23) and (24) become

$$\{-E+eFma+E_{01}-\alpha_1\}\phi_1(x_m)+\{-\gamma_1+eFB_{11}(a)\}\{\phi_1(x_m-a)+\phi_1(x_m+a)\}+eFB_{12}(0)\phi_2(x_m)+eFB_{12}(a)\times\{\phi_2(x_m-a)+\phi_2(x_m+a)\}=0; \tag{36}$$

$$\{-E+eFma+E_{02}-\alpha_2\}\phi_2(x_m)+\{\gamma_2+eFB_{22}(a)\}\{\phi_2(x_m-a)+\phi_2(x_m+a)\}+eFB_{12}(0)\phi_1(x_m)+eFB_{12}(a)\times\{\phi_1(x_m-a)+\phi_1(x_m+a)\}=0. \tag{37}$$

Interaction between the bands is described by the terms containing the B_{12}. To obtain zero-order approximations to the solutions of Eqs. (36) and (37), we consider these equations with the $B_{12}=0$. For a particular value $E=E^0$ of the energy, they can be written in the form

$$\phi_1^0(x_m-a)+\phi_1^0(x_m+a)=2\left(\frac{eFa}{\gamma_1-eFB_{11}(a)}\right)\times\left(m-\frac{E^0-E_{01}+\alpha_1}{eFa}\right)\phi_1^0(x_m); \tag{38}$$

$$\phi_2^0(x_m-a)+\phi_2^0(x_m+a)=-2\left(\frac{eFa}{\gamma_2+eFB_{22}(a)}\right)\times\left(m-\frac{E^0-E_{02}+\alpha_2}{eFa}\right)\phi_2^0(x_m). \tag{39}$$

These equations are independent equations in ϕ_1^0, and ϕ_2^0 and describe energy states which would exist if one band were present without the other. Each equation is thus of the type obtained by Katsura, Hatta, and Morita, except for γ's defined in a slightly different way and terms in B_{11} and B_{22}, which appear because a better approximation has been used here. They have recognized that such equations have the form of the recursion relations,

$$Z_{m-1}(q)+Z_{m+1}(q)=(2m/q)Z_m(q), \tag{40}$$

of the cylinder functions, $Z_m(q)$. Now $Z_m(q)$ can be written as $CJ_m(q)+DN_m(q)$. Since the $\phi(x_m)$ must approach zero as $|m|\to\infty$ and since $N_m(q)\to\infty$ as $|m|\to\infty$, D must be set equal to zero. Comparison of Eqs. (38) and (39) with Eq. (40) indicates that

$$\phi_1^0(x_m)=C_1J_{m+l_1}(-q_1),\quad \phi_2^0(x_m)=C_2J_{m+l_2}(q_2), \tag{41}$$

where

$$l_1=\frac{(E^0-E_{01}+\alpha_1)}{|eF|a},\qquad l_2=\frac{(E^0-E_{02}+\alpha_2)}{|eF|a}, \tag{42}$$

$$q_1=\frac{2(\gamma_1-eFB_{11}(a))}{|eF|a},\qquad q_2=\frac{2(\gamma_2+eFB_{22}(a))}{|eF|a}, \tag{43}$$

and where C_1 and C_2 are constants. It has been assumed that the field is applied in the negative x direction. Katsura, Hatta, and Morita have also pointed out that a Bessel function J_{m+l} will not be well behaved as $m\to\pm\infty$ unless it is of integral order; this condition quantizes the energy.

It is clear that a value of E^0 which corresponds to an integral value of l_1 may not correspond to an integral value of l_2. For such a case, C_2 would have to be set equal to zero and the zero-order solutions would be $\phi_1^0(x_m)=C_1J_{m+l_1}(-q_1)$, $\phi_2^0(x_m)=0$. Similarly, there could be energy states such that l_2 is integral and l_1 nonintegral, corresponding to solutions of the type $\phi_1^0(x_m)=0$, $\phi_2^0(x_m)=C_2J_{m+l_2}(q_2)$. On the other hand, for particular values of the field strength F, energy eigenvalues can be such as to make l_1 and l_2 simultaneously integral. This is the degenerate case and the one which will be discussed in detail here. From Eq. (42) it follows that

$$l_2=l_1-n,$$

where

$$n=(E_{02}-\alpha_2-E_{01}+\alpha_1)/|eF|a. \tag{44}$$

Thus, the condition for degeneracy is that n be an integer. In such a case, neither C_1 nor C_2 need be zero, and the zero-order wave function may be written in the form

$$\psi^0=\sum_m\{C_1J_{m+l_1}(-q_1)a_1(x-x_m)+C_2J_{m+l_2}(q_2)a_2(x-x_m)\}. \tag{45}$$

To the approximation considered above, C_1 and C_2 are undetermined; they can be fixed only by considering interaction between the bands—that is, by including the B_{12}'s in the difference equations. Now, provided that the B_{12}'s are small, we can expect Eqs. (36) and (37) to have solutions for eigenvalues E^0+E^1 where E^1 is small and such that the corresponding $\phi_1(x_m)$ and $\phi_2(x_m)$ can be written

$$\phi_1(x_m)=C_1J_{m+l_1}(-q_1)+f_m,$$
$$\phi_2(x_m)=C_2J_{m+l_2}(q_2)+g_m, \tag{46}$$

where f_m and g_m are small. Inserting these expressions for ϕ_1 and ϕ_2 into Eqs. (36) and (37), and recalling that the J's satisfy Eqs. (38) and (39), we obtain

$$\begin{aligned}&-E^1J_{m+l_1}(-q_1)+\{-E^0+eFma+E_{01}-\alpha_1\}f_m\\&+\{-\gamma_1+eFB_{11}(a)\}f_{m-1}+\{-\gamma_1+eFB_{11}(a)\}f_{m+1}\\&+eFB_{12}(0)C_2J_{m+l_2}(q_2)+eFB_{12}(0)g_m\\&+eFB_{12}(a)C_2\{J_{m+l_2-1}(q_2)+J_{m+l_2+1}(q_2)\}\\&\qquad+eFB_{12}(a)\{g_{m-1}+g_{m+1}\}=0.\end{aligned} \tag{47}$$

$$\begin{aligned}&-E^1C_2J_{m+l_2}(q_2)+\{-E^0+eFma+E_{02}-\alpha_2\}g_m\\&+\{\gamma_2+eFB_{22}(a)\}g_{m-1}+\{\gamma_2+eFB_{22}(a)\}g_{m+1}\\&+eFB_{12}(0)C_1J_{m+l_1}(-q_1)+eFB_{12}(0)f_m\\&+eFB_{12}(a)C_1\{J_{m+l_1-1}(-q_1)+J_{m+l_1+1}(-q_1)\}\\&\qquad+eFB_{12}(a)\{f_{m-1}+f_{m+1}\}=0.\end{aligned} \tag{48}$$

Second-order terms of the form E^1f_m and E^1g_m have been neglected. We now multiply Eq. (47) by $J_{m+l_1}(-q_1)$ and sum over all values of m. The first term can be simplified, using[8]

$$\sum_n J_n^2(x)=1 \tag{49}$$

for all values of x. The second, third, and fourth terms become

$$\begin{aligned}&\sum_m f_m\{-E^0+eFma+E_{01}-\alpha_1\}J_{m+l_1}(-q_1)\\&\quad+\{-\gamma_1+eFB_{11}(a)\}\sum_m f_{m-1}J_{m+l_1}(-q_1)\\&\quad+\{-\gamma_1+eFB_{11}(a)\}\sum_m f_{m+1}J_{m+l_1}(-q_1).\end{aligned}$$

By replacing m by $m+1$ in the second sum and m by $m-1$ in the third, these terms combine to yield

$$\begin{aligned}&\sum_m f_m[\{-E^0+eFma+E_{01}-\alpha_1\}J_{m+l_1}(-q_1)\\&\quad+\{-\gamma_1+eFB_{11}(a)\}\\&\quad\times\{J_{m+l_1+1}(-q_1)+J_{m+l_1-1}(-q_1)\}]=0,\end{aligned}$$

since $J_{m+l_1}(-q_1)$ satisfies Eq. (38).

Terms involving products of Bessel functions can be simplified using the addition theorem[9]

$$J_n(y+z)=\sum_m J_m(y)J_{n-m}(z),$$

and the relation of Eq. (44), $l_2=l_1-n$. Equation (47) finally becomes

$$\begin{aligned}&-E^1C_1+(-1)^neFC_2[B_{12}(0)J_n(q_1+q_2)\\&\quad-B_{12}(a)J_{n-1}(q_1+q_2)-B_{12}(a)J_{n+1}(q_1+q_2)]\\&\quad+eFB_{12}(0)\sum_m J_{m+l_1}(-q_1)g_m\\&\quad+eFB_{12}(a)\sum_m J_{m+l_1}(-q_1)\{g_{m-1}+g_{m+1}\}=0.\end{aligned} \tag{50}$$

[8] G. N. Watson, *Bessel Functions* (Cambridge University Press, Cambridge, 1944), p. 31.
[9] See reference 8, p. 30.

Similarly by multiplying Eq. (48) by $J_{m+l_2}(q_2)$, summing over all m and proceeding as above, we obtain

$$-E^1C_2+(-1)^n eFC_1[B_{12}(0)J_n(q_1+q_2) - B_{12}(a)J_{n-1}(q_1+q_2)-B_{12}(a)J_{n+1}(q_1+q_2)] + eFB_{12}(0)\sum_m J_{m+l_2}(q_2)f_m + eFB_{12}(a)\sum_m J_{m+l_2}(q_2)\{f_{m-1}+f_{m+1}\}=0. \quad (51)$$

Approximate values for C_1, C_2, and E^1 can be obtained by neglecting the terms containing f and g in Eqs. (50) and (51), which then reduce to

$$-E^1C_1+XC_2=0, \quad (52)$$

$$-E^1C_2+XC_1=0, \quad (53)$$

where

$$X=(-1)^n eF[B_{12}(0)J_n(q_1+q_2) - B_{12}(a)\{J_{n-1}(q_1+q_2)+J_{n+1}(q_1+q_2)\}]. \quad (54)$$

Consistency of Eqs. (52) and (53) requires that

$$E^1=\pm|X|; \quad C_1/C_2=\pm 1.$$

Since the f_m and g_m have been neglected in this approximation, the wave functions have the form of Eq. (45)

$$\psi=C\sum_m\{J_{m+l_1}(-q_1)a_1(x-x_m) \pm J_{m+l_2}(q_2)a_2(x-x_m)\}. \quad (55)$$

The constant C is chosen so as to normalize ψ. Using Eq. (49) and the orthogonality properties of the a's, it easily follows that $C=1/\sqrt{2}$. Thus the wave functions, corresponding to the energies $E=E^0\pm|X|$ are

$$\psi_I=(1/\sqrt{2})\sum_m\{J_{m+l_1}(-q_1)a_1(x-x_m) +J_{m+l_2}(q_2)a_2(x-x_m)\}, \quad (56)$$

$$\psi_{II}=(1/\sqrt{2})\sum_m\{J_{m+l_1}(-q_1)a_1(x-x_m) -J_{m+l_2}(q_2)a_2(x-x_m)\}. \quad (57)$$

The coefficients $J_{m+l}(q)$ are oscillatory for values of m such that $|m+l|<q$ and behave exponentially elsewhere. Thus ψ_I and ψ_{II} are oscillatory within the first permitted band (where m assumes values such that $|m+l_1|<q_1$) and within the second permitted band (where m is such that $|m+l_2|<q_2$).

D. Probability of Penetration of the Forbidden Gap

Consider now a solution of the time dependent Schrödinger equation given by

$$\psi=\psi_I\exp[-iE_It/\hbar]+\psi_{II}\exp[-iE_{II}t/\hbar].$$

From Eqs. (56) and (57), it is seen that at $t=0$, $\psi=\psi_I+\psi_{II}$ represents a wave function corresponding to an electron localized near the first permitted band. It is easily seen, however, that in a time t such that $(E_{II}-E_I)t=h/2$, $\psi=\psi_I-\psi_{II}$ corresponding to an electron localized near the second permitted band. Thus the probability per unit time Γ for an electron to cross the forbidden energy band is given by

$$\Gamma=2(E_{II}-E_I)/h=4|X|/h. \quad (58)$$

(The argument used here is similar to that used in the so-called double minimum problem of quantum mechanics[10] to obtain the probability per unit time for an electron to pass from one potential well to another.)

We now consider the expression of Eq. (54) for $|X|$. Equations (44) and (34) indicate that n is the ratio of the energy difference between the centers of the permitted bands of the unperturbed crystal to the change of the perturbing potential over a single cell of the crystal; thus for physically interesting cases, n is very large. Equation (43) indicates that q_1+q_2 is of the order of the ratio of the sum of the half-widths of the first and second permitted bands to the change in the perturbing potential over a single cell of the crystal. Since we consider here the case of narrow permitted bands and wide forbidden bands, it follows that the order of the Bessel functions which appear in Eq. (54) is greater than the argument; we may therefore use the asymptotic expression[11]

$$J_n(n\,\mathrm{sech}x)\sim e^{-n(x-\tanh x)}/[2\pi n\tanh x]^{\frac{1}{2}}. \quad (59)$$

From Eqs. (54), (58), and (59) we then obtain

$$\Gamma\sim\frac{eFa}{h}\left(\frac{eFa}{\epsilon}\right)^{\frac{1}{2}}R\exp\left\{-\frac{\epsilon}{eFa}\ln\left[\frac{2\epsilon}{\tau}-\left(1-\frac{\tau^2}{\epsilon^2}\right)^{\frac{1}{2}}\right]\right\}, \quad (60)$$

where

$$R\sim\frac{2^{\frac{1}{2}}}{\pi^{\frac{1}{2}}(1-\tau^2/\epsilon^2)^{\frac{1}{4}}}\left[\frac{B_{12}(0)}{a}-\frac{B_{12}(a)}{a}\right] \times\left\{\exp\left[-\ln\frac{2\epsilon}{\tau}+\left(1-\frac{\tau^2}{\epsilon^2}\right)^{\frac{1}{2}}\right] +\exp\left[\ln\frac{2\epsilon}{\tau}-\left(1-\frac{\tau^2}{\epsilon^2}\right)^{\frac{1}{2}}\right]\right\},$$

$$\epsilon=E_{02}-\alpha_2-E_{01}+\alpha_1,$$

$$\tau=2[\gamma_1-eFB_{11}(a)+\gamma_2+eFB_{22}(a)].$$

Since we consider narrow permitted bands, ϵ is essentially the width of the forbidden energy gap. The quantity τ is essentially the average width of the permitted bands.

It is of interest to compare Eq. (60) for Γ with the expression obtained by Zener[12] by another method and

[10] S. Dushman, *Elements of Quantum Mechanics* (John Wiley & Sons, Inc., New York, 1938), p. 214.
[11] See reference 8, p. 243.
[12] C. Zener, Proc. Roy. Soc. (London) **145**, 523 (1934).

using the approximation of nearly free electrons (narrow forbidden bands). Zener's expression is

$$\Gamma=\frac{eFa}{h}\exp\left[-\frac{\epsilon}{eFa}\left\{\frac{\pi^2 ma^2\epsilon}{h^2}\right\}\right], \tag{61}$$

where m is the electron mass. In both expressions for Γ, the important factor is the exponential and in particular the quantity ϵ/eFa of the exponent, which is just the number of cells traversed as the forbidden band is crossed. For ordinary fields, this is very large and Γ is negligibly small. In Eq. (61), $\pi^2 ma^2\epsilon/h^2$ is essentially $\sim\epsilon/\tau$, the ratio of the forbidden band width to the permitted band width, and Eq. (61) is valid when this ratio $\ll 1$. This is to be compared with $[\ln(2\epsilon/\tau)-(1-\tau^2/\epsilon^2)^{\frac{1}{2}}]$ of Eq. (60), which is valid when $\epsilon/\tau\gg 1$. Thus, if applied to a practical intermediate case, Eq. (60) will predict a smaller field for which penetration of the barrier becomes important than will Eq. (61).

E. Comparison with Experiment

The considerations of the preceding sections imply that for sufficiently high fields applied to a crystal, one should be able to observe a sudden increase in current, associated with the tunneling of electrons from the filled band to the conduction band. This has been observed in experiments carried out at Bell Laboratories by McAfee, Ryder, Shockley, and Sparks[13] on $N-P$ rectifiers formed in single crystals of germanium. They find that for fields $\sim 2\times 10^5$ volts/cm, the current in the back direction of such a rectifier increases suddenly and rapidly. They call this increase in current the Zener current and, assuming the field in the barrier to be uniform, give a theoretical expression for the current density I, which can be written

$$I=(nze/a^2)\Gamma, \tag{62}$$

where z is the number of electrons per cell and n the number of cells in the barrier. Using an expression for Γ derived by Shockley (the method of derivation is not indicated), which has the form $\Gamma\approx(eFa/h)e^{-\beta/F}$, where $\beta=(\pi^2/eh)(m/2)^{\frac{1}{2}}\epsilon^{\frac{1}{2}}$, they write I as

$$I=Ve^{\alpha-\beta/V}, \tag{63}$$

where $\alpha=\ln(e^2z/a^2h)$ and V is the applied voltage. Using Eq. (63) with appropriate constants for germanium, they find that the predicted slope of the $\ln I-\ln V$ curve is in good agreement with experiment but that the predicted field at which current should become appreciable is too high.

If one now uses Eq. (60) for Γ, one can write I in the form of Eq. (63) with

$$\alpha=\ln(e^2z/a^2h)+\ln R(eFa/\epsilon)^{\frac{1}{2}},$$
$$\beta=(\epsilon/ea)[\ln(2\epsilon/\tau)-(1-\tau^2/\epsilon^2)^{\frac{1}{2}}].$$

[13] McAfee, Ryder, Shockley, and Sparks, Phys. Rev. **83**, 650 (1951).

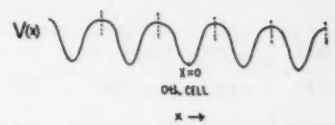

FIG. 2. Periodic potential in a one-dimensional lattice.

In comparing this new expression with the experimental current-voltage characteristic, α could be considered as essentially constant since the observed values of the field varied little. Values of α and β obtained from the experimental curve were found to correspond to $\ln R=0.3$ and $\epsilon/\tau=2.3$. The fairly large value of ϵ/τ is consistent with the assumptions made in deriving Eq. (60) but not with the known band structure of germanium.

The author is most grateful to Professor H. M. James for much valuable advice and discussion during the course of this work.

APPENDIX

The Wannier functions $a(\mathbf{r}-\mathbf{r}_k)$ are defined by Eq. (2); it should be emphasized, however, that in Eq. (2), each solution $\psi_0(\mathbf{p};\mathbf{r})$ of the unperturbed problem contains an arbitrary phase factor $e^{i\gamma(\mathbf{p})}$. It will be shown here that the $a(\mathbf{r}-\mathbf{r}_k)$ will have the desired localization about the kth atom of the crystal only if the $f(\mathbf{p})$ are appropriately chosen, a point not discussed by Wannier. It will also be shown that the Wannier functions can possess useful symmetry properties.

To obtain a more detailed knowledge of the Wannier functions they will be investigated here using a one-dimensional model originally used by Shockley[14] in discussing surface states, and later considered in more detail by James[15] in discussing solutions of the periodic and perturbed periodic wave equations.

Figure 2 shows the electronic potential energy as a function of position in the crystal. The potential is symmetric about the center of each cell. The crystal wave functions are expressed in terms of functions $g(E;x)$ and $u(E;x)$ which are solutions of the Schrödinger equation for the single potential well associated with the zeroth cell. $g(E;x)$ and $u(E;x)$ are respectively symmetric and antisymmetric about the cell center $x=0$. Moreover,

$$g(E;0)=1;\ g'(E;0)=0;\ u(E;0)=0;\ u'(E;0)=1, \tag{64}$$

where the primes signify derivatives with respect to x. Within the pass band, corresponding to an energy E, there are two independent crystal wave functions—complex conjugates of each other. In the nth cell, these are

$$\psi_n=\exp\pm(ipna/h)\{\alpha(E)g(E;x-x_n)+\beta(E)u(E;x-x_n)\}, \tag{65}$$

[14] W. Shockley, Phys. Rev. **56**, 317 (1939).
[15] H. M. James, Phys. Rev. **76**, 1602 (1949).

where

$$\frac{\beta(E)}{\alpha(E)}=\mp i\frac{g_0(E)}{u_0(E)}\left|\frac{g_0'(E)u_0(E)}{g_0(E)u_0'(E)}\right|^{\frac{1}{2}}=\mp i\delta(E). \quad (66)$$

The subscript 0 indicates the value of the function at the left edge of the 0th cell. $\alpha(E)$ is determined, except for a phase factor, by normalizing the wave function. For an energy corresponding to a band edge, one of the quantities g_0, u_0, g_0', u_0' vanishes and there is only one well-behaved wave function. Below are listed the various possibilities for band edge wave functions (in the nth cell).

1. If

$$g_0(E_e)=0, \quad \psi_n(E_e;x)=c(E_e)(-1)^n g(E_e;x-x_n). \quad (67)$$

2. If

$$g_0'(E_e)=0, \quad \psi_n(E_e;x)=c(E_e)g(E_e;x-x_n). \quad (68)$$

3. If

$$u_0(E_e)=0, \quad \psi_n(E_e;x)=c(E_e)u(E_e;x-x_n). \quad (69)$$

4. If

$$u_0'(E_e)=0, \quad \psi_n(E_e;x)=c(E_e)(-1)^n u(E_e;x-x_n). \quad (70)$$

Various bands will now be classified according to their upper and lower edges, and Wannier functions corresponding to these bands will be constructed.

Case 1:—Consider a band with edges E_{e1} and E_{e2} corresponding to $g_0'(E_{e1})=0$ and $g_0(E_{e2})=0$. The Wannier functions localized around the zeroth cell are then given in the nth cell by [Eqs. (2), (65), (66), (67), (68)]

$$a(x)=N^{-\frac{1}{2}}\sum_{p=0}^{\pi\hbar/a}\{2\cos(pna/\hbar)\alpha(E)g(E;x-x_n)$$

$$+2\sin(pna/\hbar)\alpha(E)\delta(E)u(E;x-x_n)\}, \quad (71)$$

where $\alpha(E_{e1})=\frac{1}{2}c(E_{e1})$ and $\alpha(E_{e2})=\frac{1}{2}c(E_{e2})$. (Since E is a function of p the quantities α, δ, g, and u are all functions of p.) It will now be shown that by choosing $\alpha(E)$ real and positive, the function $a(x)$ is made real and localized as desired around the zeroth cell of the crystal. In order to carry out the above summation it is necessary to know the specific potential distribution within the zeroth cell, since this determines the g's and u's. One can see qualitatively how the localization comes about, however, by examining $a(x)$ at the center of the zeroth cell, first cell $\cdots$ nth cell. At the center ($x=0$) of the zeroth cell $a(x)$ is given by Eq. (71) with $n=0$. Thus

$$a(0)=N^{-\frac{1}{2}}\textstyle\sum_p \alpha(E)g(E;0)=\sum_p \alpha(E),$$

(since $g(E,0)=1$), each term of the sum being positive. On the other hand (since $u(E;0)=0$),

$$a(x_n)=N^{-\frac{1}{2}}\textstyle\sum_p \alpha(E)\cos(pna/\hbar).$$

Now $\alpha(E)$ is a smoothly and slowly varying function of E or p. [For the special case of a constant potential, $\alpha(E)$ is constant and equal to $(Na)^{-\frac{1}{2}}$.] Since $\cos(pna/\hbar)$ becomes more and more rapidly oscillatory as n increases, the terms of the sum change sign more and more rapidly and the magnitude of the sum decreases; thus $a(x)$ is attenuated with increasing $|n|$. To get an idea of the rate of attenuation, let us compare $\sum\alpha(E)\cos(pna/\hbar)$ when $n=0$ and $n=N/2$. When $n=0$, we obtain a sum of positive terms, which can be written $N\alpha(E)_{Av}$. We now recall that in the sum, $p=sh/Na$, where $s=0, 1, 2, \cdots$. Thus, when $n=N/2$, the cosine term behaves as $(-1)^s$ and the series has a value of the order of magnitude of a single term of the series, which in turn is of the order of $\alpha(E)_{Av}$ or less. Thus, the ratio of the value of the sum in the $(N/2)$th cell to that in the zeroth cell is $\sim 1/\frac{1}{2}N$ at most; attenuation may actually be much more rapid.

It can easily be seen, using the symmetry properties of the g and u, that $a(x)$ is symmetric around $x=0$.

Case 2:—Consider a band with edges E_{e3} and E_{e4} corresponding to $u_0'(E_{e3})=0$ and $u_0(E_{e4})=0$. The Wannier functions localized around the zeroth cell can then be written [Eqs. (2), (65), (69), (70)]

$$a(x)=N^{-\frac{1}{2}}\sum_{p=0}^{\pi\hbar/a}\left\{2\cos(pna/\hbar)\beta(E)u(E;x-x_n)\right.$$

$$\left.-2\sin(pna/\hbar)\frac{\beta(E)}{\delta(E)}g(E;x-x_n)\right\}, \quad (72)$$

where $\beta(E_{e3})=\frac{1}{2}c(E_{e3})$ and $\beta(E_{e4})=\frac{1}{2}c(E_{e4})$. Since in this case the function is zero at the center of the zeroth cell, we obtain information about the function by considering its slope at the centers of the various cells. At the center of the zeroth cell, $a'(0)$ is the sum of $\beta(E)u'(E;0)$ over the permitted band. Since $u'(E;0)=1$, each term of the sum will be positive if $\beta(E)$ is chosen positive. To obtain $a'(x_n)$, however, it is necessary to sum over products $\beta(E)\cos(pna/\hbar)$ (since $g'(E;0)=0$). Using arguments analogous to those applied to the discussion of $a(x)$ in case 1, it is seen that here $a'(x)$ is attenuated with increasing $|n|$.

It can easily be shown that the $a(x)$ of Eq. (72) is antisymmetric about $x=0$.

Localized Wannier functions which are symmetric or antisymmetric around the cell centers can be similarly constructed for the other types of bands.

The Intrinsic Parity of Elementary Particles

G. C. Wick
Carnegie Institute of Technology, Pittsburgh, Pennsylvania

AND

A. S. Wightman and E. P. Wigner
Princeton University, Princeton, New Jersey

(Received June 16, 1952)

The limitations to the concept of parity of quantum-mechanical states and, in particular, of intrinsic parity of elementary particles are discussed. These limitations are shown to follow from "superselection rules," i.e., from restrictions on the nature and scope of possible measurements. The existence of such superselection rules is proved for the case of spinor fields; it is also conjectured that a superselection rule operates between states of different total charge.

THE POSSIBILITY OF INDETERMINATE PARITIES

ALTHOUGH the present quantum-field-theoretic scheme to describe elementary particles is full of mathematical holes, it possesses certain features, mainly based on invariance properties, that are believed to be of far more permanent value. The importance of these features can hardly be overestimated, since they offer the most reliable guidance that we have in classifying and interpreting the rapidly growing and already very complex experimental picture.

The purpose of this paper is to point out the possible (and in certain cases necessary) existence of limitations to one of these general concepts, the concept of "intrinsic parity" of an elementary particle. Even though no radical modification of our thinking is thereby achieved, we believe that the injection of a certain amount of caution in this matter may be useful, as it may prevent one from calling "theorems" certain assumptions, or from discarding as "impossible" forms of the theory, which under a more flexible scheme are perfectly consistent. Another possible advantage of the following considerations may be to bring a certain amount of clarity in a field in which a great deal of confusion exists.[1]

The more or less standard position seems to be that every elementary particle must have a definite "intrinsic parity" factor, which can be determined unambiguously from experiment[2] (at least in principle).

In order to understand the limitations of this viewpoint, it will be useful to recall first some simple points about the formalism.

The transformation properties (in our case, the parity) of a certain kind of particles can be described in two ways; it will be useful to keep both in mind. One can state the transformation law of the quantized field. One will say, for instance, that a certain kind of spinless particles are the quanta of a "pseudoscalar" field, i.e., a field φ such that the transformation law for an inversion at the origin is

$$\varphi'(x, y, z) = -\varphi(-x, -y, -z). \tag{1}$$

Alternatively, one can state the transformation law for the state vector or Schrödinger function F, which gives the quantum-mechanical description of the state of the field,[3] i.e., one can find the unitary operator I such that

$$F' = IF \tag{2}$$

describes the state which is the mirror image of the state described by F.

The two alternative descriptions of the transformation law are, of course, very simply related, for in quantum mechanics the "observables" or operator quantities, such as the field $\varphi(x, y, z)$ above, transform according to the law

$$\varphi' = I\varphi I^{-1}, \tag{3}$$

when the state vector transforms according to (2).

Thus the unitary operator I determines completely the transformation law for the field quantities, and conversely, the transformation law for the latter is sufficient to determine the operator I. Thus, for instance, if one states that φ is a pseudoscalar, this means that

$$I\varphi(x, y, z)I^{-1} = -\varphi(-x, -y, -z), \tag{4}$$

and from this equation one may infer that I is of the form:

$$IF = \omega(-1)^{N_0+N_1+N_2+\cdots}F, \tag{5}$$

where N_l is the number of particles (of the kind described by φ) with angular momentum l while ω is an arbitrary factor of modulus unity, which remains

[1] The origin of the present article is an address which was presented by the last author at the International Conference on Nuclear Physics and the Physics of Elementary Particles in September 1951 in Chicago and which was based on a review article which the last two authors are preparing together with V. Bargmann. In view of several inquiries concerning the above-mentioned address, the authors feel that a preliminary publication of some of the main points in the present paper is justified, even though they must refer the reader to the review article to appear later for a more exhaustive and consistent presentation of the whole subject.

[2] This is no doubt an oversimplified version even of "current" belief, especially in the case of spin $\frac{1}{2}$ particles. This case, however, will be discussed later in greater detail.

[3] In this particular kind of discussion it seems to be a good idea to avoid the chameleon-like term wave function. We shall adhere strictly to state-vector in one case and field function in the other.

indeterminate in any quantum mechanical transformation. If one arbitrarily sets $\omega=1$, the vacuum vector F_0 will satisfy

$$IF_0=F_0, \tag{6}$$

i.e., the vacuum will be an "even" state. A one-particle S-state will be "odd," etc. It is, of course, the presence of even angular momenta in the exponent of (5) which characterizes "pseudoscalar" particles, rather than the arbitrary choice of even and odd states which is conventionally determined by (6). This is, however, a convenient choice which is usually made.

Similarly, for the particles of a scalar field one finds

$$IF=(-1)^{N_1'+N_2'+N_3'+\cdots}F, \tag{5a}$$

where the N' have the same significance for the scalar particles as the N had for the pseudoscalar ones. If F describes an aggregate of pseudoscalar and scalar particles, one has, naturally

$$IF=(-1)^{N_0+N_2+\cdots+N_1'+N_3'+\cdots}F. \tag{5b}$$

We can now resume the discussion of the main point. The customary assumption is that the field quantities must obey an unambiguous transformation law, or alternatively, in the quantum mechanical case, that the unitary operator I is well defined, apart from the trivial factor ω. Once that is granted, it follows for instance that a scalar field must be either a "true" scalar or a "pseudo" scalar. Such assumptions are even believed to be a logical necessity, if symmetry operations, such as the inversion, are to have a well-defined meaning at all.

Nevertheless, everybody knows that the transformation law of spinor quantities, such as the Dirac field ψ is not unambiguous. Yang and Tiomno, in their interesting paper[4] on the inversion law for spin 1/2 fields, which has been the origin of much thinking on this matter, do in fact assume an essential ambiguity in the sign of $I\psi I^{-1}$. While the case of spin 1/2 particles offers perhaps the best substance to our doubts, it is preferable to state first our position in a quite general manner.

In our opinion, the whole question hinges on what one can say about the measurability of the field operators. In fact, if a field is measurable, then it must have a well-defined expectation value in any given state. The situation is then equivalent to the classical one, where one can argue that there must be a definite transformation law, just because the fields are regarded as well-defined physical quantities. If, however, a field quantity is not measurable—and, as we shall see below on the example of the Dirac field, there are such fields—there is no logical need for an unambiguous transformation law.

It is quite true, of course, that the assumption that "all Hermitean operators represent measurable quantities" is often presented as an integral part of the general scheme of quantum mechanics. It is also true that in the case of the ordinary nonrelativistic quantum mechanics of particles this assumption, implausible as it sounds for all but the very simplest operators, is not subject to any very serious objection. It should be hardly necessary to point out, however, that a wholesale extension of the measurability postulate to the physical abstractions with which the present field theory of "elementary" particles operates is an unwarranted and enormous extrapolation, especially in view of our scarce knowledge of the actual interaction laws.

That no intrinsic difficulties are inherent in such a position, will be apparent if one considers that it is perfectly possible to construct logical schemes in which the unrestricted measurability postulate is abandoned. It is indeed surprising, in view of the known nonmeasurability of the Dirac field, that the nature of such schemes has not been more widely discussed.

What we have in mind is the following. The usual assumption in quantum mechanics is that it is possible to carry out a "complete" set of measurements, the result of which determines the state vector F completely, except for the usual phase factor. Suppose now instead that the Hilbert space can be decomposed into certain orthogonal subspaces $A, B, C, \cdots$ such that the relative phase of the components of F along $A, B, C, \cdots$ is intrinsically irrelevant. In other words, calling these components (which are themselves vectors) F_a, F_b, F_c, $\cdots$, assume that no physical measurement can distinguish between the state-vectors

$$F_a+F_b+F_c+\cdots \tag{7}$$

and

$$e^{i\alpha}F_a+e^{i\beta}F_b+e^{i\gamma}F_c+\cdots, \tag{7'}$$

where $\alpha, \beta, \gamma, \cdots$ are arbitrary phases. It is clear then, that the expectation value of any operator that has matrix elements connecting the subspaces A and B, or A and C, etc., will be, in general, completely undefined. Hence such an operator will not correspond to a measurable quantity. Such an assumption is not incompatible with the other rules of quantum mechanics, and in particular with the superposition principle; a linear relationship between vectors will remain unaltered if all vectors simultaneously are subjected to the transformation (7'). One may indeed regard this transformation as a generalization of the ordinary multiplication of the whole vector by one phase factor.

Another, and more familiar, way of describing this situation is to say that the state described by (7') is not a pure state, but a statistical mixture, which could be best described by a density matrix.[5] The assumption presented above is that such a density matrix represents the maximum possible amount of knowledge. The system can, of course, be in a pure state in the ordinary sense, but only if only one of the components, say F_a,

[4] C. N. Yang and J. Tiomno, Phys. Rev. **79**, 495 (1950); see also E. R. Caianiello, Nuovo cimento **7**, 534 (1951); **8**, 749 (1951); **9**, 336 (1952).

[5] For this concept see J. v. Neumann, *Mathematische Grundlagen der Quantenmechanik* (Verlag. Julius Springer, Berlin, 1932), Chap. IV.

is finite. If the above is admitted, the unitary operator I representing a symmetry operation will be affected by a corresponding lack of definition. Ordinarily I will have no matrix elements connecting the subspaces A, B, C, $\cdots$; it will leave each invariant. Hence the submatrices of I in any of the subspaces A, B, $\cdots$ will contain an arbitrary factor ω_a, ω_b, $\cdots$ just as the whole I contained such an arbitrary factor. Because of the equivalence of the wave functions (7) and (7′) there will be no way to determine the ratios of ω_a, ω_b, $\cdots$; instead of the single indeterminate phase factor there will be as many as there are subspaces A, B, $\cdots$. This means that it will not be possible to make any statement as to the relative parity of states belonging to different subspaces.

It is customary to say that a selection rule operates between subspaces of the total Hilbert space if the state vectors of each subspace remain orthogonal to all state vectors of the other subspaces as long as the system is isolated. There is, for instance, a selection rule which prevents any state of an isolated system from changing its total linear momentum. Similarly, the state vectors of the subspace containing all states with total angular momentum J will remain, in a closed system, orthogonal to all states with any other total angular momentum. We shall say that a superselection rule operates between subspaces if there are neither spontaneous transitions between their state vectors (i.e., if a selection rule operates between them) and if, in addition to this, there are no measurable quantities with finite matrix elements between their state vectors. This is the situation described above; it entails that the phase factors ω_a, ω_b, $\cdots$, given above, are all unobservable. The new point which we wish to bring out is that there is definite evidence that such superselection rules exist in the present formalism of relativistic field theories. We shall outline a proof for this in one case and will suggest another case in which it is also very likely to operate.

The existence of superselection rules allows one more freedom than one would perhaps like to have. We are not especially concerned here, however, with the possibility of exploiting this freedom to the utmost limit,[6] in order to produce "monsters" with unexpected properties. Rather, we are interested in the most simple instances in which the above described situation appears to prevail. It would be quite wrong to assume that a superselection rule operates, for instance, between subspaces with different total linear momenta. The phase between such states is measurable, and every position measurement, in fact, involves the measurement of phases between states of different linear momenta.

[6] Strictly speaking, even if one assumes a definite transformation law, one cannot exclude on general grounds a more complicated transformation, such as $\varphi'(x, y, z) = \omega(N)\varphi(-x, -y, -z) \times \omega(N)^{-1}$ where the value $\omega(N) = \pm 1$ can be chosen at will for every N irrespective of the product rule. This possibility can be easily excluded only if φ is a locally measurable quantity.

SPINORS

One must introduce a superselection rule between at least two subspaces of the whole Hilbert space if one wishes to preserve the relativistic invariance of this space. The first of these subspaces, A, contains the states in which the total angular momentum of the system is an integer multiple of $\hbar$, the second subspace B contains the states with half-integer angular momenta. Let us denote the state vectors of the first subspace by f_A, g_A, $\cdots$, those of the second by f_B, g_B, $\cdots$. We shall consider states $2^{-\frac{1}{2}}(f_A + f_B)$ for which the measurement of the angular momentum gives with a probability $1/2$ an integer angular momentum and with the same probability a half-integer angular momentum. Let us imagine, furthermore, that the two states $2^{-\frac{1}{2}}(f_A + f_B)$ and $2^{-\frac{1}{2}}(f_A - f_B)$ can be distinguished by some measurement. This is what we mean by the statement that the phase between the subspaces A and B can be measured. We shall see that this assumption cannot be reconciled with the requirement of relativistic invariance.

Our proof for this will be based on the transformation of time inversion. This transforms f_A into $U_A K f_A$ and f_B into $U_B K f_B$ in which the U are unitary operators and the K indicates that one has to take the conjugate complex of the ensuing expression. The crucial point of our proof is based on the equations[7]

$$U_A K U_A K = 1; \quad U_B K U_B K = -1. \tag{8}$$

Naturally, $U_A K$ and $U_B K$ can be replaced by $\omega U_A K$ and $\omega' U_B K$ without changing the content of the theory as long as $|\omega| = |\omega'| = 1$. Such a substitution, however, will leave (8) unaffected. It is this circumstance which renders a proof based on the transformation of time inversion particularly simple.

Applying the operation of time inversion to a state $f_A + f_B$ will give $\omega U_A K f_A + \omega' U_B K f_B$ in which ω is, of course, indeterminate but ω'/ω, though unknown, will be independent[8] of the state vectors f_A and f_B. Applying now the operation of time inversion again, we must obtain a state which is indistinguishable from the original $f_A + f_B$. The result is

$$\omega'' U_A K(\omega U_A K f_A) + \omega''' U_B K(\omega' U_B K f_B), \tag{9}$$

with $\omega'''/\omega'' = \omega'/\omega$. Because of this and (8), (9) becomes

$$\omega''\bar{\omega} U_A K U_A K f_A + \omega'''\bar{\omega}' U_B K U_B K f_B = (\omega''/\omega) f_A - (\omega'''/\omega') f_B = \text{const}(f_A - f_B). \tag{9a}$$

In view of the different signs in (8), this result was to be expected; it shows that $f_A + f_B$ and $f_A - f_B$ must remain indistinguishable as long as a time inversion operator satisfying (8) exists. The same result could have been obtained by considering rotations instead

[7] See E. Wigner, Nachr. Ges. Wiss. Göttingen, p. 546 (1932).

[8] This is a crucial point which, however, has been discussed repeatedly. See E. Wigner, *Gruppentheorie und ihre Anwendung auf die Quantenmechanik der Atomspektren* (Friedr. Vieweg. Braunschweig, 1931), Appendix to Chapter XX. A simplified proof will be given in the article mentioned in reference 1.

of the time inversion. However, the consideration becomes somewhat more involved because there is no equation for rotational transformations, similar to (8), which would remain unchanged if one replaces the transformation by a multiple thereof.

It follows from the above that the measurability of any Hermitean operator ξ which has finite matrix elements $(f_A, \xi f_B)$ between the subspaces A and B (i.e., between states with integer and half-integer angular momenta) would lead to a contradiction. In fact, unless $(f_A, \xi f_B)$ is purely imaginary, the expectation values of ξ for the states f_A+f_B and f_A-f_B would be different. However, we have seen that these states are undistinguishable. If $(f_A, \xi f_B)$ is purely imaginary, the above statement applies to the pair of states f_A+if_B, f_A-if_B which can be shown to be similarly undistinguishable.

Since every spinor field ψ has the property that both $\psi+\psi^*$ and $i(\psi-\psi^*)$ connect the subspaces A and B, it follows that neither of these two quantities can be measurable (ψ itself is not Hermitean and, for this reason, its measurement need not be considered).

CHARGED FIELDS

In the present form of field theory, charged particles are represented by complex fields. If only one such field is considered, say $\varphi(x, y, z, t)$, the Lagrangean and Hamiltonian functions, including if necessary the interaction with external fields, will contain φ only in the bilinear combination $\varphi^*\varphi$, i.e., they will be invariant against multiplication of φ by a phase factor $e^{i\alpha}$. We are thus led to believe that such a factor is an intrinsically unobservable modification of the field. If several charged fields $\varphi_1, \varphi_2, \cdots$ be present, the Hamiltonian may contain terms such as $\varphi_1^*\varphi_2$, $\varphi_1^*\varphi_2^*\varphi_3^2$, $\cdots$ etc., but in all cases it is invariant against a simultaneous multiplication of all fields by the same $e^{i\alpha}$.

This property is known to be connected with the principle of conservation of the total charge and represents a very restricted type of gauge invariance. If Q is the total charge, in terms of e as a unit, multiplication of $\varphi_1, \varphi_2, \cdots$ by $e^{i\alpha}$ can be achieved by the unitary transformation

$$\varphi_s \rightarrow e^{-i\alpha Q}\varphi_s e^{i\alpha Q}. \tag{10}$$

We are thus led to postulate that: multiplication of the state vector F by the operator $e^{i\alpha Q}$ produces no physically observable modification of the state of a system of (mutually interacting) charged fields.

We can give no conclusive evidence for this assertion, and such evidence may in fact depend on a deeper understanding of the meaning of electric charges which we still lack. Assuming that the assertion is correct, it follows that the parities of states with different charges cannot be compared.

As a result, it is clear, for instance, that if certain experimental data can be interpreted on the assumption that the charged π-meson field is pseudoscalar and the other (proton, μ-meson, $\cdots$ etc.) charged fields with which it interacts have certain specified inversion properties, it must be equally possible to interpret the data on the assumption that the charged π-meson field is scalar, provided corresponding modifications in the properties of the other fields are made.[4]

APPLICATIONS

Having stressed purely negative aspects so far, let us see what one can say in an affirmative sense.

In the first place, the electromagnetic field is no doubt the one about which we know most. Once it is stated that the electric field is a polar vector,[5] one knows the properties of any state containing only photons.

The parity of a particle, like the neutral π^0, which can decay into a pure photon state, is then in principle determinable. Another way to do this is to ascertain which selection rules obtain experimentally in a reaction such as $p+p \rightarrow \pi^0+p+p$, where no other particle is created or destroyed.

If we turn now to charged particles, our considerations show that parities are to a certain extent arbitrary. This means, as it often happens, that we need a frame of reference, which is based on conventions, but is no less useful because of that. We could, for instance, agree that the $\pi^{\pm}$ mesons are to be regarded as odd. This would then reduce the arbitrariness in the inversion law for other particles. For instance, the well-known capture experiments in deuterium give indications as to parity, that can be formulated in the above frame of reference, by saying that the proton and neutron fields ψ_P and ψ_N transform in such a way that $\psi_P^*\beta\psi_N$ is a scalar.

Leaving these special examples, it is perhaps desirable to state in general what possibilities exist; this will also clarify the difference as well as the area of agreement between our standpoint and that adopted in the paper of Yang and Tiomno.[4]

The preceding remarks should demonstrate that the possibility of determining or comparing intrinsic parities is intimately connected with the possibility of performing quantum mechanical experiments which can serve to determine phase differences between different parts of a state function. If there were no superselection rules, i.e., if all phase differences could be measured in principle, the relative parities of all particles could be determined. This could be done in prin-

[5] It is, of course, true that if, in addition to the inversion I as it is usually understood, (i.e., such that the sign of the charges is preserved, and E is polar) one believes in the operation of charge conjugation C as an exact symmetry property of nature it becomes arbitrary whether one regards I or CI as the inversion law. Adopting CI, however, none of the states of atoms or nuclei, that one considers normally, would be a state of definite parity (states of definite parity would involve superpositions of states containing protons and anti-protons, etc.). The definition thus is not a convenient one to adopt. That C is an exact symmetry property is moreover still far from proved. The disturbing possibility remains that C and I are both only approximate and CI is the only exact symmetry law. This would force us to regard the electric field as an axial vector. This possibility, however, seems rather remote at the moment.

ciple, for instance, by constructing a state which is, with probability 1/2, a particle A with angular momenta J and J_z about a point and a line, with probability 1/2, another particle B in a similar state. If this state looks the same in a mirror which is parallel to the line, and if rotated by π about an axis perpendicular to the line, the parities of A and B are the same; they are opposite otherwise.[10] Less abstractly, one could try to transform A into B and keep track of the parities of the particles which were absorbed and emitted during the transformation.

The superselection rule which prevents the comparison of phases between states with half-integral and integral angular momenta makes it impossible to compare directly the parities of spinor particles with those of integral spin particles. However, if this is the only superselection rule, it remains possible to compare the joint parities of two identical particles with that of an integral spin particle. If this parity be even, one would be tempted to attribute a real parity to the individual spinor particle. If the parity is odd, one would be tempted to attribute an imaginary parity thereto. However, still proceeding on the assumption that the spinor superselection rule is the only one in existence, and that all phases can be measured, the measurement of which is not forbidden by this superselection rule, the parities of any two spinor particles can be compared. This comparison, as any comparison of parities, can yield only the results "equal" or "opposite." Hence, if one spinor particle had a real parity in the above sense, this will be true for all other spinors. Similarly, if one spinor had an imaginary parity, this will be true of all others. Less abstractly, some pairs of spinors may disintegrate in such a way that one will say that the product of their parities is even, some pairs in such a way as to make the product of their parities appear odd. Under the assumptions of this paragraph the product of their parities clearly cannot be imaginary because every pair will be able to transform into integral spin particles, possibly after absorbing some such particles. In particular, under the assumption of this paragraph, it would not be possible for one pair of identical spinors s_1 to show even, for another pair s_2, to show odd parity. In this case a pair of s_1 plus a pair of s_2 would show odd parity. This would mean, however, that the parity of a pair consisting of one s_1 and one s_2 particle would have to be indeterminate. This is contrary to our assumption.

If we assume that the phases of states with different charges cannot be compared either, i.e., assume a superselection rule for charge, there will be no direct way to compare parities of particles with different charges. However, it will be again possible (unless prevented by the spinor superselection rule) to compare the product of the parities of two particles with opposite charges, with the parity of an uncharged particle. This parity can again be the same or opposite. Since an identical pair of charged particles cannot be uncharged, the square of the parity of a charged particle cannot be determined under the present assumption. It will be possible to say that the parity of a particle of unit charge is ω, where ω may be any number of modulus 1. Still under the assumption of this paragraph, every other particle with unit charge (and the same type of spin) will then have parity ω or $-\omega$, every particle with opposite charge the parity ω^{-1} or $-\omega^{-1}$. Clearly, it will not be possible to attribute a direct physical significance to the quantity ω and one may just as well call it 1. However, there may be some advantage in keeping ω because it will remind one of the conservation law for electric charges. An interaction operator which violates this law will also appear to violate the principle of inversion symmetry. If one assumes the conservation law for heavy particles to hold and adopts a corresponding superselection rule, forbidding the observation of phase differences between states with different numbers of heavy particles, the parity of a heavy particle will have a new indeterminate factor ω' in it which again will have no immediate physical significance. Similar remarks apply to ω' as were made above for ω. It may be again desirable to keep this indeterminate phase as a useful formal device to remind one of this conservation law.

A slightly less general device is that employed by Yang and Tiomno, who by a suitable choice of factors, $\omega'=\pm 1, \pm i$ for the various particles, succeed in excluding many of the interactions that one would otherwise be tempted to assume and which are in contradiction with the conservation law for heavy particles.

[10] It is hardly necessary to point out that within a subspace A, or B, . . . the operator I^3 must be a multiple of unity, for the customary reasons; see, for example, "reference 7. Hence the parities of two states, whenever they can be compared, can only be equal or opposite.

Radiation Damage and Recovery in Cu, Ag, Au, Ni, and Ta*

J. W. MARX, H. G. COOPER, AND J. W. HENDERSON
University of Illinois, Urbana, Illinois

(Received May 26, 1952)

The electric resistivity changes induced by the 12-Mev deuteron bombardment of Cu, Ag, Au, Ni, and Ta foils were determined as functions of the integrated flux. Bombardments were carried out at about −140°C and −150°C, and differences in the two sets of measurements were traced to a thermal recovery process which was proceeding with measurable velocity even at −165°C. This low temperature reaction was characterized by an activation energy of 0.2, ±0.05 ev for Cu, Ag, and Au, and one of 0.3, ±0.1 ev for Ni and Ta. It is suggested that the migration of vacancy pairs offers a reasonable model for the initial recovery process, although other mechanisms are also discussed.

RECENT experimental work on the effects of neutron and charged particle bombardment of solids clearly demonstrates the vital contribution that such investigations can make to our understanding of fundamental solid state processes. Among the notable contributions in this field are the measurements of Billington and Siegel,[1] Blewitt and Coltman,[2] Brattain and Pearson,[3] and Lark-Horovitz[4] and his co-workers. The work of the fundamental research group at the North American Aviation laboratories is of particular interest to the present discussion. The calculations, surveys, and data of Parkins,[5] Dienes,[6] Martin,[7] Yockey,[8] and others of the NAA group, under Starr and Siegel, were available to the University of Illinois personnel interested in the investigation of radiation damage. Possession of this information contributed greatly to the selection and execution of the measurements described here.

In this investigation the resistivity changes produced by low temperature bombardment of pure metal foils by 12-Mev deuterons were studied. The metals selected were Cu, Ag, Au, Ni, and Ta, and the foil thicknesses were chosen so that about a third of the incident particle energy would be dissipated in traversing the specimen. Choice of the first three metals was dictated by the fact that their similar electronic structure would permit estimates of the Z-dependence of the processes involved, while the last two were selected to evaluate the effect of lattice binding energy on the fraction of low temperature resistivity retained at room temperature. The bombardment of the specimens was carried out at the University of Illinois cyclotron under the supervision of Professor W. Jentschke.

EXPERIMENTAL PROCEDURE

The specimens were in the form of polycrystalline foil strips about 1 mm wide and 0.07 mm thick, and the measured portion of each strip was about 5 mm in length. The copper, silver, and gold were about 99.95 percent pure, the tantalum about 99.8 percent, and the nickel about 99.5 percent after fabrication. Before mounting, the Cu, Ag, and Au specimens were annealed for about three hours at 450° C, and the Ni and Ta at 800°C, in a 10^{-6} mm vacuum.

Copper-constantan thermocouples were spot welded to the foils at top and bottom of the suspended center section to be used in the measurement. The end portions of the specimens were then sandwiched between 0.5-mil strips of mica on which a thin film of silicone grease had been placed, and, electrically insulated in this fashion, they were clamped against an aluminum target block by means of aluminum bars, as indicated in Fig. 1. This target block was fastened to the bottom of a spun copper flask, which served as a liquid nitrogen container. This entire apparatus was suspended within an evacuated target chamber by means of a thin inconel tube, which provided both mechanical support and a channel for replenishing the liquid nitrogen, as shown in Fig. 2.

The internal cryostat arrangement, i.e., flask plus target block, was electrically insulated from the walls of the vacuum chamber, and served as a Faraday cage. Particle flux was measured by passing the output current of the Faraday cage through a current integrator of standard design. The actual target area for the unfocused beam used was defined by an entrance aperture cut in a grounded aluminum plate, and the intensity distribution within that area was determined by means of copper monitor wires placed between the specimens and at each end of the target area. It was found that the deuteron flux at the target position, which was some distance beyond the regular cyclotron target box, was uniform within a 10 percent range over a target area 5 cm long and 1 cm wide.

This desirable homogeneity was obtained at the

* This research was supported by the AEC.

[1] D. S. Billington and S. Siegel, Metal Progress, 847 (December, 1950).

[2] T. H. Blewitt and R. R. Coltman, Phys. Rev. **82**, 769 (1951); **85**, 384 (1952).

[3] W. H. Brattain and G. L. Pearson, Phys. Rev. **80**, 846 (1950).

[4] W. E. Johnson and K. Lark-Horovitz, Phys. Rev. **76**, 442 (1949); Cleland, Crawford, Lark-Horovitz, and Pigg, Phys. Rev. **82**, 763 (1951); E. E. Klontz and K. Lark-Horovitz, Phys. Rev. **82**, 763 (1951).

[5] W. E. Parkins and G. J. Dienes, Phys. Rev. **81**, 650 (1951).

[6] G. J. Dienes, J. Chem. Phys. **16**, 620 (1948); Phys. Rev. **80**, 123 (1950).

[7] Martin, Austerman, Eggleston, McGee, and Tarpinian, Phys. Rev. **81**, 664 (1951); Martin, Johnson, and Goeddel, Phys. Rev. **83**, 885 (1951).

[8] Yockey, Jeppson, and Hunt, Phys. Rev. **80**, 663 (1950).

expense of the beam intensity, which never exceeded 0.5 microamperes/cm² on the target and averaged about 0.1. The low intensity of the beam made end cooling of the specimens feasible, and it was not necessary to place the center section, or measured portion of the specimen, in contact with the target block or any cementing agent. It was felt that this feature would greatly reduce the chance of chemical contamination during bombardment.

The copper leads of each thermocouple pair also served as potential leads for the resistance measurements. Because these were not true line contacts, a geometrical uncertainty is introduced into any calculation of the absolute value of the resistivity; but this cancels out wherever resistance ratios are used, and it may be assumed to be of the same sign and approximately the same magnitude for all specimens. Comparative plots of the resistivity should then be perfectly valid.

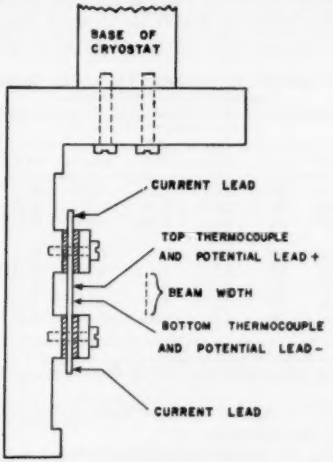

FIG. 1. Target block and sample mounting.

The measuring circuit for the case of three specimens is shown in Fig. 3. At selected intervals during the bombardment, the cyclotron beam was cut off and a one ampere measuring current was passed through the specimens. In general, a period of about twenty minutes sufficed for the temperature to become stabilized in the immediate vicinity of its reference value at about −170°C. The four potentiometers (Fig. 3) were then simultaneously balanced and their readings recorded, after which the measuring current was reversed and the procedure repeated, for each specimen. The true resistance, exclusive of any parasitic emf in the measuring circuit, was taken as the sum of the two IR drops divided by the sum of the currents of opposite polarity. After each specimen had been measured once,

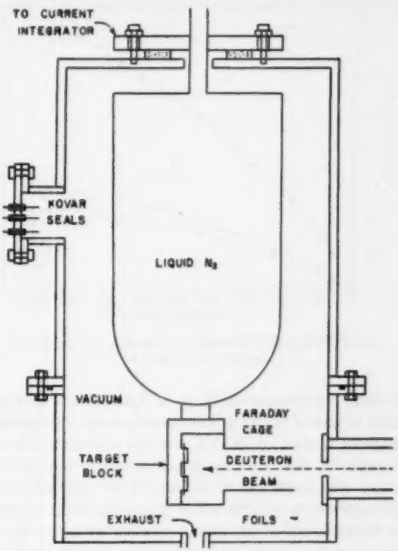

FIG. 2. Cryostat.

the entire operation was repeated, and the points plotted are, in almost all cases, the average of two complete measurements.

As soon as a set of specimens was mounted, the resistance of each specimen was measured over the range −170°C to +30°C, and precise values of dR/dT obtained in this manner were then used to correct all later measurements to an exact reference temperature. The reference temperature (T_r) was selected in the interval −165°C to −170°C so that corrections would be a minimum over the whole set of points.

Low temperature recovery phenomena were investigated by means of a pulse annealing technique. The measuring circuit of Fig. 3 was adapted so that a manually controlled ac heating current could be substituted for the dc measuring current. A high speed

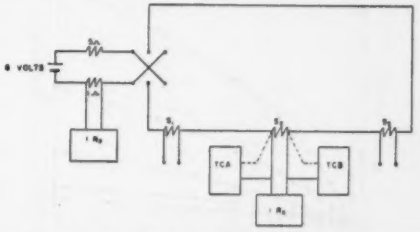

FIG. 3. Measuring circuit. The boxes represent potentiometers for measuring voltage drops across standard ohm (IR_0), top and bottom specimen thermocouples (TCA and TCB), and specimen (IR_s).

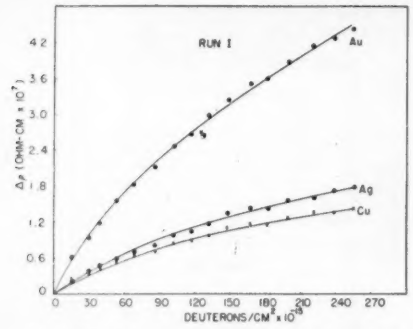

FIG. 4. Resistivity increase as a function of integrated deuteron flux. Run I.

recording millivoltmeter (L & N Speedomax) was connected to one of the two thermocouples on the specimen of highest resistance, in this case the tantalum foil, and the rate of rise to any predetermined temperature plateau was noted. It was found that specimen temperatures rose to within a few degrees of their ultimate free current value in about twenty seconds. If the current were slowly reduced after that period, the plateau temperatures could be kept within a two-degree interval for periods of an hour or more. The recording instrument was only used to stabilize the temperature on the high resistance foil; the actual plateau temperatures were measured on the entire group of foils at regular intervals with the manual thermocouple potentiometers. Pulses of one-half hour to one and one-half hours were employed. At the end of each period, the ac current was cut off and the specimens were allowed to drop back to their reference temperatures for remeasurement.

EXPERIMENTAL RESULTS

Two sets of measurements of the resistivity increase as a function of low temperature bombardment by 12-Mev deuterons were made. In the first set, denoted by "Run I," the only specimens used were Cu, Ag, and Au, following the suggestion by Koehler[9] that a comparison of these three metals might provide a basis for evaluating the Z-dependence employed by Seitz.[10] The data from Run I are shown in Fig. 4. The average bombardment temperature was about -150°C during these measurements, the maximum temperature was -142°C, and the total flux obtained was about 2.6×10^{17} deuterons per square centimeter on the target. A pronounced Z-dependency was observed for the resistivity increases.

In the second set of measurements (Run II) the investigation of Cu, Ag, and Au was repeated, and, in addition, foils of Ni and Ta were added to the target block. The relative Z-dependence observed earlier for the first three metals was confirmed, and it was further noted that the transition metals, Ni and Ta, exhibited much larger resistivity changes than the other specimens. The results of Run II are shown in Fig. 5, and the end results of both sets of measurements are given in Table I, together with pertinent information concerning the specimens.

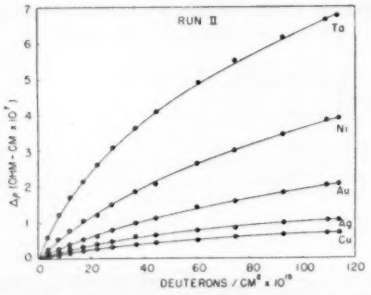

FIG. 5. Resistivity increase as a function of integrated deuteron flux. Run. II.

TABLE I. Resistivity increase induced by 12-Mev deuteron bombardment at low temperatures.

Run	Sample	Z	$\pi D/\text{cm}^2$ $\times10^{-17}$	$\Delta\rho_m$ $\mu\Omega$-cm $\times10$	$\Delta R_m/R_0$	$\Delta E/E$[a]	T_{A_T}[b] °C
I	Cu	29	2.6	1.38	0.245	0.25	−154
	Ag	47	2.6	1.78	0.322	0.26	−153
	Au	79	2.6	4.40	0.496	0.46	−151
II	Cu	29	1.1	0.68	0.119	0.25	−141
	Ni	28	1.1	3.81	0.122	0.25	−133
	Ta	73	1.1	6.69	0.151	0.35	−134
	Ag	47	1.1	1.09	0.173	0.26	−140
	Au	79	1.1	2.18	0.199	0.46	−135

[a] $\Delta E/E$ = fraction of incident particle energy dissipated in foil.
[b] T_{A_T} = average temperature of specimen during bombardment.

During the second bombardment the average temperature of the Cu, Ag, and Au foils was about -140°C and the maximum temperature about -130°C, approximately 10° higher than during Run I. The higher temperatures in the second case resulted from the use of slightly thicker mica strips to electrically insulate the specimens from the cooling block. When the data from Run II were plotted on the same scale as that from Run I, a significant discrepancy was observed. The data for gold are shown in Fig. 6, and similar differences were observed for the other duplicated specimens.

Since the only known variation in the two measurements was the difference in bombardment temperatures, it appeared that a process of ordinary thermal recovery was proceeding with appreciable velocity at the temperatures concerned. Prior to this observation it had been thought that bombardment below -100°C would effectively suppress thermal annealing and that

[9] J. S. Koehler, private communication.
[10] F. Seitz, Disc. Faraday Soc. 5, 271 (1949).

the bending of the $\Delta\rho$ *vs* n curves obtained was almost entirely caused by the thermal spike attendant on the passage of a particle through the lattice, as postulated by Billington and Siegel.[1]

LOW TEMPERATURE ANNEALING

The thermal recovery indicated in Fig. 6 could be detected even in the temperature range $-165°$ to $-170°$C, although the velocity of the reaction was very small in that region. Immediately after the bombardment was completed the specimen temperatures dropped back to their reference values in the indicated range, and they were maintained at these temperatures for a total of 173 hours. At the end of this period the percentage recovery of the radiation induced resistance increase was between 2 percent and 3 percent for Ni and Ta, and between 4 percent and 5 percent for Au, Ag, and Cu.

When the specimens were raised to temperatures in the range $-100°$C to $-120°$C by means of pulse anneals, the reaction velocity was sufficiently increased to show recoveries of the order of 2 percent in times of less than an hour. If it is assumed that the recovery is dominated by a unique rate process, the velocity equation may be written as

$$dR/dt = A(kT/h)e^{-Q/kT},$$

where A includes the concentration of the undefined reactants and an exponential entropy term, kT/h is a frequency factor[11] in which the symbols have their conventional meaning, and Q is an activation energy for the reaction. From this it follows that, if the slopes of the resistance *vs* time curves are known at the point of intersection of two isotherms, the activation energy may be computed by taking the log of the ratios of the slopes.

In Fig. 7 the $\Delta R/\Delta R_m$ *vs* t plots for two different annealing temperatures are shown for Cu, Ag, and Au. The initial points are displaced so that the curves may be distinguished, but the ordinate scale is the same. The ratio $\Delta R/\Delta R_m$ represents the fraction of the original resistivity increase still remaining after a time t. Similar data were obtained for Ni and Ta at higher annealing temperatures, but these measurements did not produce curves as well defined as those for the other three metals, and the uncertainties in the activation energy estimates were much larger. Activation energies of the order of 0.2 ± 0.05 ev appeared to characterize the recovery process for Cu, Ag, and Au, while the more uncertain data on Ni and Ta indicated values of 0.3 ∓ 0.1 ev.

TABLE II. Thermal recovery of radiation-induced resistivity increase at low temperatures.

Sample	Annealing temp., °C	Annealing time, hr	Observed decrease in percent ΔR_m	Calc. decrease percent ΔR_m	Assumed Q[a] ev
Cu	−165	173	5.2	3.5	0.15
Ag	−165	173	4.3	3.5	0.15
Au	−165	173	3.8	2.6	0.15
Ni	−161	173	2.0	1.1	0.20
Ta	−161	173	2.6	1.2	0.20

[a] Q = activation energy used in calculation.

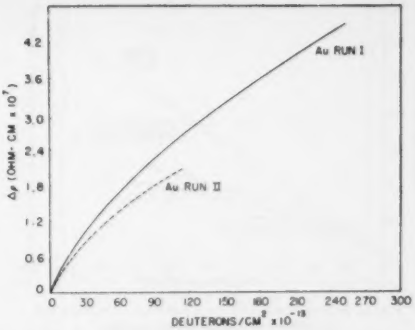

FIG. 6. Comparison of the resistivity increase produced in gold during Run I and Run II.

Using the activation energy values obtained from these pulse annealing data in the vicinity of $-100°$C, together with the initial slopes of the recovery curves in that region, the reaction velocity in the region just below $-165°$C was computed, and the amount of recovery to be expected in a 173-hour interval was calculated and compared with the measured recovery noted earlier for these conditions. Very satisfactory agreement was obtained if the activation energies for Cu, Au, and Ag were taken as 0.15 ev, and those for Ni and Ta assumed to be about 0.2 ev. These values lie on the lower limit of the uncertainty interval for the pulse annealing values quoted.

The low temperature annealing data are collected in Table II, together with the results of the calculations described above. It should be noted that the activation energies have appreciable uncertainties, as indicated, and they are not presented as precision measurements

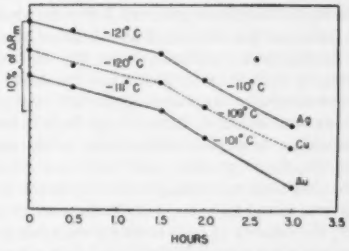

FIG. 7. Thermal recovery of the radiation induced resistivity increase in copper, silver, and gold.

[11] Glasstone, Laidler, and Eyring, *The Theory of Rate Processes* (McGraw-Hill Book Company, Inc., New York, 1951).

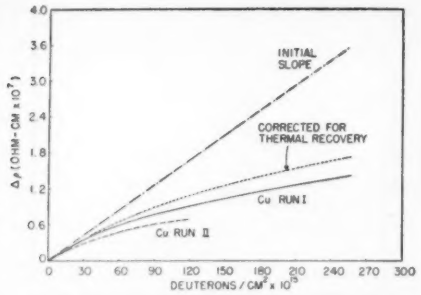

FIG. 8. Representative thermal recovery correction for resistivity *vs* deuteron flux curves.

of those quantities. No low temperature annealing data were obtained from Run I because of equipment failure.

ROOM TEMPERATURE ANNEALING

After the pulse anneals described, the liquid nitrogen was allowed to evaporate from the cryostat and the specimens reached room temperature. After standing at +28°C, ±5°, for the time intervals indicated in Table III, where these data are shown, liquid N_2 was again added and the specimens cooled to their reference temperature and remeasured. An appreciable fraction of the original resistivity increase still persists after room temperature anneals of the order of 300 hours for all specimens, and a low velocity recovery reaction is still observable after about 100 hours. The authors did not succeed in making reliable measurements of activation energies for room temperature recovery, but it seems quite apparent that the reaction or reactions involved are not the same as in the low temperature processes.

DISCUSSION

It seems reasonable to assume that the primary persistent effect of particle bombardment of pure metals is the production of interstitial-vacancy (I–V) pairs. These lattice defects are believed to be produced in atomically dispersed form, and while in that state might be regarded as impurities in solution. If the migration and agglomeration of these defect impurities could be suppressed, the number of I–V pairs produced by any given particle flux could be calculated, over the entire bombardment interval, from the expressions developed by Seitz,[10] or at least until the defect concentration became so large that significant coincidence corrections were required. Even though both bombardment annealing, from the thermal spike in the wake of each bombarding particle, and ordinary thermal recovery processes are thought to contribute to the bending over of the $\Delta\rho$ *vs* n curves in the present measurement, the velocity of both recovery reactions should be near zero when the concentration of defects is small. Therefore, the initial slopes of these curves (Fig. 4 and Fig. 5) should be governed by the production of I–V pairs in the fashion postulated by Seitz.

Working on this hypothesis and estimating the effective scattering cross sections of both I and V defects from available data on impurity increases in resistivity, Koehler[12] has obtained agreement between experiment and theory to within a factor of three. His calculations indicate that the fraction of atomic displacements in Cu, Ag, and Au was between 10^{-2} and 10^{-3} in Run I.

The activation energies obtained from the low temperature recovery process may be used to correct the bombardment curves of Figs. 4 and 5, for the purpose of ascertaining whether the entire curvature might not be accounted for by purely thermal recovery, without recourse to the thermal spike hypothesis. Figure 8 shows the result of this correction applied to the data on Cu from Run I and Run II. It is observed that this approximate correction brings the two sets of measurements into near coincidence with each other, but that it falls short of bringing the measured curve up to the extrapolated value of its initial slope. Similar results are obtained from the data on Ag and Cu. The authors feel that the major portion of that deviation from the original slope which is not accounted for by thermal annealing probably results from the action of thermal spikes, although coincidence annihilation and interdefect screening should make some contribution.

If the production of I and V defects is the fundamental damage process observed during bombardment of pure metals, then the low temperature recovery of the lattice might be formally regarded as a series of chemical reactions between these defects. Letting A represent the annihilation of an I–V pair, the primary *a priori* possibilities are:

$$I+V=A; \quad (1)$$

$$V+V=V_2; \quad (2)$$

$$I+I=I_2. \quad (3)$$

To this must be added a series of possible secondary reactions involving the products of the first group, as follows:

$$V_2+V=V_3; \quad V_2+V_2=V_4 \quad \text{etc.}; \quad (4)$$

$$V_2+I=A+V \quad \text{etc.}; \quad (5)$$

$$I_2+I=I_3 \quad \text{etc.} \quad (6)$$

TABLE III. Room temperature thermal recovery of radiation-induced resistivity increase.

Sample	$\Delta R_m/R_0$	Annealing temp., °C	$\Delta R/\Delta R_m \times 100$ 20 hr	96 hr	264 hr
Cu	0.119	28°C, ±5	12.9	8.6	4.3
Au	0.199	28°C, ±5	10.3	8.9	6.4
Ag	0.173	28°C, ±5	18.6	16.7	11.1
Ni	0.122	28°C, ±5	39.2	35.4	31.3
Ta	0.151	28°C, ±5	57.0	55.0	51.6

[12] J. S. Koehler, unpublished Progress Report, February 1, 1952, AEC Contract AT(11-1)182.

Seitz[13] has pointed out that the coalescence of interstitials, if it occurs at all, would probably produce aggregates of very low thermal mobility. On the other hand, it is possible that the simpler vacancy aggregates might have greater thermal mobility than the individual vacancies. The calculation of Huntington and Seitz,[14] together with self-diffusion data on copper, leads to the expectation that the migration activation energies for single vacancies would be about 1.0 ev in copper, appreciably larger than that for the low temperature recovery process for that metal noted here. If the results of this theoretical treatment are to be accepted, single vacancies do not appear to be the major low temperature reactants.

In a more recent work, Seitz[15] estimates that double vacancy aggregates, the V_2 "molecules" produced by Eq. (2), will be thermally stable below room temperature and that they would require an activation energy of less than 0.5 ev for migration. Presumably the larger vacancy aggregates would have reduced thermal mobility because of the greater coordination required for movement.

If the initial recovery observed here were presumed to depend solely on the migration of divacancies, it would be necessary for a sufficient concentration of the V_2 aggregates to be present in the lattice to effect a substantial reduction, something of the order of 30 percent, in the bombardment induced resistivity increase, at low temperatures. Along with the annihilation of I–V pairs, the coalescence of neighboring vacancies may possibly occur on a scale large enough to account for the data in regions energized momentarily by thermal spikes during bombardment.

Since only a limited number of the mobile divacancies would exist after the bombardment, and since their interaction, either with interstitials or other vacancies, always leaves a residue, it is not to be expected that complete thermal recovery could be achieved by this low temperature process. Pulse annealing data above -100°C seem to indicate such an exhaustion of the low temperature reactants, as shown in Fig. 9.

The existing data might also be interpreted by assigning migration activation energies of less than 0.3 ev to the interstitials. If the coalescence of I defects is prohibited, the only possible reaction, on the basis of the idealized model used here, is an annihilation process, such as reactions (1) or (5). Thus complete recovery could occur at, say, -80°C in reasonable times. All experiments seem to contradict this. If I defects also aggregate, however, then some fraction will always be immobilized as interstitial "precipitates," or extra plane segments in the lattice, and complete recovery would not be expected.

When the low temperature recovery has been effectively halted by depletion of the reactants, extensive

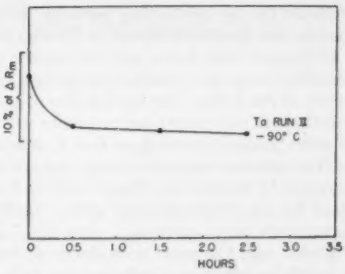

FIG. 9. Thermal recovery in tantalum, showing apparent exhaustion of the recovery mechanism.

lattice debris should still remain. The present measurement corroborates this picture. Even after extended intervals at temperatures in the neighborhood of $+30$°C, the data of Table III show that a recovery process is proceeding with appreciable velocity. The indications are that this process is governed by an activation energy of the order of 1.0 ev. It is possible that the room temperature recovery, therefore, involves the migration of single vacancies, since this is the value to be expected from the calculation of Huntington and Seitz.

The fraction of radiation induced resistivity increase which still remains in Ni and Ta after 300 hours at room temperature is strikingly large compared to that of Cu, Ag, and Au. Even though the electron scattering is of a different nature in the transition metals than in the simple metals, there is no reason to believe that fractional changes in the resistivity increase are not directly related to fractional changes in the impurity concentration for both. Thus it would appear that a major portion of the original I or V defects, or both, may still be retained in atomic dispersion in these transition metals. Experiments on such metals might yield valuable results without the great inconvenience of constant refrigeration.

It is quite possible that the occurrence of more than one recovery process in the low temperature region is concealed by the uncertainties in the activation energies reported here. The defects produced by irradiation are distributed in various states of propinquity. It is conceivable, for example, that an I–V pair whose members were immediately adjacent to each other might require only a small activation energy for annihilation. A reaction of this sort could account for the low temperature recovery without resort to the divacancy mechanism previously discussed. A larger activation energy might be required for the annihilation of an I–V pair of slightly greater separation, and so on. More precise activation energy measurements might be able to reveal the existence of such a fine structure and would be most desirable at this time.

Up to this point the original lattice has been treated as an ideal one, free from any imperfections except

[13] F. Seitz, private communication.
[14] H. B. Huntington and F. Seitz, Phys. Rev. **61**, 315 (1942).
[15] F. Seitz, Phil. Mag. Supplement, **I**, 60 (January, 1952).

those produced by the bombarding particles. Actually the materials used possessed regions of disorder in the vicinity of the grain boundaries, and presumably, additional disordered regions in the form of dislocations in the interiors of the grains. The annihilation of an I–V pair results in both mechanical and resistivity recovery, but any other process by which an I or V defect was removed from solution, such as vacancy aggregation or defect trapping by dislocations, should result in marked recovery of the electrical resistivity without producing a correspondingly large mechanical recovery. In this respect Blewitt and Coltman[2] have observed that the neutron irradiation of copper single crystals above room temperature produced only a 2 percent change in resistivity, but about a 1000 percent increase in the critical resolved shear stress, which was not completely recoverable until annealing temperatures of about 400°C were employed.

It is now known that large resistivity increases can be produced in pure metals both by low temperature particle bombardment and low temperature plastic deformation. The authors suggest that it would be of great value to know whether these effects are additive or not. It is possible that if a metal specimen, irradiated at low temperatures, were later plastically deformed at the same, or lower, temperatures, the resulting dislocation motion might result in a "sweeping out" or general trapping of some of the I and V defects. If this occurs a very interesting drop in resistivity should be observed.

If it were assumed that the only recovery occurring during bombardment is the annihilation of I–V pairs, neglecting both thermal recovery and vacancy aggregation, then the production of lattice defects, and with it the resistivity, could be described by an expression of the form

$$dN = \alpha dn - \beta N dn,$$

where N is the concentration of I–V pairs, n is the particle flux, α is the number of I–V pairs produced per unit volume by any particle, and β is the probability that any existing pair would be annihilated through the action of a bombarding particle. If $\Delta\rho$ is proportional to N, these assumptions would lead to the following integrated expression for the $\Delta\rho$ *vs* n curve:

$$\Delta\rho = A(1-e^{-\beta n}),$$

which predicts a phenomenological saturation value of $\Delta\rho_m = A$ for infinite n. Earlier data obtained by the authors, with relatively large point scatter and no thermal correction, could be approximately fitted with this expression. More precise later measurements gave better definition of the experimental curve, and it was not possible to fit the equation within the reduced point scatter. Thermal recovery corrections aggravated the misfit, and the substitution of N^2 for N in the original differential expression, which seemed reasonable in view of reaction (1), also increased the fitting discrepancy between integrated expression and data. If a third fitting parameter in the form of a term linear in n is added, all of the data obtained may be rather precisely accommodated. The resulting expression is

$$\Delta\rho = A(1-e^{-\beta n}) + Bn.$$

Since the experimental curve is of simple form, no great significance can be attached to the fitting by a three-parameter equation. However, the physical picture implied by the given expression is interesting in view of the preceding discussion. It appears to infer that, in the absence of ordinary thermal annealing, the damage process consists of simultaneous creation and destruction of primary lattice defects during bombardment, plus the gradual accumulation of a secondary type of defect which appears to be relatively immune to bombardment annealing. This latter effect could be associated with the aggregation of vacancies and consequent stranding, or abandonment, of a fraction of the interstitials.

It has been pointed out by Koehler[16] that if defect formation is assumed to follow a differential equation of the form

$$dN = \alpha dn - \beta N^{\frac{1}{2}} dn,$$

then the integrated two-parameter expression does give a reasonable fit with the data. This is also true for other exponents of N less than unity. The integrated expressions obtained by the use of these fractional exponents predict a phenomenological saturation value.

The authors are indebted to Professor J. S. Koehler and Professor C. A. Wert for their discussion, criticism, and assistance in making the measurements, to Professor F. Seitz and Dr. A. W. Overhauser for valuable discussions, to Professor P. G. Kruger and Professor D. E. Mapother for suggestions concerning the execution of the measurement, and to Mr. Roger Erickson and Mr. F. Witt for the design and construction of the target cryostat. As noted previously, the actual operation of the cyclotron during the bombardment periods was directed by Professor W. K. Jentschke. Particular acknowledgement is made of the cooperation of Professor H. L. Walker, head of the Department of Mining and Metallurgical Engineering, in establishing the research facilities used in this investigation.

[16] J. S. Koehler (private communication).

Vapor Pressures of He^3-He^4 Mixtures Below the Lambda-Point*

H. S. Sommers, Jr.
Los Alamos Scientific Laboratory, University of California, Los Alamos, New Mexico
(Received April 16, 1952)

A series of measurements of the vapor pressures of solutions of He^3 in He^4 are described. The methods used are absolute, giving directly the vapor pressure as a function of temperature, liquid phase concentration, and vapor phase concentration. The concentrations are determined from the measured abundance ratios of the room temperature gases without the necessity of withdrawing samples from the cryostat. The He^3 concentrations studied ranged up to 80 percent for the vapor phase and 13 percent for the liquid phase, while the temperature interval was 1.30–2.18°K. From these measured pressures are deduced the vapor pressures as a function of temperature and vapor phase concentration and as a function of temperature and liquid concentration, the He^3 distribution function, and latent heats of evaporation. Analysis of the experimental results on rather general grounds shows there is a significant repulsive potential energy between the two isotopes. At constant temperature the mixing should thus be accompanied by heat absorption, while adiabatic mixing should lower the temperature. On the basis of classical solution theory, the mutual repulsive potential energy leads to a separation into two liquid phases around 0.7°K.

I. INTRODUCTION

STUDIES of the properties of solutions of He^3 in He^4 give new information about He^4, information needed because of the incomplete state of the theory of liquid helium and in particular of the He II region.[1] It is true that Landau's hydrodynamic model of He II has been successful in predicting the variation of second sound with temperature,[1] and recent experiments[2] give a good agreement with his predictions as to the specific heat of liquid helium down to very low temperature; however, it is not certain these successes do not originate in certain assumptions as to specific properties of the liquid rather than in the basic concepts of his theory.

The properties of the mixtures of the two isotopes may give some idea of the influence of statistics on the abnormal properties of He^4, since the two isotopes should obey different statistics. Besides this, and probably more important, the addition of He^3 to liquid helium permits a study of He^4 under a whole new set of conditions.

The phase diagram of the solutions is important from two points of view. Its determination is a prerequisite to a quantitative study of the properties of the mixtures, for without the relation between vapor pressure and concentration one cannot deduce the composition of the sample by any simple measurements. In addition, the solubility of the lighter isotope in the heavier presents an interesting theoretical problem, as yet unsolved. It has not yet even been shown whether the peculiar behavior of the solubility with temperature could be expected of a classical mixture, whether it is a quantum effect, or whether it originates in the statistics obeyed by the two types of atoms.

Studies of the solubility of the two isotopes below the lambda-point have been hampered by the abnormal properties of the superfluid phase, and the results have differed from each other by orders of magnitude depending on the method used. The different approaches can be separated into three general categories.

1. Absolute Measurement of Solubility

The absolute method involves the deduction of the concentrations of the phases from measurements of isotopic abundance, masses, pressure, volume, and temperature.

For example, in one popular method the average concentration of the entire sample and the concentration of some gas withdrawn from the vapor phase are measured on a mass spectrograph. The liquid phase is assumed to have the same concentration as the average for the entire sample, since essentially all the gas has been liquefied.

This method is direct and reliable provided there is true equilibrium between liquid and vapor phases and provided the sample withdrawn is representative of the vapor in contact with the liquid. These conditions are probably satisfied above the lambda-point but not below, for here the results published have been highly ambiguous, with wide divergences depending on the method of sampling.

A paper by Lane and his co-workers[3] contains a bibliography of such measurements and an analysis of the reasons they have been unreliable. Apparently the failure is due to the properties of the super phase, which upset the measurements in two different ways, both of which are initiated by the presence of the Rollin film. This film, due to the reflux action of evaporation in the stem of the filling tube and recondensation at the surface of the liquid, gives an abnormal heat flux into the exposed liquid surface, which produces a heat flush in the liquid sweeping the He^3 into the liquid and

* This paper is based on work performed under University of California contract with the AEC.
[1] L. Tisza, Compt. rend. **207**, 1035 (1938); Phys. Rev. **72**, 838 (1947); L. Landau, J. Phys. (U.S.S.R.) **5**, 71 (1941); J. Exp. et Theoret. Phys. **11**, 91 (1947); F. London, Phys. Rev. **54**, 947 (1938).
[2] H. C. Kramers, Proc. Int. Conf. Low Temp. Phys. (Oxford), 93 (1951).
[3] Lane, Fairbank, Aldrich, and Nier, Phys. Rev. **75**, 46 (1949).

reducing the liquid concentration of He^3 at the liquid-vapor interface. This prevents the vapor from ever reaching equilibrium with the bulk liquid. The second difficulty is that a sample pumped out of the filling tube is not representative of the vapor immediately above the liquid but rather of the gas evaporating from the Rollin film somewhere up in the tube.

Since the film escaping into a region where the pressure is reduced below the bath pressure (the condition when one pumps the gas out of the sample tube) is essentially pure He^4,[4] a sample thus withdrawn will be depleted in He^3. Because of these difficulties, any sampling technique is open to the doubt as to whether the process of sampling has not destroyed the equilibrium and given an incorrect result.

2. Application of Equation of State

In this method, the equilibrium temperature and pressure are measured and the He^3 distribution calculated from an assumed equation of state. A check on the results is afforded by application of the principle of conservation of mass, which requires measuring the concentration of the sample at room temperature, the volumes of the liquid and vapor phase, and the total amount of gas added. The liquid and vapor densities are taken as those of pure He^4 at the temperature and pressure measured.

Apparently the method is not very sensitive to the equation of state assumed, for quite different equations of state have been justified by the mass balance. Eselson and Lasarev[5] found that the vapor pressure of their solution agreed with Raoult's law. They did not actually calculate a mass balance but showed that the mass in the vapor phase was negligible. On the other hand, Taconis[4] and his collaborators calculated a mass balance in the following way. They filled the sample holder with a known amount of helium of known concentration and measured the volumes of the liquid and gas phases. Next, known amounts of He^4 were withdrawn through a ground joint and the pressure measured after each withdrawal. This gave a series of readings of pressure for different mixtures at fixed temperature. Their result was that the pressure did not agree with that given by Raoult's law. To explain their results, they assumed the solution is indeed ideal, but that the He^3 is insoluble in the superfluid portion of the He II; this gives a modified form of Raoult's law in which the solubility of He^3 decreases very rapidly as the temperature is lowered below the lambda-point. With this equation of state, calculation of the mass of each element in each phase showed the mass of He^3 was constant throughout the experiment within the experimental accuracy.

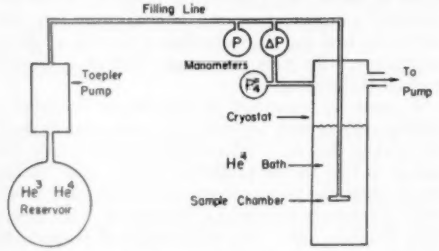

FIG. 1. Apparatus—schematic.

3. Indirect Method of Measuring Solubility

Taconis, Beenakker, and Dokoupil[6] have used the osmotic pressure of the He^3 solution in respect to pure He^4 as a measure of the concentration of He^3. This pressure was balanced by having the pure He^4 liquid at a slightly higher temperature than the mixture and connecting the solution to the pure component by a narrow slit above the liquid level. The condition for no liquid flow through the slit was then assumed to be the cancellation of the osmotic pressure of the solution by the fountain pressure of the pure component caused by the temperature difference between the two liquids. From van't Hoff's law of osmosis, they calculated the He^3 concentration in the liquid. A check on this was again afforded by applying the condition of mass balance, which was satisfied if the distribution of He^3 between liquid and vapor was given by Taconis' modification of Raoult's law.

To date, no extensive study of the phase diagram has been made, nor has agreement been reached among the various workers as to the form of the distribution function of He^3. All the measurements reviewed here have been of a survey character with low accuracy, the small amounts of He^3 available being a serious limitation to the measurements. In contrast to this, we were fortunate in having at our disposal a sufficient amount of the lighter isotope to permit a detailed study.

II. METHOD AND APPARATUS

By a modification of the absolute method of studying the He^3 distribution, we have measured the pressure of samples whose liquid phase concentration was known and of other samples of known vapor phase concentration. The apparatus is shown schematically in Fig. 1. The He^3 concentration of the gas in the reservoir is measured with a mass spectrograph. Known amounts of this gas are pumped through the stainless steel filling tube into the copper or brass sample chamber, and the pressure of the bath, P_4^0, and the difference between sample and bath, ΔP, measured. These quantities give the temperature of the bath, the sample pressure, the total mass pumped into the sample and

[4] Daunt, Probst, Johnston, Aldrich, and Nier, Phys. Rev. **72**, 502 (1947); Taconis, Beenakker, Nier, and Aldrich, Physica **15**, 733 (1949).

[5] B. N. Eselson and B. G. Lazarev, J. Exp. Theoret. Phys. **20**, 1055 (1950).

[6] Taconis, Beenakker, and Dokoupil, Phys. Rev. **78**, 171 (1950).

filling line, and the average He^3 concentration of this mass.

In general, when a mixed gas is pumped into the sample holder, the process of liquefaction will be accompanied by fractionation and the He^3 will distribute itself in some definite but unknown manner between the liquid and vapor phases. As a result, the concentration of neither phase will be known. However, there are two cases in which the composition of one of the phases is given; when all the sample is in the vapor phase or when all is in the liquid. In both cases, the composition of the phase containing the entire sample is precisely that of the gas in the reservoir.

This consideration defines the two types of measurements we made. In common with most of the other experimenters, we determined the concentration of the liquid phase by completely filling the holder with liquid. Under this condition the He^3 in the gas phase, which is confined to the filling tube, can be neglected and the liquid concentration is that of the gas in the reservoir. The vapor phase was studied by measuring the vapor pressure of the sample when the gas phase was in equilibrium with zero amount of liquid phase, that is, at the dew point. Here the vapor phase has the concentration of the initial gas.

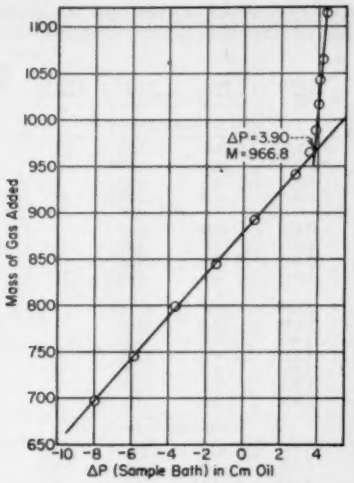

FIG. 2. Filling curve; $T=2.102°K$, $X_v=9.85$ percent.

III. MEASUREMENTS

1. Vapor Phase

As already described, the isotherms of the vapor phase were determined by measuring the dew point pressures for various vapor concentrations. This was accomplished by taking filling curves, a sample one of which is shown in Fig. 2, which shows how the pressure varies when small amounts of gas, measured by the Toepler pump, are forced into the sample holder. In this figure we have plotted the mass of gas added, in arbitrary units, against ΔP, the difference between sample and bath pressures. The sharp break indicates the start of condensation, or dew point. Up to this break, no liquid has collected and so no fractionation has occurred, which means that the concentration in the vapor phase is that originally found for the gas in the reservoir.

a. Filling Curves of He^3 Concentrations of Less Than 15 Percent.

For the low concentration samples, an apparatus with relatively large volumes was used. The sample holder, of about 55 cm^3 volume, was filled through a $\frac{1}{4}$-in. stainless steel tube from a 500-cm^3 Toepler pump. ΔP, the difference between bath and sample pressures, was measured with a manometer filled with butyl sebacate, while all other pressures were determined by Wallace and Tiernan Model FA145 pressure gauges. Although this is reasonably sensitive because of its long scale length, the hysteresis limited accurate measurements to the region above 1.60°K. Improved manometry would have permitted reaching a lower temperature, but the regularity of all the vapor phase data indicated the interpolation from the higher concentrations would always be sufficiently reliable to make further studies of the dilute vapor unnecessary.

b. Filling Curves for High Concentrations

With the higher concentrations, smaller scale apparatus was necessary. The copper sample holder had a volume of 9.5 cm^3. Again the filling tube was of $\frac{1}{4}$-in. stainless steel tubing, but the Toepler had two calibrated volumes of 39.1 and 196.1 cm^3. A Bourdon gauge measured the pressure in the Toepler, a not very critical quantity, while all other pressures were read on oil manometers. The temperature interval covered was 1.3 to 2.18°K for He^3 concentrations of approximately 40, 60, and 80 percent. The experimental data and estimated accuracies are given in Table I.

2. Liquid Phase

To determine the vapor pressure of the different liquid phase concentrations, the sample holder was completely filled with liquid at a temperature somewhat below 2.18°K and the pressure measured for different bath temperatures. The apparatus was the same as for the higher concentration vapor phase except for the sample holder and filling tube. These were a copper pill box of volume 0.98 cm^3 and a stainless steel filling line of 0.045 in. i.d. and 0.004 in. wall for the bottom twelve inches and 0.125 in. i.d. $\times$ 0.010 in. wall for the remainder. The line passed through an O-ring seal at the top of the cryostat so that the sample immersion depth could be kept constant. This sliding seal also

TABLE I. Vapor pressure for several vapor concentrations.

X_V %	Temperature °K	Vapor pressure mm Hg	$\Delta P/P$ %	Error: Instrumental %	Error: Deviation from Eq. (2) %
		A. Low concentrations			
5.21	2.153	37.5	4.73	±2	−1.1
	1.996	24.7	4.95	3	+1.0
	1.868	16.5	4.88	4	−2.0
	1.556	5.0	4.88	13	−4.8
9.49	2.102	34.0	8.84	2	+0.5
	1.804	13.8	9.20	4	+0.8
	1.801	13.6	9.10	4	−0.4
	1.545	4.9	9.43	11	+0.9
13.0	2.159	41.2	11.9	1	−0.2
	2.052	31.3	12.2	1	+0.7
	1.918	21.2	12.4	2	+1.1
	1.702	9.9	12.6	4	−0.3
	1.593	6.3	12.4	8	−2.7
	1.555	5.4	12.9	8	+0.9
	1.536	4.9	12.9	8	+0.7
		B. High concentrations			
40.5	2.155	56.4	37.0	±1.2	+0.1
	1.697	14.21	40.9	1.6	+4.3
	1.695	14.13	41.0	1.6	+3.0
	1.285	1.91	41.9	4.3	+3.8
	1.269	1.78	43.8	4.7	+8.5
58.0	1.978	48.5	54.7	1.2	+1.5
	1.662	17.02	57.0	1.4	+1.8
	1.546	10.94	59.4	1.5	+5.1
	1.486	8.20	58.8	1.7	+3.5
	1.448	6.64	58.0	1.7	+1.2
	1.260	2.33	59.6	3.0	+3.5
78.1	2.142	110.0	68.8	1.1	−1.1
	2.138	110.2	69.1	1.1	−0.7
	1.703	35.4	75.7	1.2	+2.7
	1.702	34.2	74.8	1.2	+1.3
	1.688	32.8	75.3	1.2	+1.3
	1.287	4.38	79.6	1.7	+1.9
	1.285	4.94	77.5	1.7	+3.9
	1.268	4.58	78.4	1.9	+2.1
100.0	1.000	8.68	98.6		+0.6
	1.100	13.51	97.8		+0.7
	1.200	19.93	96.2		+0.6
	1.300	28.13	95.1		+0.6
	1.400	38.33	93.9		+0.3
	1.500	50.72	92.6		+0.4
	1.600	65.0	91.2		+0.3
	1.700	82.0	89.7		−0.1
	1.800	101.5	88.1		−0.2
	1.900	123.7	86.4		−0.5
	2.000	149	84.7		−0.6
	2.100	178	83.0		−0.5
	2.200	209	81.2		−0.5

permitted raising the sample out of the bath to evaporate the bubbles which occasionally formed in the filling tube. The small size of the filling line inside the bath so reduced the amount of gas in the tube that the He^3 in this space was neglected compared to that in the liquid phase. As a check on the importance of the He^3 in the filling tube, a filling curve was run similar to those for the study of the vapor phase except that here sufficient sample was added to completely fill the sample holder with liquid. With an initial gas phase concentration of 3.6 percent He^3 and temperature of 2.118°K, the value of ΔP changed by less than 0.4 percent when the mass of gas in the sample holder was changed by 10 percent, the total mass being approximately the calculated amount to fill the sample holder. Another increase in the mass by 10 percent quadrupled the value of ΔP, showing the presence of liquid in the filling tube. In all subsequent fillings the mass of gas added was 3 percent less than that of the last point preceding the break on this trial filling curve. Since the liquid density is nearly independent of temperature, such a filling worked for all temperatures studied.

While the small diameter of the filling tube satisfactorily reduced the amount of He^3 in the vapor, it introduced an annoying pressure difference between bath and sample at low temperatures. This pressure difference was carefully studied, using pure He^4 in the sample holder, as a function of bath temperature and depth of immersion of the sample. At 1.180°K, the excess pressure inside the sample holder was 0.3 mm Hg. Above this temperature, the difference dropped as the logarithm of the bath pressure to a negligible value above 1.55°K. For deep immersion of the sample holder, the pressure difference was independent of immersion depth, and so in all measurements the depth was kept at about 10 cm.

The reason for the difference in pressure inside and outside the sample holder is not understood. A rough calculation of the thermomolecular pressure drop showed it was negligible. There also seems to be no chance of explaining the difference as a pressure drop resulting from the returning gas from the evaporation of the Rollin film. On the other hand, it is hard to believe the pressure difference represents a difference in temperature between bath and sample. The copper sample holder should not support such a gradient of temperature; moreover, we observed that increasing the surface area of the sample holder by the factor six had no appreciable effect on the pressure difference. Also a larger filling tube, which would have an increased heat leak, gave a smaller pressure difference.

In correcting the liquid phase data for this pressure difference, we assumed temperature equilibrium between bath and sample and subtracted from the sample pressure just the pressure difference found for pure He^4. The estimated errors of manometry shown in Table II include 10 percent of this pressure correction. An alternative method of making the correction would be to assume the error was due to a temperature difference arising from the Rollin film and to assign to the sample the temperature corresponding to the bath pressure plus the sample-bath difference found for pure He^4. Such a correction would certainly be too large, for the heat leak caused by the film will drop off rapidly with addition of He^3, which lowers the film flow rate.[7]

[7] B. N. Eselson and B. G. Lazarev, Doklady Akad. Nauk. SSSR, V. 72, 265 (1950). Also E. F. Hammel (private communication).

A measure of the vapor pressure of a sample of pure He^3 at 1.272°K agreed with the data of Abraham *et al.*[8] to within 0.4 mm Hg, or 1.5 percent, providing the pressure correction was made as already outlined. If instead, the correction was made assuming a temperature difference between sample and bath, the He^3 pressure would have been in error by over 2 mm Hg, while the uncorrected pressure was in error by 2.3 percent. Thus the correction as we have made it works for pure He^4 and pure He^3.

The measurements of vapor pressures and the estimated errors are given in Table II.

TABLE II. Vapor pressure of various liquid phase concentrations.

X_L %	Temperature °K	Sample pressure mm Hg	Instrumental error %
0.58	2.172	38.41	0.4
	2.066	29.47	0.4
	1.957	21.88	0.4
	1.847	15.61	0.4
	1.749	11.28	0.5
	1.658	8.13	0.5
	1.612	6.74	0.6
	1.517	4.61	0.8
	1.405	2.75	1.5
	1.395	2.60	1.5
	1.295	1.47	3.0
	1.272	1.35	3.5
1.98	2.177	41.97	0.3
	2.176	41.95	0.3
	2.146	39.31	0.4
	2.114	36.66	0.4
	2.082	34.00	0.4
	2.044	31.03	0.4
	1.960	25.12	0.4
	1.855	18.91	0.4
	1.767	14.67	0.4
	1.698	11.89	0.5
	1.667	10.79	0.5
	1.631	9.57	0.5
	1.609	8.96	0.5
	1.500	6.18	0.6
	1.384	3.99	1.1
	1.351	3.49	1.3
5.21	2.176	48.10	0.3
	2.112	42.59	0.3
	1.978	32.43	0.4
	1.788	20.82	0.4
	1.723	17.60	0.4
	1.621	13.55	0.4
	1.453	8.52	0.6
	1.441	8.18	0.7
	1.212	3.89	1.5
	1.194	3.66	1.6
9.49	2.183	58.18	0.3
	2.098	49.44	0.3
	2.044	41.61	0.3
	1.953	37.85	0.4
	1.902	34.25	0.4
	1.866	31.85	0.4
	1.799	27.77	0.4
	1.752	25.15	0.4
	1.704	22.62	0.4
	1.683	21.55	0.4
	1.632	19.21	0.4
	1.586	17.29	0.4
	1.554	15.98	0.4
	1.504	14.17	0.4
	1.402	10.83	0.6
	1.230	6.52	1.0
13.0	2.175	64.23	0.3
	2.070	52.16	0.3
	1.961	43.09	0.3
	1.850	35.35	0.4
	1.748	29.03	0.4
	1.655	23.94	0.4
	1.476	16.16	0.4
	1.394	13.11	0.5
	1.328	11.04	0.7
	1.287	9.89	0.7
	1.255	9.98	0.7

3. Evaluation of Accuracy

In the tables of data and with the empirical relations we have indicated the estimated error. Because of the wide divergence of published data on He^3-He^4 mixtures, it seems advisable to include a discussion of the errors expected in the measurements.

a. Manometry

The accuracy of the measurements of the vapor pressures for dilute vapor phase was determined by the Bourdon gauges, whose absolute accuracy in this pressure range we took as $\pm\frac{1}{4}$ mm Hg. For the high vapor concentrations and all the liquid curves, the oil manometers determined the accuracy of the pressure readings. These manometers were calibrated against a mercury manometer at 25°C. The correction to mercury at 0°C and $g=981$ cm/sec^2, amounting to 0.6 percent, was neglected. The error assigned to the oil manometers was ± 0.02 mm Hg for repeatability and ± 0.3 percent arising from the oil density.

b. Temperature

The temperature scale used throughout was the "agreed scale."[9] While it is true some doubt exists about the accuracy of this scale in the vicinity of the lambda-point, all the quantities we measured varied so slowly with temperature that the small uncertainty in the absolute temperature is unimportant.

In certain cases we found a difference in vapor pressure between the liquid in the bath and in the sample holder. For each sample holder, we checked on this effect by making measurements with pure He^4 in the sample holder and made appropriate correction to the data. For the vapor phase data, the difference between sample and bath was negligible except around 1.3°K where it reached 0.03 mm Hg. This amount was then subtracted from the measured value of ΔP. The correction for the corresponding error in the liquid phase curves has already been discussed (see Sec. III-2).

c. Mass Spectrometer

All the samples were analyzed on a Consolidated-Nier mass spectrometer with a viscous leak between the sample and the ion chamber. In a perfect viscous leak there should be a discrimination against the lighter

[8] Abraham, Osborne, and Weinstock, Phys. Rev. **80**, 366 (1950).
[9] H. van Dijk and D. Shoenberg, Nature **164**, 151 (1949).

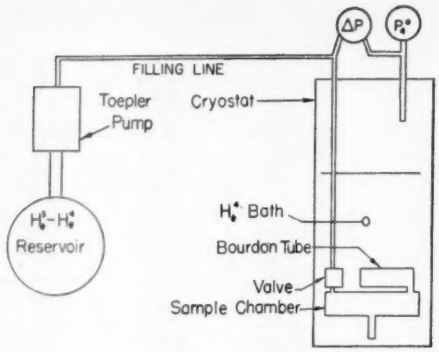

FIG. 3. Modified apparatus.

isotope, because of the higher velocity with which it passes through the electron beam, given by the ratio of the square root of the isotopic masses,[10] but there should be no change of measured abundance ratio with pressure or time. Since the latter pair of conditions was satisfied with our spectrometer, it seemed probable the leak was truly viscous.

In order to remove the possibility of any serious error in the abundance measurements with the mass spectrograph, we made up standard mixtures of helium isotopes with concentrations approximating every sample used in this study and compared each unknown sample with the appropriate standard sample.

Actually, the reading of the mass spectrograph, corrected for the difference in masses of the two isotopes, corresponded quite well with the known abundances of the standards. For our six standard samples, whose absolute abundances ranged from $\frac{1}{2}$ to 80 percent He^3, the formula for the relative abundance was $N_3/N_4 = (4/3)^{\frac{1}{2}} V_3/V_4(1-0.011)$, and the probable error of a single reading was about $\frac{1}{2}$ percent. This means the mass spectrograph reading gave the correct concentration to within 1 percent. For our data, we included the correction found from our calibration of the spectrograph but have taken ± 1 percent as the uncertainty in the absolute value of each unknown gas mixture.[11]

d. Location of Dew Point

We found no evidence for anything but a sharp break in the filling curves, Fig. 2, and the location of the dew point was always taken as the intersections of the lines drawn through the gas sector (low pressure region) and vapor sector of the graph. Repeated runs at a fixed temperature and concentration gave dew points which agreed with each other to within the accuracy expected from the manometry. As mentioned in Sec. IV-3, there is some evidence that, at low temperatures, the dew point pressure was slightly high, which might be due to our failure to observe a small curvature in the filling curve at the dew point. Such a curvature would be too small to matter at higher pressures, that is at high temperatures or high concentration, but could affect the readings in the 40 to 60 percent curves below 1.400°K. However, the high value of the 40 percent concentration at 1.7°K (see Table I) would require a mislocation of the dew point by $\frac{1}{2}$ mm Hg, and this does not seem probable. The reason for the large departure of these two independent measurements at the same temperature is not known.

Although Fig. 2 shows a representative filling curve, there were certain deviations from this shape that are worth mentioning. For higher pressures, which occur for higher concentrations and higher temperature, both the gas phase portion (pressures below the dew point) and the saturated vapor region above the dew point show a marked curvature due to gas law imperfections. In fact, measurements of the filling curves could be used to study the second virial coefficients.[12] However, in every curve studied the break was sharp and clearly defined. At the high concentrations, the change in slope at the break was small, but even here the dew points were reproducible within the error limits expected from the manometry, as can be seen in Table I.[13]

e. Thermal Equilibrium

A very troublesome source of error is failure to reach true thermal equilibrium between liquid and vapor phases in the sample. One cannot be sure that a long wait will guarantee thermal equilibrium, for it is always possible that the Rollin film and the resulting abnormal heat flux will give a serious temperature gradient in the liquid. In these measurements no stirring was attempted and the assumption was always made that, below the lambda-point of the bath, the superfluid properties of the bath would produce a constant temperature throughout the sample. The pill box shape of the liquid sample holder, 0.1 in. deep by $\frac{3}{4}$ in. diameter, gives a large area to volume ratio to improve the heat transfer from bath to sample. We always tried to wait long enough before taking a reading to assure steady-state conditions were reached, and the absence of hysteresis effects when approaching a temperature from either above or below confirmed that this was accomplished.

[10] R. E. Halsted and A. O. Nier, Rev. Sci. Instr. **21**, 1019 (1950).

[11] We wish to thank Dr. B. B. McIntyre and Dr. T. R. Roberts for their advice on the use of the mass spectrometer and their help with many of the gas analyses.

[12] Our data do not give the virial coefficients. For the small sample holder, where the sample volume was known accurately, the nuisance volume due to the filling line was uncertain; while for the largest sample holder, where the nuisance volume was known, the sample volume was uncertain due to its peculiar geometry. Measurements of the second virial coefficients by this method are under way in our laboratory.

[13] Dr. R. D. Arnold (private communication) found that the dew points were not sharp for mixtures of the hydrogen isotopes. This may be due to the fact that his measurements were relatively much closer to the critical point than were ours.

We made two observations which indicated the failure of sampling experiments[3] was due to the Rollin film, but our experiments were not appreciably affected by it. The apparatus for these observations was similar to that already described, but had two important auxiliary features, shown in Fig. 3. In the filling line immediately above the sample holder is a valve with a seat made from a single crystal of silver chloride which could be shut from outside the bath. Since AgCl remains soft at liquid helium temperatures, this valve could be closed very tightly. The one model we built did not completely stop the Rollin film, but it did reduce it to a few percent of its normal value, as judged by leakage measurements, and blocked all gas phase flow. The second feature is a Bourdon tube manometer inside the bath. The position of the end of the Bourdon tube was determined by its capacity in reference to a fixed plate. This manometer had high sensitivity, a few microns' change being easily detectable, but it was subject to slow drift which always made day-long measurements less accurate than readings of an oil manometer.[14]

The first important observation was made when we attempted to enrich part of our sample by pumping off the vapor above the liquid at a temperature well below the transition of the solution. The hope was to get a sample greatly enriched in He^3, corresponding to the concentration of the vapor phase. During the course of the day, while pumping continuously with the Toepler pump, the reading of the Bourdon tube inside the bath was observed to gradually rise as if the liquid were being enriched in He^3 rather than depleted as expected. This did, in fact, prove to be the case. While the original sample had an He^3 concentration of 3.5 percent, the sample withdrawn had, instead of the expected 25 percent, only ½ percent He^3. Apparently the gas pumped off originated in the Rollin film. The rate of pumping was no faster than one would expect the film to be able to keep up with. The pressure drop caused by pumping seemed to be effectively canceled by the evaporation of the Rollin film, for throughout the day the capacitance manometer indicated the vapor above the liquid was indeed 25 percent He^3 and its concentration was undisturbed by the pumping. This indicates that the failure of sampling experiments has not been due primarily to destruction of equilibrium through sampling, but rather to withdrawal of the Rollin film instead of the vapor above the liquid.

The second observation was that closing and opening the AgCl valve had little effect on the reading of the Bourdon tube manometer. It is true the valve did not completely stop the film flow; however, by checking the return flow of gaseous helium it did stop the flux of heat into the liquid and so prevent any heat flush effect. Unfortunately, the process of closing the valve somewhat jarred the Bourdon tube, subjecting it to the possibility of a slight zero shift, but we could safely say that any change in vapor pressure due to checking the heat reflux was less than a few hundredths of a millimeter of Hg. The best observations were made with 3.4 percent liquid at a temperature of about 1.95°K and an excess pressure of sample over bath of around 4 mm Hg. Because of this we feel that for all the more concentrated liquid samples, 2 percent and greater, we did achieve true thermal equilibrium. It is still possible that the peculiar behavior observed for the 0.5 percent sample was due to a heat flush effect, as mentioned in Sec. V.

[14] The original model of the capacitance manometer was designed and tested by Dr. J. E. Kilpatrick.

IV. VAPOR PRESSURE

1. Vapor Pressure for Fixed Liquid Concentration

Table II gives our measured vapor pressures in the temperature interval from 1.2 to 2.18°K, for liquid samples with mole fraction between ½ and 13 percent He^3, together with the estimated instrumental errors.

For each concentration, these data can be described by an Antoine equation, $\log P = A + B/(T+C)$; however, the constants are all rapidly changing functions of the concentration, and no simple relations could be deduced which would give an interpolation equation solvable for the concentration to an accuracy compatible with the precision assigned the data. Since we could discover no explicit relationship between P, T, and X_L, we used the Antoine equations for each X_L to smooth the data. Interpolation on each of these curves gave the vapor pressure isothermals for the liquid phase, Fig. 4, from which we then deduced the table of vapor pressures for the entire temperature range and liquid concentrations studied, Table III. In Table III the log of the vapor pressure is given for each one-tenth degree of temperature and each one-half percent of mole fraction, $[N_3/(N_3+N_4)]_L$. The table of $\log P$ permits linear interpolation with estimated reliability of ± 0.5 percent for $T \geq 1.5$°K and $X_L \geq 1.0$ percent; the accuracy decreases as temperature and vapor pressure drop to a greatest uncertainty of ± 3 percent for 1.2°K and 0.5 percent concentration.

2. Vapor Pressure for Fixed Vapor Concentration; Empirical

The mole fraction of He^3 in the vapor phase can be expressed as

$$X_v = (\Delta P/P)[1+F(P,T)]. \quad (1)$$

From zero to 100 percent He^3 and from 1.2 to 2.18°K, the value of $F(P, T)$ is always small compared to unity, never exceeding 0.20. A fit of $F(P, T)$ to our data for the mixtures and the data of Abraham *et al.*[8] for pure He^3 gives the relation

$$X_v = (\Delta P/P)[1+0.080\{T-1.100 +0.600(\Delta P/P)^{\frac{1}{2}}\}^2], \quad (2)$$

for $0 < X_v \leq 100$ percent and $1.300 \leq T \leq 2.2$°K.

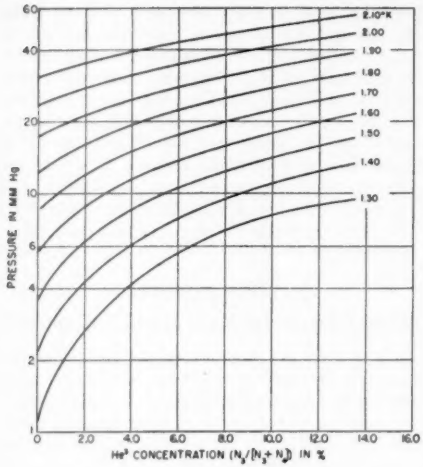

FIG. 4. Liquid phase isotherms.

This equation does not give the best mean square fit to the data, as can be seen from the last column in Table I, for at high concentration and low temperature we have purposely chosen the empirical equation to give a higher value of X_v than indicated by our experimental data. As mentioned in the next section, there is theoretical evidence that the ratio $\Delta P/PX_v$ will never exceed unity in the region studied, while at low temperatures and high concentration our data give a value of this ratio exceeding unity by about 3 percent. This slight excess we have attributed to systematic error in determining the exact dew point, as discussed in Sec. III-3. In fitting the equation to the data, we have imposed the following conditions:

1. $\Delta P/PX_v \leq 1.00$;
2. for $X_v = 1.00$ (pure He^3), $\Delta P/PX_v = 1 - P_4^0/P_3^0$;

where the superscript zero refers to the pure component. This latter equation comes directly from the definition of the terms involved. Equation 2 was made to satisfy this second condition quite closely, within $\pm\frac{1}{2}$ percent, because the data on pure He^3 [8] and pure He^4 [9] are more precise than our measurements on the mixtures. We estimate the accuracy of Eq. 2 to be ± 2.5 percent above 1.5°K and ± 4 percent below this temperature. This inaccuracy is slightly greater than the estimated instrumental error given in the fifth column of Table I.

3. Vapor Pressure for Fixed Vapor Concentration—Interpretation

Since $X_v = P_3/(P_3+P_4)$, it would be quite surprising if we found a very large difference between X_v and $\Delta P/P$. From the definition of the quantities involved, we see that

$$\Delta P/PX_v = 1 - (P_4^0 - P_4)/PX_v, \qquad (3)$$

where ΔP is the difference between sample and bath pressures and P_4^0 and P_4 are the He^4 vapor pressures over the bath and the sample.

TABLE III. Log$P$ (in mm Hg at 25°C) for even temperatures and liquid phase mole fractions (linear interpolation in log$P$).

X_L% \ T°K*	1.2	1.3	1.4	1.5	1.6	1.7	1.8	1.9	2.0	2.1	2.2
0.000	−0.200	0.083	0.332	0.555	0.751	0.929	1.091	1.237	1.370	1.489	1.599
0.50	−0.073	0.185	0.414	0.620	0.804	0.971	1.124	1.262	1.389	1.504	1.611
1.00	0.046	0.281	0.493	0.682	0.854	1.011	1.155	1.286	1.408	1.519	1.623
1.50	0.152	0.368	0.563	0.738	0.900	1.048	1.184	1.309	1.425	1.533	1.634
2.00	0.243	0.443	0.624	0.788	0.941	1.082	1.211	1.330	1.442	1.546	1.644
2.50	0.318	0.506	0.677	0.832	0.977	1.111	1.234	1.350	1.457	1.558	1.653
3.00	0.380	0.558	0.722	0.869	1.008	1.137	1.256	1.368	1.471	1.570	1.663
3.50	0.433	0.603	0.759	0.901	1.035	1.161	1.275	1.384	1.485	1.581	1.672
4.00	0.479	0.642	0.792	0.930	1.059	1.183	1.293	1.400	1.497	1.592	1.681
4.50	0.519	0.677	0.821	0.956	1.082	1.202	1.310	1.413	1.510	1.602	1.689
5.00	0.555	0.708	0.848	0.980	1.102	1.220	1.325	1.427	1.521	1.612	1.697
5.50	0.589	0.737	0.873	1.004	1.121	1.237	1.341	1.440	1.533	1.623	1.706
6.00	0.618	0.763	0.897	1.025	1.140	1.253	1.355	1.452	1.544	1.632	1.715
6.50	0.646	0.787	0.919	1.046	1.158	1.268	1.369	1.464	1.555	1.642	1.722
7.00	0.671	0.810	0.940	1.065	1.175	1.283	1.383	1.476	1.566	1.651	1.730
7.50	0.695	0.833	0.960	1.085	1.192	1.298	1.396	1.488	1.576	1.660	1.738
8.00	0.718	0.854	0.979	1.103	1.208	1.312	1.410	1.499	1.587	1.668	1.746
8.50	0.739	0.874	0.998	1.120	1.223	1.325	1.422	1.511	1.597	1.677	1.753
9.00	0.760	0.893	1.016	1.137	1.238	1.338	1.436	1.522	1.606	1.685	1.760
9.50	0.779	0.911	1.032	1.152	1.252	1.351	1.446	1.533	1.616	1.694	1.768
10.00	0.798	0.928	1.048	1.167	1.266	1.363	1.457	1.543	1.625	1.701	1.775
10.50	0.816	0.945	1.063	1.180	1.278	1.374	1.467	1.553	1.633	1.708	1.781
11.00	0.833	0.960	1.077	1.192	1.290	1.385	1.476	1.562	1.640	1.715	1.787
11.50	0.849	0.974	1.089	1.202	1.301	1.396	1.485	1.569	1.647	1.721	1.792
12.00	0.863	0.987	1.101	1.212	1.311	1.404	1.493	1.577	1.654	1.727	1.797
12.50	0.877	0.999	1.113	1.221	1.320	1.412	1.500	1.584	1.660	1.732	1.803
13.00	0.889	1.011	1.124	1.229	1.329	1.420	1.507	1.590	1.666	1.738	1.807

* Agreed temperature scale, reference 9.

We are going to evaluate this equation for small liquid concentrations, and so we will apply Raoult's law to the solvent in order to eliminate the partial pressure of He^4. This gives the substitution

$$P_4^* = P_4^{*0}(1-X_L).^{15}$$

Substitution in Eq. (3) gives

$$\frac{\Delta P}{PX_v} = 1 - \frac{1+(1-b)/bX_L}{C_v/C_L}, \tag{4}$$

where $b = P_4/P_4^*$. As throughout the paper, X refers to the mole fraction, C to the mole ratio, and the superscript zero means the pure component; the subscript v or L identifies the phase referred to.

Physically the terms in Eq. (4) have the following significance; $1-1/(C_v/C_L)$ is the complete expression for an ideal solution whose vapor phase obeys the perfect gas law, while the departure of b from unity represents the first correction to the gas law. No correction is included for departure from ideality in the solution, but since only the partial pressure of the solvent appears in Eq. (3), this neglect cannot be serious.

To evaluate Eq. (4), we have used our measured values of C_v/C_L (Sec. V) and the theoretical values of the second virial coefficients given by de Boer and co-workers.[16] It turns out that at 2.1°K inclusion of the virial coefficients gives a correction of 4 percent to the ratio $\Delta P/PX_v$.

In Fig. 5 the empirical equation, Eq. (2), is compared with Eq. (4). This plot of $\Delta P/PX_v$ against the temperature reduces all concentrations to nearly the same curve and so gives an extremely sensitive method of comparison. The solid lines show the behavior of the empirical equation for low concentrations, for $X_v = 80$ percent, and for 100 percent (pure He^3), while the dotted line is the evaluation of Eq. (4) at $X_v = 40$ percent. Both the empirical and theoretical equations predict a lowering of the curve for higher temperatures and with increasing concentration, and both give the same value for pure He^3; the agreement between the two equations is well within the experimental error.

In the preceding section, we mentioned that at low temperatures we measured values of our experimental ratio of $\Delta P/PX_v$ which slightly exceeded unity. Referring to Eq. (3), and accepting that the de Boer values of the second virial coefficients have the correct order of magnitude, this would imply that the partial pressure of He^4 over the solution exceeds that of the pure component. As such a condition seems to have no physical reality, we have concluded that near 1.3°K there does exist a small systematic error in locating the

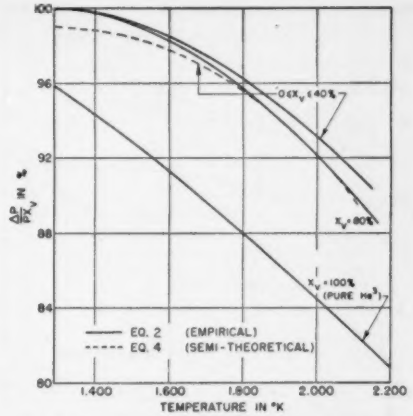

FIG. 5. Vapor pressure for various vapor concentrations.

position of the dew point. At higher temperatures, however, no sizeable error in the dew point location seems probable.

A striking feature of Fig. 5 is the large change in behavior in the range of concentrations from 80 to 100 percent compared to the change between zero and 80 percent. This effect is not inconsistent with the theoretical Eq. (3); it arises from the fact that in the region of vapor concentration above 80 percent the liquid is changing from a dilute to a concentrated solution.

V. PHASE DIAGRAM AND DISTRIBUTION FUNCTION

Our results show a reduction in the solubility of the helium isotopes similar to that which previous workers have reported for temperatures below 2.2°K.

The departure from ideality is well illustrated by the phase diagram, Fig. 6, whose solid curves show two representative liquid phase isothermals, that is, vapor pressure plotted against concentration for the temperatures of 2.100 and 1.300°K. These can be compared with the prediction of ideal solution theory, shown by the dot-dash lines. At low temperatures, the deviation from ideal solution theory is indeed large, but even at the lambda-point of pure He^4 it is appreciable.

The dashed lines give the corresponding isothermals of the vapor phase. For both the liquid and vapor curves, the region studied is indicated by the heavy lines and the arbitrary extensions to pure He^3, shown by the light lines, are included as a pictorial aid. The extent of the fractionation which occurs, especially at the lower temperatures, is extremely large.

The behavior of the liquid curve for dilute solutions is worth examining in more detail. If the solution obeys Henry's law, $P_3 = aX_L$, then the total vapor pressure should be linear in the concentration, for from the Gibbs-Duhem relations one can immediately deduce

[15] By P_4^* we mean the fugacity. Where accuracy required a calculation of the actual pressure, we used the equation given by Kilpatrick [J. E. Kilpatrick, Phys. Rev. **79**, 529 (1950)] to evaluate it from the fugacity.

[16] de Boer, van Kranendonk, and Compaan, Physica **16**, 545 (1950).

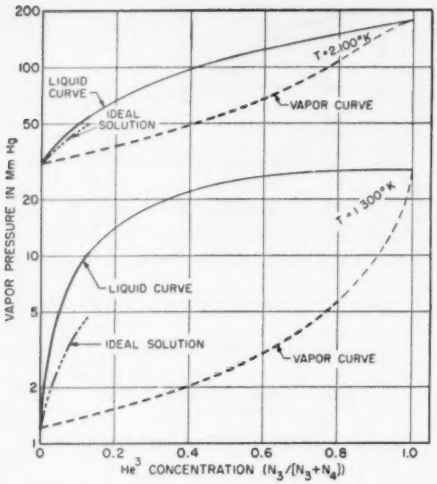

FIG. 6. Phase diagram.

that where Henry's law holds we have, neglecting the distinction between fugacity and pressure,

$$P=X_L(a-P_4^0)+P_4^0. \tag{5}$$

A linear plot of the low concentration part of the two liquid isotherms shown on the phase diagram is given by Fig. 7. The solid curves are the present measurements; the dashed lines give the behavior according to Henry's law, which is obeyed quite well for solutions of less than 4 percent He^3. The dot-dash lines give the behavior of a perfect classical solution.

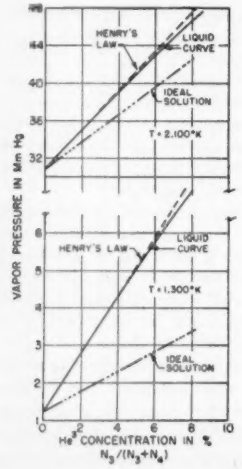

FIG. 7. Henry's law.

From the slope of the tangent to each curve at the origin comes the value of the corresponding Henry's law constant, a. According to ideal classical solution theory the constant (a) should equal P_3^0, and so one can take a/P_3^0 as a measure of the departure from an ideal solution. At 2.100°K, this ratio has the value of 1.3, while at 1.300°K the ratio is 2.8; for an ideal solution it is of course unity.

Another convenient way of examining the solubility is by evaluating the distribution function, or quotient of the mole ratios in vapor and liquid phases, defined as

$$\frac{C_v}{C_L}=\frac{(N_3/N_4)_V}{(N_3/N_4)_L}.$$

We have deduced this ratio from our unsmoothed data in the following way. Each of our measurements of vapor pressure for fixed liquid concentration gave directly the ratio $\Delta P/P$, at random temperature, Table IV, columns 1, 2, and 3. To a first approximation, this value of $\Delta P/P$ is the mole fraction of He^3 in the vapor; however, a more precise value of the vapor fraction was obtained by substituting $\Delta P/P$ in the empirical equation of the vapor phase, Eq. (2). From this mole fraction we deduced the mole ratio, C_v, and hence the values of C_v/C_L given in Table IV, column 4. The estimated rms error of each point, based on the manometry, the mass spectrograph measurements, and the uncertainty of position of the dew points, is given in the last column.

A sample distribution function is plotted in Fig. 8, our measurements for the 5.21 percent solution ($C_L=0.055$). The vertical lines give the estimated rms deviation expected from an individual point, and the arrow gives the approximate position of the lambda-point.[18] Again the extensive fractionation at low temperatures is clearly shown, as well as the observation that there is no apparent indication of the crossing of the lambda-line. In fact, in none of our measurements did we detect the occurrence of a lambda-transition. This is perhaps not surprising, since only the most precise measurements of the vapor pressure of He^4 give an indication of the transition, but it does raise a doubt about any theory of the solubility which assigns a primary role to the transition.

Figure 9 gives the change of distribution function with liquid concentration for the two temperatures of 1.300 and 2.100°K. Again the vertical lines represent the estimated rms deviation. Although the expected errors are large, there does seem to be a real increase in solubility with increasing concentration at the higher temperatures but very little change at the lower temperatures. The low values consistently found for the distribution function at the lowest concentration ($C_L=0.0058$) probably are due to systematic error; they may be an indication of the presence of heat flush

[18] J. G. Daunt and C. V. Heer, Phys. Rev. **79**, 46 (1950).

TABLE IV. He^3 distribution function for various temperatures and liquid concentrations.

X_L/C_L	T	$\Delta P/P$	C_V/C_L	rms error %
0.58%/0.58	2.172	0.0338	6.57	3.4
	2.066	0.0434	8.38	3.7
	1.957	0.0553	10.7	3.7
	1.847	0.0717	13.9	4.0
	1.749	0.090	17.6	4.2
	1.658	0.116	23.1	4.5
	1.612	0.120	23.9	4.7
	1.517	0.156	32.2	5.6
	1.405	0.196	42.2	7.6
	1.395	0.196	42.2	8.4
	1.295	0.197	42.2	12.7
	1.272	0.244	55.5	16.8
1.98%/0.0202	2.176	0.1085	6.66	2.8
	2.177	0.1072	6.57	2.8
	2.146	0.1170	7.22	2.8
	2.114	0.1260	7.82	2.8
	2.082	0.1338	8.34	2.9
	2.044	0.1453	9.13	2.9
	1.960	0.1724	11.1	2.9
	1.855	0.2121	14.1	3.3
	1.767	0.2529	17.6	3.4
	1.698	0.2910	21.2	3.4
	1.667	0.3086	23.0	3.7
	1.631	0.329	25.2	3.7
	1.609	0.346	27.1	3.7
	1.500	0.417	36.4	4.1
	1.384	0.506	51.8	4.8
	1.351	0.530	56.9	5.1
5.21%/0.0550	2.176	0.222	5.91	2.6
	2.112	0.252	6.83	2.7
	1.978	0.321	9.44	2.9
	1.788	0.431	14.9	3.2
	1.723	0.474	17.6	3.3
	1.621	0.545	23.3	3.5
	1.453	0.665	38.6	3.7
	1.441	0.673	40.1	3.7
	1.212	0.825	84.2	6.5
	1.194	0.836	103.0	6.9
9.49%/0.1049	2.183	0.345	5.82	2.6
	2.098	0.380	6.69	2.7
	2.004	0.430	8.16	2.7
	1.953	0.461	9.23	2.9
	1.902	0.493	10.5	3.0
	1.866	0.516	11.5	3.1
	1.799	0.558	13.5	3.2
	1.752	0.587	15.2	3.2
	1.704	0.618	17.4	3.3
	1.683	0.632	18.5	3.3
	1.632	0.664	21.3	3.5
	1.586	0.693	24.4	3.6
	1.554	0.712	26.8	3.6
	1.504	0.741	31.3	3.7
	1.402	0.800	44.7	4.2
	1.230	0.881	87.1	5.1
13.0 %/0.1494	2.175	0.419	5.72	2.6
	2.070	0.454	6.49	2.9
	1.961	0.515	8.23	2.9
	1.850	0.585	10.9	3.1
	1.748	0.648	14.4	3.2
	1.655	0.703	18.6	3.4
	1.476	0.801	32.8	3.7
	1.394	0.841	44.6	3.8
	1.328	0.870	58.3	4.0
	1.287	0.886	69.1	4.7
	1.255	0.899	81.6	4.9

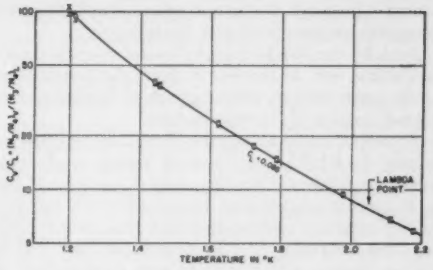

FIG. 8. Typical distribution function.

effects reported by other workers for very small concentrations.

Since our distribution function is not directly measured but is deduced from independent measurements on the two phases, its accuracy is considerably less than that of the vapor pressure data. Hence, we will draw no comparison between the distribution function and the theoretical predictions but will instead compare the predicted and observed values of vapor pressure for different liquid concentration.

VI. COMPARISON WITH SEVERAL THEORIES

From the time of the earliest measurements on the mutual solubility of the helium isotopes, when the spectacular deviations from Raoult's law became apparent, attempts have been made to explain the excessive fractionation as a nonclassical behavior. At such low temperatures and for such light masses, it seems probable that a complete theory of the solubility must include quantum and statistical effects, and perhaps because of this the predictions of classical solubility theory have not been investigated.

It should be pointed out, however, that even a so-called classical theory, such as Raoult's law, is not really classical since it takes for granted the measured vapor pressures of the pure components, which are

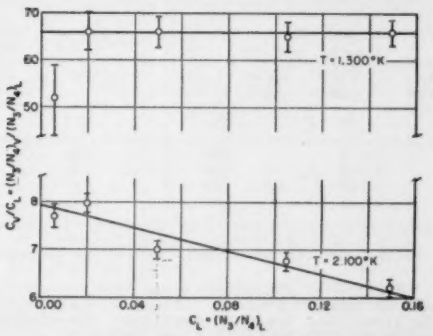

FIG. 9. Change of distribution function with liquid concentration.

probably the result of whatever quantum and statistical properties are associated with the isotopes.

Actually one should regard classical solution theory as classical only in the way it treats the perturbation to the vapor pressure resulting from an introduction of a small amount of the other isotope.

A perfect classical solution has ideal entropy of mixing $(-R\ln X)$, zero heat of mixing, and equal molecular volumes. Since the molecular volume of He^3 is 40 percent greater than that of He^4, it is not surprising to find a positive deviation from Raoult's law (i.e., the measured vapor pressure is too high).[19] Here we are dealing with a solution with positive heat of mixing, since the replacement of an He^4 atom by an He^3 atom changes the average atomic separation, raising the potential energy of the solvent; this process, at constant temperature, will be accompanied by an absorption of heat.

Classical nonideal solution theories require a knowledge of the forces between the molecules. In the theory we will evaluate, this information is deduced from the law of corresponding states, to which the objection can be raised that the helium isotopes do not obey the classical law. The objection is similar to the one against application of any classical solution theory. It is certainly true that the classical law of corresponding states fails to correctly predict the critical constants of He^3 in terms of those for He^4 and must be replaced with the quantum mechanical equation.[20] However, in this calculation we accept the measured values of the critical constants and will use the van der Waals equation to deduce from them the effective potential energy of the He^4 atoms. In justification of such an approach, one might point out that for the helium isotopes the quantity RT_c/P_cV_c comes closer to its theoretical classical value than for any other common gas. The nearest rival is hydrogen, whose isotopes also deviate appreciably from the classical law of corresponding states.

TABLE V. Van der Waals constants and interaction energies derived from critical data.

	P_c atmos	V_c cm³/mole	T_c °K	a Atmos$\left(\frac{\text{cm}^3}{\text{mole}}\right)^2$	b $\frac{\text{cm}^3}{\text{mole}}$
He^3	1.17	71.4[a]	3.35	2.21×10^4	23.8
He^4	2.26	57.7[b]	5.20	2.77	19.2

X_L %	W_3/R °K	W_4/R °K
0	1.69	1.38
5	1.66	1.40
10	1.61	1.42
15	1.58	1.45

[a] Grilly, Hammel, and Sydoriak, Phys. Rev. **75**, 1103 (1949).
[b] W. H. Keesom, *Liquid Helium* (Elsevier, New York, 1942), pp. 192, 209.

[19] The deviation from ideality arising solely from unequal molecular sizes, with zero heat of mixing, is too small to explain the present data. See E. A. Guggenheim, *Thermodynamics* (Interscience Publishers, Inc., New York, 1949), p. 212.
[20] J. de Boer and R. J. Lunbeck, Physica **14**, 510 (1948).

1. Classical Solution Theory[21]

Since the difference in the volumes of the isotopes makes perfect solution theory inapplicable to helium, we have examined the next most complicated classical theory, that of the regular solution, defined as a solution of components whose molecular volumes are somewhat unequal, which has a positive heat of mixing, but ideal mixing entropy. We shall apply the theory of van Laar, who deduced the interaction energy from the critical constants of the pure components for a liquid obeying the van der Waals equation.

In the van der Waals equation,

$$P=RT/(V-b)-a/V^2, \tag{6}$$

the constants a and b are related to the critical constants by the equations

$$b=V_c/3, \quad a=9RT_cV_c/8.$$

With this notation, van Laar's equation for the partial fugacity becomes

$$RT\ln\frac{P_1^*}{P_1^{*0}X_1}=\frac{N_2^2b_2^2b_1}{(N_1b_1+N_2b_2)^2}\left(\frac{a_1^{\frac{1}{2}}}{b_1}-\frac{a_2^{\frac{1}{2}}}{b_2}\right)^2. \tag{7}$$

The subscripts refer to the two components of the solution, X is the mole fraction, N is the number of moles, and the a's and b's are the van der Waals coefficients of the pure components. This is a particular case of the fugacity of any regular solution,

$$P_1^*=P_1^{*0}(X_1)\exp[(1-X_1)^2W_1/RT], \tag{8}$$

in which the interaction energy W_1 is given as an explicit function of the van der Waals constants and the concentration.

In the upper half of Table V we have listed the critical constants and the van der Waals constants deduced from them, while the lower half of the table is our evaluation of W_3/R and W_4/R of Eq. 8, using van Laar's formula, Eq. (7).

From these interaction energies we finally deduce the total vapor pressure, Table VI, column 4, for a 5 percent solution. This concentration was used as a compromise between the desire for large concentration so the pressure measurements are reasonably accurate, and small concentration to make dilute solution theory applicable. Reference to Fig. 7 shows that at 5 percent Henry's law is still obeyed rather well, indicating the solution is reasonably dilute.

If one rewrites Eq. (7) in Hildebrand's notation, it becomes

$$RT\ln(P_1^*/P_1^{*0}X_1)=\varphi_2^2V_1(\delta_1-\delta_2)^2. \tag{9}$$

φ_2 is the volume fraction of component 2 and δ_1 the solubility parameter of component 1. In van Laar's equation, one calculates "effective values" of these

[21] J. H. Hildebrand and R. L. Scott, *Solubility of Non-Electrolytes* (Reinhold Publishing Company, New York, 1950), Chaps. 2, 3, 7, and 8.

TABLE VI. Comparison of vapor pressure from various theories with experimental values for $X_L=0.05$.

		Calculated pressures							
	P	PCS		RCS		H and D		dB and G	
T	observed	P_c	$\frac{P_c-P}{P}$	P_c	$\frac{P_c-P}{P}$	P_c	$\frac{P_c-P}{P}$	P_c	$\frac{P_c-P}{P}$
°K	mm Hg	mm Hg	%	mm Hg	%	mm Hg	%	mm Hg	%
2.2	49.77	47.27	− 5.0	56.76	14.0	54.87	10.2	47.27	−5.0
2.0	33.19	29.16	−12.0	36.92	11.2	35.73	7.7	30.17	−9.1
1.6	12.65	8.39	−34.0	13.15	4.0	12.36	−2.3	12.91	2.0
1.2	3.59	1.56	−57.0	3.94	9.8	3.15	−12.3	5.29	47.0

PCS = Perfect Classical Solution; RCS = Regular Classical Solution (van Laar); H and D = Theory of Heer and Daunt; dB and G = Theory of de Boer and Gorter.

terms, that is, for the molal volumes used in deducing φ_2, as well as for V_1, the van der Waals volume b is used, while the solubility parameter is taken as $a^{\frac{1}{2}}/b$. As shown by Scatchard and by Hildebrand and Wood, an equation giving better agreement with the behavior of many regular solutions and one with a sounder theoretical foundation than Eq. (7) is given by Eq. (9) with the usual definition of the terms. That is, for volume one uses the measured molal volume (V_1^0), and for the solubility parameter the latent heat of evaporation per unit volume ($\Delta E^v/V_1^0$) of each pure component.

Instead of improving the agreement with our experimental values, this modification gives a still higher vapor pressure, for it increases the size of each interaction energy, W_1, of Eq. (8). The value of W_3 after van Laar was already too high, while Scatchard's value is 1.4 times as big. W_4 increases by a factor 2.3, but since our dilute solution study gives no check on W_4, the importance of this change cannot be estimated. Measurements on concentrated solutions are needed to gauge the proper value of W_4.

Similarly the theory of van Laar and H. Lorenz, which replaces b_1 and b_2 in Eq. (7) by V_1^0 and V_2^0, gives much too large an interaction energy.

In Table VI, the first column gives the temperatures, the second our observed vapor pressures for a 5 percent liquid, the third column the vapor pressure according to Raoult's law (PCS), the fourth column the pressure according to van Laar's theory of regular solutions (RCS), as just described, the fifth column (H and D) the pressure according to the theory of Heer and Daunt,[22] and the last column (dB and G) according to the theory of de Boer and Gorter.[23] The pressures tabulated are corrected for the difference between fugacity and pressure. To the right of each vapor pressure is the percentage deviation of the pressures from the experimental value.

2. Nonclassical Theories

It is clear that the deviation from Raoult's law is not due solely to the lambda-transition. At the lambda-point for pure He^4 the Raoult's law pressure is already 5 percent too small. The fact that the ideal pressure is 50 percent low at 1.2°K is then not surprising, for it is a quite general property of solutions showing a positive deviation that the departure from ideality increases as the temperature drops.

The theory of de Boer and Gorter[23] assumes the solution is ideal above the He^4 transition temperature, but that below this He^3 is soluble in only the normal component of He^4. This assumption leads to a sharp increase in vapor pressure at lower temperatures so that at 1.2°K the latter theory is as far above the measured pressure as is Raoult's law below it.

The theory of Heer and Daunt[22] is based on a smoothed potential interaction in the liquid. One important term in the vapor pressure on such a model is the chemical potential of the solvent, pure He^4. Their suggestion is that for this one takes the chemical potential of an ideal Bose fluid. As with the theory of de Boer and Gorter, the solubility at low temperature is intimately connected with the lambda-transition. The theory of H and D has the smallest mean square deviation from the experimental pressures of any of these four theories. However, if it were normalized to give the correct pressure at 2.2°K, it would then far over-emphasize any effect of the lambda-transition. This can be clearly seen in Fig. 10 in which is plotted the percent deviation of the pressure, according to each theory, from the observed vapor pressure. The deviation of the curve "H and D" changes from positive to negative around 1.65°K. In contrast to this, van Laar's theory (RCS), while its deviation at 2.2°K is larger than for H and D, does show approximately the proper trend of pressure with decreasing temperature. The theory of de Boer and Gorter, as already mentioned, gives too much importance to the effect of the lambda-transition and departs greatly from the measured pressures at lower temperatures.

None of the theories here considered achieves any great success in describing the experimental data. However, as yet there seems to be no reason to reject classical solution theory nor to attribute to the lambda-transition an important influence on the mutual solubility of the helium isotopes. It again seems to be the case that important conclusions about the role of the

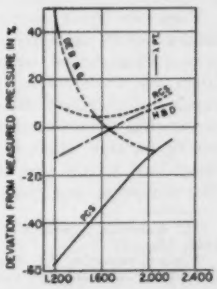

FIG. 10. Comparison of vapor pressures from various theories for $X_L=5$ percent. PCS = Perfect Classical Solution; RCS = Regular Classical Solution, theory of van Laar; H and D = Heer and Daunt; DE B and G = de Boer and Gorter.

[22] C. V. Heer and J. G. Daunt, Phys. Rev. **81**, 447 (1951).
[23] J. de Boer and C. J. Gorter, Physica **16**, 225 (1950).

statistics of the helium isotopes can only be reached after an extensive quantitative study of the solubility and complete and rigorous theoretical interpretations.

VII. LATENT HEAT OF EVAPORATION

The Clausius-Clapeyron equation defines a latent heat of evaporation from the temperature derivative of the vapor pressure curves. There are, however, a large number of such latent heats that can be defined for a solution with two volatile components.[24] Since it is not obvious which ones we will get from our vapor pressure measurements, we will derive the Clausius-Clapeyron equation for these.

Let $F=H-TS=$ Gibbs free energy. We will consider a process occurring at constant liquid phase concentration, $X_L=$constant. Then for equilibrium between liquid and vapor phases, the change in the partial molal free energy of a component in the liquid phase must be equal to its change in the vapor, giving

$$\begin{aligned} d\bar{F}_3{}^L &= \bar{V}_{3L}dP-\bar{S}_{3L}dT=d\bar{F}_3{}^v \\ &= \bar{V}_{3V}dP-\bar{S}_{3V}dT+(\partial\bar{F}_3{}^v/\partial X_3)dX_3, \\ \bar{V}_{4L}dP-\bar{S}_{4L}dT &= \bar{V}_{4v}dP-\bar{S}_{4v}dT+(\partial\bar{F}_4{}^v/\partial X_4)dX_4 \\ &= \bar{V}_{4v}dP-\bar{S}_{4v}dT+(\partial\bar{F}_4{}^v/\partial X_3)dX_3. \end{aligned} \tag{10}$$

Multiply the first equation by $N_3{}^v$, the second by $N_4{}^v$, and combine, letting $\Delta\bar{V}_3=\bar{V}_{3v}-\bar{V}_{3L}$, etc. Then

$$\begin{aligned} (N_3{}^v\Delta\bar{V}_3+N_4{}^v\Delta\bar{V}_4)dP &= (N_3{}^v\Delta\bar{S}_3+N_4{}^v\Delta\bar{S}_4)dT \\ &\quad -(N_3{}^v\partial\bar{F}_3{}^v/\partial X_3+N_4{}^v\partial\bar{F}_4{}^v/\partial X_3)dX_3. \end{aligned}$$

Since the last term is identically zero,[25] we get

$$\left(\frac{dP}{dT}\right)_{X_L}=\frac{N_3{}^v\Delta\bar{S}_3+N_4{}^v\Delta\bar{S}_4}{N_3{}^v\Delta\bar{V}_3+N_4{}^v\Delta\bar{V}_4}=\frac{\lambda_{V,L}}{T\Delta V}, \tag{11}$$

where $(\lambda_{V,L})$ is the symbol used by Ruheman[24] to denote the heat absorbed when a mole of vapor is formed from a very large amount of liquid; the concentration of the vapor so formed is, of course, that of the vapor phase.

By analogy we see also that

$$(dP/dT)_{X_V}=-\lambda_{L,V}/T\Delta V, \tag{12}$$

where $(-\lambda_{L,V})$ equals the heat absorbed when a mole of liquid is formed from a large amount of vapor.

These two latent heats will be the same if they are deduced for the same composition of material changing phase. Thus at one temperature the values of the latent heat we derive from the vapor pressures at fixed vapor concentrations will correspond to small values of X, while those from the fixed liquid concentration will be for high values of X. We give our values of latent heat for the temperature of 1.5°K in Fig. 11. The horizontal axis gives the concentration of the material changing phase; the latent heats for pure He^4 and pure He^3 come from the vapor pressure tables.[9,8] The triangles give the latent heats from $(dP/dT)_{X_L}$, the circles $(dP/dT)_{X_V}$, while the number with each point is the concentration of that phase held fixed during the pressure measurements. The change of volume used in Eqs. (11) and (12) is corrected for both the liquid volume, taken as the weighted sum of the volumes of the pure liquids, and the weighted sum of the second virial coefficients according to de Boer *et al.*[17]

No attempt has been made to evaluate the accuracy of the latent heats, but it is probably poor enough to remove any significance from the wavers in the curve. Certainly the data show the latent heat is not a linear sum of the latent heats of the two pure components (solid line of Fig. 11), indicating there is a heat of mixing.

From a consideration of the change of enthalpy on evaporation, one can readily deduce the following relation:

$$\begin{aligned} XL_3+(1-X)L_4-\lambda_{V,L} &= X[\bar{H}_3(X_L)-H_3{}^0] \\ &\quad +[1-X][\bar{H}_4(X_L)-H_4{}^0]. \end{aligned} \tag{13}$$

Here X is the composition of the material changing phase and X_L the composition of the liquid. L is the latent heat of evaporation of the pure component, $\bar{H}(X_L)$, the partial molal enthalpy of a component of the liquid solution, and H^0 the molal enthalpy of a pure component. The left-hand side of this equation is the difference between the solid and dotted lines in Fig. 11. The two terms on the right-hand side represent respectively the heats of mixing when X moles of liquid He^3 and $(1-X)$ moles of liquid He^4 are added to a large amount of liquid of composition X_L, the value of X_L being the composition of the liquid in equilibrium with vapor of concentration X. In Eq. (13) we have neglected the gas law imperfection; for the worst case this introduces an error of only 0.1 cal/mole.

To apply Eq. (13) we make the approximation of neglecting the heat of mixing due to addition of the He^4 with the justification that since the solution is always dilute, $\bar{H}_4-H_4{}^0$ is very small. The difference in slope between the solid and dotted lines of Fig. 11 then becomes the partial molal heat of mixing of liquid He^3 into a dilute solution; its value is about 3 cal/mole. Another method of deducing the heat of mixing will be presented in the next section.

It is not safe to extrapolate the dotted line to higher concentrations. The region covered by Fig. 11, although it determines $\lambda_{V,L}$ for X ranging up to 80 percent, is still the region of dilute liquid phase with X_L ranging up to only 13 percent. For the region of values of X between 80 percent and 100 percent, that is, for concentrated solutions, the dotted line through the experimental points will pass through a minimum and finally curve upward again to the value of 10.6 cal/mole for pure He^3.

[24] M. Ruheman, *Separation of Gases* (Clarendon Press, Oxford, 1949), Chap. IV.

[25] Duhem's equation, P. S. Epstein, *Textbook of Thermodynamics* (John Wiley and Sons, New York, 1937), p. 103.

VIII. SPECULATIONS ON OTHER PROPERTIES OF THE SOLUTION

The fact that the van Laar theory gives a moderately good description of the vapor pressures of the mixed isotopes permits one to make certain speculations about other properties of the solutions. For instance, the interaction energies, W_3 and W_4 of Eq. (8), determine the partial molal heats of mixing of the two component liquids from the relation $\Delta\bar{H}_1^m=(1-X_1)^2W_1$. This gives quite a large heat of mixing. At infinite dilution, $\Delta\bar{H}_3^m=1.6R=3.2$ cal/mol, which is comparable with the latent heat of evaporation at absolute zero, $(\Delta H_3^0)_{vap}=4.47$ cal/mol.[8]

If one mixed adiabatically a 10 percent solution of He^3 in He^4, starting with pure components originally at 1.0°K, the heat of mixing of approximately 0.1 $\times 1.6R$ would be sufficient to produce a considerable cooling for the mixture, whose total heat content is probably no larger than this. This might prove to be an excellent way of cooling samples of helium.[26] Since the specific heat is due mainly to the He^3, the final temperature will be nearly independent of the amount of He^3 added.

Intimately connected with the heat of mixing is the stability against separation of the liquid into two phases. Classical solution theory predicts such a separation at the temperature where $RT=W/2$, which for the helium isotopes would come between 0.7 and 0.8°K, depending on whether one used W_3 or W_4 in the criterion.[27] This is considerably lower than the temperature of 1.2°K at which Weinstock and coworkers[28] showed no separation occurred. Such a phase separation would probably prevent the achievement of very low temperatures from mixing, but there might still be a very interesting region below the normally achieved temperatures accessible to study by this cooling process.

As already mentioned in Sec. VI, the liquid solution of the helium isotopes is unusual because it obeys the van Laar vapor pressure equation more closely than it does the more successful theory of Scatchard. Both theoretical equations have the form of Eq. (9), the quantities substituted giving the different behavior of the two theories. Actually, the first and third factors on the right side of Eq. (9) have approximately the same value on either theory, and the principal difference comes from the volume used. From this point of view, one might say that the van der Waals volume, used by van Laar, is a better estimate of the space occupied by the He^3 in the dilute solution than is the molal volume of pure He^3. This is a tempting speculation; pursued further, it suggests that the forces which give the large volume for pure He^3 are not so important when the He^3 is less condensed. The van der Waals volume, which is determined from the behavior at high vapor densities, gives a volume more nearly akin to that associated with the He^3 atoms in dilute solution than does the volume of the pure liquid. Whether a similar behavior should be suggested for He^4 is uncertain; experiments on concentrated solutions might give valuable information about this.

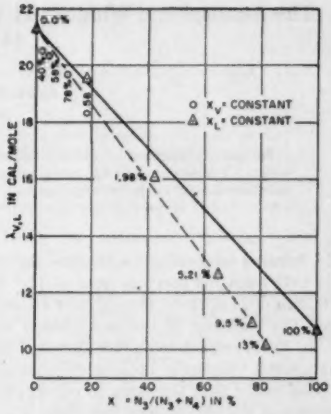

FIG. 11. Latent heat of vaporization for various He^3 concentrations from Clausius-Clapeyron equation; $T=1.500$°K.

ACKNOWLEDGMENT

It is a pleasure to be able to acknowledge the extensive contribution Dr. L. Goldstein has made to this work through continued discussion and criticism. Dr. J. E. Kilpatrick also gave considerable help in regard to the thermodynamics of mixtures. Dr. C. J. Hoffman assisted in taking part of the data and some of the analysis. A large part of the numerical computation was done by the computer group under the direction of Mr. M. Goldstein.

Finally we wish to thank Mr. Ball and his liquefier crew for the supply of liquid air and liquid helium.

[26] H. London, Proc. Int. Conf. Low Temp. Phys. (Oxford) 157 (1951), suggested reversible mixing as a means of producing low temperatures. We are not sure if this is the same process here considered, since the present suggestion gives the cooling for an irreversible mixing.

[27] The relation $RT=W/2$ for the critical temperature of mixing assumes $W_3=W_4$, a relation approximately satisfied here.

[28] Weinstock, Osborne, and Abraham, Phys. Rev. 77, 400 (1950).

The Atmospheric Window, 16 to 24 Microns, and the Second Fundamental of Nitrous Oxide*

ARTHUR ADEL
Arizona State College, Flagstaff, Arizona
(Received May 26, 1952)

Further investigation of the atmospheric window, 16–24 microns, has disclosed the presence of the second fundamental of nitrous oxide, centered at 17 microns. All three fundamentals of nitrous oxide have now been located in the telluric spectrum.

THE infrared solar-telluric spectrum was extended in 1941 from the previous limit of 13.9 microns[1] to a new limit of 24 microns, through a new atmospheric window.[2] The existence of the new window was confirmed in ONR experiments conducted from high altitude aircraft.[3] Virtually nothing of importance has been added in the past ten years to our knowledge of this segment of the atmospheric spectrum.

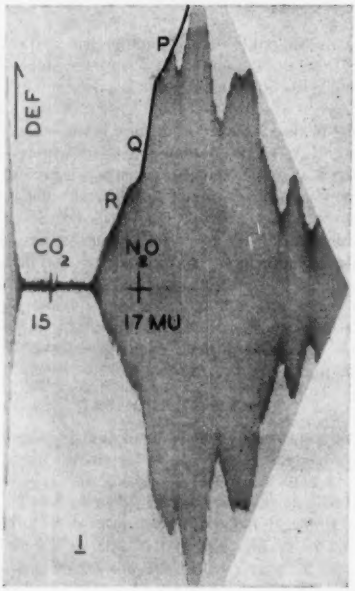

FIG. 1. Infrared solar-telluric spectrum, showing the *P*, *Q*, and *R* branches of the atmospheric 17-micron nitrons oxide band.

The window is defined by complete absorption by carbon dioxide on the short wavelength side and by complete absorption by water vapor on the long wavelength side. The amount of solar radiation arriving at the earth's surface in this spectrum interval increases sharply with diminishing precipitable water vapor content of the atmosphere. The transparency of the window has been tentatively estimated as exceeding ten percent in the 16–22 microns interval on the driest days.[4] It is thus not negligible from a meteorological point of view.

The spectral region in question is featured by great daily and seasonal change, which is related to the incessant fluctuation of water vapor content. However, a recent re-examination of this spectrum has revealed a weak absorption band whose intensity remains sensibly constant in time. Comparison with laboratory observations indicates strongly that this band is the long sought second fundamental of nitrous oxide with center at 17 microns.[5]

The *P*, *Q*, and *R* branches of the atmospheric 17-micron nitrous oxide band are indicated in the solar-telluric spectrum of Fig. 1, which was obtained through one mm of precipitable water. In moist as well as dry atmosphere observations the *R*-branch of the band appears to be completely isolated from the incursions of water vapor. Even on dry days, however, the *Q*-branch is moderately involved with water vapor absorption, and the *P*-branch is more seriously obscured.

All three fundamentals of nitrous oxide have now been located in the telluric spectrum:[6,7] ν_1 at 7.8 microns, ν_2 at 17.0 microns, and ν_3 at 4.5 microns.[8]

* This work was supported in part by a contract with the United States Air Force, through sponsorship of the Geophysical Research Division, Air Force Cambridge Research Center, Air Research and Development Command.

[1] Arthur Adel, Astrophys. J. **91**, 481 (1940).
[2] Arthur Adel, Astrophys. J. **96**, 239 (1942).
[3] Unpublished Johns Hopkins (ONR) progress report on High Altitude Infrared Transmission of the Atmosphere (January 10, 1949).
[4] Arthur Adel, J. Opt. Soc. Am. **37**, 769 (1947).
[5] E. K. Plyler and E. F. Barker, Phys. Rev. **38**, 1827 (1931).
[6] Arthur Adel, Astrophys. J. **90**, 627 (1939); Arthur Adel, Astrophys. J. **93**, 509 (1941).
[7] Shaw, Sutherland, and Wormell, Phys. Rev. **74**, 978 (1948).
[8] While this article was in the process of being cleared for publication, there have appeared two notes bearing directly upon the problem in question: (a) R. Anthony, Phys. Rev. **85**, 674 (1952), has independently confirmed the existence of the new window; (b) M. Migeotte and L. Nevin, Astrophys. J. **115**, 326 (1952) also have confirmed the existence of the new window, and, in addition, have also made an identification of ν_2 of N_2O at 17 microns.

The Alpha-Particles of Radium

FRANK ASARO AND I. PERLMAN
Radiation Laboratory and Department of Chemistry, University of California, Berkeley, California
(Received June 3, 1952)

The abundance of α_{188} of Ra^{226} was determined with an alpha-particle spectrograph to be 5.7 ± 0.3 percent. The nomenclature α_{188} refers to the alpha-group populating the excited level of the residual nucleus which is 188 kev above the ground state.

A limit of 0.1 percent was determined as the maximum abundance of any alpha-group in the region 300 to 800 kev below α_0 of Ra^{226}. A. Ghiorso, utilizing an alpha-pulse analyzer, lowered this limit to 0.02 percent in the region 400 to 1200 kev below α_0.

IN the course of the measurement of the alpha-particle spectra of a considerable number of artificial alpha-emitters using a magnetic spectrograph, some secondary standards for energy calibration have been adopted in relation to the primary standard RaA whose alpha-particle energy was determined accurately as 5.9981 $\pm$0.0008 by Briggs.[1] Among these standards is Ra^{226} which has been used primarily to determine the dispersion of the instrument by measuring the displacement between the two well-known peaks separated by 185 kev. The abundances of the alpha-groups are used in testing agreement between measured data and alpha-decay theory, and since there have been some minor differences between published values of the abundances, a new determination has been made.

That Ra^{226} has complex structure could be inferred from the early measurement of an 188-kev gamma-ray of Hahn and Meitner.[2] This gamma-ray was shown to be partially converted[3] and the gamma-ray energy determined as 186 kev by spectrographic measurement of the conversion electrons.[4]

The alpha-particle group for the transition to this excited state was observed with an alpha-ray spectrograph by Rosenblum and co-workers,[5] who reported its abundance as $\sim$6.5 percent. The abundance was confirmed as 6.5 percent in another measurement by Bastin-Scoffier.[6] Using an ionization chamber coupled to a pulse-height analyzer, members of this laboratory[7] reported a lower value (4.8 percent) for the abundance of the low energy group. In addition to this well-defined group, Rosenblum and co-workers[5,6] found some evidence for a weak group of 600 kev lower energy than the main group. In referring to alpha-groups of a particular nuclide we shall designate by α_0 that group

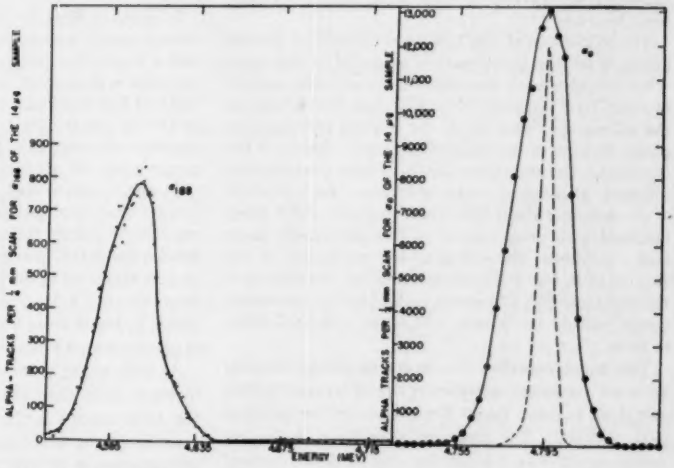

FIG. 1. · Alpha-tracks per ½-mm scan for α_{188} of the 14-microgram sample. • Alpha-tracks per ½-mm scan for α_0 of the 14-microgram sample. The ordinate scale is that shown on the center of the figure. – – – Curve showing the shape of the α_0 peak obtained with the 0.3-microgram sample. The ordinate scale is 1/20 that shown in the center of the figure. The abscissa scale is the same for all three alpha-groups.

[1] G. H. Briggs, Proc. Roy. Soc. (London) **A157**, 183 (1936).
[2] O. Hahn and L. Meitner, Z. Physik **26**, 161 (1924).
[3] E. Stahel and W. Johner (1931), quoted by P. Falk-Varaint and J. Teillac, J. phys. et radium **12**, 659 (1951).
[4] Cork, Branyan, Stoddard, Keller, LeBlanc, and Childs, Phys. Rev. **83**, 681 (1951).
[5] Rosenblum, Guillot, and Bastin-Scoffier, Compt. rend. **229**, 191 (1949); S. Rosenblum, Compt. rend. **195**, 317 (1932).
[6] G. Bastin-Scoffier, Compt. rend. **233**, 945 (1951).
[7] Karraker, Ghiorso, and Templeton, Phys. Rev. **83**, 390 (1951).

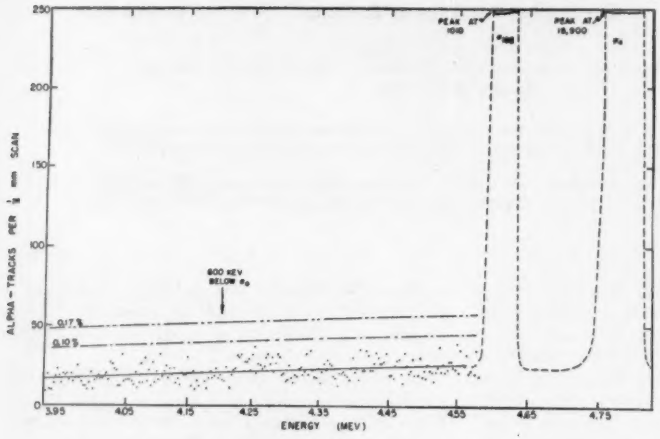

FIG. 2. · Alpha-tracks per $\frac{1}{4}$-mm scan. – – – Curve indicating the position and the abundances calculated for α_0 and α_{188} from a short exposure. —— Average background below α_{188}. – – – – A straight line parallel to the average background and 0.17 percent of the α_0 peak height above the average background. – – – A straight line parallel to the average background and 0.10 percent of the α_0 peak height above the average background.

believed to be the ground state transition, and for other groups the energy levels in kev above the ground-state to which the groups lead will be entered as subscripts.[8] The three groups mentioned would be accordingly, α_0, α_{188}, α_{600}.

The source employed in the present measurement consisted of 14 micrograms of Ra^{226} as radium chloride sublimed in vacuum onto a $\frac{1}{8}\times 1$ inch band on a platinum plate by a technique described elsewhere.[6] The magnetic alpha-particle spectrograph and its operation have also been described.[8,9]

The solid curve of Fig. 1 shows the results of 21-hour exposure for the alpha-particle spectrum in the range ~4.5–4.8 Mev with the ordinate showing the number of alpha-tracks in each $\frac{1}{4}$-mm wide (one field of view of the microscope) scan across the receiver photographic plate. Because of the disparity in track counts for the two peaks, the ordinate scales have been made tenfold different. Because of source thickness, the half-width of the peaks are about 28 kev, as compared with 5–8 kev obtained with other sources in this instrument under best conditions. Nevertheless, the resolution of the two peaks in Fig. 1 is complete, and the abundances of the alpha-groups [5.5 percent ($\pm$0.2) for the low energy group] should be reliable within the indicated limits of error.

The abundances (Fig. 1) were determined by counting all of the tracks in the low energy peak (almost 26,000) and those in every fourth $\frac{1}{4}$-mm scan for the principal peak (109,000). The measured abundance of the low energy group was 5.6 percent, but this was revised downward to 5.5 percent because of the different geometry factor applicable to the two groups. This difference is a consequence of the longer path followed by the high energy particles because the photographic plate is not normal to the trajectory of the alpha-particles but 60° to the normal. Abundance measurements were also made on three other samples for all of which fewer tracks were registered. The values obtained were 6.0, 5.8, and 5.5 percent for the abundance of the low energy group. The value that we shall adopt is 5.7$\pm$0.3 percent, which is the average of the four measurements and the limit of error encompasses all of them.

In order to illustrate the resolution attainable with thinner sources an analysis of the main peak was made with a source consisting of only 0.3 microgram Ra^{226}. The peak is shown with a broken line in Fig. 1, and the width at half-maximum is only 6 kev as compared with 26 kev for the thicker source. In this particular measurement the magnetic field was such that the low energy group did not register on the photographic plate.

As mentioned, a weak group of about 600 kev lower energy than the ground state transition has been reported,[5,6] and its abundance was given in the second publication as 0.17 percent. This group would be placed at 4.20 Mev, and in the present experiments the region from 4.0 to 4.5 Mev was examined. The results are shown in Fig. 2, from which it is deduced that no peak of greater than 0.1 percent abundance could be present.

As seen in Fig. 2 the inability to distinguish groups in lower abundance than 0.1 percent so distant from the main groups is due to an extensive and nearly constant tailing on the low energy side of the peaks. This phenomenon is as yet unexplained. Incidentally, the integrated number of alpha-tracks over this wide range is considerable, but by the same token they must come proportionally from both alpha-groups so that the ratio of abundances of the two groups would not be affected. Since the limitation of discrimination of an alpha-group

[8] Asaro, Reynolds, and Perlman, Phys. Rev. **87**, 277 (1952).
[9] F. L. Reynolds, Rev. Sci. Instr. **22**, 749 (1951).

in this region is not a great deal lower than the reported[5,6] intensity of the peak α_{600}, a definite disagreement cannot be suggested. However, A. Ghiorso in this laboratory has made a careful examination of Ra^{226} with an alpha-particle pulse analyzer over the energy range 3.6–4.4 Mev and set a limit of 0.02 percent for the abundance of any group in this interval.

We wish to acknowledge the assistance of Miss Beverly Turner in counting the alpha-tracks. This work was performed under the auspices of the AEC.

PHYSICAL REVIEW VOLUME 88, NUMBER 1 OCTOBER 1, 1952

Evaluation of Range Straggling for Heavy Particles*†

DAVID O. CALDWELL‡
Department of Physics, University of California, Los Angeles, California
(Received May 12, 1952)

From the formula developed by Lewis for the differential range distribution of heavy, charged, nonrelativistic particles, an integral range distribution is obtained. The latter is evaluated for 2- to 500-Mev protons in Al to show, in a practical way, how the distribution differs from a Gaussian, as evidenced by its shorter-than-average range tail. The extent to which this tail increases the mean range and makes it different from the most probable range is indicated. Values for the range straggling are also given.

THE deviation of the range distribution of fast, but nonrelativistic, heavy charged particles from a Gaussian form is the subject of a recent paper by Lewis.[1] Because a large fraction of a particle's energy can be lost in a single collision, this distribution has a longer tail on the side of shorter-than-average range. While the existence of the long tail is known from previous calculations[2–6] of the corresponding distribution in energy loss, this earlier work has been done assuming the total energy loss to be small compared with the initial energy.

Lewis, making the opposite approximation, finds the differential range distribution in the form

$$f(y)=(2\pi)^{-\frac{1}{2}}h(y)\exp(-y^2/2),$$

where $y=(x-\langle x\rangle)/\beta_2^{\frac{1}{2}}$ (i.e., the difference between the

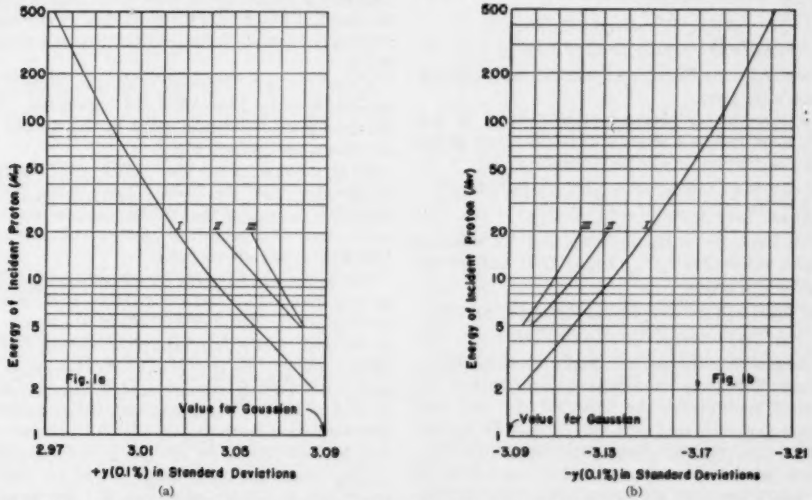

FIG. 1. Variation with incident particle energy of the positions of the 0.1 percent tails of the integral range distribution. Figure 1(a) is for $+y$ (longer than average range) and Fig. 1(b) for $-y$ (shorter than average range). Curves I are for protons in Al; II, protons in Cu; and III, deuterons in Al.

* This work was supported in part by the joint program of the ONR and AEC.
† A more complete account of this work is given in unpublished University of California at Los Angeles Technical Report No. 9 (1952).
‡ AEC Predoctoral Fellow.
[1] H. W. Lewis, Phys. Rev. **85**, 20 (1952).
[2] N. Bohr, Phil. Mag. **30**, 581 (1915); Kgl. Danske Videnskab. Selskab, Mat.-fys. Medd. **18**, 8 (1948).
[3] E. J. Williams, Proc. Roy. Soc. (London) **A125**, 420 (1929).
[4] L. Landau, J. Phys. (U.S.S.R.) **8**, 201 (1944).
[5] O. Blunck and S. Leisegang, Z. Physik **128**, 500 (1950).
[6] W. Schultz, Z. Physik **129**, 530 (1951).

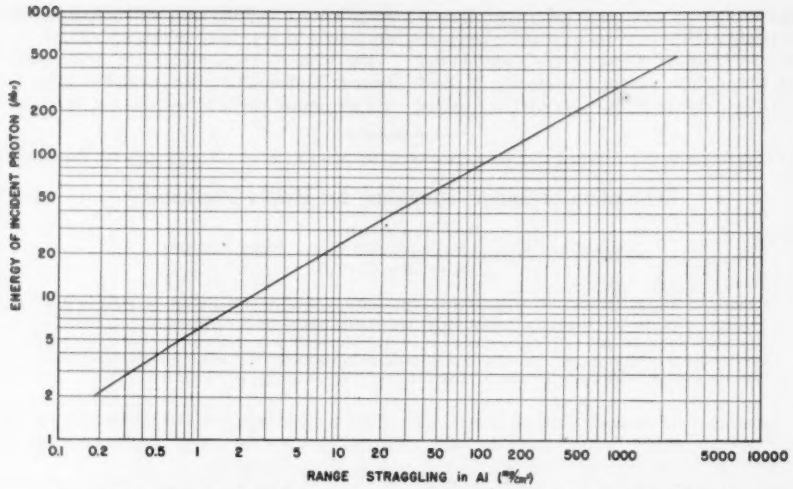

FIG. 2. The variation with initial energy of the range straggling for protons stopping in aluminum.

range, x, and the mean range, $\langle x\rangle$, in units of the standard deviation, $\beta_2^{\frac{1}{2}}$). The correction factor multiplying the normal distribution is

$$h(y)=[1]+[\gamma_3 H_3(y)]+[\gamma_4 H_4(y)+\tfrac{1}{2}\gamma_3^2 H_6(y)]+[\gamma_5 H_5(y)+\gamma_3\gamma_4 H_7(y)+\tfrac{1}{6}\gamma_3^3 H_9(y)]+\cdots, \quad (1)$$

where the $H_n(y)$ are Hermite polynomials, and formulas for the γ's are given.

If $\varphi^{(n)}(y)=(d^n/dy^n)\varphi(y)=(-1)^n H_n(y)\varphi(y)$ is put in $f(y)$, there results a series in the derivatives of the normal distribution, $\varphi(y)=(2\pi)^{-\frac{1}{2}}\exp(-y^2/2)$:

$$f(y)=[\varphi(y)]-[\gamma_3\varphi^{(3)}(y)]+[\gamma_4\varphi^{(4)}(y)+\tfrac{1}{2}\gamma_3^2\varphi^{(6)}(y)]-[\gamma_5\varphi^{(5)}(y)+\gamma_3\gamma_4\varphi^{(7)}(y)+\tfrac{1}{6}\gamma_3^3\varphi^{(9)}(y)]+\cdots. \quad (2)$$

In this form, $f(y)$ is readily integrated[7] by replacing $\varphi(y)$ with $\Phi(y)=(2\pi)^{-\frac{1}{2}}\int_{-\infty}^{y}\exp(-t^2/2)dt$ and $\varphi^{(n)}(y)$ with $\varphi^{(n-1)}(y)$, giving

$$F(y)=[\Phi(y)]-[\gamma_3\varphi^{(2)}(y)]+[\gamma_4\varphi^{(3)}(y)+\tfrac{1}{2}\gamma_3^2\varphi^{(5)}(y)]-[\gamma_5\varphi^{(4)}(y)+\gamma_3\gamma_4\varphi^{(6)}(y)+\tfrac{1}{6}\gamma_3^3\varphi^{(8)}(y)]+\cdots. \quad (3)$$

This integral distribution is usually more useful to experimentalists than the differential distribution.

In most applications, the series for $f(y)$ and $F(y)$ converges so rapidly that even the fourth of the square-bracketed terms in either gives a negligible contribution. In using tabulated[7,8] values of $\varphi^{(n)}(y)$ and $\Phi(y)$ for range values less than the mean, one needs the relations[7] $\Phi(-y)=1-\Phi(y)$, $\varphi(-y)=\varphi(y)$, and $\varphi^{(n)}(-y)=(-1)^n\varphi^{(n)}(y)$.

To show how the range distribution differs from a Gaussian, $F(y)$ has been computed for the stopping in aluminum of protons of energies from 2 to 500 Mev (roughly the range of validity of the calculation). Since the central portion of the distribution is close to Gaussian, a comparison is made of the distance, y, from the mean at which only 0.1 percent of $F(y)$ remains in either tail. These distances, $\pm y(0.1\text{ percent})$, are plotted in Fig. 1.

To put the $\pm y(0.1\text{ percent})$ values in terms of range, one multiplies by $\beta_2^{\frac{1}{2}}=\langle\Delta R^2\rangle^{\frac{1}{2}}$, the "straggling." Values, obtained from a formula given by Lewis[1] and using $I=160$ ev, are given in Fig. 2.

As an example, if one uses (7.73) (3.15) mg/cm² less Al absorber than the 20-Mev mean range thickness, then 99.9 percent of the 20-Mev protons are counted and at least 99.9 percent of protons with mean energy 19.0 Mev or less are excluded.

The protons-in-Al curve for straggling may be used for any material, Z, and any particle, z, M, within the validity of the assumptions $M\gg m$(=electron mass), $I\propto Z$, and $Z/A=Z_{Al}/A_{Al}$, provided an equivalent proton energy, $E_{p,Al}=(M_p/MZ)E_{M,z,Z}$, is taken and the following applied: $[\langle\Delta R^2\rangle^{\frac{1}{2}}]_{M,z,Z}=(M/M_p)^{\frac{1}{2}}\times(Z/Z_{Al})^{\frac{2}{3}}z^{-2}[\langle\Delta R^2\rangle^{\frac{1}{2}}]_{p,Al}$ mg/cm². If this same energy transformation is made, the $\pm y(0.1\text{ percent})$ curves may be used directly for protons in any material.

The theoretical mean range should be lengthened somewhat, as Lewis[1] points out, but the mean range increases in Al for the protons of 2, 20, and 200 Mev are only 0.050 percent, 0.029 percent, and 0.021 percent, respectively. To compensate for the short-range tail, the most probable range is longer than the mean range, but this is an even smaller effect, the difference being 1.6×10^{-4} mg/cm² for 20-Mev protons in Al.

The writer thanks Professors J. Reginald Richardson and Paul G. Hoel for helpful suggestions.

[7] H. Cramér, *Mathematical Methods of Statistics* (Princeton University Press, Princeton, 1946).

[8] J. Glover, *Tables of Applied Mathematics in Statistics* (George Wahr, Michigan, 1924).

Letters to the Editor

PUBLICATION of brief reports of important discoveries in physics may be secured by addressing them to this department. The closing date for this department is five weeks prior to the date of issue. No proof will be sent to the authors. The Board of Editors does not hold itself responsible for the opinions expressed by the correspondents. Communications should not exceed 600 words in length and should be submitted in duplicate.

Stripping and Pick-Up Differential Cross Sections

S. T. BUTLER AND E. E. SALPETER
Cornell University, Ithaca, New York
(Received August 11, 1952)

THE fact that, at small angles, the angular distributions of nuclear reactions such as (d, t) and (t, d) contain large contributions from pick-up or stripping, respectively, is evidenced by the pronounced forward structure observed[1] in the distribution for the reaction $Be^9(d, t)Be^8$. For this reason we have calculated the differential cross sections to be expected from such reactions as a result of stripping and pick-up, the method employed being identical with that used previously for (d, p) and (p, d) reactions,[2] Coulomb effects again being neglected. For simplicity we will present the results here which are derived assuming S states only in the deuteron and triton wave functions. Possible admixtures of other angular momentum states have also been considered, but for admixtures of the order to be expected negligible changes in the cross sections result.

The formula for the (d, t) and (t, d) angular distributions is very similar to that for the (d, p) and (p, d) distributions given by Eq. (34) of reference 2 (and we use the notation of reference 2). The term under the summation over l_n is identical with the corresponding term in the $(d, p)(p, d)$ case, except that now we have $Z=|\mathbf{k}_T-(M_1/M_2)\mathbf{k}_D|$ instead[3] of $|\mathbf{k}_D-(M_1/M_2)\mathbf{k}_P|$. ($\mathbf{k}_T$, $\mathbf{k}_D$, and $\mathbf{k}_P$ are the wave numbers for the triton, deuteron, and proton, respectively, in the appropriate center-of-mass systems, and M_1 and M_2 are the masses of the lighter and heavier of the initial and final nuclei, respectively.) For the other angle dependent factor in the cross section we now have a function $\varphi_T{}^2(|\frac{1}{2}\mathbf{k}_T-\mathbf{k}_D|)$ depending on the triton momentum distribution which replaces the deuteron momentum distribution $\varphi_D{}^2(|\frac{1}{2}\mathbf{k}_D-\mathbf{k}_P|)$.

The form factor $\varphi_T{}^2$ may be described as follows: Expand the (unsymmetrized) triton wave function in terms of states i of the deuteron, thus

$$\psi_T(\mathbf{r}, \mathbf{R})=\Sigma_{iL}A_{iL}\chi_{iL}(\mathbf{r})f_{iL}(\mathbf{R}). \quad (1)$$

Here $\mathbf{r}$ is the difference between the coordinates of the proton and a neutron, and $\mathbf{R}$ is the position of the second neutron with respect to the midpoint of $\mathbf{r}$. The χ_{iL} are wave functions of states i of the deuteron with spin orientations i, and both χ_{iL} and f_{iL} are assumed to include spin functions and to be normalized to unity. Then the function φ_T is merely the Fourier transform of $f_{iL}(\mathbf{R})$ ($l=0$ corresponding to the deuteron ground state) which is independent of i. Thus $\varphi_T{}^2$ is the momentum distribution (of the third particle) in a triton when it has the configuration of a deuteron ground state plus third particle.

Also, apart from known factors, the nuclear parameter $Nl_n s_n j'$ which enters under the summation over l_n is the same for (d, t), (t, d), (p, d), and (d, p) reactions between the same nuclear levels. With the same nuclear (N) factor in these cases, and with φ_T and φ_D normalized to the same number, the multiplying angle independent factors for the above four reactions are in the ratios $(4/9)m_D{}^*m_T{}^*(k_T/k_D)A_d{}^2$, $\frac{2}{3}m_D{}^*m_T{}^*(k_D/k_T)A_d{}^2$, $m_T{}^*m_D{}^*(k_D/k_P)$, and $\frac{2}{3}m_P{}^*m_D{}^*(k_P/k_D)$, respectively, where $m_T{}^*$, $m_D{}^*$, $m_P{}^*$ are the appropriate reduced masses of the triton, deuteron, and proton. Here $A_d{}^2=\Sigma_i|A_{iL}|^2$ is the probability of finding the triton in the configuration of a deuteron and third particle.[4]

The same selection rules on l_n apply in the (d, t) and (t, d) cases as in the (d, p) and (p, d). However, rather than to try to use (d, t) and (t, d) reactions for obtaining information about the spins and parities of nuclear energy levels, as is done with (d, p) and (p, d) reactions,[2] it seems more desirable in this case that information be sought concerning the triton wave function. If the angular distribution for a (d, t) reaction (say) be obtained in a case where one known value of l_n is allowed, then by dividing this distribution by the oscillatory (Bessel) factor in the formula, a plot of the function $\varphi_T{}^2(k)$ is obtained, for k ranging over the values of $|\frac{1}{2}\mathbf{k}_T-\mathbf{k}_D|$ which enter into the forward part of the distribution. The range of values of this argument can easily be varied by judicious choice of different experiments employing, for example, different incident energies or different reactions.

Once the form of $\varphi_T{}^2$ has been obtained, the factor $A_d{}^2$ can be found directly by measuring the ratio of (d, t) or (t, d) to (p, d) or (d, p) cross sections between the same two nuclear states. Thus the probability of the triton being in the configuration of a deuteron and third particle can be obtained. Although $\varphi_T{}^2$ is the momentum distribution for this configuration alone, it should give a good approximation to that of the triton as a whole *if* $A_d{}^2$ is found to be reasonably large.

Performing both a (d, t) or (t, d) and a (p, d) or (d, p) reaction between the same two nuclear states would also be advantageous in obtaining $\varphi_T{}^2$ in the first place, since the value used for the nuclear radius r_0 in the formula could be checked from the (d, p) or (p, d) case and adjusted if necessary.

By way of indicating how the (d, t) and (t, d) angular distributions depend on the form factor $\varphi_T{}^2$ we show in Fig. 1 some distributions for the reaction $C^{12}(d, t)C^{13}$ with 8-Mev (lab) deuterons. The dotted curves are the distributions resulting (a) if $\varphi_T{}^2$ had the same form as the deuteron momentum distribution $\varphi_D{}^2$ and (b) if it were constant. The actual curve should lie between these, and the solid curve is that obtained from a reasonable but approximate triton wave function. In this example $l_n=1$ and r_0 was taken to be 4.5×10^{-13} cm.

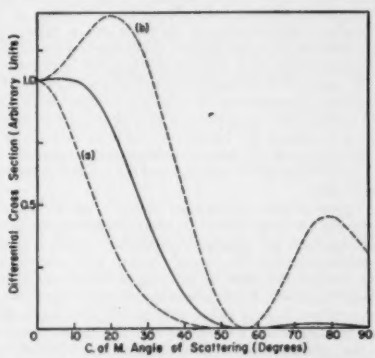

FIG. 1. Angular distributions for the reaction $C^{12}(d, t)C^{13}$ with 8-Mev (lab) deuterons. Curve (a) pertains to the case that $\varphi_T{}^2$ is the same as the deuteron momentum distribution, and curve (b) to the case that it is constant. The solid curve is the distribution more nearly to be expected. The three curves have been normalized to be equal at zero angle.

Finally, if it were possible to perform a (t, d^*) reaction in which deuterons in the singlet state are observed, the momentum distribution and the magnitude of the term $t=1$ in (1) could also be obtained. The discussion presented here applies equally well, of course, to the reactions (He^3, d), (d, He^3), (d, n), and (n, d). Full details of these calculations will be published later.

We are indebted to Dr. N. Austern for valuable discussions, and to Mrs. E. Baranger and Mrs. P. Greifinger for some numerical calculations.

[1] Tai, Middleton, and El Bedervi, Proceedings of the Chicago Nuclear Physics Conference (1951), p. 43 (reported by J. M. Cassels).
[2] S. T. Butler, Proc. Roy. Soc. (London) **A208**, 559 (1951).
[3] The ratio M_1/M_3 appearing in Z is a refinement neglected in reference 2.
[4] The maximum possible value of A_3^2 is $\frac{1}{4}$, since this is the probability of obtaining a triplet neutron-proton spin factor from the triton spin function.

X-Rays from Mesic Atoms*

M. Camac, A. D. McGuire, J. B. Platt, and H. J. Schulte
University of Rochester, Rochester, New York
(Received August 18, 1952)

SEVERAL authors[1-3] have discussed the possible formation of a mesic atom composed of a positively charged nucleus to which a negative pion or muon is bound in a Bohr-like orbit. There have been at least two experiments performed which gave indirect evidence for such phenomena.[4,5] We have found direct evidence for π-mesic atom formation with the nuclei of carbon, oxygen, and beryllium. For $Z<10$ the nuclear radius is small compared to the radii of even the lowest mesic orbits, and hence a simple Coulomb potential should suffice for calculating the expected energy levels. Such a calculation for the $2p-1s$ transition (assuming a pion mass$=276\ m_e$) gives quantum energies of 100 kev in carbon, 178 kev in oxygen, and 44.3 kev in beryllium.

We have searched for such x-rays in coincidence with the stopping of negative pions in the above elements. The fringing field of the 130-inch Rochester cyclotron was used to select and focus an external beam of 40±3 Mev negative pions produced by protons striking an internal copper target. The pions passed through three liquid scintillators and were stopped in a target of the desired element. Identification of the pions was by means of magnetic deflection and range. Beyond the stopper we placed an x-ray detector consisting of a 0.145-in. thick, 1.5-in. diameter disk of NaI(Tl) and a 5819 photomultiplier. The amplitude distribution of those NaI(Tl) pulses which were in coincidence with the three liquid scintillators was analyzed with a 24-channel discriminator. In order to reduce the background counting rate in the x-ray detector approximately five feet of brass was used between it and all parts of the cyclotron tank except for a channel in the brass to pass the pions.

0.55 g/cm^2 of lead or aluminum could be inserted between the stopper and the x-ray detector without disturbing the geometry. These absorbers are roughly equivalent in stopping power for charged particles but differ greatly in their x-ray absorption.

The energy calibration of the x-ray detector was a two-step process. 74-kev lead $K\alpha$ fluorescence radiation was used as a primary standard. A light pulser was constructed using a 5823 gas triode through which a condenser was discharged. Some of the resulting light was directed onto the 5819 photocathode, and the amplitude of the resulting pulses was adjusted to match the output of the 5819 when the NaI(Tl) was irradiated by the primary standard. The light pulser then remained permanently attached to the x-ray detector. It was possible to synchronize the light pulser with the arrival of the protons at the cyclotron target so that the energy calibration and resolution could be checked at the time of maximum background counting rate in the crystal. By this means an energy calibration of about 10 percent accuracy was established. Somewhat less accurate calibrations were also made at 44, 100, and 140 kev. The energy spread indicated in the spectrum in Fig. 1 is consistent with that observed during light pulser calibration.

Representative pulse-height spectra obtained during our most recent runs are shown in Fig. 1. Each curve represents 65,600 pions stopped in carbon. The data were taken in a total of 26 runs by alternating the lead and aluminum absorbers. The aluminum-lead differences with standard deviations due to counting statistics are also plotted. The calculated transmission in our geometry at 100 kev was 0.018 for the lead and 0.79 for the aluminum. Similar

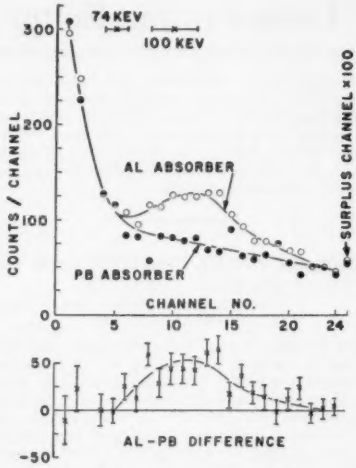

FIG. 1. Pulse-height spectrum from carbon.

spectra have been taken with the pions stopping in a water cell. A third series of runs was made with the pions stopping either in beryllium or carbon.

In all three elements x-rays were observed at the expected energies within the limits of our energy calibration. In carbon and water quantitative yield measurements were possible. The yield from beryllium is uncertain in amount at this time because of the large background counting rate at 44 kev. In carbon the number of x-rays emitted per stopped pion is 0.13±0.03. The corresponding yield for water is 0.21±0.07.

The largest uncertainty in our measurements is in determining the number of stopped pions which can contribute to the x-ray yield. Less than 2 percent of the particles stopping are muons. The yield from carbon agrees well with the predictions of Marshak and Messiah.[6] If the nuclear absorption from the $2p$ state were comparable in carbon and oxygen, the oxygen yield should be roughly 0.6 of the carbon yield, contrary to our measurement. This may indicate the operation of a special selection rule for negative pion absorption in the "magic number" oxygen nucleus. Work is continuing in attempts to improve the energy resolution, decrease the yield uncertainties, and extend the investigations to other low Z materials.

* Work supported jointly by the University of Rochester and AEC.
[1] E. Fermi and E. Teller, Phys. Rev. **72**, 399 (1947).
[2] J. A. Wheeler, Revs. Modern Phys. **21**, 133 (1949).
[3] R. E. Marshak, *Meson Physics* (McGraw-Hill Book Company, Inc., New York, to be published).
[4] W. Y. Chang, Revs. Modern Phys. **21**, 166 (1949).
[5] Panofsky, Aamodt, and York, Phys. Rev. **78**, 825 (1950).
[6] R. E. Marshak and A. M. L. Messiah (private communication).

Activation Energy of Heat Treatment Introduced Lattice Defects in Germanium*

R. M. Baum† and C. S. Hung‡
Purdue University, Lafayette, Indiana
(Received July 31, 1952)

RECENTLY Dunlap[1] and DeSorbo[2] reported on resistivity measurements of heat-treated germanium single crystals at hydrogen temperatures. They found that the activation energy for thermally introduced acceptors is about 0.03 ev; i.e., considerably higher than for chemical acceptors.[3] Some time ago,[4] at the

suggestion of K. Lark-Horovitz, we measured both the Hall coefficient and the resistivity of heat-treated germanium single crystals at low temperatures. The single crystals were prepared and heat treated by Taylor. The heat treatment consisted of holding the samples which were originally n-type in a vacuum of about 10^{-3} mm Hg at 695°C for several hours and then quenching them in ethyl alcohol.

TABLE I. Room temperature resistivity, Hall coefficient, Hall mobility, and carrier density of three typical samples before and after heat treatment.

Sample		ρ ohm-cm	R cm³/coulomb	b cm²/volt-sec	N No./cm³
44 B22	Before	6.80			3.4×10^{14}
	After	1.40	+ 3280	2000	2.2×10^{15}
44 B3	Before	3.60			6.4×10^{14}
	After	1.20	+ 3600	2350	2.0×10^{15}
45 I20	Before	4.16	−17,600	3600	4.2×10^{14}
	After	1.68	+ 4830	2440	1.5×10^{15}

Table I shows the room temperature properties of three typical samples before and after heat treatment.

Note the high Hall mobility of the N- and P-type samples comparable with drift mobilities.

Resistivity and Hall measurements were first carried out between room and liquid nitrogen temperatures. The samples were then cooled to liquid hydrogen or liquid helium temperatures and heated up to specified temperatures. Around 30°K most samples showed marked inhomogeneity. Measurements at temperatures less than this were not considered reliable. Figure 1 shows the Hall and resistivity curves of two samples. Figure 2 shows mobility plots determined from experimental R and ρ values. The analysis of the experimental data was carried out according to two methods, both assuming the simultaneous presence of donors and acceptors[5]; from the analysis of the Hall curves the activation energy of thermally introduced acceptors was calculated to be 0.058 and 0.047 ev, respectively. Inasmuch as the activation energies are considerably higher than one observes with chemically

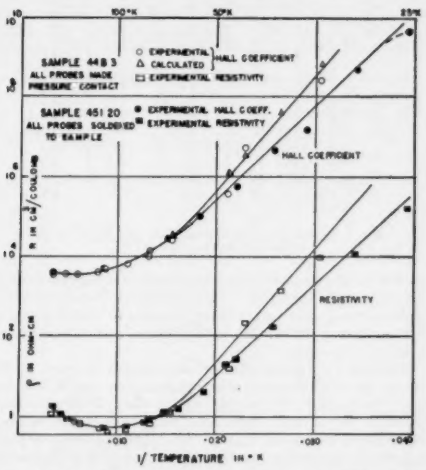

FIG. 1. Hall coefficient and resistivity vs $1/T$ for samples 44B3 and 45I20 Ge single crystals, originally n-type alcohol quenched from 968°K, then p-type.

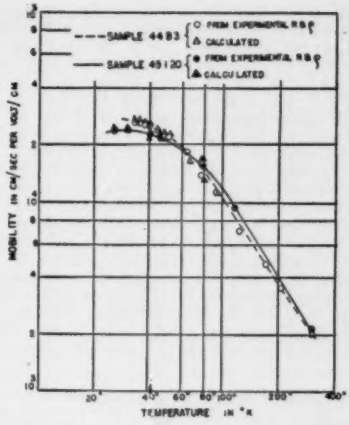

FIG. 2. Mobility vs temperature curves for samples 44B3 and 45I20 Ge single crystals, originally n-type alcohol quenched from 968°K, then p-type.

introduced acceptors, our results are in agreement with those reported by Dunlap and DeSorbo. However, the analysis of low temperature experimental data is subject to the following criticisms.

At low temperatures scattering by both ionized and neutral impurity centers should be considered.[6] One should also remember that the lattice and the impurity mean-free paths are different functions of the carrier velocity.[7] It is therefore difficult to make exact calculations, as has already been pointed out by Shockley and mentioned by Pearson and Bardeen.[8]

The authors wish to thank Dr. P. H. Keesom for providing them with liquid hydrogen and liquid helium.

* Supported in part by Signal Corps Contract.
† Now with Sylvania Electric Products Company, Newton, Massachusetts.
‡ Now at the University of Leiden, Leiden, Holland.
[1] W. C. Dunlap, Jr., Phys. Rev. **87**, 190 (1952).
[2] W. DeSorbo and W. C. Dunlap, Jr., Phys. Rev. **83**, 879 (1951).
[3] Such high activation energies were observed by the Purdue group sometime ago, both after heat treatment and after nucleon bombardment. [For a summary see H. N. James and K. Lark-Horovitz, Z. physik. Chem. **198**, 112 (1951)].
[4] R. M. Baum, thesis, Purdue University, 1951 (unpublished).
[5] C. S. Hung and V. A. Johnson, Phys. Rev. **79**, 535 (1950).
[6] G. L. Pearson and G. Bardeen, Phys. Rev. **75**, 881 (1949); C. Erginsoy, Phys. Rev. **79**, 1013 (1950).
[7] V. A. Johnson and K. Lark-Horovitz, Fourth Quarterly Report, Purdue University (1949); Phys. Rev. **82**, 977 (1951).
[8] G. L. Pearson and J. Bardeen, reference 6, p. 881.

The Solidification Curve of Helium II*·†·‡

B. M. CWILONG
Department of Physics, University of British Columbia, Vancouver, Canada
(Received June 27, 1952)

ALL experimenters who have measured various properties of helium II under pressure conveyed the pressure to the investigated sample of helium by a "helium wire" (an expression used by Keesom in his papers on heat conductivity of helium II), that is, a column of helium under pressure enclosed in a capillary and connecting an experimental chamber, containing liquid or solid helium, with a compression chamber, containing compressed helium gas. A considerable temperature difference between the experimental chamber and the compression chamber is inevitable in such arrangements for the maintenance of the pressure. Thus were obtained the melting curve, specific heat, latent heat of melt-

ing, density, heat conductivity, etc. In all these experiments, the temperature of the sample was identified either with the temperature of the surrounding bath or with the temperature of the thermometers attached to the outside of the walls of the container, on the assumption that the thermal gradient across the walls is negligible. In view of the exceptionally high heat transport in helium II, any walls containing the "helium II wire" can be considered rather as a thermal shield than a conductor. In such conditions, the temperature of an experimental chamber may drop only a little below the λ-temperature, even when the temperature of the bath is much lower, and the thermal gradient across the walls will be most significant. The heat necessary for the maintenance of such a gradient will be transported along the "helium II wire," and it will be supplied from the warmer surroundings across the walls of the capillary near the compression chamber.

To check the influence of this effect and to eliminate it, an apparatus has been designed for retracing the solidification curve of helium II. In this apparatus, pressures are conveyed mechanically, by a compression of metal sylphon bellows, totally immersed in the helium bath, Fig. 1. A glass piezometer (A) is used

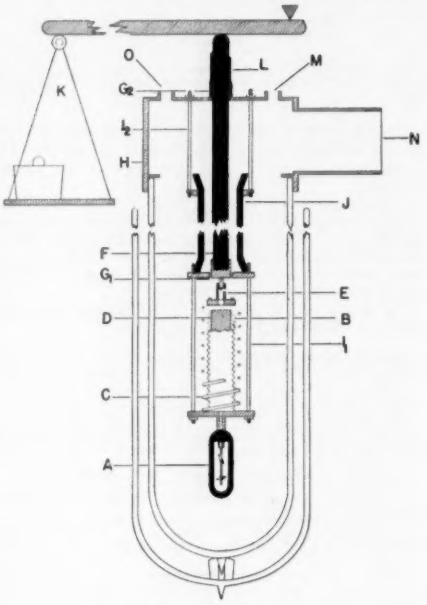

FIG. 1. Sketch of apparatus.

as an observation chamber. It contains two magnetized needles which can be moved by a bar magnet from outside. The solidification of helium in the piezometer is indicated by their immobility. The piezometer is connected by a Kovar sleeve to a metal sylphon bellows (B), initially extended by the spring (C). A solid brass bar (D) is placed inside the bellows to reduce the dead volume of helium under pressure. The bellows are sealed at the top by a steel needle valve (E), which is fitted tightly to the rigid glass rod (F). The rod (F) is located by the clearances (G_1) and (G_2), which leave it free to turn and to move vertically. The bellows are attached rigidly to the cap (H) by series of stainless steel rods (I_1) and (I_2), and also by means of the glass sleeve (J). The pressure is conveyed to the sample of helium by the steel-yard (K) pressing on the glass rod (E). The clearance between the glass rod and the Dewar cap is sealed by an elastic rubber sleeve (L). The Dewar cap has three openings: (M)—for the sylphon feeding liquid helium, (N)—to the vacuum pump, and (O)—to the manometers.

The experimental procedure is as follows. The apparatus is precooled in a liquid nitrogen bath and the helium Dewar and its contents thoroughly evacuated, with the needle valve open. The Dewar is filled with liquid helium and the temperature of the helium bath is lowered by pumping. The needle valve is closed; weights are added to the pan of the steel-yard until helium solidifies in the piezometer. The temperature of the helium bath is slowly raised and the melting point of helium observed. After this, the whole operation can be repeated for the next point of the melting curve. The temperature is measured by the vapor pressure of the helium bath. Because of the higher heat conductivity of the Kovar sleeve, the upper magnetic needle of the piezometer, which is nearer to the sleeve, responds first. The experiment can be carried out in such a way that the lower needle is stuck in solid helium continuously. This allows the use of points of solidification (as well as of melting) for reliable data, as the presence of solid helium in the lower part of the piezometer eliminates the chance of supercooling.

The melting branch, as obtained from three series of measurements, is shown in Fig. 2; in comparison with Swenson's curve,[1]

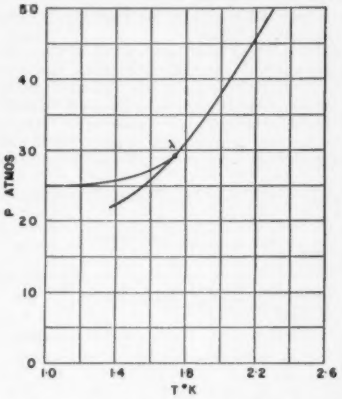

FIG. 2. Melting pressure curve of He II. The upper curve is that of Swenson (reference 1).

each series gave a slightly deviating curve. The slope of the melting curve also in the region of the "triple point" is continuous. The main source of error (±1/4 atmos) was due to the friction of the bellows against the bar (D), as the bellows tend to buckle somewhat under pressure.

Although the "helium II wire" heat leakage is absent in this set-up, the method employed introduces a new type of heat leakage. This is due to the mechano-caloric effect. It seems very improbable that a really tight valve for helium II can be made; therefore, a certain amount of the "superfluid" was probably leaking out of the valve in this apparatus, too. This phenomenon will cause heating of the sample of helium inside the bellows and, as it will be more pronounced at lower temperatures, it is probable that the true melting curve lies lower still and is less curved. As the valve was turned for each series of measurements, the "superfluid" leak was probably different for each series; this may account for the slight deviation of each experimental branch.

From these results, it can be concluded that not only the melting curve but also all other curves formerly obtained for helium II under pressure are considerably stretched along the temperature axis towards 0°K. All these curves really represent much shorter and steeper sectors.

As the new melting curve, corrected somewhat arbitrarily for the mechano-caloric heat leakage, cuts the temperature axis about 0.4°K when extrapolated, it seems reasonable to check for the triple point of helium (the "ordinary" triple point) in the magnetic region of cooling.

* This work is carried out under a grant from the National Research Council of Canada.
† A brief account of this work was given at the meeting of the Physics Section of the Royal Society of Canada on June 3, 1952.
‡ After writing this letter, the author read in a recent article in the Physical Review [P. Closmann and R. T. Swim, Phys. Rev. 86, 576 (1952)] that Dr. K. Mendelssohn, F. R. S., suggested an experimental investigation of the thermal gradient in the "helium wire." The experimental results reported there are in complete agreement with views expressed in this letter.
[1] C. A. Swenson, Phys. Rev. 79, 626 (1950).

Geiger-Nuttall Relation and α-Ray Spectra

M. L. Chaudhury
Department of Theoretical Physics, Indian Association for the Cultivation of Science, Calcutta, India
(Received July 14, 1952)

ATTEMPTS have been made by Berthelot and others[1,2] to improve the original Geiger-Nuttall[3] curves by choosing the "same charge number Z," instead of the "same neutron-excess" as the basis for joining the points. However, recently Perlman *et al.*[4] showed that in fact all nuclei except the even-even ones deviate considerably from the above linear relation. Besides, the deviations of the spectral components of lower intensities are usually more serious.

In view of this well-known difficulty in correlating different elements, we consider here each alpha-spectrum (i.e., each element) individually with regard to the relation $\log\lambda$ *vs* decay energy E. Partial α-decay constants λ_i are plotted against the corresponding decay energies of all the spectral components, and the points for the "same Z and same mass-number A" have been joined. The curves obtained will be discussed in detail in a separate paper, while some typical ones are shown here in Fig. 1

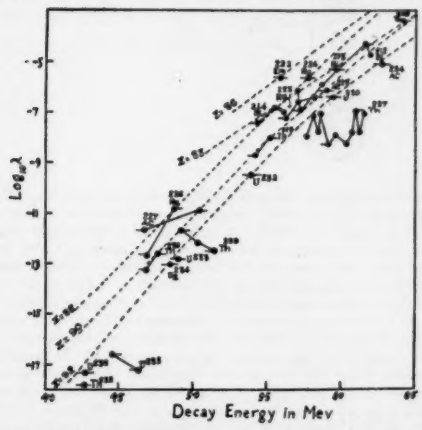

FIG. 1. A dotted line is the usual Geiger-Nuttal curve for the same Z, while a solid line represents a $\log\lambda_i$ *vs* E curve for an α-spectrum. -●- represents an α-spectrum with single line. ●- represents a maximum intensity group, -● a minimum intensity group, and ● means a group of intermediate intensity of an α-spectrum.

(solid lines), along with the usual Geiger-Nuttal curves (dotted lines).

It may be seen from the solid line curves in the figure that in α-ray spectra, instead of the positive gradient of the Geiger-Nuttal relation (i.e., a linear increase of $\log\lambda$ with increasing E), both positive and negative trends exist in the variation of λ with E. In this respect striking similarity is exhibited by all the fifteen α-spectra known at present. The simplest spectra are the doublets, which give either the positive trend only (e.g., Th spectra) or the negative trend (e.g., U^{238}). For the triplet spectra, a positive trend is followed by a negative one (e.g., Bi^{214}) or vice versa, while in the case of the Th^{229} triplet only a negative trend exists. For more complex spectra (a typical example being Th^{227} in Fig. 1), regular alternations of the two opposite trends occur in general.

Now from a theoretical standpoint these negative trends present serious difficulties. For the α-decay theories of Gamow[5] and others gave λ as a function of Z, nuclear radius r_0, and decay energy E. In an α-sprectrum, since Z and r_0 ($\partial A^{\frac{1}{3}}$) are constant, λ becomes an exponential function of E alone, giving only a steep rise in λ with increasing E. From the above discussion it follows that some compensation of the increasing effect of E on λ should be postulated. In the paper to be published we have theoretically discussed the nonlinear curves for α-spectra in the light of various recent suggestions, *viz.*, nonzero values of azimuthal quantum number (Gamow[5]) or delay in formation of the α-particle (Perlman *et al.*[4]), etc., which have been made in connection with the stated deviations from the Geiger-Nuttal relation. It will be seen that none of these is very useful in the case of α-spectra.

It may be pointed out that so far in α-decay theories, the field outside the nucleus has been assumed to be purely Coulombian. However, when the alpha-particle is just emitted, a short-range Yukawa field, say V', would operate between the four nucleons of the emitted α-particle and those on the surface of the residual nucleus. So if the resultant field outside the nucleus is taken to be $\{2(Z-2)e^2/r-V'\}$, the wave equation for the α-particle would be

$$\Delta\psi+(8\pi^2M_\alpha/h^2)[E+V'-2(Z-2)e^2/r]\psi=0.$$

Obviously, in the final formula for λ, V' would be involved. Now what form of V' would lead to a fluctuation of λ or to the observed negative trend is a matter for further study. It is, however, probable that since V' is spin-dependent, the excitation shells within the nucleus of the four nucleons forming the alpha-particle may have different spin values and affect V' differently in the different cases, as observed.

Finally, I wish to express my gratitude to Professor M. N. Saha, F. R. S., for his kind interest in this work and for his encouragement. I wish also to thank Dr. D. Basu for the facilities and encouragement given.

[1] A. Berthelot, J. phys. et radium 3, 17 (1942).
[2] S. Biswas, Indian J. Phys. 23, 51 (1949).
[3] H. Geiger and J. M. Nuttal, Phil. Mag. 22, 613 (1911).
[4] Perlman, Ghiorso, and Seaborg, Phys. Rev. 77, 26 (1950).
[5] G. Gamow and C. L. Critchfield, *Theory of Atomic Nucleus and Nuclear Energy Sources* (Clarendon Press, Oxford, 1949), p. 173.

Shock Waves in Low Pressure Spark Discharges*

Richard G. Fowler, William R. Atkinson, Walter D. Compton, and Robert J. Lee
University of Oklahoma, Norman, Oklahoma
(Received July 31, 1952)

ASSUMING that an expansion of hot gas follows the passage of a columnar current through a gas at low pressure, a shock wave should precede the advancing hot gas front (through the quiescent medium surrounding the column). Treating the expanding gas as a moving piston and measuring its velocity of advance by means of its own luminosity,[1] the Rankine-Hugoniot equations will give the velocity of advance of the shock front.

We have found two situations in which the shock fronts make themselves visible by the excitation they produce, and computations of the sort suggested above verify the correctness of this description of the expanding spark channel. A mirrorgram which shows both situations at the same time is shown in Fig. 1. In the first case the shock fronts become self-luminous upon reflection from an obstacle to the flow so that the original shock path can be inferred by the point at which the reflection occurs. In the

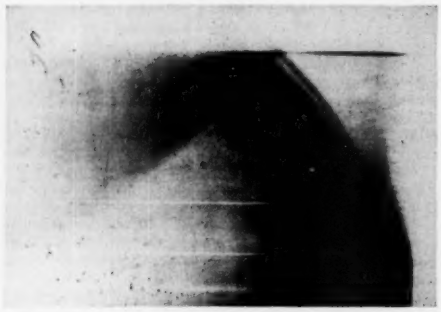

FIG. 1. Mirrorgram showing expanding luminous gas, preceded by a luminous shock front which reflects with intensified luminosity at a piston and then intersects the oncoming luminous gas flow.

second case, with a careful choice of discharge pressure, the shock waves are directly visible in their own light. Argon was the gas employed.

Table I gives among other things a comparison of the measured shock velocities with the computations from the luminous gas flow velocity. Also included are a few computations of temperature and pressure behind the shock in the case of both the original and the reflected shock, computed on an ideal gas law. These latter figures give some idea of the origin for the observed luminosity. It is probable that we have to deal here almost exclusively with Saha temperature excitation processes.

TABLE I. Comparative thermodynamic data for spark expansions. W = capacitor energy; p_0 = initial pressure; U_c = contact velocity (luminosity); U_s = calculated shock velocity; U_s^1 = measured shock velocity; p_1 = shock pressure; T_1 = shock temperature; p_2 = reflected shock pressure; T_2 = reflected shock temperature. Units used are joules, mm Hg, km/sec, 1000°K.

W	p_0	U_c	U_s	U_s^1	p_1	T_1	p_2	T_2
30	10	1.6	2.2	2.0	560	4.5	2100	10
120	0.8	4.0	5.4	5.1	280	27	1600	64
10	17	1.0	1.4	···	380	1.9	1900	4.2
120	17	2.1	2.8	2.9	···	···	···	···
120	2	2.5	3.4	4.0	···	···	···	···
120	0.3	2.65	3.5	3.5	···	···	···	···
120	3.4	1.35	1.6	2.7	···	···	···	···
120	1.1	2.60	2.9	3.6	···	···	···	···

Examination of a series of mirrorgrams in which controlled reflection of the advancing gas was studied shows that at high initial densities the description given above is adequate, i.e., an optionally luminous shock front precedes an expanding, hot, luminous gas. At low densities, however, this description is inadequate, and a strongly self-luminous shock front is by far the principal manifestation of the expansion. This result explains the anomalies which are present in our earlier reports,[1,2] where we have described the expanding post-discharge luminosity of the spark as being in some cases a ball of flame and in others more nearly a luminous tongue or jet. We believe that this transition in the post-discharge disposal mechanism of surplus excitation energy, which occurs in the vicinity of an initial density of 5×10^{16} particles per cc, may well be a critical point for the definition of the term, low pressure spark discharge.

Recent work by Kantrowitz[3] and by Laporte,[4] has shown the possibility of producing luminosity even in conventional shock tubes.

The authors desire to express their gratitude to Dr. Otto Laporte for his valuable suggestions concerning this work.

* Supported by the ONR.

[1] Fowler, Goldstein, and Clotfelter, Phys. Rev. **82**, 879 (1951).
[2] R. J. Lee and R. G. Fowler, Phys. Rev. **81**, 457 (1951).
[3] Resler, Jr., Petschek, Lin, and Kantrowitz, Phys. Rev. **87**, 909 (1952).
[4] Hollyer, Jr., Hunting, Laporte, Schwarcz, and Turner, Phys. Rev. **87**, 911 (1952).

Cavitation Effect in Helium II*

B. M. CWILONG, J. LEES, AND F. D. MANCHESTER
Department of Physics, University of British Columbia, Vancouver, Canada
(Received August 11, 1952)

DURING some work on the properties of helium at temperatures in the magnetic region of cooling, apparatus was constructed (Fig. 1) containing a few grams of a powdered paramagnetic salt (iron ammonium alum) in a glass capsule 8 mm in diameter, enclosed in a vacuum jacket. The capsule and the jacket could be pumped independently with a pumping speed of up to 2 liters per second, and provision was made for the condensation of helium in the capsule. Usually the liquid helium meniscus in the capsule was kept just above the level of the salt. The top of the salt and the helium level could be observed through a gap in the silvering of the Dewars and the capsule. The salt was cooled by adiabatic demagnetization from a maximum field of 10,000 oersteds and an initial temperature of about 1.2°K.

The effect observed with this apparatus was that, invariably, after demagnetization, the meniscus of the helium in the capsule

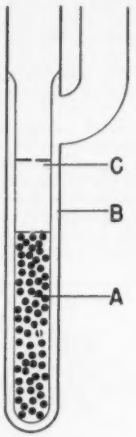

FIG. 1. A schematic diagram of the capsule and vacuum jacket. A—powdered paramagnetic salt, B—vacuum jacket, C—membrane.

suddenly rose above the salt, as high as 2 cm in some cases—this apparent volume increase being comparable with the amount of helium present in between the grains of the powdered salt. After one or two seconds, the meniscus dropped again and then immediately rose, going through several oscillations. When demagnetization was performed in several stages, the time of the rise of the meniscus correlated with each step of demagnetization.

In a series of experiments, a thin glass membrane, with a pinhole of diameter varying from 100 to 300μ, was introduced as a partition in the tube connecting the capsule with the pumping system. With this arrangement, the initial temperature of the capsule could be lowered to about 0.8°K. When the membrane was 6 cm above the level of the salt, a much diminished effect (1 mm) was observed. When the membrane was 3 cm above, no rise of the meniscus could be observed, but the surface of the helium during every demagnetization appeared very confused, showing lively ripples due to vigorous undercurrents. In all cases, however, if the pumping of the capsule was stopped a few seconds before demagnetization, the effect reappeared.

As no other sources of helium comparable with the amount in the salt are present in the system, the necessary conclusion is that the liquid helium is expelled from the powder. In this connection, it may be mentioned that the effect was absent when the powdered

salt was replaced by a specimen cut from solid crystal, either hollow or having wall clearances.

As the existence of a helium II film in the tube connecting the capsule with the pumping system (up to 40 cm of its length in helium II bath when a membrane was not used, and 6 cm of its length in vacuum jacket when the diminished effect was observed) is a necessary condition for the appearance of the phenomenon, it could be perhaps considered as an extreme case of the fountain effect, producing cavitation of the helium II within the powder. The oscillations could then be explained by assuming consecutive coolings of the helium II film and warmings of the helium II in bulk, above the powder, with re-entries of the liquid into the colder powder.

In view of these observations, caution should be exercised with remote control experiments in assuming thermal equilibrium when a powdered paramagnetic salt is diluted with helium.

* This work was carried out under a grant from the National Research Council of Canada.

$p-n$ Junctions Produced by Growth Rate Variation

R. N. Hall
General Electric Research Laboratory, Schenectady, New York
(Received July 29, 1952)

MORE than a hundred uniformly spaced $p-n$ junctions have been produced in an ingot of germanium by periodically varying the rate of growth of the crystal from a properly doped melt. The amount of an impurity picked up by a growing crystal is determined by the segregation constant k,[1] which has been observed to depend upon the growth rate even when the accumulation of impurities ahead of the ingot is made negligible by thorough stirring of the melt.[2] The preparation of $p-n$ junctions by growth rate variation requires the presence of two opposite type impurities whose segregation constants vary at different rates with growth velocity.

Pronounced growth rate effects have been observed in the segregation of antimony during the solidification of ingots of germanium, as shown in Fig. 1. These data were obtained by con-

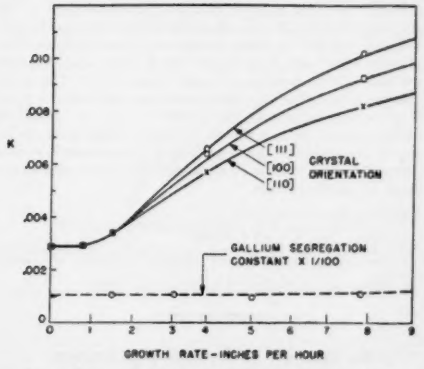

FIG. 1. Effect of growth rate upon the segregation of antimony during the growth of a germanium crystal.

ductivity measurements of a tri-crystal grown from a melt, using a bundle of three differently oriented seed crystals. Concentration of impurities in the melt ahead of the growing interface was made small by rotating the ingot at 200 rpm to provide thorough stirring.

Most p-type impurities such as Ga and In show much smaller changes in segregation constant. It follows that an ingot grown from a melt doped with the proper amount of antimony and either gallium or indium will be p-type when grown slowly and n-type when grown rapidly. By cycling the growth rate of an ingot, it is possible to produce a large number of uniform and evenly spaced $p-n$ junctions, each cycle producing two junctions having somewhat different characteristics. A wide variety of impurity distributions may be produced by changing the shape and amplitude of the growth cycles. In particular, this technique makes possible the growth of junctions having much smaller impurity concentration gradients than are produced by techniques previously reported.[3] Gradients less than 10^{-16} cm^{-4} are readily obtained and give rise to junctions having very low barrier capacities and high Zener breakdown voltages.

It is believed that the change in segregation constant with growth rate shown in Fig. 1 results largely from nonequilibrium conditions which prevail within the crystal near its growing surface. When the crystal is growing very slowly, the ratio of the impurity content in the solid to that in the liquid is given by the equilibrium segregation constant k_0. Because of the difference in binding energy at the surface of the crystal, it is to be expected that the composition of the surface layer of the crystal will be different from that in its interior. After each surface layer of the growing crystal is covered by a new layer, its composition will tend to approach the equilibrium value for the solid. If new layers are added too rapidly, however, the impurities have insufficient time to exchange with the surface, and material having a nonequilibrium composition will be grown.

The above mechanism leads to the following variation of segration constant with growth rate:

$$k=k_0+(k_s-k_0)\exp(-v_i/v).$$

Curves fitted to this equation are drawn through the experimental points in Fig. 1. The constant v_i is the growth rate for which the time interval between the deposition of successive layers to the crystal is equal to the relaxation time for the change in impurity content of a layer which has just been covered up. This time interval is comparable with the time required for antimony to diffuse a few angstroms in solid germanium as estimated from its measured diffusion constant.[4]

[1] R. N. Hall, Phys. Rev. **78**, 645 (1950).
[2] The dependence of segregation constant upon melt stirring was discussed by J. A. Burton and W. P. Slichter at the IRE and AIEE Conference on Semiconductor Device Research in June, 1952 (unpublished).
[3] Teal, Sparks, and Buehler, Phys. Rev. **81**, 637 (1951).
[4] W. C. Dunlap and D. E. Brown, Phys. Rev. **86**, 417 (1952).

Production of Photomesons in Deuterium*

James Keck and Raphael Littauer
Newman Laboratory of Nuclear Studies, Cornell University, Ithaca, New York
(Received August 20, 1952)

THE reaction

$$\gamma+d\rightarrow\pi^-+p+p' \qquad (1)$$

is being studied by detecting the meson in coincidence with a recoil proton. Since the deuteron is a loosely bound structure, it was expected that in a fair fraction of the cases the process should be characteristic of that for a neutron moving with the momentum distribution of the deuteron, the role of the proton being only that of a spectator. The present letter is a report of an investigation primarily of this "spectator process."

The experimental arrangement is shown in Fig. 1. 0.50-cm targets of D_2O and H_2O were irradiated by 310-Mev bremsstrahlung. Mesons emitted at $90\pm10°$ with an energy of 56 ± 9 Mev were identified by their specific ionization and range in a coincidence-anticoincidence telescope of three scintillators. The recoil protons were counted by a Na(Tl) crystal 6.55 g/cm^2 thick, a range corresponding to that of a 69-Mev proton. Their energy was measured with a pulse-height analyzer. The cross section for the process (1) was obtained as a function of both the proton energy and angle by making a D_2O-H_2O subtraction. The H_2O count was about 30 percent of that for the D_2O.

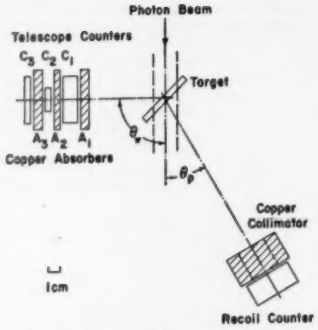

FIG. 1. Schematic diagram of the experimental arrangement.

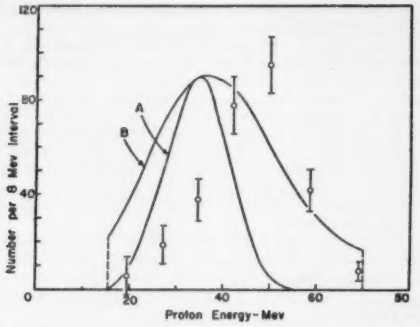

FIG. 3. Energy distribution of recoils at 30° counted in coincidence with a 56-Mev meson at 90°. See text for explanation of curves.

Figure 2 shows the angular distribution of the protons integrated over the energy spectrum. Curve A shows the distribution to be expected with our geometry for meson production from a free neutron at rest; curve B takes into account the internal momentum of the deuteron, assuming the zero-range wave function and no momentum transfer to the "spectator" proton. The cross section for meson production was assumed constant over the energy and angular intervals employed. The agreement of curve B with the experimental points is satisfactory, supporting the assumption of negligible momentum transfer to the "spectator" proton.

Figure 3 shows the energy spectrum of the recoil protons observed at 30°±6°. Curves A and B were computed as for Fig. 2. The experimental points differ significantly from the theoretical curve in this case; they appear to be shifted from 10 to 15 Mev towards higher energy.

Considerable time has been spent in an effort to resolve this discrepancy. The proton counter was calibrated (1) by measurement of the Cs^{137} photoelectric peak at 0.67 Mev; (2) by measurement of pulses produced by cosmic-ray mesons at 9.5 Mev[1]; and (3) by extrapolation of the number-bias curve for an inhomogeneous beam of protons to the high energy cutoff at 69 Mev.[2] All these methods agreed to ±5 percent. Further checks were made by using different crystals for the proton counter and by direct range measurements on the protons.

An error in the definition of meson energy[3] could be produced if mesons were being scattered around the anticoincidence counter C_3. To check this point, experiments were performed with two different telescopes, in one of which C_3 had twice the area of the other. The results with the two telescopes were identical.

Assuming the angular distribution of recoils to be correctly given by curve B of Fig. 2, one can compute the differential cross section for the production of negative pions accompanied by correlated recoil protons. The value obtained is 10.8±1.0 μb/sterad for production at 90° in the laboratory by 236-Mev photons. The error quoted is the standard statistical deviation. We have also determined the cross section for the production of negative pions without the requirement of a correlated recoil, using the π^-/π^+ ratios of Littauer and Walker[4] to separate the π^- and π^+ contributions in the telescope. The value so obtained is 11.8±1.2 μb/sterad. The agreement between the two cross sections may be taken as evidence that the "spectator process" does indeed account for a substantial fraction of the meson production in the deuteron at the angles and energies here involved.

The correctness of the interpretation is, of course, still in doubt due to the failure to fit the energy distributions of the recoils. In closing, we might mention two possible explanations of this discrepancy which have been considered and found unsatisfactory. The first is that the low energy protons are preferentially removed by Coulomb scattering in the target. This is a small effect and there is a tendency for *scattering in* to cancel *scattering out*. The second is that the cross section for meson production might vary in such a way as to favor high energy recoils. Here the difficulty is that the photon energy in the c.m. system is defined within fairly narrow limits by the meson energy, regardless of the momentum state of the struck nucleon, and the cross section is unlikely to vary steeply enough within these limits.

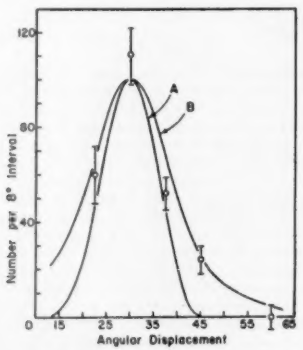

FIG. 2. Angular distribution of recoils counted in coincidence with a 56-Mev meson at 90°. See text for explanation of curves.

* Work supported by the ONR.
[1] W. L. Whittmore and J. C. Street, Phys. Rev. **76**, 1786 (1949).
[2] J. C. Keck, Phys. Rev. **85**, 410 (1952).
[3] In obtaining a range-energy curve for mesons from that for protons a small correction was made for the increased importance of Coulomb scattering.
[4] R. Littauer and D. Walker, Phys. Rev. **86**, 838 (1952).

An Anomaly in the Low Temperature Atomic Heat of Silver*

P. H. KEESOM AND N. PEARLMAN
Purdue University, Lafayette, Indiana
(Received July 21, 1952)

IN measurements of the atomic heat of the semiconductors Ge and Si at very low temperatures, the problem arose of distinguishing between two possible sources of deviations from a cubic dependence of the atomic heat on temperature: (a) electronic heat capacity (due to the presence of impurities); (b) polycrystal-

line structure of the material. To determine the influence of the crystalline state of material on the specific heat, K. Lark-Horovitz suggested measuring the atomic heat of a very pure single crystal of Ag, for comparison with the results of earlier measurements on polycrystalline Ag by Keesom and Kok.[1]

We have therefore measured the atomic heat of a single crystal of Ag[2] at liquid helium temperatures. The results are identical, within experimental error, with those obtained earlier by Keesom and Kok.[1] On a plot of C_v/T against T^2 (see Fig. 1), it is not possible to fit all the data below 4.2°K with one straight line. Below 2.2°K, both sets of data can be represented by the solid line, which has the equation

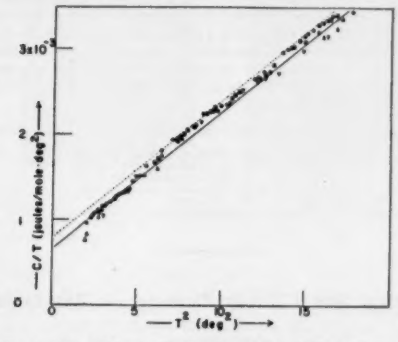

FIG. 1. C_v/T *vs* T^2 for Ag: ▽—Keesom and Kok, 1932; △—Keesom and Kok, 1933; □—this measurement, 1/25/52; ○—1/30/52.

$$C_v = 1.619\times10^{-4}T^3 + 6.45\times10^{-4}T \text{ joules/mole degree}, \quad (1)$$

while above 2.5°K, the dashed line, which has the equation:

$$C_v = 1.598\times10^{-4}T^3 + 7.82\times10^{-4}T \text{ joules/mole degree}, \quad (2)$$

fits both sets of data.

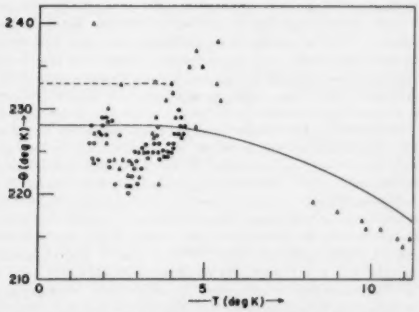

FIG. 2. Debye θ *vs* T for Ag; △—Keesom and Kok; ○—this measurement; ——Leighton's calculated curve; - - - $\theta(E)$ calculated from elastic constants (this calculation is valid only in the true T^3 region).

While this anomaly is also evident in the data of Keesom and Kok, it becomes obvious only in a plot of C_v/T *vs* T^3. However, as was common at the time of their experiments (which provided the first proof of the existence of electronic heat capacity in metals), they analyzed their results only with a plot of θ *vs* T.

Several alternatives suggest themselves for the explanation of this effect. Gerritsen and Korringa[3] have suggested that the rise of resistance observed in some metals at very low temperatures is due to the presence of a very small concentration of paramagnetic impurity atoms, such as Mn. They also predict an additional contribution to the atomic heat in the form of a Schottky curve[4] arising from electronic transitions between states whose degeneracy has been removed by the paramagnetic atoms. Their predicted effect, however, would be much too small compared with that observed, if our single crystal had the purity stated for it (99.999 percent). It also seems unlikely that both our sample and that of Keesom and Kok would contain the same type and amount of impurities.

Katz[5] has suggested that lattice perturbations (due to work hardening, mosaic structure, impurities, etc.) can result in deviations from the Debye vibration spectrum at very low temperatures and provide anomalous contributions to the atomic heat. He has discussed in this way apparent irregularities in the curve of θ *vs* T (see Fig. 2) for Ag, but Keesom and Kok do not believe them to be significant in view of their experimental error. Such perturbations, moreover, must have a considerable degree of order themselves, so that they may form a "superlattice" capable of affecting the spectrum in this way. It is hard to imagine a perturbation of this type which would be identical in Keesom and Kok's polycrystalline material and our single crystal.

Leighton[6] has calculated the elastic spectrum for face-centered cubic crystals and finds that for T less than 4°K, θ for Ag is practically constant at 228°K. This agrees very well with the experimental values, 229°K for the solid line and 230°K for the dashed line, and with the value $\theta(E)=233$°K calculated from elastic constants[7] by the method of Hopf and Lechner.[8] It is therefore unlikely[4] that deviations from the Debye vibration spectrum due to the nature of the Ag lattice itself are responsible for the anomaly.

It seems reasonable to interpret the behavior shown in Fig. 1 as a change in γ, the coefficient of the linear term, occurring between 2.2°K and 2.5°K, with the cubic term remaining constant. A general expression for γ per mole is[9]

$$\gamma = (\pi^2k^2/3)Vf(\zeta), \quad (3)$$

where k is Boltzmann's constant, V is the atomic volume, and $f(\zeta)$ is the density of electronic states at the Fermi level. An increase in γ could correspond to an increase in $f(\zeta)$. This increase could come about as a result of overlapping of allowed bands, and the position of the overlap and the density of levels in the higher band should be derivable from the observed increase in γ (21 percent) and the temperature at which it occurs. Unfortunately, however, no detailed calculation of the band structure of Ag on the basis of electronic wave functions is available for comparison. If such a calculation were made, it would be of great interest to compare the electronic heat capacity predicted from it with our experimental results.

* Work performed under contract with the Signal Corps.

[1] W. K. Keesom and J. A. Kok, Commun. Kamerlingh Onnes Laboratory, University of Leiden, No. 219d (1932); No. 232d (1933).

[2] The single crystal weighed about 90 grams and was kindly supplied to K. Lark-Horovitz by Dr. R. Maddin of The Johns Hopkins University.

[3] A. N. Gerritsen and J. Korringa, Phys. Rev. **84**, 604 (1951).

[4] W. Schottky, Physik. Z. **23**, 448 (1922).

[5] E. Katz, J. Chem. Phys. **19**, 488 (1951).

[6] R. B. Leighton, Revs. Modern Phys. **20**, 165 (1948).

[7] Landoldt-Bornstein, *Physikalisch-Chemische Tabellen* (Verlag Julius Springer, Berlin, 1927), fifth edition.

[8] L. Hopf and G. Lechner, Verhandl. deut. physik. Ges. **16**, 643 (1914).

[9] F. Seitz, *The Modern Theory of Solids* (McGraw-Hill Book Company, Inc., New York, 1940), pp. 150–151.

A Further Test of the Shell Model*

J. S. KING AND W. C. PARKINSON
H. M. Randall Laboratory of Physics, University of Michigan, Ann Arbor, Michigan

(Received August 15, 1952)

As an additional test of the accuracy of the shell model in ascribing definite orbital angular momentum states to nucleons in a nucleus[1,2] we have measured the angular distribution of the protons associated with the ground state in the reaction $Cl^{35}(d, p)Cl^{36}$. As pointed out by Bethe and Butler, the selection

rules for this reaction allow the neutron to carry into the residual nucleus an orbital angular momentum of 0, 2, or 4 units, while the shell model requires that $l_n=2$, corresponding to the addition of a $d_{3/2}$ neutron to the configuration of Cl^{35}.

The experimental data are plotted in Fig. 1 along with the angular distribution of the protons predicted by the Butler[3]

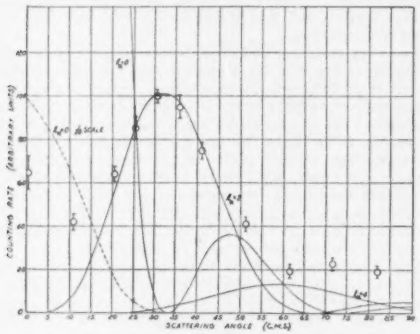

FIG. 1. The angular distribution of the protons associated with the ground state for the reaction $Cl^{35}(d, p)Cl^{36}$. The solid curves are calculated from the Butler theory.

theory for values of $l_n=0$, 2, and 4. The theoretical curves were computed using values of $r_0=5.5\times10^{-13}$ cm, $a=0.23\times10^{13}$ cm^{-1}, and $b=1.4\times10^{13}$ cm^{-1}. The incident deuteron energy was 6.90 Mev (c.m. system) and the Q of the reaction was measured to be 6.3 Mev in good agreement with Shrader and Pollard[4] and with Ennis.[5]

The target, a foil of silver chloride 0.0003 inch thick, was rolled from a pure silver chloride crystal. The background counting rate was obtained by substituting for the silver chloride target a foil of pure silver containing very nearly the same amount of silver per square centimeter as that of the target. It was negligible at all angles except 0°, where it accounted for 35 percent of the total counting rate. In Fig. 1 the vertical lines through the experimental points represent the standard deviations as determined from the

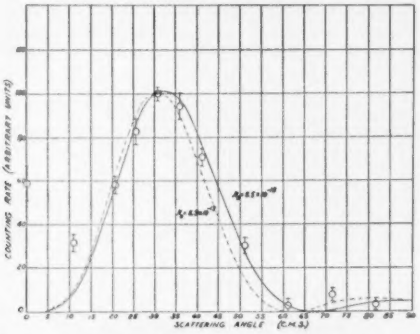

FIG. 2. The angular distribution of Fig. 1 replotted after subtracting from each point the constant "background" counting rate at 65°. The solid curves are calculated from the Butler theory for two values of r_0.

total number of counts and do not represent the over-all uncertainty of the data.

Although (d, p) reactions proceed mainly by means of a stripping process, other processes, such as compound nucleus formation, offer competition. These, however, do not show such marked angular dependence.[6] Because of the competitive processes the measured values do not become zero where indicated by the Butler curves. Since it is difficult to obtain a reliable estimate of the relative cross sections, we subtracted from each point of Fig. 1 an amount equal to the counting rate at 65° and replotted the renormalized data in Fig. 2. The theoretical curves for $l_n=2$ for two values of r_0 are included. Much better agreement is obtained for angles of 20° and larger.

The results of the measurement indicate that the neutron carries mainly two units of orbital angular momentum into the residual nucleus and is presumably a $d_{3/2}$ nucleon as required by the shell model. Assuming that the ground state is a single level (there is some evidence of a doublet structure as in the case of P^{32}), the amount of admixture of $l_n=0$ appears to be less than 4 percent. It is difficult to set a limit on the $l_n=4$ admixture, particularly because of the uncertainty in the "background." It is, however, presumably small.

* This work was supported in part by the AEC and the Michigan Memorial Phoenix Project.

[1] H. A. Bethe and S. T. Butler, Phys. Rev. **85**, 1045 (1952).
[2] Parkinson, Beach, and King, Phys. Rev. **87**, 387 (1952).
[3] S. T. Butler, Proc. Roy. Soc. (London) **A208**, 559 (1951).
[4] E. F. Shrader and E. Pollard, Phys. Rev. **59**, 277 (1941).
[5] W. W. Ennis, Phys. Rev. **82**, 304 (1951).
[6] L. Wolfenstein, Phys. Rev. **82**, 690 (1951).

Nuclear Spin of V^{50} by Paramagnetic Resonance*

C. KIKUCHI,† M. H. SIRVETZ, AND V. W. COHEN
Brookhaven National Laboratory, Upton, New York
(Received August 15, 1952)

WE have investigated the hfs in the paramagnetic resonance absorption spectrum of a Tutton salt of vanadium, enriched to 22.83 percent of V^{50}, and find evidence that the spin of V^{50} is 6. This nucleus, consisting of 23 protons and 27 neutrons, was expected on the basis of Nordheim's rule[1] to have a spin of 7, or near this maximum value. Hitchcock[2] has recently made shell-theoretical calculations based on various potential functions and finds that the state $I=6$ lies lowest for a δ-function potential.

The crystals of $V(NH_4)_2(SO_4)_2\cdot6H_2O$ diluted in the corresponding zinc salt were grown from a solution prepared by using 10 mg of V_2O_5 with a V:Zn ratio of about 1.5:100. A sample of V_2O_5 enriched in V^{50} was supplied by the Stable Isotopes Research and Production division of the AEC. Measurements were performed on several specimens, each approximately 5 mm long and 2 mm in diameter, inserted axially into a cylindrical transmission cavity operating in the TE_{011} mode at approximately 23,000 Mc/sec. The rf was kept constant in frequency while the magnetic field was modulated at 60 cps over a range of approximately 80 gauss.

The observed spectrum consisted of 8 strong lines, corresponding to $I(V^{51})=7/2$,[3] and a number of weak components which have been assigned to V^{50}. The intensity ratio of weak to strong lines was approximately 1:5 and their relative splittings 0.39. The spectrum can be calculated from the known g-values[4,5] and isotopic abundance for various V^{50} spin values. Figure 1 shows the spectrum that is expected for $I(V^{50})=6$ and 7. The calculated relative splitting is 0.38 and the intensity ratio, for $I=6$, is 1:5.5.

In all samples used we observed the components corresponding to $-6\leq m\leq6$, excepting those for $m=\pm4$, which, according to

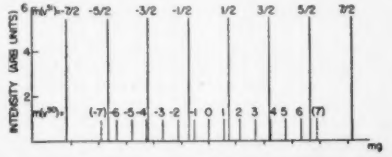

FIG. 1. Theoretical hfs spectrum of V^{50} and V^{51}. The solid V^{50} lines are those to be expected for $I=6$. For $I=7$, the additional dotted lines would appear.

theory, should almost coincide with the strong V^{51} lines. The lines for $m=\pm 7$ were not observed, and considerable effort was directed towards demonstrating that these components would have been observed if present. In Fig. 2(a) we show the lines $m=5/2$ of

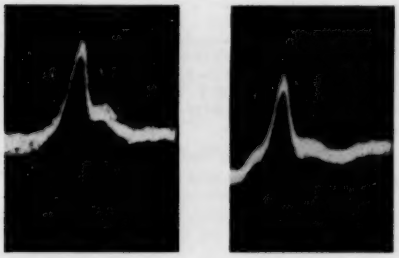

(a) (b)

FIG. 2. Photographs of two sections of spectrum. (a) The line $m=-5/2$ of V^{51} and the satellite $m=-6$ of V^{50}; (b) lines $m=1/2$ of V^{51} and $m=1$ and 2 of V^{50}.

V^{51} and $m=-6$ of V^{50} separated by 20 gauss. Figure 2(b) shows that line $m=+1/2$ of V^{51} with the partially resolved lines $m=+1$ and $+2$ of V^{50}, the measured separations from the main peak being 21 and 14 gauss. Therefore, we conclude that the line for $m=-7$ would have been observed if V^{50} spin were 7. No line attributable to $I>7$ was observed.

* Work done at Brookhaven National Laboratory under the auspices of the AEC.
† On leave from Michigan State College.
[1] L. W. Nordheim, Revs. Modern Phys. **23**, 322 (1951).
[2] A. Hitchcock, Phys. Rev. **87**, 664 (1952).
[3] Bleaney, Ingram, and Scovil, Proc. Phys. Soc. (London) **A64**, 601 (1951); C. A. Hutchison, ONR Technical Report (1951) (unpublished).
[4] W. Knight and V. W. Cohen, Phys. Rev. **76**, 1421 (1949); W. G. Proctor and F. C. Yu, Phys. Rev. **81**, 20 (1951).
[5] Walchli, Leyshon, and Scheitlin, Phys. Rev. **85**, 922 (1952).

High Energy Nuclear Reactions and the Goldberger Model*

J. W. MEADOWS
Cyclotron Laboratory, Harvard University, Cambridge, Massachusetts
(Received August 14, 1952)

ACCORDING to a model first proposed by Serber[1] and developed in greater detail by Goldberger,[2] high energy nuclear reactions are usually considered as occurring in two steps. First, a high energy particle (100 Mev or greater) may pass through a nucleus, perhaps knocking out one or more nucleons and leaving the residual nucleus in an excited state. Second, this excited nucleus may evaporate other nucleons or emit photons according to the statistical theory. If we can determine the probabilities of the various processes in the first step and the distribution of excitation energy in the residual nucleus, it should be possible to apply the statistical theory to calculate reaction cross sections. Estimates for (p, n), $(p, 2n)$, $(p, 2p)$, and (p, pn) reactions for incident protons of 100 Mev have been made in the region of $A=64$.

Reactions of the above types can proceed in one or more of the following ways:

$$\begin{aligned}
&p+A\rightarrow C_1^*+p; && C_1^*\rightarrow B_1+n\\
&\qquad && C_1^*\rightarrow B_2+p\\
&p+A\rightarrow C_2^*+n; && C_2^*\rightarrow B_3+n\\
&\qquad && C_2^*\rightarrow B_1+p\\
&\qquad && C_2^*\rightarrow B_4+\gamma\\
&p+A\rightarrow C_3^*+2p; && C_3^*\rightarrow B_2+\gamma\\
&p+A\rightarrow C_4^*+2n; && C_4^*\rightarrow B_3+\gamma\\
&p+A\rightarrow C_5^*+p+n; && C_5^*\rightarrow B_1+\gamma
\end{aligned}$$

TABLE I. Calculated distribution of various knock-out processes, for 100 incident protons.

Particles ejected	No. of cases
p	11
n	12
$2p$	8
$2n$	5
pn	25

where A is the target nucleus, C^* is the excited residual nucleus, and B is the product nucleus. The contribution from deuteron pick-up is not included, although experiments by Hadley and York[3] indicate that it may be appreciable.

The probabilities of the various initial knock-out processes were calculated on the basis of the model developed by Goldberger.[2] The calculations were performed for $A=64$, $Z=32$, and $R=(1.4\times 10^{-13})A^{\frac{1}{3}}$ cm. The maximum Fermi energy is 24 Mev. If an average binding energy of 8 Mev is assumed, the total well depth is 32 Mev. For protons there is an additional 7 Mev representing the Coulomb barrier. The mean free path as a function of energy was calculated from experimental $n-p$ and $p-p$ cross sections. The value of the $n-n$ cross section used was that obtained from a $n-d$, $n-p$ subtraction by Dejuren and Knable.[4] The calculations followed the technique described by Goldberger[2] and Bernardini *et al.*[6] The results for 100 incident protons applicable to these calculations are shown in Table I and Fig. 1. The secondary evaporation processes were calculated from the statistical theory using constants given by Blatt and Weisskopf.[6]

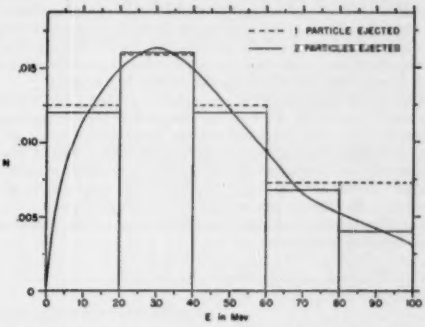

FIG. 1. Distribution of excitation energy in the residual nuclei.

The experimental cross sections were obtained by a previously described method[7] using enriched isotopes[8] in the case of copper and the natural element in the case of zinc. A comparison of the experimental and calculated cross sections is given in Table II.

There are two factors which may account for the discrepancy between the observed and calculated values. (1) At incident proton energies of 25 Mev, where the statistical model alone should account for all reactions, the observed value is twice the calculated value for the p, pn reactions and about one-half the calculated value for the p, $2n$ reactions. (2) The same distribution of the

TABLE II. Comparison of calculated and experimental cross sections.

Reaction	σ in millibarns calc.	expt.
$Cu^{63}(p, pn)Cu^{62}$	23	98
$Cu^{63}(p, 2n)Zn^{62}$	20	7
$Cu^{63}(p, n)Zn^{63}$	6	8
$Cu^{63}(p, pn)Cu^{61}$	34	120
$Zn^{64}(p, 2p)Cu^{63}$	4	14

excitation energy was used in all cases, although here is some indication that the distribution curve should be shifted to lower energies when a single proton is ejected and to higher energies when a neutron is emitted. The statistical accuracy of these calculations is not sufficient to show any definite difference. Since only the lower excitation energies contribute to these reactions, such a change would cause a decrease in the p, n and $p, 2n$ cross sections and an increase in the others.

A more detailed report will be published shortly.

* Assisted by the joint program of the ONR and AEC.
[1] R. Serber, Phys. Rev. **72**, 1114 (1947).
[2] M. L. Goldberger, Phys. Rev. **74**, 1269 (1948).
[3] J. Hadley and H. York, Phys. Rev. **80**, 345 (1950).
[4] J. Dejuren and N. Knable, Phys. Rev. **77**, 606 (1950).
[5] Bernardini, Booth, and Lindenbaum, Phys. Rev. **83**, 669 (1951).
[6] J. M. Blatt and V. F. Weisskopf, Massachusetts Institute of Technology Technical Report No. 42, May 1, 1950 (unpublished).
[7] N. M. Hintz, Phys. Rev. **83**, 185 (1951).
[8] Obtained from Oak Ridge National Laboratory, Oak Ridge, Tennessee.

Nuclear Forces in Pseudoscalar Meson Theory

K. NAKABAYASI AND I. SATO
Physics Institute, Tohoku University, Sendai, Japan
(Received August 1, 1952)

WE have performed a perturbational calculation of nuclear potentials up to the fourth order in coupling constants, assuming pseudoscalar meson theory. In the pseudoscalar theory, the second-order potential is anomalously small, so it is incorrect to discuss the validity of the perturbation theory only by comparing the second order with the fourth order; rather the second plus fourth order should be regarded as the "lowest order."

The fourth-order potentials have been calculated by several authors,[1-4] neglecting, however, nucleon recoil in the intermediate states in spite of its importance in the pseudoscalar theory. We first calculated the fourth-order part of Dyson's S matrix subtracted by the "iteration" of the second-order effective Hamiltonian.[5] Terms of order $(v/c)^2$ relative to the main terms were neglected. But the nucleon recoil in the intermediate states was taken into account correctly. The fourth-order nuclear potential thus obtained is as follows:

$$V_4=\mu(M/\mu)^2\sum_{\rho,\sigma=1}^{4}\beta_\rho\beta_\sigma[\tau_\rho{}^{(1)}\tau_\sigma{}^{(1)}\tau_\rho{}^{(2)}\tau_\sigma{}^{(2)}J_A(\xi) +\tau_\rho{}^{(1)}\tau_\sigma{}^{(1)}\tau_\sigma{}^{(2)}\tau_\rho{}^{(2)}J_B(\xi)], \quad (1)$$

where ξ is the distance between nucleons in units $\hbar/\mu c$. The coupling parameters β_σ and the functions J_A, J_B are given by

$$\beta_\sigma=(f_\sigma{}^2/4\pi)(\mu/2M)^2, \quad \begin{matrix}(\pi/4)J_A=-j_1+j_2,\\ (\pi/4)J_B=2j_3-4j_5,\end{matrix} \quad (2)$$

for the case of pseudoscalar coupling; and

$$\beta_\sigma=f_\sigma{}^2/4\pi, \quad \begin{matrix}(\pi/4)J_A=-2j_1+j_2+4j_3+j_4,\\ (\pi/4)J_B=-j_1+6j_3-j_4-4j_5,\end{matrix} \quad (3)$$

for the case of pseudovector coupling,[6] where

$$\begin{aligned}
&j_1=K_1(2\xi)\xi^{-3},\\
&j_2=(M/\mu)^2\xi^{-1}\int_0^1 du\, u^{-4}[2(\mu/M)^2f^2\\
&\qquad+(1-u^2)^2(1+4u^2+u^4)(1+u^2)^{-2}]K_0(2\xi f),\\
&j_3=(M/\mu)^2\xi^{-1}\int_0^1 du\, u^{-1}(1-u)K_0(2\xi f), \quad (4)\\
&j_4=\xi^{-3}\int_0^1 du\, uf K_1(2\xi f)-2(M/\mu)^2\xi^{-1}\int_0^1 du\, u^{-1}(1-u)^2K_0(2\xi f),\\
&j_5=(M/\mu)^4\int_0^1 du\, u^{-3}(1-u)^2f^{-1}K_1(2\xi f),
\end{aligned}$$

with

$$f=u^{-1}[(M/\mu)^2(1-u)^2+u]^{\frac{1}{2}}.$$

V_4 represents a central force, but contains a charge-exchange part, even for charge symmetrical theory, in contrast with references 1 and 4. Even for pseudovector coupling, no tensor force appears in V_4, in contrast with references 2 and 3. j_2, which is essentially a recoil effect and has hitherto been overlooked, has the strongest singularity ($\sim\xi^{-5}$), and the isotopic spin operator multiplied by J_A in V_4 takes always positive values. Therefore, V_4 is always strongly repulsive at small distances, so that the singularity of the second-order tensor potential becomes completely of no effect. Furthermore, the "hard core" character of V_4 ensures the saturation property of nuclear forces.

For pseudoscalar coupling, the adiabatic approximation corresponds to making $M/\mu\to\infty$ in j_i. Then, j_2 and j_4 tend to zero, while both j_3 and j_5 approach $(2/\pi)K_1(2\xi)\xi^{-3}$. For charge symmetrical theory, we thus have

$$V_4{}^{\text{ad}}=-(3/2\pi)\mu(f^2/4\pi)^2(\mu/M)^2\xi^{-2}K_1(2\xi), \quad (5)$$

in agreement with Lévy's result[4] in the same approximation.

Taking, e.g., the symmetrical theory and $\beta=0.089$, the potentials (including the second-order ones) in even states are plotted in Fig. 1. For pseudovector coupling, the too strong repulsive central

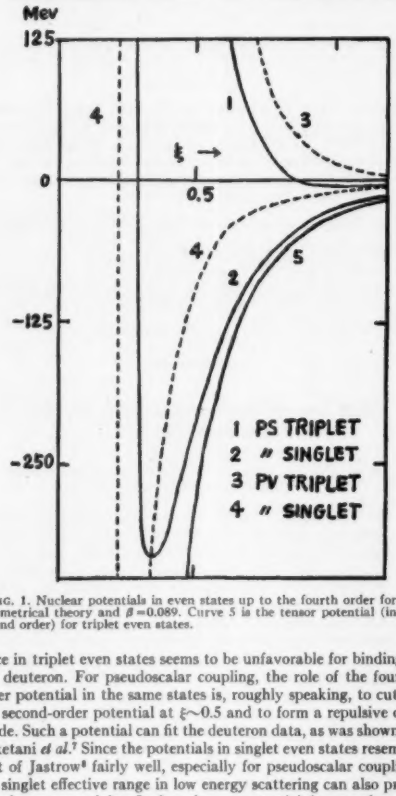

FIG. 1. Nuclear potentials in even states up to the fourth order for the symmetrical theory and $\beta=0.089$. Curve 5 is the tensor potential (in the second order) for triplet even states.

force in triplet even states seems to be unfavorable for binding of the deuteron. For pseudoscalar coupling, the role of the fourth-order potential in the same states is, roughly speaking, to cut off the second-order potential at $\xi\sim0.5$ and to form a repulsive core inside. Such a potential can fit the deuteron data, as was shown by Taketani *et al.*[7] Since the potentials in singlet even states resemble that of Jastrow[8] fairly well, especially for pseudoscalar coupling, the singlet effective range in low energy scattering can also probably be accounted for. In fact, in our potential for pseudoscalar coupling, which approximates $-375\exp(-4.05\xi+1.4)$ Mev for $0.4\lesssim\xi\lesssim1.0$, the well depth is shallower, but the well range, as well as the core radius, is shorter instead.[8] For pseudovector coupling, our potential seems to have too small a core radius.

In triplet odd states, besides the strong tensor repulsion, there acts a central potential similar to that in singlet even states. On

the other hand, a repulsive force acts in singlet odd states. These central forces in odd states are in marked contrast with the Serber potential.[10] For high energy scattering, these circumstances require further study.

A full report and more detailed discussion will be puslished soon by one of us.

[1] K. M. Watson and J. V. Lepore, Phys. Rev. **76**, 1157 (1949).
[2] K. Nishijima, Prog. Theoret. Phys. **6**, 801, 911 (1951).
[3] Taketani, Machida, and Onuma, Prog. Theoret. Phys. **6**, 638 (1951).
[4] M. Lévy, Compt. rend. **234**, 1671 (1952).
[5] Y. Nambu [Prog. Theoret. Phys. **5**, 614 (1950)] has also referred to this point. In reference 1, the subtraction of the iteration was not taken into account.
[6] Unrenormalizable divergent integrals in the fourth-order S matrix for pseudovector coupling are of the form

$$\int d^4x \Big[A\bar{\psi}(x)\psi(x)\bar{\psi}(x)\psi(x)+B\bar{\psi}(x)\gamma_\mu\psi(x)\bar{\psi}(x)\gamma_\mu\psi(x) + C\frac{\partial}{\partial x_\mu}(\bar{\psi}(x)\gamma_\mu\psi(x))\frac{\partial}{\partial x_\mu}(\bar{\psi}(x)\gamma_\mu\psi(x))\Big],$$

where A, B, and C are divergent constants, so they do not contribute to the potential for finite distances and were omitted. The iteration of the second-order effective Hamiltonian is divergent in momentum space even for pseudoscalar coupling, owing to the strong singularity in the second-order potential, but converges in configuration space for both couplings. The strong repulsive core arises from this subtracted iteration. One part of this, which appears only for pseudovector coupling, has been neglected in (3), since its effect is only to make the core somewhat harder.
[7] Taketani, Machida, and Onuma, Prog. Theoret. Phys. **7**, 45 (1952).
[8] R. Jastrow, Phys. Rev. **81**, 165 (1950).
[9] J. M. Blatt and J. D. Jackson, Phys. Rev. **76**, 18 (1949).
[10] R. S. Christian and E. W. Hart, Phys. Rev. **77**, 441 (1950); R. S. Christian and H. P. Noyes, Phys. Rev. **79**, 85 (1950).

Comparison of Electron Density in Different Regions of a dc Glow Discharge*

BURTON J. UDELSON AND JOHN E. CREEDON
National Bureau of Standards, Washington, D. C.
(Received May 27, 1952)

PRELIMINARY investigations of the relative densities of the various regions of a hydrogen dc glow discharge have been made using microwave techniques.

From theoretical considerations of a microwave cavity in which a conducting medium is present, it can be shown that the real and imaginary components of the complex conductivity of the medium are proportional, respectively, to the change of conductivity Δg and the shift of resonant frequency Δf of the cavity caused by the presence of this conducting medium in the cavity.[1] For an undercoupled cavity in which the coupling section from the wave guide to the cavity is assumed to be lossless, the conductivity of the cavity is equal to the VSWR measured at resonance.

In gas discharges in which the collision frequency is assumed to be independent of electron energy, it has been shown by Everhart and Brown,[2] on the basis of work done by Margenau,[3] that the real and imaginary components of complex conductivity are both proportional to the electron density. The assumption that the collision frequency is independent of electron energy holds well in a hydrogen discharge.[4] Thus, by placing a hydrogen gas discharge in the field of a microwave cavity, measurements of Δg and Δf using standard microwave techniques will determine the relative electron density of the discharge.

An S-band microwave re-entrant cavity was designed such that there was a small cylindrical hole through the center of the cones of the cavity, so that a thin discharge tube could be inserted into the cavity. The rf field of the cavity couples through the glass walls of the discharge tube to whichever region of the dc discharge is located in the 0.040-in. gap between the cones of the cavity. The glass walls of the discharge tube have no effect on the microwave field except to add to the dielectric loss of the cavity. By manipulating the discharge tube back and forth, a detailed examination of the relative electron density distribution along the length of the hydrogen dc glow discharge tube is possible. In making these measurements, the strength of the microwave field must be sufficiently small so that it does not change the nature of the dc discharge.

Δg and Δf are determined by placing a discharge tube in the S-band cavity and measuring the change of conductivity and shift of resonant frequency of the cavity caused by operation of the dc discharge. The values of Δg and Δf, both proportional to electron density, are plotted in Fig. 1 as a function of the position of hydrogen dc discharge in the S-band cavity. The hydrogen discharge tube was filled with 14 mm Hg and operated at a current of 1.0 ma. Unfortunately, owing to an oversight, no measurements were made in the negative glow proper. It can be seen from Fig. 1 that:

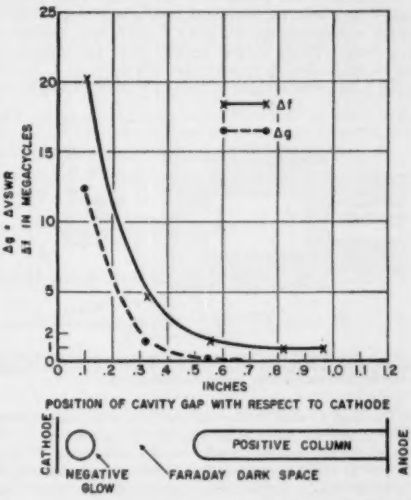

FIG. 1. Change of resonant frequency (Δf) and of conductivity (Δg) of an S-band cavity as a function of the region of a dc hydrogen discharge exposed to the rf field of the cavity gap. Frequency = 2962 Mc; gap height = 0.040 inch; gas pressure = 14 mm Hg; tube current = 1.0 ma; tube voltage = 945 volts; tube diameter = 0.18 inch I.d.

1. The electron density along the length of the nonstriated positive column is a constant.

2. The electron density adjacent to the negative glow is greater than that in the positive column by a factor of about 20.

3. The Faraday dark space is effectively a transition region between the negative glow and the positive column.

Measurements of the proportionality factors between Δg and Δf and the real and imaginary components of the complex conductivity are being undertaken, so that a determination of the absolute values of electron density in the different regions of dc discharges will be possible.

* Sponsored by Bureau of Ships, Navy Department.
[1] J. C. Slater, Revs. Modern Phys. **18**, 473 (1946).
[2] E. Everhart and S. C. Brown, Phys. Rev. **76**, 840 (1949).
[3] H. Margenau, Phys. Rev. **69**, 508 (1946).
[4] R. B. Brode, Revs. Modern Phys. **5**, 257 (1933).

Neutrons Produced in the Absorption of Negative π-Mesons at Rest*

V. COCCONI TONGIORGI AND D. A. EDWARDS
Cornell University, Ithaca, New York
(Received August 11, 1952)

THE process of absorption of negative π-mesons at rest has been discussed by several authors, and the charged particles produced have been extensively investigated in photographic plates.[1] The present experiment was performed to obtain information concerning the neutrons produced in this process. Since our

apparatus would detect efficiently only neutrons with energies between about 0.5 and 15 Mev, the results refer to the knock-on and evaporation neutrons lying in this range and exclude neutrons of higher energies which may be produced in the absorption mechanism.

The π-mesons were produced by the 315-Mev bremsstrahlung beam of the Cornell synchrotron incident on a Be target. Negative mesons, with energies between about 30 and 75 Mev, were selected by a double-focusing magnet system.[2] After the magnets, the mesons passed through three trays of GM counters, A, B, and C in Fig. 1, and were brought to rest in the absorber Σ, which was

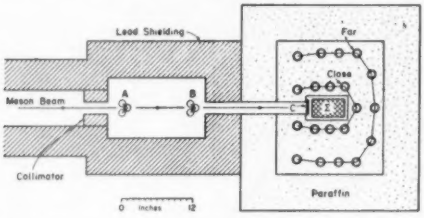

FIG. 1. Side view of the experimental arrangement. A, B, and C are GM counters; Close and Far are groups of BF_3 proportional counters connected in parallel. Σ is the absorber in which π-mesons stop.

thick enough to stop 90-Mev mesons. Neutrons emitted from Σ following the absorption of the meson by a nucleus were thermalized by the surrounding paraffin (total volume about 3 ft×3 ft ×2.5 ft) in which were embedded 20 BF_3 proportional counters. The counters were divided into two groups, designated as "Close" and "Far," and the counters of each group were connected in parallel. About 2 Mev and 10 Mev were needed for neutrons to reach counters "Close" and "Far," respectively.

Coincidences $A+B+C$ triggered the sweep of a cathode-ray tube gated to have a length of 600 μsec, spread over a path of 60 cm. The amplified pulses of the neutron counters were applied to the deflecting plates of the CRT in such a fashion that counters "Close" and "Far" produced pulses of opposite sign. A camera, triggered by $A+B+C$, took pictures of the sweep.

The experiment was run at a beam intensity sufficiently low for the neutron background to be smaller than 5 percent. The background was estimated by analyzing the distribution in time of the neutrons appearing on the 600-μsec sweep, using the experimental information that the neutron lifetime in the detector was (150±5) μsec. The estimate of the background was found in agreement with the results obtained in 500 pictures taken with the magnets set to select positive mesons.

The contamination of the π-meson beam by μ-meson, resulting from the decay in flight of the π's, was estimated to be not larger than 4 percent; our results have been corrected accordingly, using the results of Widgoff for neutrons produced by μ-meson absorption.[3]

The results are listed in Table I. The first five rows give the corrected numbers of pictures in which n neutrons were observed. The efficiencies ϵ of the apparatus for detecting each neutron were determined with a RaαBe source placed at various points in the absorbers Σ. The largest uncertainty in these determinations arises from the fact that the energy spectra of the neutrons emitted by the various absorbers will in general differ from the spectrum of the RaαBe source. The values of the ratios of the recorded rates "Close" and "Far" are given as an indication of the relative hardness of the neutron spectra in the various absorbers. With the RaαBe source located in the absorbers, such ratios were between 4.5 and 5. Therefore, the efficiencies listed for Pb and Sn are underestimates, and those for Al and C overestimates. In row 8 are given the average numbers $\langle\nu\rangle$ of neutrons with $E<\sim$15 Mev emitted per π-meson absorbed; i.e., $\langle\nu\rangle=\langle n\rangle/\epsilon$. The errors given are statistical only. The spread in the distribution of the ν's around $\langle\nu\rangle$ is given by the standard deviation σ computed according to

$$\sigma^2=\langle\nu^2\rangle-\langle\nu\rangle^2=[\langle n^2\rangle-\langle n\rangle^2-\langle n\rangle(1-\epsilon)]/\epsilon^2.$$

For comparison, in row 10 are given the average numbers of neutrons $\langle\nu_\mu\rangle$ produced by absorption of a negative μ-meson.[3]

The present data support the interpretation that the starless meson tracks observed in plates (about 30 percent of all meson tracks ending in the emulsion) are associated with emission of neutrons only. By interpolating our data to $A=100$, one gets $\langle\nu\rangle=5.2\pm0.4$ and $\sigma\approx2$, which is not inconsistent with the data obtained from plates and with calculations of LeCouteur[4] ($\langle\nu\rangle=4.5$ and $\sigma=1.9$) and with recent detailed calculations of Puppi *et al.*[5] ($\langle\nu\rangle\approx5$). The energy spectrum of the neutrons as calculated in reference 5 is also not inconsistent with the recorded ratio Close/Far.

TABLE I. Data on neutrons produced by various nuclei in the absorption of negative mesons at rest.

		Pb	Sn	Al	C
1.	$n=0$	484	425	950	1128
2.	$n=1$	234	150	125	128
3.	$n=2$	78	36	6	4
4.	$n=3$	21	3	1	1
5.	$n=4$	5	0	0	0
6.	$\epsilon(\%)$	6.2	6.3	6.5	7.0
7.	Close/Far	7.8±1.1	6.0±1.1	3.5±0.7	3.2±0.6
8.	$\langle\nu\rangle$	9.3±0.5	6.1±0.4	2.0±0.2	1.6±0.2
9.	σ	5.5±0.8	2.3±1.0	1.4±0.5	1.2±0.5
10.	$\langle\nu_\mu\rangle$	2.1±0.2	1.5±0.2	0.9±0.2	···

* Work supported by the ONR.

[1] E.g., see bibliography quoted in: R. E. Marshak, *Meson Physics* (McGraw-Hill Book Company, Inc. New York, to be published).
[2] M. Carmac, Rev. Sci. Instr. **22**, 197 (1951).
[3] M. Widgoff, Ph.D. thesis, Cornell University, 1952 (unpublished).
[4] K. J. LeCouteur (private communication).
[5] Puppi, De Sabbata, and Manaresi (private communication).

Magnetic Double Refraction at Microwave Frequencies

M. T. WEISS AND A. G. FOX
Bell Telephone Laboratories, Holmdel, New Jersey
(Received August 12, 1952)

WE have recently observed a magnetic double refraction effect at microwave frequencies similar to the well-known Voigt and Cotton-Mouton effects at optical frequencies. This magnetic double refraction was evidenced by a conversion from linear to elliptical polarization of a dominant TE wave in a section of circular wave guide filled with ferrite and subjected to a dc magnetic field H_0 transverse to the direction of propagation and at 45° to the input polarization.

This double refraction is to be explained by the difference between the rf permeabilities of the medium along the dc field $\mu_\parallel$ and at right angles to the dc field $\mu_\perp$. In order to compute these permeabilities we shall make the simplifying assumption that we are dealing with a uniform TEM wave in an infinite medium of ferrite. It is believed that the results should apply rather closely for the wave-guide case, just as the analysis for the infinite plane wave Faraday effect applies fairly closely to wave guides, as found by Hogan.[1] Furthermore, it is assumed that the ferrite is saturated and has no magnetic losses.

For the above conditions, the wave whose magnetic vector is parallel to H_0 sees a relative permeability of one, independent of the magnitude of H_0. However, an rf magnetic vector $H_\perp$ perpendicular to H_0 sees a permeability $\mu_\perp$, which depends on the magnitude of H_0 as shown in the ferromagnetic resonance papers of Kittel.[2] This dependence is caused by the uncompensated electron spins in the ferrite, which are oriented by H_0 and have a natural precession frequency given by $\omega_0=\gamma H_0$, where γ is the spectroscopic splitting factor.

In order to calculate the permeability for the rf $H_\perp$, we decompose the $H_\perp$ into two circularly polarized components whose permeabilities are shown by Polder[2] to be, (in rationalized units)

$$\mu_+/\mu_0 = 1+\gamma M/(\omega_0-\omega),$$
$$\mu_-/\mu_0 = 1+\gamma M/(\omega_0+\omega), \quad (1)$$

where M is the saturation magnetization of the sample and ω is the operating frequency. Knowing μ_+ and μ_-, it can be shown that the effective $\mu_\perp$ is given by[3]

$$\mu_\perp = \frac{2\mu_+\mu_-}{\mu_++\mu_-} = \left[1+\frac{\gamma M\omega_0+\gamma^2M^2}{(\omega_0^2-\omega^2)+\gamma M\omega_0}\right]\mu_0. \quad (2)$$

It is interesting to note that $\mu_\perp$ becomes infinite, not when $\omega=\omega_0=\gamma H_0$ as for an infinite medium magnetized in the direction of propagation, but when $\omega=\omega_0(1+\gamma M/\omega_0)^{\frac{1}{2}}$. Thus, the maximum magnetic displacement in the medium will occur at different frequencies depending upon the direction of the dc magnetic field relative to the field vectors of the wave.[3] This is due to the fact that for a uniform plane wave there is no rf B in the direction of propagation as can be seen from Maxwell's curl equation. The electrons therefore experience a restraint from turning their spin axes in a longitudinal direction, since there will be an rf H along the z axis opposing their alignment in this direction. This restraint is equivalent to a demagnetizing force which raises the resonant frequency. No such restraint to electron precession exists when the H_0 is in the direction of propagation.

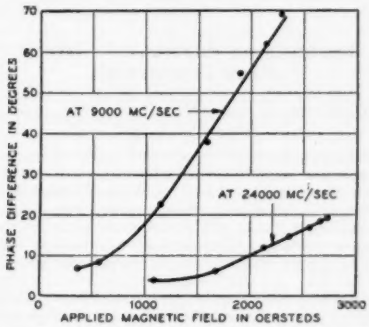

FIG. 1. Phase difference as a function of applied magnetic field, at 24,000 Mc/sec and 9000 Mc/sec.

If ω is much higher than the resonance frequency, so that ω_0^2 and $M\gamma\omega_0$ can be neglected compared to ω^2, the above equation can be simplified to

$$\mu_\perp = [1-(\gamma M\omega_0+\gamma^2M^2)/\omega^2]\mu_0. \quad (3)$$

The relative phase retardation of the wave with its magnetic vector parallel to H_0, with respect to the wave whose magnetic vector is perpendicular to H_0, is therefore given by

$$\theta_\gamma = 2\pi l\left(\frac{1}{\lambda_{11}}-\frac{1}{\lambda_\perp}\right) = \frac{l(\epsilon\mu_0)^{\frac{1}{2}}}{2}\left[\frac{\gamma^2M^2}{\omega}+\frac{\gamma^2MH_0}{\omega}\right]. \quad (4)$$

This is to be compared to the Faraday rotation angle given by Hogan:[1]

$$\theta_F = \tfrac{1}{2}l(\epsilon\mu_0)^{\frac{1}{2}}[\gamma M]. \quad (5)$$

It is thus seen that far above resonance, the double refraction effect will be much smaller than the Faraday rotation and will be inversely proportional to frequency. It is also to be noted that the relative phase retardation is a linear function of the applied steady magnetic field after the material is saturated, unlike the Voigt and Cotton-Mouton effects which are quadratic functions of the magnetic field, since these latter deal with nonsaturable materials.

In the experimental setup to check the above relations, the ferrite sample is placed in a dominant mode circular wave guide with reflections eliminated by proper tapering and with cross polarizing absorbers used to prevent cross-polarized reflections from the rectangular guide ends. The transverse magnetic field is applied at 45° to the rf E vector. The phase difference is measured by noting the ellipticity of the output with linearly polarized input. The results for measurements made at 24,000 Mc/sec and at 9000 Mc/sec are shown in Fig. 1. The measurements at these two frequencies were made with the same type of ferrite but with somewhat different geometrical shapes. From the results one notes that the phase difference is a linear function of the magnetic field over the high field range and that the effect is much smaller at the higher frequencies as predicted by the above analysis.

[1] C. L. Hogan, Bell System Tech. J. 31, 1 (1952).
[2] C. Kittel, Phys. Rev. 71, 270 (1947).
[3] D. Polder, Phil. Mag. 40, 99 (1949).

Internal Conversion of the Sr^{88} Gamma-Rays*

F. R. METZGER† AND H. C. AMACHER
Physics Department, University of Illinois, Urbana, Illinois
(Received August 14, 1952)

WHEN investigating the decay of 105-day Y^{88}, Peacock and Jones[1] determined the internal conversion coefficients of the 0.9- and 1.85-Mev Sr^{88} gamma-rays as 2.7×10^{-4} and 1.3×10^{-4}, respectively. Using the theoretical data then available, these authors characterize the 1.85-Mev transition as electric dipole, the 0.9-Mev transition as magnetic dipole. Ling and Falkoff[2] based their analysis of the angular correlation data[3] on this assignment and showed that the spin combination 2–1–0 with a mixture of $E2$ and $M1$ for the 900-kev transition fits the experimental results.

Recently Bunker, Langer, and Moffat[4] found that the disintegration of Rb^{88} leads to the same levels in Sr^{88}. They assigned even parity to all the levels in Sr^{88}, discarding the conversion experiments.

In view of this disagreement we decided to reinvestigate the internal conversion of the Sr^{88} gamma-rays. This seemed the more important, as at least one experiment had indicated an electric dipole transition which is a type of transition rarely found in radioactive decays.

Using a Y^{88} source obtained from the MIT cyclotron group,[5] we compared with a lens spectrometer of 2.5 percent resolution the internal conversion electron peaks with the photoelectron peaks from a gold converter of known efficiency. In Table I the experimental conversion coefficients are compared with the theoretical values of Rose *et al.*[6] The agreement between the two experiments is satisfactory. The conversion coefficients characterize the 900-kev transitions as $E1$, the 1.85-Mev transition as $M1$ or $E2$.

TABLE I. Internal conversion coefficients of the Sr^{88} gamma-rays. The experimental values are total conversion coefficients, the theoretical values K-conversion coefficients.

	Experiment α		Theory α_K			
	Peacock and Jones	This paper	$E1$	$E2$	$M1$	$M2$
$10^4\times\alpha_K$ (0.9 Mev)	27	34±7	28	68	66	165
$10^4\times\alpha_K$ (1.85 Mev)	13	17±4	7.8	15	15.5	29

For the explanation of the angular correlation experiments one is now faced with the necessity of having to mix $E1$ and $M2$. If such a mixture occurs, it provides us with information concerning the reduction of the $E1$ matrix element. However, before this question can be decided, better angular correlation data are necessary.

It might turn out that the first excited state of Sr^{88} has spin 2, even parity in accordance with the Goldhaber-Sunyar rule.[7] This would remove the last[8] of the four even-even nuclei with spin one in the first excited state which were quoted by Goldhaber and Sunyar[7] as exceptions to their rule.

* Supported in part by the joint program of the AEC and ONR.
† Now with the Bartol Research Foundation, Swarthmore, Pennsylvania.
[1] W. C. Peacock and J. W. Jones, AEC Report AECD 1812 (unpublished).
[2] D. S. Ling and D. L. Falkoff, Phys. Rev. **76**, 1639 (1949).
[3] E. L. Brady and M. Deutsch, Phys. Rev. **74**, 1541 (1948).
[4] Bunker, Langer, and Moffat, Phys. Rev. **81**, 30 (1951).
[5] The authors are grateful to Professor M. Deutsch and Mr. T. R. Bulkley of the MIT radioactivity group for their kind cooperation.
[6] Rose, Goertzel, and Perry, Oak Ridge National Laboratory Report ORNL 1023 (unpublished).
[7] M. Goldhaber and A. W. Sunyar, Phys. Rev. **83**, 906 (1951).
[8] Mo^{98}, Te^{124}, and Hg^{198} all have spin 2, even and not spin 1, odd. See P. Preiswerk and P. Staehelin, Helv. Phys. Acta **24**, 300 (1951); P. Staehelin, Phys. Rev. **87**, 374 (1952); and F. R. Metzger, Phys. Rev. **83**, 842 (1951); **86**, 435 (1952).

A Variational Method for Radiationless Transitions

B. H. Bransden and A. Dalgarno
Department of Physics and Department of Applied Mathematics, Queen's University of Belfast, Belfast, Northern Ireland
(Received July 11, 1952)

RADIATIONLESS transitions are usually formulated by means of a time independent perturbation theory. Since the initial state is unstable, the corresponding wave function may be written as a sum of terms, several of which are not closed. The system formed is, therefore, analogous to a "collision complex" whose break-up may be described by a time independent theory.

Consider, in particular, the auto-ionization of an excited atomic system. Suppose $\Psi_i(1\cdots n)$ is a properly antisymmetrical closed wave function, normalized to unity, and $\Psi_f(1\cdots n)$ is a wave function describing the final (unbound) state for which the transition probability is required. Then, if only these two terms are included, the total wave function Ψ corresponding to an energy E may be written as the linear combination

$$\Psi = c\Psi_i + d\Psi_f,$$

where the correct Ψ satisfies the appropriate Schrödinger equation

$$(H-E)\Psi = 0;$$

c, d are constants and $\Psi_f \sim \chi(2\cdots n)\phi(1)\,\sigma(1\cdots n)$, where $\chi(2\cdots n)$ is the core wave function $\sigma(1\cdots n)$ the spin wave function for the whole system, and $\phi(1)$ represents an outgoing spherical wave

$$\phi(1) = r_1^{-1}\exp[i(kr_1 - \alpha\log 2kr_1)]P_l(\cos\theta).$$

Ψ_f may be normalized so that

$$\int \Psi_f^*(k')\Psi_f(k)\,d\tau = \frac{4\pi^2}{(2l+1)}\delta(k-k'),$$

so that the constants c, d are related to P, the probability of auto-ionization per atom per unit time, by the equation

$$P = \frac{\hbar}{2m}\frac{8\pi}{(2l+1)}k\left|\frac{d}{c}\right|^2\left(1+\left|\frac{d}{c}\right|^2\right)^{-1}.$$

The variational methods developed by Hulthén[1] and Kohn[2] for collision problems may be extended for the computation of the ratio d/c and hence P. Using the notation of Kato,[3] we define

$$L \equiv H - E,$$

and Ψ_t, a trial wave function depending on p constants a_m, the final state wave function having the same boundary conditions as Ψ_f with the exception that d_t replaces d.

It follows that, if $\omega \equiv \Psi_t - \Psi$,

$$I(a_m, d_t) \equiv \sum_{\text{spin}} \int \Psi_t^* L[\Psi_t]\,d\tau$$

$$= -\frac{\hbar^2}{2m}(8\pi ik)d^*(d-d_t) + \sum_{\text{spin}} \int \omega^* L[\omega]\,d\tau.$$

This is the finite form of the usual variational equation, the integral on the right-hand side being of the order ω^2.

Following Hulthén, we may require $d_t - d \to 0$ and then the best function $\Psi_t(a_m, d_t)$, of the trial form chosen, and the best value of $|d/c|$ may be found from the equations

$$I(a_m, d_t) = 0,$$
$$\partial I/\partial a_m = 0, \qquad m = 1, 2, \cdots p,$$

which (as d_t, a_m need not be real) are $(2p+2)$ in number.

Kohn's method may also be applied, leading to the equations

$$\partial I/\partial a_m = 0, \quad m = 1, 2, \cdots p,$$

$$\partial I/\partial d_t = \frac{\hbar^2}{2m}\frac{8\pi ik}{(2l+1)}d^*,$$

$$d^*d = d_t^* d_t - \frac{2m}{\hbar^2}\frac{(2l+1)}{8\pi ik}I.$$

A comparison of these variational methods and the usual perturbation treatment is being carried out for a number of auto-ionizations undergone by helium.

The authors wish to thank Professor D. R. Bates for his interest in the problem.

[1] L. Hulthén, Kgl. fysiograf. Sällskap. Lund, Förh. **14**, No. 21 (1944).
[2] W. Kohn, Phys. Rev. **74**, 1763 (1948).
[3] T. Kato, Prog. Theoret. Phys. **6**, 394 (1951).

The Minimum of Electrical Resistance at Low Temperatures

D. K. C. MacDonald
Division of Physics, National Research Council, Ottawa, Canada
(Received July 10, 1952)

THE initial discovery[1,2] of a resistance minimum at low temperatures in gold has been followed since the war by increasing interest in the analogous phenomenon in other metals.[3-7] An extended investigation has been in progress over the past two years on alloys of Cu, Ag, and Au, and some aspects have already been reported.[8] More recently particular attention has been paid to a very characteristic minimum in Cu occurring generally at about 10.5°K.

The following conclusions have now been definitely established through experiments on a rather wide range of alloys specially prepared from spectrographically pure metals. As solute, elements were chosen which tend to occur as traces in very pure samples of the parent.

(1) Pure copper and gold as parent metals do not exhibit the characteristic minimum.

(2) A variety of different solute elements when alloyed with the parent metal are capable of producing the minimum.

(3) The initial introduction of an effective "impurity" causes characteristic general scattering and a proportionately increasing resistive minimum together with a corresponding rise in the temperature of the minimum. The second effect, however, "saturates" very rapidly as the appropriate concentration (in the order of $<10^{-2}$ atomic percent to 10^{-1} percent dependent on solute and solvent) is approached. Thereafter the only further effect is to provide additional random scattering while both the magnitude and location of the minimum stay constant.

(4) In particular, it has been established in the case of copper-rich alloys that: (a) oxygen, silver, and nickel as solutes do not produce the minimum; (b) tin (which enters into homogeneous solid solution) and (c) carbon, lead, and bismuth (which at best have very small solid solubility) all produce the minimum.

(5) Also in the case of copper-rich alloys, very dilute ternary solutions of carbon and tin can almost annul the minimum over a short range of solute concentration. At the same time, anomalous behavior is observed in the over-all residual resistance.[8] (See following letter.)

Previous theoretical proposals[9-11] to account for the general minimum phenomenon appear to be inadequate when considered in the light of these results.

I am grateful to Dr. W. B. Pearson for much help in the preparation of the copper alloys.

[1] de Haas, de Boer, and van der Berg, Physica **1**, 1115 (1933).
[2] D. J. van der Berg, thesis, Leiden (1938)(unpublished).
[3] D. K. C. MacDonald and K. Mendelssohn, Proc. Roy. Soc. (London) **A202**, 523 (1950).
[4] A. N. Gerritsen and J. O. Linde, Physica **17**, 573, 584 (1951).
[5] E. Mendoza and J. G. Thomas, Phil. Mag. **42**, 291 (1951); Proc. Intern. Conf. on Low Temp. Phys., Oxford, 1951, p. 39 (unpublished).
[6] I. M. Templeton and D. K. C. MacDonald, Phil. Mag. **42**, 432 (1951); D. K. C. MacDonald, Proc. Intern. Conf. on Low Temp. Phys., Oxford, 1951, p. 58 (unpublished).
[7] H. E. Rorschach and M. A. Herlin, Phys. Rev. **81**, 467 (1951).
[8] D. K. C. MacDonald and W. Pearson, Phys. Rev. **88**, 149(L) (1952).
[9] J. C. Slater, Phys. Rev. **84**, 179 (1951).
[10] D. K. C. MacDonald, Phil. Mag. **42**, 756 (1951).
[11] A. N. Gerritsen and J. Korringa, Phys. Rev. **84**, 604 (1951).

Residual Resistance in Dilute Copper Alloys

D. K. C. MacDonald and W. B. Pearson
Division of Physics, National Research Council, Ottawa, Canada
(Received July 10, 1952)

EXAMINATION of the resistance minimum occurring at ~10°K in dilute alloys of copper (reported above[1]) demanded as a check on alloy purity and concentration the detailed investigation of the resistance ratios $R_{4.2°K}/R_{273.2°K}$, and further of $R_{77.7°K}/R_{273.2°K}$ and $R_{90.2°K}/R_{273.2°K}$ for comparison with the classical results of Linde.[2] In general such data are of fundamental value when interpreted as cross sections,[3] for electron scattering and prominent deviations found from Linde's results forced us to undertake a systematic investigation. It is significant that all differences found so far are in the direction of lower cross section.

After extensive tests, alumina crucibles for high vacuum melting were chosen which caused no measurable contamination. Control spectrographic and chemical analyses were conducted during the experiments.

Linde's scattering determinations were based on measurements between liquid oxygen and room temperature, dependent on an assumed validity of Matthiessen's rule. Departures from this law, however, are now well known, particularly in the case of copper, and further confirmed by our experiments.

We find the following:

(1) In order to avoid serious errors due almost certainly to oxygen contamination, the final strain-relieving anneal after rolling or drawing must be carried out in a very high continuous vacuum, the specimen being freely suspended in a glass vessel. Following this technique in our work, pure (H.S.) Hilger copper (lab. No. 11,184) always yielded $R_{4.2°K}/R_{273.2°K}=2.9(\pm0.3)\times10^{-4}$ over a wide range of annealing temperatures and times. On the other hand, when a rolled strip received the final anneal in a fresh crucible sealed in an evacuated silica tube, a residual resistance some fortyfold greater was found, agreeing in magnitude with the range of specific resistance variation found by Linde using his annealing technique.

(2) Present results on dilute Cu–Sn alloys with oxygen contamination suggest that the absorbed atoms provide additional scattering centers approximately proportional to the number of already present (Sn) scattering centers. Apart from the general importance of such behavior, it follows that such experiments can yield an artificially high (but approximately constant) scattering cross section. We suggest that this explains the consistent but high cross sections which follow from Linde's work in certain cases.

(3) The figure illustrates some results obtained with dilute Cu–Ni (*A*), Cu–Sn (*B*), Cu–Ag (*C*), and Cu–C–Sn (*D*), alloys. The cross sections deduced for Ni and Ag call for little comment here; in particular, the scattering by Ni agrees very well with that of Linde. However, in the case of Sn (also Sb, not shown), which differs strongly in chemical valency from copper, the scattering as discussed above is much lower than found by Linde. The major theoretical interest involved leads us to extend the work to the solute series: Zn→As and Cd→Sb.

(4) Investigation of carbon as an impurity led to curve *D* in Fig. 1 obtained for Sn alloys melted in spec-pure graphite crucibles. That the initial additional scattering was indeed the result of carbon was confirmed by the inclusion of powdered graphite in a pure Cu melt (*E*). The remarkable fact emerges that, particularly for very low Sn concentrations, the scattering is far from additive. Excluding the virtually untenable hypothesis at these very low concentrations of a mutually ordered lattice structure, one is led to consider the possibility of some novel electron-ion interaction additional to the screened electrostatic potential (e^2e^{-qr}/r) normally postulated in the theory of metallic resistance.[3] In view of the associated anomaly in the resistance minimum remarked above it appears possible that some type of "resonant" interaction is involved, perhaps analogous to that proposed by Gerritsen and Korringa[4] as a special case in Ag–Mn alloys.

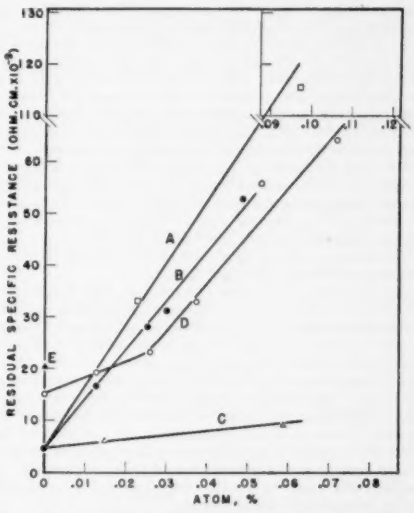

FIG. 1. Residual resistance of dilute alloys. *A*: Cu–Ni alloys; *B*: Cu–Sn alloys; *C*: Cu–Ag alloys; *D*: Cu–Sn alloys melted in spec-pure graphite crucibles; *E*: pure Cu melted with excess powdered graphite. (Specific resistances calculated on basis of 1.58×10^{-6} ohm cm for pure Cu at 0°C.)

We thank Mr. F. W. Richardson for able technical assistance in the above experiments.

[1] D. K. C. MacDonald, preceding letter, Phys. Rev. **88**, 148 (1952).
[2] J. O. Linde, Ann. Phys. **15**, 219 (1932).
[3] See, e.g., N. F. Mott, Proc. Cambridge Phil. Soc. **32**, 281 (1936) and N. F. Mott and H. Jones, *Properties of Metals and Alloys* (Oxford University Press, London, 1936), p. 292.
[4] A. N. Gerritsen and J. Korringa, Phys. Rev. **84**, 604 (1951).

The Quenching-in of Lattice Vacancies in Pure Gold*

J. W. Kauffman and J. S. Koehler
University of Illinois, Urbana, Illinois
(Received August 11, 1952)

ALTHOUGH diffusion in close-packed lattices probably occurs as a result of the migration of vacancies, direct experimental evidence is meager. At present the main support for the theory stems from the Kirkendall effect[1] and from the agreement with

experiment obtained by Huntington and Seitz[2] who calculated the activation energy for self-diffusion in copper on basis of a vacancy mechanism. The following experimental measurements provide preliminary data on the disorder produced at elevated temperature, presumably vacancies, in pure gold.

Gold wires, 99.999 percent pure, of 16-mil diameter were quenched in a blast of gaseous helium to room temperature. The wires were then immediately immersed in liquid nitrogen. The time required for the quench from the high temperature was 7 ± 3 milliseconds. About a third of a second was required to get the wire from room temperature to liquid nitrogen temperature.

After quenching, an increase in the residual electrical resistivity at liquid nitrogen temperature was detected. Measurements were made on the annealing of the quenched-in resistance. About one-third of the resistance increase can be annealed at temperatures in the vicinity of room temperature. The resistance at liquid nitrogen temperature was measured as a function of the annealing time at -21.7°C and also at -2.7°C. From these data the energy required to move a vacancy is 0.4 ev$\pm$0.14 ev.

The remaining two-thirds of the resistance anneals out at some temperature between 100°C and 500°C.

Quenches were made from five different high temperatures, from 920°C to 690°C and the increment in resistance quenched in from these temperatures varied, respectively, from 0.82 percent to 0.065 percent. The large change in the amount of resistance quenched-in with the temperature from which the quench was made indicates that stresses arising from thermal gradients are not the source of the resistance increase. Further, these data may be used to determine the energy required for the production of a vacancy. However, errors in measuring the temperature from which the quenches are made give rise to large errors for the energy to form a vacancy, and with this difficulty we can at present only estimate this energy as lying between 1 ev and 2 ev. More accurate measurements are in progress.

We would like to thank Professor F. Seitz for valuable discussions and Mr. D. Magnuson for aid in making the measurements.

* This work was supported by the AEC.

[1] See, for example, F. Seitz, *Phase Transformations in Solids*, edited by R. Smoluchowski *et al.* (John Wiley and Sons, Inc., New York, 1951).

[2] H. B. Huntington and F. Seitz, Phys. Rev. **61**, 315 (1942); see also H. B. Huntington, Phys. Rev. **61**, 325 (1942).

Some Experiments on Ge^{75} and Ge^{75m}†

ALAN B. SMITH, R. S. CAIRD, AND ALLAN C. G. MITCHELL
Indiana University, Bloomington, Indiana
(Received August 11, 1952)

Ge^{75} has not been investigated by spectroscopic means. The half-life is known[1-3] to be 80 min and the beta-ray end point has been measured by aluminum absorption and found to be[1,2] 1.3 Mev.

In the present investigation germanium enriched in Ge^{74} was bombarded by neutrons, and measurements were made with the help of a magnetic lens spectrometer, scintillation spectrometer, and coincidence counting techniques. In all of the work the activity was quite weak.

The beta-ray spectrum was measured in the lens spectrometer and two beta-ray groups were found having end-point energies, relative abundances, and logft values of 1.137 Mev, 85 percent, logft=5.2; 0.614, 15 percent, logft=4.5. In addition, two internal conversion lines were seen. There was a well-resolved line at 0.408 Mev and an unresolved group at about 0.520 Mev.

The gamma-rays were measured from observations of photoelectrons from a uranium radiator. A line at 0.265 Mev was found and also a Compton distribution for a line around 0.600 Mev. The line at 0.265 Mev was confirmed with the help of a scintillation spectrometer. In addition, weak lines at 0.418 and 0.572 Mev were seen on the scintillation spectrometer.

Beta-gamma coincidence experiments were performed using ordinary counters. No coincidences were found between the high energy group of beta-rays and gamma-rays showing that the high energy group leads to the ground state.

Some of the gamma-rays seen in Ge^{75} are also seen in the transition[4-7] $Se^{75}\rightarrow As^{75}$. Those which appear in both are the ones at 0.265 and 0.408 Mev. Although a careful search for internal conversion lines of low energy was made, none was seen.

Since the ground state of As^{75} has a configuration $p_{3/2}$, and the transition from the ground state of Ge^{75} to the ground state of As^{75} is allowed, the configuration of the ground state of Ge^{75} is probably $p_{1/2}$. The fact that the higher states of As^{75} are excited by the K-capture transitions from Se^{75} infers that the ground state of Se^{75} has the configuration $g_{9/2}$. It is interesting to note that both beta-ray groups of Ge^{75} have logft values corresponding to allowed transitions.

We have produced a metastable state of Ge^{75}. This state was produced both by a Ge^{74} (separated) (n, γ) reaction and $As^{75}(n, p)$ reaction. The energy of the gamma-ray was measured photographically on a scintillation spectrometer and was found to be 0.175 Mev. The half-life of the state was found by setting on the line with a scintillation spectrometer connected to a differential pulse-height selector. The half-life is 48 ± 2 sec. While this experiment was in progress a similar experiment was reported by Flammersfeld.[8]

Assuming the radiation to be $E3$, using the empirical lifetime formula of Goldhaber and Sunyar,[9] and the expected conversion coefficient and K/L ratio, the half-life comes out 88 sec compared with the measured half-life of 48. If, on the other hand, this radiation has been assumed to be $M4$, the half-life would have been of the order of 10^6 sec.

† Supported by the joint program of the ONR and AEC.

[1] McCown, Woodward, and Pool, Phys. Rev. **74**, 1311 (1948).
[2] Seaborg, Livingood, and Friedlander, Phys. Rev. **59**, 320 (1941).
[3] S. A. Reynolds, Oak Ridge National Laboratory Report ORNL-867, 24 (1950) (unpublished).
[4] Ter Pogossian, Robinson, and Cook, Phys. Rev. **75**, 995 (1949).
[5] Cork, Rutledge, Branyan, Stoddard, and LeBlanc, Phys. Rev. **79**, 889 (1951).
[6] Jensen, Laslett, and Pratt, AEC Report AECD 1836, April 1948 (unpublished).
[7] Jensen, Laslett, Martin, Hughes, and Pratt (to be published).
[8] A. Flammersfeld, Z. Naturforsch. **7a**, 295 (1952).
[9] M. Goldhaber and A. W. Sunyar, Phys. Rev. **83**, 906 (1951).

K^{40} Radioactive Decay: Its Branching Ratio and Its Use in Geological Age Determinations*

A. K. MOUSUF
Geophysics Laboratory, Department of Physics, University of Toronto, Toronto, Canada
(Received June 30, 1952)

THE ratio of K-capture to beta-emission for the naturally occurring radioactive isotope K^{40} has been determined. For this purpose argon was extracted from four different samples of microcline and purified. The volume of the extracted argon was measured by means of a McLeod gauge built into the apparatus, and the amount of radiogenic A^{40} was ascertained by mass spectrometric analysis of the isotopic abundances in the extracted argon. The potassium contents of the samples of microcline were determined by chemical analysis and the amount of K^{40} has been estimated using the recent value[1] of Nier, 0.0119$\pm$0.0001 percent, as the isotopic abundance of K^{40} in potassium.

Previous determinations of the branching ratio by direct measurements have used counting techniques,[8-9] whereas those based on indirect measurements have used age data coupled with either Ca^{40} or A^{40} extraction data to get the branching ratio,[10-12] except Inghram *et al.*,[13] who measured both A^{40} and Ca^{40} to get the branching ratio.

The argon was extracted by heating a sample of known weight of powdered microcline (75 g in each case) with metallic sodium in vacuum to about 600°C, and it was purified by treating the gas in a calcium furnace to constant volume. The results of the isotopic analysis of argon thus obtained are shown in Table I. All

TABLE I. Isotopic analysis of argon from samples of microcline.[a]

Sample No.	Locality	Run	A^{40}/A^{36}	Radiogenic argon, %	Average
1	Hybla, Ont.	1	39800±4000	99.3±0.1	99.4±0.1
		2	59400±5000	99.5±0.1	
2	Frontenac Co., Ont.	1	3790±320	92.0±0.7	92.7±0.5
		2	4460±220	93.4±0.3	
3	Monteagle Twp., Ont.		>90000	100.0±0.1	100.0±0.1
4	Leeds Co., Ont.		6310±520	95.3±0.4	95.3±0.4

[a] In column 4 the errors given are mean deviations of observations.

of them contain a very high percentage of radiogenic argon and two of them contain nearly pure radiogenic argon.

The extraction of argon from the first two samples (Table I) was repeated and the volumes measured agreed within less than 3 percent. Mass spectrometric analyses were carried out for each separate run and the amounts of radiogenic argon calculated from these analyses showed agreement within 1.5 percent for each pair of runs for each sample. For one sample, purity of argon was tested spectroscopically. Occurrence of faint band spectra indicated the presence of some impurities whose identifications were not definite. The same sample was then analyzed in the mass spectrometer, scanning the entire mass range from 14 to about 100. Traces of impurities at masses 18 and 28 were detected whose total effect was not more than one percent.

All the samples of microcline used in this investigation are from the Grenville area where ages range from about 850 to 1050×10^6 yr, but since they were not collected from pegmatite veins which have been precisely dated no exact values can be assigned for the ages of the minerals. However, for one sample (Hybla), a fairly definite value for its age (t) may perhaps be given because the locality of Hybla is close to Wilberforce and a pegmatite at Wilberforce has been accurately determined to be 1030×10^6 yr old by both chemical and isotopic lead determinations.[14–16] The age of the Hybla sample has, therefore, been taken to be 1030×10^6 yr. As no more definite value for t can be assigned to the rest of the samples, they have been assumed to be of the same age as the Hybla sample and the branching ratio calculated with the results given in Table II. However, it is quite possible that the real ages of these samples are younger and lie in the range 850 to 1050×10^6 yr, in which case it is interesting to note that the variations in the values of the branching ratio are similar to this possible spread in the age value of the samples.

The volume measurements of the extracted argon are believed to have been made within an accuracy of one percent. The values of the branching ratio have been calculated using the total half-life for K^{40} of 12.7×10^9 years obtained by Sawyer and Wiedenbeck.[6] The results are in good agreement with the low range of values of the branching ratio obtained by some workers using direct measurements[4, 9] and also with those obtained by Aldrich and Nier.[13] The results are consistent within the range expected from the spread in the age data, and the author is hopeful that further work may establish the branching ratio with the precision required for its application to geological age determinations. For this purpose, samples of potassium bearing minerals are needed from localities which are well dated by other reliable radioactive methods. Further work using such samples is in progress.

TABLE II. Volume of argon from microcline samples and calculated branching ratio of potassium 40. The last column (B.R.) gives the branching ratio for total half-life 12.7×10^9 yr. Each sample had a total weight of 75 g and was assumed to have an age of 1030×10^6 yr.

Sample No.	Potassium[a] grams	Argon[b] std. cc	Radiogenic A^{40} std. cc	g radio-A^{40} / g K^{40}	B.R.
1	7.88	0.0246	0.0244	4.65×10^{-3}	0.066
2	7.84	0.0230	0.0214	4.10×10^{-3}	0.059
3	7.85	0.0204	0.0204	3.90×10^{-3}	0.055
4	7.62	0.0204	0.0193	3.80×10^{-3}	0.053

[a] Estimated from chemical analysis.
[b] Measured with McLeod gauge.

The author gratefully acknowledges the assistance and advice of Professor J. T. Wilson, Dr. C. B. Collins, Mr. R. D. Russell, and Mr. R. M. Farquhar. Thanks are due Professor E. W. Nuffield of the Department of Geology, University of Toronto, who supplied the samples of mineral used in this experiment, to D. A. Moddle of the Ontario Department of Mines, who made the chemical analysis for potassium, and to R. H. Chappell for technical assistance.

[*] This research has been supported by the National Research Council of Canada and by the Research Council of Ontario.

[1] A. O. Nier, Phys. Rev. **77**, 789 (1950).
[2] E. Bleuler and M. Gabriel, Helv. Phys. Acta **20**, 67 (1947).
[3] O. Hirzel and H. Wäffler, Phys. Rev. **74**, 1553 (1948).
[4] J. J. Floyd and L. B. Borst, Phys. Rev. **73**, 1106 (1949).
[5] W. R. Faust, Phys. Rev. **78**, 624 (1950).
[6] T. Gráf, Phys. Rev. **79**, 1014 (1950).
[7] Houtermans, Hazel, and Heintze, Z. Physik **128**, 657 (1950).
[8] G. A. Sawyer and M. L. Wiedenbeck, Phys. Rev. **79**, 490 (1950).
[9] Ceccarelli, Quareni, and Rostagni, Phys. Rev. **80**, 909 (1950).
[10] L. H. Ahrens and R. D. Evans, Phys. Rev. **74**, 279 (1948).
[11] H. E. Suess, Phys. Rev. **73**, 1209 (1948).
[12] L. T. Aldrich and A. O. Nier, Phys. Rev. **74**, 876 (1948).
[13] Ingram, Brown, Patterson, and Hess, Phys. Rev. **80**, 916 (1950).
[14] H. V. Ellsworth, Rare-element Minerals of Canada, Geol. Surv. Canada, Ec. Geol. Series No. 11 (1932).
[15] A. O. Nier, Phys. Rev. **55**, 150 (1939).
[16] C. B. Collins and J. R. Freeman, Trans. Roy. Soc. Canada, **45**, 23 (1951), Series III, Sec. IV.

The Very Long Lifetime of C^{14} β-Decay*

A. M. L. MESSIAH
University of Rochester, Rochester, New York
(Received August 19, 1952)

THE very long lifetime of C^{14} is one of the difficulties of β-decay theory which still remains. The spins of C^{14} and N^{14} have been measured to be 0 and 1, respectively. The interpretation of the forward angular distributions associated with the reactions $C^{13}(d, p)C^{14}$ and $C^{13}(d, n)N^{14}$, along the line of Butler's theory,[1] leads to the conclusion that C^{14} and N^{14} both have even parity. One expects therefore an allowed β-decay according to the G. T. selection rules. The spectrum actually has the allowed shape; however, the ft value is very large: $\log ft=9$ to compare, among other cases, with the β-decay of He^6 where $\log ft=2.95$ (super-allowed).[2]

An explanation of the C^{14} anomaly in terms of "L-forbiddenness" has been proposed.[3] It is assumed that in the light nuclei, the orbital angular momentum L is a very good quantum number; then $C^{14}\rightarrow N^{14}$ is supposed to be a $^1S_0\rightarrow{}^3D_1$ transition, whereas $He^6\rightarrow Li^6$, for example, is $^1S_0\rightarrow{}^3S_1$. The allowed shape of the C^{14} spectrum is then explained either by assuming a small admixture (very small indeed) of $^3S_1$ in the N^{14} ground state or by showing that the transition $^1S_0\rightarrow{}^3D_1$ is governed by a matrix element which simulates the allowed shape.

L is certainly a rather good quantum number in the very lightest nuclei (deuteron, H^3, He^3), whereas strong noncentral effects show up in heavy nuclei, as evidenced by the success of Mayer's model. It is quite reasonable, therefore, to assume that L is a good quantum number in the medium light nuclei considered above. The question arises, then, whether the L assignments which have been proposed to explain the β-decay are consistent with other experimental data and whether they can be tested by further experiments.

In fact, the electric properties of N^{14} and Li^6 are consistent with $^3D_1$ and $^3S_1$ assignments, respectively. In those nuclei which have isotopic spin $T=0$, the magnetic moment is given by the simple expression (in units $e\hbar/2Mc$):

$$\mathbf{M}=\tfrac{1}{2}\mathbf{L}+(\mu_P+\mu_N)\mathbf{S},$$

which gives 0.33 for $^3D_1$ whereas $\mu_{N^{14}}=0.40$ and 0.85 for $^3S_1$ whereas $\mu_{Li^6}=0.82$. Whether the small differences can be explained in terms of relativistic effects, exchange moment effects, or in terms of noncentral forces remains to be seen. The quadrupole

moments of Li^6 and N^{14} have also been measured;[4] the rather small upper limit for Li^6 is consistent with a vanishing quadrupole moment characteristic of a pure $^3S_1$; the finite value found for N^{14} is an indication in favor of $L \neq 0$. However, it is not possible to draw more precise conclusions since the quadrupole moment, in contradistinction to the magnetic moment, is not uniquely determined by the values of L, S, J even when $T=0$.

In order to experimentally test the L assignments of C^{14} and N^{14}, one may use Butler's theory of stripping in the following way: Let us assume that C^{13} is even and $^1S_0$. The reaction $C^{13}(d, p)C^{13*}$ leading to the first excited state of C^{13} has been studied very thoroughly;[5] it exhibits an "$l=0$" angular distribution, showing that C^{13*} is in an even $^2S_{\frac{1}{2}}$ state. If N^{14} is in a pure $^3D_1$ state, one expects a pure "$l=2$" angular distribution in reaction $N^{14}(n, d)C^{13*}$, rather than a mixture of "$l=0$" and "$l=2$" predicted on the basis of total angular momentum and parity conservation alone; similarly, one expects a pure "$l=0$" in $C^{14}(p, d)C^{13*}$. At any rate, one would expect a striking difference in the angular distributions from the reactions $N^{14}(n, d)C^{13*}$ and $C^{14}(p, d)C^{13*}$, in contradistinction to the almost identical shapes found for $C^{13}(d, p)C^{14}$ and $C^{13}(d, n)N^{14}$.

Finally, it must be noted that the long life of C^{14} is very hard to understand in terms of existing one-particle models. The shell model with $j-j$ coupling fails completely:[6] it assigns to C^{14} and N^{14} the configuration $s_{\frac{1}{2}}^4$, $p_{\frac{1}{2}}^8$, $p_{\frac{3}{2}}^2$, and leads to an "allowed" ft value. The shell model with Russell-Saunders coupling, where C^{14} and N^{14} are assigned the configuration $(1s)^4(1p)^{10}$ and the degeneracy in zeroth order is removed by a charge-independent central potential coupling the nucleons in the unfilled p-shell, is the only model consistent with the "L-forbiddenness" picture discussed above. It leads, however, to a definite contradiction no matter what perturbing potential is chosen, because it predicts the same ft value for the C^{14} and the He^6 β-decay. In fact, He^6 and Li^6 possess the complementary configuration $(1s)^4(1p)^2$; it follows from the properties of complementary configurations that the matrix elements for the β-decays between the ground states $He^6 \rightarrow Li^6$ and $C^{14} \rightarrow N^{14}$ are equal.[7] In fact the property of complementary configurations which is used here still holds when the perturbation potential contains a tensor force part; therefore the contradiction cannot be removed by considering an unorthodox shell model with tensor coupling. On the other hand, we assume here that the p nucleons have the same radial wave function in both configurations, a necessary condition for them to be complementary. This cannot be strictly correct since the nuclear radii are somewhat different, and a change in the order of the levels, such that the ^3D is brought below the ^3S level when the nuclear radius increases, is not completely ruled out.

I with to thank Dr. R. E. Marshak and Dr. P. M. Noyse for helpful comments and Dr. R. Christy, Dr. T. Lauritsen, and Dr. F. Ajzenberg for a critical reading of the manuscript.

* This work was assisted jointly by the AEC and the French Direction des Mines.

[1] S. T. Butler, Proc. Roy. Soc. (London) **A208**, 559 (1951); D. A. Bromley and L. M. Goldman, Phys. Rev. **86**, 790 (1952).

[2] New ft value cited in F. Ajzenberg and T. Lauritsen [Revs. Modern Phys. (to be published)].

[3] R. Bouchez, Compt. rend. **231**, 225 (1950).

[4] E. P. Wigner, lecture notes, Wisconsin (1951) (unpublished).

[5] J. Rotblat, Proceedings of the Chicago Conference, September 17 to 22, 1951, p. 38 (unpublished).

[6] Note also that it predicts $\mu_{N^{14}}=0.38$, $\mu_{Li^6}=0.62$, a vanishing quadrupole moment for N^{14} and a nonvanishing one for Li^6, in rather bad agreement with experiment.

[7] A. M. L. Messiah, AEC Report NYO-3212 (unpublished).

Proceedings of the American Physical Society

Minutes of the Meeting of the New England Section at Tufts College, Medford, Massachusetts, May 24, 1952

THE thirty-eighth meeting of the New England Section of the American Physical Society was held at Tufts College, Medford, Massachusetts, on Saturday, May 24, 1952. Approximately 100 members of the Section were in attendance. The program consisted of four invited papers and fourteen contributed papers. The invited speakers were F. L. Friedman, C. L. Hogan, E. H. Land, and Erwin Mueller. The abstracts of ten of the contributed papers are appended hereto, those of the other four having been sent to the *American Journal of Physics*.

A. G. Hill
Secretary-Treasurer
New England Section

1. A Probe Technique for Measuring Ion Densities in the Afterglow of a Pulsed Discharge.* Morton A. Levine and Winston H. Bostick, *Tufts College*.—This laboratory has been using a probe for measuring ion densities in the afterglow of an induction-excited discharge in He and N_2 in a toroidal discharge tube. The technique involves a mechanical relay which electrically connects the probe to the amplifier and voltage source only during an examining interval which can be variably delayed with respect to the main excitation pulse of the discharge. This technique yields what we believe to be suitable probe voltage *vs* probe current characteristics in the afterglow region at pressures of 0.02 to 2 mm of Hg. Saturated positive-ion current to the probe can be used to measure the ion density as a function of time.

* This work has been performed under contract with the Geophysics Research Division of the USAF Cambridge Research Center of the Air Research and Development Command. O. T. Fundingsland, supervisor of the contract in that organization, suggested the use of the technique of electrically switching the probe.

2. Direct Observation of the Presence of Magneto-Hydrodynamic Waves in Ionized He Gas.* Winston H. Bostick and Morton A. Levine, *Tufts College*. Magneto-hydrodynamic standing waves and noise have been observed by means of a transient probe technique in the afterglow of discharges in He, N_2, and H_2 at pressures of about 0.02 mm of Hg with toroidal dc magnetic fields up to 800 gauss. The discharge is produced by pulsed, induction excitation of the gas in a toroidal discharge tube in which the peak currents can go as high as 8000 amperes. Under favorable circumstances standing waves are apparently set up around the toroid. The observed frequency of these waves of 10^4 cycles/sec agrees approximately with the frequency for the standing waves calculated from the tube dimensions and the velocity of propagation, $V=H_0(4\pi\rho)^{-\frac{1}{2}}$ cm/sec, where H_0 is the dc magnetic field in gauss and ρ is the gas density in g/cc. Under less favorable conditions when standing waves cannot be set up, magneto-hydrodynamic noise is observable. Photographs of probe-current traces on a synchroscope will be shown.

* This work has been performed under contract with the Geophysics Research Division of the USAF Cambridge Research Center of the Air Research and Development Command.

3. Thermal Conductivity of Sapphire and Rutile as a Function of Temperature.* Kathryn A. McCarthy, Stanley S. Ballard, and Edward C. Doerner, *Tufts College*.—The thermal conductivities of sapphire and rutile have been measured in the temperature range −50°C to 100°C. The method[1] of measurement is a comparative one in which heat flow through the samples under test is compared with that through *Z*-cut crystalline quartz, for which the values of thermal conductivity are well-established. Thermal conductivity varies with direction in the crystal, for crystals other than those in the cubic system. For crystals of the hexagonal, tetragonal, and trigonal classes, the thermal conductivity is defined in terms of two values: that with heat flow parallel to the optic axis of the crystal, and that with heat flow perpendicular to the optic axis. For sapphire, rutile, and quartz, the former value is greater than the latter. Data are presented which show that both values of the thermal conductivity of sapphire and rutile decrease with increasing temperature, in the temperature range covered. These data also show that the ratio of the thermal conductivity with heat flow perpendicular to the optic axis to that with heat flow parallel to the optic axis varies with temperature, rather than being a constant for a given material.

* Assisted by a grant from the Penrose Fund of the American Philosophical Society.
[1] Ballard, McCarthy, and Davis, Rev. Sci. Instr. **21**, 905–907 (1950); Ballard, McCarthy, and MacLeod, J. Opt. Soc. Am. **41**, 871(A) (1951).

4. Inelastic Deformation (Cold Flow) of Certain Crystalline Materials Under Flexural Stress.* Lewis S. Combes, Stanley S. Ballard, and David L. Honkonen, *Tufts College*.—Data have previously been reported[1] on elastic properties of cubic crystals of the NaCl, CsCl, and CaF_2 types, and typical stress-strain curves were presented for cyrstals of each type. Measurements have also been made of the cold flow of these same crystals when each was subjected to a constant flexural stress of the order of magnitude of its apparent elastic limit. Each test was continued for a period of at least 50 hours. Typical strain *vs* time curves will be shown for crystals of the NaCl and CsCl types. Only two crystals of the CaF_2 type were available, namely, CaF_2 and BaF_2, and each of these showed no cold flow whatever for stresses up to its modulus of rupture. All tests were made at a temperature of 30°C.

* This work has received support from the Permanent Science Fund of the American Academy of Arts and Sciences.
[1] Combes, Ballard, and McCarthy, "Comparative elastic studies of single crystals of the NaCl type," Phys. Rev. **86**, 623(A) (1952); "Comparative elastic studies of single crystals of the CaF_2 and CsCl types," Phys. Rev. **87**, 201(A) (1952).

5. Effective Mass of Electrons in Polar Crystals. E. P. Gross, *Massachusetts Institute of Technology*.—Frohlich, Pelzer, and Zienau[1] have studied the interaction of slow electrons with the optical modes of polar crystals and have concluded that the effective mass is close to that of free electrons. Landau and Pekar,[2] using the same Hamiltonian, find, by a semiclassical treatment, an effective mass of about 400 for alkali-halide crystals. The F.P.Z. solution is completely quantum-mechanical but includes only zero and one-quantum terms in the wave function. In the present work we set up the Fock equations[3] which make possible a systematic treatment according to the number of quanta included in the wave function. The lowest approximation gives the F.P.Z. solution which is shown to be valid for interaction strengths less than one-fifth the value for alkali halides. A solution is obtained which includes effects of two and three quanta and is valid for strengths one-half of the value for alkali halides. At this value the effective mass is *ca* 5. This

solution may be of quantitative value for crystals less polar than the alkali halides. For the latter the results indicate a very high effective mass and that terms involving many quanta must be included, thus providing evidence for the approximate validity of the semiclassical treatment.

[1] Frohlich, Pelzer, and Zienau, Phil. Mag. **41**, 221 (1950).
[2] L. Landau and S. Pekar, J. Exptl. Theoret. Phys. **18**, 420 (1948).
[3] V. Fock, Z. Physik **75**, 622 (1932).

6. Measurements of the Lateral Distribution of Extensive Air Showers. MORTON A. LEVINE, *Tufts College.*—Extensive cosmic-ray showers have been measured with ionization chambers, and it has been found that within the rather large experimental error the lateral distribution agrees with the Moliere function. Four pulse ionization chambers were used in a triangular geometry with one chamber in the center. This arrangement gave enough information to over-determine the axis of the shower.[1] Thirty-five showers were measured and analyzed at sea level.

[1] Robert W. Williams, Phys. Rev. **74**, 1689–1700 (1948).

11. Confirmation of Polymer and Dimer Absorptions in the Ultraviolet Spectra of Alcohols.* GLADYS A. ANSLOW, IRENE S. WHITE, AND RIKA SARFATY, *Smith College.*—Conclusive evidence of the origin of the long wavelength absorptions in the ultraviolet spectra of alcohols, suspected as impurities.[1] result from the comparison of Beckman spectrophotometer curves of distillates of *n*-propanol and *n*-butanol, produced over silica gel and metallic Na. Both processes remove water; with silica gel the absorptions ascribed to the hydrogen bridge[2] tend to increase, indicating further polymerization; whereas with Na, which cracks the polymers, the spectra type changes from the polymeric to the dimeric form, curves being nearly smooth in intermediate stages. The rate of change of type varies with the cube or the square of the concentration with polymers and dimers, respectively. Discrete absorptions in the 35,000–38,000 cm^{-1} region, in the spectra of numerous isomers of all alcohols, are at the frequencies of the $\Delta\nu = 1, 2, 3$ members of the $^2\Sigma - {}^2\pi$ transition of unassociated OH. The stronger absorption ($D \sim 10$) initiated in *n*-propanol, butanol, pentanol, hexanol, and octanol at approximately 38,800, 35,500, 33,100, 30,000, and 28,000 cm^{-1}, respectively, may be predissociation spectra.

* Supported by the ONR and by the Research Corporation.
[1] Disc. Faraday Soc., No. 9, 333 (1950).
[2] See reference 1, pp. 299–318.

12. High Frequency Electromechanical Filters.* C. R. MINGINS, S. BARTNOFF, AND L. A. HOWARD, *Tufts College.*—Although filter structures were probably developed first in electrical form, there is basically no reason why they must be fully electrical, even for the selection of frequency ranges of electrical oscillations. Functional analogies exist between electrical and mechanical components, and they find expression both in mathematical similarities and in the external evidences of internal behavior associated with a combined system. In seeking a bandpass arrangement which cuts off sharply, the desirability of using electromechanical systems is indicated by a consideration of the low internal dissipation of energy in vibrating mechanical components. At frequencies above one mcps, available dimension ratios are not favorable as at lower frequencies, and one must use a thickness mode of vibration. The high conversion efficiency of piezoelectric crystals, as well as the ready possibility of cutting them with zero temperature coefficient of frequency, makes them offer promise for use as transducing elements. Furthermore, previous extensive studies at Tufts College have demonstrated that secondary modes can be displaced in frequency and undesired ones can be eliminated by appropriately shaping the surfaces. Several possible electromechanical arrangements are considered.

* This work is sponsored by the U. S. Signal Corps.

13. The Equivalent Electrical Network of a Quartz Plate Used as a Filter.* A. D. FROST, C. R. MINGINS, AND R. W. PERRY, *Tufts College.*—Studies have been conducted on the frequency-selective properties of piezoelectric quartz plates with multiple electrodes, when used as two-terminal-pair electric wave filters at high frequencies. In connection with analyses of the performance of these units, an effective electric network representation has been proposed. Measurements of the frequencies of the normal-mode resonances and the terminal impedances of the system have provided specific values for individual components of the circuit. From this and other evidence it appears that the bandpass behavior observed is due to the excitation of both the fundamental thickness shear and the 1, 2, 1 mode of vibration.

* This work is sponsored by the U.S. Signal Corps.

14. Stepped-Surface Piezoelectric Filters.* R. R. MCDONOUGH, D. W. MACLEOD, AND G. A. LARSON, *Tufts College.*—In investigating the use of a single quartz plate with divided electrodes as a bandpass filter, it is found that modifications of the shape of the plate cause changes in the filter transmission characteristic. A symmetrical reduction of the thickness of the plate in strips parallel to the electrode division has been found to increase the bandwidth. The effect is discussed from both electrical and mechanical points of view. The use of added impedance elements to improve the transmission curve is also reported.

* This work is sponsored by the U. S. Signal Corps.

MINUTES OF THE 1952 SUMMER MEETING AT DENVER, COLORADO, JUNE 30 TO JULY 3, 1952

(Corresponding to *Bulletin of the American Physical Society*, Volume 27, No. 4)

THE 314th meeting of the American Physical Society, being the only summer meeting of 1952, was held in Denver, Colorado, on Monday, Tuesday, Wednesday, and Thursday, June 30 to July 3, 1952, with an attendance of 350. This was a meeting of an unusual type, of which the first two days were devoted to invited and contributed papers in our usual fashion, while the last two days were mainly used for three discussions and one symposium. Two of the discussions were in the field of cosmic rays; they were led by E. Fermi and B. Rossi. The third discussion was in the field of phenomena of the upper atmosphere; its leader was J. Kaplan. Discussions of this type have been held at only one previous meeting of the Society. They were well attended and well enjoyed, and it seems worthwhile to hold similar discussions from time to time in the future. The titles of these discussions and the names of some of the participants will be found in the following pages. The reader will also find the program of the meeting held by the Society in Denver 51 years ago, which is inserted to show the contrast in the activity of the Society between 1901 and 1952.

We owe so much to so many people that it is impossible to give due credit to all. First place must go to Professor Byron E. Cohn, who together with J. Kaplan took the first steps toward the organizing of the discussions, and who as chairman of the local committee directed the immense amount of work involved in the meeting. Thanks are expressed to the University of Denver, which provided halls for some of our meetings; the others were held in two hotels. The Denver Fire Clay Company furnished projectors and other equipment, and the Adolph Coors Company provided favors at the banquet. Miss Beatrice Brewster and Miss Annabelle Kyffin gave us music at the banquet. The Lieutenant Governor of Colorado and the Mayor of Denver attended the banquet at considerable personal inconvenience to themselves. Over a dozen Denver people helped at the registration desk and in operating the lanterns. A wonderful pleasure and unique event was a reception tendered to members of the Society and their families by Mr. and Mrs. John Evans in their Denver home, which will always be remembered with delight.

The banquet was held on Tuesday evening in the Student Union of the University of Denver. Lieutenant Governor Allott and Mayor Newton made gracious speeches, and Dr. Manuel Sandoval Vallarta gave us an account of physics in Mexico and closed his speech by inviting the Society to meet in Mexico City in June, 1955.

The Council met on Monday and on Tuesday. It elected 154 candidates to membership and seven to fellowship. Their names follow at the end of these minutes.

The Council reversed its action of April and decided to increase the income of the Society otherwise than by raising membership dues. Membership dues will continue at $15, and Fellowship dues will be raised to $25 instead of $30. The additional revenue will be obtained by imposing an extra charge on members who receive *The Physical Review* or any journal they choose as an alternative to *The Physical Review*. The extra charge will be $5 per year for *The Physical Review*, and other amounts for the other journals which may be taken as alternatives. Full details will be given in a notice which will be sent to all members of the Society before these Minutes appear in print.

Remembrance is bespoken for Eileen Fahey, who worked diligently and well for two years in the office of the Society at Columbia University, and at the age of eighteen met a tragic death in that office on the morning of July 14, 1952.

Elected to Fellowship: Walter Betteridge, F. W. Brown, J. H. Coon, J. G. Daunt, W. L. Davidson, F. N. Frenkiel, Elizabeth R. Graves.

Elected to Membership: Ko Aizu, Harold Briggs Almond, Dorman W. Arnold, Frederick Eugene Bailey, Jr., Andrew Newton Baker, Jr., Walter Baltensperger, Lee Fenichel Barash, Saul Abraham Basri, Egil Kristoffer Bjornerud, Warren Bloomfield, Jacques Marcel Blum, Leland Sheaff Bohl, Rudolf F. Brill, James Hughes Brown, Martin John Brown, Harvey Jerome Brudner, John Paul Buckley, Margaret Elizabeth Carncrose, Raymond A. Carpenter, Sheldon Shou-lien Chang, Janet M. Cisar, Nathan Lebovitz Cohen, George A. Contos, Charles Falk Cook, Eugene A. Cotton, Clyde Lorrain Cowan, Jr., Hugh Joseph Curnan, Worbert James Dabrowski, Michael Danos, Norman R. Davidson, William Donald Davis, Amiello Francis De Meglio, Malcolm Eugene Ennis, Ronald McCunn Farquhar, Jacques Rene Favereau, Alvin E. Fein, Thomas Lassfolk Finch, John Victor Florio, John Major Fowler, Octavio Rafael Foz-Gazulla, June Fujimura, Andrew Francis Gabrysh, Harold Wells Gandy, Joleroy Gauger, Wayland Dale George, Julian Howard Gibbs, Forrest Richard Gilmore, Solomon Jack Glass, Leo Goldberg, Benjamin G. Goldring, Charles David Goodman, Osamu Hara, Akira Harasima, Chushiro Hayashi, LeRoy Heaton, Lester C. Hehn, Edwin Wendell Hill, Donald Frank Holcomb, George Robert Holzman, Chieh Su Hsu, Raymond Jancel, Kenneth Alan Johnson, Harold S. Johnston, David Reese Jones, Keith W. Jones, Koichi Kamata, Paul H. Keck, Ernest Ray Keown, James Claude King, Joe Douglas Kingston, Jr., Hideji Kita, Donald Alvin Konler, Alan Charles Kolb, Akira Komatsusawa, Hiroo Komori, Irving Korobkin, David Alexander Kottwitz, William Eric Krag, Arnold Guy Kramer, Albin Gustaf Lagerqvist, David Dayton Lanning, Antoine M. Leveque, Fred Marcus Lurie, Bruce Charles Lutz, George John Lutz, David Willis Martin, Charles Walter McCutchen, Charles Alexander McDonald, Jr., Joseph Tinsley Meers, Lael Merlin Meixsell, Brian Miles, Edwin J. Miller, Charles W. Misner, Walter Edwin Mochel,

George J. Mohn, Eugene Joseph Moscaret, Marvin Moskowitz, Yasuo Munakata, Russell James Nash, Yukihisa Nogami, Theodore George Northrop, Richard Oberdorfer, Nobuo Oda, Allen Charles Odian, Thomas Jefferson O'Donnell, Akira Okaya, Hisaichiro Okonogi, Ingrid Ulrika Olsson, George J. Ourada, Jr., Kenneth Lee Perkins, Martin Melvin Perlman, Herbert Reynold Philipp, Harry E. Pickett, Reuel Platt, Jr., William B. Pohlman, Gordon Wayne Repp, Carlton Phillip Roberts, Charles Edwin Roos, Francis Xavier Roser, Richard Doncaster Russell, Charles Philip Sargent, Tatuya Sasakawa, John Frederick Schuler, Morton Shepetin, Amon Mann Short, Gerald Bruce Shpeen, Donald Brandis Sill, Jan Philip Simpelaar, Chester Wallace Spencer, Benjamin H. J. Stallwood, James Rufus Stevenson, Takehiko Takabayasi, Yasushi Takahashi, Makoto Takeo, David Millar Thomson, Robin Christopher Giles Thornton, Robert Geoffrey Uebergang, Tunemaru Usui, Leo von Gottfried, Woldemar Franz von Jaskowsky, John Wells Wachter, Robert Thomas Wagner, John Vincent Walsh, Karl H. Wieland, Mary-Camilla Williams, Robert Wochinger, Richard Forrest Woodcock, William Jacob Worthington, Jr., Eiji Yamada, Kazuo Yamazaki, Arthur Peck Young, Philip Geneuus Youngner, Robert John Zentner, Sidney Fred Zimmerman, Jr.

KARL K. DARROW, *Secretary*
American Physical Society
Columbia University
New York 27, N. Y.

MINUTES OF THE SPECIAL BUSINESS MEETING OF THE AMERICAN PHYSICAL SOCIETY HELD AT DENVER, COLORADO, ON JUNE 30, 1952

A SPECIAL Business Meeting of the American Physical Society was convoked at Denver, Colorado, on the evening of June 30, 1952, so that the Council of the Society might recommend to it the adoption of certain amendments to the By-Laws. The attendance compared favorably with what is usually recorded at the regular Business Meetings held in conjunction with the Annual Meetings of the Society. After ample discussion the members present modified by unanimous vote two sections of the By-Laws, which follow in their new forms.

ARTICLE I, Section 2. The membership of a newly elected Fellow or Member, with respect to membership subscriptions and reduced-rate subscriptions, shall commence on the first of January of the year of his election if his annual dues are received before August first (September first for people residing elsewhere than on the North American continent) of that year, and on the first of January of the year after his election if his annual dues are received after July thirty-first (August thirty-first for people residing elsewhere than on the North American continent) of the year of his election.

ARTICLE VI, Section 1. Each member of the Society who has paid his dues in full shall be entitled to receive *The Physical Review*, or some other journal specified on the dues card, by payment of an extra charge to be fixed by the Council. Members residing in countries to which the postage rates are greater than domestic postal rates shall be required to pay, in addition to dues and the extra charge defined above, an amount for foreign postage to be fixed by the Managing Editor. The Council shall be empowered to fix the terms on which members of the Society shall receive *Physics Abstracts* or *Electrical Engineering Abstracts*.

Errata Pertaining to Papers A8, B4, D11, D12, E12, H1, H5, I9, and L6

A8, by William B. Kennedy. In line 11, instead of ". . . relatively large magnitude (greater than 30 m/sec) . . .," read ". . . relatively large magnitude (greater than 25 m/sec). . . ." In line 13, instead of ". . . were of lesser speeds (less than 30 m/sec) . . .," read ". . . were of lesser speeds (less than 25 m/sec). . . ." In footnote *, instead of "This research is sponsored by the Geophysical Research Directorate of the Air Force, Cambridge Research Center," read "The research reported in this paper has been sponsored by the Geophysics Research Division of Air Force Cambridge Research Center under Contract AF19(122)-252)"

B4, by M. E. Battat and F. L. Ribe. In the last line, instead of "0.83±0.3 second," read "0.83±0.03 second."

D11, by Stirling A. Colgate. In line 11, instead of the formula $E-E/\{[2/(E+1)^{\frac{1}{2}}]\}$, read $E-\{[2(E-1)]^{\frac{1}{2}}/\pi\}$.

D12, by F. C. Gilbert and Stirling A. Colgate. In line 17, instead of "This cross section is ½ that corresponding to the two events observed in nuclear emulsion above," read "This cross section is 1/6 that corresponding to the two events observed in nuclear emulsion above."

E12, by W. E. Henry. In reference 1, instead of "L. Brillouin, J. Phys. (USSR) **8**, 74 (1927)," read "L. Brillouin, J. phys. **8**, 74 (1927)."

H1, by C. N. Chou. In line 22, instead of "mu-meson," read "pi-meson."

H5, by Stephen S. Friedland and Henry S. Katzenstein. The following footnote is added: "This work was supported by a joint program of the AEC and the Research Corporation."

I9, by John K. Long, M. L. Pool, and D. N. Kundu. The last two sentences should be deleted.

L6, by Herman Hoerlin and Frank Kaszuba. Footnote * should read "Work performed under subcontract 31-109-38-193 with the Argonne National Laboratory."

PROGRAMME

MONDAY MORNING AT 10:15

Shirley-Savoy

(J. KAPLAN presiding)

Atmospheric Physics

A1. Recombination Processes in Oxygen.* JOSEPH KAPLAN AND MARX BROOK, *University of California, Los Angeles.*—The suggestion by M. Dufay that Krassovsky's observation of a night airglow emission at 9976A can be interpreted as the O−2 band of the forbidden atmospheric system of O_2, continues to confirm the fact first discovered by Kaplan in O_2 afterglows, that the $v'=0$ level of the $^1\Sigma$ state is probably exclusively observed, since bands originating on $v'>0$ are very weak or absent. The suggestion by D. R. Bates that selectivity could be produced by a secondary mechanism $O_2{}^1\Sigma(v'>0)+O_2{}^3\Sigma(v''=0)=O_2{}^3\Sigma(v''>0)+O_2{}^1\Sigma(v'=0)$ is discussed in the light of current ideas regarding the Herzberg and Vegard-Kaplan bands in the night airglow. The relationship between these observations in O_2 and the afterglows associated with very weak electrical discharges in N_2 and in N_2-O_2 mixtures is discussed, since the $v'=0$ selectivity was first discovered in the latter. This discussion indicates that the primary three-body recombination process is directly responsible for the $v'=0$ selectivity and that no secondary process is required. Experiments designed to clarify the mechanism responsible for the selectivity in O_2 will be described.

* This work has been sponsored by the Geophysical Research Division of the U. S. Air Force.

A2. Observation of Non-Rayleigh Scattering in the Very Near Infrared Spectrum of the Day Sky. ROMUALD ANTHONY, *Inyokern.*—Spectra of the day sky were obtained at several different azimuth angles away from the sun for approximately constant solar elevation. The region from 0.55μ to 2.2μ was recorded using a PbS cell receiver. By comparing the sky spectrum with the direct solar spectrum recorded a few minutes earlier, it was possible to observe the change in the spectral distribution that appears for different regions of the sky. The change is indicated by a graph which is a plot of the $\log(I_s/I_d)_\lambda$ *vs* $\log\lambda$ where I_s and I_d are the recorded sky and direct solar intensities, respectively. Experimental data of the solar spectrum and the sky spectrum published by Arthur Adel[1] were plotted in the same manner. Both curves are similar showing a pronounced discontinuity at approximately $\lambda=0.85\mu$ with a sudden increase in slope toward 1.2μ. Computed values of the "reduced scattering functions" $\sigma'(\varphi)$ *vs* α published by H. Holl[2] show a curve of precisely the same form.

[1] A. Adel, Phys. Rev. **76**, 446 (1949).
[2] H. Holl, Optik **4**, 173 (1948–49).

A3. Radiative Transfer and Equilibrium Associated with Far Infrared Bands in the Atmosphere.* J. I. KING, *University of Utah.*—Earlier theories of radiative heat transfer and equilibrium did not take into account the proportionality of line width with pressure. Within the region, however, where collision broadening prevails (up to heights of about 40 km) the pressure and hence line width decreases by a factor of about 200. Strong and Plass[1] recently considered this effect for an isothermal stratosphere, neglecting mutual overlapping of neighboring lines. We have been able to set up in analytical terms the equations of radiative transfer and equilibrium for pressure-broadened lines, both without and with overlapping. The latter case is a generalization of the earlier absorption formula of Elsasser for equal, equidistant lines. Numerical solutions of these equations are now being worked out. In addition we have proved a theorem stating that all such radiative equilibrium configurations have temperatures monotonically decreasing with height. Hence a near-isothermal stratosphere seems to require sources of heat other than far infrared transfer, e.g., the ultraviolet absorption of ozone.

* Supported by the Geophysics Division, Air Force Cambridge Research Center.
[1] J. Strong and G. N. Plass, Astrophys. J. **112**, 365 (1950).

A4. Spectral Solar Energy in the Near Infrared.* DAVID M. GATES, ROBERT F. CALFEE, AND BYRON E. COHN, *University of Denver.*—The spectral solar energy distribution in the near infrared between 1.0 and 6.0 microns was determined using a Perkin-Elmer Model 12C infrared spectrometer with NaCl optics. The solar radiation and the radiation from a Globar operated at 1441°K were alternately focused on the spectrometer entrance slit. At a given wavelength position and a fixed slit width the instrumental response to the Globar was determined and the solar energy attenuated by means of an iris diaphram aperture situated in the solar beam to give the same response. From the diameter of the aperture, the geometry of the system, and the known Globar emission the apparent solar emission in ergs/cm²/sec/unit wavelength interval was calculated. The values determined represent only apparent energies as seen through the earth's atmosphere. From 1.5 to 1.7 microns where atmospheric absorption is small the energies approach those characteristic of a blackbody at 7000°K. Determinations were made in Denver, Colorado, during periods of reduced atmospheric moisture during December, 1951 and January, 1952.

* The research reported in these papers has been sponsored by the Geophysics Research Division of the Air Force Cambridge Research Center.

A5. Atmospheric Water Vapor Determination by Means of Infrared Solar Spectroscopy.* ROBERT F. CALFEE, DAVID M. GATES, AND BYRON E. COHN, *University of Denver.*—The Perkin-Elmer Model 12C infrared spectrometer was used to obtain data concerning the atmospheric absorption of solar radiation in the region between 0.9 and 2.0 microns. Determinations were made with the atmospheric water vapor content ranging from one millimeter to one centimeter of precipitable water in the zenith direction. The earlier work of F. E. Fowle on transparency of aqueous vapor was essentially substantiated with some corrections. The spectrographic findings were compared with the meteorological soundings taken daily at Lowry Air Force Base at Denver, Colorado. Calibration curves for each telluric water band ρ, ϕ, and ψ were established. In order that reliable results should be obtained certain precautions with respect to slit width, recording speed, amplifier gain and other parameters need to be observed.

* The research reported in these papers has been sponsored by the Geophysics Research Division of the Air Force Cambridge Research Center.

A6. Atmospheric Ion Monitor. J. D. GRAVES, W. R. KETLER, AND R. I. CONDIT, *Broadview Research and Development.*—A compact, portable instrument to measure the concentration of ions in the atmosphere has been developed.[1] It consists of an ion chamber of cylindrical symmetry open to the atmos-

phere and provided with a blower for forcing air through the chamber. Electrical charges from the atmospheric ions are collected on the central electrode as the air passes through the chamber. Charges thus collected in this dynamic ion chamber are equivalent to those in a static ion chamber of much larger volume. The flow of air may be increased for greater sensitivity until disturbances within the air stream cause the formation ions. For sensitivity and freedom from fluctuations, a non-turbulent flow is desired. Since the insulator supporting the collecting electrode is exposed to the atmosphere, special precautions were taken in the design with respect to its voltage gradient, composition, temperature, and the circulation of air in its vicinity. The electric current resulting from the collected charge is amplified and indicated by conventional electrometer circuits. The completed device operates as a detector of high sensitivity (large collecting volume) free from absorbing walls or windows (open to the atmosphere).

[1] Initiated and supported in part by the Wesix Electric Heater Company of San Francisco, California.

A7. Local Atmospheric Ion Concentrations as a Basis for Personnel and Plant Protection. R. I. CONDIT, *Broadview Research and Development.*—The existing measurements of the ion concentrations in the atmosphere[1] have emphasized the natural conditions which exist free from the disturbances of man. In addition to these natural phenomena, however, the local ion concentrations within the confined spaces of buildings may be an effective and convenient indicator of certain industrial hazards. The local ion concentration is generally increased by the action of ionizing agents (flames, electrical discharges, nuclear radiation, ultra-violet light, static electricity); effected one way or the other by reactive gases (electropositive or electronegative); and influenced by certain dispersions of dust. Thus the atmospheric ion monitor may serve to guard against fire, escaping gases, electrical disturbances, radioactive contamination, and a variety of special technical hazards. In principle, the same monitor may even serve simultaneously to guard against several of the more likely dangers in a given plant. For example, a particular installation may be set up to monitor continuously the effectiveness of static electricity suppression around rotating machinery, while operating at the same time as a standby detector for the outbreak of fire and/or the explosion of an atomic bomb.

[1] J. A. Fleming, *Terrestrial Magnetism and Electricity* (Dover Publications, Inc., New York, 1949), Chapter IV.

A8. Wind and Temperature Measurements Above the Lower Isothermal Region of the Atmosphere by Acoustic Propagation Studies (July 1950–May 1951).* WILLIAM B. KENNEDY, *University of Denver* (introduced by Robert S. Bradford).—During the period July, 1950 through May, 1951, three sets of data per month were obtained from field observations sufficient for the determination of high level winds and temperatures. The method of operation and calculation employed was developed by A. P. Crary.[1] These studies show that, in the winter months, the upper winds (20 to 50 km) were of relatively large magnitude (greater than 30 m/sec) from the Northwest, and in the summer months, these winds were of lesser speeds (less than 30 m/sec) and Easterly. An analysis of results obtained show that the annual mean temperatures in the 20 to 45 km region were as shown in Table I.

TABLE I.

Altitude above sea level (km)	Annual mean temperature (C)
20	−61
25	−58
30	−49
35	−34
40	−14
45	−2

* This research is supported by the Geophysical Research Directorate of the Air Force, Cambridge Research Center.
[1] A. P. Crary, J. Meteorol. 7, 233 (1950).

Invited paper

A9. The Theory of Infrared Radiation in the Atmosphere. W. M. ELSASSER, *University of Utah.* (30 min.)

MONDAY MORNING AT 10:15

Cosmopolitan

(N. E. BRADBURY presiding)

Reactions of Transmutation

B1. Determination of the Cross Section of the Reaction $H^3(d, n)He^4$. J. P. CONNER, T. W. BONNER, AND J. R. SMITH, *Rice Institute.*—The reaction $H^3(d, n)He^4$ has been studied with bombarding deuterons for energies of 10 kev up to 1700 kev. Thin zirconium-tritium targets have been used. The cross section shows a pronounced peak at 109 kev and at this energy the total cross section was measured to be 5.1 ± 0.2 barns. From very low energies up to 800 kev a good fit to the experimental curve was given by the Breit-Wigner formula. Cross sections above this energy were larger than predicted by the one level formula.

B2. Cyclotron Bombardments with 21-Mev He^3. T. W. DONAVEN, D. N. KUNDU, JOHN K. LONG, AND M. L. POOL, *Ohio State University.*—A small amount of He^3 obtained from Oak Ridge was introduced into the cyclotron tank and accelerated to 21 Mev as calculated from the frequency of 13.5 Mc/sec. A recirculation cycle was worked out in course of which the oil diffusion pump was backed by two mercury diffusion pumps in parallel. The gas from the exhaust outlet of the mercury pumps was freed by a liquid hydrogen trap from the air which entered the system through natural leakage. The He^3 gas was then reinjected into the system. Neutrons and gamma-rays from a Be target were used to detect initially the resonance of the He^3 beam. A prominent 20-minute positron activity was produced from Be presumably from the reaction $Be^9(He^3, n)C^{11}$. A strong 1.8-hour positron activity of F^{18} was evident in all targets bombarded. This is attributable to small traces of oxygen on the targets.

B3. Angular Distribution of Protons from the Reaction $He^3(d, p)He^4$.* J. L. YARNELL, R. H. LOVBERG, T. F. STRAT-

TON, AND W. R. STRATTON, *University of Minnesota.*—The differential cross section for the production of protons by the reaction $He^3(d, p)He^4$ has been measured in the energy range 0.25 to 3.5 Mev. Monoergic deuterons from the Minnesota electrostatic generator were used to bombard a thin gaseous target of He^3. The protons emerged from the reaction chamber through a thin window and were detected in a NaI scintillation counter. Observations were made between the angles of 16° and 137° in the C-M system. The total cross section exhibits a broad maximum at 430±30 kev, and decreases slowly with energy above the resonance. The differential cross section above 1.5 Mev shows a minimum which moves to smaller angles as the energy is increased. Preliminary measurements show that the angular distribution at the peak of the resonance is anisotropic. Further data being taken at low energies will be reported.

* Supported by the joint program of the AEC and ONR.

B4. Cross Sections for $Li^6(n, p)He^6$, $Li^7(n, d)He^6$, and $Be^9(n, \alpha)He^6$ for 14-Mev Neutrons.* M. E. BATTAT AND F. L. RIBE, *Los Alamos Scientific Laboratory.*—Formation of He^6 by bombardment of Li^6, Li^7, and Be^9 with 14-Mev neutrons has been observed. The He^6 was identified by its 0.85 second half-life[1] and the decay observed on a ten-channel time-delay analyzer with channel widths of 0.4 and 1.0 second. The He^6 beta-rays were detected by means of a thin-walled aluminum proportional counter filled to 65-cm pressure with a Kr-CO^2 mixture. An over-all counting efficiency was determined by using the $Cu^{63}(n, 2n)Cu^{62}$ reaction, the cross section for which is known to an accuracy of 7 percent.[2] The effect of scattering and absorption of the beta-rays in Li and Be was measured. Targets of Be, normal Li, and enriched Li^6 and Li^7 were used. The cross sections determined for the $Li^6(n, p)$, $Li^7(n, d)$, and $Be^9(n, \alpha)He^6$ reactions were 6.7±0.8, 9.8±1.1, and 10±1 millibarns, respectively. The half-life of He^6 was found to be 0.83±0.3 second.

* Work performed under the auspices of the AEC.
[1] Natl. Bur. Standards Circular 499 (1950).
[2] S. G. Forbes, private communication.

B5. Low-Lying Levels of Al^{25} Observed from the $Mg^{24}(d, n)Al^{25}$ Reaction.* E. GOLDBERG,† *University of Wisconsin.*—A 67-kv Mg^{24} target was bombarded with 4.007-Mev deuterons and the neutrons from the $Mg^{24}(d, n)Al^{25}$ reaction were detected at seven angles with Ilford C2 emulsions. Preliminary readings of 1200 tracks at two angles indicate the presence of at least seven levels of Al^{25} of energies less than 3.4 Mev. Three of these are virtual and confirm previous findings from the $Mg^{24}+p$ elastic scattering[1] and capture[2] data. It is anticipated that additional information will be available from the emulsions exposed at the five other angles.

* Work supported in part by the Wisconsin Alumni Research Foundation and in part by the AEC.
† AEC Predoctoral Fellow.
[1] Mooring, Koester, Goldberg, Saxon and Kaufmann, Phys. Rev. **84**, 703 (1951).
Grotdal, Lönsjö, Tangen, and Bergstrom, Phys. Rev. **77**, 296 (1950).

B6. An Absolute Low Energy Cross Section Experiment.* J. A. PHILLIPS, W. R. ARNOLD, G. A. SAWYER, E. J. STOVALL, JR., AND J. L. TUCK, *Los Alamos Scientific Laboratory.*—A 5-millimeter-diameter pencil of collimated and analyzed deuterons passes through an 8-millimeter-diameter SiO window 7 $\mu g/cm^2$ thick into the target gas at 1-millimeter pressure. The beam current is measured on the high vacuum side of the film uncomplicated by neutral gas and charge exchange effects and with effective guard ring precautions. In the gas a length of the beam is viewed at 90° by two diametral proportional counters. The measured small divergence of the beam together with a measured counter slit system gives a definite target volume and calculable geometry. The gas temperature and pressure are observed continuously, the latter by a sensitive diaphragm micromanometer continuously calibrated against an absolute fluid manometer. The beam energy and its distribution in the target volume are determined separately by allowing the beam to continue into a retarding field and measuring the current as a function of a retarding potential. Cross sections for the reactions DDp, DDn, DT, DHe^3 have been completed.

* Work performed under the auspices of the AEC.

B7. DD Cross Sections 14–110 Kev.* W. R. ARNOLD, J. A. PHILLIPS, G. A. SAWYER, E. J. STOVALL, JR., AND J. L. TUCK, *Los Alamos Scientific Laboratory.*—Measurements have been obtained at 50 points over the above range with 1 percent statistics and 6 percent estimated over-all accuracy above 25 kev. By changing the gas pressure and window thickness in the proportional counters, and using a 6-channel recorder, protons and He^3 nuclei, and, as a check, H^3 were separately counted. The observations were made at 90°, and the integrated cross sections derived from the angular distributions of Bretscher and French.[1] A selection of the results are given in Table I. $\sigma_{DD\ total}$ lies on a Gamow plot of slope 19.34 $\log_{10}$ barns kev/kev[1] close to the theoretical value. The branching ratio $\sigma_{DDn}/\sigma_{DDp}$ approaches a steady value of 0.94 at the lowest energies.

TABLE I.

E_D kev	15	30	45	60	75	90	105
σ_{DDp} millibarns	0.079	1.17	3.6	6.7	10.1	13.4	16.4
σ_{DDn} millibarns	0.074	1.10	3.4	6.5	9.8	13.1	16.1

* Work performed under the auspices of the AEC.
[1] E. Bretscher and A. P. French, Phys. Rev. **75**, 1154 (1949).

B8. TD Cross Sections 15–125 Kev.* E. J. STOVALL, JR., W. R. ARNOLD, J. A. PHILLIPS, G. A. SAWYER, AND J. L. TUCK, *Los Alamos Scientific Laboratory.*—Using 99 percent tritium gas in the target chamber, about 50 measurements at 90° have been obtained over the above energy range with 1 percent statistics and 6 percent estimated over-all accuracy above 25 kev. A selection of the cross sections obtained, assuming an isotropic angular distribution, appears in Table I.

TABLE I.

E_D kev	15	30	45	60	75	90	105
σ_{TD} barns	0.0154	0.28	1.0	2.2	3.6	4.6	4.94

σ_{TD} shows a peak at 107-kev E_D, with magnitude 4.95 barns, and at 25 kev has a Gamow coefficient of 19.35 $\log_{10}$ barns kev/kev[1] close to that of DD and to the theoretical value.

* Work performed under the auspices of the AEC.

B9. He^3D Cross Sections 35–100 kev.* J. L. TUCK, W. R. ARNOLD, J. A. PHILLIPS, G. A. SAWYER, AND E. J. STOVALL, JR., *Los Alamos Scientific Laboratory.*—Using 99 percent He^3 gas in the target chamber, the He^3D cross section has been measured at 25 points with 1 percent statistics and 6 percent estimated over-all accuracy counting alpha-particles. A selection of the cross sections calculated, assuming an isotropic angular distribution, appears in Table I. The Gamow plot is

TABLE I.

E_D kev	35	45	55	65	75	85	95
σ_{He^3D} millibarns	0.109	0.51	1.5	3.4	6.4	10.5	16.0

linear with slope 38.9 $\log_{10}$ barns kev/kev^4. This is 2.01 times the DD slope measured previously in satisfying agreement with the theoretical value of 2. The deuteron energies cited above are sugject to a downward revision of a few hundred volts due to the energy loss in the He^3 gas. Appropriate energy loss cross sections are being measured using the same apparatus.

* Work performed under the auspices of the AEC.

B10. Photo Protons from Heavy Elements. W. E. STEPHENS AND M. E. TOMS, *University of Pennsylvania.**—The photoprotons ejected from bismuth, cerium, and barium by the 24-Mev bremsstrahlung from the University of Pennsylvania betatron have been measured in nuclear emulsions. Preliminary results give yields of approximately $16 \cdot 10^4$ and $23 \cdot 10^4$ protons per mole per roentgen unit for Ce and Ba, respectively. A second run with better statistics than our previous data gives $4 \cdot 10^4$ $p/m/r$ from bismuth. The yields calculated from an evaporation process are roughly $0.4 \cdot 10^4$, $0.07 \cdot 10^4$, and $0.09 \cdot 10^4$ $p/m/r$ for Bi, Ce, and Ba, respectively. The angular distribution of the bismuth photoprotons is markedly asymmetric with three times as many protons at 30° and 50° as at 130° and 150°. If these asymmetric protons are ascribed to a direct photoelectric effect, then at least half of the bismuth yield is due to such an effect. It would seem reasonable then to associate the high yields from Ce and Ba also with a direct effect. The angular distribution of the photoprotons from Ce and Ba will be measured to examine this further.

* Assisted by the Air Research and Development Command and by the joint program of the ONR and AEC.

MONDAY MORNING AT 10:00

University of Denver

(HARVEY FLETCHER presiding)

General Physics; Fluid Dynamics

C1. Utah Digital Computer.* D. C. EVANS AND W. M. ELSASSER, *University of Utah.*—Recent developments have made available machines of large arithmetical capacity which can be operated by an individual physicist. Our installation now consists of the digital differential analyzer made commercially by the Northrop Aircraft Corporation, and an input-output device constructed by us. The latter is operated automatically by the machine and uses punched paper tape as external memory. We are now supplementing these devices by a 10×10 size linear-secular equation solver (analog machine; expected accuracy 0.1 percent). The digital differential analyzer has a capacity comparing favorably with that of a very large mechanical analyzer; its accuracy is variable and directly proportional to running time. For typical problems and conventional three-digit accuracy, running time is of the order of some minutes. The arithmetical methods used in our devices are much closer to processes of traditional mathematical analysis than is the case for most digital machines; this feature makes it possible to operate these machines without the benefit of experts in numerical computing. Our experience to date has convinced us that the aim of a physicist to do his computing personally rather than to relay it to a separate organization can eventually be achieved.

* Supported by the Geophysics Division, Air Force Cambridge Research Center.

C2. A Table Model Computer for Fourier Synthesis. BARTON J. HOWELL.—An analog computer is described for Fourier synthesis using optical methods, and is discussed on the basis of its utility in computing the projection of crystal structures from x-ray data. The computed two-dimensional structure is recorded photographically. The instrument is based on the principles of the "multiple projector"[1] using "modified Huggins masks"[2] but differs in the methods of obtaining multiple light sources with individual intensity controls. The major advantages of this instrument are (a) its small size; (b) the reproducibility of all components in manufacture; (c) independence from ambient or permanent power conditions; and (d) ease of adjustment and rapid computations.

[1] Dan McLachlan, Jr., and Roscoe H. Woolley, Rev. Sci. Instr. **22**, 423 (1951).
[2] Howell, Christensen, and McLachlan, Jr., Nature **168**, 282 (1951).

C3. Kinks in Gases. GEORGE ANTONOFF.— As in solids and liquids kinks are also observed in gases. The value PV (pressure-volume) can be easily measured with five significant figures. Only three of them show themselves reproducible. To assure the last two figures the substance must be suitably conditioned. Change in properties with time may be observed, until the system reaches the equilibrium. The process is accelerated by impurities, such as water. In drastically dried systems (J. B. Baker) properties can be fixed for long. For reproducibility the impurities must be standardized and the time factor considered. The discrepancies observed are not due to inaccuracy in measurements.

C4. On the WKB Method. STANLEY C. MILLER, JR., AND R. H. GOOD, JR., *University of California, Berkeley.*—Ordinarily the WKB method is used both to demonstrate the classical limit of quantum mechanics and to obtain approximate solutions of the one-dimensional Schrödinger equation. At the expense of losing the classical limit demonstration, an improved approximation may be obtained. The usual procedure of substituting $\psi(x) = \exp i\hbar^{-1}[S_0(x) + \hbar S_1(x) + \cdots]$ into the Schrödinger equation and expanding for small $\hbar$ can be modified by using a more appropriate function than the exponential. For example, to discuss the Schrödinger equation for a potential well with two turning points, one can take, instead of the exponential, the functions arising in the harmonic oscillator problem, where the potential is of the same general type. There results an approximate wave function, continuous even across the turning points, which, far from the turning points, approaches the usual WKB function. The eigenvalue condition is identical with the ordinary WKB condition. The potential barrier problem can be treated similarly giving, for small penetration, the ordinary WKB transmission coefficient, but giving a different result for an energy near the peak of the barrier.

C5. Euclidean Tensors. WESLEY E. BRITTIN AND JAMES H. MARABLE, *University of Colorado.*—The n-dimensional Euclidean group $0(n)^1$ may be represented by the set of all matrices, E, of the form $\begin{bmatrix} 0(n) & t \\ 0 & 1 \end{bmatrix}$, $0(n)$ being an $n \times n$ orthogonal matrix, t an $n \times 1$ matrix, and 0 the $1 \times n$ zero matrix. E

may be considered as the matrix of a coordinate transformation relating two equivalent Euclidean frames of reference. Quantities defined in every frame and transforming under E as $ExEx\cdots xExE'^{-1}x\cdots xE'^{-1}xE'^{-1}$, a prime denoting the transpose, will be called Euclidean tensors. (A more modern definition would be based on an arbitrary representation of $0(n)$[1], but the present definition is sufficient for many applications and parallels the term, Cartesian tensor.) In certain applications where Euclidean relativity is required, the Euclidean tensors arise quite naturally. (In the pseudo-Euclidean space of special relativity 0(4) must be taken to be a Lorentz matrix.) Second-order skew-symmetric Euclidean tensors correspond to the motors of line geometry. An application to the dynamics of rigid bodies will be made, and the results compared with the corresponding but more complicated motor treatment.

C6. On the Phase Space of a Nonlocalizable Elementary Particle. E. J. SCHREMP, *Naval Research Laboratory*.—By considering the projective properties of the complex essential parameters q^1/q^0, q^2/q^0, q^3/q^0 of the proper Lorentz group (where $q=e_0q^0+e_1q^1+e_2q^2+e_3q^3$ is a general complex quaternion of norm Pe^{iS}), one may show that these parameters determine and are determined by two canonically conjugate quaternions $p=e_0p^0+i(e_1p^1+e_2p^2+e_3p^3)$, $x=e_0x^0+i(e_1x^1+e_2x^2+e_3x^3)$, with real coordinates p^k, $x^k(k=0, 1, 2, 3)$ in the tangent space T_4 to space-time (the corresponding rays through the origin of T_4 being equivalent, respectively, to the actual and ultra-infinite points of a real hyperbolic 3-space). These coordinates p^k, x^k have been identified with the external momentum and internal configuration variates of a single nonlocalizable elementary particle; and the real gauge P has been interpreted as the particle's coefficient of probability of phase $P(p;x)$, and the imaginary index S as the integral $\int(p\,d\bar{x}+dx\,\bar{p})$.[1] For $P>0$, the quaternion transformation $p\bar{q}=q\bar{e}^{iS}$, $2x=(q/\bar{q}^0)p-p(q/q^0)$ so determines p and x that their norms, $p\bar{p}=m^2(=1)$ and $x\bar{x}=-r^2$, are absolute and relative invariants, respectively (the only invariant constraint upon x^k, for $r>0$, being the null-polarity $p\bar{x}+x\bar{p}=0$). The inverse transformation, valid for $P\not\equiv 0$, is $q/q^0=(\bar{x}/x^0)(e_0-pe^{\pm iS_0})$, where $\cos S_0=p^0-x^0$ and $q^0/\bar{q}^0=e^{i(S\mp S_0)}$.

[1] In taking the complex conjugate, denoted by the bar (¯), it is here understood that the quaternion units e_0, e_1, e_2, e_3 are real.

C7. Fast Jets from Collapsing Cylinders. F. J. WILLIG, F. A. LUCY, AND R. G. SHREFFLER.—A method is described for producing fast jets from the collapse of metal-line cavities in high explosives. The behavior of these jets suggests that they cannot be accounted for by the simple hydrodynamical considerations that have in the past been successful when applied to slower type jets. Various experiments, including time resolved spectrographic observations, show the jets to be, at least in part, of a gaseous nature. Velocities as high as 90 km/sec have been observed for beryllium jets, with heavier elements exhibiting lower velocities in inverse order of their atomic weights.

C8. A Study of Impinging Liquid Jets in a Liquid Stream. GEORGE G. KRETSCHMAR AND HENRY W. WEDAA, *Inyokern*.—Two miscible organic liquids are injected into a vertical tube containing the mixture of the two liquids. The volume ratio of injection is maintained constant by means of a positive displacement hydraulic injection equipment. The injector is of a fixed geometry as regards size of injector holes and the angle of impingement. A study of the mixing of the two liquids has been carried on by an optical method making use of a modified schlieren system. The liquid stream is in a round glass tube which is contained in a rectangular glass-sided cell filled with liquid of about the same index of refraction as the glass tube. This masks the refractive effect of the glass tube and much of the lens effect of the round cross section of the stream. It is shown that for a definite minimum energy of injection, the mixing becomes essentially complete at the end of the mixing region. The region of mixing appears in the photographs as a region of special turbulence above the jet openings, in which the jet energy is being dissipated.

C9. Dependence of Pfeifenton (Pipe Tone) Frequency on Pipe Length, Orifice Diameter, and Gas Discharge Pressure. A. B. C. ANDERSON, *Inyokern*.—When a pipe terminated in an orifice is attached to a large vessel containing gas, a spectrum of acoustic notes is produced inside the pipe as the gas pressure in the vessel is either raised or lowered. These notes differ from ordinary organ pipe notes in that they are produced in and by the gas discharging continuously from the orifice. Most studies related to this phenomena were made during the last century and the oscillations were then called *Pfeifentöne*. Measured dependences of the *Pfeifenton frequency* on static flow pressure, orifice diameter, and pipe length are presented here, based upon studies of air flowing through pipes terminated in various orifices. Frequency measurements were made of the vibrations inside the pipe. The *Pfeifentöne* are not a series of discrete single valued harmonics. Each covers a range of frequencies, any specific value of which is determined by the discharge flow-velocity or pressure. When the orifice diameter approaches zero the behavior of the *primary Pfeifenton* frequencies is as if they were produced by an open-closed organ pipe; when the orifice diameter approaches that of the pipe, the behavior is as if they were produced by an open-open organ pipe. A mechanism for the excitation of the *Pfeifentöne* is proposed.

C10. Analog Computation in a Theory for Critical Stability of a Fluid. F. T. ROGERS, JR., AND H. L. MORRISON, *Inyokern*.—Reference 1 derives two simultaneous linear differential equations in mixed variables and nonconstant coefficients, which, with suitable boundary conditions, define the thermal environment at critical stability of a fluid (heated from below) in a porous medium. It also presents a solution of the system as got by the beginning of successive approximations. At the suggestion of, and with the advice of, Dr. R. H. Olds, two limiting cases have been solved on the N.O.T.S. analog computer, one for $\nu=0$ and $\varphi=0$, the other for $\varphi=0$; notation is that of reference 1. Since the system represents a characteristic value problem, analog computation involved the automatic generation of dependent variables by the machine, for various values of the parameter whose characteristic value was sought. Examination of charts of generated dependent variables served to identify those forms which satisfied boundary conditions, and hence the desired characteristic value. We wish to report that for each limiting case above referred to, analog computation led to results which are essentially indistinguishable from those listed in reference 1.

[1] Rogers, Schilberg, and Morrison, J. Appl. Phys. **22**, 1476 (1951).

C11. Application of a Generalization of Heisenberg's Model of Turbulence to Critical Reynold's Numbers. E. N. PARKER, *University of Utah*.—It is possible to generalize the turbulence model proposed by Heisenberg for isotropic homogeneous turbulence fields, to the case of anisotropic inhomogeneous fields. Application of the resulting equations to computation of critical Reynold's numbers has been carried out on the belief that it poses a critical test of the model. In particular, the critical Reynold's number for flow through a pipe has been calculated and is found to agree with experiment. The somewhat more complicated problem of flow past a plate has been carried out, the results again being in agreement with experiment and results obtained by Lin[1] and others directly from the Navier Stokes equations. The advantage of the model is, first, the ease with which results may be obtained, and

second, the clear physical insight afforded by the simple calculations involved.

[1] C. C. Lin, Quart. Appl. Math. 3, 117, 218, 277 (1945).

C12. Scabbing of Metals Under Explosive Attack: Multiple Scabbing.* JOHN S. RINEHART, *Inyokern.*—Further quantitative data bearing on the scabbing of metals under explosive attack are presented in this paper. In particular, the mechanics of the generation of multiple scabs is established. Experimental data have been obtained that show that multiple scabbing will occur whenever the maximum stress σ_0 in the transient wave that impinges on a free surface is more than double the critical normal fracture stress σ_c of the material. The number of scabs that will be formed will be equal to the first whole number smaller than the quotient σ_0/σ_c. The thickness of each scab is governed by the shape of the stress wave.

* Work supported by Armament Branch, ONR.

C13. Rayleigh Disk Measurements in He^3–He^4 Mixtures. JOHN R. PELLAM, *National Bureau of Standards*, AND BERNARD WEINSTOCK, *Argonne National Laboratory.*—Observations of second sound propagation in a four percent mixture of helium 3 in helium 4 have been carried out. Both wave velocity and mechanical energy density of second sound waves have been observed by means of the disk in the temperature range from 2°K down to 0.9°K. Our extension of measurements beyond the range of Lynton and Fairbank[1] (0.8 percent of He^3 concentration and down to 1.2°K) have shown no decrease in velocity as predicted by Pomeranchuk;[2] rather for this new region the velocity tends to rise even more rapidly down to the lowest temperatures reached (about 38 m/s at 0.9°K) as predicted by Dingle.[3] The prediction of Koide and Usui[4] that torque on the Thermal Rayleigh disk would drop markedly (for constant heat current) has been confirmed. Our observations show that at 0.9°K, for example, the presence of 4 percent helium 3 decreases the mechanical energy density (and thus the torque) from the pure helium 4 value by more than two orders of magnitude.

[1] E. Lynton and H. Fairbank, Phys. Rev. **80**, 1043 (1950).
[2] L. Pomeranchuk, J. Exptl. Theoret. Phys. USSR **19**, 42 (1949).
[3] R. Dingle, Phil. Mag. **42**, 1080 (1951).
[4] S. Koide and T. Usui (to be published).

MONDAY AFTERNOON AT 2:00

Cosmopolitan

(W. W. HAVENS presiding)

Neutrons and General Nuclear Physics; Positronium

D1. Inelastic Scattering of 7.7-Mev Protons.* J. A. HARVEY,† *M.I.T.*—Inelastic protons have been observed from targets (several mg/cm² thick) bombarded with 7.7-Mev protons from the M.I.T. cyclotron. The inelastic proton spectra were measured with aluminum absorbers and previously described equipment.[1] The following targets have been studied: lithium, beryllium, carbon, fluorine (Teflon), sodium, magnesium, aluminum, calcium, titanium, vanadium, nickel, and zirconium. For the targets where excited levels are already known the inelastic proton groups agreed with the known levels. The first excited level observed in Ca^{40} occurred at 3.8 Mev. Angular distributions of the inelastic proton groups are approximately isotropic over the angles studied. The inelastic protons from the 1.38-Mev level in Mg^{24} have also been measured with 5.9- and 6.8-Mev protons and the angular distributions vary with energy. Cross sections of the inelastic protons have been measured relative to the elastically scattered protons from a thin gold target. The total cross sections range from 200–500 mb except for vanadium which is only 40 mb. This is probably due to the low (p, n) threshold of vanadium.

* Supported in part by the ONR and AEC.
† Now at Brookhaven National Laboratory.
[1] Boyer, Gove, Harvey, Deutsch, and Livingston, Rev. Sci. Instr. **22**, 311 (1951).

D2. Neutron-Proton Scattering Using Organic Crystal Scintillation Detectors.* M. E. REMLEY,† W. K. JENTSCHKE, AND P. G. KRUGER, *University of Illinois.*—Organic scintillation crystals of anthracene and stilbene have been used as both a source and detector of recoil protons to investigate the angular distribution of protons recoiling from fast neutrons. Neutrons of 13.7 and 28.4 Mev were obtained from the $D(d, n)He^3$ and $T(d, n)He^4$ reactions with deuterons accelerated by the University of Illinois cyclotron. The amplified output of a 5819 photomultiplier was analyzed with a twelve channel pulse amplitude analyzer. Using the known pulse height *vs* energy relation for protons incident on the crystals, the data were converted to angular distributions. The corrections required for the finite size of the crystals were calculated and applied to the data. The angular distribution obtained at 13.7 Mev is consistent with spherically symmetric scattering in the center-of-mass system, while the results at 28.4 Mev show an anisotropy with a favoring of scattering in the backward direction. This anisotropy appears somewhat greater than that predicted by Christian and Hart,[1] using a Yukawa potential with exchange forces plus the inclusion of a tensor force. However, the results are consistent with previously reported results at 27 Mev.[2]

* Assisted by the joint program of the ONR and AEC.
† Now at North American Aviation, Inc., Downey, California.
[1] R. W. Christian and E. W. Hart, Phys. Rev. **77**, 441 (1950).
[2] Brolley, Coon, and Fowler, Phys. Rev. **82**, 190 (1951).

D3. Total Cross Sections for 14-Mev Neutrons. J. H. COON, E. R. GRAVES, AND H. H. BARSCHALL, *Los Alamos Scientific Laboratory.*—The total cross sections of over 50 elements were measured for 14-Mev neutrons in a geometry in which the effect of scattering through angles greater than 2° was observed. A plot of the square root of the total cross sections *versus* the one-third power of the atomic weight shows deviations from the linear relationship predicted by statistical theory.[1] The deviations are most pronounced for low and high atomic weights.

* Work performed under the auspices of the AEC.
[1] H. Feshbach and V. F. Weisskopf, Phys. Rev. **76**, 1550 (1949).

D4. Response of Organic Crystals to Neutrons. T. W. BONNER, A. B. LILLIE AND H. L. TAYLOR, *Rice Institute.*—Recoil-protons from monoenergetic neutrons have been observed in anthracene, stilbene, terphynl, and diphenylacetylene crystals. The ratio of pulse sizes from 580-kev recoil-protons in these crystals has been compared to that from 660 kev gamma-radiation. The largest proton pulses relative to gamma-ray pulses were observed in anthracene;

the other crystals followed in the order of stilbene, terphynl, and diphenylacetylene. 60-kev recoil-protons from threshold neutrons of the reaction $H^3(p, n)He^3$ were observed in an anthracene crystal. 1.5-Mev carbon recoils from 4.5-Mev neutrons were also detected in anthracene.

D5. The Two-Plate Method of Measuring Anisotropic Fast Neutron Spectra.* JOHN E. EVANS, *Los Alamos Scientific Laboratory*.†—Anisotropic, as well as isotropic, fast neutron spectra can be measured by exposing two nuclear plates in planes 90° apart. In plate No. 1 tracks $\leq 45°$ (unprocessed emulsion) from the emulsion plane are measured at all azimuth angles. In plate No. 2 tracks are measured if their directions fall in the supplementary double cone. The sum of tracks from equal volumes of both plates constitute all proton recoils which originate in that volume of emulsion and the formula of Reines[1] gives the neutron density spectrum. No tracks with angles $>45°$ from the emulsion plane must be measured. Small length corrections[2] (0 to 7 percent) must be made to tracks between 25° and 45° from the emulsion plane, since the track shrinkage differs from the emulsion shrinkage at these angles. By measuring tracks which start in the central 20-micron layer in a 200-micron emulsion spectra can be measured from 600 kev to 4.1 Mev. 1050 tracks have been measured from a pair of plates exposed to two groups of monoenergetic neutrons about 500 kev apart. Two well separated peaks were obtained.

* Work done under the auspices of the AEC.
† Present Address: Phillips Petroleum Company, Idaho Falls, Idaho.
[1] F. Reines, Phys. Rev. **74**, 1565 (1948).
[2] J. Rotblat and C. T. Tai, Nature **A164**, 835 (1949).

D6. Mirror Measurement of the Neutron-Electron Interaction. D. J. HUGHES, J. A. HARVEY AND M. D. GOLDBERG, *Brookhaven National Laboratory*.*—In the method[1] of measurement of the neutron-electron interaction by reflection of neutrons from a bismuth-liquid oxygen interface, the principal uncertainties arise from the measured values of the critical angle and the free atom cross sections of bismuth and oxygen. The accuracy of the critical angle measurement has now been improved to the extent that the uncertainty in the well depth (now 4250 volts) of the interaction from this source is only 250 volts. The present values of the bismuth and oxygen free atom cross sections, based on separate transmission measurements for each element, contribute a somewhat larger error. Because the difference of the oxygen and bismuth scattering amplitudes enter the expression for the critical angle, only the *relative* transmissions are needed accurately. The relative transmissions are now being measured by a self-monitoring method, involving two pile beams, in which high counting rates can be used with no dead-time correction. The present 4250-ev result may change slightly but the final error, including all uncertainties, will be about 400 ev. When 4100 ev for the Foldy effect (magnetic dipole interaction) is subtracted, the mesonic effect is extremely small.

* Research carried out under contract with the AEC.
[1] Harvey, Hughes, and Goldberg, Bull. Am. Phys. Soc. **27**, No. 3, 44 (1952).

D7. The Paramagnetic Neutron Scattering Cross Section of Various Transition Group Ions at Long Neutron Wavelengths.* R. R. SMITH, *Columbia University and Brookhaven National Laboratory*, AND T. I. TAYLOR AND W. W. HAVENS, JR., *Columbia University*.—The paramagnetic neutron-scattering cross section has been determined for the following ions; Fe^{+++} in FeF_3 and $ZnFe_2O_4$, and Mn^{++} in MnF_2 and MnO. Because of the high intensity of subthermal neutrons available from the Brookhaven reactor, it was possible to carry out measurements at neutron wavelengths long enough for the paramagnetic scattering to become isotropic. For this limiting condition, theory indicates a cross section of 21 barns per ion for uncoupled paramagnetic ions.[1] Such was found to be the case with FeF_3, $ZnFe_2O_4$, and MnF_2. The cross-section variation with wavelength found for the Mn^{++}-ion in MnF_2 was in excellent agreement with the theoretical.[1] The paramagnetic scattering of the Mn^{++}-ion in MnO behaves differently. Because the electron spins are partially coupled in this compound, many of the collisions will be inelastic. Thus, instead of a form factor increase of scattering with wavelength a $1/v$ dependence is to be anticipated. This was found to be the case. The lattice vibrational inelastic scattering was estimated from slight $1/v$ dependences of the experimental curves at wavelengths long enough for the paramagnetic contribution to be constant.

* Research carried out under AEC contract with Columbia University.
[1] O. Halpern and M. H. Johnson, Phys. Rev. **55**, 898 (1939).

D8. Nuclear Relaxation Time of Hydrogen Gas. MARTIN E. PACKARD, *Varian Associates*, AND HARRY E. WEAVER, *Stanford University*.—The nuclear relaxation time T_2 of hydrogen gas has been measured as a function of pressure over the range of $\frac{1}{4}$ atmosphere to 40 atmospheres. The data below 3 atmospheres was taken by measuring the nuclear magnetic resonance line width as recorded by a phase sensitive detector. The data above 4 atmospheres was obtained from a direct line-width measurement recorded photographically from an oscilloscope having a very slow sweep. This data was corrected for the broadening effects of the magnet. Spin echo measurements of T_1 were made at the higher pressures and were found to agree within experimental error to the line width measurements of T_2 at the same pressures. The relaxation time T_2 is found to be almost directly proportional to the pressure[1] and to have as representative values a T_2 of $(1.0\pm0.2)\times10^{-4}$ second at 1 atmosphere, and $(1.2\pm0.2)\times10^{-3}$ second at 10 atmospheres.

[1] N. Bloembergen, *Nuclear Magnetic Relaxation* (Martinus Nijhoff, 1948), p. 103.

D9. The Roughness of the Nuclear Energy Surface. JOHN A. ELDRIDGE AND RICHARD J. BRUNDY, *State University of Iowa*.—When a proton or neutron is added to a nucleus the binding energy ($B.E.$) of the two particles differ because they differ in mass, because they change the isotopic number oppositely, and because of a specific preference for certain proton and neutron numbers (p, n). By allowing for the first two effects we obtain values (D_s) which show the depression increments (in Mev) of the energy surface of the nuclides below a smooth parabolic valley. As typical, values are given for two particular nuclide chains along the energy surface.

	H^3	H^4	H^5	He^6	He^8	Li^9	Li^7	Be^9
(p,n)	(1,0)	(1,1)	(1,2)	(2,2)	(2,3)	(3,3)	(3,4)	(4,4)
ΔD_s	−17	12.7	14.1	3.2	1.7	9.5	15.6	
$B.E.$	2.18	6.2	19.8	−0.8	4.5	7.2	17.2	

	N^{14}	O^{15}	O^{16}	F^{17}	F^{18}	F^{19}	F^{20}	Ne^{21}
(p,n)	(7,7)	(8,7)	(8,8)	(9,8)	(9,9)	(9,10)	(9,11)	(10,11)
ΔD_s	10.6	13.2	3.2	6.7	9.8	7.6	12.6	
$B.E.$	7.3	15.6	0.51	9.1	10.3	6.4	13.0	

The consistently larger (underlined) values of D_s when either p or n changes from odd to even show the effect of pairing.

D10. A New Conception of Nuclei and Elementary Particles. ENOS E. WITMER, *University of Pennsylvania*.—The masses of nuclei and elementary particles in all states are given by Mm, where m is the rest mass of the negative electron and M is a rational number. For this reason the writer has proposed the idea[1] that there are no particles in the nucleus. Fundamentally the nuclei and so-called elementary particles are on a par. To explain the good results obtained with individual particle models, we propose a *new correspondence principle*, according to which an individual particle model of any assumed compound structure of nuclear character may give good results in many respects whenever the transition to

a state in which any of the assumed constituent particles exist in the free state does not involve neutrinos. It seems reasonable to add the requirement that the binding energy per particle in the assumed compound structure shall be only a small fraction of the rest mass of the assumed constituent particles. This principle rules out electrons as satisfactory constituent particles, but not protons, neutrons, and alpha-particles. In any case such an assumed particle model is only an approximation to what actually exists.

[1] E. E. Witmer, Bull. Am. Phys. Soc. **27**, No. 3, Abstract SP2, Washington Meeting, 1952.

D11. The Use of Annihilation of Positrons in Flight to Give a Peaked Gamma-Ray Spectrum. STIRLING A. COLGATE, *University of California, Berkeley.*—The theoretical behavior of the annihilation of positrons in flight with a negative electron at rest was derived by Dirac.[1] The total cross section at high energy is qualitatively checked by the experiment (above), so that the theoretical gamma-ray spectrum can be relied upon. This spectrum is strongly peaked at the high and low energy ends. In one-half the annihilation events, one of the two gamma-rays has an energy greater than $E-E/\{\pi[2/(E+1)^{\frac{1}{2}}]\}$ where E is the total energy of the positron. The spectrum of annihilation plus bremsstrahlung for positrons passing through low Z materials is favorable from 10 Mev up to 200 Mev for threshold type experiments. 10-Mev positrons passing through $\frac{1}{2}$ cm of LiH will give an annihilation spectrum peak 10 percent (full width and 50 times the intensity of the upper 10 percent) of the bremsstrahlung spectrum. 200-Mev positrons passing through 1/100 radiation lengths (30 cm) of liquid hydrogen give a peak 6 times the bremsstrahlung intensity and 3 percent wide.

[1] P. A. M. Dirac. Proc. Cambridge Phil. Soc. **26**, 361 (1930).

D12. The Annihilation of Positrons in Flight at 100 and 200 Mev. F. C. GILBERT AND STIRLING A. COLGATE, *University of California, Berkeley.*—The two disappearances observed by Gilbert *et al.*[1] of 200-Mev electrons in flight in nuclear emulsion prompted the following investigation by counters of the general question of the annihilation in flight of positrons and electrons. A poor geometry absorption experiment was performed in Be and LiH in absorbers thin compared to the processes multiple scattering, single scattering, and bremsstrahlung. Three small proportional counters in a magnetic field determined the momentum of electrons or positrons from a radiator in the bremsstrahlung beam of the Berkeley synchrotron. A fourth large counter backed up a small absorber and by anticoincidence indicated the absorption of the particle. The cross section for the theoretically known process of annihilation in flight by positrons at 200 Mev agreed with theory ±25 percent. This cross section is $\frac{1}{3}$ that corresponding to the two events observed in nuclear emulsion above. The disappearance of electrons in flight at 200 Mev was $\frac{1}{3}$ the positron annihilation cross section and corresponded to the approximate bremsstrahlung loss. At 100 Mev, positron annihilation doubled in agreement with theory and electron disappearances were the same. Better statistics are anticipated.

[1] Violet, Gilbert, Deutsch and Barkas, Phys. Rev. **85**, 756 (1952).

D13. Magnetic Quenching of the Three-Quantum Annihilation of Positronium. OTTO HALPERN, *University of Southern California.*—Observations on the change in the number of three-quantum processes of annihilation of positronium in a constant magnetic field have been reported by Deutsch and Dulit[1] and recently in a summary form by Wheatley and Halliday.[2] The theory of this quenching process has been extended to include the assumption that transitions between the three states of ortho-positronium are produced by collisions with a rate that is not vanishingly small as compared with the various rates of annihilation. This refinement of the theory may be required to account for the observation[3] that the number of three-quantum processes decreases to one-half of its original value for large magnetic fields. We have also worked out a more detailed theory for the influence of an additional alternating magnetic field;[3] formulas for the determination of the splitting of the energy-levels of para- and ortho-positronium[4] and a comparison with the experiments[3] will be presented.

[1] M. Deutsch and E. Dulit, Phys. Rev. **84**, 601 (1951).
[2] J. Wheatley and D. Halliday, Bull. Am. Phys. Soc. **27**, 59, Y4 (1952).
[3] M. Deutsch and S. C. Brown, Phys. Rev. **85**, 1047 (1952).
[4] A. Klein and R. Karplus, Bull. Am. Phys. Soc. **27**, 59, Y3 (1952).

MONDAY AFTERNOON AT 2:00

University of Denver

(E. J. WORKMAN presiding)

Electronic and Solid-State Physics

E1. On the Relation Between the Conductance and the Noise Power Spectrum of Certain Electronic Streams. J. J. FREEMAN (*introduced by* Harold Lyons).—The noise power spectrum of a diode with a temperature-limited current and also for a diode with a retarding field is shown to be the sum of two parts. One, the "pure" shot effect, is the spectrum that would obtain if the electrons were all emitted with zero velocity, that is, if the cathode were at zero temperature (and still maintained the same emitting properties). The second is the thermal contribution; namely, $4kTg$, where T is the cathode temperature and g is the conductance of the electron stream.

E2. Notes on a Radiofrequency Mass Spectrometer. JAMES C. AXTELL,* EMMETT H. WILEY,† AND S. W. BASS, *Texas College of Arts and Industries.*—Using a design based on a modification of the ion mobility apparatus of Tyndall and Powell,[1] the authors have constructed a radiofrequency mass spectrometer which has been able to separate the isotope of neon of atomic weight 22, with an over-all ion current of 100 milliamperes (measured at the source). The total through-put of the spectrometer was only 10 microamperes, showing an ion efficiency of only 0.01 percent. The device shows considerable promise of serving as an efficient isotope separator.

* Now at Southwest Research Institute.
† Now at General Electric Research Laboratory.
[1] Tyndall, Starr, and Powell, Proc. Roy. Soc. (London) **A121**, 172 (1928)

E3. The Range-Energy Relation for Heavy Ions. P. M. STIER AND G. E. EVANS, *Oak Ridge National Laboratory.*—The extrapolated ionization ranges of a number of heavy positive ions (H^+, He^+, N^+, Ne^+, N_2^+, and A^+) have been measured in a number of stopping gases (He, N_2, A, and air), at energies from about 50 to 300 kev. A monoenergetic beam of heavy ions

from a Cockcroft-Walton accelerator enters the range chamber by passing through three 0.030-inch pinholes, which form a highly collimated beam and act as barriers for a differential pumping system. Ionization-range data were obtained by using a movable parallel plate ionization chamber, 3 inches in diameter, whose "entrance foil" was a high transparency grid. For a majority of the incident ion-stopping gas combinations studied, the range-energy curve is approximately linear. It has been found that the range is not exactly inversely proportional to the pressure. An interpretation of this "pressure effect" based upon elastic scattering and geometrical factors, is proposed which accounts for the observed effects without recourse to any postulates concerning the mechanism of ionization.

E4. Space Distribution of Ionization. G. E. Evans and P. M. Stier, *Oak Ridge National Laboratory.*—The space distribution of ionization produced by a beam of positive ions entering a gas volume has been measured, using the same incident ions, stopping gases, and energies described in preceeding abstract. Relative ionization density was measured as a function of axial distance (R) and radial distance (r) using a small (*ca* 1 mm³) ionization chamber, eccentrically mounted so as to permit motion in three dimensions. Integration of ionization density data over planes normal to the beam axis yields results in good agreement with previously measured ionization range curves. Empirical relations have been established between relative ionization density, axial distance (R), radial distance (r), and pressure. It has been found that the axial attenuation of the ionization is approximately exponential, whereas the radial attenuation is approximately Gaussian. This is in qualitative agreement with the behavior to be expected if the primary mechanism of energy transfer is by elastic scattering.

E5. Measurements of Ionization Efficiencies. Willard H. Bennett, *Naval Research Laboratory.*—The nonmagnetic mass spectrometer[1] is being applied to the measurement of ionization efficiencies for multiple ionization. All voltages throughout the tube are held constant except the voltage through which the ionizing electrons are accelerated in the ion source. The various orders of ionization are separately measured by varying the frequency only of the rf potential used in the mass spectrometer. It can be shown when all voltages in the analyzer of the mass spectrometer are held constant, that the small deviations from a straight line path through the tube for any charge-to-mass ratio, when the appropriate frequency of the rf potential is applied to enable that charge-to-mass ratio to reach the collector, are identical with those for any other charge-to-mass ratio at its appropriate frequency. For this reason the instrument used in this way permits the relative ionization efficiencies for the different orders of ionization to be measured free of the errors that are unavoidable in any method requiring the use of slits.

[1] J. Appl. Phys. **21**, 143 (1950).

E6. Efficiencies of Multiple Ionization of Mercury. Boyd W. Harned and Willard H. Bennett, *Naval Research Laboratory.*—The relative efficiencies of multiple ionization of mercury vapor have been measured using the nonmagnetic mass spectrometer for electron energies up to 5 kilovolts. The total ionization as a function of ionizing electron energy has the same form as the results published by Compton and Van Voorhis,[1] P. T. Smith,[2] and J. W. Liska[3] but disagrees with the results of W. Bleakney,[4] as do the results of the others. The ion currents for each order of ionization also differ from the results of Bleakney in a similar manner, being smaller than Bleakney's at low voltages and larger at high voltages. An explanation for the discrepancy will be suggested.

[1] Compton and Van Voorhis, Phys. Rev. **27**, 724 (1926).
[2] P. T. Smith, Phys. Rev. **37**, 814 (1931).
[3] J. W. Liska, Phys. Rev. **46**, 169 (1934).
[4] W. Bleakney, Phys. Rev. **35**, 139 (1930).

E7. Total Specific Ionization in Air, Argon, and Hydrogen from 17.5-Mev Electrons. J. Ovadia, J. S. Laughlin, J. W. Beattie, and W. J. Henderson, *University of Illinois.*—The total specific ionization produced in air, argon, and hydrogen by a beam of monoenergetic electrons whose kinetic energy was varied from 9.0 to 17.5 Mev has been measured. The electrons were accelerated in a betatron, and the energy was varied by controlling the expansion time. An absolute energy calibration was obtained by observing known electrodisintegration thresholds. A thin lens magnet focused the electrons into a nearly parallel beam of 3-mm diameter, which then passed through a parallel plate ionization chamber and into a Faraday cage. Guard electrodes insured the uniformity of the collecting field in the chamber. The electron and ion currents were amplified in dc current amplifiers and their absolute values read directly. The ratio of these currents together with a knowledge of the pressure, temperature, and path length of the electrons in the chamber yields the total specific ionization. The total specific ionization in air and hydrogen was found to increase by 5 percent when the kinetic energy of the electron is raised from 9 Mev to 17.5 Mev. The following values of the total specific ionization produced by 17.5-Mev electrons were obtained in these gases: air, 64; argon, 101; hydrogen, 8.4; all the values are in ion pairs per cm at NTP.

E8. Average Energy Loss per Ion Pair of Slow Electrons in Helium. C. E. Nielsen, *Ohio State University;* R. H. Frost, *University of Missouri;* and W. J. Choyke, *Ohio State University.*—Either total or specific ionization produced by a low energy electron in an expansion chamber can, under suitable conditions, be obtained by the count of drops formed on the diffused ions. We have determined from a count of drops per cm of path the specific ionization of electron tracks of β from 0.3 to 0.8. Momentum was determined from measurements of curvature in a magnetic field perpendicular to the camera axis. From these results and application of the Bethe-Bloch theory one obtains a value of 26 ev per ion pair in He. We have determined from count of the number of drops per cluster the total ionization in ion clusters produced by x-ray photoelectrons of known energy. The preliminary value of average energy loss is 25 ev per ion pair.

E9. New Data on Electrical Phenomena Associated with the Freezing of Dilute Aqueous Solutions. Marvin E. Backman, *Inyokern.*—It was discovered by Workman and Reynolds[1] that electrical phenomena accompany the freezing of dilute aqueous solutions of ionic compounds. The exact nature of the effect is unknown and in order to obtain further information on the effect a study has been made of the dependence of the shape and magnitude of these curves on the concentration of the solute. A set of curves was obtained for a range of concentrations from 10^{-6} normal to 10^{-2} normal. The equipment used was the same electrometer apparatus used for earlier[2] investigation of the effect. Special techniques in the handling and preparation of solution were used to avoid CO_2 contamination.

[1] E. J. Workman and S. E. Reynolds, Phys. Rev. **78**, 254 (1950).
[2] M. E. Backman, Phys. Rev. **85**, 759 (1952).

E10. Lifetime of Injected Carriers in Germanium.† D. Navon, Ralph Bray, and H. Y. Fan, *Purdue University.*—The lifetime of carriers injected into germanium samples by the application of square voltage pulses across the rhodium plated ends has been measured. The decay of conductance of

the sample from its value just after applying the pulse to its pre-pulse value is observed on an oscilloscope. An analysis of this curve gives a value for the lifetime of the injected carrier. Using this method, the variation of lifetime with sample dimension and surface condition was studied for holes injected into a 19 ohm-cm single crystal of *N*-type Ge. The recombination velocity[1] for the ground surface was $\sim 10^4$ cm/sec. The etched surface lifetime was a few hundred microseconds and showed no significant variation when the cross section was decreased from 0.74×0.37 cm down to 0.48×0.06 cm, indicating that a bulk lifetime was measured. The surface recombination velocity should be <100 cm/sec, much lower than values previously reported.[1] Tests were made on the effects of quenching from temperatures of 500°C and above. Many-fold changes in bulk lifetime were observed before the electrical resistivity was noticeably increased. Additional heat treatment results will be discussed.

† Supported by Signal Corps Contract.

[1] Shockley, *Electrons and Holes in Semiconductors* (D. Van Nostrand Company, Inc., New York, 1950), pp. 321, 324.

E11. Alpha-Particle Bombardment of PbS Semiconductors. F. K. ODENCRANTZ, *Inyokern.*—The conductivity of a thin film of PbS was measured during bombardment with polonium α-particles. The conductivity initially increased several percent and then decreased slowly to about one-third of its initial value. Recovery of the PbS after bombardment required several days. Conductivity *vs* bombardment time curves show a temperature dependence.

E12. Anomalous Paramagnetism of Copper Sulfate Pentahydrate. W. E. HENRY, *Naval Research Laboratory.*—The magnetic moment of an aggregate of quantized, noninteracting paramagnetic ions can be represented[1] as a function of (H/T), where H and T are the magnetic field and absolute temperature. Previous work[2] has shown that the Brillouin function very closely represents the magnetic moment for Cr^{+++} in potassium chromium alum (free spin) and Fe^{+++} in iron ammonium alum (free ion) in the range near magnetic saturation. The same experimental technique has been employed to study, at fixed temperatures in the helium range, the magnetic field dependence of the state of magnetization of Cu^{++} in one sample of crystalline copper sulfate pentahydrate. Observations were made for magnetic fields ranging from 3 to 50 kilogauss. When relative moments are plotted against H/T, curves drawn through experimental points for different values of T do not superimpose. This implies that the magnetic moment is not a unique function of (H/T). The apparent anomaly is examined in terms of possible[3] effects of crystalline field splitting, dipole-dipole, exchange and nuclear interactions.

[1] J. H. Van Vleck, *Electric and Magnetic Susceptibilities* (Oxford University Press, London, 1932), p. 257; L. Brillouin, J. Phys. (U.S.S.R.) **8**, 74 (1927).
[2] W. E. Henry, Phys. Rev. **85**, 487 (1952); Bull. Am. Phys. Soc. **27**, No. 1, 53 (1952); **27**, No. 3, 53 (1952).
[3] K. S. Krishnan and A. Mookherji, Phys. Rev. **54**, 533 (1938); Bagguley, Griffiths, and Price, Nature **162**, 538 (1948); R. D. Arnold and A. F. Kipp, Phys. Rev. **75**, 1199 (1949); T. H. Geballe, Ph.D. dissertation, University of California, 1950.

E13. Low Temperature Thermal Expansion of Uranium.* HENRY L. LAQUER AND ADAM F. SCHUCH, *Los Alamos Scientific Laboratory.*—The length changes of a number of samples of polycrystalline uranium have been measured between room temperature and various fixed low temperatures, using a dial gauge dilatometer. It appears that uranium has a density maximum somewhere between 20° and 60°K. Certain speculative explanations of this rather anomalous behavior are offered.

* Work performed under University of California contract with the AEC.

E14. Mathematical Studies of Thermal Processes Relating to Reaction Rates in Solid Fuels. R. H. OLDS AND G. B. SHOOK, *Inyokern.*—With the aid of a differential analyzer the equation,

$$k\frac{d^2T}{dx^2}+\rho c v\frac{dT}{dx}+I_{0\alpha}\varepsilon^{-\alpha x}+\rho H s\varepsilon^{-E/RT}=0,$$

describing the dependence of temperature upon heat transfer by thermal diffusion, radiant absorption, and chemical action, is being investigated for conditions representative of steady-state burning of solid fuels in rocket motors. Values for the physical and chemical parameters are estimated from experimental data, considerable uncertainty being introduced by extrapolation of the data to conditions assumed to prevail at the burning surface. The primary objective of the mathematical study is to determine the ranges of values for the physical and chemical parameters that yield solutions to the above equation in accordance with the observed behavior of solid fuels. The results so far are proving useful in revealing the relative importance of the various parameters so as to guide research toward the investigation of the more significant factors.

E15. Measurement of Reaction Rates for Solids. G. B. SHOOK AND R. H. OLDS, *Inyokern.*—A rapid method has been developed for determining the constants s and E in the Arrhenius term $s\exp(-E/RT)$ describing the temperature dependence of chemical reactions. The method is limited in the present apparatus to solids in which the reaction is not primarily dependent on a diffusion process, although a correction may be easily applied for low diffusion rates. The apparatus consists of a flow chamber containing the sample, a difference thermocouple providing a control signal to a heater linked to a servo system, a thermocouple providing a signal to a recording potentiometer, and a sweep gas metering and heating system. The sample is allowed to change temperature adiabatically or with a predetermined departure from adiabaticity. Temperature control is effected through the sweep gas passing through the flow chamber, the gas being maintained at, or a given incremental amount different from the temperature of the sample. The corrected rate of temperature change is then interpreted to represent the rate of chemical reaction in the sample. The usable range in rate of temperature change is at present approximately 0.001°C/sec to 2°C/sec. Typical data obtained for the thermal decomposition rate of organic nitrates are presented.

MONDAY AFTERNOON AT 2:00

Shirley-Savoy

(C. D. ANDERSON presiding)

Invited Papers

F1. Experiments on Penetrating Cosmic-Ray Showers. V. H. REGENER, *University of New Mexico.* (30 min.)

F2. Thunderstorm-Precipitation Growth and Electrical-Charge Generation. S. E. REYNOLDS, *New Mexico Institute of Mining and Technology.* (30 min.)

F3. A Review of Tropospheric Propagation Data at Distances Far Beyond the Horizon. G. R. CHAMBERS, *National Bureau of Standards, Boulder.* (60 min for F3-F4-F5 altogether.)

F4. Recent Developments in the Theory of Electromagnetic Wave Propagation through Spherically Stratified Media. J. FEINSTEIN, *National Bureau of Standards, Washington.*

F5. The Effect of Scattering by a Turbulent Atmosphere on the Received Field Deep in the Shadow Region. H. STARAS, *National Bureau of Standards, Washington.*

MONDAY EVENING AT 8:30

Cosmopolitan

(J. A. WHEELER presiding)

Invited Paper

G1. Physics and Atomic-Bomb Tests. A. C. GRAVES, *Los Alamos Scientific Laboratory.* (50 min.)

TUESDAY MORNING AT 9:30

Cosmopolitan

(J. W. BROXON presiding)

Apparatus of Nuclear Physics; Mesons

H1. Internal Absorption of Fluorescent Light in Large Plastic Scintillators.* C. N. CHOU, *University of Chicago.*—The preparation and performance of comparatively small plastic scintillators have been reported by several authors.[1] In a series of experiments large plastic scintillators were constructed; the samples had the form of a rod 3.5 cm in diameter and 20 cm long. These samples were compared with liquid phenylcyclohexane solution (plus 0.3 percent *p*-terphenyl and 0.001 percent diphenylhexatriene) of the same dimensions. The pulse-sizes were observed in an oscilloscope from the output of a 5819 photomultiplier attached to one end of the sample. Radiation from a Co^{60} source passed through the sample perpendicularly to its axis. A sample of anthracene in polystyrene of diameter 4.1 cm and as long as 30 cm showed relatively small absorption (within about 15 percent) of light output throughout the whole length. This makes it possible to use scintillators of this kind in cosmic-ray counter telescopes, for triggering cloud chambers and for locating weak radioactive sources, etc. Pyrene in polystyrene was found to be almost as good as anthracene in polystyrene for small thicknesses; however, it showed greater absorption at greater lengths. With the 130-Mev mu-meson beam of the Chicago cyclotron no saturation occurred for the plastics up to twice minimum ionization. Measurements in the proton beam of the cyclotron are in progress, in order to study the saturation effect at higher ionization losses.

* Supported by the joint program of the ONR and AEC.

[1] M. G. Schorr and E. C. Farmer, Phys. Rev. **81**, 891 (1951); W. S. Koski, Phys. Rev. **82**, 230 (1951).

H2. The Minimum Temperature Gradient Required for the Formation of Tracks in a Cloud-Ion Chamber. H. L. MORRISON AND G. J. PLAIN, *Inyokern.*—The radial and vertical distribution of temperature in a cylindrical diffusion cloud chamber (filled with air and 95 percent ethyl alcohol vapor at atmospheric pressure) has been determined during operation by reading twenty-two copper constantan thermocouples supported by a light Bakelite framework. Readings were taken at regular time intervals, beginning with the addition of the solid CO_2, through thermal equilibrium, and until the chamber had ceased to operate upon the depletion of the refrigerant. The vertical temperature gradient in the sensitive volume (the lower one-third of the chamber) was found to be approximately 13°C/cm during thermal equilibrium. Tracks were no longer visible when the gradient had diminished to 9.7°C/cm. It is therefore concluded that a gradient of at least 10°C/cm is required for the formation of tracks. The addition of heat to the top of the chamber has negligible effect on the vertical temperature gradient in the bottom third of the chamber, and hence changes the depth of the sensitive volume only slightly. There appears to be no appreciable horizontal temperature gradient.

H3. Low Pressure Helium Diffusion Cloud Chamber. W. J. CHOYKE AND C. E. NIELSEN, *Ohio State University.*—The diffusion cloud chamber is stable only when the density gradient is positive downward. This requirement sets a maximum of approximately −20°C for the top temperature of a diffusion chamber employing ethanol in helium, at atmospheric

pressure, and an even lower temperature if the partial pressure of helium is below atmospheric. We have designed a chamber employing liquid nitrogen refrigeration that operates at pressures of helium down to one-fifth atmosphere with a sensitive region 1–3 cm deep. This chamber is being employed in a magnetic field in the study of a β-ray spectrum too weak to be measured in the usual β-ray spectrometer.

H4. A Low Pressure Cloud Chamber Investigation of Range-Energy Relations. ROBERT G. MILLS, *University of California, Berkeley.*—An expansion cloud chamber has been developed which operates at a total pressure before the expansion of about 45 millimeters. Because the rate of evaporation of water is high and the temperature of the gas very low during the sensitive time, the density of the gas is actually higher after the expansion than before. When the chamber is operated with oxygen and water vapor, the stopping power of the gas during the sensitive time is 7.6 percent that of NTP air. When it is operated with helium and water vapor, the stopping power is 5.7 percent that of NTP air. The chamber has been applied to the problem of the low energy range-energy relations for protons, alpha-particles, and oxygen ions. Monoenergetic neutrons are produced by bombarding thin lithium films with protons from the Berkeley Van de Graaff generator. These neutrons pass through the cloud chamber, producing elastic recoils of nuclei present in the gas. The energy of a recoil is determined by measuring the angle between its direction and the direction of the neutron trajectory. The range-energy curves found are in essential agreement with previous work of other investigators.

H5. The Deterioration of Self-Quenching Counters. STEPHEN S. FRIEDLAND AND HENRY S. KATZENSTEIN, *University of Connecticut.*—To determine the effects of dissociation of the polyatomic vapor used in self-quenching counters, two counters connected together through a stopcock were prepared and one was run for 10^{10} counts till it no longer acted as a good counter. The deteriorated gas was pumped into the second counter and its characteristics obtained. The old shell was treated and the gas put back into it. A mass spectrometer was used to study the dissociation products of the gas, and the results so obtained are used to explain the nature of the operating characteristics of the counters.

H6. Temperature Effect on the Counting Rate of Boron Neutron Counters. AUREL GOODWIN, JR., AND MARIO IONA, *University of Denver.*—The counting rate of BF_3 neutron counters was found to be dependent on the temperature in experiments supported in part by the Research Corporation and by the Geophysical Research Division of the Air Force Cambridge Research Center. An analysis of this effect was undertaken by measurements of differential pulse-height distributions which were obtained by using an amplifier of variable calibrated gain and selecting pulses of a narrow size interval by means of a two-channel discriminator circuit. The differential pulse-height distribution shows a large number of small pulses due to the gamma-rays of the Ra-Be neutron source. In addition there are large pulses of varying size from the boron disintegrations due to neutrons. At room temperature the two parts are separated by a distinct minimum of almost zero. An increase in temperature will change the counting rate due to changes in neutron density and change in cross section of the boron neutron reaction. However, the counting rates are changed also by a shifting of the pulse-height distribution toward smaller pulses. The larger pulses being more affected than are the smaller ones.

H7. μ-Meson-Electron Scattering.* W. D. WALKER, *University of California, Berkeley.*—The spectrum of knock-on electrons produced by high energy μ-mesons is being measured. The experiment has extended the previous measurements[1] to higher electron energies. The primary particles are required to traverse 1200 g/cm^2 of lead in order to trigger the apparatus. The knock-on electrons are produced in a carbon plate placed in the middle of a cloud chamber which is in a magnetic field of 1500 gauss. Preliminary results agree with the calculated spectrum.

* Assisted by the joint program of the ONR and AEC.
[1] Walker, Hammel, Sinclair, and Sorrels, Phys. Rev. **83**, 655 (1951).

H8. Lifetimes of the μ^- Meson Stopped in Light Elements —Apparatus. W. E. BELL* AND E. P. HINCKS, *Chalk River Laboratories.*—Cosmic-ray μ-meson lifetimes are being determined with apparatus designed to record the time delays in the emission of decay electrons with good stability and high accuracy. Both meson and electron are detected in an arrangement, previously described,[1] of 3 counter trays *A*, *B*, and *C* under 5½-in. lead and 2-ft concrete. The meson absorber is placed in a 2-in. space between trays *B* and *C*. Discharges of *B or C* following, with a short delay, the coincident discharge of *A* and *B*, but not *C*, are observed, and the distribution of delays between 1 and 11 μsec is recorded with a 10-channel "interval analyzer." A calibration to determine the delay limits appropriate to each counting channel is made daily using a high precision double-pulse generator. Pairs of fast-rising pulses are derived from a continuous sine wave generated by an *RC* type oscillator, and are repeated at a suitable low rate. The oscillator frequency is continuously variable over a range 40:1, and is checked at several points against quartz crystals. The interval between the test pulses of a pair is determinable with an uncertainty <0.3 percent.

* Now with Newmont Exploration Ltd., Jerome, Arizona.
[1] W. E. Bell and E. P. Hincks, Phys. Rev. **84**, 1243 (1951).

H9. Lifetimes of the μ^- Meson Stopped in Light Elements —Results. E. P. HINCKS AND W. E. BELL,* *Chalk River Laboratories.*—Absorbers of Li, Be, and C were used in turn to stop μ-mesons, and with the apparatus described in the preceding abstract the distribution of delays for about 30,000 decay electrons was observed for each. After correcting for accidental events, and to standard channel gate widths, the decay curves appear to be single exponentials, the mean lifetimes (μsec) being for Li, 2.20±0.02, for Be, 2.15±0.02, and for C, 2.12±0.03. Allowing for μ^+ mesons that decay in the absorber (the excess of μ^+ mesons of ~500 Mev at sea level is taken as 20 percent) counter walls and supports with a mean life 2.22±0.02 μsec,[1] the mean life (τ^-_{Li}), of slow μ^- mesons in Li is 2.15±0.09 μsec—not significantly different from the μ^+ lifetime. Assuming that the lifetimes for *decay* of μ^+ and μ^- mesons are, in fact, equal, it follows that the *capture* rate (A_{Li}) by a Li nucleus of a μ^- meson in its *K* orbit is $<3.5\times10^4$ sec^{-1} (with 85 percent probability.) Similar analyses of the results for Be and C yield the following values: $\tau^-_{Be}=2.05\pm0.06$ μsec; $\tau^-_C=1.98\pm0.08$ μsec. The corresponding capture rates are $A_{Be}=(3.7\pm1.5)\times10^4$ sec^{-1}; $A_C=(5.5\pm2.1)\times10^4$ sec^{-1}.

* Now with Newmont Exploration Ltd., Jerome, Arizona.
[1] W. E. Bell and E. P. Hincks, Phys. Rev. **84**, 1243 (1951).

H10. Lifetimes of the π^- and π^+ Mesons.* H. LOAR, R. DURBIN, AND W. W. HAVENS, JR., *Columbia University.*—The lifetimes of the π^- and π^+ mesons have been measured under similar conditions. A 73-Mev meson beam of either sign is collimated and monitored by a 10-ft telescope of three thin stilbene counters, 1¼-in. in diameter. An 8-in. diameter liquid scintillation counter is placed at a variable distance *L* behind the telescope. The number of fourfold coincidences per threefold monitor count is then measured as a function of *L*. The fourfold count rate decreases with increasing *L* due to the decay in flight of the π-mesons in the collimated beam. For decay at a distance greater than about 20 in. from the 8-in. counter, the μ-meson has a very small probability of being

counted. This probability is known from the kinematics of the reaction. The lifetimes were found to be $(2.55\pm0.19)\times10^{-8}$ sec for the π^- meson, and $(2.44\pm0.18)\pm10^{-8}$ sec for the π^+ meson.

* Sponsored by the joint program of the ONR and AEC.

H11. The Interaction Mean Free Path of π-Mesons in Lead.* FRITZ E. FROEHLICH AND KURT SITTE, *Syracuse University.*—An experiment is carried out at Echo Lake, Colorado (altitude 3260 m) to detect a possible difference between the interaction mean free paths of π-mesons and of nucleons. While the N-component incident from the atmosphere can be expected to contain in the energy region around 10 Bev, and at this altitude, only a few percent of π-mesons, this fraction would be considerably increased after "filtering" through a thick absorber if the mean free path of π-mesons exceeds that of protons. Consequently, one would then expect to observe a mean free path of the shower-producing radiation which increases with the absorber thickness, at least for absorbers of several times the proton mean free path. No such variation would be expected for less energetic showers since their primaries are practically all protons. The barometer effect offers a further check. Preliminary results of a run under 660 g/cm² show an increase in the interaction mean free path beyond the usual 165 g/cm², the reality of which will be discussed.

* Supported by the Air Force Cambridge Research Center.

H12. Multiple Scattering of Fast Pions in Photographic Emulsions. MEERA BACKUS AND J. J. LORD, *University of Chicago.*—The small angle multiple scattering of 218±10 Mev negative pions in 200-micron thick Ilford G-5 emulsions has been measured by the sagita method. In order to test the theory at very long cell lengths, ninety pion tracks of average length about 9000 microns were measured at cell lengths of 250, 500, 750, 1000, and 2000 microns. The average scattering factor[1] for cells of 500 and 750 microns was found to be 25.2±0.8 in an interval where spurious scattering corrections are negligible for these particles. This is in good agreement with the scattering factor obtained from monoenergetic protons from the Berkeley cyclotron.[2] The dependence of the average scattering angle upon the cell length is in fair agreement with theory. Comparison of these measurements with similar ones for cyclotron accelerated carbon nuclei of 1.1 Bev will be given.

[1] Martin Berger, sent for publication to *The Physical Review.*
[2] Berger, Lord, and Schein, Phys. Rev. **83**, 850 (1951).

H13. The Cosmic Radiation at Great Depths. WALTER GOAD, *Duke University and Los Alamos Scientific Laboratory.*—Greisen[1] has pointed out that the "knee" in the absorption curve of cosmic rays underground is probably due to the competition between nuclear collision and μ-decay of π-mesons after they have been produced. When one assumes that the mean free path for production of π-mesons by the primaries is equal the mean free path for interaction of π-mesons with nuclei, only two parameters enter this effect, the e-folding distance of the atmospheric density and the lifetime of the π-meson. With this assumption we have obtained from the underground data an energy spectrum with which π-mesons are produced in the range $10^{10}-10^{12}$ ev which is free of adjustable parameters. The effects of $\pi-\mu$ decay, and of all relevant electromagnetic processes have been included. The implications of these results for the properties of primary events involving multiple (or plural) production of mesons will be discussed.

[1] Kenneth I. Greisen, Phys. Rev. **73**, 521 (1948).

H14. Ionization Loss at Relativistic Velocities in Nuclear Emulsions. MAURICE M. SHAPIRO AND BERTRAM STILLER, *Naval Research Laboratory.*—Conflicting results have been reported on the variation of specific ionization I with velocity in nuclear emulsions (as measured by grain density g) at kinetic energies >2 rest masses. Interpretation of certain high energy phenomena requires a knowledge of this variation; yet the very existence of a rise in g above its minimum value $g_{\min}$ has been controversial. In 400μ Ilford G-5 emulsions exposed in the stratosphere we have measured g along the primary tracks of meson showers and along the shower tracks themselves. The frequency distribution in g of the shower tracks shows a peak at $g_{\min}$, whereas the primaries of showers with multiplicity ≥5 show a well-resolved peak at about $g=1.10$ $g_{\min}$. This indicates that for energies >10 rest masses, I exceeds $I_{\min}$ by $\simeq10$ percent. High energy electron tracks provide corroborative evidence. These findings support those of Voyvodic[1] on the existence of a rise in ionization above $I_{\min}$ to a "plateau" at higher energies. Implications for the theory of ionization and for the identification of particles are discussed.

[1] L. Voyvodic, Conference on V-Particles and Heavy Mesons, Bristol, December, 1951.

TUESDAY MORNING AT 10:00

University of Denver

(E. TELLER presiding)

Radioactive Substances

I1. K/L Internal Conversion Ratio in $M4$ Transitions.* G. A. GRAVES, L. M. Langer, AND R. D. MOFFAT, *Indiana University.*—It is observed that the $K/L+M$ internal conversion ratios for $M4$ transitions fall somewhat lower than the empirical curve of Goldhaber and Sunyar[1] in the region of low values of Z^3/E. The observations were made with the large magnetic spectrometer with measured resolutions of from 0.5 to 1.1 percent, depending on source thickness. The following values were obtained for the energy of the transition and for the $K/L+M$ ratio: Y^{91}, 551.2 kev, 6.00; Sr^{87}, 388.2 kev, 5.79; Y^{87}, 381.3 kev, 5.41; Ba^{137}, 661.4 kev, 4.64; In^{115}, 391.7 kev, 4.21 and In^{116}, 334.6 kev, 3.76. These points fall on a curve which joins smoothly with the empirical curve at high values of Z^3/E.

* Assisted by a grant from the Frederick Gardner Cottrell Fund of the Research Corporation and by the joint program of ONR and AEC.
[1] M. Goldhaber and A. W. Sunyar, Phys. Rev. **83**, 906 (1951).

I2. The Tritium Beta-Spectrum and the Mass of the Neutrino.* L. M. LANGER AND R. D. MOFFAT, *Indiana University.*—A direct determination of the beta-momentum spectrum of H^3 has been made in the large magnetic spectrometer. The

source is a thin and uniform layer of tritiated succinic acid[1] thermally deposited in vacuo onto a 1.5-microgram/cm² Zapon backing. A G-M counter with a 1.5-microgram/cm² Zapon side window is used for detection. The spectrometer was operated with a resolution of 0.7 percent. The Fermi plot of the data obtained with the thickest source (about 1 mC) is straight from about 7 kev out to the end point. Preliminary measurements indicate that the rest mass of the neutrino is less than 0.1 percent the mass of the electron, if it is the antineutrino that accompanies negatron emission. On the basis of the *Th A* line at $H\rho = 533.66$,[2] the maximum energy of the H^3 spectrum, obtained with a grounded source, is 18.0 ± 0.4 kev. It is anticipated that more precise data will be available in time for the meeting.

* Assisted by a grant from the Frederick Gardner Cottrell Fund of the Research Corporation and by the joint program of ONR and AEC.
[1] We wish to acknowledge the cooperation of E. S. Robinson and J. G. Povelites of Los Alamos Scientific Laboratories in preparing the tritium sources.
[2] H. Craig, Phys. Rev. **85**, 688 (1952).

I3. Low Energy Portion of the S^{35} Beta-Spectrum. G. J. PLAIN, H. L. MORRISON AND F. T. ROGERS, JR., *Inyokern.*—The low energy portion of the S^{35} beta-spectrum has been observed after the general method of H. O. W. Richardson and Alice Leigh-Smith, using a radioactive vapor in a continuously sensitive diffusion cloud-chamber. The activity was carried on trace quantities of labeled ethyl mercaptan.* One thousand low energy beta-tracks were measured, out of approximately 25,000 tracks recorded on nonstereoscopic photographs. Only those tracks which were well defined and in focus over their entire length were selected. From the observed spectrum it appears that there are few, if any, beta-particles from S^{35} having energies below 10 kev.[1]

* Obtained under AEC authorization No. 11695.
[1] Cook, Langer, and Price, Phys. Rev. **74**, 548 (1948).

I4. The Beta Spectrum of As^{76}. E. P. TOMLINSON AND S. L. RIDGWAY, *Princeton University.*—The As^{76} spectrum was investigated for information bearing on the interpretation of angular correlation measurements (abstract JA2 of the 1952 Washington meeting). Using the high resolution Siegbahn type double-focusing spectrometer, data on the highest energy spectrum (end point 2.98 ± 0.01 Mev) gave a Kurie plot originally curved, rectified by the $p^2 + q^2$ factor, indicating a transition of type $\Delta J = 2$, (yes). Subtraction gave for the next highest energy transition an end point at 2.40 ± 0.03 Mev. K conversion electrons were observed with energy corresponding to a transition of 558 ± 6 kev. Accepting Siegbahn's[1] decay scheme, the K conversion coefficient is $(2.0 \pm 0.2) \times 10^{-3}$ implying electric quadrupole according to Rose *et al.*[2] Assuming a zero even ground state of Se^{76} these date give two even for the first Se^{76} excited state and two odd for As^{76}. This work was supported in part by the AEC, and the Higgins Scientific Trust Fund.

[1] K. Siegbahn, Arkiv. Mat. Astron. Fysik, **34A**, No. 7 (1948).
[2] Rose, Goertzel, and Perry, ORNL Report 1023.

I5. Photoproduction of the Isomeric Pair of Bromine^{80}. ERICH M. HARTH, *U. S. Naval Research Laboratory.*—The relative yields of Br^{80} and Br^{80m} have been investigated by Fairhall,[1] using different nuclear reactions. It seemed desirable to obtain the ratio σ_g/σ_m of the number of nuclei produced in the ground state and the metastable state when they originate in a (γ, n) reaction. Bromine samples shielded with cadmium were irradiated with the bremsstrahlung spectrum from a 22-Mev betatron. The decay curves of the activities induced in the sample could be readily resolved by a subtraction method into the 4.4^h half-life of Br^{80m}, the 18^m half-life of Br^{80}, and a 6^m activity due to the $Br^{79}(\gamma, n)Br^{78}$ reaction. The ratio σ_g/σ_m was then obtained from the extrapolated initial 4.4^h and 18^m activities and the length of irradiation. Some of the ratios thus obtained are given in Table I as functions of the maximum photon energy. The values are in very good agreement with those obtained by Katz and others[2] using a similar method.

TABLE I.

E_{max}(Mev)	10.5	10.7	10.8	11.0	11.2	11.7	14.2	18.3	22.2
σ_g/σ_m	14	18	28	18	13	8.5	4.2	2.2	1.8

[1] A. W. Fairhall and C. D. Coryell, Bull. Am. Phys. Soc. **27**, No. 3, 39 (1952).
[2] Katz, Pease, and Moody, Bull. Am. Phys. Soc. **27**, No. 3, 20 (1952), and private communication to Dr. L. Seren.

I6. Radiations of Rh^{99} and Ga^{67}. S. C. FULTZ, R. J. NASH, R. L. WOODWARD, AND M. L. POOL, *Ohio State University.*—Radiations from Rh activities produced by bombardment of Ru metal with 6.3-Mev protons, were examined in a 180° focusing spectrometer. Internal conversion peaks corresponding to gamma-rays with energies of 0.144 ± 0.005 and 0.286 ± 0.005 Mev were observed and their half-lives measured. Both gamma-rays were found to decay with a long half-life of 4.3 days, corresponding to Rh^{101}, but the 0.286-Mev gamma-ray also decayed with a shorter half-life of 4.5 hours. Lack of positrons observed from Rh^{101} would indicate that the 0.286-Mev gamma-ray arises from Rh^{99} and is not an isomer of Rh^{101}. The gamma-rays of Ga^{67} have been examined by the coincidence method. The 295- and 180-kev gamma-rays have been confirmed as being in cascade, but the 90-kev gamma-ray is not in coincidence with the harder gamma-rays. Preliminary x-ray−gamma-ray delayed coincidence measurements made on a scintillation spectrometer indicate that the 90-kev gamma-ray is metastable, with a half-life in the microsecond range. Disintegration schemes for Ga^{67} and Rh^{99} will be presented.

I7. The Angular Correlation of the Gamma-Rays Emitted from the Excited States of Cd^{114}.* ROLF M. STEFFEN AND W. ZOBEL, *Purdue University.*—The angular correlation of the 548- and 715-kev gamma-rays of In^{114} has been measured using sources of $InCl_3$, $In_2(SO_4)_3$, and In metal sources. In spite of the short lifetime of the intermediate state ($< 2 \times 10^{-9}$ sec) an appreciable effect of the chemical state of the In^{114} sources on the angular correlation has been observed, the metal sources giving the supposedly unperturbed angular correlation: $f(\vartheta) = 1 + 0.09\cos^2\vartheta + 0.07\cos^4\vartheta (\pm 0.01)$. This correlation function is in good agreement with that reported before,[1,2] however the more accurate data make a revision of the former interpretation necessary. The observed angular correlation can be described in terms of a 4–2–0 cascade in which the 4–2 transition is a mixture of octupole and quadrupole radiation, or in terms of a 2–2–0 cascade in which the 2–2 transition is a mixture ($\delta = 0$) of quadrupole (4.4 percent) and dipole radiation (95.6 percent). In both cases the 2–0 transition to the ground state is by quadrupole radiation. The investigation of the 73-sec In^{114} ground state, produced directly by deuteron bombardment of In and Cd, showed conclusively that the gamma-cascade follows the K capture decay of the 72-sec In^{114} ground state indicating a spin 2 for the 1.26-Mev level of Cd^{114}.

* Work supported by the AEC.
[1] Rolf M. Steffen, Phys. Rev. **83**, 166 (1951).
[2] Johns, Cox, and McMullen, Bull. Am. Phys. Soc. **27**, No. 1 (1952).

I8. The Disintegration of Ce^{144} and Pr^{144}. FRED T. PORTER AND C. SHARP COOK, *Washington University.*—The radiations from the radioactive chain $Ce^{144} \rightarrow Pr^{144} \rightarrow Nd^{144}$ have been investigated, using chemically purified sources. Ce^{144} (295-day half-life) decays to the ground state of Pr^{144} through a 70 percent abundant beta-group having a maximum energy of 304 ± 2 kev. Conversion electrons have been observed which indicate

that within the praseodymium nucleus there are transitions having energies 33.7, 53.5, 80.7, 100.3, and 134.2 kev. The predominant number of the Pr^{144} beta-transitions go directly to the ground state of Nd^{144} through a 2.97 ± 0.01 Mev beta-group. Conversion electrons from a weak 60.3-kev transition in neodymium have been observed. Very weak gamma-radiation having energies 0.696, 1.5, and 2.185 Mev have been observed. The beta-spectrum indicates that less than 2 percent of the beta-transitions go to excited states of neodymium at 0.696 and 2.185 Mev. Using the evidence available a disintegration scheme will be proposed.

* Supported by the joint program of the ONR and AEC.

I9. Radioactivity of Pm^{143}, Pm^{145}, Pm^{146}, Pm^{148}, and Sm^{146}. JOHN K. LONG, M. L. POOL, AND D. N. KUNDU, *Ohio State University*.—7-Mev proton bombardments have been performed on enrichments of the isotopes of neodymium. An activity has been observed with a half-life of 250–280 days in Pm^{145}. The activity consists largely of electromagnetic radiation and is therefore believed to be K capture. In Pm^{143}, a K capture activity was observed with a half-life of 300–350 days. Pm^{146} has been found to have a positron activity of 0.45 ± 0.05 Mev with a half-life of 14–18 days. Pm^{148} decays by negative beta-particle emission of energy 0.75 ± 0.10 Mev with a half-life of 1½–2½ years. Samples of neodymium bombarded with deuterons in years past now show a low intensity alpha-particle activity, which supports the expectation that Sm^{146} may decay to the magic number nucleus Nd^{142}. The alpha half-life is calculated to be 10^{4}–10^{6} years.

I10. Radioactivity of Osmium. J. B. SWAN AND R. D. HILL, *University of Illinois*.*—Osmium activities of 15-day and 32-hour half-lives, which were previously ascribed to Os^{190} and Os^{191}, respectively, have now been positively assigned to Os^{191} and Os^{193}. Using ordinary osmium metal, both activities were shown to be present when samples were irradiated by pile neutrons, whereas the 32-hour activity was absent from samples activated by γ-rays from a 20-Mev betatron. A 14-hour activity, associated with a γ-transition of 74.2 kev, was also observed with both of the above irradiations. Conversion electron energies placed this activity in osmium. A growth of the 15-day activity, consistent with a parent half-life of 14 hours, showed that the 14-hour activity was in Os^{193}. The measured half-life of the 14-hour osmium activity probably identifies it as an $M4$ isomeric transition. It was confirmed that γ-rays of 41.7 and 129.1 kev follow the 15-day β-decay of Os^{193}. The 41.7-kev transition was identified as $E2$, and the 129.1-kev transition as an $M1$, $E2$ mixture. Long-lived γ-radiations of 650 and 228 kev have also been observed. These are probably associated with a previously reported 878 kev cross-over γ-transition in Os^{185}.

* Assisted by joint ONR and AEC programs.

I11. Radiations of Bi^{212}, Pb^{209}, and Tl^{209}. F. WAGNER, JR., M. S. FREEDMAN, D. W. ENGELKEMEIR, AND L. B. MAGNUSSON, *Argonne National Laboratory*.—The electron spectrum of the beta-active daughters in equilibrium with a sample of 10-day Ac^{225} was determined with a double lens spectrometer. The Kurie plot of the continuum was resolved into four components: 1.99 Mev, assigned to Tl^{209}; 1.39 and 0.96 Mev, assigned to Bi^{212}; and 0.62 Mev, assigned to Pb^{209}. Conversion electron lines were found at 417, 341, 200, 118, and 80 kev. A study of the equilibrium sample with a scintillation spectrometer showed gammas at 435, 230, and 165 kev and K x-rays. In a separated Bi^{212} sample gammas were found at 435 and at 120 kev. Coincidence measurements showed the 120-kev gamma to be in cascade with the 1.39-Mev beta. A study of the Pb^{209} beta-spectrum on a separated sample with the use of an anthracene scintillation spectrometer gave a Kurie plot with an end point of 640 kev. The 230- and 165-kev gammas are assigned to the alpha-activities present.

TUESDAY MORNING AT 10:00

Shirley-Savoy

(R. J. SEEGER presiding)

Invited Papers

J1. Recent Advances in the Theory of Magnetization. R. M. BOZORTH, *Bell Telephone Laboratories*. (45 min.)

J2. Noise in Electron Beams at Microwave Frequencies. D. A. WATKINS, *Hughes Research and Development Laboratories*. (45 min.)

TUESDAY AFTERNOON AT 1:45

Cosmopolitan

(W. B. PIETENPOL presiding)

Cosmic Rays

K1. Mass Determinations of Fast Cosmic-Ray Particles in Emulsions. L. VOYVODIC, *National Research Council of Canada*.—The mass spectrum of fast particles recorded in Ilford G5 emulsions is being investigated by means of the grain density-multiple scattering method, with particular emphasis on long tracks and precision measurements in order to obtain high mass resolution. Preliminary results are reported on shower particles and isolated tracks in 600-micron emulsions flown at high altitude. Besides pi-mesons and protons, two particles of intermediate mass have been found so far, with apparent masses of $1210\pm180m_e$ and $1330\pm200m_e$. The former event resembles the charged V-particle tracks occasionally observed

in cloud chambers, showing a change in direction through 20° with no visible recoil. The detailed analysis of this event is discussed.

K2. Collision Cross Sections in Cosmic-Ray Interactions. KURT SITTE, *Syracuse University*.—For heavy materials, counter experiments yield collision cross sections that are geometrical for very energetic primaries, and decrease with decreasing energy. Light nuclei are found to be "transparent" also at high primary energies. On the other hand, observations in cloud chambers and nuclear emulsions show large collision cross sections even for shower secondaries. Recently obtained data* are used to show that this discrepancy cannot be explained in terms of differences in primary energies, but is due to the inefficiency of counter experiments in eliminating preceding interactions. If due corrections are made, it appears that the counter data for heavy materials are compatible with a geometrical collision cross section for all primary energies above ~0.75 Bev. An upper limit of (0.25 ± 0.15) can be deduced for the probability of charge exchange in collisions of cosmic-ray protons and neutrons. While present data do not permit a quantitative analysis of counter experiments with light materials, it can be concluded that the "transparency" effect has been overestimated, and that the cross sections are at least closer to the geometrical value than the usual estimate.

* Harth, Froehlich, and Sitte, Bull. Am. Phys. Soc. **27**, No. 1, 15 (1952).

K3. Collisions of Heavy Primary Nuclei in Emulsions. N. L. ALLEN* AND E. PICKUP, *National Research Council, Canada*.—A survey will be given of the different types of collisions of incoming primary nuclei with target nuclei in Ilford G5 emulsions exposed at about 85,000 feet. Some collisions appear to be with hydrogen nuclei. A few events will be described in detail, together with an interpretation of the disintegration and the nature of the products.

* National Research Council of Canada Fellow.

K4. A High Energy Nuclear Interaction.* J. E. NAUGLE, *University of Minnesota*.—A very energetic nuclear disintegration due to a primary nucleus with a charge of 7 ± 1 has been observed in an emulsion pellicle. 127 ± 5 tracks with a grain density at or near minimum originated at or within 0.25 radiation lengths of the point of disintegration. All but three of the particles were contained in a cone of half-width 3°. The existence of only 3 slow evaporation particles indicates that the primary collided with a light nucleus of the emulsion or made a grazing collision with Ag or Br. By following the shower through 3 cm of glass, it was possible to δ-ray and grain count on the fragment of the incident heavy. The charge of the heavy after the collision was (5 ± 1). If one assumes that the charged mesons are emitted symmetrically in the backward and forward directions with relativistic velocities in the center of mass system, then one can calculate the energy of the incoming primary from the shape of the angular distribution in the laboratory system. This method gives an energy of 1.4×10^{14} ev/nucleon for the incident particle and is obviously independent of the theory of meson production assumed. The angular distribution and multiplicity is consistent with that predicted by Fermi[1] if 4 or 5 nucleons of the incident nucleus suffered collisions with nucleons of the target nucleus.

* This work supported by the joint program of the AEC and the ONR.
[1] E. Fermi, Phys. Rev. **81**, 683 (1951).

K5. Narrow Angle Pairs from Nuclear Disintegrations. J. J. LORD, D. M. HASKIN, AND MARCEL SCHEIN, *University of Chicago*.—An investigation is in progress to study the nature of very narrow angle pairs of particles emitted from nuclear interactions in Ilford emulsions. Out of 160 meson-produced stars, one produced by a cyclotron accelerated 135-Mev negative pion consisted of a 17-Mev proton track and a pair of 0.005 ± 0.001 radian angular divergence. Each track is of minimum ionization within a statistical precision of 15 percent. From multiple scattering measurements the first of these particles must be less massive than about $\frac{1}{2}$ that of a muon while the upper limit of the mass of the other is approximately that of a muon. The pair is emitted at an angle of 110° with the direction of travel of the incident pion. If the particles are assumed to be electrons, then the total energy $(205\pm36$ Mev), the opening angles, and the angle of emission are not incompatible with the process that the incident negative pion is converted in an interaction with a proton of the nucleus to produce a 60-Mev neutron and a 230-Mev gamma-ray which in turn is internally converted to a pair of electrons in the Coulomb field of this nucleus. On the basis of our previous knowledge the probability of this process should, however, be extremely low. Other similar narrow angle pairs from cosmic-ray induced stars will be discussed.

K6. Interactions of Secondary Particles from Penetrating Showers.* N. M. DULLER, W. D. WALKER,† AND J. D. SORRELS,‡ *Rice Institute*.—The mean free path for penetrating shower production has been measured for secondary particles from showers in carbon and heavier elements. For charged secondaries from carbon showers the mean free path is found to be 400 ± 100 g/cm² in carbon and 750 ± 200 g/cm² in lead. The mean free path of secondary particles from showers starting in lead, iron or brass is 1000 ± 200 g/cm² in carbon and 900 ± 200 g/cm² in lead. The preliminary results seem to indicate that a sizeable fraction of the secondary particles from carbon penetrating showers have a cross section close to the geometric. Secondary particles from iron or lead have a smaller cross section for the production of penetrating showers, probably because they have, on the average, lower energy than secondaries from carbon. There are four times as many secondary penetrating showers produced by charged secondaries as by neutral secondaries.

* Supported in part by a grant from the Research Corporation.
† Now on leave at the University of California, Berkeley, California.
‡ Now at California Institute of Technology, Pasadena, California.

K7. Nuclear Transparency and Nucleon Cross Section for Penetrating-Shower Producing Cosmic Radiation.* DAROL FROMAN, *Los Alamos Scientific Laboratory*.—Assuming incident particles react independently with individual nucleons with effective cross section, $\sigma_0=\alpha\pi k^2$, and using $\sigma_n=\pi k^2A^{\frac{1}{3}}$ for the nuclear cross section, the effective collision length becomes $L_e=A^{\frac{1}{3}}/N\pi k^2[1-\exp(-\alpha A^{\frac{1}{3}})]$. Using $\alpha=0.44$ and $k=1.45\times10^{-13}$ cm, L_e agrees better than the "geometric" collision length, $L_g=A^{\frac{1}{3}}/N\pi(\hbar/\mu c)^2$, especially for light materials, with published measurements of collision lengths in CH_2, H_2O, C, air, Al, Fe, Au, and Pb for both charged and neutral incident particles. These values give a mfp for incident particles in nuclear matter of $\lambda=4k/3\alpha=4.4\times10^{-13}$ cm. Cocconi[1] uses $\lambda\approx4\hbar/\mu c=5.5\times10^{-13}$ cm to fit his observed and calculated collision lengths in Pb, Fe, and C. Fernbach, Serber, and Taylor[2] find $\lambda=4.5\times10^{-13}$ cm for 90-Mev neutrons. Choosing $\sigma_0=\alpha\pi k^2=29$ mb would lead to lower multiplicities of meson production in nucleon-nucleon interactions than Fermi's[3] estimates based on $\sigma_0=\pi(\hbar/\mu c)^2=60$ mb.

* Work performed under the auspices of the AEC.
[1] G. Cocconi, Phys. Rev. **75**, 1074 (1949).
[2] Fernbach, Serber, and Taylor, Phys. Rev. **75**, 1352 (1949).
[3] E. Fermi, Prog. Theoret. Phys. **5**, 570 (1950); Phys. Rev. **81**, 683 (1951).

K8. Close Pairs of Tracks in Showers in Emulsions. J. Y. MEI* AND E. PICKUP, *National Research Council, Canada*.—In an analysis of the showers of minimum ionization particles associated with energetic cosmic-ray stars there appear to be more close pairs of particles ($\lesssim4°$ separation) than would be expected on a statistical basis, taking into account the average angular distribution for the shower particles. We have made measurements[1] for showers with n particles, where $6<n\lesssim20$,

and it is hoped to give results for a more extended analysis. Possible interpretations for this effect will be discussed, including the recent suggestion of an intermediate, short-lived neutral meson.[3] Some of the particles have been identified as pions.

* National Research Council of Canada Fellow.
[1] J. Y. Mei and E. Pickup, Phys. Rev. (to be published).
[2] Danysz, Lock, and Yekutieli, Nature **169**, 364 (1952).

K9. Angular Distribution of Penetrating Secondary Particles from Showers in Carbon and Lead.* W. D. WALKER,† N. M. DULLER, AND J. D. SORRELS,‡ *Rice Institute.*—A comparison has been made between the angular distribution of penetrating secondary particles of showers originating in carbon and in lead. The angular distributions are very similar with the following exceptions. Showers from carbon have relatively more particles within a narrow cone in the direction of the primary particle. Showers from lead have relatively more particles projected at angles of 40° or more from the direction of the primary particle. Several cases have been found showing pairs of penetrating secondary particles separated by angles of the order of 3° or 4°. Sometimes these pairs are found at wide angles, with respect to the direction of the primary. Similar events have been described by Danysz *et al.*[1] as the decay of a particle with low Q and very short lifetime. More pairs of particles appear to come from showers in carbon than in lead.

* Supported in part by a grant from the Research Corporation.
† Now on leave at the University of California, Berkeley, California.
‡ Now at the California Institute of Technology, Pasadena, California.
[1] Danysz, Lock, and Yekutieli, Nature **169**, 364 (1952).

K10. On the Lateral Structure of Electronic Showers in Air. M. H. KALOS AND J. M. BLATT, *University of Illinois.*—The distribution of particles at any depth and energy as a function of distance from the shower axis can be shown to satisfy an integro-differential equation which does not involve the angular distribution of the particles.[1] A similar equation will be presented for the angular distribution at any depth and energy (integrated over the lateral distance). A variation-iteration technique which converges to the solution can be formulated. A result for the tracklength value of the angular distribution is obtained by inserting a plausible trial function into the diffusion equation. Iteration of this result provides an estimate of its validity. A general explicit formula has been derived for the $2n$th moment of the tracklength value of the lateral distance in approximation $\frac{A}{}$ ($\beta \ll E \ll E_0$). The first 8 moments (up to and including r^{16}) have been computed using the ORDVAC electronic digital computer. These moments disagree with the ones derived from Molière's[2] function for monoenergetic electrons. The true distribution appears to have more of a "tail." Further work toward the solution of the corresponding diffusion equation will be reported.

[1] Echo Lake Cosmic Ray Symposium, paper no. 66 (June, 1949).
[2] G. Molière, in W. Heisenberg's *Cosmic Radiation* (New York, 1946), Chapter 3.

K11. Effects of the Atmosphere on the Penetrating Cosmic Radiation. H. O. CURTIS AND E. S. COTTON, *Air Force Cambridge Research Center.*—Data obtained with a cosmic-ray telescope operated continuously from October 9 to November 22, 1950, has been analyzed to determine more completely than previously[1] the effects of the atmosphere on the radiation observed. For each day in the period the average height for the production of the mu-mesons was computed by weighting the heights of various pressure levels according to the probable distribution of originating levels obtained by Sands.[2] The average density of the air confronting the pi-mesons was computed for each day by weighting the actual densities at increasing pressure levels exponentially to account for the absorption of the pi-mesons. The mean hourly counting rate, the station pressure, and the two parameters above were analyzed for statistical correlation. The results of this analysis will be presented.

[1] E. S. Cotton and H. O. Curtis, Phys. Rev. **84**, 840 (1951).
[2] M. Sands, Phys. Rev. **77**, 180 (1950).

K12. Burst Production in Material of Low Atomic Number by Cosmic Rays at Sea Level.* F. E. DRIGGERS,† *University of Michigan* (*introduced by* W. E. Hazen).—A large ionization chamber has been used to obtain an integral burst size-frequency distribution by amplifying and recording the electron pulses produced. A comparison of the integrated burst rate from the upper hemisphere with that produced by primaries with a small zenith angle permitted an estimate of the burst rate resulting from interactions of the N component. Calculations were made of the expected burst distributions arising from the electromagnetic interactions (bremsstrahlung, knock-on, and direct pair production) of spin 0 and spin $\frac{1}{2}$ μ-mesons. About $\frac{1}{4}$ of the observed bursts were attributed to the N component. The remaining burst rate agreed with the rate calculated for spin $\frac{1}{2}$ mesons to within the estimated uncertainty of the calculations—about 15 percent. Only if it is postulated that at least $\frac{1}{2}$ of the bursts generally attributed to μ-mesons arise from specifically nuclear force interactions are these results consistent with a spin of 0 for the μ-meson. If this possibility could be eliminated, these data would indicate a spin of $\frac{1}{2}$.

* Supported in part by the joint program of the AEC and ONR and by an AEC fellowship.
† Now with E. I. du Pont de Nemours & Company, Argonne National Laboratory.

K13. New Barometric and Temperature Coefficients for Small Cosmic-Ray Bursts. JAMES W. BROXON, *University of Colorado.*—Measurements and statistical procedures have been described.[1] Records for three months of the 1947–8–9 series were read by a fifth reader with improved conditions. For two of these, considerably better correlation was indicated. Previously noted disagreement among the readers, however, was augmented. Partial barometric and temperature coefficients were determined for the 1-mm bursts of the 1938–9 series, for each of the 18 months. These, also, were predominately negative. Comparison of monthly coefficients for the two series indicates that there was no considerable dependence of the coefficients upon the magnitudes of the different 1-mm bursts. In spite of the much smaller number of bursts, having only two readers appears to have provided vastly superior statistical reliability for coefficients based upon the entire period of the 1938–9 series. The best value for the barometric coefficient is about −4.6 percent/mm Hg and for the temperature coefficient, −2.5 percent/°C, based on daily average values. Using monthly averages, −9.1 percent/mm and −2.2 percent/°C are obtained. The latter are less reliable, but have significance ratios above the 1 percent level. Earlier positive long-time temperature coefficients are believed to have been caused by differences among readers.

[1] J. W. Broxon, Phys. Rev. **81**, 555 (1951).

TUESDAY AFTERNOON AT 2:15

University of Denver

(W. M. ELSASSER presiding)

Optical Physics

L1. A Survey of Isotope Shift in OI.* LEE W. PARKER AND JOHN R. HOLMES, *University of Southern California.*—An O^{18}-enriched oxygen sample (donated by A. O. Nier) has allowed examination of isotope structure in 18 atomic lines between 2000 and 10,000A. Strong sharp lines were obtained in a liquid nitrogen-cooled electrodeless quartz discharge tube containing about 0.2 mm of oxygen and 2 mm of helium excited by a 10-mc oscillator. The discharge was photographed through an external Fabry-Perot interferometer in series with a large prism spectrograph. The shifts were found to range from zero to as high as 0.5 cm^{-1} for λ2884. A semi-quantitative check on the mass effect theory is furnished by shifts in lines connecting states of the $2p^33p$ configuration through intermediate states of opposite parity. The specific mass effect should be the same for all states arising from the $2p^33p$ configuration, assuming Russell-Saunders coupling.[1] Thus the observed relative shifts between pairs of such states should be given by the normal mass effect alone. This is found to be true in two out of three cases, within experimental accuracy. Some newly resolved fine structure will be reported later.

* Supported by the ONR.
[1] See J. H. Bartlett, Jr., and J. J. Gibbons, Jr., Phys. Rev. **44**, 538 (1933), whose treatment of the $2p^33p$ configuration in Ne can be applied to $2p^33p$ in oxygen.

L2. Infrared Rotational Spectrum of Hydrogen Sulfide.* E. E. BELL, R. L. HANSLER,† AND R. A. OETJEN, *The Ohio State University.*—The infrared rotational spectrum of H_2S from 65 cm^{-1} to 250 cm^{-1} has been obtained and correlated with the energy levels predicted by Crawford and Cross.[1] The goodness of this correlation will be discussed.

* These measurements were obtained with a far infrared spectrograph constructed under contract between Wright Air Development Center and the Ohio State University Research Foundation.
† Eastman Kodak Research Fellow.
[1] B. L. Crawford and P. C. Cross, J. Chem. Phys. **5**, 621 (1937).

L3. Microwave Absorption and Dielectric Relaxation in Some Long-Chain Esters.* P. L. MCGEER, A. J. CURTIS, G. B. RATHMANN, AND C. P. SMYTH, *Princeton University.*—Dielectric constants and losses between 3° and 90° have been measured at wavelengths of 1.25, 3.22, and 10.0 cm and 577 m for thirteen long-chain esters. The critical wavelength, at which the loss is a maximum, increases with molecular length and with viscosity, as observed previously for alkyl bromides. The viscosities of the esters are slightly lower than those of alkyl bromides of approximately the same molecular length, but the critical wavelengths are only about half as large. This shows a greater ease of orientation of the esters, which may be due, in part at least, to the fact that the orienting dipole in the esters does not occur at the end of the molecular chain. Orientation of polar molecular segments, presumably, occurs by rotation around carbon-carbon bonds, which gives rise to a distribution of relaxation times. The distribution increases with increasing size of the ester molecule and decreases with increasing temperature.

* Supported in part by the ONR.

L4. The Spectral Distribution of Energy in the Fluorescence of Sodium Fluorescein. EARL H. GILMORE, *Inyokern.*—In most instances the experimentally observed emission band of sodium fluorescein is altered considerably by self-absorption. A study has been made to determine photometrically the character of the unaltered band. The emissions from solutions of differing concentrations were studied spectrally with a combination photomultiplier-tube monochromator. Integrated forms of Beer's law equations were used to arrive at the final results. The final curve obtained closely resembles that obtained by Nichols and Merritt[1] by visual photometry. Their observations were made on a line perpendicular to the exiting beam, whereas in the present work the observations were from the front and from the rear of the cell and on a line 45 degrees from the exiting beam.

[1] E. L. Nichols and E. Merritt, Phys. Rev. **30**, 328 (1910).

L5. Instantaneous Measurement of Transient Flame Temperatures.* GEORGE W. BAUSERMAN, *University of Denver* (*introduced by* Robert S. Bradford).—An instrument has been developed to determine the time-temperature relationships of sub-explosive flames of short duration. This instrument is based on a modification of the line-reversal method of temperature measurement. Descriptions will be given of the line-reversal method and of the modification of this method upon which the instrument is based. The design of the optical system and the electronic components of the instrument will be described, along with the method of producing test flames for use with the instrument. The method of calibration and determination of the accuracy of the measurements, and typical results obtained with the instrument, will also be discussed.

* This research is supported by the Ordnance Department of the United States Army.

L6. Wavelength Independent Photographic Dosimeter Employing Terphenyl Intensifying Screens.* HERMAN HOERLIN AND FRANK KASZUBA, *Ansco Research Laboratories.*—The emission of several organic scintillators has been investigated under gamma and x-ray excitation in the $\lambda_{eff} = 0.01$ to 0.60A range. Their fluorescent efficiency decreases rapidly with increasing wavelength. This trend is in marked contrast with the response of photographic film to the same radiation which is known to be low for the shorter and high for the longer wavelengths. The characteristics of intensifying screens and of film can therefore be matched to yield a dosimeter having fully wavelength independent response in the indicated range. Mechanically rigid and highly efficient screens containing 145 mg/cm^2 terphenyl powder, 105 mg/cm^2 Lucite and 4 mg/cm^2 $PbCl_2$[1] were made by a simple molding technique. Screens are placed in contact with both sides of a special, double coated monitoring film designed for medium light sensitivity and for very low reciprocity law failure in the 1-second to 40-hour exposure range. This dosimeter permits the monitoring of gamma- and x-ray dosages of 0.02 to 10 roentgens with a maximum interpretation error of 25 percent.

* Work supported by subcontract with the Argonne National Laboratory.
[1] Addition of $PbCl_2$ recommended by J. E. Rose and L. D. Marinelli, Chicago.

L7. Contrast and Color in Interference Fringes. H. W. WEDAA AND E. W. PRICE, *Inyokern.*—In applications using the Mach-Zehnder interferometer, the use of an approximately monochromatic light results in a loss of identity of the zero-order fringe so that the fringes all appear alike. This is a

serious disadvantage since a particular fringe can no longer be traced across discontinuities in the picture nor can it be identified in sequences of pictures. In recent work using a magnesium spark and a 4481A interference filter, it has been found that the zero-order fringe can be identified either by eye or with a photometer provided the interferometer is adjusted so that the color disperion in each branch of the interferometer is exactly the same. The dispersive effect of an excess of 2×10^{-4} inches of glass in one branch of the interferometer is illustrated by the lack of symmetry of color dispersion about the order zero in white light fringes using color films and the lack of contrast in fringes using a filtered spark. The excess glass is produced by rotating one of the interferometer plates on its horizontal axis through a small angle.

L8. Multiple-Beam Interferometric Study of Topaz Cleavage Faces and Polished Glass Surfaces. W. F. KOEHLER, *Inyokern.*—Multiple-beam fringes of equal chromatic order were formed by the film between the surface being investigated and an appropriately silvered optical flat. Crystal cleavage steps were determined from measurements of fringe steps. The c-dimension of the unit cell of topaz was determined by a method of successive approximations to be 8.77 ± 0.04A which agrees with the x-ray value within the experimental error. The local smoothness of polished glass surfaces in the range of several angstrom units, was measured using these techniques. The contours of the surfaces studied thus far do not indicate flow of glass during polishing, which is contrary to the Beilby Flow Theory.

Post-Deadline Papers, if Any

TUESDAY AFTERNOON AT 2:15

Shirley-Savoy

(K. K. DARROW presiding)

Invited Papers

M1. The Perception of Speech by Deafened Listeners and Its Relation to the Design of Hearing Aids. HARVEY FLETCHER, *Brigham Young University.* (30 min.)

M2. Shock-Wave Phenomena. R. J. SEEGER, *National Science Foundation.* (30 min.)

TUESDAY EVENING AT 7:00

University of Denver

(E. FERMI presiding)

Banquet of the American Physical Society

WEDNESDAY MORNING AT 9:30

Cosmopolitan

(E. FERMI presiding)

Session P

Discussion on the Components of the Cosmic Radiation

Discussion Leader: E. FERMI.

Members of the Panel: K. GREISEN, W. E. HAZEN, H. V. NEHER, E. P. NEY, E. TELLER, M. S. VALLARTA, J. A. WHEELER, and others to be chosen by the Discussion Leader.

WEDNESDAY AFTERNOON AT 2:00

Shirley-Savoy (Empire Room)

(A. C. GRAVES presiding)

Invited Papers

Q1. Measurements of Neutron-Spectra Using Nuclear-Emulsion Techniques. LOUIS ROSEN, *Los Alamos Scientific Laboratory.* (30 min.)

Q2. The Los Alamos Fast Reactor and Its Experimental Use. D. B. HALL, *Los Alamos Scientific Laboratory.* (30 min.)

Q3. Precision Measurement of the Annihilation Radiation and Decay Schemes of Tantalum 182 and Iridium 192. H. C. HOYT, *California Institute of Technology.* (30 min.)

WEDNESDAY AFTERNOON AT 2:00

Cosmopolitan

(J. A. VAN ALLEN presiding)

Symposium on Temperature, Composition and Motions of the Upper Atmosphere

R1. The Distribution of Atmospheric Ozone between 25- and 65-km Altitude. J. A. VAN ALLEN, *Iowa State University.* (25 min.)

R2. Study of Upper Atmospheric Winds by the Echo Methods. L. A. MANNING, *Stanford University.* (25 min.)

R3. Lunar Tides in the Ionosphere. A. G. MCNISH, *National Bureau of Standards.* (25 min.)

R4. Atmospheric Temperatures and Pressures at High Altitudes. H. NEWELL, JR., *Naval Research Laboratory.* (25 min.)

R5. Gravitational Separation in the Upper Atmosphere. L. M. JONES, *University of Michigan.* (25 min.)

THURSDAY MORNING AT 9:30

Shirley-Savoy

(J. KAPLAN presiding)

Session S

Discussion on Composition, Winds, Pressures, and Temperatures of the Upper Atmosphere

Discussion Leader: J. KAPLAN.

Members of the Panel: R. A. CRAIG, C. T. ELVEY, H. E. NEWELL, JR., MARCUS O'DAY, R. PENNDORF, and others to be chosen by the Discussion Leader.

THURSDAY AFTERNOON AT 2:00

Shirley-Savoy

(E. ROSSI presiding)

Session T

Discussion on the New Unstable Particles in Cosmic Radiation

Discussion Leader: B. ROSSI.

Members of the Panel: C. D. ANDERSON, E. FERMI, W. B. FRETTER, R. B. LEIGHTON, R. E. MARSHAK, C. PEYROU, M. SCHEIN, R. W. THOMPSON, H. YUKAWA, and others to be chosen by the Discussion Leader.

SUPPLEMENTARY PROGRAMME

SP1. The Use of a Radioactive Vapor in a Continuously Operating Diffusion Cloud Chamber.* G. J. PLAIN AND H. L. MORRISON, *Inyokern.*—A mixture of radioactive S^{35}† in the compound ethyl mercaptan and ethyl alcohol has been used in a diffusion type cloud chamber. Because of condensation of vapor on the bottom, extreme care must be exercised to prevent overloading. An activity of 8 mc in a volume of 1.18 cc of ethyl mercaptan had to be diluted with ethyl alcohol to one part in 10^3. It was observed during operation that a potential difference is developed between the top and bottom plates of the chamber. This potential difference influences the formation of the beta-tracks. Measurements indicated that if the bottom was one volt negative with respect to the top the quality of the tracks was noticeably reduced. When the bottom was made two volts negative track formation ceased. The best tracks were obtained when the top and bottom plates were maintained at the same potential.

* Obtained under AEC authorization.
† To be given at the end of Session H if the Chairman rules that time permits.

SP2. Experimental Demonstration of Kinks. GEORGE ANTONOFF.*—The discovery of kinks appears to be in contradiction with the classical view, which assumes the properties *vs* temperature change continually. For this reason the experimental results are distrusted by most people, inclined to attribute them to the experimental errors. This effect is purely psychological. The liquid must be brought into equilibrium by keeping it in a thermostat for some time. The thermo-control within 0.1°C is quite sufficient. Weighing of a pycnometer of 25 ml on an analytical balance will show the kinks quite distinctly and unquestionably. The effect is perfectly reproducible if the above conditions are followed. My theory, now forty years old, predicted the kinks and has shown itself in perfect agreement with the experimental evidence [see J. chim. phys. (Paris), Feb. (1952)].

* To be given at the end of Session C if the Chairman rules that time permits.

The First Denver Meeting of the American Physical Society

Every one of the first ten meetings of the American Physical Society was held in New York City; but when the Society at last decided to quit the confines of Manhattan, it bounded all the way to Denver. No Bulletin was issued for that eleventh meeting; and the omission of fifty-one years ago is now repaired by printing here in toto *the Minutes thereof. It is a pleasure to record that one of the authors of papers presented at that meeting—Professor Gordon Ferrie Hull—is still a Fellow of the Society. The paper given at this meeting was the first disclosure of the Nichols-Hull observations of the pressure of light.*

A joint meeting of the American Physical Society and Section B of the American Association for the Advancement of Science was held in the High School Euilding at Denver, Colorado, Thursday morning, August 29th, 1901.

In the absence of the President and Vice-President, Edward L. Nichols was made Chairman, *pro tempore.*

Benjamin W. Snow was elected Secretary, *pro tempore.*

The following papers were presented.

1. **Note on the Supposed Elongation of a Dielectric in an Electrostatic Field.** L. T. MORE.
2. **On Electro-Striction.** J. S. SHEARER (read by E. L. NICHOLS).
3. **The Pressure of Heat and Light Radiation.** E. F. NICHOLS and G. F. HULL (read by B. W. SNOW).
4. **The Heat of Combustion of Acetylene.** H. A. RANDS (read by title).
5. **The Fall of Temperature Through a Wedge-Shaped Wall of Glass.** ARTHUR BALL (read by title).
6. **On a New Method of Determining the Curve of Luminosity by Homogeneous Comparison.** D. B. BRACE.

BENJAMIN W. SNOW
Secretary, *pro tempore*

Author Index to Papers Presented at the Denver Meeting

Allen, N. L. and E. Pickup—K3
Anderson, A. B. C.—C9
Anthony, Romuald—A2
Antonoff, George—C3, SP2
Arnold, W. R., J. A. Phillips, G. A. Sawyer, E. J. Stovall, Jr., and J. L. Tuck—B7
Axtell, James C., Emmett H. Wiley, and S. W. Bass—E2
Backman, Marvin E.—E9
Backus, Meera and J. J. Lord—H12
Battat, M. E. and F. L. Ribe—B4
Bauserman, George W.—L5
Bell, E. E., R. L. Hansler, and R. A. Oetjen—L2
Bell, W. E. and E. P. Hincks—H8
Bennett, Willard H.—E5
Bonner, T. W., A. B. Lillie, and H. L. Taylor—D4
Bozorth, R. M.—J1
Brittin, Wesley E. and James H. Marable—C5
Broxon, James W.—K13
Calfee, Robert F., David M. Gates, and Byron E. Cohn—A5
Chambers, G. R.—F3
Chou, C. N.—H1
Choyke, W. J. and C. E. Nielsen—H3
Colgate, Stirling A.—D11
Condit, R. I.—A7
Conner, J. P., T. W. Bonner, and J. R. Smith—B1
Coon, J. H., E. R. Graves, and H. H. Barschall—D3
Curtis, H. O. and E. S. Cotton—K11
Donaven, T. W., D. N. Kundu, John K. Long, and M. L. Pool—B2
Driggers, F. E.—K12
Duller, N. M., W. D. Walker, and J. D. Sorrels—K6
Eldridge, John A. and Richard J. Brundy—D9
Elsasser, W. M.—A9
Evans, D. C. and W. M. Elsasser—C1
Evans, G. E. and P. M. Stier—E4
Evans, John E.—D5
Feinstein, J.—F4
Fermi, E.—Session P
Fletcher, Harvey—M1
Freeman, J. J.—E1
Friedland, Stephen S. and Henry S. Katzenstein—H5
Froehlich, Fritz E. and Kurt Sitte—H11
Froman, Darol—K7
Fultz, S. C., R. J. Nash, R. L. Woodward, and M. L. Pool—I6
Gates, David M., Robert F. Calfee, and Byron E. Cohn—A4
Gilbert, F. C. and Stirling A. Colgate—D12
Gilmore, Earl H.—L4
Goad, Walter—H13
Goldberg, E.—B5
Goodwin, Aurel, Jr., and Mario Iona—H6
Graves, A. C.—G1
Graves, G. A., L. M. Langer, and R. D. Moffat—I1
Graves, J. D., W. R. Ketler, and R. I. Condit—A6
Hall, D. B.—Q2
Halpern, Otto—D13
Harned, Boyd W. and Willard H. Bennett—E6
Harth, Erich M.—I5
Harvey, J. A.—D1
Henry, W. E.—E12
Hincks, E. P. and W. E. Bell—H9
Hoerlin, Herman and Frank Kaszuba—L6
Howell, Barton J.—C2
Hoyt, H. C.—Q3
Hughes, D. J., J. A. Harvey, and M. D. Goldberg—D6
Jones, L. M.—R5
Kalos, M. H. and J. M. Blatt—K10
Kaplan, J.—Session S
Kaplan, Joseph and Marx Brook—A1
Kennedy, William B.—A8
King, J. I.—A3
Koehler, W. F.—L8
Kretschmar, George G. and Henry W. Wedaa—C8
Langer, L. M. and R. D. Moffat—I2
Laquer, Henry L. and Adam F. Schuch—E13
Loar, H., R. Durbin, and W. W. Havens, Jr.—H10
Long, John K., M. L. Pool, and D. N. Kundu—I9
Lord, J. J., D. M. Haskin, and Marcel Schein—K5
Manning, L. A.—R2
McGeer, P. L., A. J. Curtis, G. B. Rathmann, and C. P. Smyth—L3
McNish, A. G.—R3
Mei, J. Y. and E. Pickup—K8
Miller, Stanley C., Jr., and R. H. Good, Jr.—C4
Mills, Robert G.—H4
Morrison, H. L. and G. J. Plain—H2
Naugle, J. E.—K4
Navon, D., Ralph Bray, and H. Y. Fan—E10
Newell, H., Jr.—R4
Nielsen, C. E., R. H. Frost, and W. J. Choyke—E8
Odencrantz, F. K.—E11
Olds, R. H. and G. B. Shook—E14
Ovadia, J., J. S. Laughlin, J. W. Beattie, and W. J. Henderson—E7
Packard, Martin E. and Harry E. Weaver—D8
Parker, E. N.—C11
Parker, Lee W. and John R. Holmes—L1
Pellam, John R. and Bernard Weinstock—C13
Phillips, J. A., W. R. Arnold, G. A. Sawyer, E. J. Stovall, Jr., and J. L. Tuck—B6
Plain, G. J. and H. L. Morrison—SP1
Plain, G. J., H. L. Morrison, and F. T. Rogers, Jr.—I3
Porter, Fred T. and C. Sharp Cook—I8
Regener, V. H.—F1
Remley, M. E., W. K. Jentschke, and P. G. Kruger—D2
Reynolds, S. E.—F2
Rinehart, John S.—C12
Rogers, F. T., Jr., and H. L. Morrison—C10
Rosen, Louis—Q1
Rossi, B.—Session T
Schremp, E. J.—C6
Seeger, R. J.—M2
Shapiro, Maurice M. and Bertram Stiller—H14
Shook, G. B. and R. H. Olds—E15
Sitte, Kurt—K2
Smith, R. R., T. I. Taylor, and W. W. Havens, Jr.—D7
Staras, H.—F5
Steffen, Rolf M. and W. Zobel—I7
Stephens, W. E. and M. E. Toms—B10
Stier, P. M. and G. E. Evans—E3
Stovall, E. J., Jr., W. R. Arnold, J. A. Phillips, G. A. Sawyer, and J. L. Tuck—B8
Swan, J. B. and R. D. Hill—I10
Tomlinson, E. P. and S. L. Ridgway—I4
Tuck, J. L., W. R. Arnold, J. A. Phillips, G. A. Sawyer, and E. J. Stovall, Jr.—B9
Van Allen, J. A.—R1
Voyvodic, L.—K1
Wagner, F., Jr., M. S. Freedman, D. W. Engelkemeir, and L. B. Magnusson—I11
Walker, W. D.—H7
Walker, W. D., N. M. Duller, and J. D. Sorrels—K9
Watkins, D. A.—J2
Wedaa, H. W. and E. W. Price—L7
Willig, F. J., F. A. Lucy, and R. G. Shreffler—C7
Witmer, Enos E.—D10
Yarnell, J. L., R. H. Lovberg, T. F. Stratton, and W. R. Stratton—B3

THE AMERICAN INSTITUTE OF PHYSICS

INCORPORATED

57 East 55 Street New York 22, N.Y.

MEMBER SOCIETIES:

American Physical Society
Karl K. Darrow, *Secretary*, Columbia University, New York 27, New York

Optical Society of America
Arthur C. Hardy, *Secretary*, Massachusetts Institute of Technology, Cambridge, Massachusetts

Acoustical Society of America
Wallace Waterfall, *Secretary*, 57 East 55th Street, New York 22, New York

Society of Rheology
G. J. Dienes, *Secretary*, Brookhaven National Laboratory, Upton, Long Island, New York

American Association of Physics Teachers
R. F. Paton, *Secretary*, University of Illinois, Urbana, Illinois

AFFILIATED SOCIETIES:

American Crystallographic Association
American Society for Metals
Electron Microscopy Society of America
Physical Society of Pittsburgh
Physics Club of Birmingham
Physics Club of Minneapolis
Cleveland Physics Society
Physics Club of the Lehigh Valley
Sigma Pi Sigma

ASSOCIATES:

Over seventy-five leading industrial corporations and other institutions which contribute to the support of the Institute.

JOURNALS:

The Physical Review
S. A. Goudsmit, *Editor*, Brookhaven National Laboratory, Upton, Long Island, New York

American Mineralogist
J. W. Stout, *Editor*, University of Minnesota, Minneapolis, Minnesota

Journal of the Optical Society of America
Wallace R. Brode, *Editor*, National Bureau of Standards, Washington 25, D. C.

The Journal of the Acoustical Society of America
Floyd A. Firestone, *Editor*, 57 East 55th Street, New York 22, New York

American Journal of Physics
Thomas H. Osgood, *Editor*, Michigan State College, East Lansing, Michigan

The Review of Scientific Instruments
Gaylord P. Harnwell, *Editor*, Randal Morgan Laboratory of Physics, University of Pennsylvania, Philadelphia 4, Pennsylvania

The Journal of Chemical Physics
Joseph E. Mayer, *Editor*, Institute for Nuclear Studies, University of Chicago, Chicago 37, Illinois

Journal of Applied Physics
Elmer Hutchisson, *Editor*, Case Institute of Technology, Cleveland 6, Ohio

Physics Today
Gaylord P. Harnwell, *Editorial Director*; Beatrice S. Bunce, *Managing Editor*, American Institute of Physics, 57 East 55 Street, New York 22, New York

OFFICERS

George B. Harrison, *Chairman*
Massachusetts Institute of Technology

George B. Pegram, *Treasurer*
Columbia University

GOVERNING BOARD

Karl K. Darrow
G. J. Dienes
S. A. Goudsmit
G. P. Harnwell
George B. Harrison
P. V. Hunt
Rudolph Kingsbury
Hugh S. Knowles
C. C. Lauritsen
F. W. Loomis
William F. Meggers
George B. Pegram
I. I. Rabi
Duane Roller
Frederick Seitz
Francis G. Slack
John C. Stehman
Richard M. Sutton
Mark W. Zemansky

Committee on Physics
Melvin Lax

ADMINISTRATIVE STAFF

Henry A. Barton, *Director*
Wallace Waterfall, *Executive Secretary*
Theodore Vosburgh, *Advertising Manager*
Ruth F. Bassler, *Publication Manager*
Betty H. Goodenough, *Assistant Secretary*
Bertie B. Nunemaker, *Circulation Manager*
Katherine Seitz, *Assistant Treasurer*

THE American Institute of Physics was founded in 1931 as a federation of leading societies in the field of Physics. It combines into one operating agency those functions on behalf of physics which can best be done by the societies jointly. Its purpose is the advancement and diffusion of physics and its applications to human welfare. To this end it promotes for itself or the Societies the nine journals listed on this page; it promotes unity and effectiveness of effort among all who are interested in physics; renders numerous direct services to physicists and to the public; and cooperates with government agencies, national associations, educational institutions, technical industries, and others in such manner as to realize the opportunities and fulfill the responsibilities of physics as an important and constructive human activity.